Predictive Computational Modelling of the c-myc Gene Regulatory Network for Combinatorial Treatments of Breast Cancer

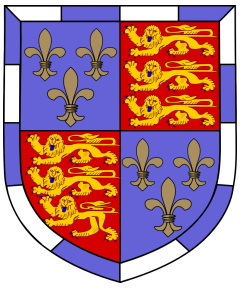

Matthew Alan Clarke

Supervisor: Dr. J. Fisher

Department of Biochemistry
University of Cambridge

This dissertation is submitted for the degree of
Doctor of Philosophy

Christ's College

September 2018

Predictive Computational Modelling of the c-myc Gene Regulatory Network for Combinatorial Treatments of Breast Cancer

Matthew Alan Clarke

As cancer tumours develop, competition between cells will favour those with some mutations over others, creating a dynamic heterogeneous system made up of different cell populations, called sub-clones. This heterogeneity poses a challenge for treatment, as this variety serves to ensure there is almost always a portion of the cells which are resistant to any one targeted therapy. This can be avoided by combining therapies, but finding viable combinations experimentally is expensive and time-consuming. However, there is also cooperation between sub-clones, and being able to better model and predict these dynamics could allow this interdependence to be exploited.

In order to investigate how best to tackle tumour heterogeneity, while avoiding acquired resistance, I have developed the first comprehensive computational model of the gene regulatory network in breast cancer focused on the c-myc oncogene and the differences between sub-clones. I model the system as a discrete, qualitative network, which can reproduce the conditions in heterogeneous tumours, as well as predict the effect of perturbations mimicking mutations or application of therapy.

Together with experimental collaborators, I apply my computational model to an *in vivo* mouse model of MMTV-Wnt1 driven breast cancer, which has high and low c-myc expressing sub-clones. I show that the computational model is able to reproduce the behaviour of this system, and predict how best to target either one sub-clone individually or the tumour as a whole. I show how combination therapies offer more paths to attack the tumour, and how two drugs can work synergistically. For example, I predict how Mek inhibition will preferentially affect one sub-clone, but the addition of COX2 inhibition improves effectiveness across the tumour as a whole.

In this thesis, I show how a computational network model can predict treatments in breast cancer, and assess the effects on different clones of different treatment combinations. This model can be easily extended with new data, as well as adapted to different types of cancer. This therefore represents a novel method to find viable combination therapies computationally and speed up the development of new cancer treatments.

I would like to dedicate this thesis to my loving parents, for all their help, care and inspiration.

Declaration

I hereby declare that except where specific reference is made to the work of others, the contents of this dissertation are original and have not been submitted in whole or in part for consideration for any other degree or qualification in this, or any other university. This dissertation is my own work and contains nothing which is the outcome of work done in collaboration with others, except as specified in the text and Acknowledgements. This dissertation contains fewer than 60,000 words excluding appendices, bibliography, footnotes, tables and equations.

Matthew Alan Clarke
September 2018

Acknowledgements

Firstly I would like to thank my parents for instilling in me the skills, values and insatiable curiosity that inevitably drove me to pursue science. I thank them for all the support and advice that helped me to succeed so far in life. It is thanks to them that I am able to be part of this endeavour to understand our world, and I wouldn't have it any other way. I would further like to thank all my friends and family for all their support in everything so far. I couldn't have done it without you.

I was incredibly fortunate to be working with such helpful and knowledgeable colleagues as I found in the Fisher Lab. I would like to especially like to thank Dr Nir Piterman and Dr Ben Hall for their tireless help in building the computational tools I needed to do my work, and helping me to understand the theoretical underpinnings of modelling networks. Dr Steven Woodhouse not only helped with the above, and was a key partner in developing the techniques used to analyse tumour evolution, but as someone who had recently gone through a PhD in the same lab, was helpful with all the questions I had about how to pursue the work and enjoy it.

But I was uncommonly fortunate in that I was able to benefit from two labs being behind me. The Evan Lab took me in and helped me as though I were one of their own. Professor Gerard Evan's help and advice was invaluable in guiding me through my PhD, and I am grateful for every moment of his time. I am thankful for helpful conversations with the whole group, but especially Dr Deborah Burkhart, Dr Catherine Wilson, Dr Ana Rebocho, Dr Luca Pellegrinet, Dr Nicole Sodir and Dr Roderik Kortlever, who all helped me navigate the world of myc. I am also grateful to the support from my fellow students in the lab, Ben Lam, and now Dr Dan Lu. I would also like to thank the Part III students who I had the privilege of supervising, Victoria Wang, Moritz Reiterer and Simon Lam. I am sure I learnt as much from you as you did from me, if not more, and I wish you all the best in the future. I would like to thank my advisor Dr Trevor Littlewood for his patient advice on myc and experimental design. Finally, I am immensely thankful to all the work of Dr Peter Kreuzaler, as well as his student Elizabeth Brown, whose mouse model of heterogeneous breast cancer was the foundation of this work.

Of course, none of this would have been possible without the help and support of the Mathematical Genomics and Medicine program, funded by the Wellcome Trust. I heartily thank the program directors, Professor Simon Tavaré, Professor John Todd, Dr Gos Micklem, Dr Richard Durbin, Dr Jeffrey Barrett, Dr Marc Tischkowitz, and Dr Chris Wallace, as well as those who run the program on their behalf and who helped me with any problems I had, with especial thanks to Joanne Heritage, Kati Sexton and Elizabeth McIntyre of the Clinical and Academic Training Office. I would also like to thank my rotation supervisor, Dr Joanna Howson, from whom I learned a lot.

The University of course provided excellent support, resources and training during my time at the Department of Applied Mathematics and Theoretical Physics and the Department of Biochemistry. I am grateful to Ben Stokell and Oliver Feng from the Statistical Laboratory for their help and advice. I am especially thankful to the members of my Graduate Thesis Panel, Professor Stephen Oliver, Dr Chris Smith and Dr Marc de la Roche, for their invaluable guidance. Microsoft Research Cambridge, where I spent much of my time, was an excellent place to learn research and an example of how partnership between industry and academia can work for all. I would also like to thank my PostDoc mentor, Dr Sarah Caddy, who helped me push myself harder and go outside my comfort zone. A special place in my heart will always remain for Christ's College, whose staff, students and Fellows have shaped so much of my time here in Cambridge, and always for the better. I would like to especially thank Dr Alan Winter, who persuaded me to teach Undergraduate Supervisions, which I found more fulfilling than I could have imagined. The College motto may be *Souvent me Souvient*, but I shall remember always.

Finally, none of this would have been possible without my supervisor Dr Jasmin Fisher, and her tireless help, guidance and insight into every aspect of myc and modelling. But most of all, for teaching me how to be the best researcher I could be.

Abstract

As cancer tumours develop, competition between cells will favour those with some mutations over others, creating a dynamic heterogeneous system made up of different cell populations, called sub-clones. This heterogeneity poses a challenge for treatment, as this variety serves to ensure there is almost always a portion of the cells which are resistant to any one targeted therapy. This can be avoided by combining therapies, but finding viable combinations experimentally is expensive and time-consuming. However, there is also cooperation between sub-clones, and being able to better model and predict these dynamics could allow this interdependence to be exploited.

In order to investigate how best to tackle tumour heterogeneity, while avoiding acquired resistance, I have developed the first comprehensive computational model of the gene regulatory network in breast cancer focused on the c-myc oncogene and the differences between sub-clones. I model the system as a discrete, qualitative network, which can reproduce the conditions in heterogeneous tumours, as well as predict the effect of perturbations mimicking mutations or application of therapy.

Together with experimental collaborators, I apply my computational model to an *in vivo* mouse model of MMTV-Wnt1 driven breast cancer, which has high and low c-myc expressing sub-clones. I show that the computational model is able to reproduce the behaviour of this system, and predict how best to target either one sub-clone individually or the tumour as a whole. I show how combination therapies offer more paths to attack the tumour, and how two drugs can work synergistically. For example, I predict how Mek inhibition will preferentially affect one sub-clone, but the addition of COX2 inhibition improves effectiveness across the tumour as a whole.

In this thesis, I show how a computational network model can predict treatments in breast cancer, and assess the effects on different clones of different treatment combinations. This model can be easily extended with new data, as well as adapted to different types of cancer. This therefore represents a novel method to find viable combination therapies computationally and speed up the development of new cancer treatments.

Table of contents

List of figures

List of tables

Papers arising from this PhD

1. **Mechanistic insights into myc heterogeneity in breast cancer.** Peter Kreuzaler, Matthew Clarke, Elizabeth Brown, Nir Piterman, Trevor Littlewood, Gerard Evan and Jasmin Fisher. (2017). *In preparation*

2. **Using State Space Exploration to Determine How Gene Regulatory Networks Constrain Mutation Order in Cancer Evolution.** Matthew Clarke, Steven Woodhouse, Nir Piterman and Jasmin Fisher. (2017). *In preparation*

Nomenclature

Roman Symbols

N	Granularity of a variable in a Qualitative Network
s	A state of a Qualitative Network
T	Set of Target Functions in a Qualitative Network
V	Set of all variables in a Qualitative Network
v	Variable in a Qualitative Network

Other Symbols

$\wedge$	Logical and
$\exists$	There exists
$\forall$	For all

Acronyms / Abbreviations

4-OHT	4-hydroxytamoxifen
ACTB	β-Actin
AIC	Akaike Information Criterion
ANOVA	Analysis of Variance
BDD	Binary Decision Diagram
BDT	Binary Decision Tree
bHLHZ	Basic-helix-loop-helix zipper

BIC	Bayesian Information Criterion
BMA	Bio Model Analyzer
CAG	A synthetic promoter used to ensure high gene expression
CC3	Cleaved Caspase-3
ChIP-seq	Chromatin Immunoprecipitation-sequencing
CldU	5-Chloro-2′-deoxyuridine, used to detect proliferation
Co-IP	Protein complex immunoprecipitation
COSMIC	Catalogue of Somatic Mutations in Cancer
Cre	Cre-recombinase, a virally delivered topoisomerase which triggers the recombination of loxP genes and so excision of Lox-Stop-Lox (LSL) cassettes
DMSO	Dimethyl sulfoxide
EGF	Epithelial Growth Factor
ER+	Cells with Oestrogen receptor
ER-	Cells without Oestrogen receptor
ER	Oestrogen receptor
FACS	Fluorescence-activated cell sorting
FBS	Fetal Bovine Serum (a.k.a Fetal Calf Serum)
GAPDH	Glyceraldehyde 3-phosphate dehydrogenase
GFP	Green Fluorescent Protein
GST	Glutathione S-transferase, GST used as tag to purify a protein of interest
GUI	Graphical User Interface
IdU	5-iodo-2′-deoxyuridine, used to detect proliferation
IL11	Interleukin-11

IP	Intraperitoneal Injection, used to administer drugs to animal models
KEGG	Kyoto Encyclopedia of Genes and Genomes
Lico	COX2 inhibitor Licofelone
loxP	Recognition site for Cre-recombinase
LSL	LoxP-STOP-LoxP cassette
LTR	Long Terminal Repeat
MEF	Mouse embryonic fibroblast
mG	Membrane-targeted green fluorescent protein
MI	Mutual Information
ML	Maximum Likelihood
MMTV	Mouse Mammary Tumour Virus
mTmG	A Cre reporter gene which expresses mT before activation by Cre-recombinase and mG after
mT	Membrane-targeted tandem dimer Tomato
MycER^{T2}	A fusion protein of c-myc and a murine N-terminally truncated ER gene, dependent on 4-OHT
ODE	Ordinary Differential Equation
PD	Mek Inhibitory PD-0325901
pRb	Retinoblastoma Protein
PR	Progesterone Receptor
PTEN	Phosphatase Tensin Homologue
PUMA	p53 Upregulated Modulator of Apoptosis
QN	Qualitative Network
REML	Restricted Maximum Likelihood

RFP	Red Fluorescent Protein
RNAi	RNA interference
ROSA26	A locus used to express a gene ubiquitously and constitutively in mice
RT-PCR	Reverse transcription polymerase chain reaction
RT-qPCR	Real time quantitative Polymerase Chain Reaction
SAT	Boolean Satisfiability Problem
SCID	Severe Combined Immunodeficiency
sd	Standard Deviation
shRNA	Short hairpin RNA
siRNA	Small interfering RNA
SMT	Satisfiability modulo theories
TBP	TATA-box Binding Protein
TF	Target Function
TNBC	Triple Negative Breast Cancer
TukeyHSD	Tukey Honest Significant Difference
VMCAI	Fast algorithm for checking stability, first presented at International Conference on Verification, Model Checking, and Abstract Interpretation
Wnt1	Wingless-related integration site 1

Chapter 1

Introduction

A human being is the most complex piece of machinery we know of. It is capable of growing from a single cell into an adult of trillions of cells, each of which must work in harmony to stably provide for one another an environment suitable to life. Further, these cells must form tissues capable of, at the macro level, outrunning a threat, while at the micro level being able to counter invasion by pathogens, and many things in between.

This leaves us with four key questions. How do cells, which all share the same basic genetic code, make the decisions necessary to adapt to these many and varied challenges? How do cells ensure that they make decisions as tissues and organs together, promoting cooperation, rather than competition? How do these decision making processes go wrong and result in disease? And how can we change these decisions in order to correct or counter this damage, and so save lives?

In this thesis I aim to investigate these questions in the case of breast cancer. Specifically, how breast epithelial cells make decisions about when to divide and when to die, and how this process fails in cancer. I also explore competition and cooperation between different tumour cells, focussing on heterogeneity in expression of the oncogene c-myc. It has been observed in breast cancer that one population of cells, or sub-clone, within the tumour often has higher c-myc expression. This is unsurprising as it is a potent oncogene, but that it does not dominate the cancer implies that there is a complex relationship between this and other sub-clones. This presents the opportunity to understand this relationship further through computational modelling, and to investigate whether or not it can be taken advantage of for therapy.

In order to do this, I build a discrete, qualitative network model of the gene regulatory network of breast cancer, which I describe in Chapter 3, and validate its behaviour against that of breast cancer cell lines. My collaborators in the Evan Lab (Department of Biochemistry,

University of Cambridge) created a mouse model designed to mimic such c-myc heterogeneity, described in Chapter 2. I further compared my model to this system to ensure it could reproduce the behaviour of breast cancer *in vivo*. This model then allows me to investigate the effect of therapy, modelled by perturbing the network. In Chapter 4, I focus on how the effects of drugs differ between different sub-clones. I show how different targeted therapies might affect one sub-clone preferentially, or affect tumour as a whole.

However, cancers can develop resistance to such targeted therapies. This can be countered by applying them in combination. In Chapter 5, therefore, I use the model further to assess how these treatments interact in combination, in order to identify those that cooperate to provide the best treatment, as well as eliminate those which interfere with one another. These predictions were then tested in the mouse model, and show that the model successfully predicts the treatment dynamics of both mono- and combination therapy.

The model can therefore be used to adapt to and take advantage of the heterogeneity of tumours by providing an understanding of the effects of treatments on different sub-clones. In Chapter 6 I demonstrate how the model can further be used to model the evolution of a tumour. This allows the identification of mutations which occur early in that evolution, and so are likely to be found in all the sub-clones that develop within the tumour. Therefore in addition to showing how to compensate for heterogeneity in treatment, the model also shows how one might best circumvent it entirely.

In summary, this thesis has three main goals: to build and test a model of heterogeneous breast cancer, to predict and test the most effective targeted therapies for this cancer, and to model the evolution of such cancers in order to provide better diagnosis and prognosis.

1.1 Challenges and Opportunities in Cancer Therapy

1.1.1 Need for Modelling

Cancer is one of the leading causes of mortality worldwide. It was responsible for causing 8 million deaths in 2010, increasing by 38% since 1990 [296]. Unlike pathogenic diseases, it is not caused by an external agent, which can be treated by exploiting differences between our biology and that of the pathogen. Nor is it a disease caused by a single malfunction within our bodies. Rather it is a disease of a cell performing too well. All multi-cellular organisms must control proliferation within their tissues, to prioritise procreation of the organism over that of the individual cell. Cancer occurs when cells escape these controls, and it continues to change and adapt under selection pressure within the organism, gaining new features to

better ensure its survival and growth [190]. This means that many of the mechanisms and redundancies that have evolved to ensure our survival are turned against us, giving cancer unrivalled resilience in the face of treatment. To understand how best to treat cancer requires the understanding of how the cell as a whole makes decisions in response to its environment, about when to divide and when to die, and how these are subverted by cancer. Further, it requires understanding of how these pathways interact to respond to treatment. This is a problem of enormous complexity, given the number of genes and proteins involved in these pathways, and the number of combinations of perturbations to consider. This is compounded by the variation between patients, but also within tumours [23]. All these factors suggest that even with a perfect understanding of the cell biology, there would be no one treatment, nor would any one treatment remain effective, as the cancer will continually evolve and adapt. This problem is ripe for the methods of computational biology, allowing the modelling of the response to treatment by the cell. In this thesis, I focus in particular on modelling breast cancer, with the aim of predicting the evolution and behaviour of tumours both with and without treatment, in order to guide experiment and drug target selection.

1.2 Tumour Heterogeneity

Tumours are diverse collections of diseased, healthy but co-opted, and immune cells [170, 321, 164]. This mixture changes as the tumour responds to pressure from its environment and to treatment, creating a complex, moving target for therapy. Heterogeneity also provides a pool of diverse mutations that can allow the tumour to quickly gain resistance to therapy [183]. It further results in complex relationships of cooperation and competition, where different sub-clones of a tumour might provide different functions necessary for a successful cancer (see Fig. 1.1). For example, sub-clones can provide paracrine and juxtacrine signalling between each other, becoming mutually dependent [49, 510], shaping the micro-environment [235], or allowing a small group of malignant cells to recruit a larger group of non-malignant cells [441, 154]. Heterogeneity is also a predictor of disease progression [312]. This means that ignoring this complexity jeopardises treatment success through imbalanced effects on one sub-clone over others (see Fig. 1.2). For example, allowing a small resistant sub-clone to support regrowth of sensitive sub-clones [263, 203]. In other cases a small population of cells may drive cancerous behaviour in surrounding cells, which are have no direct mutations. These co-opted cells are more treatable, while the cells driving the tumour may not be highly proliferative and so are not sensitive to conventional chemotherapy [441, 154].

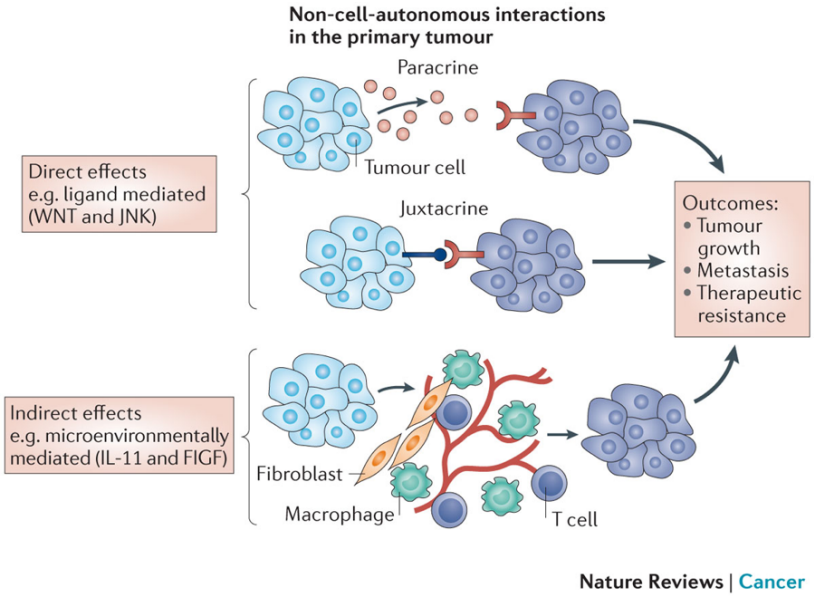

Fig. 1.1 Illustration of different ways in which tumour sub-clones can support one another, either directly through supply of growth factors, or indirectly by shaping the microenvironment of the tumour. In this thesis I consider a system in which both effects are present. (Reprinted by permission from Springer Nature: Nature Reviews Cancer, Tabassum and Polyak [431] © 2015)

This means that considering heterogeneity in planning treatment is a necessity, but it is also an opportunity (see Fig. 1.2). Taking advantage of this opens up new avenues for treatment. For example, Marusyk et al. [317] show how a tumour can be driven by supportive growth factors from a single sub-clone within the tumour. Targeting this sub-clone specifically removes this support and causes the tumour to collapse, as shown in Figure 1.3. Targeted therapies are also beneficial for a new therapy paradigm of Adaptive Therapy, as presented by Gatenby et al. [168] and demonstrated by Enriquez-Navas et al. [132]. In this case, rather than trying to eliminate a tumour entirely, the aim is to restrict and stabilise its growth, turning it into a chronic but manageable disease. This relies on being able to alternate focus on different sub-clones within the tumour in order to restrict growth, but also prevent the emergence of resistance by periodically removing the selection pressure against one of the drugs. This can be achieved by modulating the dose of a single drug, but would benefit from being able to target different sub-clones specifically. Both these methods have the advantage of targeting a smaller population of cells at a time and so providing fewer opportunities for resistance to develop [45]. All these methods would benefit from not only targeted therapies, but as wide range of options for targeted therapy as possible. This presents an opportunity for computational methods to identify such therapies, as a single model can

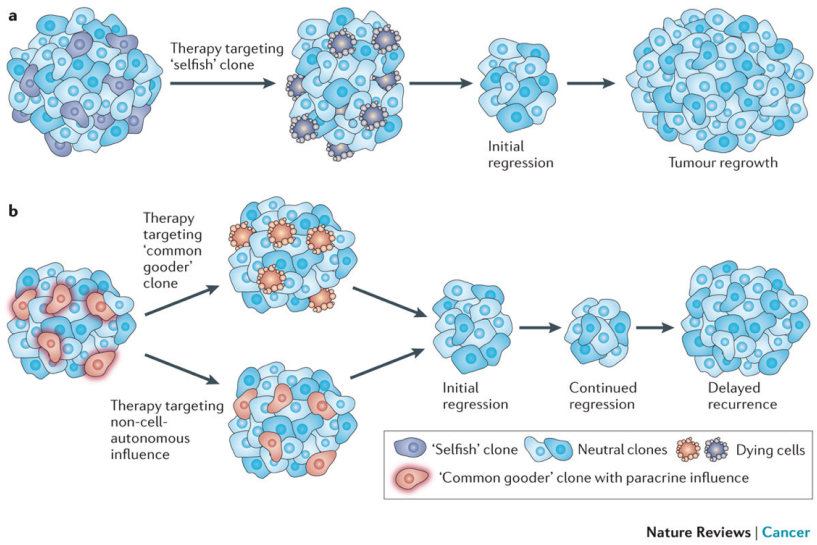

Fig. 1.2 Methods by which tumour heterogeneity and interdependence among sub-clones can pose a risk to the long term efficacy of targeted therapy, but can also be taken advantage of. In a) the targeting of a selfish clone does not treat the cancer as a whole, and may prompt competitive release. In b) basing targeting on disrupting cooperation improves long term effect. (Reprinted by permission from Springer Nature: Nature Reviews Cancer, Tabassum and Polyak [431] © 2015)

identify many potential treatments and so save time and expense over a more brute-force experimental search.

1.3 Targeted Therapy and Resistance

In order to exploit tumour heterogeneity, therapies are required that are capable of affecting a single sub-clone specifically as well as those which target all sub-clones broadly. There exist therapies, which, rather than attacking a proliferative cells in general, attack specific pathways or mutated proteins. Such targeted therapies are an exciting new development in cancer therapy; they show significant improvement in pathologic complete response [455, 186], 3-year event-free survival [173] and progression free survival [182, 179]. Accordingly, in the period from 2001-2011 their use has risen from 13% to 43% in the United States [405], and they have become an increasing focus in clinical trials (see Fig. 1.2). These treatments also promise fewer side-effects than chemotherapy [26, 459, 353] and reduced metastatic recurrence when used as adjuvant treatment following primary therapy [363, 376]. However, despite dramatic effects at the start of treatment, use of a single targeted therapy drug quickly leads to the emergence of resistance in many cases [72, 204, 464], and so new strategies are required for these therapies to reach their full potential (see Fig. 1.4). For example, different

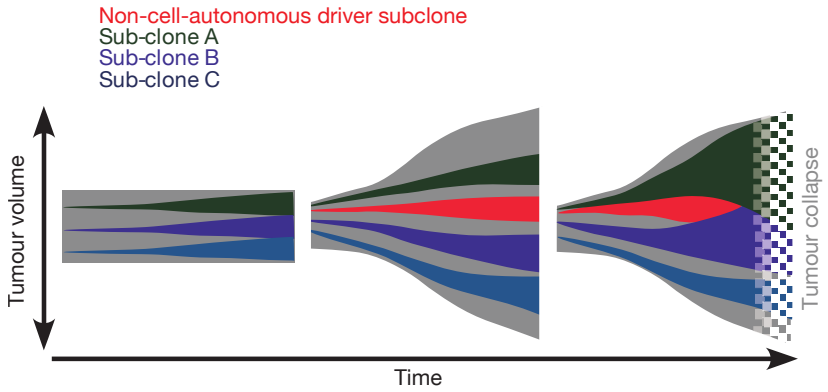

Fig. 1.3 Marusyk et al. [317] generated a model of cancer in mice in which one sub-clone supported the others through expression of interleukin-11 (IL11). They did this by first purposely culturing indolent tumours from the MDA-MB-468 breast cancer cell line, and then generating a panel of sub-lines secreting different factors. In the original tumour, volume remained steady (left), but that the addition of the IL11 expressing sub-line caused rapid growth (centre). Subsequent elimination due to competition from the other sub-clones it supported caused collapse of the tumour, implying addiction. This highlights the importance of even a small sub-clone in tumour dynamics. (Reprinted by permission from Springer Nature: Nature, Marusyk et al. [317] © 2014)

targeted therapies can be applied sequentially, forcing the tumour to acquire more resistance mechanisms in order to survive. This also allows the benefit of multiple treatments without the risk of toxic pharmacological interactions, unlike combining multiple therapies at once. However, combination therapy offers a greater chance of success (see Fig. 1.6a) [326].

The evolution of a tumour in response to treatment can also be taken advantage of. Basanta et al. [17] demonstrate how sufficient knowledge of how a tumour adapts to different treatments can be used to force it into a more treatable state, and so enable elimination because of the response to treatment, rather than in spite of it.

I present a method for using my model to predict tumour evolution in Chapter 6. I focus on the emergence of cancer, but the method could be adapted to the acquisition of resistance mutations in a developed tumour.

1.4 Combination Therapy

The specificity of action for which targeted therapies are valued also plays a role in the emergence of resistance. For any part of a pathway that is disrupted, this interference can often be effectively counteracted by mutations up- or down-stream in the same pathway. While in some cases this resistance emerges as a dynamic response to therapy [348, 57],

Fig. 1.4 Resistance to the targeted therapy of BRAF mutant melanoma with Vemurafenib (a.k.a PLX4032). A shows patient prior to therapy, B 15 weeks after therapy and C 23 weeks after therapy. (Reprinted with permission. © (2011) American Society of Clinical Oncology. All rights reserved. Wagle et al. [464])

it has become apparent that it is primarily due to the selection of a sub-clone containing pre-existing resistance mutations [451, 450, 224].

However, if two independent treatments are administered together, then there is no single mutation that can provide resistance, and the probability of both resistance mutations existing in a single cell is dramatically lower, increasing the probability of successful treatment. Mathematical modelling of tumours suggests that only a pair of drugs is sufficient to drastically reduce the chances of resistance, as shown by Bozic et al. [45] (see Fig. 1.6b), and Komarova et al. [256]. This benefit is not attained by changing drugs in response to resistance, as in the sequential therapy paradigm [45] (see Fig. 1.6a). Such combination therapies have been demonstrated in clinical trials; in the case of melanoma, for which single therapy produces rapid resistance [464], a combination of nivolumab-plus-ipilimumab increases progression-free survival to 11.5 months compared to 6.9 and 2.9 for either alone [275]. In the period from 2008-2012, 25% of US clinical trials in oncology were focussed on combination therapy [486].

Simply combining effective single treatments is not sufficient, as they may share a single resistance mutations (see Fig. 1.6). An understanding of the underlying mechanisms of cellular decision making to distinguish between truly independent and synergistic pairs of treatments is required, which I aim to provide with my model. Nevertheless, while

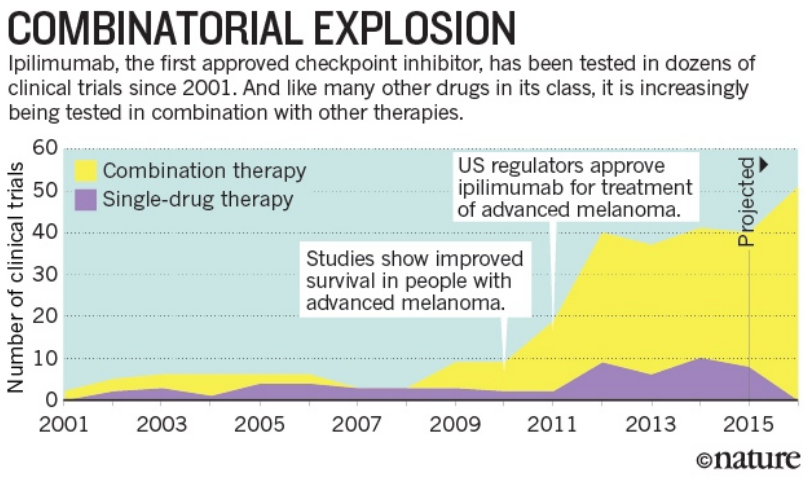

Fig. 1.5 Recent trends in clinical trials for anti-cancer drugs shows recent interest in combination therapy. (Reprinted by permission from Nature Publishing Group: Nature, Ledford [281] © 2016.)

synergistic combinations, those which are only effective together, are more likely to be defeated by a single resistance mutation, they are still likely to be more effective than single drug treatments [256]. Further, they are better tests of understanding of the network as they rely upon the cross talk between different pathways. Combination therapy also runs the risk of adverse interactions between drugs, which are hard to predict [150]. This makes testing drug combinations expensive. This, combined with the difficulty in distinguishing between truly independent and synergistic drug combinations, requires us to have a robust method of drug discovery that minimises the chances of false positives. The only way to do this is to understand the complex interactions of the gene regulatory network of the cell.

1.5 Breast Cancer

Breast cancer is the second most common cancer worldwide at 11.9% of cancer diagnoses in 2012, and the cause of over 500,000 deaths globally per year [144]. There has been a decline in breast cancer mortality in the UK of around 30% between the late 1980s and 2006 [13], as a result of a combination of the introduction of screening [222] and Tamoxifen therapy [46]. However, of the major breast cancer sub-types, both basal and triple negative (TNBC) breast cancers are frequently estrogen-negative (ER-) and so not treatable by Tamoxifen. These sub-types have higher mortality [414] and have fewer treatment options [220]. In order to better understand the development of such tumours, and so improve treatment, a better understanding of their evolution and response to treatment is required.

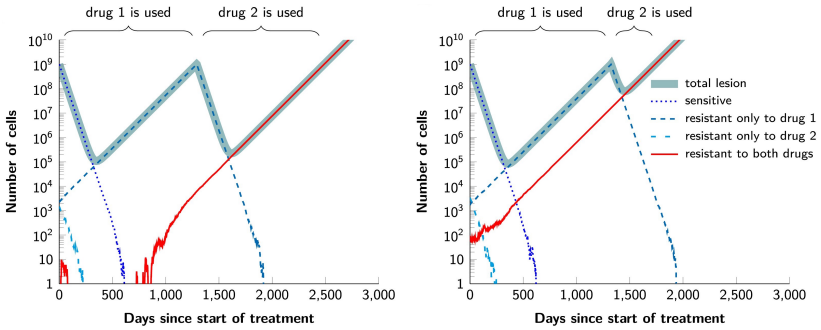

(a) Example simulations show that for a tumour of a detectable size, the rate of cell death from simulated therapy is insufficient to avoid tumour resistance emerging, and although sequential extends the time for which therapy is effective, it does not results in elimination. In the first example simulation (left), a mutation for resistance to both drugs only emerges later, while resistance to the first drug applied is pre-existing, and so combination therapy may have performed better. In the second simulation (right) a single mutation providing resistance to both drugs is pre-existing showing the limitations of combination therapy. (This Figure is from the supplement to Figure 5.)

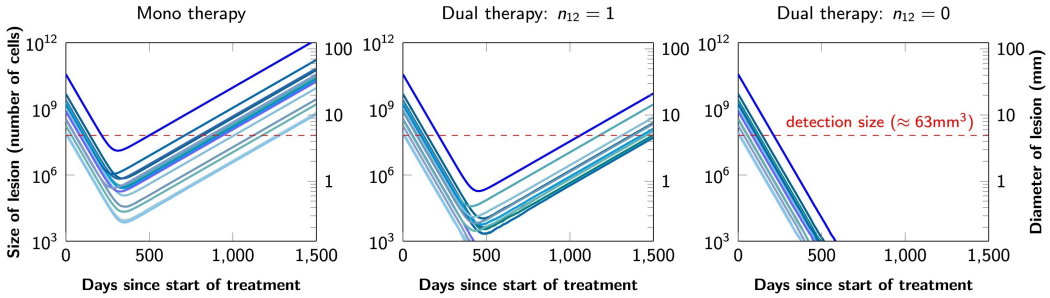

(b) Example simulations of combination therapy show that a pair of drugs reduces the chance of a resistance mutation pre-existing within the a cell of the tumour, and of one emerging during treatment. This improves the chance of tumour elimination, particularly in the case where there is no single mutation providing resistance to both drugs ($n_{12} = 0$), although there is still some benefit if this is the case ($n_{12} = 1$).

Fig. 1.6 Bozic et al. [45] (CC BY 3.0) constructed a mathematical model of cell division, death and mutation under treatment, and simulated the effect of sequential therapy (1.6a) and combination therapy (1.6b). Both drugs applied had 50 possible point resistance mutations, and the cell had a mutation rate of 10^{-9}, allowing the simulation of the acquisition of resistance in both treatment paradigms.

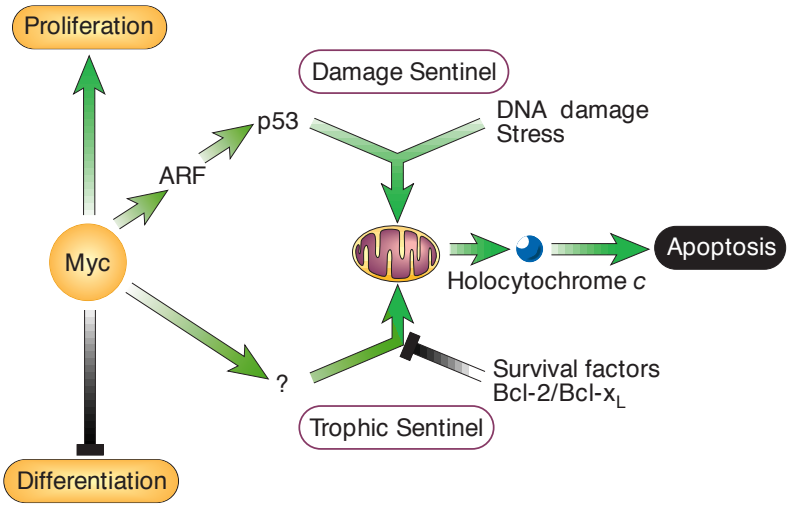

Fig. 1.7 High c-myc expression produces cancerous phenotypes by driving proliferation and suppressing differentiation. However, it also increases apoptotic signalling, through p53-dependent and -independent methods. This means that c-myc driven proliferation alone overcomes the influence of survival factors, leading to cell death in a process referred to as the Trophic Sentinel by Evan and Vousden [135] (Figure reprinted by permission from Springer Nature: Nature, Evan and Vousden [135] © 2001).

Furthermore, breast cancers often exhibit heterogeneity in oncogene expression between sub-clones. In order to successfully treat the tumour as a whole, the cooperation and competition between these sub-clones, and how these dynamics affect treatment effectiveness on individual sub-clones, requires a mechanistic model of tumour behaviour in response to treatment. In this Thesis I build, test and predict therapies from such a model, as well as use it to predict the order in which tumours acquire mutations. I especially focus on the effects of heterogeneity in the c-myc oncogene amongst tumour sub-clones.

1.5.1 c-myc

c-myc (henceforth myc) is a key driver of the cell cycle, and plays a key role in many cancers [340]; being overexpressed in 45% of breast cancers, 67% of colon cancers and 70% of prostate cancers. Expression of myc alone is sufficient to increase proliferation [128] although it must still cooperate with other oncogenes in order to form tumours [273]. It also encourages de-differentiation of cells [146]. This is an important marker of breast cancer stage [228], and is important in the emergence of putative cancer stem cells [159]. However, overexpression of myc can also trigger apoptosis [136]. These contradictory functions imply a fine degree of control by the decision making processes of the cell, expressed as the

network of interactions between transcription factors. To understand myc also requires an understanding of how its pathways interact with the rest of the gene regulatory network, to be able to predict why in cancer proliferation overcomes apoptosis, and how this might be corrected.

Myc, unlike other oncogenes, may be essential to tumour proliferation, and so if targeted for therapy could not be replaced [466], making resistance difficult. Because of this, and the prevalence of its overexpression in cancer, myc presents a tempting target for therapy [415]. Unfortunately, as with many transcription factors, myc has proven hard to drug [212, 101]. There have been promising developments in indirect myc inhibition using bromodomain inhibitors [365]. In this Thesis I explore the pathways controlling myc, and its effectors, for routes to treatment despite its resistance to targeted therapy.

1.5.2 Myc Heterogeneity in Breast Cancer

Despite the powerful oncogenic effects of myc, there are many cases where it is only expressed in one sub-clone of a heterogeneous breast cancer. Gupta et al. [187] found that in triple negative breast cancer cell lines and primary patient tumours, there exist distinct populations of SOX2 expression, which they show is driven by heterogeneity in myc expression. They saw similar patterns in ER+ breast cancer [485], oesophageal cancer [508] and ALK-positive anaplastic large cell lymphoma [169]. They further found that higher proportions of high-myc cells correlated with worse patient outcome. Glöckner et al. [177] found that in all cases of myc amplification in breast cancer, there was also intratumoural heterogeneity for this amplification, with Pavelic et al. [357] showing similar results. Finally, Leung et al. [285] demonstrate that tumours induced by MMTV-Myc perform better when one sub-clone loses myc expression. As myc is a strong promoter of proliferation, this observed heterogeneity raises the question of why high myc sub-clones do not out-compete other sub-clones and dominate the tumour. to explore this further, I not only model the gene regulatory network focussing on myc, but also aimed to model the methods by which high myc expressing sub-clones might provide non-cell autonomous support, and receive the same, from other sub-clones within the tumour. I then compare this to a mouse model of breast cancer heterogeneous in myc, created by Dr Peter Kreuzaler.

1.6 Tumour Evolution

I further apply my network to modelling tumour evolution. Multicellular organisms, in particular long long-lived ones such as mammals, must assure the survival and procreation of the organism as a whole over the individual survival of a single cell. As such, organisms have evolved robust mechanisms to control proliferation and to detect and remove damaged or malfunctioning cells [59]. Consequently, no single mutation is believed to suffice to elicit tumour formation; rather cells require several key changes in order to escape these controls, out-compete healthy cells, and adapt to the new environment that emerges as a tumour forms [190]. These controls, and the different characteristics that are favoured at different stages of tumour evolution, will restrict which mutations are selected for and observed at different stages. In addition to using my model to search for effective treatments in a developed cancer, it can also be used to model the evolution of a cancer.

This evolution is not linear; while fitter sub-clones out-compete their neighbours they do not necessarily dominate and many tumours become highly heterogeneous, with competition [183] and cooperation [431] between clones. As discussed in Section 1.2, this poses a problem for treatment, with the degree of heterogeneity being a predictor of poor prognosis [312] and serving as a pool of possible adaptations to therapy, leading to the rapid emergence of acquired resistance [45], particularly in the case of targeted therapy [72].

Nonetheless, tumours largely come from a single cell, even in cases of strong environmental factors such as smoking, or where there is a germline mutation that causes a predisposition [105]. In testimony to the efficiency of the body's tumour surveillance mechanisms, this also suggests that despite heterogeneity there will be shared mutations, with the order in which mutations emerge determining which are the most prevalent among tumour sub-clones [449]. As these are also likely to be driver mutations, treatments targeting these would be more broadly effective against the entire tumour. Furthermore, existing treatment may preferentially affect late, sub-clonal mutations. For example, Sun et al [425] observe that in acute myeloid leukaemia, cells carrying early mutations persist and may play a part in relapse, with similar results from Ding et al [113]. This suggests that targeting founder mutations may help avoid this pool of early mutations and reduce rates of relapse.

In order to take advantage of this commonality underlying tumour heterogeneity, there is a need to understand the constraints on the acquisition of tumour promoting mutations as the tumour progresses. This allows the prediction of which mutations occur early in tumour development and so are best for treatment. In Chapter 6, I present a method to study how positive and negative selection influences the evolution of tumours, and so determines the

order of mutations, based on the gene regulatory network. I apply this to my model of breast cancer.

1.7 Gene Regulatory Networks

In order to find the best combination treatments for heterogeneous breast cancer, as well as to study the evolution of such cancers, I look to the genetic regulatory network of cells. This is a combination of DNA and protein interaction networks, which regulate one another in response to the environment. For example, a growth factor might trigger a phosphorylation cascade in proteins already in the cell, which results in a transcription factor being able to bind the DNA and make new protein required to respond to the situation.

Cell behaviour needs to be predicable and robust to noise, so that tissues and organs form and function properly. In a healthy cell, protein-protein and protein-DNA interactions will form feedback loops to ensure homeostasis, and that any response to the environment is proportional. How this can be accomplished has been demonstrated in synthetic circuits by Becskei and Serrano [22] and Bleris et al. [42]. These authors demonstrate small sub-networks, or motifs, which form the basic building blocks of larger networks. Similar motifs have been observed in animals, with interactions forming simple logic gates. This is reviewed by Davidson [104] in the context of development. As such, gene regulatory networks must have robust stable states to which they return, associated with cell fate [218].

As these motifs are combined in the network, they allow the cell to respond in complex ways to a changing environment [223]. There has been much interest in how to manipulate these networks to guide stem-cell development for better production of experimental cell lines, and one day tissue [366], and reprogram cells to be used as therapies [288]. In the same way, understanding such networks can lead to more efficient interventions to change cancer cell behaviour. To gain such understanding, it is necessary to model these systems to predict how they react to perturbations. What is the best way to model these interactions, and how can experimental data be used to produce them?

1.8 Modelling Gene Regulatory Networks

1.8.1 Level of Abstraction

In a perfect world, it would be possible to model a system precisely and quantitatively. However, this is often infeasible due to limitations on the data available to build and test

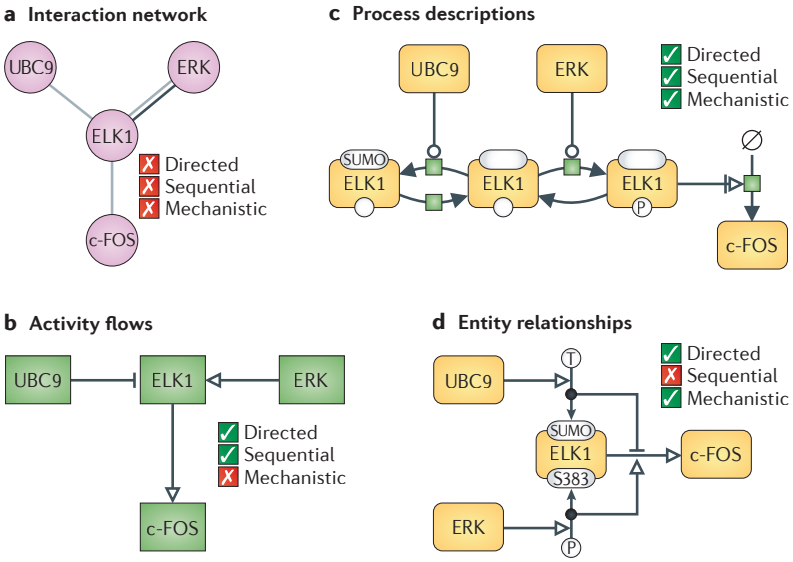

Fig. 1.8 Examples of different levels of abstraction in biological systems (reprinted by permission from Springer Nature: Nature Reviews Genetics, Le Novere [280] © 2015). a) A non-directional representation of interactions between proteins, b) a representation with directionality but without mechanistic logic for the interactions, c) a detailed model of all the processes characterising the interactions, d) a model focusing on rule-based relationships between entities, rather than continuous chemical processes. These models produce increasingly detailed predictions, but also require increasingly detailed prior knowledge.

the model, as well as the computational complexity of using it. As such, the first important choice in modelling a system is to choose the level of abstraction which will allow one to answer the questions at hand [148]. For example, for engineering a new semi-conductor, taking quantum effects into account is a necessity, but for designing a table, it is likely excessive, and classical mechanics will suffice.

In systems biology, there are problems requiring different levels of abstraction as well. Considering a metabolic network, for example, one will likely have high quality quantitative data for many of the components, such as reaction kinetics. This gives the parameters needed for it to be modelled quantitatively, such as modelling the Tricarboxylic Acid Cycle using a system of Ordinary Differential Equations (ODE) [6]. When considering the interaction networks of transcription factors, a logical model may be more appropriate, such as a Boolean Network [172]. This reflects the key aspects of the interaction being modelled, whether a gene is off or on, and can be built from data which is noisier or less complete. A Boolean network can also be larger and still remain computationally tractable, compared to a system of ODE, especially if the ODE are non-linear [176, 103]. Between these extremes are many possible choices of abstraction, which will be appropriate for different problems and different

data sets, as reviewed by Le Novere [280]. However they can be broadly broken up into Continuous and Discrete.

1.8.2 Continuous versus Discrete Models

A continuous system uses quantitative data to predict precise values. Such models have also traditionally been the way in which systems are modelled in physics and mathematics, and so there are a wide range of tools and knowledge for their analysis. These have the advantage of being a closer model of the system, as well as being able to model the effect of small changes on the initial values or parameters. Their results can be also compared directly to experimental data. Finally, they are most suitable for cases in which one needs to understand how a system changes over time, as they can model this as a continuous quantity rather than abstract time-steps.

However, continuous systems also have disadvantages. They require precise data for both the parametrisation and testing of the model. Further, the solution space may be infinite, and so a continuous model cannot give bounds about all possible results. That is to say, they can precisely predict the results for a set of initial conditions, but may not be able to show whether a given state is possible, and what initial conditions would be required for this. For this a discrete system may be more appropriate.

Discrete systems necessarily require more abstraction, namely breaking the data into discrete states. However, this may still be a good representation of the system, as in many cases biological systems have evolved to produce for discrete levels of behaviour. For example, it is beneficial for a cell to become committed once it enters a stage of the cell cycle, not maintain some characteristics of the stage but only partially. Thus this is discretised, rather than existing on a continuum. Gene regulatory networks cannot be too sensitive to small changes in initial conditions, as they need to be able to reliably and consistently produce the correct behaviours throughout tissues. This is supported by the observation of canalisation [406] and genetic buffering [192] in these systems.

A discrete model is also less suitable for modelling temporal changes, as it will need to progress in time-steps, which may not be able to be matched to real time. However, they also have a finite solution space, so they can give precise answers about what solutions are possible. This also allows one to check solutions for all initial states to the model by applying and model checking techniques from Computer Science [77, 78, 499, 58]. Such systems are easier to scale while remaining computationally tractable, and can take more heterogeneous

data. Therefore, they are more suitable to systems in which there is a broad range of data, but insufficient depth for a quantitative continuous model.

In this thesis I aim to model the gene regulatory network in heterogeneous breast cancer. To model the interdependency between sub-clones requires a broad network comprising many different pathways, which may have been characterised to different levels of detail. Quantitative data sufficient to model some pathways as continuous systems exists, for example the cell cycle [453]. However, other key pathways are not characterised to this level of detail. Indeed, new interactions emerged as my collaborators were investigating the system (see Chapter 3.5), such as the suppression of Wnt1 by c-myc (see Chapter 3.5.1). This meant that I needed to be able to integrate these diverse sources of information, and as I was interested in the overall phenotypes of the cells involved in a stable state, I chose to use a discrete model. However, a simple entity relationship model was insufficient, as a key aim was to be able to have a mechanistic understanding of the reason why the system behaved in the way it did. As such I chose an executable modelling system, that is to say a system in which the interactions had a logic which allowed interactions to be analysed and simulated. This allowed me to take into account the details of interactions such as a protein only activating another above a certain threshold, or in certain contexts but without requiring precise reaction-kinetic data.

1.8.3 Executable Network Models

Boolean Networks

The simplest type of logic-based, executable, discrete network model is the Boolean Network. These consist of nodes that can take only two values: 0 (off) and 1 (on). These nodes are connected by edges, which can be activatory or inhibitory. Activatory edges ($\rightarrow$) transmit the value of their parent node, while inhibitory edges ($\dashv$) the inverse (acting as a NOT operator). The state of each node is determined by an update function which is a boolean function of these incoming values. For example, for the network in Figure. 1.9, *Out* might have the update function: On if a AND NOT b. It is possible to map all the possible transistions of a Boolean Network, as shown in Figure 1.9b, and so visualise the behaviour and stable states, as shown in Figure 1.9. Despite their simplicity they are still very powerful, and have been used to model the immune response to infection [440], extracellular matrix dynamics [482] and cortical development [172]. Many elements of gene regulatory networks are well abstracted as Boolean, for example, single cell transcription data shows many transcription

factors activate genes in a binary manner, and so this data can be used to build a network capable of modelling such complex processes as haematopoiesis [330].

As such this is a popular system to represent signalling and transcriptional networks, and there are many tools to analyse both synchronous and asynchronous Boolean networks [167, 210]. However, they are limited in the complexity of the interactions they can model, as each node can only take two values, so their utility depends on whether the system can be binarised without losing key functionality.

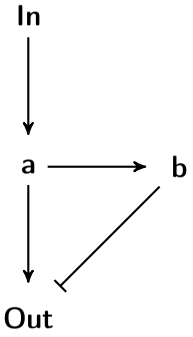

(a) A simple Boolean network, where a single input *In* activates an output via *a*, but only transiently due to the suppression via *b*. *a* and *b* are active if their parent node is, *Out* is active If *a* AND NOT *b*.

In	*t*			*t+1*		
	a	b	Out	a'	b'	Out'
0	0	0	0	0	0	0
	0	0	1	0	0	0
	0	1	0	0	0	0
	1	0	0	0	1	1
	0	1	1	0	0	0
	1	0	1	0	0	1
	1	1	0	0	1	0
	1	1	1	0	1	0
1	0	0	0	1	0	0
	0	0	1	1	0	1
	0	1	0	1	1	0
	1	0	0	1	1	1
	0	1	1	1	0	0
	1	0	1	1	1	1
	1	1	0	1	1	0
	1	1	1	1	1	0

(b) The *State Transition Table* for 1.9a. This shows how the nodes change in the timestep $t+1$ based on the values in t, and the initial condition *In*. Note that at $t+1$ the node values are based on those at t only. Thus if *a* turns on then *Out* does not turn on in the same time-step as this signal has not propagated yet.

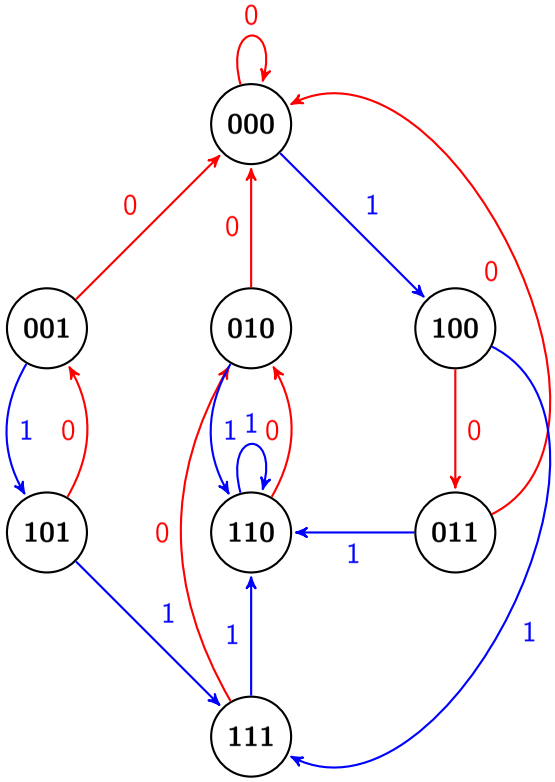

(c) The *State Transition Diagram* for the network shown in 1.9a. Values within the nodes refer to *a*, *b* and *Out* respectively, and edges represent transitions in the case that *In* is either 0 (red), or 1 (blue). This makes clear the two stable states for the system, 000 for $In = 0$ and 110 for $In = 1$.

Fig. 1.9 A simple Boolean network and representations of how it evolves under different initial conditions (*In*).

Qualitative Networks

I choose to model the gene regulatory network of heterogeneous breast cancer as a Qualitative Network (QN) [390], an extension of Boolean Networks. These have nodes that still take a discrete integer value within a finite range, but where the range is larger than 0 to 1. The range over which a node can vary is referred to as the granularity, where the granularity is the number of values within the range. So a Boolean network has nodes which take values 0 or 1 and so has granularity 2. This allows more complex interactions between nodes, such as activation only above a certain threshold, or comparing mean activity of different sets of nodes. The mathematical definition of how a node interacts with other is called the Target Function of the node. This is an equation that determines the value a node will take in the next time-step, based on the current values of nodes to which it is connected. These are explained in detail for QN in Chapter 2.1.5.

As with Boolean Networks, QN have a fixed topology; the wiring between nodes does not change. However, contextual interactions can be modelled using the Target Functions, which allow inactivation of edges selectively. Further, they are deterministic. This has the advantage of giving predictable responses to initial conditions, but may lose some accuracy in the dynamics of signalling networks. For example, a long cascade of signalling molecules is more susceptible to a fluctuation part way along the chain causing a false positive [289, 287]. Conversely, stochasticity may improve the robustness of signalling networks in some circumstances [307]. However, as the aim of my model is to reproduce the overall behaviour of connections drawn from the literature, rather than to predict new interactions, this is an acceptable compromise.

Finally, the system is synchronous. An asynchronous network allows different parts of the network to be updated independently. This is more realistic, as there is nothing ensuring all the components of a cell change at the same rate, and allows more complex loops. However, the number of possible transitions between states is larger for the asynchronous network, and it can be much more complex to find the stable states [166, 513]. For the system I am trying to model, in which I am interested in the behaviour under treatment and so there is time for the whole system to enter a stable state, I do not believe an asynchronous model would provide increased fidelity which would outweigh the reduced computational tractability.

I model this system in Bio Model Analyzer, the capabilities of which are explained in detail in Chapter 2.1.3. Existing models built in this system are, for example, models of *C. elegans* tissue development by Fisher et al. [147] and Hall et al. [189], metabolism in diabetes and obesity by Beyer et al. [33], Chronic Myeloid Leukemia by Chuang et al. [75] and Acute Myeliod Leukemia by Silverbush et al. [408].

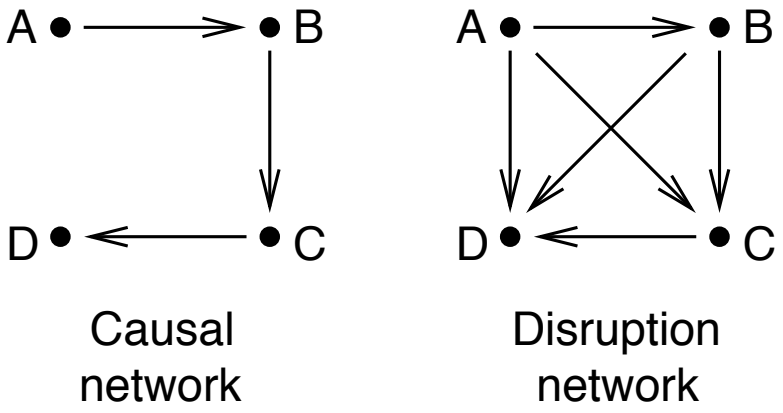

Fig. 1.10 Network inference from gene expression data begins with information about coexpression of genes. Adding information on how expression changes under perturbation allows the addition of directionality to the network. However, perturbation to one node, e.g. A, will disrupt the expression of many of the nodes downstream, B, C and D, due to both direct and indirect interactions (right), rather than showing the direct interactions (left). Discrimination between the two by inference from expression data remains challenging (from Markowetz and Spang [314] (CC BY 2.0).

1.8.4 Model Inference and Synthesis

The data available determines the model which can be built. A ready source of data comes from gene expression micro-array and RNA sequencing. This kind of data has been used successfully to construct gene interaction networks using co-expression and Bayesian-inference based methods. Co-expression network inference often uses Mutual Information (MI). In information theory, this is a measure of the dependence between two variables. Unlike covariance, MI can show non-linear relationships between variables. Genes whose expression has a high MI, e.g. those which tend to only become active together, are assumed to be linked. By comparing this under different perturbations, the regulatory relationship underlying the co-expression can be inferred. However, there is still mixing between the network of disruption and that of direct interactions between genes and proteins (see Fig. 1.10). A popular example of such methods is ARACNE [313]. However, methods based on MI, and similar methods, do not produce directed graphs, and so must be further processed to produce simulations of the response to perturbation. Increasing the accuracy of such methods, when applied in an unsupervised manner, remains challenging [309].

These data can also be analysed by Bayesian Inference methods, which offer to produce directed, although acyclic networks. Here, the probability that a network would produce the observed behaviour is evaluated, and then the network iteratively improved to attempt to maximise the score. The acyclic nature of the results of this method is a significant limitation

as feedback mechanisms are key to cellular behaviour and cancer resistance mechanisms. Bayesian Inference is more computationally intensive than MI based inference, and so is less suited to large networks. These methods are reviewed and compared by Markowetz and Spang [314], Smet and Marchal [412] and Emmert-Streib et al. [131], and an example of using Bayesian Inference to find gene regulatory networks from expression data is presented by Peña et al. [359].

These methods are well suited to gene expression data, but run the risk of producing large, over-determined networks, due to the difficulty of distinguishing between direct and indirect connections. This makes them less suitable for my aims, as they are less able to provide a mechanistic network. Further, myc binds to promoters for many genes, [291, 342], although the degree to which regulatory control by myc can be derived from this remains controversial [294, 264].

An alternative is to synthesise the network from more detailed single cell expression data. In this case, it is possible to reconstruct the state transition diagram of the network by comparing expression from cells at different time points. This then makes it possible to synthesise a network that reproduces precisely the behaviour observed, and which can be directed and cyclic. A successful example of such a method to derive the network determining fate-determination in haematopoiesis is presented by Moignard et al. [330]. Single cell data can alternatively allow more sophisticated inference techniques as opposed to synthesis. For example, Chan et al. [62] propose a new method based on MI which takes advantage of the unique features of single cell expression data sets, and which relies on fewer assumptions than many other methods proposed for network construction from single cell data. More and more single cell data is becoming available and will enable further use of such techniques in the future, as reviewed by Angerer et al. [10], Babtie et al. [15].

Another technique is to focus not on the pattern of expression, but on co-mutation of genes. Zhou et al. [515] extract a network of co-mutated and mutually exclusively mutated genes from the COSMIC (Catalogue of Somatic Mutations in Cancer) database [156]. This can highlight which mutations synergise to the benefit of the cancer, and so may conversely be targeted together for treatment. Such mutation data can be combined with expression data to improve the accuracy of network inference techniques, as laid out by Paull et al. [356] and applied to prostate cancer by Drake et al. [119]. Cho et al. [71] present a similar method to combine network models derived from different sources of data.

These methods are being continually improved, for example, Molinelli et al. [331] demonstrate the use of methods from statistical physics, namely belief propagation, to increase the scale at which network inference can be applied, while Kabir et al. [237]

use evolutionary algorithms to converge on a network which matches experimental data. However, while these methods offer certain improvements on the more common inference and synthesis methods outlined above, they also share their inherent weaknesses.

However, due to a need to understand the mechanistic relationship between nodes in the network so as to better guide experiments, and due to the complexities of regulation by myc, the above methods were not applicable. I chose to build my network from direct measurements of interactions in the literature, as described in Chapter 3. Other examples of models built from the literature include, for example, metabolic models of *Aspergillus niger* by Andersen et al. [9] and *Homo sapiens* Duarte et al. [120].

1.8.5 Analysis of Networks

Once a network has been constructed, it must be analysed. For a large network, possibly undirected or non-mechanistic, one can analyse the network structure and topology. This can be used to identify important nodes by looking for hubs and inferring regulatory features by looking for network motifs [16]. This can then be used to identify the key regulators of branches of the network [152], and driver mutations in disease [65]. Such networks can also elucidate Gene Ontologies, as demonstrated by Dutkowski et al. [123]. An extension of such analysis is to consider expression data not as a source for network inference, but as something to be interpreted in the context of an existing, static protien-protein interaction network. West et al. [477] use this combination to measure the difference in network entropy between the parts of the network active in healthy and diseased cells. The underlying network topology was assumed to remain constant, gene expression data providing edge weights. The authors show that an increase in network entropy is characteristic of cancer, and that this may lead to further insights into the differing dynamics of cancer compared to healthy cells. Methods of analysis of the structure of networks is further reviewed by Furlong [161].

For a simple but mechanistic network, one can look at the whole state transition diagram, as shown in Figure 1.9. However, for large networks this can become unwieldy. This can be especially difficult if the number of possible values of a node, or the granularity, is large. A network of n nodes with granularity g has a state space of g^n, and so the state space rapidly increases in size as more nodes are added.

One of the key determinants of cell behaviour will be the stable states of the gene regulatory network, as demonstrated experimentally by Huang et al. [218]. Finding and characterising the stable states of the network under different initial conditions can be tied to phenotypes such as proliferation and apoptosis, and so be used to make predictions about

cell behaviour in different circumstances. Therefore, my analysis of the network model I present in this thesis focusses on what the stable states for the network are given certain initial conditions, and which initial conditions result in a given state. This remains a difficult problem, and one which may not be computationally tractable in all cases. I discuss a range of analysis techniques which balance accuracy and time needed to run in Chapter 2.1.6.

1.8.6 Testing the Model

In order to test the validity of the model, I compare it to known behaviour. I first collate a specification of observed results both from the literature (see Chapter 3.4.2) and from experiments conducted by my collaborators (see Chapter 3.5.2). This is analogous to the formal specification of the behaviour required a program, as used in software engineering.

To then assess how well the model reproduces these results it is necessary to analyse what states, on the state transition graph described by the model (Fig. 1.9c), are reachable, for a given set of conditions. This represents the possible behaviours of the system under those conditions, which should be the same set of possible behaviours as is observed experimentally for the same conditions. As described in Section 1.8.5, due to the size of the graph, I focus on the stable states, or attractors (see Chapter 2.1.6), of the model, and therefore the overall behaviours of the cell such as proliferation and apoptosis, as opposed to transient changes in individual pathways.

The specification places two constraints upon the model which must be assessed. Firstly, that the model must be able to reach those stable states which are observed in experiments. Secondly and conversely, that the model does not reach states which are inconsistent with the observed results. In Chapter 2.1.8 I describe how it is possible to place bounds on all states a model can reach for all possible initial conditions, and in Chapter 2.2 how this can be applied to validate the model. This allows me to assess how accurately the responses of the model match, and do not contradict, the responses of the real system being modelled, and thus obtain an assessment of the quality of the model. If the model cannot reach observed states or produces states which contradict the specification, I then re-examine the assumptions of the model, and iterate. I report the results of this validation in Chapter 3.4 and 3.5.2. It is then further tested by the experimental application of the predictions of the model (see Chapter 5.7).

1.8.7 Other Abstractions and Consequent Limitations

Any model is necessarily a simplification of the reality it models. Choices about which complexity is necessary, or in which cases a simpler model is sufficient, will not always fit into the above categories. This means that the model relies on assumptions about what is and is not necessary to answer the specific biological questions being addressed. As these assumptions may differ in future applications of the model, before any such extension it would be important to address these. I therefore provide details of such limitations in Chapter 3.2.8, specifically pertaining to the auto-regulatory loop of p53 and mdm2 and the simplification of the cell cycle. I also detail how the model could be expanded in Chapter 7.2.3.

1.9 Existing Models of Cancer

There are many existing models of different cancers with divergent goals. Here, I focus especially on computational models of breast cancer, as well as models and studies focussed on drug discovery and tumour evolution in general. In addition to the specific examples below, the use of network methods for biology is further reviewed by Wynn et al. [489], Jong [232]. Zañudo et al. [504] focus on network methods for studying cancer specifically, while Csermely et al. [94] review the applications of such methods to drug discovery.

1.9.1 For Drug Target Prioritisation and Prediction of the Effects of Therapy

As finding and testing drugs is such a long and expensive process, with a high failure rate [380], there is a need to eliminate as many low-priority targets as possible computationally. Especially required are models able to give a mechanistic explanation of why predicted therapies work. This allows information about which drugs fail in clinical trials and for what reasons can be fed back in and used to improve target selection. There are several main ways in which network models can be used for this.

Firstly, one can focus on the structure of the network in order to identify central proteins, and those which serve as a bridge between key clusters, and so might represent a bottleneck which the cell would find it hard to avoid if targeted for therapy. Such clustering maps have been produced, for example, by Jonsson and Bates [233]. Further, Farkas et al. [141] show that such central proteins often overlap with existing drug targets, so may be a good way to predict new drugs.

Second, comparison between network structures can be used to identify patient-specific drug targets. This has been demonstrated in breast cancer by Zaman et al. [502], who mapped patient-specific expression data onto existing human signalling network data. They then demonstrated that differences in which proteins acted as hubs between patients predicted differences in the effectiveness of therapy targeting those hubs.

However, neither of these methods provide a mechanistic understanding of why a certain treatment works better than another. Further, focussing on single perturbations of hubs may not overcome the robustness of the network, with studies in yeast and *E. coli* showing that multiple hits to peripheral parts of the network are more effective than a single perturbation of a highly connected hub [2]. This not only reinforces the need for combination therapy, but for network models that can predict the effect of perturbation.

An effective example of this is the simulation of the metabolic network in cancer by Folger et al. [153]. This was then used to evaluate perturbations to disrupt the metabolism of cancer and find cytostatic drugs. Similarly, Jackson et al. [225] model the cell cycle as a system of differential equations to find combination therapies focussing on the cell cycle. For example, simulating the effect of combining a drug which preferentially places cancer cells in a specific phase of the cell cycle, combined with a cytotoxic drug preferential for that stage, can reduce effects on healthy cells. This demonstrates the benefits of a continuous model, in that it can model the duration in which cells stay in different stages of the cycle, which a logical model could not do as well. However, it also shows the disadvantage, as it is difficult to assess why certain combinations are better than others, as in the case of a combination of Actinomycin D and Paclitaxel in this study.

Kirouac et al. [250] built an ODE based model of ErbB-family signalling network, which governs the response to epithelial growth factor (EGF). They focused on feedback mechanisms that can provide resistance to therapy, and the different time-scales over which they come into effect. This provides precise predictions of dose dependent effects, but is focused on a small part of the gene regulatory network, and is hard to scale up. Nevertheless, this model was detailed enough to correctly predict that a single inhibition of EGFR and HER2, higher upstream in a pathway, is more effective than combination therapy against the two downstream branches with Mek and Akt inhibitors, due to the interaction of the feedback mechanisms. Heiser et al. [199] constructed a static-network from a combination of rules for the interaction between genes and proteins, and expression data for the initial conditions of these proteins in different cell lines. They were able to then synthesise a network to satisfy these constraints, and analyse the structure and topology to identify Pak1 as a key regulator of MAPK signalling, and found that expression levels of Pak1 predicted response to therapy.

Another network formalism is that of the Petri net [361]. These are more complex than Boolean networks in that they are bipartite graphs, modelling systems through the movement of tokens between places, controlled by transitions. Places and transitions are two kinds of node, with tokens denoting activity. These have a long history of use in computing and engineering, particularly in modelling concurrency. These are now being applied in biology, as laid out by Sackmann et al. [384], Zevedei-Oancea and Schuster [506] and Júlvez et al. [234]. Petri nets have an advantage in biological applications as biological systems have many concurrent processes interactions which need to be handled carefully. However, unlike a synchronous boolean or qualitative network, they can have infinitely many configurations, making analysis more difficult. The advantages of Petri Nets in a biological context are further considered by Peleg et al. [358], while some of the issues which must be considered in their application are discussed by Krepska et al. [262].

Ruths et al. [381] construct a synchronous, stochastic, Petri net model of breast cancer, and used this model to predict the response of the EGFR pathway to perturbation of TSC2 and mTOR-Raptor. However, the initial states of this model must be chosen explicitly, either being set to no initial activity (tokens) for all places, set at random or set from experimental data, with all three paradigms producing different results. This contrasts with the method which I present, in which it is possible to make statements about network behaviour for all possible initial states (Chapter 2.1.8). Nevertheless, the authors were able to predict the response of other nodes in the network when TSC2 was perturbed.

Layek et al. [279] construct a Boolean network model of the various growth factor signalling pathways. The authors use this to enumerate the possible ways in which these pathways can malfunction, how this relates to cancer, and how to correct these malfunctions with targeted drug interventions. Notably, their use of a Boolean network model allows them to predict treatments to specific malfunctions, allowing for personalised treatments. Fumiã and Martins [160] perform a similar analysis on a broader network, and further consider the effects of different micro-environmental conditions in colorectal cancer.

Samaga et al. [387] converted an existing network describing the stoichiometry of the EGFR/ErbB pathway into a Boolean network. This was then used to find nodes which are strongly coupled within the network, as well as to identify the minimal mutations of the network that stimulate a proliferative response in the absence of any ligands, promoting cancer. However, this model was not specific to any tissue or cell type, and so may be over general in which interactions it includes. Nonetheless in making testable predictions of the response to perturbation, it demonstrates the potential of these techniques. In this Thesis, I aim to build upon this potential by using a qualitative network model to similarly predict

treatments based on mutations applied to the network, using the flexibility of the qualitative network formalism to incorporate the effects of different sub-clones interacting.

1.9.2 For Tumour Evolution

Existing studies, such as Kuukasjärvi et al. [267] and Shah et al. [400], have tried to shed light on the temporal evolution of tumours by comparing metastases to primary tumours. This shows the late adaptations of the tumour needed for successful metastasis, rather than the overall evolution of the tumour. Other studies have analysed sequencing data from primary tumours for genetic recombinations [184, 343, 468], comparing regions within biopsies [497] and single-cell sequencing [165]. However, these studies either have very few time-points within tumour evolution, or must rely on reconstruction of a history that has been distorted by selective sweeps over the history of the tumour. This, coupled with a lack of biopsy data for early, asymptomatic, stages of tumour evolution, makes identification of the early behaviour of the tumour more difficult [417].

Several studies model the evolution of tumours from a game-theoretic perspective. The application of game theory to modelling the effects of selection pressure rather than rational decisions of conscious actors in various contexts is reviewed by Hummert et al. [219] and discussed by Cleveland et al. [80]. The authors examine how evolutionary game theory can predict how populations of cells, such as those in a tumour, evolve to maximise fitness under the constrains of different interacting populations. In this application, "strategies" for the game are different mutations within the population, and the choice of strategy consists of said mutations being selected by evolution.

Many of these models focus on competition between two populations, such as Basanta et al. [18] where proliferation rate and other similar variables are able to change directly. This allows insight into the overall population dynamics of cancer, but not the underlying genetics of the emergence of more fit populations. A similar approach is applied to a more complex system of different cell types by Pacheco et al. [350]. Such an approach can also be used to model cooperative relationships, as demonstrated by Wu et al. [484]. The authors show how game theory can be used to model the interrelated population dynamics of cancer and supportive stromal cells, and how this is perturbed by drug intervention, and how this influences resistance. However, this focuses on changes to the clonal composition of the tumour, but not to mutations of the sub-clones.

Another approach to modelling tumour evolution is taken by Wodarz et al. [481], who examine the relation between abstract driver and passenger mutations using cell automa. They

consider a scenario in which two mutations of a specific gene are required for cells to gain an advantage that allows a cancer to form, but a single mutation is neutral or disadvantages. There is therefore a fitness valley between healthy and cancerous cells. Using a stochastic, agent based model they demonstrate how it is possible for neutral, passenger mutations in such a scenario can accelerate the emergence of a double mutant of the oncogene.

In contrast to the above examples, I focus on the different orderings of specific mutations within a genetic regulatory network, as opposed to abstract changes in overall fitness or generic mutations. I instead propose a method based upon a biological understanding of the gene regulatory network of the cell to model the defining constraints on early tumour development, and focus on how this affects the order in which mutations emerge, as opposed to the population dynamics of different cell types. This allows me to better map out this stage using *in silico* models. However, as different sub-clones may emerge due to different order of mutations, with different fitnesses, such an approach could be combined with a population level model.

1.10 Summary of Aims

In this Thesis, I aimed to apply the methods of executable, qualitative network modelling to the questions of how to find the most effective combination therapies to treat breast cancer heterogeneous in myc expression, as well as to predict its evolution. As such, I present a model of heterogeneous breast cancer focussed on myc. I first show the evidence used to build and test the model in Chapter 3. I then present the application of this computational model to a mouse model of MMTV-Wnt driven breast cancer, which is heterogeneous in myc expression. In Chapter 4 I assess the effects of targeted therapy on proliferation and apoptosis in high- and low-myc expressing sub-clones, focussing on how one might target each specifically. In Chapter 5 I show how such treatment might be improved by combination with a second drug, and further demonstrate the effectiveness of therapies predicted by my computational model in the mouse model.

Overall, I present a method for computational driven drug selection, focussing on compensating for and taking advantage of the heterogeneity of cancers. However, rather than compensating for such heterogeneity, it may also be possible to avoid it entirely. Cancers evolve from a single cell, and so necessarily heterogeneity increases as it develops. In Chapter 6 I demonstrate how the same computational model can be used to find the order in which tumours acquire mutations, and so be better able to supply diagnosis and prognosis for such

tumours. Knowledge of which mutations are likely to be among the founder mutations of the cancer also allows one to target those as the most likely to be common amongst sub-clones.

I therefore present a root and branch approach to finding new treatments for cancer with discrete qualitative network models. All the methods I present to analyse my network model can be applied equally well to any other qualitative network model, and so can be readily applied to different cancers.

Chapter 2

Materials and Methods

2.1 Building and Analysing Gene Regulatory Networks with Bio Model Analyzer

2.1.1 Qualitative Network Modelling

I model the system as a Qualitative Network, an extension of the Boolean Network formalism [390]. In a Qualitative Network, nodes can take many values rather than 0 or 1. These values must be natural numbers, hence Qualitative, and within a fixed range defined when building the network. Nodes can be of different ranges, henceforth referred to as the granularity. Let N be the upper bound of the node, then the granularity is $N+1$. Therefore, a Boolean network variable would have a granularity of 2, with the upper bound being 1 and the lower bound 0, but a Qualitative Network could allow a node to have granularity 5 i.e. take values $\{0,1,2,3,4\}$. This granularity can have a non-zero lower bound, but this does not occur in any of the models discussed in this thesis. This allows the modelling of variables which have distinct effects at different levels of activity, beyond simply being active or inactive. For example, p53 can be inactive, active enough to be promoting growth arrest, or at higher activity promoting apoptosis. It therefore requires a granularity of at least 3.

2.1.2 Formal Definition of Qualitative Networks

As laid out in Schaub et al. [390] and Cook et al. [88], a Qualitative Network is defined as an object $Q(V,T,N)$. This consists of: *variables*: $V = \{v_1, v_2, \ldots, v_n\}$, representing genes and proteins in the regulatory network. Their behaviour is defined by a set of *Target Functions* (TF): $T = \{T_1, T_2, \ldots, T_n\}$, and as such each variable $v_i \in V$ has a target function $T_i \in T$

associated with it: $T_i : \{0,1,\ldots,N\}^n \to \{0,1,\ldots,N\}$. Here, I consider the case where all variables have the same range $\{0,\ldots,N\}$, and so a granularity of $N+1$, but variables may have different ranges (see Section 2.1.5). A state of the network consists of the value of each variable: $s : V \to \{0,1,\ldots,N\}$. Every variable is updated synchronously and in parallel each time-step as the network is simulated, as determined by their respective target functions. Thus the network moves from a state $s = (u_1, u_2, \ldots, u_n)$ to a the next state $s' = (u'_1, u'_2, \ldots, u'_n)$, where u_i is the value of variable v_i. This is determined by the target functions as:

$$u'_i = \begin{cases} u_i + 1 & u_i < T_i(s) \text{ and } u_i < N, \\ u_i - 1 & u_i > T_i(s) \text{ and } u_i > 0, \\ u_i & \text{otherwise} \end{cases} \tag{2.1}$$

This means that each variable can only update its value by a maximum of ± 1 per time-step. Then $s' = T(s)$ where $T(s)$ is a function applying all the Target Functions T_i to the variables V_i at state s. All the Target Functions are applied synchronously. Note that this uniquely determines the next state for each current state, and so network behaviour must eventually converge on either a single fixed point or a loop.

2.1.3 Building Models in Bio Model Analyzer

I choose to build and run the model in Bio Model Analyzer (BMA) [27]. This is open-source software that is being developed at Microsoft Research Cambridge for modelling QNs. The tool can be used online at http://biomodelanalyzer.org/ while source code is found at https://github.com/Microsoft/BioModelAnalyzer. An example of the components of a network built in BMA is shown in Figure 2.1. BMA includes a graphical user interface (GUI) to build the model and perform analysis (VMCAI algorithm, SMT solver and Simulation, see 2.1.6). Further, there is a downloadable version of the tool which allows more in-depth and automated analysis. Both versions of the tool store networks in `.json` file format. This means that a model can be quickly and easily built and prototyped in the GUI and then exported for further analysis in the offline version of the program.

A network is built in BMA from nodes, corresponding to variables in Section 2.1.2, and edges, which connect them. Edges connect nodes and determine which nodes influence their behaviour, and which nodes they influence in turn. Edges may be activatory ($\to$) or inhibitory ($\dashv$).

To build the network, I collated information on nodes and edges from the literature (see Chapter 3.2), and tested the network against *in vitro* (Chapter 3.4.2) and *in vivo* data

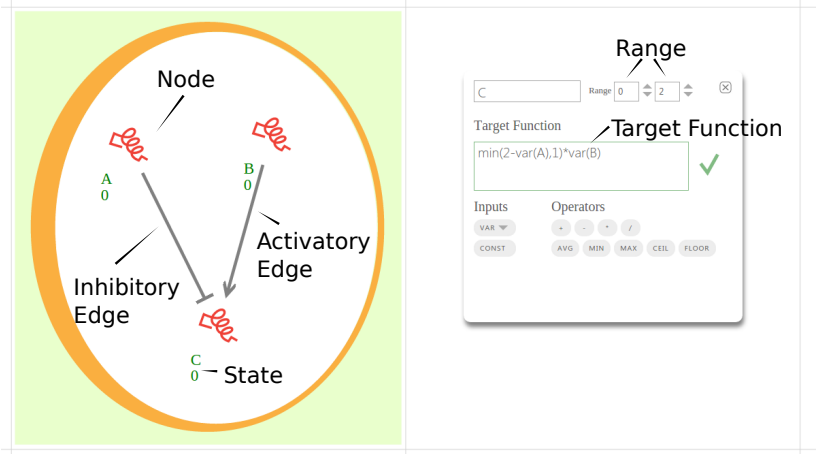

Fig. 2.1 Components of a Qualitative Network in BMA. Left: A representation of the network. Red symbols represent *variables*, or *nodes*, which may be genes or proteins. These are connected to one another with *edges*, which may be activatory (→) or inhibitory (⊣). Whether an edge is activatory or inhibitory determines the behaviour of the default target function (see Section 2.1.5). When the network is assessed for stability (see Section 2.1.6) the *state* of the network is shown by the green number by each variable, showing the *value* or range of values to which that variable can be restricted. The variables are enclosed by an orange circle which can be used to denote different functional modules for convenience, but which have no impact on the working of the model.
Right: A control panel for determining the behaviour of a variable, in this case variable C. Here the name of the variable can be set, as well as the *range* of values it can take. The target function is defined here also (see Section 2.1.5). This can be any equation that can take discrete variables, using the *Operators* provided below the text box. The variables in the target function must correspond to those connected to the variable for which the target function is being defined, these are listed as *Inputs*.

(Chapter 3.5.2). In the case of contradiction, I reviewed the literature to see if this could be resolved with more detail which had already been tested, or made hypotheses about unknown connections. I repeat this iteratively until the network matches experimental data (Fig. 2.2).

In this Chapter I describe how to analyse a generic network, and in Chapter 3 I describe how I built the network for my specific aims.

2.1.4 Sourced of Bias when Incorporating Literature Data

Model building can broadly take two approaches. The model can be inferred or synthesised from a genome-wide or similarly broad data set from the "top-down", or alternatively prior knowledge about small modules of a network, such as individual pathways, can be built and combined into a larger whole to attempt to explain such a data set, from the "bottom-up". These two approaches are compared, when applied to modelling epithelial mesenchymal transition, by Jolly and Levine [231]. Top-down, data-driven approaches have the advantage

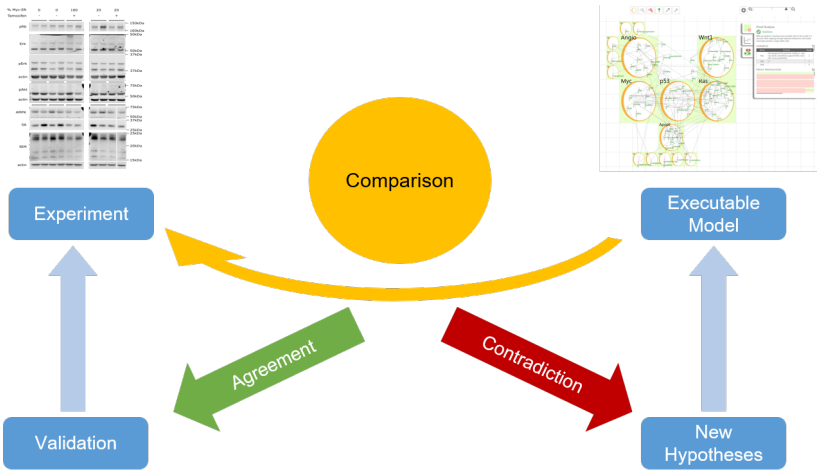

Fig. 2.2 In order to build the model, I added nodes and edges based upon information in the literature. I then compared this to *in vitro* and *in vivo* experiments. In the case of disagreement, I sought further guidance from the literature, or if there was no other way, hypothesised new connections or target functions which could later be followed up experimentally.

that they do not require any prior knowledge, and so are less susceptible to bias by existing assumptions about the underlying network. However, one must be careful of bias from the axioms taken in the creation of algorithms used to analyse such data sets. Further, care must be taken over sources of bias inherent in the techniques used to produce such data. For example, analysis of Chromatin Immunoprecipitation-sequencing (ChIP-seq) must account for its bias towards GC-rich areas of the genome [354].

In the case of GRN construction specifically, a common technique is to use correlation or mutual information to find co-expressed genes in expression data, and then to infer the relationships between them on this basis. However, this can confuse direct and indirect interactions, as discussed by Markowetz and Spang [314]. Such approaches also often result in undirected network, without information as to the nature of the interactions. An alternative is to attempt to synthesise a network, that is to search for the simplest network which can reproduce all the expected behaviour, while minimising unexpected behaviour. This approach is demonstrated by Moignard et al. [330]. Both these approaches suffer from difficulties in scaling. This is because, as the number of variables n in a network increases, the number of edges that could connect them, and which must be considered, increases as $n(n-1)$. Therefore these approaches are better suited to modelling a small number of nodes in depth than a broad network.

The alternative, bottom-up approach, is to use a source or sources of prior-knowledge, and then test this against known behaviour of the network, for example building from pathway databases or other literature data [120]. This has the advantage of allowing integration of

disparate sources of data, with different techniques applied to best suit the needs of different kinds of genes, proteins and interactions. The nature of interactions can also be indicated from an experiment focusing solely on that interaction (see Chapter 3.2).In order to answer the questions posed in this Thesis, I needed to build a broad network able to integrate the different possible methods of cooperation between sub-clones. Further, I needed the flexibility to integrate different sources and kinds of data. For example, finding the targets of myc by high-throughput methods has been inconclusive, as discussed further in Chapter 3.2.1. As discussed in Chapter 1.8.4, I therefore use literature data as this source of prior knowledge.

I used an existing pathway database, KEGG (Kyoto Encyclopedia of Genes and Genomes) [240, 241, 239], to get the initial framework of the network. I then supplemented this with reviews of the pathway being modelled in order to get an overview of open questions and areas of contention. Finally, I investigated individual interactions using searches of Google Scholar and PubMed for the variables in question; both in general and in mammary tissue and mammary cancers in particular.

However, such an approach brings with it several sources of bias. These include:

Publication bias Significant results are more likely to be published than null results [125]

Observational Bias A tendency to look in places where one expects to find results, also known as the Streetlight Effect or the Drunkard's search [243]

Confirmation bias Favouring evidence which supports ones preferred conclusion [341]

Anchoring A propensity to favour early evidence over late when forming a hypothesis [452, 158]

These can be mitigated, but not completely eliminated. A model built from the literature will suffer from observational and publication biases, as the literature itself does. In the case of publication bias, as null results are less likely to be published, there will be a bias towards the existence of an interaction, and a paucity of evidence against it. A bias towards positive results can be detected in meta-analyses, however, many meta-analyses do not adequately control for this [3], and meta-analyses of the literature are not available for many of the interactions modelled. Observational bias will affect the model in that the model can only be based on behaviour for which there exists evidence already. However, there are likely to be interactions which have not yet been observed, which may be key to reproducing the overall observed behaviour of the cell. After building the initial version of the model, I test the whole behaviour of the model against overall cell behaviour (see Section 2.2), both drawn

from the literature (see Table 3.10) and from the experiments of my collaborators (see Table 3.12). This allowed the removal of interactions which did not fit the observed behaviour of the whole system, introduced due to the above biases, and is documented in Appendix D. Further, it allowed the possibility of hypothesising new interactions to fit observed behaviour, which could then be searched for experimentally.

There are also the similar issues of confirmation and anchoring bias. In order to counter these I started with a broad overview of the pathway with KEGG and review articles, and focussed in on the details of specific interactions. This allowed me to get an overview of competing hypotheses for a how a pathway functions at the beginning of its implementation into the network model. For example, the indirect activator versus direct activator-derepressor models for apoptosis (see Chapter 3 3.2.7). As with observation and publication biases, the need for the network to reproduce observed behaviour helped eliminate spurious interactions.

However, despite these efforts at mitigation, a literature-based approach will likely remain vulnerable in part to the above effects. In the future, more steps can be taken to further mitigate the above concerns. For the control of publication bias, an assessment can be made of the unpublished, or "grey" literature for different interactions [211]. To better counter confirmation and anchoring bias more pathway databases can be integrated, the range of which are reviewed by Chowdhury and Sarkar [74]. A systematic comparison of original to final versions of pathways in the network could also highlight if anchoring bias has taken effect. Further, the scope of this project changed and enlarged over its course, but it would be preferable in the future to be able to define systematically what searches will be conducted and where, and all the results collated, in order to further reduce confirmation and anchoring bias, for example as laid out by the Agency for Healthcare Research and Quality [1].

2.1.5 Target Functions

Every node in the network has a Target Function (TF) which defines how its state changes as a result of the nodes connected to it. Many are simple activatory or inhibitory relationships, for which a default target function is used:

$$avg(pos) - avg(neg) \tag{2.2}$$

Here the node compares the average state of all the nodes that connect to the current node via an activatory, i.e. positive edge, to the average state of all the nodes that connect via an inhibitory, i.e. negative edge. This is suitable for many connections within the network.

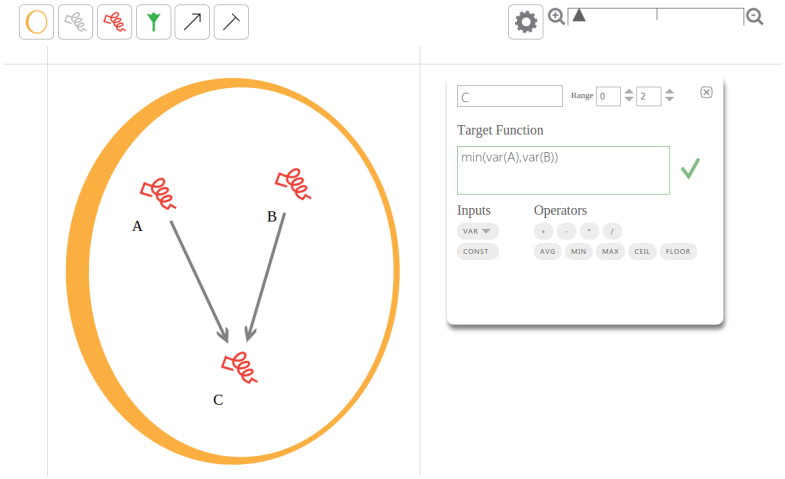

Fig. 2.3 Example of the BMA representation and Target Function for a dimer.

However, Target functions can be used to model much more complex interactions. These can be any equation that can take discrete variables, using the following operators:

- $var()$: an operator that denotes a node, so node A is referred to by $var(A)$
- The standard arithmetic operations: $+$, $-$, $*$, $/$
- $const()$: A constant value
- $min()$ and $max()$: take 2 arguments and give the minimum or the maximum of the two respectively
- $ceil()$ and $floor()$: round up or down respectively to the nearest integer to ensure the target function produces discrete values
- $avg()$: takes the average

For example, the limiting factor on the amount of a dimer will be the lower activity of the two components of said dimer. This is produced with the Target Function shown in Equation 2.3, shown in BMA in Figure 2.3.

$$min(var(A), var(B)) \tag{2.3}$$

It is also possible to model more conditional interactions. Consider the case of a protein, A, which inhibits another protein, C, only when at high level (2) but not below. Otherwise

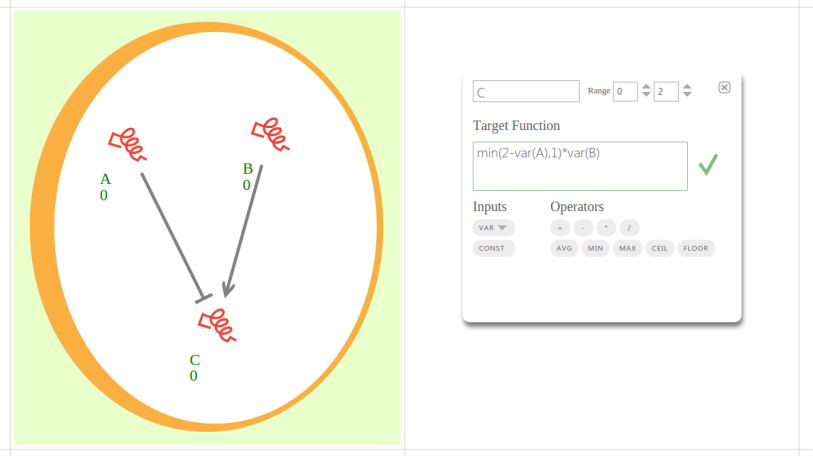

Fig. 2.4 Example of Conditional Inhibition within BMA.

C is activated by *B*. This results in the Target Function shown in Equation 2.4, as shown in Figure 2.4.

$$min(2-var(A),1)*var(B) \tag{2.4}$$

Here $min(2-var(A),1)$ is 1 when *A* is at low or normal activity (0 or 1), and so the target function follows the value of node *B*, denoted by $var(B)$. However, if *A* is highly expressed (2) then $min(2-var(A),1)$ will be 0 and so the whole Target Function is 0. Then C is at 0 and is so inhibited by *A*, only when *A* is at its maximum level of activity, as required. Such thresholds are a common feature of my model, as shown in Chapter 3.3.

Range Conversion

As nodes do not need to have the same granularity, there needs to be a way to convert values being passed between nodes whose granularity is unequal. Otherwise, a node which is, for example, at activity 3 and granularity 10, might maximally activate a node of granularity 2, which would be misleading. When passing values between nodes of unequal granularity, the value is converted as a function of the range. Consider node X with a range a to b, and Y range c to d. Then let X' be the value of X converted to match the granularity of Y. I.e. Y will interpret the value of X as X' in its Target Function, where:

$$X' = \frac{(X-a)(d-c)}{(b-a)+c} \tag{2.5}$$

2.1.6 Methods of Analysis supported by BMA

As the network is deterministic and has a finite number of nodes, there are a finite number of states it can take. As such, it will always eventually converge to an *attractor* where it repeats *n*-states indefinitely. If this attractor is of length 1, where the activity of each node remains the same for each time step once it has entered the attractor, the network has entered a *fixed-point*. If the attractor is of length greater than 1, then the network has entered *oscillation*. Analysis of the network consists of finding the attractors which result from different conditions and perturbations of the network.

I can use BMA to characterise the behaviour of the network in two main ways: simulation (see Section 2.1.7) and stability analysis. Simulation shows what the next states of the model will be for a single initial state, while stability analysis finds the stable states of the model for all, or a set of, initial states. BMA supports three methods for stability analysis discussed in Sections 2.1.8 (VMCAI), 2.1.9 (SMT Solver) and 2.1.10 (BDD analysis).

2.1.7 Simulation

As the network is entirely deterministic, BMA can simulate the future behaviour of the network. This simply takes the current state of every node and calculates what the next state must be, by applying the target functions repeatedly for as many time steps as desired. This is more specific than the methods to find and characterise attractors, as it only shows behaviour of the network for these precise initial states. However, it is useful for seeing what causes a bifurcation, how long it takes a network to stabilise or to quickly test different target functions.

For large networks, it is unlikely that experimental data for the initial state for every node in the network will be available, and so this becomes less useful, as it will only show the behaviour of the network in one of many possible cases. Instead, it is necessary to assess which attractors are reachable from a range of initial states. In addition to fixed-points and oscillations, this creates a third option, that different initial conditions within this range will create different stable states. In this case, the network is said to have undergone *bifurcation*, although there may be more than two stable states.

Such analysis of attractors from a range of initial states can become extremely complex if attempted by brute force. Even simple questions, such as finding the smallest attractor in a Boolean Network, are NP-Hard [511]. As such, in order to analyse the behaviour of the network for all possible initial states, BMA employs three different methods, each with different advantages and disadvantages.

2.1.8 Fast Algorithm - VMCAI

One of the key questions which one might wish to ask about a network is whether there exists some single state towards which it tends, representing the homeostatic behaviour of the cell in those conditions. In order to answer this, BMA attempts to use modular proofs to restrict the behaviour of small subsets of the network, and then see if this restricts the overall behaviour of the network. That is, it attempts to prove stability for small parts of the network, and combine these proofs to prove overall stability. This is not guaranteed, but is fast and scalable. This was presented at the International Conference on Verification, Model Checking, and Abstract Interpretation (VMCAI) and so is henceforth referred to as the VMCAI algorithm [89].

To find a fixed-point attractor, it needs to be determined whether:

$$\exists\ s \text{ such that } T(s) = s \tag{2.6}$$

In other words, a state such that the next state, after applying the Target Functions to all variables, is the same as the current state.

The VMCAI algorithm assesses how much the Target Function of a node restricts the range of values it can take. Once it has done this, it will iterate, as the restriction of one node may place further bounds on another node dependent upon it. Once no more restriction is possible, if the range of values each node can take is zero, then Condition 2.6 (that there is a state for which applying the Target Functions results in no change) is satisfied, and so a unique fixed-point is found and returned. Otherwise, the restrictions that were able to be proven for each variable are returned, with further analysis possible with the SMT solver (see Section 2.1.9). This algorithm is formally defined in Cook et al. [89].

The advantages of this are that it is very quick if it works, and so can be applied to many different variations of the network, corresponding to perturbations by, for example, drugs. However, it will not always find a fixed-point if one exists, and it does not give detailed information about network behaviour, for example details of oscillations or bifurcations within this range in the case that it does not identify stability. Nevertheless, a restriction of key variables is often still useful in predicting cell behaviour. In order to get a definite solution, at the expense of exponential time for the algorithm to run, I turn either to the SMT solver (Section 2.1.9) or BDD Analysis (Section 2.1.10).

2.1.9 SMT Solver

The question of network stability can also be formulated as a Boolean Satisfiability problem (SAT). A SAT problem is to find a possible assignment of values to variables such that a Boolean statement is true. For example, if x AND $y = TRUE$, this can be satisfied with with the assignment of the values $x = y = TRUE$.

However, SAT problems are NP-Complete [90], meaning that they can be extremely time-consuming to solve. There is no known algorithm that can solve all SAT problems in a useful period of time. Nonetheless, there are SAT solving algorithms capable of handling a large subset of very complex SAT problems efficiently, and as they provide an exact solution, such methods are worth applying to my models. BMA uses an extension of SAT to more quantitative problems, to account for the non-Boolean nature of QN, which are called Satisfiability modulo theories (SMT). The particular SMT solver used is Z3 [107].

If the VMCAI algorithm fails to find a fixed-point attractor, the SMT solver first checks for either a bifurcation or a loop attractor. Proof of this can then be sought using an SMT solver implemented in BMA.

It first checks for the case of a bifurcation, by querying the SMT solver to find whether there exist states such that:

$$\exists\, s,t \text{ such that } T(s) = s \wedge T(t) = t \text{ where } s \neq t \tag{2.7}$$

i.e. that there are at least two unique states which do not change when T is applied.

If this is true then there is at least a bifurcation, therefore there is no unique stability point and the SMT solver stops. If this is not able to be satisfied for any possible pair s,t then there is likely a loop. In which case BMA asks the SMT solver to show whether:

$$\exists\, s \text{ such that } T^n(s) = s \tag{2.8}$$

where it checks $\forall n <$ maximum possible loop length . That is, there is some state s which is repeated after T is applied n times, which means there is a loop attractor of length n.

It is possible that the fast algorithm could not find a fixed-point attractor, but that one does still exist. If the SMT solver cannot satisfy Condition 2.7 (that there are at least two states for which applying the Target Functions causes no further change) or Condition 2.8 (that there is a state s where applying the Target Functions n times returns to state s) then it will revert to satisfying Condition 2.6 used by the VMCAI algorithm. Therefore, the SMT solver will try and provide a counter-example to a fixed point attractor if one exists, and if not, provide the fixed-point attractor itself. However, this may not complete in reasonable

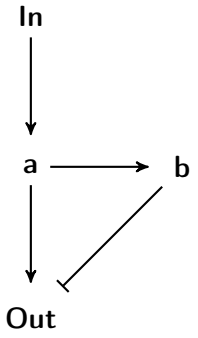

(a) A simple Boolean network, where a single input *In* activates an output via *a*, but only transiently due to the suppression via *b*. *a* and *b* are active if their parent node is, *Out* is active If *a* AND NOT *b*.

In	*t*			*t+1*
	a	b	Out	Out'
0	0	0	0	0
	0	0	1	0
	0	1	0	0
	1	0	0	1
	0	1	1	0
	1	0	1	1
	1	1	0	0
	1	1	1	0
1	0	0	0	0
	0	0	1	1
	0	1	0	0
	1	0	0	1
	0	1	1	0
	1	0	1	1
	1	1	0	0
	1	1	1	0

(b) Truth Table of the *Out* variable for small example network, see Fig. 1.9 for Network and State Transition Diagram representations, and Fig. 2.6 for how this is represented as a Binary Decision Tree and Diagram.

Fig. 2.5 An example network, and the Truth Table describing the transitions of the *Out* node.

time, hence the use of the VMCAI Algorithm primarily. Note also that while the SMT solver will provide one counter example, it will not provide all the attractors. For example, there could be multiple loops, but Condition 2.8 only searches for one.

2.1.10 Attractor Analysis with Binary Decision Diagrams

Towards the end of my PhD, Dr Steven Woodhouse, a collaborator at Microsoft Research Cambridge, implemented a technique for finding attractors in QN using Binary Decision Diagrams (BDD). This method was originally developed by Garg et al. [166] and extended by Dr Woodhouse to cover QN in BMA.

Much as the behaviour of a network can be written out as a Truth Table (see Fig. 1.9 for the original network, and Table 1.9b for the Truth Table), it can also be represented by a

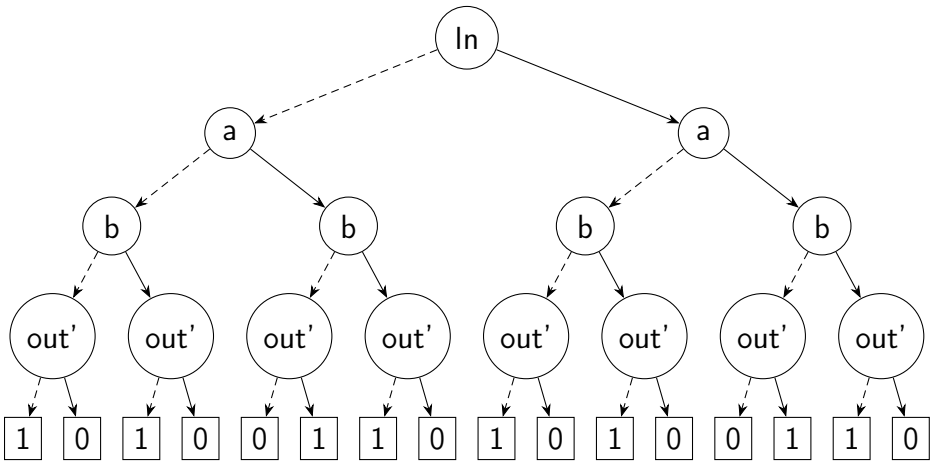

(a) Binary Decision Tree (BDT) representation of the *Out* variable at *t+1* for all possible states at t. Solid arrow corresponds to True (1) and dashed to False (0), where True is a combination of values that is a possible state of the network, and False is an impossible combination. For example, if $In = a = b = 1$ and $Out' = 1$ then the BDT returns 0 as b should block activation of *Out*, so Out' should be 0.

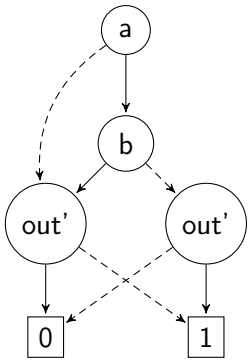

(b) Binary Decision Diagram (BDD) representation of the *Out* variable at *t+1* for all possible states at t. This is the compressed form of the BDT. Note that *In* is not in the BDD as the behaviour of a is entirely determined by *In* and so having both nodes is redundant.

Fig. 2.6 Binary Decision Tree (BDT) and Binary Decision Diagram (BDD) representations of the *Out* node for the network example given in Fig. 1.9, with the Truth Table for the *Out* node given in Fig. 1.9b. Each node has its own BDT and BDD representation which combine to represent the network.

Binary Decision Tree (BDT). This shows which transitions for *Out* to *Out*$'$ are possible in the network, according to the values of *In*, *a*, and *b* at time *t*. An example of such a Binary Decision Tree (BDT) for the *Out* variable of this network is shown in Figure 2.6a. Here the 1 and 0 variables represent True and False statements respectively about which values of *Out* are possible at time $t+1$ (i.e. the value of *Out*$'$). So, for example, if $In = a = b = 1$ and $Out' = 1$ then the BDT returns 0 as *b* should block activation of *Out*, so *Out*$'$ should be 0. This tree therefore represents the Truth Table of *Out*, and so the logic of which values it can transition to based upon the values of the other variables in the network.

A BDD is a compressed representation of the BDT, and is shown for the *Out* variable in Figure 2.6b. This shows which are the critical components that determine the transitions of *Out*, but does not show the stable states as clearly as a visualisation as a State Transition Diagram (Figure 1.9c). The advantage of the BDD representation, is that it can still be operated on in its compressed form, and different BDDs can be combined by logical operators. Much as the example Boolean Network can be converted to a BDD, so can a QN, although a BDD must remain Boolean, so they are more complex. Each variable of granularity $N+1$ is converted into $\lceil \log_2(N+1) \rceil$ variables in order that the BDD remains Boolean. A BDD may, in the worst case, require exponential space to represent all the possibilities of a network, making it impossible to work with, much as the SMT solver may require exponential time. However, in many cases it offers a substantial improvement over other methods, and the ability to find attractors more quickly.

The implementation of BDDs to find attractors in BMA works as follows. Much as Figure 2.6 shows the transitions allowed for *Out* to *Out*$'$ according to the values of *In*, *a* and *b*, so too can a BDD be used to represent all possible transitions for a network. The algorithm starts by choosing an arbitrary state *s*, and then iteratively applying the transition function BDD, to explore states reachable from *s*. This results in a second BDD representing all states reachable from the initial states. The process can also be reversed, to find states which can reach *s*. This is continued until there is an intersection between the forward-reachable and backward-reachable BDDs of sets of states. The intersection is the set of states which are both upstream and downstream of *s*. This set of states is therefore constitutes an attractor. The algorithm can then exclude these states from subsequent searches, choose another state and begin again. If there is only one attractor of length 1, this is a fixed point, if the length is $n > 1$, a loop, if multiple attractors, a bifurcation. This takes advantage of the fact that a BDD is a compressed form of a set of states or transitions, and so these manipulations are much easier to compute than explicit computation of states and transitions. In this manner all

attractors are found, unlike the SMT solver or VMCAI, but a solution in a reasonable time is not guaranteed.

2.2 Reproducing Experimental Conditions

To simulate an experimental perturbation of the cells in the model, I fix the values of nodes representing mutations, as well as external factors such as EGF, to a constant value by changing the Target Function for the relevant nodes. For example, if there were a node of granularity 3 (able to take values $\{0,1,2\}$), then to show high constant activity of this node, such as due to high exposure to a growth factor, I would use the Target Function $const(2)$. I then examine the stable state of the model and compare to experiment using the SMT algorithm (Section 2.1.9) or in cases that this does not find a solution in a reasonable time, the VMCAI algorithm (Section 2.1.8). This could also be used to account for the effect of drugs, by perturbing the node which drugs act upon to mimic their effect. This also allows a background of mutations such as those found in cell lines to be applied. The output of the model is compared to the experimental data, and in case of mismatch iterated by changing Target Functions, or searching for missing edges, until it was able to match all experiments drawn from the literature (see Chapter 3.4.2). This panel of experiments thus forms a specification for what behaviour I am able to model, defining its scope. I chose these to cover as wide a range of key nodes and behaviours in the network, under as many different circumstances as possible. To be able to test effectively, I required as exact a mutational profile of the cells or tissues used as possible, to be able to correctly set the mutations of the model. As such, I focussed on cell lines for my validation. While these are not completely stable, they have been studied to find instances of mutations, amplifications and copy number variations which translate into differences of node activity in the model, which would not be feasible with primary tissue data.

2.3 Using Bio Model Analyzer to Test Single and Double Combinations of Perturbations

In Chapters 4 and 5, to assess effective targeted mono- and combination therapies, I performed single and pairwise activation (set Target Function to constant max to show a node continuously active, such as under the effect of a mimetic drug) and inhibition (set Target Function to zero to simulate a drug blocking activity) of all nodes in the network.

The choice to model inhibition and activation as the extremes of activity for a node is for two reasons. Firstly, for the majority of the nodes of the network, I chose a granularity of 0 to 2, allowing the representation of lower, normal, and higher-than-normal activity. While in reality, different drugs may have different effectiveness, and some will be less effective than as to be able to fully block all activity, they will have some effect beyond keeping a node at normal activity. The granularity these nodes means that the only way to model this is to take the activity of the node to 0 or 2, or to increase granularity. However, this would make it more difficult to map experimental data to the model consistently, as discussed in Chapter 3.2.

Secondly, by assuming maximal effectiveness this screen can identify not only possible targets for use with existing treatments, but also areas which it would be most fruitful to attempt to target in the future, were a maximally effective treatment available. This can therefore help guide future research. It is for this reason that I also examined the effect of activation, as opposed to inhibition, despite this being a less common type of intervention (discussed further in Chapter 4.2.1, and shown in Appendix B).

Every possible combination of activations and inhibitions are performed for every combination of pairs of nodes; i.e. 4 per node. For each perturbation, I find the stable state of the network, or the smallest range to which the node can be constrained, using a script to access the command line version of BMA using the VMCAI algorithm (Section 2.1.8). In order to compare different tumour sub-clones, I also added a background set of mutations that are unaffected by the above mutations. If BMA could not restrict the value of the node to a single value, for example if there is an oscillation between two levels of activity, I used the mean of the minimum and maximum value in the heat-maps, and show the range in a separate heat-map. Due to the size of the network, the SMT solver could not always constrain the range of the final state of every node in a reasonable amount of time, so I used the VMCAI algorithm. The BDD algorithm was not available in time to aid these analyses. For cases of most interest, I can then run through the SMT or BDD algorithms for an exact solution. The results of these pairwise mutations were filtered by searching for those which showed a change to proliferative or apoptotic behaviour.

2.3.1 Filter by Druggable Targets

In order to focus on those targets which could be tested experimentally, I filtered out those nodes that were not druggable, according to the Drug-Gene Interaction Database [465]. For

this I needed to consider the genes corresponding to each node, and the number of known drugs which target them, both shown in Chapter 4.2.1 and in further detail in Appendix A.1.

This database considers any drug which interacts with the target queried, including those which may also have other off-target effects. It is therefore best suited to eliminate those genes which are most difficult to affect, but less likely to remove a gene which might be able to be usefully targeted, but in a less specific manner. This suits the questions I wish to answer, as I prioritise including interesting nodes, even those which may only be targetable in the future, over excluding those which cannot yet be targeted, while still wishing to focus on those most likely to be able to be able to be pursued in the future. However, it is also likely that the database is incomplete, and it is always possible there are errors. Therefore the full results for all nodes are included in Appendix B. In the future, it the network could be alternatively filtered more strictly, for only those genes which are specifically targetable, as opposed to simply druggable in some manner. For increased reliability, other databases of druggable genes could be included, and only those which are present on the majority of databases consulted included.

2.4 Reconstructing the Order of Mutations

In order to reconstruct tumour evolution, shown in Chapter 6, I used the BDD algorithm (Section 2.1.10) to analyse all the attractors for every possible combination of mutations in a cancer. To find combinations of mutations known to result in cancer, I used the mutational profiles of common breast cancer cell lines, as collated by Hollestelle et al. [207]. My model was not large enough to cover all the mutations seen in [207], e.g. I did not cover Epithelial–Mesenchymal Transition and so the network did not include E-cadherin. However, I chose cell lines to match the capabilities of the network as closely as possible.

For each set of mutations from a cell line, I create the powerset of all possible combinations of mutations of all possible lengths. I also include a baseline set of perturbations to the network to simulate the growth factor background, for all these experiments this was EGF and Wnt1 at 1. This is applied in addition to the mutations the cancer acquires, and when applied alone simulates the Healthy state of the cell. As the cancer evolves, it passes from the healthy cell to different partial sets of mutations, until it has acquired all the mutations of a cell line. An example of this is shown in Figure 2.7.

I can then see what the phenotype of the cell, namely level of proliferation and apoptosis, is for each combination of mutations that can be passed through on the route to the full set of mutations for a cell line.

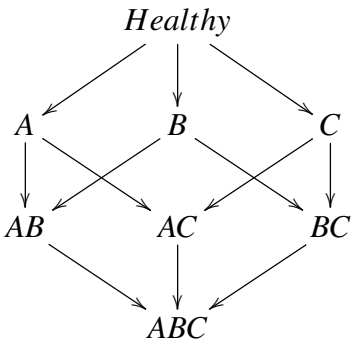

Fig. 2.7 To explore the order of mutations ABC, I apply them in all possible orders by constructing a powerset. Paths in this powerset network represent different orders in which mutations can be acquired. I then analyse the network at each node of the path to see if any of these intermediate states have high apoptosis or low proliferation, and so may block evolution following this path.

To find the behaviour of the network as the tumour evolves, I first find all the attractors for the healthy state. In the case of my breast cancer model, there is only one attractor for the healthy state, and all the cases examined in Chapter 6 start from this state. For each subsequent set of mutations, I then find all the attractors reachable from one of the previous states, with the addition of one of the mutations connected to it by an edge in the powerset. This means I find what new attractors for the network there are given the current stable state and one node which changes value due to perturbation. This is repeated until the algorithm reaches the final state of the powerset, which is equivalent to the mutational profile of the cell line.

Note that this is not the same as finding all the attractors for every node of the powerset, as there will be some attractors which can only be reached from initial states excluded from the attractor found in the previous step. For example, if the network has only 3 nodes, A, B and C, then under mutation A it might have two attractors, one in which it stabilises in if the initial state of B is 0, and the other if the initial state of B is 1. If the initial state of B is 0 in the healthy state however, then upon mutating A the second attractor is not reachable and the network will always stabilise to the first. This determines the edges which denote possible transitions between sets of mutations. This requires finding all possible attractors at each stage, as in cases of bifurcation, different attractors for the same set of mutations may have different reachable states under the next set of mutations. This was only possible with the BDD algorithm, but was possible as it only required a small number of BDD analyses, as opposed to the analysis described in Section 2.3.

2.4.1 Visualisation and Analysis

Once I have found all the attractors for each stage of the powerset, I visualise these data by showing the level of proliferation and apoptosis at each vertex of the powerset. If the attractor is a loop, I show the mean level of the phenotype over the loop. In the case of bifurcations, each receives its own vertex in the powerset. This shows which paths can be taken while minimising apoptosis, and maximising proliferation as early as possible, as the cancer develops. This allows us to find the optimal order of mutations, or the optimum path through the powerset, for each cell line.

2.5 MMTV-Wnt1 Mouse Mammary Tumours heterogeneous in Myc

2.5.1 Generation of a Traceable Model of Myc Heterogeneity

In order to test the predictions produced by the model, using the methods I describe above, I compared my predictions to *in vivo* data. Below I describe the methods used by my collaborators to produce these data.

Dr Peter Kreuzaler, with the assistance of Dr Catherine Wilson, developed a traceable, *in vivo* model of an MMTV-Wnt1 driven heterogeneous tumour containing high and low myc-expressing clones, through selective expression of a switchable MycER^{T2} construct. I used this to check the model, and to validate my predictions.

The heterogeneous model is generated in three broad stages:

1. Tumours are generated using MMTV-Wnt1
2. Cells are extracted and formed into two populations, one with high myc expression (myc-high) and one with normal myc expression (myc-low)
3. Different ratios of myc-high and myc-low are inserted into a new host to generate heterogeneous tumours

Generation of MMTV-Wnt1 driven tumours

Initial tumours are generated in triple transgenic mice carrying the Rosa26-CAG-lox-STOP-lox-MycERT2/ Rosa26-mTmG/ MMTV-Wnt1 alleles. MMTV-Wnt1 consists of the Long Terminal Repeat (LTR) of the Mouse Mammary Tumour Virus (MMTV) upstream of a Wnt1

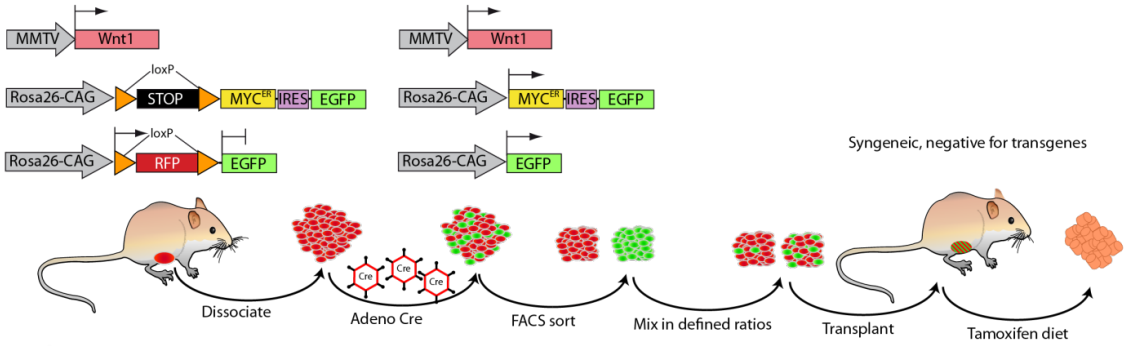

Fig. 2.8 Rosa26-CAG-lox-STOP-lox-MycER^{T2}/ Rosa26-mTmG/ MMTV-Wnt1 cells are harvested from a spontaneous tumour. These are pretreated with Tamoxifen to ensure ER negativity, as Tamoxifen will be used throughout the study. Cre-recombination activates the MycER^{T2} gene, as well as the mTmG cassette. This results in two populations of cells, one without MycER^{T2} expression, which also produces RFP, and one with MycER^{T2} which expresses GFP. These are then seperated by FACS sorting, and implanted in another mouse in as a mixture. Tamoxifen is later administered to these mice to activate MycER^{T2} to induce formation of heterogeneous tumours. (Figure produced by Dr Peter Kreuzaler)

gene [446]. MMTV-Wnt1 tumours are often ER+, which could confound the results due to the use of 4-OHT to activate Myc. It was ensured they were ER- by exposing mice to Tamoxifen during tumour generation, which is known to lead to rapid loss of ER+ clones. Once tumours were palpable, they were excised and cryopreserved as small fragments in fetal bovine serum (FBS) with 10% dimethyl sulfoxide (DMSO), thus creating a bio-bank of transplantable tumours.

As the triple transgenic mice used for tumour generation were on a mixed genetic background, tumour transplants could only be carried out into immunocompromised SCID mice (CB17/Icr-*Prkdc*^{scid}/IcrIcoCrl from Janvier Labs) to avoid rejection [44]. This also meant that I did not prioritise immune evasion in the construction of the network model as it would not represent a constraining factor on tumour growth under these conditions.

Heterogeneity in c-Myc Expression

To create two population of cells with different levels of myc expression, secondary tumours were generated, by orthotopic implantation of stored tumour fragments into the mammary fatpad of recipient mice. Once these secondary tumours were palpable, they were surgically removed and dissociated into single cell suspensions. These suspensions were then infected with attenuated adenovirus carrying Cre recombinase. Cre is a virally delivered topoisomerase which triggers the recombination of loxP genes and so excision of Lox-Stop-Lox (LSL)

cassettes. This activates the Rosa26-CAG-lox-STOP-lox-MycER^{T2}/ Rosa26-mTmG genes, which has the following elements:

ROSA26 a locus used to express a gene ubiquitously and constitutively in mice

CAG a promoter used to ensure high gene expression

LSL a cassette used to ensure expression occurs only after addition of Cre-recombinase

MycER^{T2} myc gene fused to a murine ER gene, which is activated by 4-hydroxytamoxifen (4-OHT) but not natural ligand estradiol [293]

Rosa26-mTmG Leads to cells expressing red fluorescent protein (RFP) prior to CRE recombination, and green fluorescent protein (GFP) thereafter

As such, this results in a population of cells which are unrecombined, express RFP and are unresponsive to 4-OHT (myc-low), and a population expressing GFP and which switch on Myc expression in response to 4-OHT. Note that myc-low cells still have endogenous myc, which will respond as normal to the signalling of the gene regulatory network. As shown in 2.8, this allows the creation of tumours with controlled ratios of cells with MycER^{T2} and without.

Injection of cells to produce secondary tumours

Cells were injected into the uncleared fat pad of tertiary recipient SCID mice, which had none of the transgenes. Thus tumours developed only from the injected cells. Tumours were left to grow until they were approximately 1cm^3 in volume, at which point MycER^{T2} was activated by injections of Tamoxifen twice daily for three consecutive days. Resultant tumour histology could discriminate between myc-high and myc-low cells by their fluorescence, and cells from the recipient mouse by their lack thereof. Mice with pure myc-low and myc-high tumours were created to investigate the isolated behaviour of these sub-clones, as well as heterogeneous tumours containing a mixture of 20-30% myc-high cells.

2.5.2 Characterisation of Pure Myc-High and Myc-Low Tumours

In order to understand the differences between tumour sub-clones, pure tumours were removed, cross sectioned, and assayed for proliferation, cell death, and the activity of key genes. This could then be compared to behaviour of the network model (see Chapter 3.5.2).

All surgeries, tumour collection, and fluorescence activated cell sorting were carried out by Dr. Peter Kreuzaler, with qPCR and Western Blotting performed with assistance of Elizabeth Brown.

Immunohistochemistry and Immunofluorescence was used to assay HIF1α, Cleaved Caspase 3, ARF, β-catenin, Myc, and p53. Proliferation was assayed with IdU staining.

Quantitative real-time PCR (qRT-PCR) was used to analyse PUMA, Noxa, ARF, p21, BIM and Wnt1 expression. GAPDH, TBP and ACTB were used as controls initially. While these are commonly used housekeeping genes, there is evidence of variation in different contexts and different tissues. GAPDH has been observed to vary little in breast cancer [322], while TBP has been observed to be stable but recommended to be used only in combination with other housekeeping genes [303]. GAPDH and TBP have also been assessed to be stable housekeeping genes to use when assessing myc expression, although ACTB, while widely used, is more variable and less suitable in this context [283]. Further, there is evidence that many commonly used housekeeping genes may vary more than expected, for example in hypoxic situations [55]. My collaborators compared results with these different controls to assess their suitability. None of the controls when compared inverted observed trends relative to one another, nor showed difference in expression based on sub-clone. Therefore GAPDH was settled upon as the control for all subsequent experiments.

Western Blotting was used to asses p53 and Wnt1 activity.

2.5.3 Testing Predicted Therapies

To test the effects of drugs predicted by the network model, heterogeneous tumours were created as above by Dr Kreuzaler. When tumours reached 8×8mm in size, 4-OHT was administered for 2 days to activate MycER^{T2}. On the third day, drugs were administered for four days, with 4-OHT treatment also continuing to ensure that MycER^{T2} continued to function. To inhibit COX2, Licofelone (Lico), potassium salt (Calbiochem #435801) was freshly suspended in sunflower oil at a concentration of 20mg/ml and given by oral gavage at a dose of 100mg/kg/day. To inhibit Mek, PD0325901 (PD) (Selleckchem #S1036) was dissolved in DMSO at 20mg/ml. The working solution was diluted to 2mg/ml in water with 0.5% final concentration of Hydroxyethyl-cellulose as thickener, as well as 0.2% Tween and administered at (10mg/kg/day via oral gavage).

2.5.4 Statistical Analysis of Predicted Therapies

Measured Variables

The tumours were assessed for response to treatment by measuring overall growth, proliferation and apoptosis. Tumour growth was measured based upon the cross-section, assuming an ellipsoid shape and that the tumour depth is equal to its width.

$$Tumour\ Volume = \frac{4}{3}\ \pi\ length \times width \times depth$$

Proliferation was measured by percentage of IdU positive nuclei in a tumour cross-section, and apoptosis by percentage of Cleaved Caspase 3 positive pixels in a tumour cross-sections. Tumour growth was measured at the beginning of treatment (Day 0) and for each subsequent day (Day 1-3). Treatment was continued for 3 days as the mice were unable to tolerate longer treatment.

Analysis of Proliferation and Apoptosis by Analysis of Variance

I compared how results differed for different treatment regimes, for each sub-clone individually. I modelled the presence or absence of PD or Lico as two separate factors to allow the assessment of their interaction. In the case of tumour growth, to account for the effect of replicate measurements over time I fit a linear mixed-effects model, see the below. In the case of proliferation and apoptosis data I apply Analysis of Variance (ANOVA) [149], as these had only one time-point. This is because these responses could only be measured by immunohistochemistry of tumour sections, and thus only after treatment.

ANOVA allows me to test the null hypotheses that: there is no difference in the group means due to each factor, and that there is no difference due to the interaction of factors Quinn and Keough. [369, p232].

ANOVA relies upon three assumptions:

1. Normality: that the observations are normally distributed.
2. Homoscedasticity: that the variance of the errors is similar in each group
3. Independence: that measurements are independent within and between groups

For tests of normality and homoscedasticity I use graphical methods, quantile-quantile plots and residual plots respectively, over formal tests. While tests such as the Shapiro–Wilk test for normality [402] and Levene's test for homoscedasticity [286] can be useful, I follow

the advice of Quinn and Keough. [369, p192] that such tests tend to be less informative than graphical methods and overly sensitive to skewness for which an ANOVA is still robust. This also concurs with discussion in the literature over the use of preliminary tests for homoscedasticity in the context of t-tests [518]. For all the results I discuss in Chapter 5.7 I include these assessments in Appendix C.

These data came from individual mice, so comparisons between treatment types, for one sub-clone, were independent. However, in some cases these data did not conform to the assumptions of normality and homoscedasticity. Specifically, they were heteroscedastic with an error which increased with the mean (see, for example Figure C.14a). In cases such as these, it is recommended by Quinn and Keough. [369, p65], Grafen and Hails [180, p159], Dytham [124, p43] and Sokal and Rohlf [413, p213] that a re-scaling transform is applied to the dependent variable in order to conform to these assumptions. As the heteroscedasticity showed an increase in variance with the mean, I employed a log_{10} transform to correct this, as advised by Sokal and Rohlf [413, p215].This is also the transform suggested by Sachs [383, p517] for the cases of frequency data, such as number of proliferating nuclei, and time-dependent data respectively.

The significance of the interactions indicates whether there is likely to be a synergistic effect between the two drugs applied, beyond what could be expected additively. However, transformation may hide such interactions. For example, a log_{10} transform changes an multiplicative relationship between factors into an additive one [327, p141], [369, p249]. Caution must be applied when interpreting these results therefore. In cases where there was such a significant interaction between the two factors I further considered pairwise comparisons between these factors to see which showed significant differences, using Tukey Honest Significant Difference (TukeyHSD) [448], [369, p200]. This controls for the Type I error rate introduced by the multiple unplanned comparisons.

Comparison of Proliferation and Apoptosis between Sub-clones

In order to compare the effects of treatments on the myc-low and the myc-high sub-clones, I use Welch's t-test [475] (see Appendix C.3). This is an extension of Student's t-test [423] which is more reliable in the case of unequal variances. I assume such inequality of variance and apply Welch's t-test directly, as suggested by Zimmerman [518]. This relies upon an assumption of normality, which I test for by a quartile-quartile plot. As proliferation and apoptosis for different sub-clones were measured in the same tumour, I use a dependent or paired test. In cases where this is violated, I correct for this by square-root or log_{10} transformation.

As I compare sub-clones for each treatment, I apply the Holm method [209] to control the family-wise error rate due to multiple comparisons. For this purpose I consider proliferation and apoptosis separately, as they are subject to different hypotheses, following Quinn and Keough. [369, p49].

Analysis of Tumour Growth with Linear Mixed Effects Modelling

I applied a linear mixed-effects model in the case of tumour growth data [369, p305], [124, p127], [93, p699], [19, p27], as this could be measured with callipers during treatment. This was necessary to account for the temporal change. I use the Day of treatment, as well as presence or absence of PD and Lico as before, as my fixed effects, with the mouse to which treatments were repeatedly applied as a random effect. Further, there was one more mouse which was able to be measured for tumour size in the combination treatment group than any of the other groups, and linear mixed-effects models are robust to unbalanced sample sizes [82]. As in the case of the quantification of proliferation and apoptosis, I apply a transform to correct homoscedasticity. I In the case of the tumour growth data, I found a negative inverse transform [180, p166], [249, Ch3] better fit assumptions, using the negative inverse to preserve the ordering of results. I then analyse the p-values of fixed-effects using Type III Analysis of Variance with Satterthwaite's method [301]. These tests were carried out using the lme4 [20] package, and it's extension lmerTest [268] in R [370].

In the case that comparison of the significance of different main effects and interactions by a Type III ANOVA with Satterthwaite's method shows that some are insignificant, I attempt to fit a simpler model, following the principle of marginality [339].

Finally, in the case of significant interaction between the factors, I explore the pairwise contrasts using least square means [193, 395] and correcting for multiple testing by Tukey's HSD test. For this I use the R package lsmeans [284].

Chapter 3

Building and Validating the Computational Model of the Gene Regulatory Network

3.1 Introduction

My goal is to understand how the cell makes decisions about its behaviour in response to internal and external stimuli, and how this goes wrong in cancer. These decisions are encoded in the interactions between, and levels of expression of, different genes and proteins in the cell. The sum of these states translates into overall cell behaviour such as proliferation or apoptosis.

There are many ways to model the network of interactions within the cell, with different advantages and disadvantages. All of them require that I choose certain abstractions in order to make modelling the system feasible. It is not possible, for example, to model every protein in the system at an atomic level, and indeed this would not be useful as there is no way to measure the real system accurately enough to validate this. By modelling the system as a Qualitative Network, I focus on the discrete activation states of the components of the network, retaining enough information to be useful while maximising the data available for building the model.

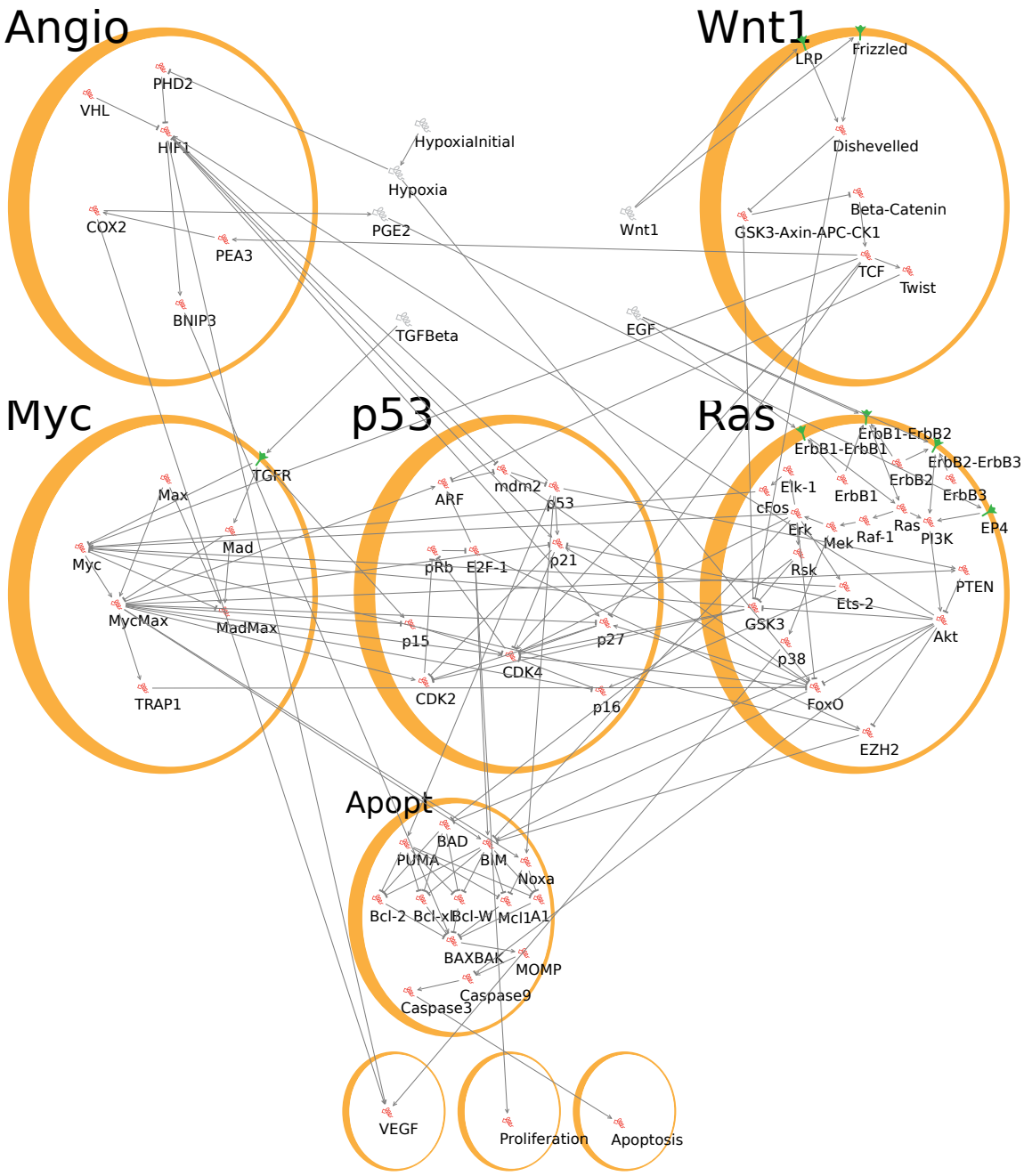

Fig. 3.1 Breast Cancer Model as seen in the Bio Model Analyzer. Red nodes represent genes or proteins within the cell, grey are extracellular. Different pathways are organised into modules (orange circles) for ease of use. Phenotypes of the cell are placed in their own module at the bottom of the network diagram.

3.2 Building the Model from Literature Data

In order to build the model I collated two data sets. Firstly I required evidence of how the key nodes and pathways interacted, and so collected evidence from the literature for every edge in the network. This is explained in more detail in this section, and tables of the literature used are included. I include an expanded version of these tables, with more details of the experiments, in Appendix A.1.2. Many of the experiments described here also help to suggest how the nodes interact, and so determine the Target Functions of the nodes (see Section 3.3). I ensured that for interactions specific to breast cancer I found evidence from breast cancer systems specifically, but for some of the core accepted interactions there were no tests in breast cancer for which I could find evidence.

Secondly, I needed to be able to test the behaviour of the network. To do this I created a specification of experimental behaviour which the model was required to match. This required experiments in which multiple nodes were perturbed, and effects measured which were far from these. So rather than testing whether a transcription factor controls expression by observing the effect of over-expressing or interfering with said transcription factor, these were experiments where the whole behaviour of the cell, such as rate of proliferation and apoptosis, was affected. The results of such experiments are dependent upon the cross-talk between pathways, so could not be directly encoded into the model, making them the best way of testing it. For this I used data on experiments primarily conducted in cell lines. This was because, in order to set the initial conditions for the network, I required a mutational profile of the cancer in order to know which genes to constitutively activate or knock out. These data are not usually available to primary tissue or *in vivo* models. These experiments and the results of my model in the same conditions are collected in Table 3.12.

However, the mutations which are required for a successful cell line do not align with those of a cancer *in vivo*. Furthermore, they do not allow testing of how the cancer cells interact with their microenvironment, e.g. through angiogenesis and hypoxia, and are sustained by high levels of growth and survival factors. To test this required an *in vivo* model with known characteristics and mutational profile. Dr Peter Kreuzaler, of the Evan Lab (Department of Biochemistry, University of Cambridge), was developing such an *in vivo* model as I was developing my computational model. I describe this *in vivo* model in Chapter 2.5 and he, with assistance of Dr Cathy Wilson and Elizabeth Brown, measured the activity of 13 nodes, and how they change between a tumour of pure myc-low and pure myc-high cells. I then compared this to my network model to ensure that it could reproduce this system as well (Section 3.5.2). However, there were some specialisations made for the *in*

vivo version of the model. My collaborators believed that the tumours were HER2 negative, so this node was removed. I also allowed VEGF and angiogenesis to control hypoxia by feedback, which is not the case in the *in vitro* case.

Target Functions are guided by the literature, but cannot map directly from a continuous system to my discrete model. In cases where the literature was ambiguous, I chose these to best fit the experiments to which I compare the model in Sections 3.4.2 and 3.5.2. For example, in many cases it is sufficient to take the average of positive inputs minus the average of negative inputs to find the activation level of a node. But in cases where there are many genes which activate a node, but they are rarely active together, this may unrealistically dilute the influence of each activatory input. In such a case it may make more sense to take the maximum rather than the average of the inputs, if this produces behaviour that better matches experiment. The reasoning behind any Target Functions which differ from the default are explained in Table 3.8.

As a Qualitative Network can have nodes with any granularity, and a mixture of granularities within the network, I had to choose a level which was appropriate to model the breast cancer gene regulatory network. For most of the nodes of the network, I chose a granularity of 0 to 2 to represent lower, normal, and higher-than-normal activity. This gave me the resolution required to model the behaviours of interest, but also avoided the need to map a more fine-grained granularity to the wide range of experimental data used to build the model. This allowed me to be more consistent in translating this data to the model than if I had needed to choose between the data showing myc being expressed at level 12 or 13 out of 20, for example. However, for phenotypes, and the nodes which integrated many other signals from the network in order to determine the phenotype, such as the BAXBAK, a higher level of granularity was required. The minimum for apoptosis would be 0 to 3 as I needed to represent the levels of apoptosis from p53 activity with PUMA or Noxa knock-outs, which were all measurably different, as well as no apoptosis signalling. In order to best model the data from the mouse model, I chose a range of 0 to 6 for phenotypes, as a smaller range did not have the sensitivity to integrate all the signals from across the cell and show the differences observed by my collaborators. The range of each node is shown in Table 3.8.

3.2.1 Myc

Table 3.1 Evidence for edges in the myc pathway of the network model.

From	To	Type	Cell Line/Tissue	Evidence
Myc	MycMax	Activatory	Review	Grandori et al. [181]
	MadMax	Inhibitory	Review	Grandori et al. [181]
Max	MycMax	Activatory	Review	Grandori et al. [181]
Max	MadMax	Activatory	Review	Grandori et al. [181]
Mad	MycMax	Inhibitory	Review	Grandori et al. [181]
	MadMax	Activatory	Review	Grandori et al. [181]
MycMax	TRAP1	Activatory	WI38 Fibroblasts	Coller et al. [84]
MycMax	ARF	Activatory	MEF	Zindy et al. [519]
MycMax	p21	Inhibitory	WI38 Fibroblasts	Coller et al. [84]
MycMax	p21	Inhibitory	SKBR3 breast cancer epithelial	Mitchell and El-Deiry [328]
MycMax	PTEN	Activatory	IMEC Immortalised Epithelial Mammary Cells	Kaur and Cole [245]
MycMax	p27	Inhibitory	Primary Human Mammary Tissue and Mouse Mammary Cell Lines HC14	Nass and Dickson [338]
MycMax	p27	Inhibitory	Hs578T breast cancer cells	Yang et al. [495]
MycMax	CDK4	Activatory	Rat1 Fibroblasts	Hermeking et al. [200]
CDK4	Proliferation	Activatory	HCA2 Human Fibroblasts	Morris et al. [332]

Table 3.1 continued from previous page

MycMax	CDK2	Activatory	WI38 Fibroblasts	Coller et al. [84]
MycMax	CDK2	Activatory	Primary Human Mammary Tissue and Mouse Mammary Cell Lines HC14)	Nass and Dickson [338]
MycMax	BIM	Activatory	MEF	Muthalagu et al. [336]
MycMax	BIM	Activatory	BT474, SKBR3 and MCF7	Campone et al. [52]
MycMax	Noxa	Activatory	MDA-MB-231	Nikiforov et al. [344]
TRAP1	FoxO	Inhibitory	MCF7	Kim et al. [247]
TGFBeta	TGFR	Activatory	Review	Hinck [202]
TGFR	Myc	Inhibitory	MDA-MB-468	Fernandez-Pol et al. [145]
TGFR	Mad	Activatory (Indirect)	NMuMG mouse mammary epithelial	Siegel et al. [407]
TGFR	p15	Activatory	HaCaT	Seoane et al. [399]
MycMax	p15	Inhibitory	HaCaT	Feng et al. [143]
MycMax	p16	Inhibitory	Review	Amati et al. [7]

Myc is a key driver of proliferation [230, 345, 324] and prevents exit from the cell cycle [244]. Conversely, loss of myc expression inhibits the growth of healthy and cancerous tissue [466]. As such it is overexpressed in 45% of breast cancers, 67% of colon cancers and 70% of prostate cancers [457]. In my network, the main effectors of this are by direct induction of CDK2-CyclinE and CDK4-CyclinD1, as well as suppression of p21 and p27.

However, myc expression also primes the cell for apoptosis [136], increasing signalling along many apoptotic pathways, both via p53 [519] and p53-independent [336], and so lowering the threshold at which insults will cause cell death. This acts as a fail-safe against myc overexpression. This means that in order for myc to drive cancer, it must cooperate with other driver genes, such as Ras [273]. It is this balancing of roles that convinced me that

a network model was the best way to address questions of myc function in cancer, as it is necessary to account for and be able to explain how signals from across the gene regulatory network determine which effect of myc wins out.

The targets by which myc effects these changes are still being identified, and there is controversy over the extent of the transcriptional regulation by myc. Myc is a basic helix–loop–helix zipper (bHLHZ) protein and primarily activates and represses genes by binding to the E-box sequence CACGTG [302]. However, ChIP-seq studies of myc binding suggest a large number of targets, and potentially that it upregulates all genes which are being actively expressed at the time of myc activation [291, 342]. As suggested by Littlewood et al. [294] and Kress et al. [264], c-myc activation under this model would lead to a "lock-in" of existing behaviour if myc were a universal amplifier, and a stronger expression of the characteristics of the differentiated cell. Instead myc causes changes in cell behaviour, namely de-differentiation and proliferation, casting doubt on this hypothesis. An alternate hypothesis is that while high levels of expression can cause binding at many sites along the DNA, we do not yet know how many of these are functional, and there is a subset for which it acts as a more traditional transcription factor [100, 382]. I focus on this subset in building the model.

Myc regulation is also complex, responding to many growth signals, such as EGF [145] and Wnt1 [196], but also to regulation of its dimerisation partners. Myc homodimers have little activity, rather Myc binds to DNA by forming a dimer with Max. Max expression is constitutive, and so the level of Myc is still rate limiting for its interaction with DNA. However, it must compete with other dimerisation partners of Max from the Mad family of proteins [181, 14]. These also vary in expression in response to growth factors such as TGF-β [407]. Their expression can influence the activity of Myc through competition, although the level of effect is debated [87]. This relationship forms the basis of the Target Functions for MycMax and MadMax (see Table 3.8), which model the competition between Myc and Mad for Max.

3.2.2 Ras

Table 3.2 Evidence for edges in the Ras pathway of the network model. Citations marked with a (*) come from a model initially jointly developed with student Victoria Wang.

From	To	Type	Cell Line/Tissue	Evidence
EGF	ErbB1-ErbB1	Activatory	Review	Yarden and Sliwkowski [496]
ErbB1-ErbB1		Expression in breast	MCF10A	Dong et al. [116]
EGF	ErbB1-ErbB2	Activatory	T47D	Klapper et al. [251]
EGF	ErbB2-ErbB3	Activatory	SKBR3, MDA-MB-361, BT474	Holbro et al. [206]
ErbB1	ErbB1-ErbB1	Activatory	Review	Yarden and Sliwkowski [496]
ErbB1	ErbB1-ErbB1	Activatory	A431 Human Squamous Carcinoma	Low-Nam et al. [295]
ErbB1	ErbB1-ErbB2	Activatory	Review	Yarden and Sliwkowski [496]
ErbB1	ErbB1-ErbB2	Activatory	T47D	Klapper et al. [251]
ErbB2	ErbB1-ErbB2	Activatory	Review	Yarden and Sliwkowski [496]
ErbB2	ErbB1-ErbB2	Activatory	T47D	Klapper et al. [251]
ErbB2	ErbB2-ErbB3	Activatory	Review	Yarden and Sliwkowski [496]
ErbB2	ErbB2-ErbB3	Activatory	T47D	Klapper et al. [251]

Table 3.2 continued from previous page

ErbB3	ErbB2-ErbB3	Activatory	Review	Yarden and Sliwkowski [496]
ErbB3	ErbB2-ErbB3	Activatory	T47D	Klapper et al. [251]
ErbB1-ErbB1	Ras	Activatory	HeLa	Schulze et al. [393]*
ErbB1-ErbB2	Ras	Activatory	HeLa	Schulze et al. [393]
ErbB2-ErbB3	PI3K	Activatory	SKBR3, MDA-MB-361, BT474	Holbro et al. [206]
Ras	Raf-1	Activatory	3T3 Fibroblasts	Jelinek et al. [227]*
		Activatory	Primary Breast Tissue	McGlynn et al. [320]
Raf-1	Mek	Activatory	3T3 Fibroblasts	Jelinek et al. [227]*
		Activatory	Primary Breast Tissue	McGlynn et al. [320]
		Activatory	3T3 Fibroblasts	Kyriakis et al. [270]*
Mek	Erk	Activatory	Review	Cobb [83]*
		Activatory	Primary Breast Tissue	McGlynn et al. [320]
Erk	Elk-1	Activatory	3T3 Fibroblasts	Aplin et al. [12]
Elk-1	cFos	Activatory	3T3 Fibroblasts	Hill and Treisman [201]*
cFos	Myc	Activatory (Indirect)	MCF7	Lu et al. [297]
Erk	Myc	Activatory	REF52 Fibroblasts	Sears et al. [396]*

Table 3.2 continued from previous page

Erk	Rsk	Activatory	MCF10A Breast	Doehn et al. [115]
Rsk	GSK3	Inhibitory	3T3 Fibroblasts	Eldar-Finkelman et al. [129]
Rsk	GSK3	Inhibitory	Primary Human Colon Carcinoma	Ding et al. [114]
Rsk	BAD	Inhibitory	Primary mouse mammary epithelial cells	Gilmore et al. [175]
Ets-2	p16	Activatory	TIG3, Hs68 Human Fibroblasts	Ohtani et al. [346]
Erk	Ets-2	Activatory	SKBR3	Al-azawi et al. [4]
Ets-2	Myc	Activatory	SKBR3	Al-azawi et al. [4]
Mek	p38	Activatory	Primary Human Breast Tissue	Esteva et al. [134]
Ras	p38	Activatory (indirect)	MDA-MB-231	Kwon et al. [269]
Ras	p38	Activatory (indirect)	MCF10A	Kim et al. [248]
p38	VEGF	Activatory	MCF7, SKBR3	Xiong et al. [490]
Erk	FoxO	Inhibitory	MCF7	Yang et al. [493]
Erk	BIM	Inhibitory	MCF10A	Collins et al. [85]
Erk	CDK4	Activatory	Review	Whitmarsh and Davis [479]
Erk	CDK4	Activatory	3T3 Fibroblasts	Cheng et al. [69]

Table 3.2 continued from previous page

Erk	CDK4	Activatory	Human Lung Fibroblast	Shen et al. [404]
Ras	PI3K	Activatory	COS-7	Pacold et al. [351]*
PI3K	Akt	Activatory	Review	Franke et al. [157]*
Akt	HIF1	Activatory	MDA-MB-468	Blancher et al. [40]
Akt	p21	Inhibitory	MDA-MB-453	Zhou et al. [514]
Akt	GSK3	Inhibitory	MCF7	Knuefermann et al. [254]*
Akt	BAD	Inhibitory	MCF7	Knuefermann et al. [254]
Akt	EZH2	Inhibitory	IMEC Immortalised Epithelial Mammary Cells	Kaur and Cole [245]
Akt	Apoptosis	Inhibitory	Rat1 Fibroblasts	Zundel and Giaccia [521]
Akt	Caspase9	Inhibitory	293T HEK	Cardone [56]
Akt	Caspase9	Inhibitory	MCF7	Li et al. [290]
Akt	FoxO	Inhibitory	MCF7	Sunters et al. [428]
EZH2	BIM	Inhibitory	MCF7	Wu et al. [488]
EZH2	Myc	Inhibitory	IMEC Immortalised Epithelial Mammary Cells	Kaur and Cole [245]
PTEN	Akt	Inhibitory	IMEC Immortalised Epithelial Mammary Cells	Kaur and Cole [245]
EZH2	BIM	Inhibitory	MCF7	Wu et al. [488]

Table 3.2 continued from previous page

FoxO	BIM	Activatory	MCF7, MDA-MB-231	Sunters et al. [427]
FoxO	CDK4CylindD	Inhibitory	MEF	Schmidt et al. [392]*
FoxO	p21	Activatory	MCF7	Zou et al. [520]
FoxO	p27	Activatory	Ba/F3 Murine pre-B-cell	Dijkers et al. [112]
FoxO	p27	Activatory	MCF7, MDA-MB-231	Sunters et al. [427]
GSK3	MycMax	Inhibitory	MCF7	Rodrik et al. [375], Yeh et al. [498]*

KRAS (henceforth Ras) is another key effector of cell growth [117] and cooperates well with Myc [273]. Ras mutation is comparatively rare in breast cancer, but the pathway is often highly active through mutations of growth receptors EGFR and HER2 [461]. Indeed some of the most successful targeted therapies in breast cancer target these receptors, with Trastuzumab targeting the HER2 receptor [458] and Gefitinib the EGFR receptor [491]. Ras signalling has two main branches: the MAPK pathway and the PI3K-Akt pathway. The MAPK pathway drives cell growth and proliferation [110], partly through myc activation, while the PI3K-Akt pathway inhibits growth antagonists such as p21 and p27, as well as countering apoptotic signalling. These branches are not independent however and interact at various points, such as regulation of GSK3β and FoxO.

Regulation of Ras in breast cancer comes via the EGFR family, as well as other receptors such as those for Oestrogen and Progesterone. However, I focus on the former, as the *in vivo* model to which I compare my model is of basal breast cancer, which usually lacks Oestrogen and Progesterone receptors [98], and so these are not included in the model. The EGFR receptor is made up of a homodimer of ErbB1 proteins. These can also dimerise with other members of the family, most importantly the ErbB2 or HER2 protein [496]. ErbB2 cannot bind ligands alone [251], but when dimerised with ErbB1 increases the strength and duration of its signalling. Hence it is often upregulated in breast cancer [410]. I also include the ErbB2-ErbB3 dimer, as this can be activated by EGF, whereas the ErbB4 containing dimers are more strongly dependant on neuregulin [426].

3.2.3 Wnt1

Table 3.3 Evidence for edges in the Wnt1 pathway of the network model.

From	To	Type	Cell Line/Tissue	Evidence
Wnt1	Frizzled	Activatory	Mammary (Review)	Boras-Granic and Wysolmerski [43]
			Mammary (Review)	Smalley and Dale [411]
			Drosophila, Human Embryonic Kidney (HEK293)	Bhanot et al. [34]
Wnt1	LRP	Activatory	Mammary HC11 Cells	Goel et al. [178]
			Human Embryonic Kidney (HEK293)	Tamai et al. [436]
Frizzled	Dishevelled	Activatory	Mammary (Review)	Boras-Granic and Wysolmerski [43]
			Mammary (Review)	Smalley and Dale [411]
			HeLa	Bilic et al. [36]
LRP	Dishevelled	Activatory	Mammary (Review)	Boras-Granic and Wysolmerski [43]
			Mammary (Review)	Smalley and Dale [411]
			HeLa	Bilic et al. [36]
Dishevelled	GSK3-Axin-APC-CK1	Inhibitory	Mammary (Review)	Boras-Granic and Wysolmerski [43]
			Mammary (Review)	Smalley and Dale [411]
			Review	MacDonald and He [304]
Dishevelled	GSK3		Review	MacDonald and He [304]

Table 3.3 continued from previous page

			Human Fibroblast 3T3 cells	Taelman et al. [432]
GSK3-Axin-APC-CK1	Beta-Catenin	Inhibitory	C57MG mouse mammary epithelial	Farago et al. [140]
Beta-Catenin	TCF	Activatory	Mammary (Review)	Boras-Granic and Wysolmerski [43]
			Mammary (Review)	Smalley and Dale [411]
			Xenopus	Behrens et al. [25]
			HT29 Colon Cancer	Korinek et al. [259]
TCF	Myc		HT29 Colon Cancer	He et al. [196]
			Mouse Mammary	Teuliere et al. [439]
TCF	CDK4	Activatory	MCF7	Lin et al. [292]
Wnt1	p27	Inhibitory (Indirect)	Neuronal cells	Castelo-Branco et al. [61]
Wnt1	p27	Inhibitory (Indirect)	3T3 Fibroblasts	Rimerman et al. [373]
TCF	PEA3	Activatory	Mouse Mammary Epithelial	Howe et al. [214]
TCF	Twist	Activatory	HC11, C57MG mouse mammary and *in vivo*	Howe et al. [215]
Wnt1	Twist	Activatory (Indirect)	Human Primary Breast Cancer samples	Watanabe et al. [469]
Twist	p53	Inhibitory (Indirect)	MCF7	Stasinopoulos et al. [419]
Twist	p53	Inhibitory	HNE1-T3 and HNE1 nasopharangeal cancer	Wang et al. [467]

Table 3.3 continued from previous page

Twist	Apoptosis	Inhibitory	HNE1-T3 and HNE1 nasopharangeal cancer	Wang et al. [467]
Twist	ARF	Inhibitory	Review (Neuroblastoma)	Puisieux et al. [367]
Twist	Apoptosis	Inhibitory	Human breast cancer (unpublished data)	Puisieux et al. [367]
Twist	ARF	Inhibitory	MEFs	Maestro et al. [308]

Wnt signalling plays an important role in breast development, as well as murine breast cancer. It regulates proliferation, as well as acting as a survival factor [67]. There are many members of the Wnt family, as well as three main pathways which respond to Wnt signalling, the Canonical, Planar Cell Polarity and Wnt/Calcium pathways. The Canonical pathway is the most focussed on proliferation, with the latter pathways playing roles in cancer through influence on invasiveness and metastasis [257, 106, 91]. I focus on the canonical pathway as this is the most relevant and well characterised, and Wnt1 as it is the family member used in the *in vivo* model.

In mammary epithelial cells, β-catenin is constitutively produced, but is also continually degraded by the GSK3β-Axin-APC-CK1 complex. This complex is disrupted by Wnt1 signalling, causing β-catenin to build up, and then activating the transcription factor complex TCF/LEF (TCF in the network). TCF/LEF then in turn activates proliferation via myc and CDK4-CyclinD1, as well as inflammation and invasiveness via COX2. There are further connections to invasive behaviour, but I do not focus on this phenotype in the model. GSK3β plays an important role in other pathways, and it is an open question how much cross-talk there is between these and the Wnt1 pathway. There is some evidence that while Wnt1 signalling results in direct phosphorylation of GSK3β, this only affects a subset of the GSK3β in the cell [362]. This is therefore best modelled by disruption of the GSK3-Axin-APC-CK1 complex. However, there is also evidence of Wnt1 signalling affecting all the GSK3β in the cell directly, so placing any GSK3β regulated pathways partly under control of Wnt1 signalling [432]. In this case Wnt1 signalling should disrupt GSK3β in general. This is summarised by MacDonald and He [304]. There is also evidence of cross-talk in the opposite direction, namely, regulation of GSK3β by other pathways having an effect on β-catenin [114]. I therefore include both mechanisms in the network, so as to have the

option of removing one if this would result in a better fit to my specification. The model could be expanded by explicitly modelling the contribution of other parts of this complex. However these are likely to play less of a role in breast cancer; for example, APC mutations are more common in colon cancer [162].

In the course of charactering the heterogeneous tumours *in vivo* (see Chapter 3.5.2), one of the key results seen by my collaborators was that ARF is suppressed by Wnt1 expression. I include this in the model as the action of the Twist, a target of Wnt1 signalling in breast [469, 215]. Twist is a bHLH transcription factor which inhibits p53 [419, 467] and through this apoptosis [367]. Work in MEFs suggests this occurs via ARF [308]. This also supports the evidence that Wnt1 acts as a survival factor [67] in breast [438], and against myc-induced apoptosis in particular [194, 500].

3.2.4 Hypoxia

Table 3.4 Evidence for edges in the Hypoxia pathway of the network model.

From	To	Type	Cell Line/Tissue	Evidence
HypoxiaInitial	Hypoxia			Used to fix external pressures on the cell
Hypoxia	FoxO	Inhibitory	MCF7	Kim et al. [247]
Hypoxia	PHD2	Inhibitory	CAL51 breast epithelial	Berra et al. [30]
PHD2	HIF1	Inhibitory	CAL51 breast epithelial	Berra et al. [30]
VHL	HIF1	Inhibitory	BT474 Mammary Epithelial human	Kong et al. [258]
HIF1	BNIP3	Activatory	Review	Greijer and van der Wall [185]
HIF1	BNIP3	Activatory	MCF7	Sowter et al. [416]
BNIP3	Apoptosis (Indirect)	Activatory	MCF7	Sowter et al. [416]

Table 3.4 continued from previous page

BNIP3	BAXBAK	Activatory	Review	Mellor and Harris [323]
HIF1	p53	Activatory (Indirect)	MCF7	An et al. [8]
HIF1	mdm2	Inhibitory	MEF	Chen et al. [64]
HIF1	p21	Activatory	HCT116 cells	Koshiji et al. [261]
HIF1	p21	Activatory	MEF	Mack et al. [305]
HIF1	p21	Activatory	MCF7, MDA-MB-231	Fanale et al. [139]
HIF1	p27	Activatory	MEF	Mack et al. [305]
HIF1	VEGF	Activatory	MCF7	Laughner et al. [277]
PEA3	COX2	Activatory	Mouse Mammary Epithelial	Howe et al. [214]
COX2	Akt	Activatory (Indirect)	MCF-7, SKBR3	Majumder et al. [311]
COX2	PGE2	Activatory	Mouse Mammary Epithelial	Kundu et al. [266]
PGE2	EP4	Activatory	C3L5 Mouse Mammary	Timoshenko et al. [444]
EP4	PI3K	Activatory	Review (breast)	Reader et al. [372]
COX2	VEGF	Activatory	MCF7	Yang and Han [494]
VEGF	Angiogenesis	Activatory	Review	Hoeben et al. [205]

Tumours develop a microenvironment with several differences to that of normal tissue. One of the challenges for a tumour is that the growth of so many cells in a part of a tissue not adapted for such a number places stresses on the existing infrastructure, and so reduces available nutrients and oxygen. Therefore one of the hallmarks of cancer is to increase angiogenesis so as to prevent hypoxia, with many putative treatments aimed at countering this [53]. I therefore include the key elements of the hypoxia response, regulated by HIF1α,

as well as modelling the effect of VEGF on angiogenesis and the subsequent amelioration of hypoxia. In order to set the initial level of hypoxia to which a tumour is subject, I have the HypoxiaInitial node, which remains fixed to model the continuing pressure on a tumour to induce angiogenesis as it outgrows existing vasculature. This is necessary as otherwise Hypoxia would drop to zero due to no incoming edges. This connects to a Hypoxia node, which is free to vary in response to angiogenesis, and so reflects mutations which help the tumour adapt to its microenvironment.

HIF1α mainly responds to hypoxia via PHD2 and VHL [258, 30] but there is also hypoxia-independent regulation through Akt [40]. Akt in turn regulates p53 via mdm2 [8, 64] and this then regulates HIF1α [38]. HIF1α promotes apoptosis through BNIP3, although the precise mechanism of action of BNIP3 is still being investigated [323]; and while BNIP3 interacts with Bcl-2 proteins, this does not appear to be functional. Instead I focus on the direct interaction with BAX and BAK (represented together in the network as BAXBAK due to similar function and regulation).

3.2.5 p53

Table 3.5 Evidence for edges in the p53 pathway of the network model.

From	To	Type	Cell Line/Tissue	Evidence
mdm2	p53	Inhibitory	HCA2 Fibroblasts	Blaydes and Wynford-Thomas [41]
ARF	mdm2	Inhibitory	MEF	Weber et al. [472]
p53	PUMA	Activatory	MCF7	Nakano and Vousden [337]
p53	PUMA	Activatory	MEF	Villunger et al. [456]
p53	Noxa	Activatory	MEF	Villunger et al. [456]
p53	p21	Activatory	HCT116 Human Colorectal	Bunz et al. [48]
p53	PTEN	Activatory	SAOS-2 Osteosarcoma	Stambolic et al. [418]

Table 3.5 continued from previous page

p53	HIF1	Inhibitory	MCF7 Breast Cancer	Blagosklonny et al. [38]
mdm2	FoxO	Inhibitory	MCF7 Breast Cancer	Yang et al. [493]
p53	PTEN	Activatory	MEF	Stambolic et al. [418]

p53 is one of the most important tumour suppressors, triggering both growth arrest, via p21, and apoptosis, via PUMA and Noxa, in response to abnormal behaviour and DNA damage [48, 456]. As a barrier to cancer development, it is found to be mutated in approximately 50% of human breast cancers [512]. p53 is constitutively expressed, but is inactivated by mdm2, which binds to and blocks the p53 active site, as well as ubiquitinating it, marking it for degradation [236]. Thus much of p53 regulation is focussed on regulation of mdm2, for example by ARF.

In this model I focus on the gross regulation of p53 activity by mdm2 binding. However, there is evidence of further complexity in that different post-translational modifications of p53 may affect function, particularly the strength activation of growth arrest over apoptosis [86]. This could be scope for expansion of the model.

Similarly, the connection between ARF, mdm2 and p53 may not need be direct, with evidence for ARF independent regulation of p53 by myc, perhaps depending on differences between mouse and human models [191]. Again, as the precise details and exceptions of this relationship are still being determined, I modelled the canonical case. Any differences were not enough to cause significant deviation from the specification or from comparison to the *in vivo* mouse model.

Finally, mdm2 is modelled as constitutively expressed, and then repressed by p53. In reality, it is expressed in response to p53. This however leads to the two nodes oscillating when modelling the healthy cell. While there is such oscillation in biology, the degree in the model, due to the limited granularity of the nodes, was misleading. I therefore chose to abstract this relationship with mdm2 being assumed as being expressed. There were no cases of regulation within the network affecting this connection. Accordingly, this does not affect the behaviour of the model.

3.2.6 Cell Cycle

Table 3.6 Evidence for edges in the cell cycle for the network model.

From	To	Type	Cell Line/Tissue	Evidence
p21	CDK4	Inhibitory	MCF7	He et al. [195]
p21	CDK2	Inhibitory	MCF7	He et al. [195]
p27	CDK4	Inhibitory	Mv1Lu Lung Epithelial	Ray et al. [371]
p27	CDK2	Inhibitory	BT-474 Cells	Lane et al. [274]
p16	CDK4	Inhibitory	BALB/c mice	Lukas et al. [300]
p15	CDK4	Inhibitory	Human Mammary Epithelial Cell (HMEC)	Sandhu et al. [389]
GSK3	CDK4	Inhibitory	Cell Free, 3T3 Fibroblasts	Diehl et al. [111]
GSK3	CDK2	Inhibitory	Cell Free, Rat Fibroblasts	Welcker et al. [476]
CDK2	pRb	Inhibitory	Review	Draetta [118]
CDK4	pRb	Inhibitory	Review	Weinberg [474]
pRb	E2F-1	Inhibitory	Review	Weinberg [474]
E2F-1	ARF	Activatory	SAOS-2 Osteosarcoma	Bates et al. [21]
E2F-1	Proliferation	Activatory	REF52 Rat	Johnson et al. [229]
E2F-1	EZH2	Activatory	MCF7	Wu et al. [488]

The cell cycle is itself a complex network, worthy of its own model. There have been attempts to model all the elements as a mathematical, ODE based model, such as by Tyson et al. [453]. I chose not to model this system in this level of detail. While the change in the length of different stages of the cell cycle is important for some paradigms of cancer therapy, such as cyclotherapy [225], it was most important, and most feasible, to measure the general rate of proliferation. I therefore modelled the regulators of key checkpoints, CDK2-CyclinE and CDK4-CyclinD, for which there was evidence of regulation by pathways in the model, and their downstream effectors in pRb and E2F-1. Signalling which increases the rate at which the cell cycles or passes through these checkpoints was considered proliferative, and the efficacy of this model checked by comparison to my specification (see Table 3.10) and

the *in vivo* data (see Table 3.12) from my collaborators. There are some positive feedback mechanisms in the interactions between these components, which in the cell ensure that once a stage of the cycle has been started, the cell remains committed and does not stop due to small environmental fluctuations. In my case, this would cause some initial conditions for cell intrinsic signals to lock the model into high proliferation. As modelling the cell passing in and out of stages of the cycle is not useful, only the overall cycle rate, this was omitted.

3.2.7 Apoptosis

Table 3.7 Evidence for edges in the apoptosis pathway for the network model.

From	To	Type	Cell Line/Tissue	Evidence
PUMA	Bcl-2	Inhibitory	DLD1, SW48, HCT116 Colorectal	Yu et al. [501]
PUMA	Bcl-2	Inhibitory	SAOS-2 Osteosarcoma	Nakano and Vousden [337]
PUMA	Bcl-2	Inhibitory	All (cell free) and MEFs	Chen et al. [66]
PUMA	Bcl-xl	Inhibitory	All (cell free) and MEFs	Chen et al. [66]
PUMA	Mcl1	Inhibitory	All (cell free) and MEFs	Chen et al. [66]
PUMA	Bcl-W	Inhibitory	All (cell free) and MEFs	Chen et al. [66]
PUMA	A1	Inhibitory	All (cell free) and MEFs	Chen et al. [66]
BIM	Bcl-2	Inhibitory	All (cell free) and MEFs	Chen et al. [66]
BIM	Bcl-xl	Inhibitory	All (cell free) and MEFs	Chen et al. [66]
BIM	Mcl1	Inhibitory	All (cell free) and MEFs	Chen et al. [66]
BIM	Bcl-W	Inhibitory	All (cell free) and MEFs	Chen et al. [66]

Table 3.7 continued from previous page

BIM	A1	Inhibitory	All (cell free) and MEFs	Chen et al. [66]
BAD	Bcl-2	Inhibitory	All (cell free) and MEFs	Chen et al. [66]
BAD	Bcl-xl	Inhibitory	All (cell free) and MEFs	Chen et al. [66]
BAD	Bcl-W	Inhibitory	All (cell free) and MEFs	Chen et al. [66]
Noxa	Mcl1	Inhibitory	All (cell free) and MEFs	Chen et al. [66]
Noxa	A1	Inhibitory	All (cell free) and MEFs	Chen et al. [66]
Bcl-2	BAXBAK	Inhibitory	All (Co-IP)	Oltvai et al. [347]
Bcl-xl	BAXBAK	Inhibitory	Cell free	Billen et al. [37]
Mcl1	BAXBAK	Inhibitory	MEF, HeLa	Germain et al. [171]
Bcl-W	BAXBAK	Inhibitory	Mouse Myeloid Cells	Gibson et al. [174]
Bcl-W	BAXBAK	Inhibitory	Mouse Sertolli	Ross et al. [378]
A1	BAXBAK	Inhibitory	Review	Vogler [460]
A1	BAXBAK	Inhibitory	Co-IP, GST assay	Zhai et al. [507]
A1			Expressed in human breast	Beverly and Varmus [32]
			Expressed in human breast	Campone et al. [51]
A1	Apoptosis	Inhibitory (Indirect)	Mouse breast	Capuco et al. [54]
BAXBAK	MOMP	Activatory	MEF	Wei et al. [473]
BAXBAK	MOMP	Activatory	MEF	Dewson et al. [109]
MOMP	Apoptosis	Activatory	Review	Tait and Green [433]
Caspase9	Caspase3	Activatory	Review	Tait and Green [433]

Table 3.7 continued from previous page

Caspase3	Apoptosis	Activatory	Review	Tait and Green [433]

Apoptosis is the process of controlled cell death initiated in cases of stress, damage, immune response, or as part of tissue formation. Tumour suppressors imitate apoptosis as the last resort to prevent a malfunctioning cell from developing into a tumour. As such, the avoidance of apoptosis is vital to model as part of how a cancer develops and responds to changes in environment, how sub-clones might cooperate, and how treatments of cancer take effect.

Apoptosis is regulated by the pro-apoptotic BH3-family of proteins such as p53-targets PUMA and Noxa. These in turn regulate the anti-apoptotic Bcl-2-family proteins, which are constitutively expressed and inactivate the BAXBAK complex. There are two primary models of the interaction between these two families. In the indirect activator model BH3-only proteins inactivate Bcl-2 proteins, and these in turn inhibit BAX and BAK. In the direct activator-derepressor model the BH3-only proteins directly activate BAX and BAK, but are inhibited by the Bcl-2 only proteins, which also inhibit BAX and BAK directly. However, the Bcl-2 only proteins are also inhibited by some of the BH3-only proteins as before, forming a complex feedback loop. These are compared by Tait and Green [433].

The indirect activator model alone was sufficient to match the observed behaviour against which the model was tested (see Section 3.4.2 and 3.5.2). To choose the direct activator-derepressor model would therefore be to make the model more complex than was necessary to model observed behaviour. The simpler model, given that it fits the data as well as the more complex one, is preferred because a complex model can produce a greater variety of outcomes and is more likely to reflect results by chance, as discussed by MacKay [306, Ch28]. Also, the indirect activator model is less dependent on initial conditions and so less likely to cause the model to be sensitive to small changes in initial conditions, which would be a poor fit to biological evidence, as apoptosis is tightly controlled. I therefore used the indirect activator model.

Different interactions with the Bcl-2 family of proteins explain different abilities to prompt apoptosis for different BH3-only proteins. For example, Noxa binds to fewer members of the family than PUMA and has less ability to prompt apoptosis [66]. To best model these different levels of apoptotic signalling, I required a higher level of granularity. It is shown that p53 causes apoptosis when activated, which is abrogated more by PUMA knock-out than Noxa knockout. As there must also be a state for no apoptosis, this cannot be accommodated with granularity less than 4, and so I use this for phenotypes and the nodes which feed directly

into them. In the case of apoptosis this is Caspase3, Caspase9, MOMP and BAXBAK. I kept most nodes in the network at a granularity of 3 for unambiguous comparison to biological data. I do not include the external cell death pathway in the model as this is primarily relevant in the immune response to tumours, but I am primarily aiming to model cell lines and tumours grown in SCID mice, which have impaired immune response.

3.2.8 Limitations of the Model

In building the model choices were necessarily made about what to include, and to what degree of complexity each component should be modelled. This results in limitations on the overall applicability of the model. While I believe these were the best choices for the questions I address in this Thesis, it is important to make these clear so that the model is appropriately used in the future.

One such simplification is the relationship between p53 and mdm2. As discussed in Section 3.2.5 I modelled mdm2 as constitutively expressed, when its expression is in part dependent on p53. As discussed in Section 3.2.5, although p53 influences the activity of mdm2, I modelled mdm2 as constitutively expressed. Modelling this loop would cause oscillations in p53 and mdm2, which due to the discrete nature of the model were large and so were amplified in the rest of the network unrealistically. This abstraction relies on the following assumptions, which hold for this Thesis, but may not for all applications of the model: that one does not wish to model regulation of p53 by the gene regulatory network of the cell independent of mdm2; that setting p53 to maximum, as described in Chapter 2.2 and 2.3, is effective independent of mdm2 status; and that oscillations are not a result of interest.

The first assumption is key if extending the model, as there is evidence that p53 can be activated by preventing p53-mdm2 binding by phosphorylating p53 [60]. The second assumption is important when considering interpretation of the model, as p53 activation might be compensated for by a concomitant activation of mdm2. However, when considering strong activation of p53, such as described in Chapter 2.3, this does not seem to occur, as discussed by Blagosklonny and El-Deiry [39]. The final assumption would be interesting to model further, as it may be that changes in the frequency of oscillations of p53 may change its downstream effects [191, 368] but how this may be encoded and interpreted down-stream is still under investigation. Further, the dynamics of such oscillations vary with species and so may not be strongly conserved [422]. The overall importance of oscillations in p53 signalling is yet to be determined.

Similarly, the discrete nature of the network makes the modelling of the full complexity of the cell cycle difficult. Further, this is constantly in flux, and I focus on the overall stable state of the system. This is due to its complex network of positive and negative feedbacks. These have been broken down into different modules, described by ODEs, by Tyson et al. [453], but recently have been further converted into a discrete formalism by Paterson et al. [355]. It was not necessary in this project to predict cell cycle dynamics, only the overall effect on proliferation. However, this work could be used to expand the model to include such dynamics, which would be key to considering how differences between healthy and cancerous cell's cycle dynamics could be used to target therapy [225].

3.3 Target Functions

I also defined Target Functions for each of the nodes to govern their interactions. For many nodes there was no indication in the literature of a more complex interaction than activation or inhibition, and the default BMA Target Function ($avg(pos) - avg(neg)$), was sufficient to reproduce the specification of expected results when the model was tested (see Section 3.4.2 and 3.5.2). However, where there was evidence in the literature to support it, more complex interactions were needed, as detailed in Table 3.8. In some cases, different inputs had more effect, and so simply taking the average was inappropriate. Few comparisons of the "weights" of different inputs have been made. In these cases they have been made in order to best fit the specification (see Section 3.4.2 and 3.5.2).

Table 3.8 Table of Target Functions and the maximum values of nodes. All nodes have a minimum value of 0.

Node	Max	Target Function	Evidence	Reasoning
A1	2	$floor(2 - avg(var(Noxa), var(PUMA), var(BIM)))$	Chen et al. [66]	Constitutively active, suppressed by PUMA, BIM and Noxa. Without floor() this is too sensitive to small changes
Akt	2	$avg(pos) - avg(neg)$		
Angiogenesis	2	$avg(pos) - avg(neg)$		
Apoptosis	6	$avg(pos) - avg(neg)$		
ARF	2	$max(var(MycMax), (var(E2F-1) * min(1, (var(E2F-1)-1)))) - var(Twist)/2$	Zindy et al. [519]	Activated by MycMax
		$\vdots$	Bates et al. [21], Trimarchi and Lees [445]	Activated by E2F-1 above threshold
		$\vdots$	Maestro et al. [308]	Inactivated by Twist
		$\vdots$		max is needed as in avg() E2F-1 blocks effect of high myc signalling, which does not match specification
BAD	2	$2 - max(var(Akt), var(Rsk))$	Knuefermann et al. [254]	Inactivated by Akt and Rsk, no major activators therefore assume constitutive activity otherwise

Table 3.8 continued from previous page

		⋮	Gilmore et al. [175]	Inactivated by Akt, no major activators therefore assume constitutive activity otherwise
		⋮	Gilmore et al. [175]	Phosphorylation by MAPK pathway on Serine-112 or Serine-155 is sufficient to block BAD, therefore take max() of Rsk (which leads to these phosphorylations) and Akt (which phosphorylates Serine-136)
BAXBAK	6	$ceil(6 - avg(var(Bcl-2), var(Bcl-xl), var(Mcl1), var(Bcl-W), var(A1)) + var(BNIP3))$	Oltvai et al. [347]	Constitutively active, inhibited by Bcl-2
		⋮	Billen et al. [37]	Constitutively active, inhibited by Bcl-xl
		⋮	Gibson et al. [174], Ross et al. [378]	Constitutively active, inhibited by Bcl-W
		⋮	Germain et al. [171]	Constitutively active, inhibited by Mcl1
		⋮	Vogler [460], Zhai et al. [507]	Constitutively active, inhibited by A1

Table 3.8 continued from previous page

		⋮	Sowter et al. [416], Mellor and Harris [323]	Activated by BNIP3
		⋮		Ceil() is used so that can reach maximum apoptosis in case where majority of Bcl-2 family is inhibited, rather than strictly when all are
Bcl-2	2	$floor(2 - avg(var(PUMA), var(BIM), var(BAD)))$	Chen et al. [66]	Constitutively active, suppressed by PUMA, BIM and BAD. Without floor() this is too sensitive to small changes
Bcl-W	2	$floor(2 - avg(var(PUMA), var(BIM), var(BAD)))$	Chen et al. [66]	Constitutively active, suppressed by PUMA, BIM and BAD. Without floor() this is too sensitive to small changes
Bcl-xl	2	$floor(2 - avg(var(PUMA), var(BIM), var(BAD)))$	Chen et al. [66]	Constitutively active, suppressed by PUMA, BIM and BAD. Without floor() this is too sensitive to small changes
Beta-Catenin	2	$2 - var(GSK3\text{-}Axin\text{-}APC\text{-}CK1)$	Farago et al. [140], MacDonald and He [304]	Beta-Catenin is constitutively expressed and degraded

Table 3.8 continued from previous page

BIM	2	$avg(pos) - avg(neg)$		
BNIP3	2	$avg(pos) - avg(neg)$		
Caspase3	6	$avg(pos) - avg(neg)$		
Caspase9	6	$var(MOMP) - 2 * var(Akt)/3$	Tait and Green [433]	Activated by MOMP
		$\vdots$	Zundel and Giaccia [521], Cardone [56], Li et al. [290]	Inhibited by Akt, but not completely, to match specification
CDK2	3	$ceil(var(MycMax) - avg(var(p21), var(p27), var(GSK3)/2))$		Ceil() prevents getting stuck in an oscillatory loop
		$\vdots$	Nass and Dickson [338]	Activated by MycMax
		$\vdots$	He et al. [195]	Inhibited by p21
		$\vdots$	Lane et al. [274]	Inhibited by p27
		$\vdots$	Won and Reed [483]	Inhibited by GSK3, less strongly than GSK3 inhibits CDK4 to match specification
CDK4	3	$avg(pos) - avg(neg)$		
cFos	2	$avg(pos) - avg(neg)$		
COX2	2	$avg(pos) - avg(neg)$		
Dishevelled	2	$min(var(Frizzled), var(LRP))$	MacDonald and He [304], He et al. [197]	Both receptors are required
E2F-1	2	$6 - var(pRb)$	Weinberg [474]	Inhibited by pRb

Table 3.8 continued from previous page

EGF	2	Set as an Initial Condition		
Elk-1	2	$avg(pos) - avg(neg)$		
EP4	2	$avg(pos) - avg(neg)$		
ErbB1	2	1	Yarden and Sliwkowski [496]	Constitutively expressed, can be over-expressed in cancer
ErbB1-ErbB1	2	$min(var(ErbB1), var(ErbB1)) * var(EGF)$	Yarden and Sliwkowski [496]	minimum reflects heterodimer, so smallest of the pair is rate limiting
ErbB2	2	1	Yarden and Sliwkowski [496]	Constitutively expressed, can be over-expressed in cancer
ErbB1-ErbB2	2	$min(var(ErbB1), var(ErbB2)) * var(EGF) * var(ErbB2)$	Yarden and Sliwkowski [496]	minimum reflects heterodimer, so smallest of the pair is rate limiting
		$\vdots$	Yarden and Sliwkowski [496]	ErbB2 increases effect of EGF binding, represented by multiplication
ErbB3	2	1	Yarden and Sliwkowski [496]	Constitutively expressed, can be over-expressed in cancer
ErbB2-ErbB3	2	$min(var(ErbB2), var(ErbB3)) * var(EGF) * var(ErbB2)$	Yarden and Sliwkowski [496]	minimum reflects heterodimer, so smallest of the pair is rate limiting
		$\vdots$	Yarden and Sliwkowski [496]	ErbB2 increases effect of EGF binding, represented by multiplication
Erk	2	$avg(pos) - avg(neg)$		
Ets-2	2	$avg(pos) - avg(neg)$		

Table 3.8 continued from previous page

EZH2	2	$avg(pos) - avg(neg)$		
FoxO	2	$1 - avg(var(Akt), min(var(mdm2), var(Erk))) + min(1, (var(Akt))) * (var(Hypoxia) - var(TRAP1))$	Sunters et al. [428]	Constitutive Expression, but downregulated by Akt
		⋮	Yang et al. [493]	Constitutive Expression, but downregulated by mdm2 and Erk cooperation
		⋮	Kim et al. [247], Brunet et al. [47], Lehtinen et al. [282]	Activation by Hypoxia, compensated for TRAP1 in Akt dependent manner
Frizzled	2	$avg(pos) - avg(neg)$		
GSK3	2	$2 - avg(var(Rsk), var(Akt), var(Dishevelled))$	Eldar-Finkelman et al. [129], Ding et al. [114]	Constitutive Expression, inhibition by Rsk
		⋮	Knuefermann et al. [254]	Inhibition by Akt
		⋮	MacDonald and He [304], Taelman et al. [432]	Inhibition by Dishevelled

Table 3.8 continued from previous page

GSK3-Axin-APC-CK1	2	$min(1, var(GSK3)) * (2 - var(Dishevelled))$	Boras-Granic and Wysolmerski [43], Smalley and Dale [411]	Primarily disrupted by Dishevelled
		⋮	Ding et al. [114]	GSK3 required for function
HIF1	2	$1 + var(Akt) - var(VHL) * (var(PHD2)) - (var(p53.active) * min(1, (var(p53.active) - 1)))$	Semenza [398]	Activated by Akt
		⋮	Blancher et al. [40], Ziello et al. [517], Laughner et al. [277]	Suppressed by VHL and PHD2,
		⋮	Blagosklonny et al. [38]	Suppressed by p53 when p53 is above a threshold
Hypoxia	2	$var(HypoxiaInitial) - var(Angiogenesis)/2$		Hypoxia is countered by angiogenesis
HypoxiaInitial	2	Set as an Initial Condition		Represents pressure on tumour to prevent hypoxia
LRP	2	$avg(pos) - avg(neg)$		
Mad	2	$avg(pos) - avg(neg)$	Grandori et al. [181]	
MadMax	2	$min(var(Mad), var(Max)) - min(1, floor(min(var(Mad), var(Max)) * min(var(Myc), var(Max))/2))$	Grandori et al. [181]	Competition between Myc and Mad for Max

Table 3.8 continued from previous page

Max	2	Constitutively Expressed	Grandori et al. [181]	
Mcl1	2	$floor(2 - avg(var(PUMA), var(BIM), var(Noxa)))$	Chen et al. [66]	Constitutively active, suppressed by PUMA, BIM and Noxa. Without floor is too sensitive to small changes
mdm2	2	$2 - var(ARF) - var(HIF1)/2$	Weber et al. [472]	Constitutively active due to p53, suppressed by ARF
		⋮	Chen et al. [64]	Constitutively active due to p53, suppressed by HIF1
Mek	2	$avg(pos) - avg(neg)$		
MOMP	6	$avg(pos) - avg(neg)$		
Myc	2	$floor(avg(var(TCF), var(cFos), var(Ets-2), max(0, var(Erk) - var(GSK3))) - avg(var(TGFR), min(1, var(EZH2))))$	Teuliere et al. [439]	Activated by TCF
		⋮	Lu et al. [297]	Activated by cFos
		⋮	Al-azawi et al. [4]	Activated by Ets-2
		⋮	Kyriakis et al. [270], Rodrik et al. [375], Yeh et al. [498]	Activated by Erk, but GSK3 blocks this specifically
		⋮	Fernandez-Pol et al. [145]	Inactivated by TGF-Beta

Table 3.8 continued from previous page

		⋮	Kaur and Cole [245]	Inactivated by EZH2, but not completely, to accord with in vivo data
MycMax	2	$min(var(Myc), var(Max)) - min(1, floor(min(var(Myc), var(Max)) * min(var(Mad), var(Max))/2))$	Grandori et al. [181]	Competition between Myc and Mad for Max
Noxa	2	$avg(pos) - avg(neg)$		
p15	2	$avg(pos) - avg(neg)$		
p16	2	$avg(pos) - avg(neg)$		
p21	2	$var(p53.active) - avg(var(Akt), max(0, (var(MycMax) - var(HIF1))))$	Bunz et al. [48]	Activation by p21
		⋮	Zhou et al. [514]	Suppressed by Akt
		⋮	Koshiji et al. [261], Coller et al. [84], Mitchell and El-Deiry [328], Dang et al. [99]	Suppressed by MycMax, but this is countered by HIF1
p27	2	$avg(var(FoxO), var(HIF1)) - avg(var(TCF), max(0, (var(MycMax) - var(HIF1))))$	Sunters et al. [427]	Activated by FoxO
		⋮	Mack et al. [305]	Activated by HIF1

Table 3.8 continued from previous page

		⋮	Castelo-Branco et al. [61], Rimerman et al. [373]	Suppressed by TCF
		⋮	Nass and Dickson [338], Yang et al. [495], Dang et al. [99], Huang [217]	Suppressed by MycMax, but this is countered by HIF1
p38	2	$avg(pos) - avg(neg)$		
p53	2	$2 - var(mdm2)$	Blaydes and Wynford-Thomas [41]	Constitutively Expressed, suppressed by mdm2
PEA3	2	$avg(pos) - avg(neg)$		
PGE2	2	$avg(pos) - avg(neg)$		
PHD2	2	$2 - var(Hypoxia)$	Semenza [398]	Constitutively expressed, O2 dependent
PI3K	4	$avg(pos) - avg(neg)$		
pRb	6	$6 - ceil(avg(var(CDK2), var(CDK4)))$	Draetta [118]	Inhibited by CDK4
		⋮	Weinberg [474]	Inhibited by CDK2
Proliferation	6	$avg(pos) - avg(neg)$		
PTEN	2	$avg(pos) - avg(neg)$		
PUMA	2	$avg(pos) - avg(neg)$		
Raf-1	2	$avg(pos) - avg(neg)$		
Ras	2	$avg(pos) - avg(neg)$		

Table 3.8 continued from previous page

Rsk	2	$avg(pos) - avg(neg)$		
TCF	2	$avg(pos) - avg(neg)$		
TGFBeta	2	Set as an Initial Condition		
TGFR	2	$avg(pos) - avg(neg)$		
TRAP1	2	$avg(pos) - avg(neg)$		
Twist	2	$avg(pos) - avg(neg)$		
VEGF	3	$var(HIF1) + avg(var(COX2), var(p38))/2$	Laughner et al. [277]	Increased by HIF1
		⋮	Yang and Han [494]	Increased by COX2, less than HIF1 to match specification
		⋮	Xiong et al. [490]	Increased by p38, less than HIF1 to match specification
VHL	2	⋮	Semenza [398]	Constitutively expressed
Wnt1	2	Set as an Initial Condition		

The nodes, edges and target functions described above are sufficient to define the model. I next test this model against *in vitro* and *in vivo* data.

3.4 Testing the Model

3.4.1 Building a Specification

In order to validate the model, I tested it against a specification of expected results from *in vitro* and *in vivo* data. This defined the behaviours the model is expected to produce. This tested the model, and also bounds its expansion to parts of the cells genetic regulatory network not relevant to the aims of the model. I focus on changes in proliferation and apoptosis in response to perturbation, as well as the response of key nodes in the network which feed into these phenotypes.

3.4.2 Validating the Model against a Specification of *in vitro* Data

In order to test the model against *in vitro* data, I used experiments with cell lines. This was to give me a mutational profile [242, 207], shown in Table 3.9, which is not possible with most primary tumour data in the literature. I apply a background of survival factors to simulate the high levels found in serum (EGF and Wnt1 set at 2). I then reproduced experiments by fixing the value of nodes as required by the mutational profile for whichever cell line was used in the experiments, and adding further perturbations in line with experiment, as shown in Table 3.10.

In mapping the experimental results to the model, I focus on the changes within the experiment, but not between them. This is because many of the experiments are not directly comparable, due to differences in experimental procedure and different assays. This means my assessments of high and low activity are made within the context of that experiment, and I do not compare between them. Attempting to map the degrees of difference observed between groups to levels of activity in the model would incorporate all the systematic and random errors of both groups. Restricting to the change, such as from higher to lower production of some secreted factor, within an experiment only includes the random errors, and helps control for any constant systematic error. Further, the measurements made may have been semi-quantitative to begin with, for example, a Western blot is best used to provide a relative comparison of protein expression, rather than give an absolute value [310]. Therefore high and low activity refer to the context of the assay for that experiment, and may rank differently were all experiments to be performed together.

Table 3.9 Baseline mutational profile, as applied in the network model, for cell lines used in *in vitro* testing.

Cell Line	Source	Initial Conditions										
		Wnt1	ErbB1	ErbB2	p53	EGF	PI3K	Ras	Raf-1	Myc	ARF	p16
MDA-MB-231	Kao et al. [242], Hollestelle et al. [207]	2	2		0	2		2	2		0	0
MDA-MB-453	Kao et al. [242], Hollestelle et al. [207], Vranic et al. [462]	2		2	0	2	2	2				0
SKBR3	Kao et al. [242], Hollestelle et al. [207]	2		2	0	2				2		

Table 3.10 Experiments from cell line data to which I compared model behaviour. Numbers in brackets are the levels of activity of the relevant nodes.

Experiment	Cell Line	Source	Changes in addition to baseline	Expected Results	Model Results
Myc inhibition slows proliferation	MDA-MB-231	Watson et al. [471]	Control	High proliferation and low apoptosis	High proliferation (5) and low apoptosis (0)
	MDA-MB-231	Watson et al. [471]	Myc inhibition (0)	Lower proliferation	Lower proliferation (2)
Knockdown of Wnt causes slower growth	MDA-MB-231	Matsuda et al. [319]	Control	High proliferation and low apoptosis	High proliferation (5) low apoptosis (0)
	MDA-MB-231	Matsuda et al. [319]	Wnt1 Knockdown (0)	Lower proliferation	Lower growth (2) increased apoptosis (1)
Myc and Ras Cooperate to form tumours	Mouse infected with MMTV/v-Ha-ras and MMTV/c-myc	Sinn et al. [409]	EGF and Wnt (1), Myc 2	Cooperation best for tumour formation	Proliferation (2) Apoptosis (3)

Table 3.10 continued from previous page

	Mouse infected with MMTV/v-Ha-ras and MMTV/c-myc	Sinn et al. [409]	EGF and Wnt (1), Ras 3	Cooperation best for tumour formation	Proliferation (4) Apoptosis (5)
	Mouse infected with MMTV/v-Ha-ras and MMTV/c-myc	Sinn et al. [409]	EGF and Wnt (1), Myc and Ras at 2	Cooperation best for tumour formation	Proliferation (5) Apoptosis (5), better growth than either alone
PUMA knockouts were more resistant to apoptosis than Noxa knockouts	MEF	Michalak et al. [325]	EGF and Wnt1 (2), p53 activation (2)	Highest apoptosis	Highest apoptosis (5)
	MEF	Michalak et al. [325]	EGF and Wnt1 (2), p53 activation (2), Noxa knockout (0)	Lower apoptosis	Lower apoptosis (3)

Table 3.10 continued from previous page

	MEF	Michalak et al. [325]	EGF and Wnt1 (2), p53 activation (2), PUMA knockout	Lowest, but still non-negligable, apoptosis	Lowest apoptosis (2)
PI3K confers resistance to Trastuzumab in SKBR3 cells	SKBR3	Berns et al. [29]	Control	High proliferation and low apoptosis	High proliferation (6) and low apoptosis (0)
	SKBR3	Berns et al. [29]	Trastuzumab (ErbB2 (0))	Trastuzumab reduces growth of SKBR3 cells	Lower growth (5) and increased apoptosis (3)
	SKBR3	Berns et al. [29]	Trastuzumab (ErbB2 (0)), activation of PI3K (2)	PI3K confers resistance	Same growth (5) and protection from apoptosis (1)
Akt loss lowers proliferation and and increases apoptosis	MDA-MB-453	She et al. [403]	Control	High proliferation and low apoptosis	High proliferation (5) and low apoptosis (0)
	MDA-MB-453	She et al. [403]	Akt suppression (0)	Lower proliferation and increased apoptosis	Lower proliferation (4) and increased apoptosis (2)

Table 3.10 continued from previous page

Akt loss lowers proliferation and and increases apoptosis	SKBR3	She et al. [403]	Control	High proliferation and low apoptosis	High proliferation (6) and low apoptosis (0)
	SKBR3	She et al. [403]	Akt suppression (0)	Lower proliferation and increased apoptosis	Same proliferation (6) and increased apoptosis (2)
Lapetinib downregulates Akt and CyclinD1 and upregulates FoxO3a	SKBR3	Hegde et al. [198]	Control	High Akt and CDK4, low FoxO	Akt(1) CDK4 (3) FoxO (0)
	SKBR3	Hegde et al. [198]	Lapatenib (ErbB1 and ErbB2 (0))	Low Akt and CDK4, High FoxO	Akt(0) CDK4 (2) FoxO (1)
p53 induction kills SKBR3 cells	SKBR3	Blagosklonny and El-Deiry [39]	Control	High proliferation and Low apoptosis	High proliferation (6) and low apoptosis (0)
	SKBR3	Blagosklonny and El-Deiry [39]	p53 activation (2)	Low proliferation and High apoptosis	Lower proliferation (5) and high apoptosis (5)

Table 3.10 continued from previous page

Inhibition of ErbB2 reduces VEGF production	SKBR3	Petit et al. [360]	Control	Normal VEGF production	Normal VEGF production (2)
	SKBR3	Petit et al. [360]	ErbB2 (0)	Lower VEGF production	Lower VEGF production (1)
Hypoxia increases VEGF production	MDA-MB-231	Scott et al. [394]	Control	Control	Normal VEGF production (2)
	MDA-MB-231	Scott et al. [394]	Hypoxia	Increased VEGF production	Higher VEGF production (3)
	MDA-MB-453	Scott et al. [394]	Control	Control	Normal VEGF production (2)
	MDA-MB-453	Scott et al. [394]	Hypoxia	Increased VEGF production	Higher VEGF production (3)
	SKBR3	Scott et al. [394]	Control	Control	Normal VEGF production (2)
	SKBR3	Scott et al. [394]	Hypoxia	Increased VEGF production	Higher VEGF production (3)

My model was able to reproduce well the changes observed in these *in vitro* experiments. This includes the correct response to knock-out of key genes such as Myc and Wnt1 demonstrated by Watson et al. [471] and Matsuda et al. [319] respectively. It also includes reproduction of both the effect of treatment and resistance mechanisms in the case of Berns et al. [29]. There was one case in which the correct behaviour was partially absent, in that Akt inhibition in the SKBR3 cell line did not inhibit proliferation. This is likely due to the difference in Myc activity in SKBR3 versus the *in vivo* model, as discussed in Section 7.2.2. However, as shown in the next Section, this fits the behaviour of the mouse model exactly. As I have more information about this system than the cell lines, I prioritise these results.

I also include the behaviour of p53, PUMA and Noxa in MEF, as this was an important interaction to correctly predict the behaviour of the *n vivo* model, which had functional p53, but none of the widely tested breast cancer cell lines had wild-type p53.

3.5 Application to MMTV-Wnt1 Mouse Mammary Tumours

My aim was to apply this model to the case of heterogeneous breast cancer tumours, specifically in the case of the mouse model created by my collaborators, as described in Chapter 2.5 to investigate how the these sub-clones work together.

In order to ensure the model was a good fit to this case, I first compared it to the behaviour of pure myc-high and myc-low tumours, and then use this to predict the behaviour of the heterogeneous tumours under single (Chapter 4) and combination therapy (Chapter 5).

In order to model this *in vivo* case, I added feedback from VEGF to the Hypoxia node (see Table 3.8) to show the effects of angiogenesis. As my collaborators expected these tumours to be HER2 negative, so I removed the ErbB2 (a.k.a. HER2), ErbB1-ErbB2, ErbB3, ErbB2-ErbB3, nodes from the model for the *in vivo* perturbations.

3.5.1 Reproducing the conditions of the *in vivo* Model

Myc-high, Myc-low and Heterogeneous Tumours

In order to set the initial conditions for the myc-high and myc-low pure and heterogeneous tumours, I had to take into account several key properties of these tumours. The first is that there is a difference of myc expression between the tumours, as myc expression is strongly driven by MycER^{T2} in the myc-high cells. The myc-low cells still have endogenous myc,

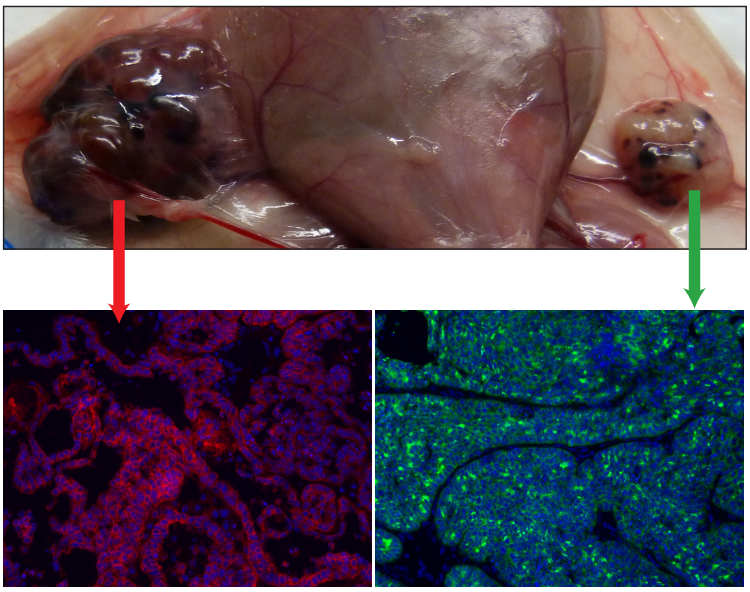

(a) (Left) Pure Myc-low tumour, showing severe necrosis. (Right) Pure Myc-high tumour after 3 days of Tamoxifen I.P, showing a reduction in hypoxia from myc activation. However, these tumours still had high levels of apoptosis from myc signalling.

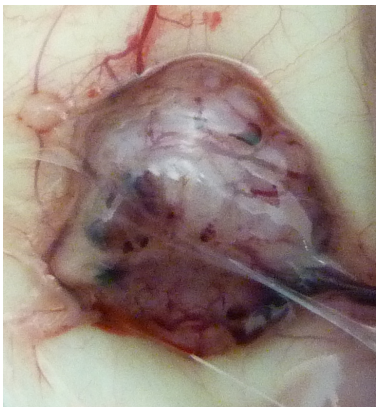

(b) Morphology of a heterogeneous tumour, showing improved growth from the cooperation of both sub-clones.

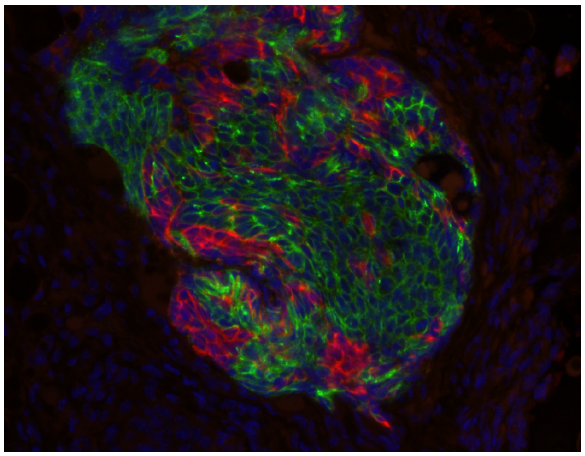

(c) Heterogeneous tumour, showing myc-low cells (red) and myc-high cells (green). Mixing of the two sub-clones allows Wnt1 signalling from the myc-low sub-clone, driven by MMTV-Wnt1, to compensate for suppression of endogenous Wnt1 by myc signalling in the myc-high sub-clone. This means the myc-high sub-clone can proliferate faster with a lower rate of apoptosis.

Fig. 3.2 Examples of tumour morphology and structure for pure myc-low and myc-high tumours, and a heterogeneous tumour.

and so it is allowed to vary freely in response to the rest of the network. MMTV-Wnt1 causes high Wnt1 expression in the myc-low cells, however, in the course of characterising the tumours my collaborators discovered that myc suppresses Wnt1 expression in the myc-high tumours. There is precedent for this in the literature [492, 76], and further investigation confirmed that this was not an effect specific to MMTV-Wnt1. This was done by testing the effect of high myc against endogenous Wnt1 in the 67NR cell line. My collaborators showed that pure myc-high tumours have lower Wnt1 expression, while pure myc-low tumours have high Wnt1 expression from MMTV-Wnt1. There is endogenous Wnt1 expression as well and so we model the myc-high tumours as having normal, rather than high Wnt1 signalling.

Each pure tumour therefore has something the other lacks, as myc suppression of Wnt1 prevents it from benefiting from MMTV-Wnt1. Wnt1 acts as a survival factor in many tissues [67, 81, 308] and there is evidence it is involved in tissue remodelling during post-lactational involution [438, 470, 271], which is a strong sign it acts as a survival factor in breast also [377]. This suggests that inhibition of Wnt1 by myc may be another aspect of the pro-apoptotic effects of myc, placing constraint on its ability to form tumours when mutated alone. The heterogeneous tumours therefore show cooperation between the myc-high cells, which gain Wnt1 from paracrine signalling by adjacent myc-low cells. This was observed by my collaborators using β-catenin staining, and extended to a maximum of four cell layers into the myc-high clone from the myc-low. Hence these cells have Wnt1 at maximum as an initial condition. My collaborators also observed that the heterogeneous tumours had better vascularisation than the pure tumours. It was initially thought this was due to VEGF expression from the myc-high tumours; however, they had lower VEGF expression than the myc-low. This may be due to the fact the model shows the final stable state, and VEGF may increase transiently as the tumour first grows. Further investigation is needed to find the exact factor which reduces hypoxia in the heterogeneous tumours. Nevertheless, to model the fact that vascularisation is higher, and hypoxia lower at the start of treatment, the heterogeneous tumours are modelled with a lower HypoxiaInitial.

I model these different initial conditions as shown in Table 3.11, allowing me to model the pure cases, as well as each sub-clone individually in the heterogeneous case. As shown in Section 3.5.2 this allows the model to reproduce the behaviour of the pure tumours, and as I explore in Chapter 4 and 5 I also show how the cooperation between these tumours means that the heterogeneous case has the highest proliferation, driven by the myc-high sub-clone supported by signalling from the myc-low sub-clone, and is the most robust against single and combination therapy. As the model can discriminate between sub-clones in the heterogeneous case, I can also predict differential effects from drugs on the different sub-

Table 3.11 Initial conditions applied, by fixing the Target Function to a constant value, for different sub-clones

Sub-clone	EGF	Wnt1	Myc	HypoxiaInitial	Description
Healthy	1	1			Normal growth factors and normoxia.
Pure myc-low	1	2		2	Endogenous Myc and high Wnt from MMTV-Wnt1. High hypoxia due to low vascularisation.
Heterogeneous myc-low	1	2		1	Endogenous Myc, hypoxia from the growing tumour, and high Wnt from MMTV-Wnt1. Lower hypoxia due to higher vascularisation.
Heterogeneous myc-high	1	2	2	1	High Myc from MycER^{T2}, high Wnt from paracrine signalling of myc-low cells. Lower hypoxia due to higher vascularisation.
Pure myc-high	1	1	2	2	High Myc from MycER^{T2}, suppressing Wnt from MMTV-Wnt1. High hypoxia due to low vascularisation.

clones. Key predictions of the model are tested in Chapter 5.7. The morphology of the pure tumour is shown in Figure 3.2a, while the mixing of sub-clones that allows this cooperative relationship is shown in Figure 3.2c.

At this stage it was also observed that ARF was suppressed in the heterogeneous case, which in the model is due to Twist (see Section 3.2.3).

3.5.2 Comparison to Myc-Low and Myc-High Tumours

My collaborators measured proliferation and the output of key nodes in the network in both the myc-low and the myc-high case. These were differential measurements, showing which increased or decreased in the myc-high compared to the myc-low. I then compared these to my models predictions, using the initial conditions for the pure myc-low and myc-high tumours as described in Table 3.11. Note particularly that proliferation is similar in both pure tumours, as the proliferative effects of myc are countered by its suppression of Wnt1. Note also that BIM, a target of myc [336, 52], does not increase in the myc-high case due to

compensatory regulation via E2F-1 and EZH2. As with the *in vitro* data, I iterated my model till it reproduced these results, by re-examining the assumptions of the model. This included comparing the edges to those reported in the literature, assessing whether the model needed to be expanded to incorporate more pathways to properly reproduce the experimental results, and adjusting the target functions to better reflect the underlying biology. I prioritised the *in vivo* data over the *in vitro* data, as this was the experimental system for which my model would be used to guide experiment. I include a log of the major changes made as the model was built and tested in Appendix D.

Table 3.12 Results from *in vivo* model data to which I compared model behaviour.

Node	Model Prediction in Myc-Low	Model Prediction in Myc-High	Change from Myc-Low to Myc-High *in vivo*	Measurement
Proliferation	4	4	Steady	CdU/IdU
ARF	0	2	Increase	qPCR
PUMA	0	2	Increase	qPCR
Noxa	1	2	Increase	qPCR
TRAP1	1	2	Increase	qPCR
PTEN	1	2	Increase	qPCR
p21	0	1	Increase	qPCR
VEGF	3	1	Decrease	qPCR
BNIP3	1	0	Decrease	qPCR
p27	0	0	Steady	qPCR
BIM	0	0	Steady	qPCR
pRb	2	2	Steady/Increase	Western
Erk	1	1	Steady/Increase	Western
BIM	0	0	Steady	Western

3.6 Conclusions

In this Chapter I demonstrate how it is possible to build and test a model of breast cancer from literature data. I further show that this model is able to reproduce the changes observed in both the *in vitro* and *in vivo* data. This places strong bounds not only on the final phenotypes of the model, but the internal decision making they depend on, and so gives strength to my

predictions on the effect of perturbations of this regulatory network, shown in the next two Chapters.

Chapter 4

Identifying Effective and Sub-clone Specific Therapies for Breast Cancer

4.1 Introduction

The earliest anti-cancer chemotherapies targeted dividing cells in general [246]. Recently, more targeted molecular therapies have become available. These can target cancer in a specific tissue based on pathway differences, such as 5-fluorouracil for liver cancer, or specific mutations, such as Imatinib for the Bcr-Abl mutation in chronic myelogenous leukemia [163]. In breast cancer a key targeted therapy is Trastuzumab, targeting the ErbB2/HER2 receptor protein. This offers fewer side-effects on healthy tissue [480]. While targeting a specific mutation can be very effective, it is also inflexible if its target mutates further. Targeting the differences between the activations of different pathways in different cancers is likely to provide more uses for the same drugs, as well as more options for therapy for any specific cancer.

My model is best suited to search for such targeted therapies, as I can perturb any node or combination of nodes to simulate the effects of drugs. Furthermore, I can discriminate between the effects on different sub-clones. As shown in Chapter 3.5.1, my collaborators had found key differences in the conditions under which the different tumour sub-clones developed. For example, the level of myc was a cell autonomous difference due to the activation of MycER^{T2} in the myc-high clone only. There was also a non-cell autonomous difference between the pure and heterogeneous cases in the level of hypoxia and the availability of Wnt1 signalling. Myc-high cells only experience high Wnt1 signalling from paracrine signalling from the myc-low cells and so only in the heterogeneous case. These different conditions could be translated to different settings for the network that allowed it to model

the different sub-clones, both in the pure and the heterogeneous case, separately. I fixed the values of key nodes as shown in Table 3.11 and so was able to differentiate between the sub-clones, and find the differences in response to treatment between them. In this Chapter I use my breast cancer model to search for single targets for therapy which can be perturbed to provide treatment which is specific either to cancer over healthy tissue, or to one sub-clone of the cancer specifically. This specificity is based on the differences in the behaviour of the sub-clones, rather than targeting specific mutations I know to be present, such as MMTV-driven Wnt1. While the behaviour of the model which I examine in this Chapter is dependent upon these specific mutations, the method for finding treatments is general and so can be applied to other cancers for which BMA models exist, such as those presented by Chuang et al. [75] and Silverbush et al. [408].

To assess the efficacy of therapies, I look at two key phenotypes predicted by the model; the proliferation and apoptosis of the cell. Cytotoxic therapy, i.e. high apoptosis, has traditionally been favoured on the basis that it offers the fastest route to tumour regression [379]. But this also increases the selection pressure for the emergence of resistance, compared to lowering proliferation with cytostatic therapies. Further, effects on healthy cells are worse than in the case of cytostatics. Cytostatic therapies have been shown to be very effective against breast cancer, such as with Trastuzumab [459]. These may have fewer side-effects, as there is less off-target cell death, although cytostatic drugs have been shown to be cardiotoxic in the long term [503, 397].

4.2 Identifying Effective Monotherapies

4.2.1 Drug Gene Interactions

To identify the key nodes controlling the proliferation and apoptosis of cancer cells, as well as assess their viability as cancer treatments, I screened the model with all possible knock-outs (set Target function to 0). These mimic possible drug interventions. I further restrict the nodes considered initially to those with known interactions in the Drug-Gene Interaction database [465], (see Fig. 4.1, and Table A.1). While not all of the interactions in the data base are likely to be clinically actionable, these do indicate which are likely to be able to be tested *in vivo*, and thus the model can help find those which are worth pursuing beyond tests in mice. I did not look for methods to disrupt GSK3-Axin-APC-CK1 other than GSK3β, as I did not fully model the other pathways feeding into this complex, and so cannot model the side effects of such disruption.

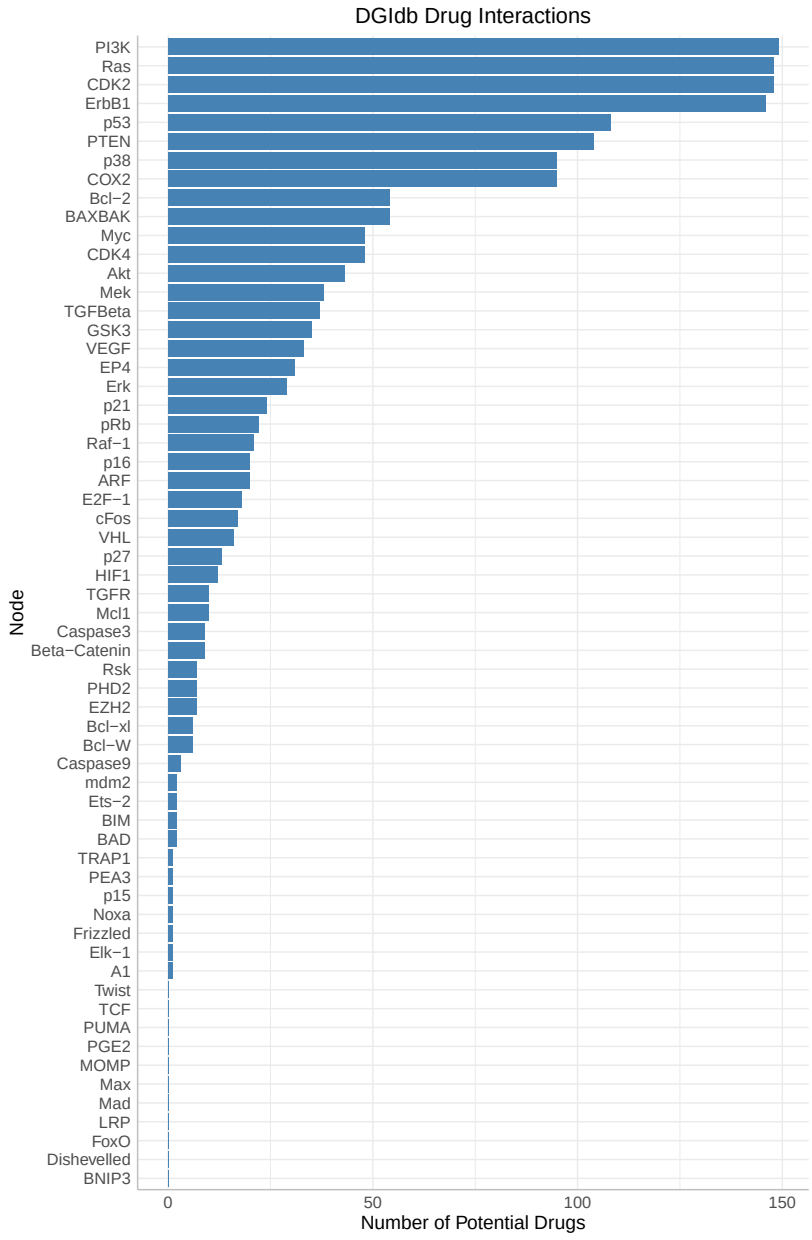

Fig. 4.1 Number of distinct drugs which interact with genes according to the Drug-Gene Interaction Database [465] accessed using the package rDGIdb [443].

As discussed in Chapter 2.3.1, my aim was to minimise the exclusion of nodes which may be at all druggable, so I included all results found in the database. However, some of these interactions will have been more thoroughly verified than others. The Drug-Gene Interaction database provides a score, based on the number of unique publications that assert an interaction for a particular drug with a particular gene, which could be used for more stringent selection of druggable targets.

I examine the effects of perturbations of the network which act on nodes known to be druggable in this Chapter. I also include the full results including activations, as heat maps similar to those in Figure 4.2 and 4.3, in Appendix B.1. This indicates which nodes might be targeted therapeutically by mimetic drugs, for example those targeting BH3 anti-apoptotic proteins [73]. Further, emerging technologies also offer the opportunity to activate rather than inhibit genes, and it is imperative that the best targets for these are identified in order to best demonstrate their capabilities. Gene therapy of specific organs and tissues might be targeted towards cancer [102] or RNA-based drugs could increase expression of key proteins [238] For example, Swisher et al. [430] demonstrated that insertion of wild-type p53 DNA by adenovirus in in lung cancer was possible, and that subsequent radiotherapy activated p53-dependent responses and tumour regression.

I consider pure as well as heterogeneous tumours, as these are likely to occur early in the progression of the cancer, or as a response to treatment which is more effective against one type of cell than the other, and so understanding how the tumour responds at different stages can provide a complete view of potential therapies.

4.2.2 Cytostatic Therapy is More Effective Against Myc-Low Sub-clone

I first consider the effects of single interventions on proliferation. These are shown in Figure 4.2, with every row corresponding to a perturbation of a node of the network. The @ symbol denotes the level to which the node is fixed, here I focus on inhibitions (e.g. Myc @ 0), but I also show activations in Appendix B.1 (e.g. Myc @ 2). In these figures I refer to the different sub-clones by the following abbreviations: wt for healthy cells, lo and hi for the pure myc-low and myc-high tumours, and het_lo and het_hi for the heterogeneous myc-low and myc-high tumours. Darker blue indicates higher proliferation, with maximum proliferation (6) being the darkest, while no proliferation (0) is white. This is the same for later heat maps in the thesis, except that those examining apoptosis have darker red for higher apoptosis. This means that rows which are uniformly light correspond to a treatment which is effective

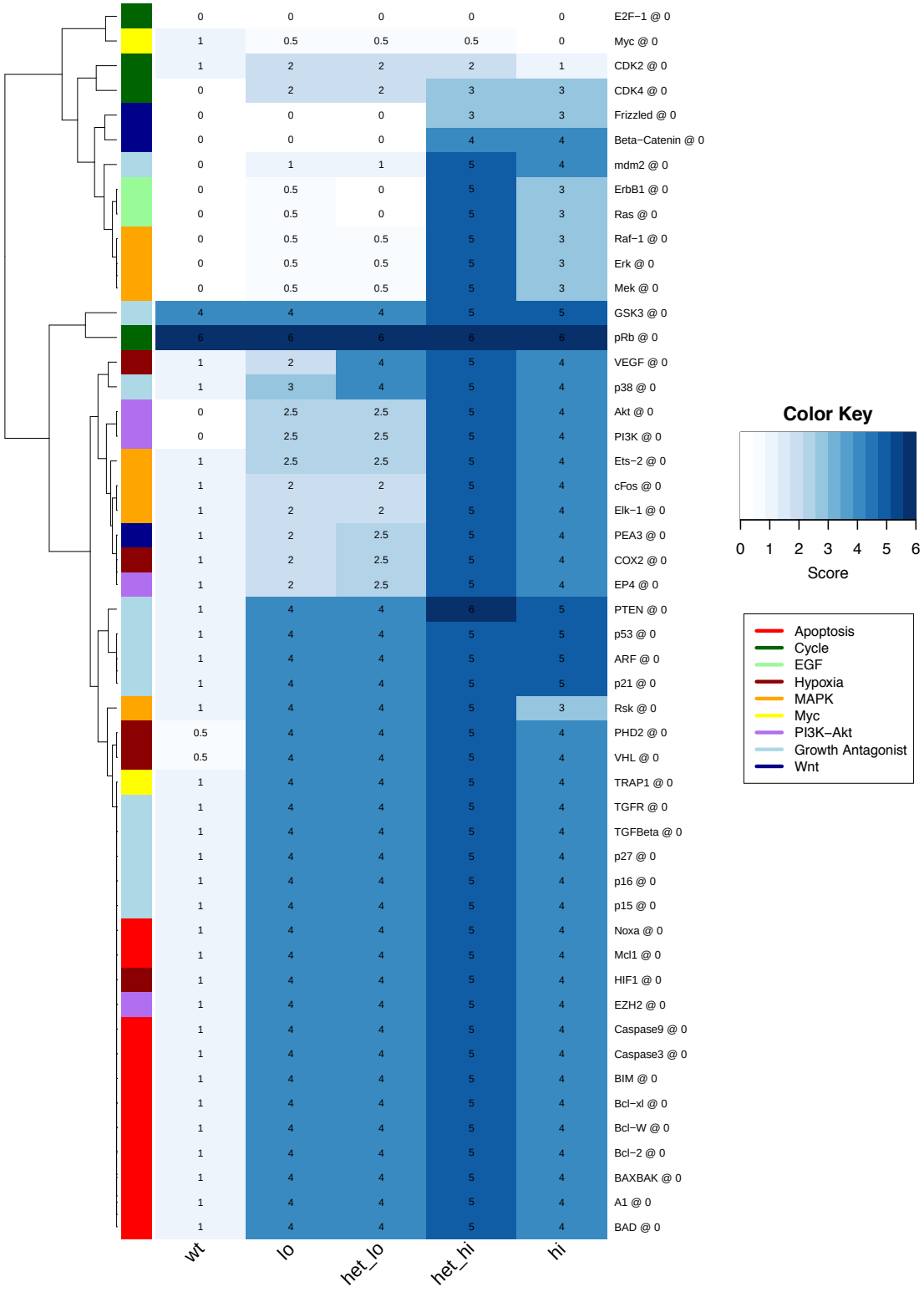

Fig. 4.2 Heat map showing the mean value of proliferation under all perturbations for which there are drugs, for the different possible sub-clones and the healthy cell (wt), shown as columns. Darker blue indicates higher proliferation, with colours on the left giving an indication of the pathways for the nodes perturbed. Results are clustered by Euclidean hierarchical clustering, as shown by the dendrogram on the left. I further show how results cluster by general node categories, as given in Appendix A.2. In cases where the VMCAI algorithm (see Chapter 2.1.8) does not find a single fixed point, the range to which the value can be restricted in shown in Appendix B.3.

across multiple sub-clones, such as for Myc inhibition (Myc @ 0). Rows which show more variation indicate treatments which are more effective in one case than others, such as PI3K inhibition; which is more effective against the pure myc-low tumours (lo) and the heterogeneous myc-low sub-clone (het_lo), than against the myc-high cells (het_hi and hi). Results are clustered by Euclidean hierarchical clustering, as shown by the dendrogram on the left. I further show how results cluster by general node categories shown by the colours next to the dendrogram. These colours correspond to categories given in Appendix A.2. In cases where the VMCAI algorithm (see Chapter 2.1.8) does not find a single fixed point, the range to which the value can be restricted in shown in Appendix B.3.

In order to assess all these perturbations of the network for all sub-clones, I cannot use the SMT solver as it does not find solutions in a reasonable time for many cases. Instead I use the VMCAI algorithm, which scales well to this purpose. This restricts the range in which the phenotypes of interest vary. In cases where the range over which the phenotype can vary is 0, there is a single fixed point attractor, and so analysis is easy. If there is a larger range, the upper and lower bounds are returned, but the algorithm does not give information on how different attractors are distributed within this range. For the purpose of comparing these perturbations, I assume that they are distributed evenly within the range, and so show the mean of the upper and lower bounds as the activity. This still indicates the overall change in the behaviour of the network, and whether a phenotype is increasing or decreasing. In cases where there is no single fixed point, if the perturbation is of particular interest, it is possible to investigate further using the SMT and BDD algorithms, and I do this in Chapter 5.6, to see whether the distribution of attractors in which the system can stabilise affects the prediction of the effectiveness of treatment. I show the range to which nodes are restricted in Appendix B.2 (i.e. the difference between the upper and lower bounds) to indicate cases in which the model has more complex behaviour than a single fixed point, which may need to be investigated further.

The benefits of the cooperation between sub-clones is clear, with the myc-high cells in the heterogeneous context showing the highest proliferation (Figure 4.2). These cells also show the most robustness against single perturbations. This in part reflects the nature of the mouse model more than it might a real cancer, however. In the network model I fix Myc expression at maximum, to reflect the strong over-expression by MycER^{T2}. In a naturally occurring tumour, there might be more possibility for regulation of even an oncogenic mutation of Myc. However, it also reflects that in the heterogeneous case there are two semi-independent pathways driving proliferation, both Wnt1 and Myc, and so both must be disrupted to successfully counter this. For example, blocking β-catenin is more

effective against the myc-low. This is also shown by there being higher proliferation under more treatments in the heterogeneous myc-high sub-clone than the pure myc-high tumours. This protective effect is seen in experimental testing of therapies predicted by this model in Chapter 5.7.2, where proliferation is consistently higher in the myc-high sub-clone, despite drug treatment.

Treatments broadly effective across both sub-clones

Overall, the key nodes controlling proliferation are activation of Myc and the core cell cycle machinery, as well as interference with the genes that regulate them, such as GSK3β, PTEN and the Ras pathway. The best treatments to affect both sub-clones would be inactivation of Myc or the cell cycle machinery. Myc remains hard to target [212], so it is important to consider ways to work around its effects. Examples of how to attempt this are presented by Posternak and Cole [365] and Whitfield et al. [478], and the model presents further possibilities.

Attacking the CDK2-CyclinE complex is more effective against the heterogeneous myc-high sub-clone than targeting the CDK4-CyclinD complex. Inactivation of GSK3β or PTEN however would increase the proliferation of the tumour, and so represent mutations that might be selected for in the further evolution of the tumour. Indeed, PTEN mutations are common in cancer [108], although more commonly in HER2 positive cancers [421]. Further, GSK3β inactivation has been shown to be oncogenic in mammary epithelium [140], consistent with the model.

Treatments Specific to one sub-clone

As there are few actionable cytostatic treatments which affect both sub-clones, I further looked for treatments which are specific to one sub-clone. This could allow targeting of the supporting sub-clone of a cancer, and so minimise the number of cells targeted and so also the chance of resistance [45]. It also offers the opportunity to attempt to stabilise tumour growth, rather than eliminate it. Gatenby et al. [168] and Enriquez-Navas et al. [132] present a method of Adaptive Therapy, in which they attempt to maintain drug-sensitive sub-clones to compete with, and restrict the growth of, drug-resistant sub-clones. They achieve this with variable dosing of a single drug, but it could benefit from being able to more accurately target different sub-clones with drugs specific to their mutational profile. Another possible method of treatment that may benefit from better understanding of how targeted therapies affect different sub-clones preferentially is presented by Basanta et al. [17]. Here the authors

model how one therapy might be used to guide the evolution of the tumour to make it more vulnerable to a second therapy. As the behaviour of the tumour depends on the cooperation and competition between the sub-clones, this approach necessitates an understanding of the sub-clone specific effects of therapy.

All possible treatments have a stronger effect on the myc-low tumours than the myc-high tumours, regardless of heterogeneity. There are options to maximise the difference between the two. This might be useful in our specific case in that restricting myc-low growth restricts access to Wnt1, the survival factor upon which myc-high cells are dependent (see Chapter 3.5.1). As expected, highly myc-low specific treatments include interference with the Wnt1 pathway, as expected as this is the primary driver in this sub-clone, but also interference with the MAPK pathway. This is likely as this pathway helps to drive Myc expression in these cells, which is not required in the myc-high case.

Interfering with the PEA3-COX2 pathway has a lesser, but still specific effect, partly through its effect on prostaglandin expression. Disrupting the Akt/PI3K pathway is similarly mildly effective against the myc-low tumours, due to de-repression of FoxO, as well as myc regulation by EZH2, as described in breast cancer by Kaur and Cole [245]. However, these have no effect on the myc-high sub-clone.

Considering activation of nodes shown in Figure B.1, p53 activation is more effective against the myc-low clones. This supports the work demonstrating p53-restoration as a possible therapy [316]. p21 and p27 are also effective against the myc-low sub-clone, but unlike the PI3K-Akt inhibition does have a small effect on the myc-high sub-clone. This is in fact more effective against myc-high than p53 activation. This is because direct activation avoids inhibition via Myc of p21 and p27, to which these nodes are vulnerable when p53 is activated. However, this inhibition may still have an effect against a putative p21 mimetic, unlike setting it to a constant value in the model. Finally, activation of HIF1α is more effective against the myc-high sub-clone than the myc-low. This happens because it cooperates with myc activation of p53 via ARF, which is normally suppressed in this sub-clone due to Wnt1 suppression of ARF via Twist. In the absence of myc, HIF1α does not activate p53 to the same degree.

Effect on healthy tissue

The optimum treatment would not be specific just to one sub-clone, but also to the tumour in general. As such a treatments tend to have better toxicity profile [480], they could be better tolerated and so be applied at higher doses and for longer, making it more effective [379]. While this is possible in the cytotoxic case (Section 4.2.3), there are no such treatments

which are less cytostatic for healthy cells than they are for tumour cells. However, inhibition of the PI3K/Akt or PEA3/COX2 pathways do not lower the healthy cell proliferation below its normal level for the model, and so would likely be better tolerated. Nonetheless, this should not remove other treatments from consideration as existing treatments which slow proliferation in healthy tissue do not appear to have such side-effects as to preclude their use. For example, Trastuzumab, does not have major side effects on healthy tissue, with the exception of cardiotoxicity [503, 397]. This, while serious, appears to be reversible [137].

In summary, the model predicts that in the case of putative cytostatic treatments, there are few which are broadly effective against both sub-clones of the heterogeneous tumour due to the constitutive expression of MycER^{T2} in the myc-high sub-clone. However, targeting the myc-low sub-clone, most effectively by targeting the MAPK pathway but also through PI3K/Akt or PEA3/COX2, is also viable. Of these, the latter is less effective but may be preferable in that it spares healthy tissue.

4.2.3 Cytotoxic Therapy Allows Specific Targeting of the Myc-High Sub-clone

In the same analysis for apoptosis, shown in Figure 4.3, there were more opportunities for single therapy, as well as more opportunities for targeting a single sub-clone specifically. This is shown by the broader range of reachable apoptotic states (see Section 4.3.2), although it is clear that the myc-low sub-clone has more variability in response. In accordance with the behaviour *in vivo*, the pure myc-high case has the highest apoptosis, and susceptibility to perturbation. The heterogeneous clones are less prone to death under treatment, but the myc-high case is still more vulnerable even in this context where it has the advantage of paracrine Wnt1 signalling from neighbouring myc-low cells.

Treatments broadly effective across both sub-clones

Key nodes raising apoptosis are mdm2, VHL and PHD2. The former is a key regulator of p53, and so when inhibited initiates an aggressive tumour suppressive response. In the latter case there is a direct activation of HIF1α and through it the pro-apoptotic factor BNIP3. Attacking EGFR (ErbB1) or Ras is also broadly effective against both sub-clones, and less dangerous to healthy cells. This is expected given the efficacy of Gefitinib in treating breast cancer [334, 188].

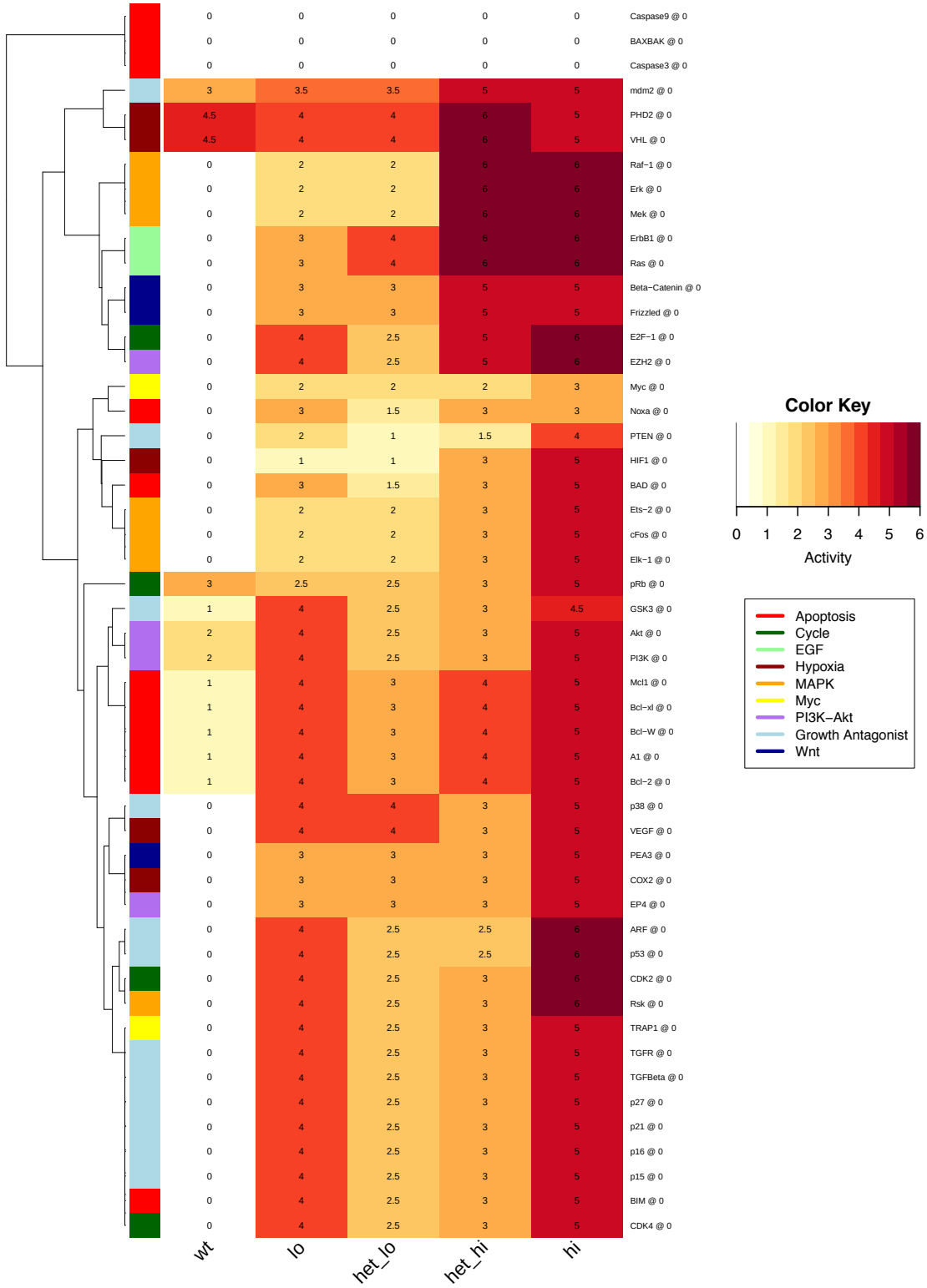

Fig. 4.3 Heat map showing the mean value of apoptosis under all perturbations for which there are drugs, for the different possible sub-clones and the healthy cell (wt), shown as columns. Darker red indicates higher apoptosis, with colours on the left giving an indication of the pathways for the nodes perturbed. Results are clustered by Euclidean hierarchical clustering, as shown by the dendrogram on the left. I further show how results cluster by general node categories, as given in Appendix A.2. In cases where the VMCAI algorithm (see Chapter 2.1.8) does not find a single fixed point, the range to which the value can be restricted in shown in Appendix B.4.

Treatments Specific to one sub-clone

There are more opportunities for sub-clone specific therapies when aiming for cytotoxicity. The MAPK pathway shows the clearest difference between sub-clones, triggering maximum apoptosis in the myc-high case, but much lower in the myc-low case. The Wnt1 pathway, also provides a way to target myc-high clones, although it is both slightly less effective against the myc-high clone, and more effective against the myc-low clone. The effect of this inhibition is to remove the key benefit of heterogeneity for the myc-high clone, the effect of Wnt1, and so it reverts to the behaviour of the pure myc-high tumours, which had high apoptosis and grew poorly (see Chapter 3.5). Interfering with the regulation of BIM by inhibiting E2F-1 or EZH2 is also effective in the myc-high clone, as BIM is a myc target [336, 52]. Finally, inhibiting the Bcl-2 family proteins, is slightly more effective against the myc-high clone, taking advantage of the higher tendency towards apoptosis engendered by myc [136].

In the case of cytostatic treatments, only one sub-clone could be targeted specifically, but cytotoxic effects show more flexibility. Knockout of VEGF, or its activator p38 increases apoptosis in the myc-low sub-clone more than the myc-high, in the heterogeneous case. This is due to cell autonomous inhibition of HIF1α by myc, as seen in the lower HIF1α observed during the characterisation of the pure tumours, despite lower VEGF expression (see Chapter 3.5.2).

Effect on healthy tissue

As in Sec. 4.2.2, it is necessary to consider the effects of treatment on healthy cells. This is more important in the case of cytotoxic effects, but most of the possible treatments outlined above are restricted to tumour cells in their effect. Only activation of HIF1α via VHL or PHD2 raises healthy cell apoptosis to levels high enough that I would consider them to no longer be useful to treat a tumour.

While my main interest in this analysis is to find viable treatments, it is also useful to see which loss-of-function mutations might be tumour promoting by lowering apoptosis. An inactivation of myc is trivially effective at lowering apoptosis, but not as likely to be selected for in the evolution of the tumour. PTEN inactivation is also protective, and also has a pro-growth effect (see Figure 4.2). Indeed, PTEN is often lower in breast cancer than healthy tissue and lower expression correlates with lower 2-year disease-free survival [509]. Inactivation of the tumour suppressors in the model, either by ARF or p53 is also effective, and also often observed [207, 31].

4.3 Reachable States of Proliferation and Apoptosis Under Single Perturbation

In order to better understand what the possibilities of treatment are; how high could apoptosis be pushed in different sub-clones, I compare the reachable states for proliferation and apoptosis in both sub-clones of the heterogeneous case. Here I map the level of both phenotypes in each sub-clone on the x- and y-axes, for all druggable nodes. I also remove treatments, either cytostatic or cytotoxic, which raise apoptosis above 3 in the healthy cell as having too great an effect on normal tissue.

4.3.1 Cytostatic Treatments show more variation in effect on the Myc-Low Sub-Clone

Figure 4.4a shows how much easier it is to affect proliferation in the myc-low sub-clone compared to the myc-high sub-clone, with more variation in the x-direction than in the y-direction. In contrast, there are no points in the lower-right of the plot, reflecting that only the myc-low sub-clone can be targeted specifically. The largest point shows high proliferation in both clones, demonstrating that even when restricting ourselves to genes for which drugs have been developed, indicating a certain level of importance, most monotherapies are ineffective.

Breaking down perturbations by pathway (Fig. 4.4b) shows that the most effective mutations, near 0 on both axes, are either targeting c-myc or CDK/cyclins directly. Other effective mutations are in the EGFR and MAPK pathways.

4.3.2 Cytotoxic Treatments show greater range of effect

In the case of cytotoxic treatments, (Fig. 4.5a) a wider spread of points is observed, reflecting that it is easier to cause apoptosis in both sub-clones than to slow growth across the whole-tumour. However, it shows that monotherapy cannot increase apoptosis as much in the myc-low sub-clone as in the myc-high. As with the cytostatic case, many of the treatments have no effect, and leave apoptosis in the middle of the range.

In Figure 4.5b there are points corresponding to knock-out of ErbB1 or Ras in the top-right, and then to the left a group of points for the MAPK pathway, demonstrating how moving down this branch of Ras signalling increases specificity.

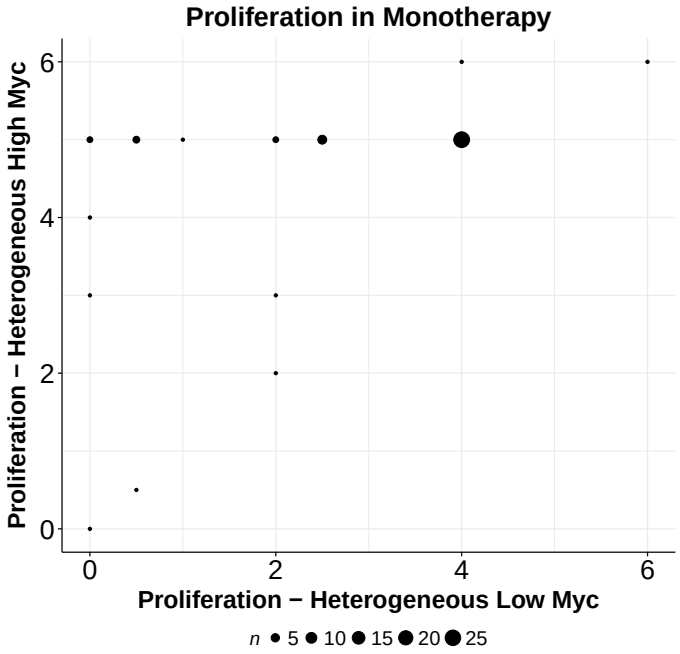

(a) Number of treatments which bring proliferation to different levels in heterogeneous myc-low vs heterogeneous myc-high case. Size of the point indicates number of treatments, for which drugs exist.

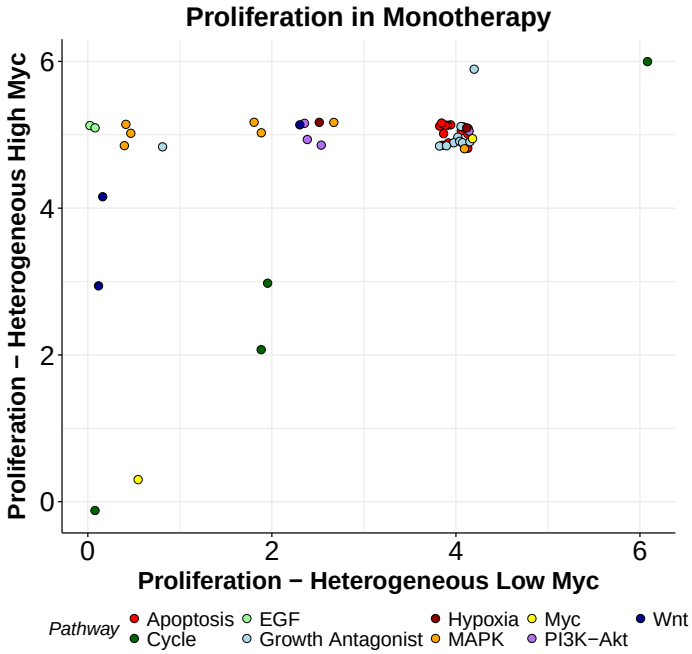

(b) Pathways of the nodes and the level of proliferation under treatment in heterogeneous myc-low vs heterogeneous myc-high case. Colour indicates the pathway of the treated node (see Appendix A.2). Small amount of noise added to points to prevent overlap, for exact values see Figure 4.4a.

Fig. 4.4 Number and type of treatment, with level of effectiveness, in heterogeneous tumour subclones, affecting proliferation.

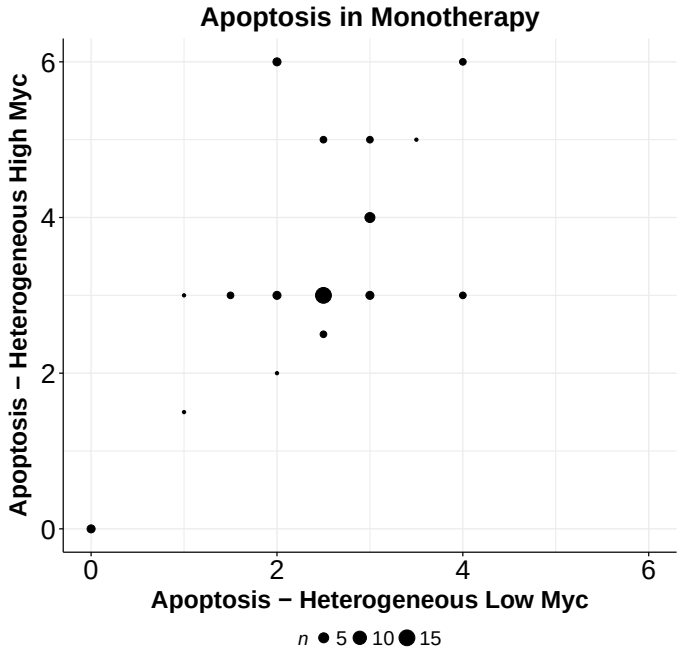

(a) Number of treatments which bring apoptosis to different levels in heterogeneous myc-low vs heterogeneous myc-high case. Size of the point indicates number of treatments, for which drugs exist.

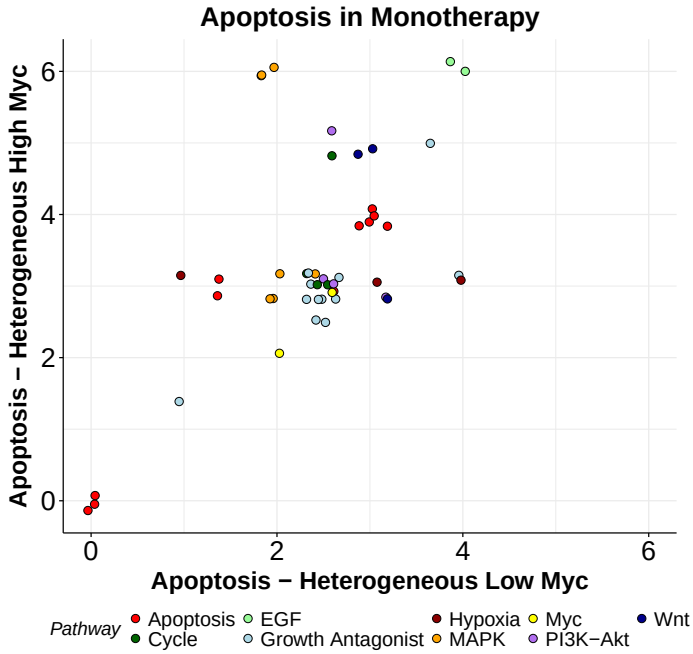

(b) Pathways of the nodes and the level of apoptosis under treatment in heterogeneous myc-low vs heterogeneous myc-high case. Colour indicates the pathway of the treated node (see Appendix A.2). Small amount of noise added to points to prevent overlap, for exact values see Figure 4.5a.

Fig. 4.5 Number and type of treatment, with level of effectiveness, in heterogeneous tumour subclones, affecting apoptosis

4.4 Pathways Involved in Effective Treatments

I further compared the proportion of successful treatments which involved different pathways. Here I define successful as those which lower proliferation below the baseline for the respective sub-clone, or apoptosis above the baseline. I also include a breakdown by absolute number of successful treatments in Appendix Figure B.29.

4.4.1 Cytostatic

The vulnerability of the myc-low subclone compared to the myc-high sub-clone is apparent in Figure 4.6a with many more pathways leading to lower proliferation in the myc-low sub-clone. The only way to affect proliferation in the myc-high sub-clone is via perturbation of the driving pathways, myc and Wnt1, or via direct interference with the cell cycle. The myc-low sub-clone is much more vulnerable to MAPK and PI3K-Akt perturbations, as myc is downstream of these and these tumours must rely on activating the endogenous myc to sustain proliferation. Cells in the myc-low sub-clone must also inhibit growth antagonists such as p21 and p27 through the PI3K-Akt pathway in order to benefit from the Wnt1 pathway, whereas myc suppresses these in the myc-high sub-clone.

4.4.2 Cytotoxic

The effective treatments for each sub-clone are more similar when considering apoptosis (Fig. 4.6b). However, the best pathways for specific treatments are also clearly apparent, with MAPK only being present in the myc-high case, or the hypoxia/angiogenesis response pathway in the myc-low case. There is also a small effect from the Cycle pathway on myc-high as E2F-1 inhibition helps deregulate BIM. This represents an alternate route to specificity in addition to targeting the MAPK pathway.

4.5 Conclusions

In this Chapter I demonstrate the effect of perturbations of single nodes in my model, corresponding to targeted therapy of single genes and proteins. I show that it is possible to affect the proliferation and apoptosis of both sub-clones, for example by inhibition of CDK4 for example by Ribociclib [213] or by blocking EGFR signalling (ErbB1) by Gefitinib [188]. The myc-high sub-clone can be targeted to increase apoptosis, such as with Mek inhibition by Trametinib [374]. This also decreases proliferation in the myc-low sub-clone.

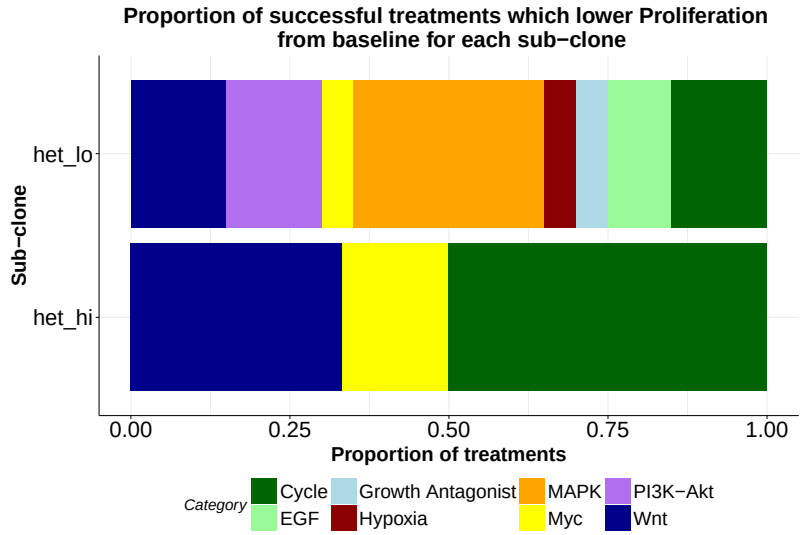

(a) Proportion of successful cytostatic treatments involving different pathways.

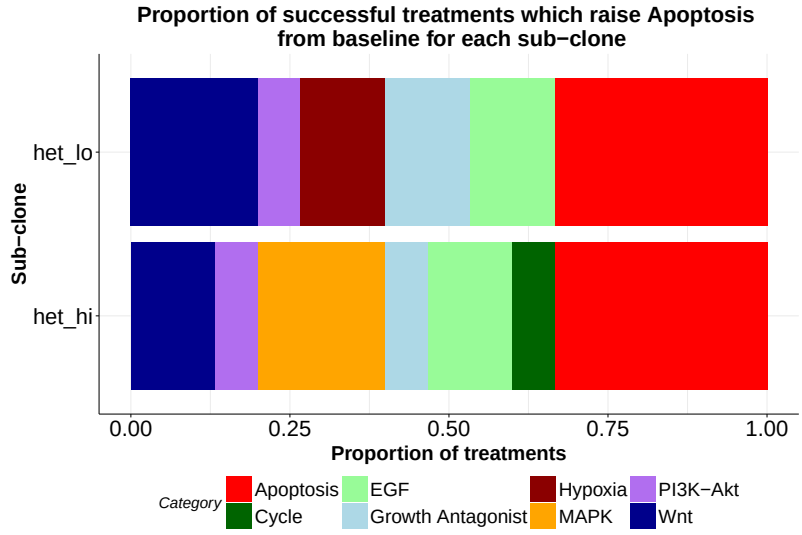

(b) Proportion of successful cytotoxic treatments involving different pathways.

Fig. 4.6 Proportion of successful cytostatic and cytotoxic treatments involving different pathways. Successful are those which lower proliferation below the baseline for the respective sub-clone, or apoptosis above the baseline. How I group nodes in the network into pathways is broken down in Appendix A.2. Note that sections of the bar indicate all the treatments which fit that category, rather than being cumulative. I.e. in 4.6a about 30% of treatments of the het_hi case involve the myc pathway, not 50%.

Alternatively, it is possible to specifically target proliferation in the myc-low sub-clone, without concomitant apoptosis in the myc-high sub-clone, for example by inhibiting PI3K such as Buparlisib [318].

However, monotherapies are vulnerable to acquired resistance. Can the addition of a second therapy improve the effects and enhance specificity, or complement a specific treatment to make it more broadly effective? I investigate such dynamics of combination therapy in the next Chapter.

Chapter 5

How Combination Therapies Interact and Can be Selected for Increased Effectiveness

5.1 Introduction

To investigate how to enhance the effects on proliferation and apoptosis identified above, I applied two treatments in combination. This simulates the interaction of two drugs to find the best avenues for research into combination therapies. These combinations may exploit novel synergies, which could allow more treatment options for sequential therapy, prolonging patient survival. There may also be combinations of independently effective treatments which do not conflict, which would reduce the chances of acquired resistance, as resistant cells would need two resistance mutations, which is much less likely to occur [45, 256]. Those treatments which are effective when applied alone but which do conflict when combined are important to identify and eliminate prior to clinical trials.

5.2 Inhibition of Druggable Genes in Combination

For clarity I consider mainly the heat maps showing only druggable interactions in this Section, as in Chapter 4. However, activations of nodes can be useful to visualise how a monotherapy might be countered by a mutation in the tumour, and so predict possibilities for acquired resistance. The full heat maps, showing every activation and inactivation combination for all nodes, are included in Appendix B.3.

5.2.1 Cytostatic

Comparison of sub-clones

As with the single perturbations, the difference in susceptibility to treatment is evident in comparing the heat-maps across the different backgrounds, with heterogeneous tumours being the most proliferative in general and robust to treatment (Fig. 5.1), and similarly the least apoptotic (Fig. 5.4).

Conversely, in the myc-high case (Fig. 5.6), we see that only interventions affecting myc or the core cell cycle machinery will lower proliferation below the baseline for this background, and the reachable set of states is quite constrained (Fig. 5.7); so combination of treatments is insufficient to counter proliferation driven by the consitutive expression of MycER^{T2}.

I next consider the two most interesting cases individually, the tumour sub-clones in the heterogeneous context.

Heterogeneous Myc-Low

I first examine the effect of combination therapy on proliferation in the myc-low sub-clone of the heterogeneous tumour (Fig. 5.2). Overall in this heat map there are many combination of treatments which are effective alone (lighter areas) and still effective together (upper left quadrant), and many combinations in which one treatment drives the effect while the other makes no difference, (the top and left rows). Conversely, there is a cluster in which there is no effect (darker blue i.e. higher proliferation), in the lower right quadrant. However, the most interesting areas are the inconsistencies in these patterns where treatments either enhance or counter one another's effects. I examine broad patterns here, and such interactions between treatments in more detail in Section 5.4.2.

Many of the patterns seen in Chapter 4 still hold in the case of combinations of perturbations of the network. That is to say, in most cases a second treatment or mutation neither enhances or counters an effect, and is merely a passenger. So, as expected, mutation of ErbB1 or Ras is effectively counter-proliferative, and in Figure 5.2 form a cluster of low proliferation regardless of partner. However, it now becomes possible to see regions which change the effect of single node perturbations, often corresponding to pathways which have a similar effect and therefore are clustered together in the heat map. For example, in Figure 5.2 it is possible to identify sets of nodes which when disrupted, enhance the effect of inhibiting the PI3K/Akt pathway, such as inhibiting c-Fos or Elk-1.

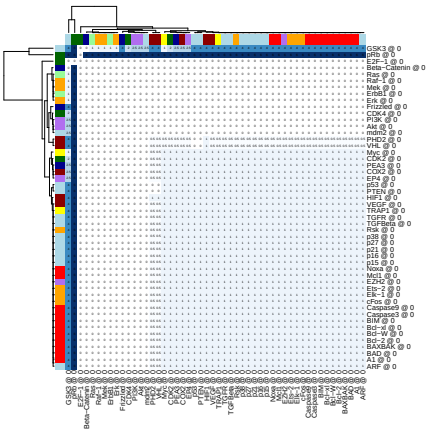

(a) Healthy Tissue

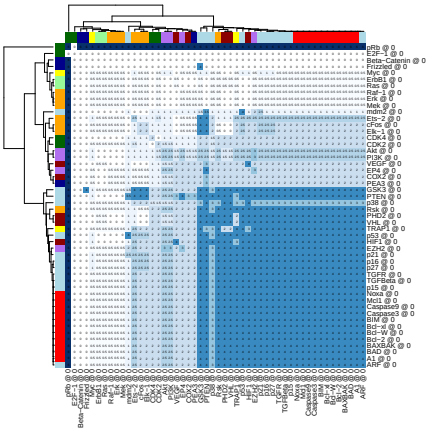

(b) Pure myc-lo tumour

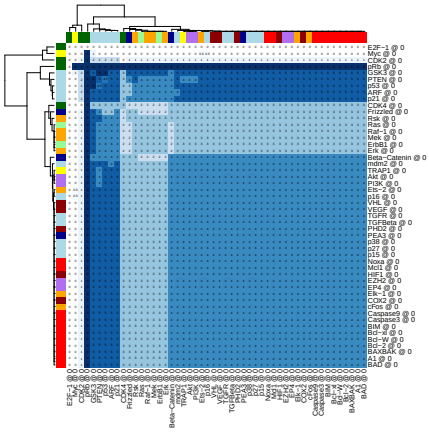

(c) Pure myc-high tumour

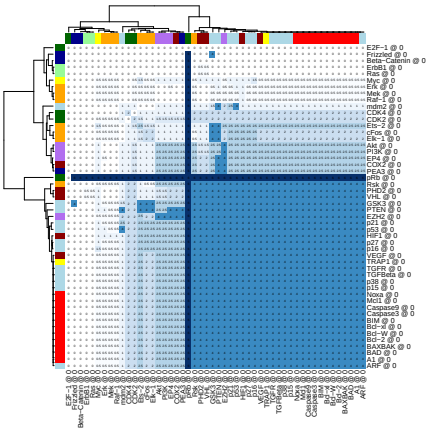

(d) Heterogeneous myc-low tumour

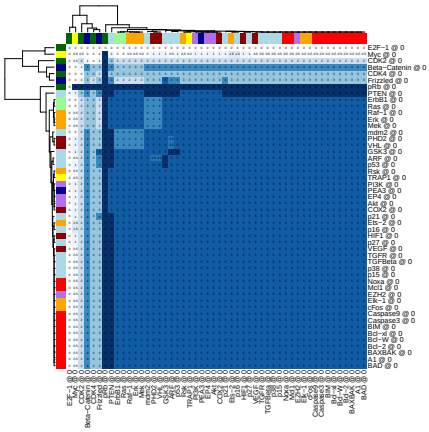

(e) Heterogeneous myc-high tumour

Fig. 5.1 Proliferation under treatment of druggable nodes for the different sub-clones and healthy tissue, simulated by the setting of nodes to constant values, as detailed in Chapter 2.3. Darkness of colour indicates the strength of predicted proliferation under the treatments. Shown here to compare overall trends between cases, full versions of these heat maps are shown in this Chapter and in Appendix B.3. The show how the general pattern of proliferation is higher under many treatments in the heterogeneous myc-high case than in the pure myc-high, while there is less difference between the heterogeneous and pure myc-low.

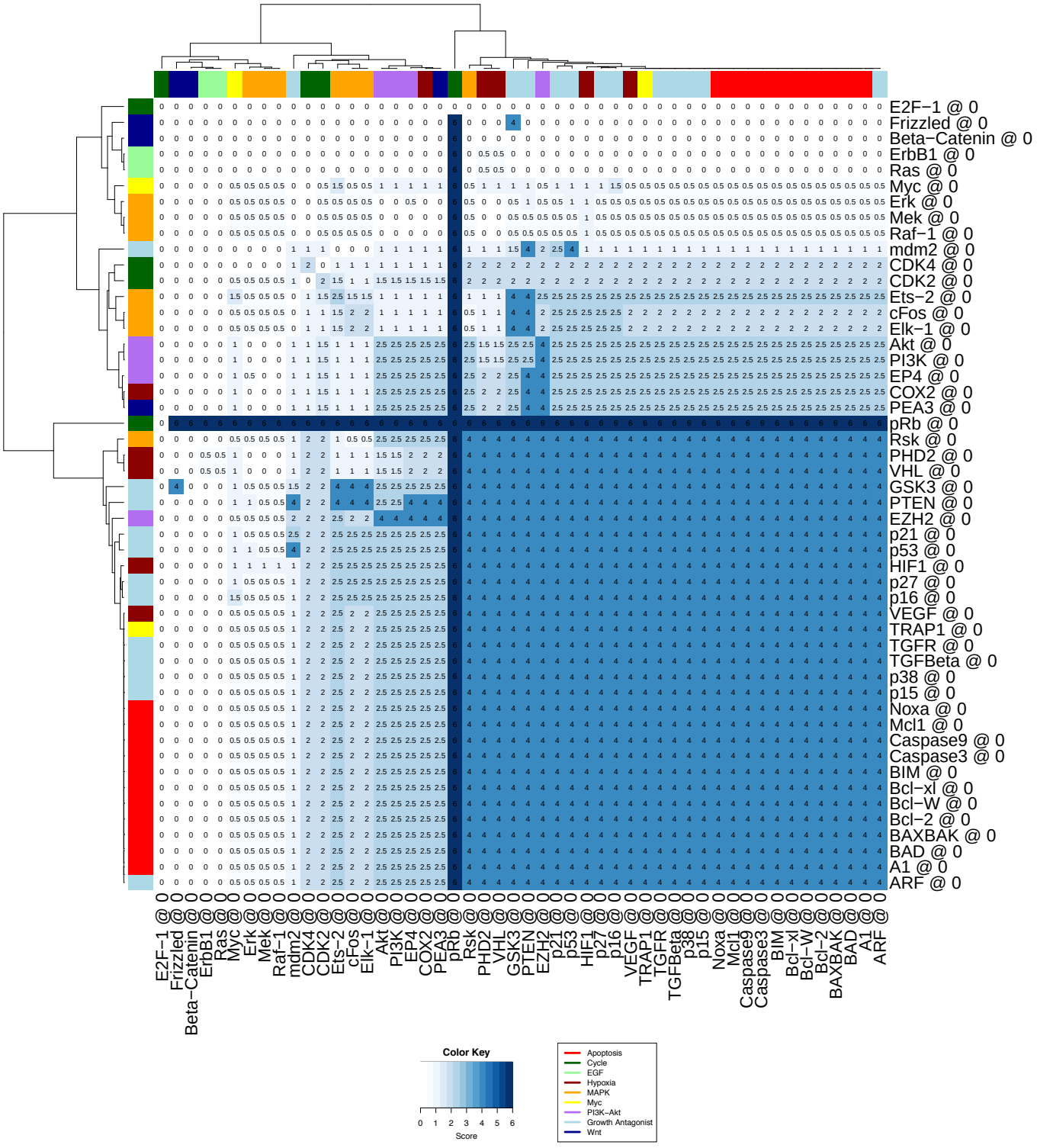

Fig. 5.2 Proliferation under combination of treatment of druggable nodes for the myc-low sub-clone in a heterogeneous tumour. In cases where the VMCAI algorithm (see Chapter 2.1.8) does not find a single fixed point, the range to which the value can be restricted in shown in Appendix B.3. The clusters of this heat map highlight areas where treatments have similar effects despite their partners, either effective (the top and left rows) or ineffective (darker blue i.e. higher proliferation). Breaks in this pattern, representing more interesting combinations, are discussed in Section 5.2.1.

Areas in which such improvement can be seen also includes the MAPK pathway, which can be improved with PI3K/Akt pathway inhibition, as expected given the effectiveness of Ras inhibition. Inhibition of one of the cell cycle complexes in the network model combines well with MAPK inhibitions but less with PI3K/Akt.

There are also cases where one perturbation of the network cancels another. This can be thought of as showing how a mutation in the tumour might counter an applied treatment, leading to resistance. There are, for example, several islands of high proliferation driven by PTEN where otherwise a mutation such as mdm2 maintains low proliferation with almost all other partners. This can be investigated further in the full version of the heat map (see Appendix B.7) where one can see a a cluster of high proliferation cutting through the clusters corresponding to otherwise effective treatments. Activation of the MAPK pathway is as effective at protecting the tumour as inhibition is for treating it.

Heterogeneous Myc-High

In the case of heterogeneous myc-high (Figure 5.3), there is less scope for treatment, even with a second line of attack. However, it is clear when comparing the pure myc-high to the heterogeneous case in Figure 5.20 that the Wnt1 pathway is key to the high proliferation of the myc-high tumour, which matches the observation that the heterogeneous tumours are more proliferative than either the pure myc-high or myc-low tumours. Therefore,while constitutive myc puts a very strong floor on how low we can force proliferation in this sub-clone; it is not sufficient for the highest growth alone.

Including activation creates further opportunities. Activation of HIF1α (through knockout of VHL or PHD2), or activation of p53 through interference with mdm2 creates a small cluster of lower proliferation.

It is also interesting to note that in the healthy cell (Fig. B.5) there are comparatively few combinations which increase proliferation. This is to be expected as cancer incidence is so rare when considering the number of cells, that the routes from a healthy cell to a cancerous state must be tightly constrained. There are many possible combinations of proliferative mutations, but only a small subset, such as Myc and Wnt1, can work together and evade tumour suppression to promote rapid, cancerous growth. Even with Myc constitutively active, there are only a few small clusters where proliferation is 5 or 6, with activation of the Wnt1 pathway being one route to this. I explore this further in Chapter 6.

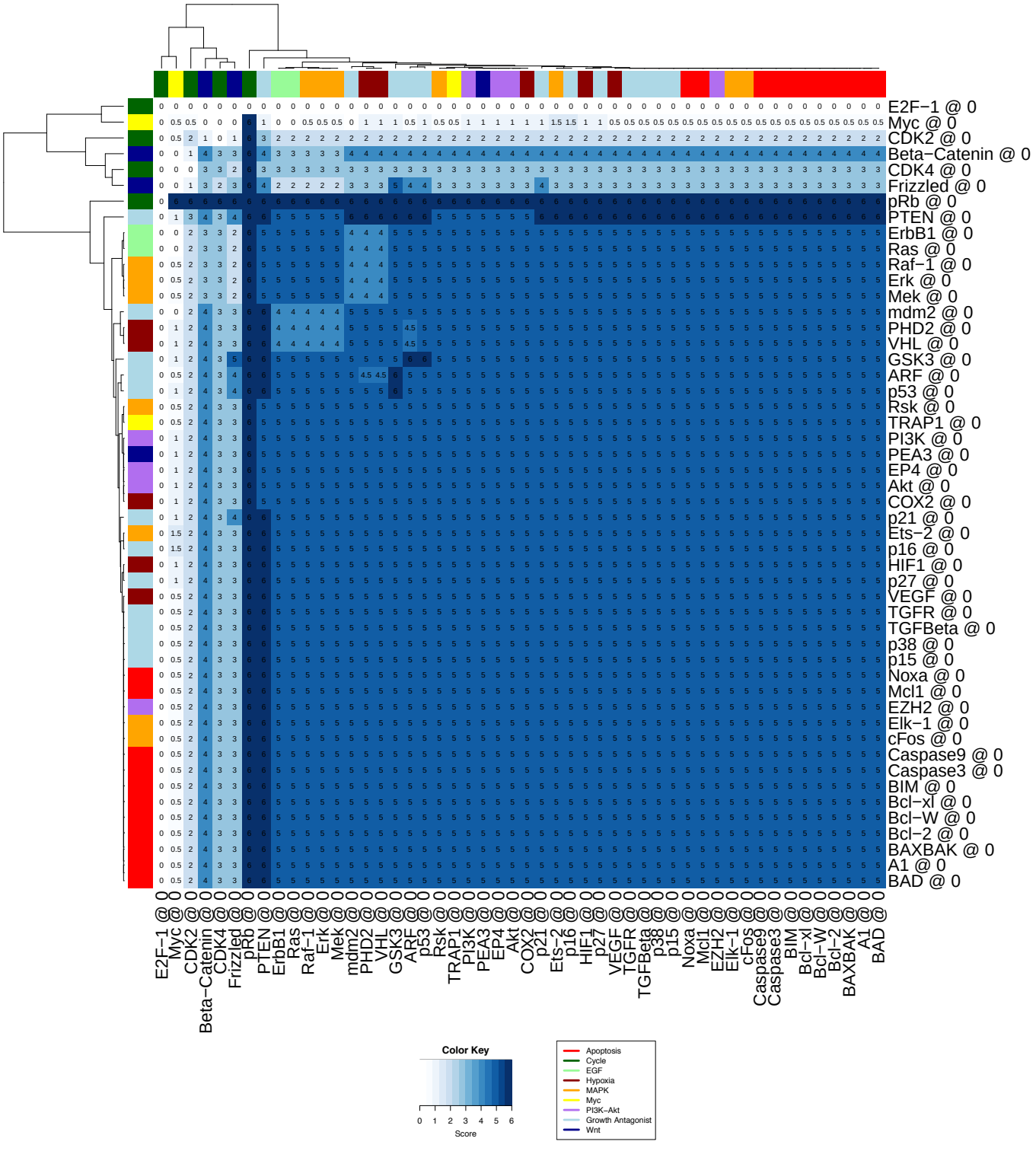

Fig. 5.3 Proliferation under combinations of treatment of druggable nodes for the myc-high sub-clone in a heterogeneous tumour. In cases where the VMCAI algorithm (see Chapter 2.1.8) does not find a single fixed point, the range to which the value can be restricted in shown in Appendix B.4. From the large cluster of dark blue (high proliferation) combinations, irt is apparent that there are fewer effective combinations against this sub-clone than in the myc-low (Fig. 5.2). Breaks in this pattern, representing more interesting combinations, are discussed in Section 5.2.1.

5.2.2 Cytotoxic

Comparison of clones

As with proliferation, examining the effect of combination treatment on apoptosis in all the sub-clones and the healthy cells (see Figure 5.4) shows that the heterogeneous case is the most robust to therapy.

There are large blocks of apoptotic behaviour representing single targets that promote apoptosis with many partners, for example up-regulation of the HIF1α pathway through inhibition of VEGF or PHD2 (Fig. 5.5 & 5.6). However, unlike the proliferative case, we do not see large breaks in this behaviour, i.e. there are fewer universally effective resistance mutations (see also Appendix B.3.2 to see that this also holds when considering activations of nodes). This means that apoptotic treatments may be more difficult to escape, and therefore more effective.

Heterogeneous Myc-Low

Figure 5.5 shows that the biggest determinants of apoptosis are activation of p53 and the hypoxia pathways, as well as the knock-out of survival promoting pathways such as Ras. There is also a cluster of higher apoptosis for interference with COX2, which combined well with many other treatments. Considering activations (see Fig B.12), resistance to apoptosis comes mainly through activation of the Akt pathway, as it both affects apoptosis directly through FoxO but also restricts proliferation which may lower p53 signalling through, for example, E2F-1.

Heterogeneous Myc-High

Figure 5.6 shows that the treatments which produce large clusters of high apoptosis in the myc-low case are equally if not more effective in the myc-high case. However, as with the case of single treatments, there are treatments which are uniquely effective in this sub-clone, such as Ras and MAPK mutations. Clusters of treatments that enhance one another include pairs of the Bcl-2 family proteins, and inhibition of the Wnt1 pathway combined with the regulators of BIM; E2F-1 and EZH2.

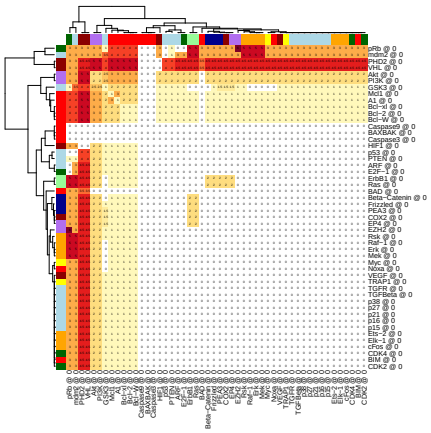

(a) Healthy Tissue

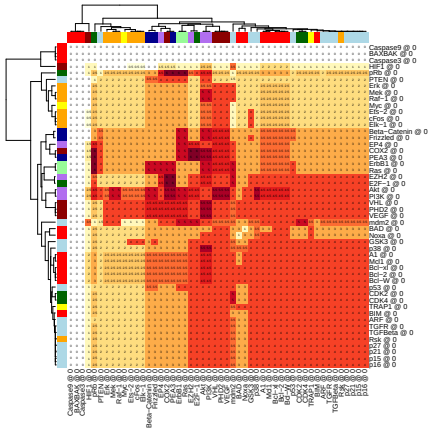

(b) Pure myc-lo tumour

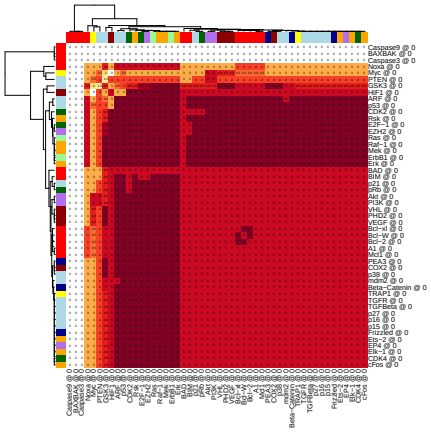

(c) Pure myc-high tumour

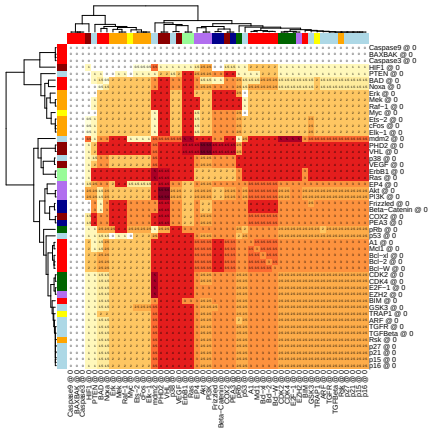

(d) Heterogeneous myc-low tumour

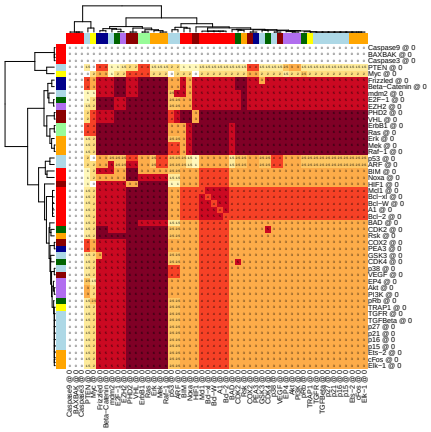

(e) Heterogeneous myc-high tumour

Fig. 5.4 Apoptosis under treatment of druggable nodes for the different sub-clones and healthy tissue, simulated by the setting of nodes to constant values, as detailed in Chapter 2.3. Darkness of colour indicates the strength of predicted proliferation under the treatments. Shown here to compare overall trends between cases, full versions of these heat maps are shown in this Chapter and in Appendix B.3. These show how the general pattern of apoptosis is lower under the different possible combination treatments for the heterogeneous cases than the pure cases.

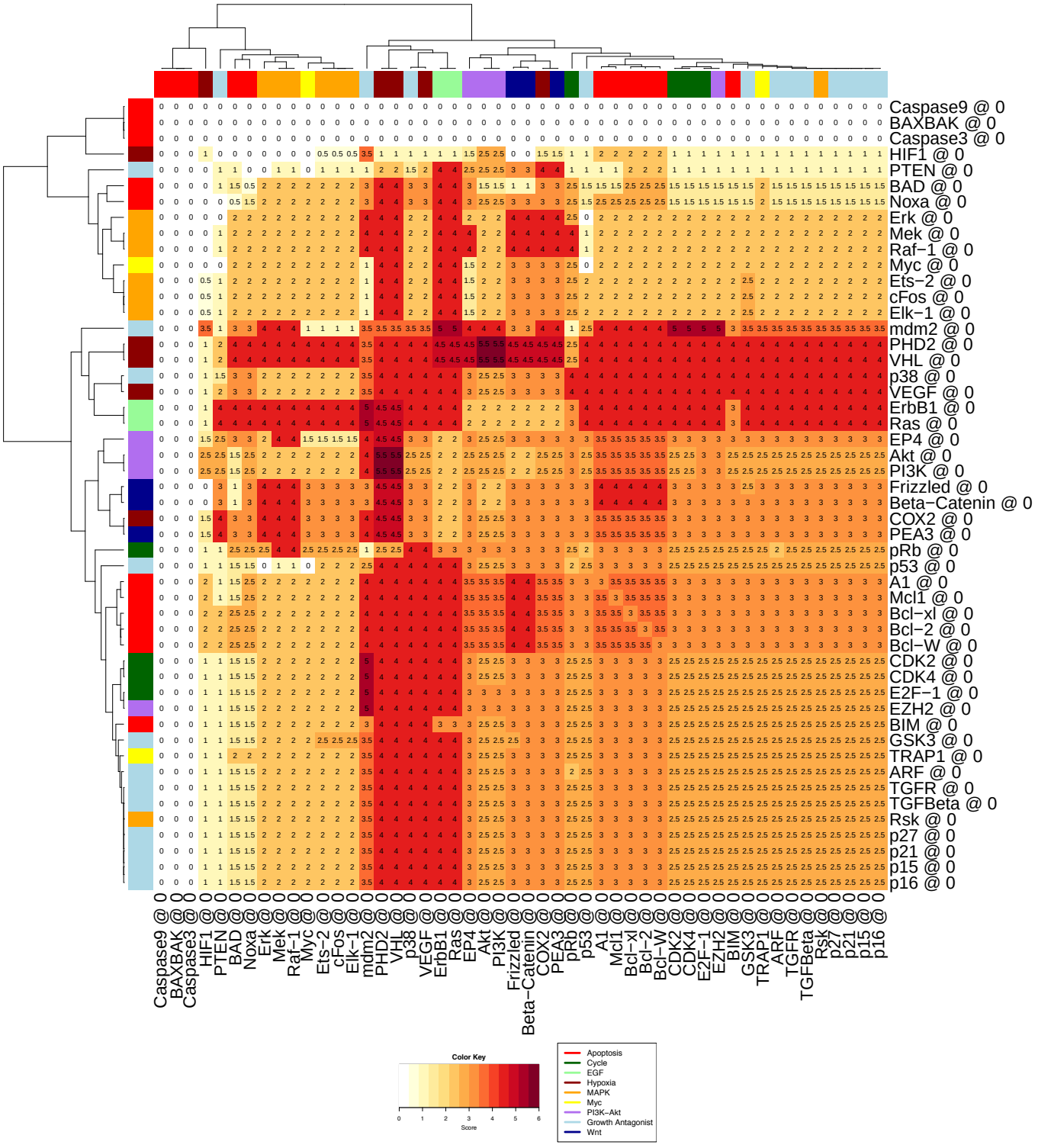

Fig. 5.5 Apoptosis under treatment of druggable nodes for the myc-low sub-clone in a heterogeneous tumour. In cases where the VMCAI algorithm (see Chapter 2.1.8) does not find a single fixed point, the range to which the value can be restricted in shown in Appendix B.4. The clusters of this heat map highlight areas where treatments have similar effects despite their partners, either ineffective (the top and left rows) or effective (darker red i.e. higher apoptosis). Breaks in this pattern, representing more interesting combinations, are discussed in Section 5.2.2.

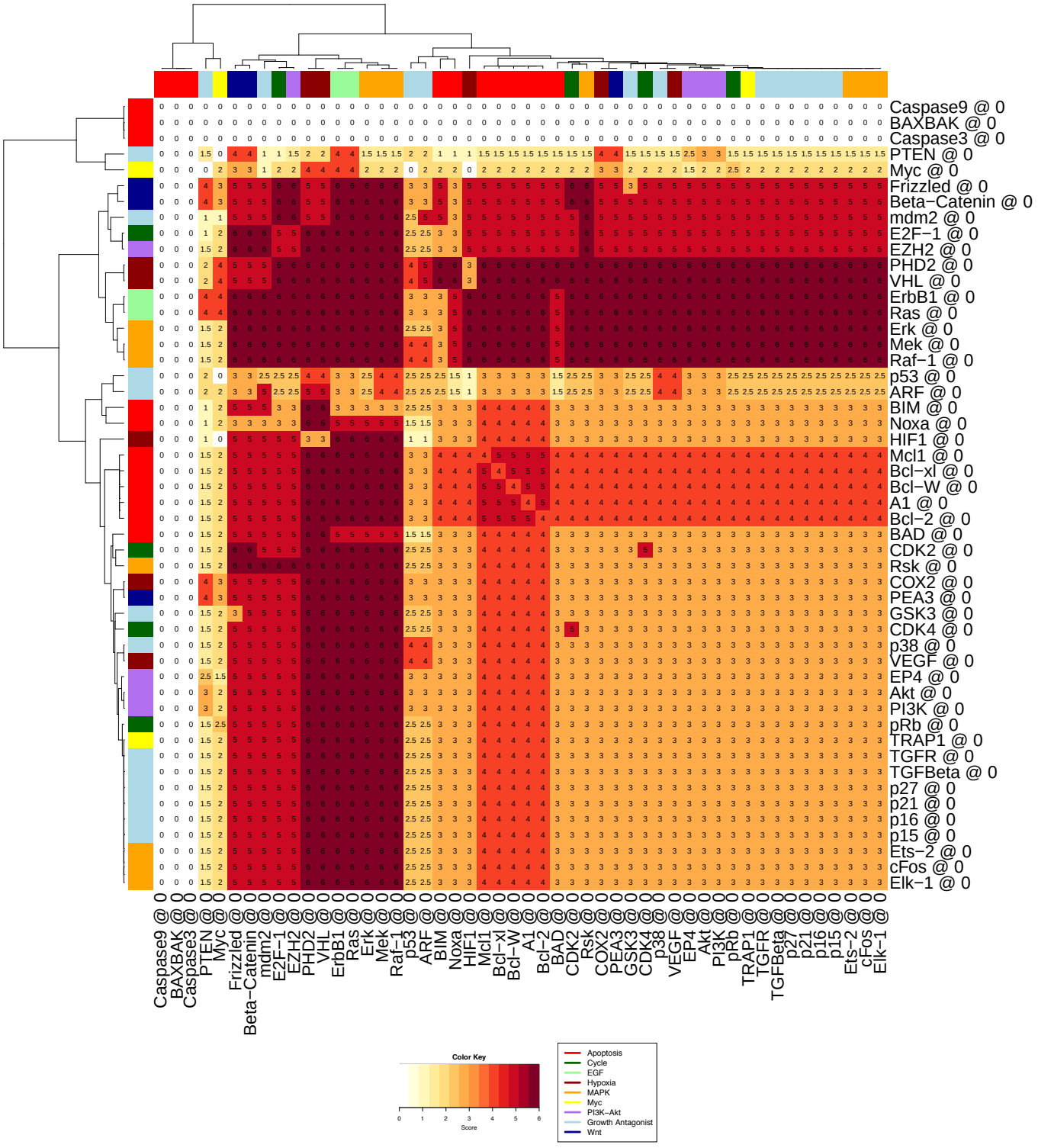

Fig. 5.6 Apoptosis under treatment of druggable nodes for the myc-high sub-clone in a heterogeneous tumour. In cases where the VMCAI algorithm (see Chapter 2.1.8) does not find a single fixed point, the range to which the value can be restricted in shown in Appendix B.4. The clusters of this heat map highlight areas where treatments have similar effects despite their partners, either ineffective (the top and left rows) or effective (darker red i.e. higher apoptosis). Breaks in this pattern, representing more interesting combinations, are discussed in Section 5.2.2. The darkest areas are larger than in the case of the myc-low (Fig. 5.5) suggesting that it is easier to induce apoptosis in this sub-clone.

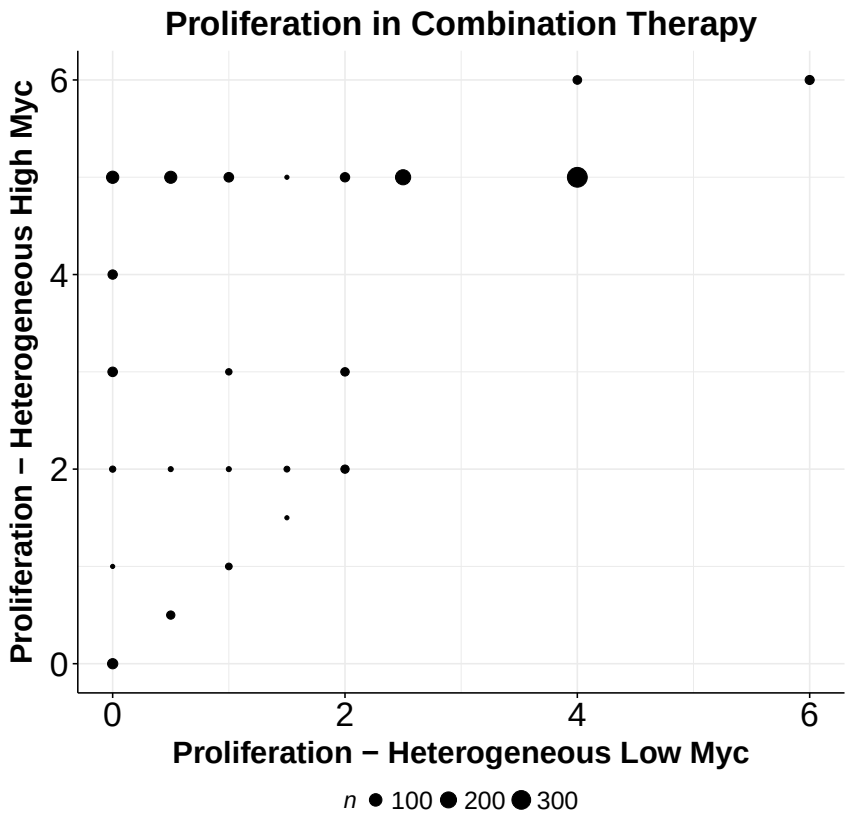

Fig. 5.7 Scatter plot of the proliferation in each sub-clone for each treatment, showing which levels of proliferation are reachable by combination therapy. In cases where multiple combinations have the same effect, the number of combinations is represented by the size of the point.

5.3 Reachable States

As in Chapter 4.3, I map the level of both phenotypes in each sub-clone on the x- and y-axes, for all druggable nodes, to show what the possibilities of treatment are. As before, I remove treatments, either cytostatic or cytotoxic, which raise apoptosis above 3 in the healthy cell as having too great an effect on normal tissue.

5.3.1 Cytostatic

The reachable proliferative states for combination therapy is very similar to monotherapy (see Fig. 5.7 and 4.4a respectively). This suggests that the addition of a second drug is not sufficient to increase the specificity of treatment, for example, there are still no therapies more effective agains the myc-low than the myc-high sub-clone. However, there are more possibilities in the lower-left quadrant of the plot, with proliferation less than 2. This implies

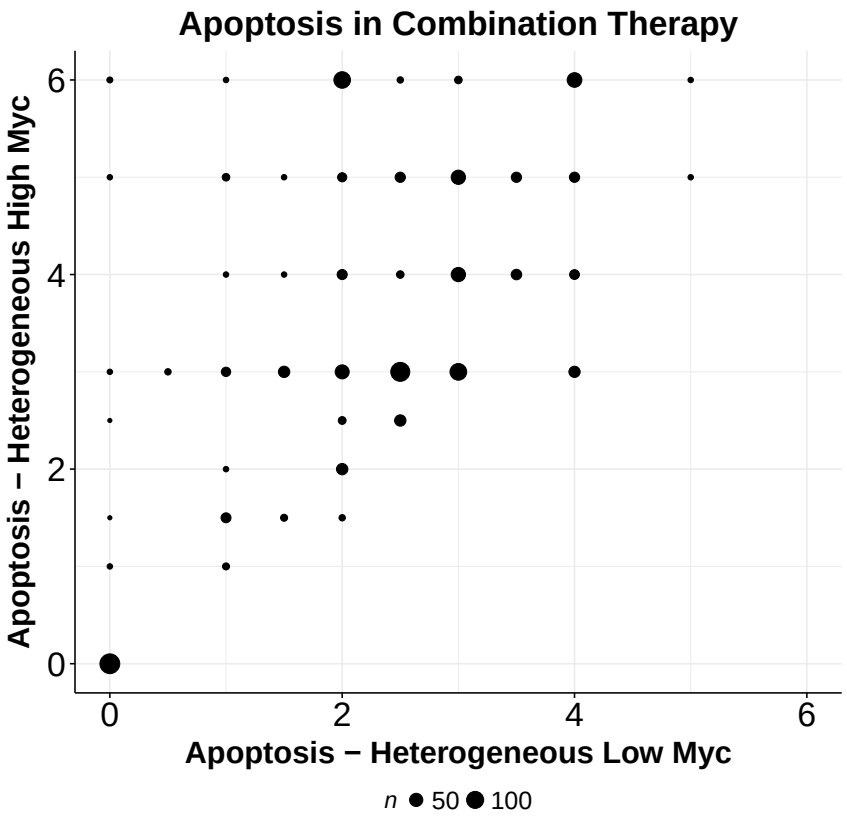

Fig. 5.8 Scatter plot of the apoptosis in each sub-clone for each treatment, showing which levels of apoptosis are reachable by combination therapy. In cases where multiple combinations have the same effect, the number of combinations is represented by the size of the point.

that there are changes in the effectiveness of treatments when combined, which is analysed further in Section 5.4.2.

5.3.2 Cytotoxic

There is more of an effect in adding a second drug on the reachable states for apoptosis than for proliferation. In Fig. 5.8 there is more variation in the myc-high sub-clone, with the possibility for most levels of apoptosis even with low apoptosis in the myc-low sub-clone. Therefore, adding a second drug can be used to increase the specificity of a therapy to one sub-clone over the other. Further, there are more points in the upper-right quadrant, suggesting that combinations can enhance one another (see further in Section 5.4.2).

5.4 Benefits of Combination Therapy

5.4.1 Number of effective treatments

The overall patterns relating to which treatments are effective in combinations largely follows that established in monotherapy. However, there are also many cases where there are large blocks of similar behaviour, indicating where most combinations do not change based on the partner, i.e. where only one of the perturbations is driving the behaviour.

I categorise the results from Chapter 4.2 and Section 5.2 into those predicted to be effective and ineffective, where success indicates that proliferation is lower than the baseline for that sub-clone, or apoptosis higher. I plot the proportion which are effective for mono- and combination therapy, assessing the cytostatic and cytotoxic effects in Figure 5.9a and 5.9b respectively. I use the proportion so as to be able to compare the mono- and combination therapy cases, as there are necessarily more possible combinations than there are monotherapies. If none of the therapies interacted, then the proportion of successes would be expected to be the same. However, as Figure 5.9 shows, the proportion of effective predicted therapies is higher in the combination case. Therefore the model predicts that combining treatments leads to interactions where there is a greater effect more often than a null or cancelling effect.

This is only an assessment of the behaviour of the model; in order to apply this to biological systems there must be an assessment of how reliable the models predictions are, as false negatives in the monotherapy case or false positives in the combination case would lead to incorrect proportions. To assess if the predicted difference is significant requires knowledge of the accuracy of these predictions. In Section 5.7 I evaluate experimental testing of some model predictions, but to test all combinations was not feasible. An alternative is to assess the stability of these predictions to further perturbation. This is difficult to assess in for all combinations, as would be required in this case, as testing the sensitivity to the combination therapy to further perturbation will take a prohibitively long time to compute. Increasing the number of perturbations to combine increases the time to run the VMCAI analysis non-linearly, enough to be prohibitive even going to 3 perturbations of the network in all combinations. However, more limited assessment of the sensitivity of the model can be made, which I discuss in Section 5.6.2.

Those interactions between treatments which the model predicts can be examined further to find the best candidates to test experimentally. There are three main categories of combination therapies that are of interest:

1. Independent Combinations: Treatments which are effective as monotherapies and display the same or improved effectiveness when combined

2. Enhanced Combinations: Treatments where an effective monotherapy is combined with a drug which is ineffective alone and shows improved effectiveness on combination

3. Cancelling Combinations: Treatments which are effective alone but ineffective when combined

Combining two treatments which are independently effective when used alone is best for preventing resistance, as this increases the chance that two independent mutations are required for a cell to counter these drugs, and this is much less likely to occur in a tumour of typical size [45]. However, the best test of the model comes from cases in which two treatments combine to have a greater effect than either individually. This may be an additive effect in the case of treatments which were relatively effective alone, or true synergy if they are ineffective as monotherapies. Therefore I focus on finding these enhancing combinations for testing in the next Section.

In order to find the best combinations to increase therapeutic effect, I consider the relative change in the phenotypes when going from one to two drugs.

5.4.2 Combinations of Effective Monotherapies

In order to find the most effective combinations, I compare the effect of a monotherapy to that of a combination therapy. To do this I take the effect of a monotherapy applied alone, and find the difference in the phenotype of interest when a second treatment is applied. I display this difference in the heat maps below (Figures 5.10 to 5.15), with a decrease being red and an increase being blue. The y-axis shows the first treatment, and the x-axis the treatment which is being added on top of this. In order to prevent the heat maps showing cases where the first treatment is counter-productive, and then is rescued by a second treatments, and so showing a misleading large "improvement", I ensure that the first therapy applied is always one that improved the phenotype of interest when applied alone. I also remove cases where this combination would increase apoptosis for the healthy cells are greater than half the maximum apoptosis (i.e. greater than 3). These are shown as grey numberless cells. Inhibition of PHD2 or VHL cause high apoptosis with any partner other than each other, and are removed as this otherwise prevents clustering of the heat maps. So, for example, in Figure 5.10, the y-axis shows treatments that have some effect alone, but the red cluster in the lower left shows

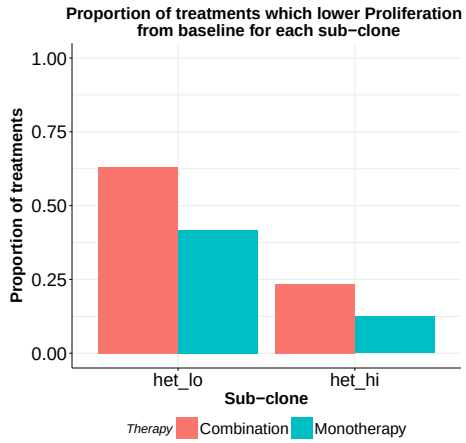

(a) Proportion of treatments which lower proliferation below baseline for respective sub-clone in mono- and combination therapy

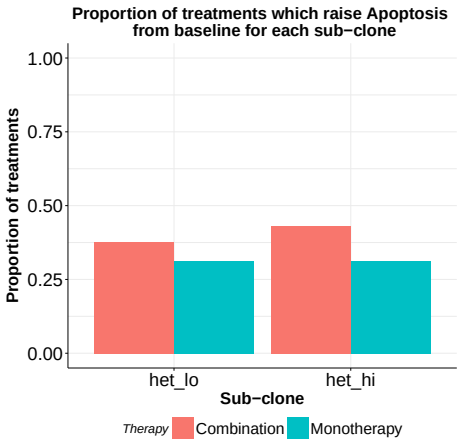

(b) Proportion of treatments which increase apoptosis above baseline for respective sub-clone in mono- and combination therapy

Fig. 5.9 Comparison of the proportion of all possible treatments which the model predicts are effective at moving the phenotypes in a direction beneficial for treatment in mono- and combination therapy, not counting those which increase apoptosis in healthy cells above 3. If the addition of a second mutation had no effect, then the proportion of effective treatments would be expected to be the same for mono- and combination therapy, so this illustrates the overall trend in the effect of interaction between mutations.

where there are partners that lower proliferation further. For the unfiltered analysis for all nodes, see Appendix B.5.

Cytostatic

Combinations which better lower proliferation in heterogeneous myc-low (red areas in Fig. 5.10) include combining both branches of the Ras pathway, with a greater improvement going from PI3K/Akt inhibition. Alternative partners for the MAPK pathway include COX2 inhibition, although the benefit is less as MAPK inhibition is more effective than PI3K inhibition to begin with. Conversely, the blue areas of the diagram show possible resistance mutations, such as PTEN and EZH2.

For heterogeneous myc-high (Fig. 5.11) there are fewer opportunities. However, this Figure shows that GSK3, PTEN or p53 inactivation raise proliferation when combined with some of the most effective monotherapies. This includes a monotherapy targeting myc or the Wnt1 pathway via Frizzled. This implies that they might be selected for as resistance mutations to these therapies.

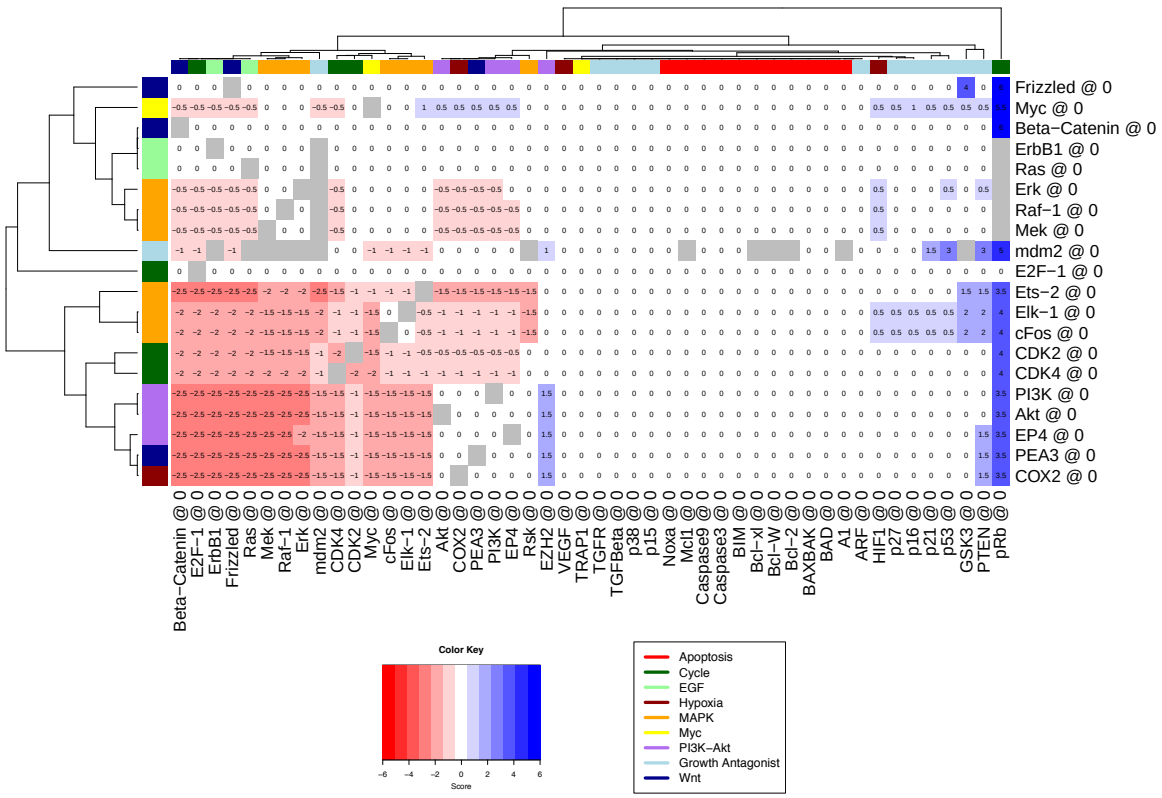

Fig. 5.10 Change in proliferation in the heterogeneous myc-low sub-clone when adding a second drug to a drug shown to be effective in monotherapy, compared to the effect of the first treatment applied alone, as predicted in Chapter 4. y-axis shows first drug, x-axis the drug which is added in combination. Grey boxes are combinations which are nonsensical (two different treatments of the same node), or cause apoptosis above 3 in the healthy cells. This identifies those combinations which create the greatest difference compared to monotherapy, as opposed to simply the most effective overall. Red indicates a drop in proliferation, and therefore a more cytostatic treatment.

Cytotoxic

Figure 5.12 shows combinations which raise apoptosis (blue areas) in the heterogeneous myc-low case. These include combining a Wnt1 pathway knock-out with inhibition of the Bcl-2 family proteins, or combining inhibition of any pair of Bcl-2 family proteins. Wnt1 pathway or COX2 inhibition, also combine well with perturbations of the MAPK pathway. However, MAPK pathway inhibition reduces the effectiveness of Bcl-2 family inhibition by lowering myc activity and so reducing the apoptotic signalling from this node. Increasing hypoxia by blocking VEGF is also effective.

Note that there are also combinations which counteract one another. For example, combining ErbB1 and Frizzled inhibition lowers apoptosis in this sub-clone in comparison to inhibition of either node alone. Therefore we cannot simply combine treatments which are

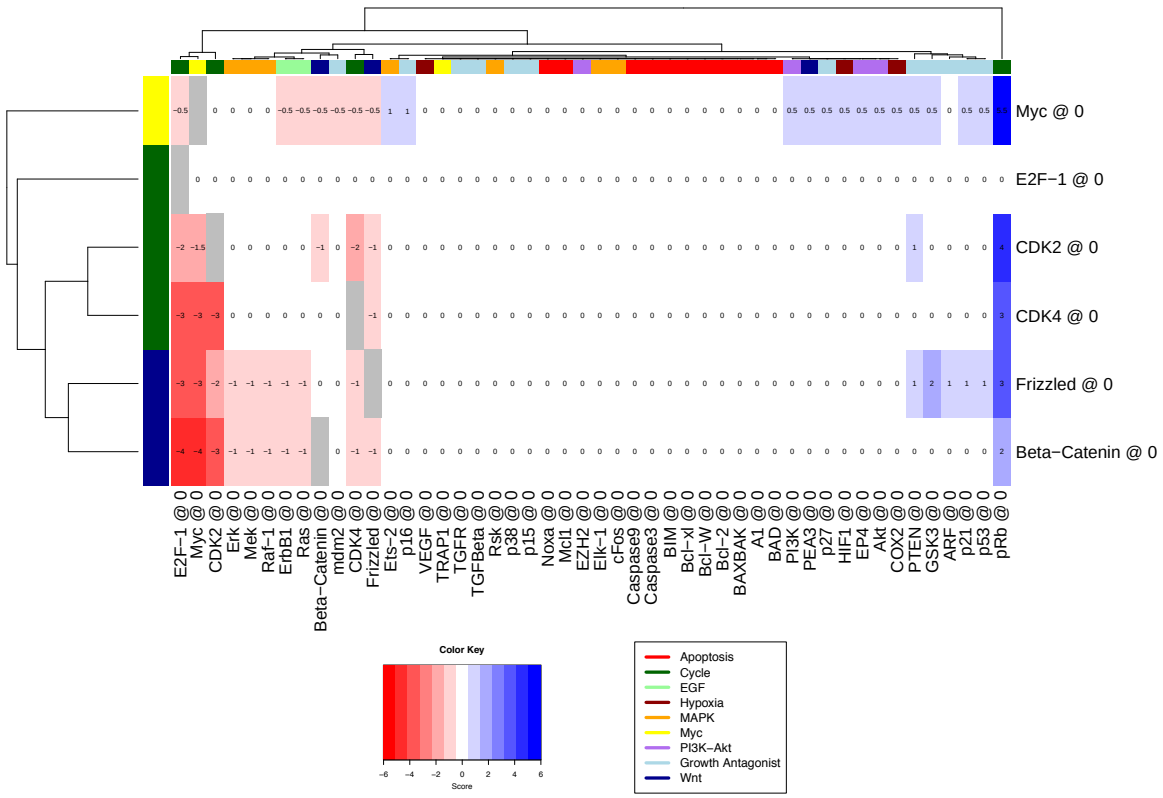

Fig. 5.11 Change in proliferation in the heterogeneous myc-high sub-clone when adding a second drug to a drug shown to be effective in monotherapy, compared to the effect of the first treatment applied alone, as predicted in Chapter 4. y-axis shows first drug, x-axis the drug which is added in combination. Grey boxes are combinations which are nonsensical (two different treatments of the same node), or cause apoptosis above 3 in the healthy cells. This identifies those combinations which create the greatest difference compared to monotherapy, as opposed to simply the most effective overall. Red indicates a drop in proliferation, and therefore a more cytostatic treatment.

effective when applied alone, highlighting the necessity of a mechanistic understanding of the interactions between treatments, as provided by my model.

In the heterogeneous myc-high case (Fig. 5.13)the MAPK pathway appears more effective, but this is because these perturbations are already maximally effective in the single perturbation case, as shown by the rows containing these genes being only 0 or below. Otherwise the best improvements are seen by combining two of the Bcl-2 family proteins or by deregulating BIM by inhibiting E2F-1 or EZH2.

Broadly Effective Combinations

Given that many monotherapies are more effective against one sub-clone than another, I searched for which combinations can best supplement these to attack the tumour as a whole.

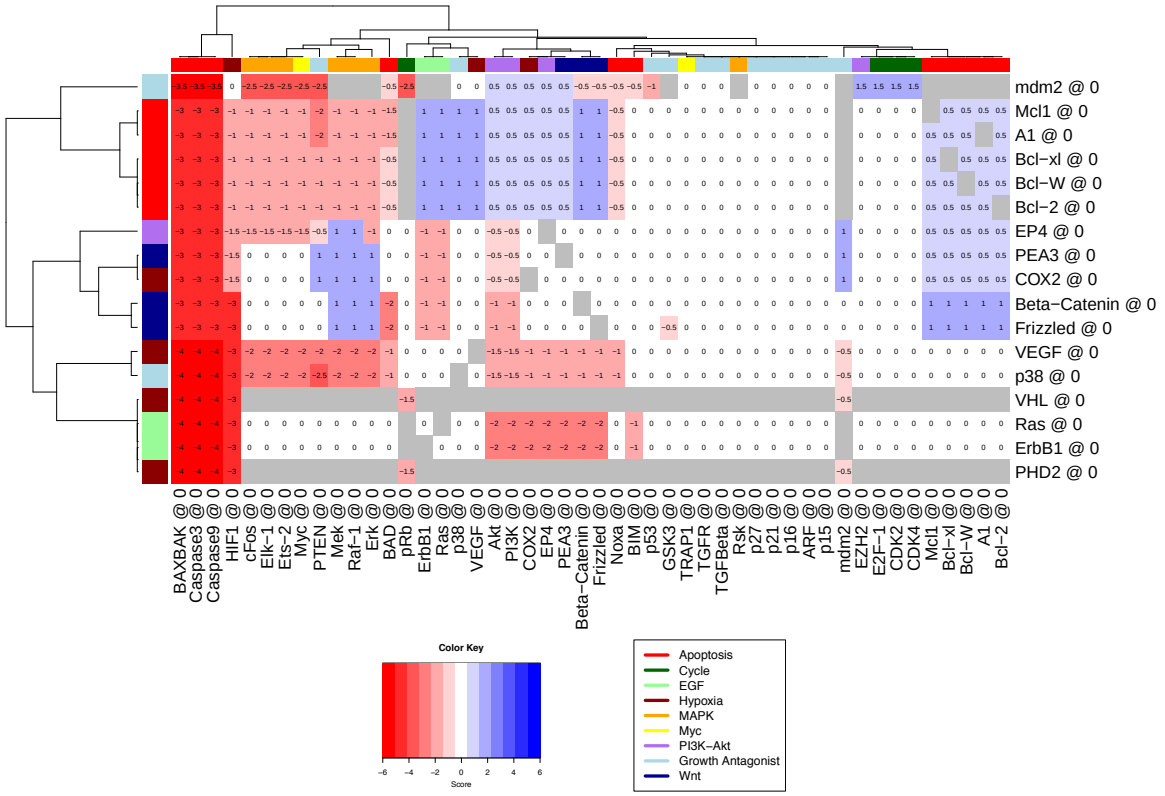

Fig. 5.12 Change in apoptosis when adding a second drug to a drug shown to be effective in monotherapy in the heterogeneous myc-low sub-clone, compared to the effect of the first treatment applied alone, as predicted in Chapter 4. y-axis shows first drug, x-axis the drug which is added in combination. Grey boxes are combinations which are nonsensical (two different treatments of the same node), or cause apoptosis above 3 in the healthy cells. This identifies those combinations which create the greatest difference compared to monotherapy, as opposed to simply the most effective overall. Blue indicates an increase in apoptosis, and therefore a more cytotoxic treatment.

To find these, I repeat the same analysis, but comparing the average of the phenotype across both sub-clones, before and after the addition of a second drug.

For proliferation, Figure 5.14 shows that a mutation in the COX2, MAPK and PI3K pathways combine well with one another.

Figure 5.15 further shows that for apoptosis the largest change is going from COX2 pathway inhibition alone to a combination with MAPK pathway inhibition. Given that MAPK inhibition also showed a high degree of specificity as a monotherapy, this combination demonstrates how a specific therapy can be made broad with a combination. Furthermore, this combination is more effective against the heterogeneous myc-low case than either of these treatments applied alone. I describe this interaction further in Section 5.6. mdm2 inhibition is also effective at increasing the effect on both sub-clones for many monotherapies.

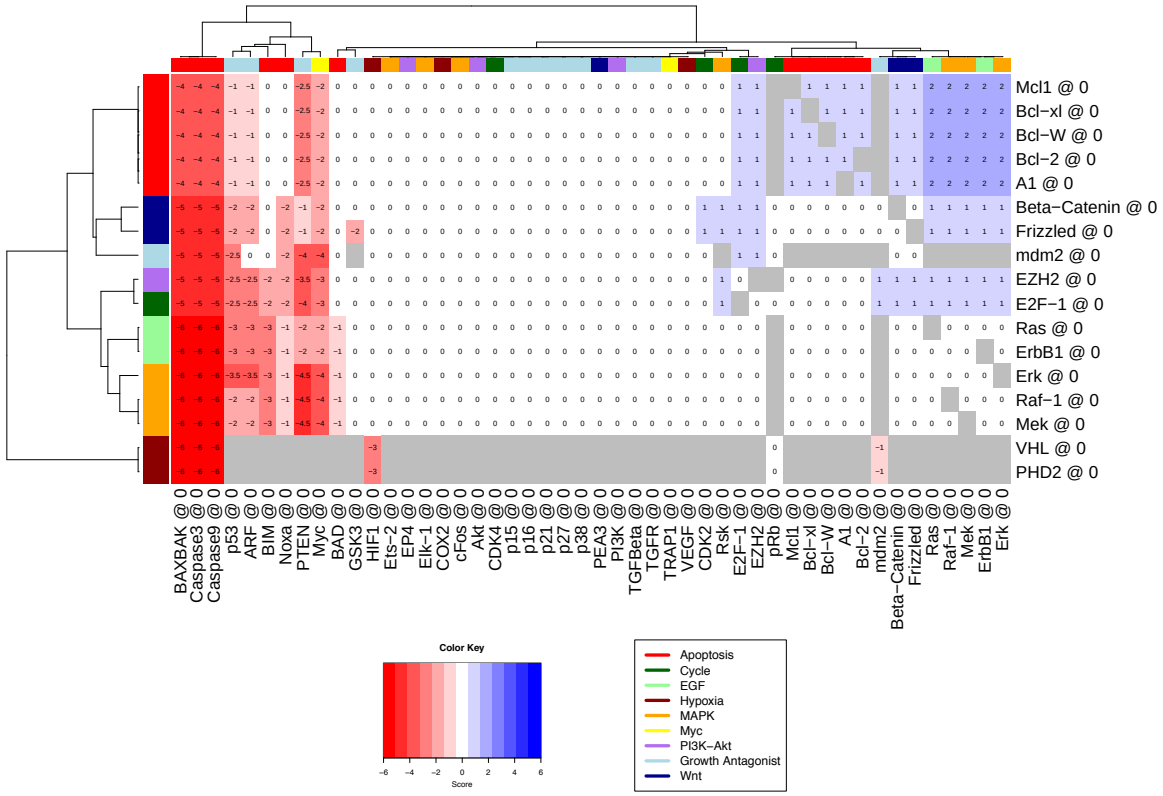

Fig. 5.13 Change in apoptosis when adding a second drug to a drug shown to be effective in monotherapy in the heterogeneous myc-high sub-clone, compared to the effect of the first treatment applied alone, as predicted in Chapter 4. y-axis shows first drug, x-axis the drug which is added in combination. Grey boxes are combinations which are nonsensical (two different treatments of the same node), or cause apoptosis above 3 in the healthy cells. This identifies those combinations which create the greatest difference compared to monotherapy, as opposed to simply the most effective overall. Blue indicates an increase in apoptosis, and therefore a more cytotoxic treatment.

As posited in Section 5.4.1, the model predicts combinations which are independently effective and can be combined to improve their effectiveness in combination, such as combining members of the Bcl-2 family in the heterogeneous myc-low sub-clone (Figure 5.12). In the same sub-clone, there are also cases of a treatment which is ineffective alone, but which enhances the effect of another treatment when applied in combination. For example, Mek is ineffective at promoting apoptosis in myc-low when used alone, but enhances the effect of COX2 inhibition. Finally, there are combinations which inhibit one another in this sub-clone despite being effective alone, such as ErbB1 and Frizzled. These examples demonstrate the power of the model to classify combination therapies into these three groups, each of which has different implications for treatment. Those which counteract one another should

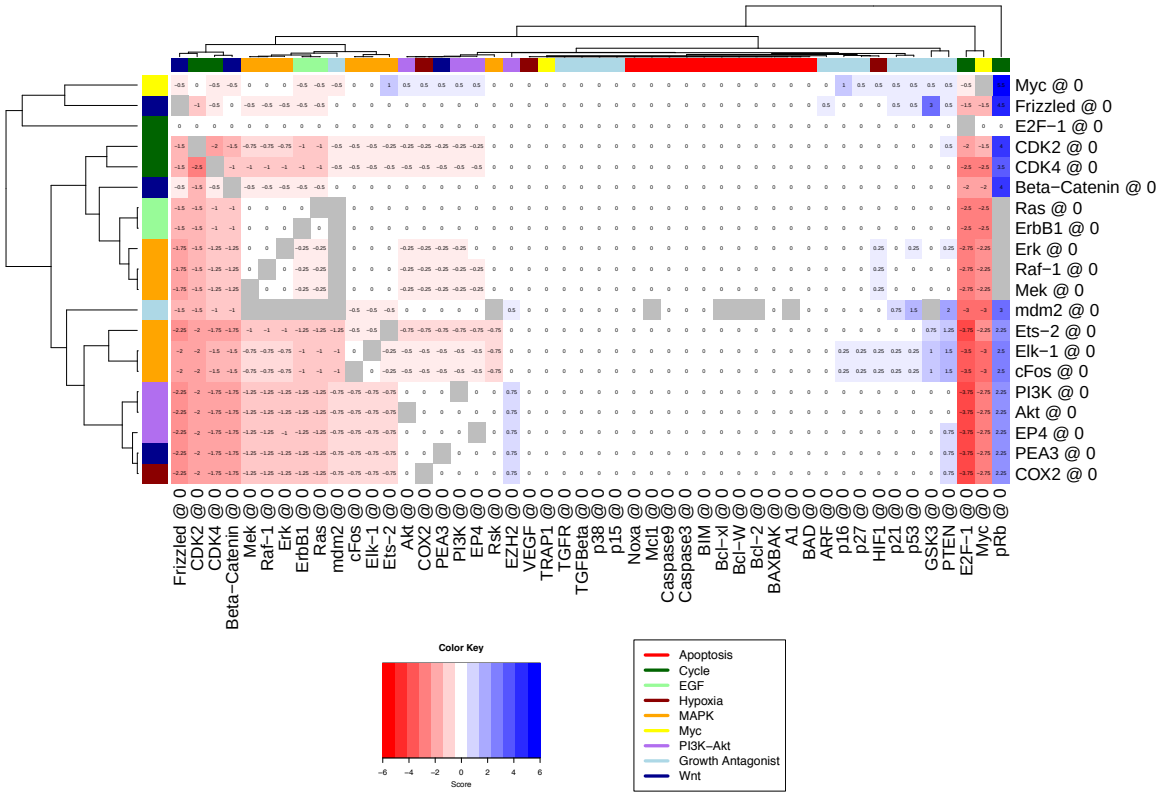

Fig. 5.14 Change in mean proliferation across heterogeneous sub-clones when adding a second drug to a drug shown to be effective in monotherapy, compared to the effect of the first treatment applied alone, as predicted in Chapter 4. y-axis shows first drug, x-axis the drug which is added in combination. Grey boxes are combinations which are nonsensical (two different treatments of the same node), or cause apoptosis above 3 in the healthy cells. This identifies those combinations which create the greatest difference across both sub-clones compared to monotherapy, as opposed to simply the most effective overall. Red indicates a drop in proliferation, and therefore a more cytostatic treatment.

be avoided, but those in which one target only enhances the other may be easier to acquire resistance to than those in which each drug is effective individually.

5.5 Pathways involved in effective treatments

As in Chapter 4 I further compared the proportion of successful treatments which involved different pathways (see Figures 5.16 and 5.17). Here I define successful as those which lower proliferation below the baseline for the respective sub-clone, or apoptosis above the baseline. I look only at those which improved over the monotherapy case to avoid describing the effects of a monotherapy and a neutral passenger. I also include a breakdown by absolute number of successful treatments in Appendix Figure B.30.

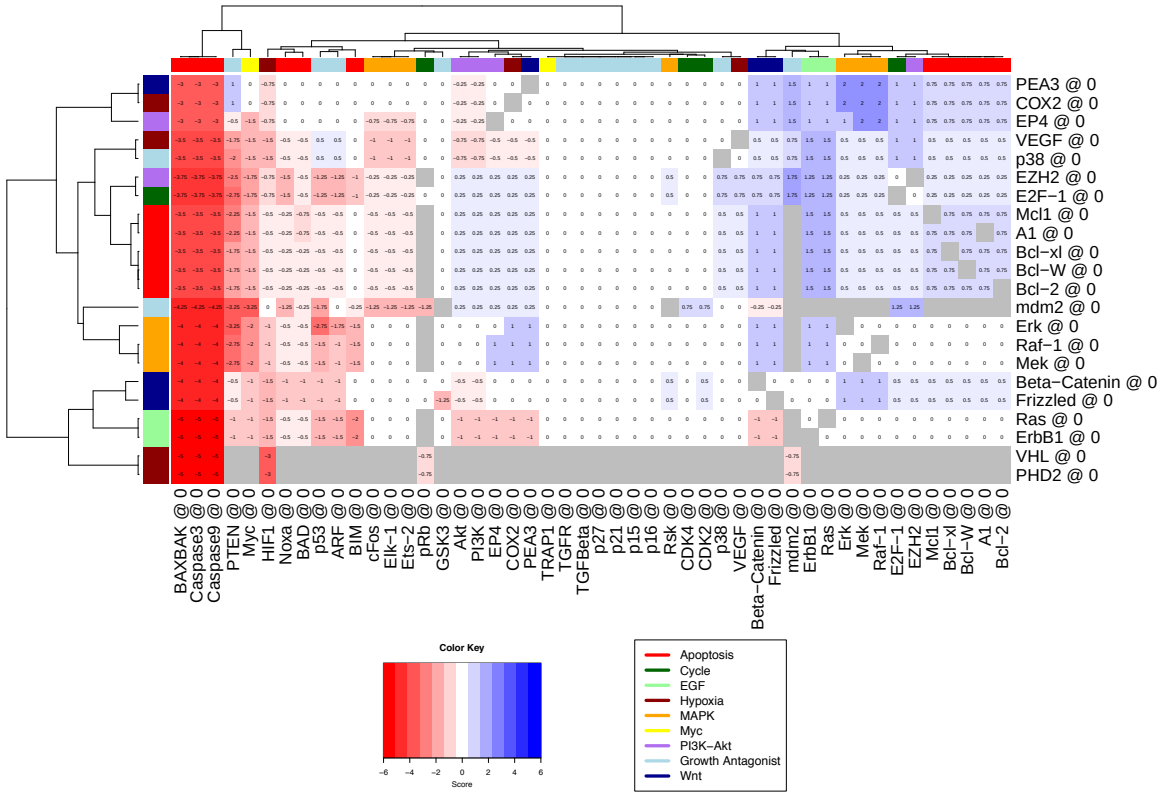

Fig. 5.15 Change in mean apoptosis across heterogeneous sub-clones when adding a second drug to a drug shown to be effective in monotherapy, compared to the effect of the first treatment applied alone, as predicted in Chapter 4. y-axis shows first drug, x-axis the drug which is added in combination. Grey boxes are combinations which are nonsensical (two different treatments of the same node), or cause apoptosis above 3 in the healthy cells. This identifies those combinations which create the greatest difference compared to monotherapy across both sub-clones, as opposed to simply the most effective overall. Blue indicates an increase in apoptosis, and therefore a more cytotoxic treatment.

5.5.1 Cytostatic

In the case of cytostatic therapies (see Fig. 5.16) there is more diversity in which pathways can be used to lower proliferation in the heterogeneous myc-high sub-clone. For example, MAPK is represented here but not in the monotherapy case (Figure 4.6a). As shown in Figure 5.11, this is because combining a MAPK inhibition with a treatment which was effective alone can improve the effect. For example, Raf-1 inhibition has no effect on myc-high proliferation alone (Figure 4.2), but lowers proliferation further when combined with β-catenin than β-catenin alone. This further demonstrates the possibilities of using combination therapy to find new uses for treatments which would not be effective alone.

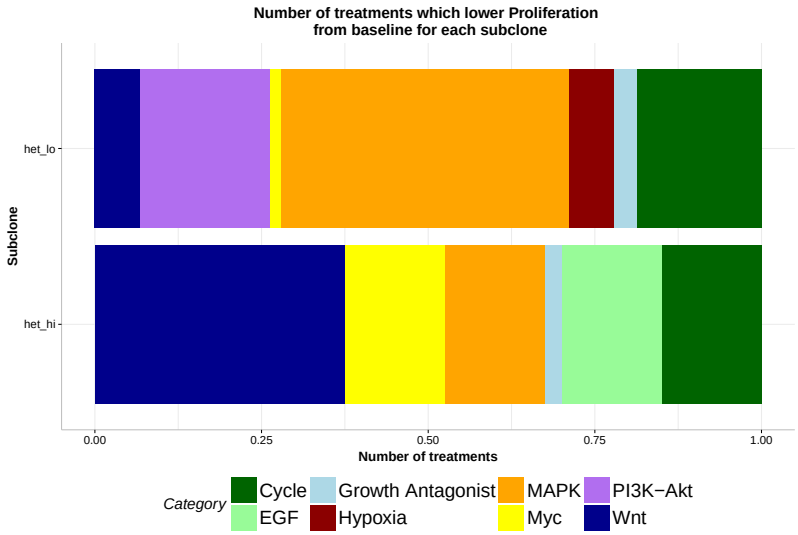

Fig. 5.16 Proportion of cytostatic treatments which lower proliferation below the baseline for the respective sub-clone involving different pathways. This includes only those which improved over the monotherapy case to avoid describing the effects of a monotherapy and a neutral passenger.

5.5.2 Cytotoxic

For cytotoxic therapies, shown in Figure 5.17, inhibition of the PI3K-Akt pathway is more effective in the myc-low case. This is likely as this was less effective than other monotherapies, and so there are more ways to improve this treatment. Similar to the cytostatic case, there is more variety in the number of pathways which affect the myc-low sub-clone when treatments are combined than when applied alone (Figure 4.6b). For example, Mek inhibition can be combined with COX2 inhibition to affect the myc-low sub-clone more than either alone, whereas Mek inhibition is ineffective against this sub-clone when applied as a monotherapy. This again shows how combination treatments provide more options.

5.6 Predictions of best treatments

In order to best treat heterogeneous breast cancers, of the kind modelled *in vivo* by my collaborators, I seek to find the most effective therapies for two strategies. Firstly, I investigated which treatments are best able to attack one sub-clone of the tumour preferentially. This has a number of possible benefits for cancer treatments, such as reducing the number of cells under pressure to acquire resistance and so reducing the number of opportunities for a resistance mutation to emerge before elimination of the tumour [45]. In Chapter 4.5 I identify the best monotherapies for attacking one tumour specifically. It is clear that for cytostatic

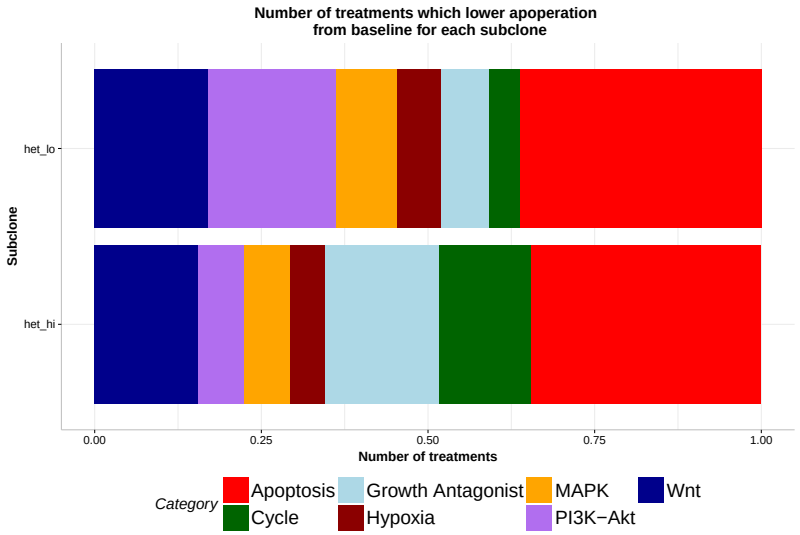

Fig. 5.17 Proportion of cytotoxic treatments which raise apoptosis above the baseline for the respective sub-clone involving different pathways. This includes only those which improved over the monotherapy case to avoid describing the effects of a monotherapy and a neutral passenger.

therapies, Ras and the MAPK pathway are good targets to inhibit to target the myc-low sub-clone. Considering the cytotoxic effects of therapies, one can also target the myc-low sub-clone by disrupting the pathways allowing the tumour to compensate for its hypoxic microenvironment by targeting VEGF or p38.

Cytotoxic therapies allow the targeting of the heterogeneous myc-high sub-clone directly. Disrupting the survival factor upon which this sub-clone depends, namely the Wnt1 pathway, is highly effective and specific. This is to be expected from the experiments of my collaborators, where the paracrine Wnt1 signalling from the myc-low sub-clone to the myc-high sub-clone was shown to be key to these cells increased survival and proliferation in heterogeneous compared to purely myc-high tumours. This is also consistent with evidence that Wnt1 acts as survival factor in breast tissue in general [438] and against myc-induced apoptosis in particular [194, 500]. However, disrupting this pathway directly might encourage resistance in this pathway, which may disrupt myc suppression of Wnt1, and so reduce the need for cooperation in the tumour. This therefore encourages the tumour to evolve in manner that reduces future opportunities for treatments, and should be avoided if possible. Even more effective, and less prone to reduce reliance on Wnt1, is to disrupt the MAPK pathway. This shows very high apoptosis in the myc-high clone alone.

As the myc-high clone is the most proliferative, yet the smaller component of the tumour, it is likely the preferred target for any specific therapy. Further, while it is possible to slow

the growth of the myc-low clone, which has a supportive effect on the myc-high clone through Wnt1 signalling, it does not appear to be easy, according to my computational model, to preferentially eliminate it. A more slowly proliferating myc-low clone would likely constrain the myc-high tumour, but Wnt1 signalling would persist and so continue to support it, allowing it to grow, evolve and possibly metastasise. Further, my collaborators observed that in long-term studies of pure-myc high tumour, some cells would eventually lose MycER^{T2} expression, and so revert to a myc-low sub-clone. This removes the suppression of Wnt1 by myc in these cells (see Chapter 2.5.1). This means that the tumour develops into a heterogeneous form, and growth increases. Attacking the myc-low clone preferentially can be avoided by a similar mechanism. Moreover, eliminating the myc-low clone entirely would not necessarily cause the myc-high clone to regress. While these cells have a very high level of apoptosis, when my collaborators attempted to create tumours of only these cells, they are able to use Wnt1 from the stroma to survive. This was far less effective than when cooperating with myc-low cells however, but suggests that targeting the myc-low sub-clone specifically may not be sufficient to cause the myc-high clone to collapse entirely. Conversely, without the myc-high clone, myc-low clones are highly necrotic, and would likely regress. Nevertheless, clinically there may be advantages to prioritising cytostatic over cytotoxic treatments, as it is likely that there are fewer side effects [480] and less pressure to evade the treatment mechanism and develop resistance, making these treatments effective for longer. For the case of proving the usefulness of the model, differences in apoptosis are likely to be clearer and are therefore prioritised.

Therefore, we focus on demonstrating specificity in the myc-high clone, and choose to use Mek inhibition to do this. This is already a well developed method for treating melanoma [133] and so well understood drugs are already available, such as Trametinib [374], making it a good candidate for a successful demonstration of model predictions *in vivo*.

Combination therapy presents the possibility of increasing the specificity of treatment, but in practice I find few combinations which have a higher difference in effect on the myc-high sub-clone compared to the myc-low, while having as much of an effect on myc-high, as MAPK inhibition alone. Those that do exist are primarily cases where the increase in specificity is by the addition of a second mutation which protects the myc-low sub-clone, such as combining β-catenin inhibition with HIF1α inhibition. I also do not find any combinations that increase the myc-low specificity of p38 or VEGF inhibition. However, the model does offer the opportunity to demonstrate the possibility of synergistic combinations, as well as how to maximise the effects on both sub-clones for drugs that are ineffective as a broad monotherapy, i.e. one which is effective against both sub-clones.

I look for treatments which are effective against both sub-clones when combined. As with monotherapy, when looking for candidates for testing by my collaborators, I prioritised cytotoxic effects. As there are no such therapies which are more effective against the myc-low than the myc-high sub-clones when applied singly, it is not as simple as to choose a pair of drugs where one is specific to each sub-clone. Instead, I searched for cases in which the combination increased the effectiveness in the myc-low case. As shown in Fig. 5.12 COX2, of slight effectiveness against myc-low alone, can be improved by combination with inhibition of MAPK, or of PTEN. PTEN is effective partly due to deregulation of myc, and has no effect on proliferation, whereas MAPK inhibition does not have the disadvantage. Therefore, this combination shows good effectiveness against both sub-clones, and also has a large difference compared to either applied alone to the myc-low sub-clone, demonstrating how combination therapy can enhance effects of two drugs beyond their monotherapy effects. Note that while the combination is the most effective way to use these drugs, both do have an effect alone, and so this would also decrease the chances of resistance emerging. This is because there are fewer single mutations that can block the effects of both drugs than if they were truly dependent upon one another.

Considered from the opposite perspective, as Mek is already as effective against myc-high as it can be, we can look for the best partners for it in myc-low and see that COX2 is among the best (see Fig. 5.15). Further, neither this combination, nor either inhibition alone, increases apoptosis in the healthy cells, making it a better tolerated treatment.

As both Mek and COX2 inhibition in the monotherapy case do not show a single fixed point of stability (see Fig. B.3 and B.4), I further analyse them with the BDD algorithm (see Section 2.1.10) to observe the exact stable states. These are shown in Appendix A.1.3. They show that the system has several loop stable states for these inhibitions. I take the mean of these over the loop as characteristic of the level of the phenotype. As there is no reason to believe any of these loops are any more likely than the others, I then take the mean value over the loops. This results in overall predictions of the mean level of proliferation and apoptosis shown in Table 5.1.

Proliferation is lower and apoptosis higher in the myc-low sub-clone with these two drugs in combination compared to either applied singly, making them an effective demonstration of the increased effects made possible by combination therapy.

Table 5.1 Comparison of the effects of Mek and COX2 inhibition applied singly or in combination. Cases in which there were bifurcations are given as the mean over the different attractors, to 3 significant figures, and full attractors are shown in Appendix A.1.3. Integers indicate a single fixed point attractor.

Sub-clone	Phenotype	COX2 at 0	Mek at 0	COX2 and Mek at 0
Heterogeneous myc-low	Proliferation	2.82	0.491	0
	Apoptosis	2.97	2.76	4
Heterogeneous myc-high	Proliferation	5	5	5
	Apoptosis	3	6	6

5.6.1 Mechanism of Action of Mek and COX2 inhibition

It is possible to induce apoptosis in a sub-clone either by increasing pro-apoptotic signalling, or decreasing anti-apoptotic signalling. The level of apoptotic signalling in each sub-clone in the heterogeneous case differs before treatments begins, and so a treatment can target a specific sub-clone by exacerbating these existing differences. The myc-high sub-clone has more pro-apoptotic signalling from myc, which must be balanced by anti-apoptotic signalling, such as from Akt, as well as suppression of BIM, specifically by Erk and EZH2. In the heterogeneous case this also comes from Wnt1 signalling by the myc-low sub-clone. This blocks p53-dependent apoptosis by blocking ARF. Therefore suppression of Wnt signalling would cause the myc-high sub-clone to revert to the highly apoptotic behaviour observed in the pure case. However, to attack Wnt directly would likely encourage the tumour to evolve to be independent of the myc-low sub-clone, so the resistant version would be worse.

Myc also signals along the pro-apoptotic BIM pathway, which is blocked by MAPK signalling. Interference with this pathway primarily affects the myc-high sub-clone by reducing this anti-apoptotic signalling. Therefore MAPK inhibition is effective against the myc-high sub-clone, but does not increase pro-apoptotic signalling in general. This means that the myc-low clone, which has a lower background of pro-apoptotic signalling, is relatively immune. Also, Mek inhibition lowers myc signalling, but this cannot happen in the myc-high clone as MycER^{T2} is constitutively expressed, whereas this lowers proliferation but also myc-induced apoptotic signalling in the myc-low sub-clone. As such, Mek inhibition has a cytotoxic effect which is specific to the myc-high sub-clone.

COX2 inhibition alone raises pro-apoptotic signalling by reducing VEGF production, but this is partially compensated for by the lower hypoxia pressure in the heterogeneous case. Furthermore, the initial characterisation of the tumours was inconclusive as to whether VEGF was the sole factor driving angiogenesis in this system (see Chapter 3.5). COX2 also signals

via PI3K-Akt due to the action of prostaglandin E2 (PGE2). This suppresses apoptosis via Akt. As such inhibiting COX2 increases pro-apoptotic signalling by increasing hypoxia and reducing anti-apoptotic signalling by reducing PGE2 production. In combination with Mek inhibition, this also activates BIM and HIF1α in the myc-low sub-clone, and so increases apoptosis in this sub-clone above the level induced by either treatments alone. Thus these combine to create a treatment broadly effective across both sub-clones.

5.6.2 Sensitivity of Predictions to Assumptions and Parameters

The model will be sensitive to the initial state of the network. This consists of the values the nodes take at time 0, as defined in Chapter 2.1.2, not the mutations applied by fixing the target functions to a constant value for all time-points. As detailed in Chapter 2.1.8, the results of the VMCAI algorithm algorithm are valid for all initial states. However, the results partition into two groups, those with a single, fixed point attractor, and those where there is either a loop or a bifurcation. In the latter case, the level of nodes will not be constant, and in the case of a bifurcation, there will be different attractors for different initial states. This latter group is shown in Appendix B.2 and Appendix B.4 by those cases where the range to which the value of proliferation or apoptosis can be restricted is greater than 0. Which attractor a network stabilises in will then be dependent on the initial state, unlike the case for a fixed point attractor.

In the case of the predictions in Table 5.1, I further investigated these attractors, and as shown in Appendix A.1.3, there are multiple attractors for single therapy in the heterogeneous myc-low sub-clone. As, which attractor is chosen will depend on the initial state, I assume that each attractor is equally likely, as all initial states are equally likely, however, if there are unknown mutations or environmental factors which skew the distribution of states of other nodes, then these may prejudice certain attractors over others. These predictions are therefore more sensitive to unknown factors than the fixed-point attractors, which hold regardless of the initial state.

Another way to test the sensitivity of the conclusions, is to see how they change under perturbation of the parameters. However, the parameters of the model are encoded in the topology, and the target functions, with the latter being amenable to change in a variety of ways which are not easily combined. For example, one could change the overall weight of a node, or the weighting of different terms within the target function in different combinations, or instead of taking the maximum of two inputs, take the average and so forth. In the analysis presented in Chapter 4 and Chapter 5, I have assessed the effect of coarse changes

to the network topology by knocking out certain nodes. It is possible to see what the single treatments are sensitive to by seeing which mutations cause a change in their behaviour along a row or column of the heat-maps shown in Section 5.2. This shows that the the predictions about monotherapy are sensitive to other mutations as follows.

The effect of COX2 inhibition on myc-low proliferation can be enhanced by blocking the Wnt1 or Raf-1/Mek/Erk pathways, but also countered by mutation of GSK3, PTEN or pRb (see Figure 5.2). However in myc-high the result is less sensitive to other mutations, and does not effect other perturbations except to block the effects of PTEN inhibition (Fig. 5.3).

For Mek inhibition, the effect on proliferation in myc-low is insensitive to other mutations, only being countered by pRb (Fig. 5.2). In myc-high it is enhanced by mdm2, PHD2, or VHL inhibition, and enhances the effect of Frizzled inhibition (Fig. 5.3).

In the case of apoptosis, COX2 inhibition in myc-low can be countered by inhibition of the Caspases or BAXBAK complex, but is can be enhanced by the Ras/Mek/Erk pathway, mutations in the Bcl-2 family of proteins, inhibition of PTEN, VHL or PHD2 (Fig. 5.5). In myc-high, the pattern is similar, but the effects of another enhancing inhibition are more pronounced (Fig. 5.6).

The cytotoxic effect of Mek inhibition in myc-low is similarly dependent on functioning Caspases and BAXBAK, and can be enhanced by mutation in ErbB1, Ras, mdm2, PHD2, VHL, and the Wnt and COX2 pathways. In myc-high, the effect is insensitive to further perturbations, only being strongly blocked by inhibition of BIM, myc, Frizzled, or the Caspases and BAXBAK. As these mutations may be present but not able to be measured in a system to which this model is applied, they increase the sensitivity of these predictions to unknown factors.

5.7 Experimental Validation of Model Predictions

In order to test the predictions of the model of which therapies would be specific to one tumour sub-clone, and broadly effective against both sub-clones, my collaborators applied a Mek inhibitor, PD-0325901 (PD), and a COX2 inhibitor, Licofelone (Lico), to heterogeneous tumours both singly and in combination.

5.7.1 Combination Therapy Promotes Tumour Regression

Tumour growth under each treatment regime was measured over the course of treatment, over four days, labelled by the number of days since the beginning of treatment. Growth relative

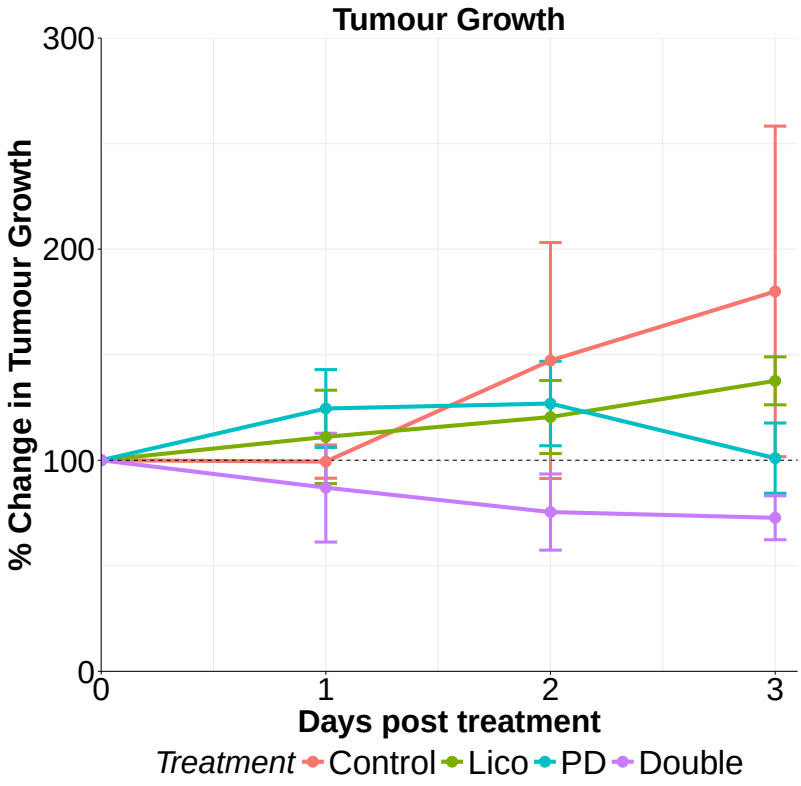

Fig. 5.18 Tumour growth in mice with heterogeneous tumours under no treatment (Control, green), Mek inhibition (PD, pink), COX2 inhibition (Lico, orange) and combination therapy of Mek and COX2 inhibition (Lico+PD, red).
Tumour growth under each treatment regime was measured over the course of treatment. Tumour volume is calculated assuming tumour is ellipsoid and is as deep as it is wide. Treatment was applied over four days, labelled by the number of days since the beginning of treatment. Growth relative to the size of the tumours at the beginning of treatment, Day 0, is presented as percentage change. Treatment was only continued for this short time period, because as an initial experiment, the dose used was high to gauge if the drugs were at all effective, and to continue any longer would be to subject the mice to unnecessary harm. There were five mice treated with both drugs, and four for each other case, due to loss of mice during the experiment. Further, in the case of the mice treated with combination therapy, one was unable to be assayed for proliferation and apoptosis. Error bars are standard deviation. Raw data, and mean and standard deviation for each treatment regime on each day, are shown in Appendix C.1.

to the size of the tumours at the beginning of treatment, Day 0, is presented in 5.18. This suggests that the growth of tumours was inhibited by each monotherapy, but most effectively by combination therapy, however, I test the significance of the differences with control below. COX2 inhibition (Lico) appeared the least effective, which would be as expected as the model predicted it would have a lower cytotoxic effect, although better spread across the sub-clones, as well as being a less effective cytostatic drug. Mean tumour growth under this treatment was lower than Control, but did not fall below the original size of the tumours, so there was no suggestion of regression. Mek inhibition (PD) appeared more effective, and showed the tumour a downward trend at the third day post treatment, but the mean size was not below the initial tumour size at the beginning of treatment. The combination therapy (PD+Lico) appeared the most effective, with immediate tumour regression, as expected given our prediction of high apoptosis in both sub-clones.

In order to assess whether the observed differences were significant, I fitted a linear mixed effects model, also known as a repeated measures ANOVA, as described in Chapter 2.5.4. This incorporates the data over all time points, and took into account the effect of making repeated measurements of the same mouse, and is robust to the unequal sample sizes. I describe fitting this model in Appendix Table C.2. This showed that there were significant interactions with PD and Lico with time and each other (see Appendix Table C.11). This indicates that both change the tumour volume over time. Interpretation of this interaction is complicated by the fact that I applied a non-linear transform to the data to control heteroscedasticity, and so is not an indication of synergy between these two drugs. This is more clear for the case of proliferation (see Section 5.4.2).

I also compared the pairwise difference between the growth curves, and found that the difference between the combination therapy and either of the monotherapies or the control, was significant (see Appendix Table C.12). However, there is no significant difference between the two treatments applied alone with one another, or with control. This is evident in the morphology of the tumours, in which the combination therapy reduces them to a mostly necrotic remnant (Fig. 5.19d), while the monotherapies still show some tumour tissue three days after the start of treatment. However, as part of the cell death was due to this necrosis, some of the tumour shrinkage is likely due to this as well. As necrosis was not explicitly included in the network model, the tumour shrinkage observed may be in excess of that predicted by the model.

Nevertheless, my collaborators also measured proliferation and apoptosis specifically, with IdU and CC3 staining specifically, see Sections 5.7.2 and 5.7.3. Further, the significant

difference between the combination therapy versus each single therapy matches the models prediction that this would be the most effective against both sub-clones.

5.7.2 Mek and COX2 inhibition applied alone are more Cytostatic in the Myc-Low than Myc-High sub-clone

To further analyse the predictions of the model, my collaborators quantified proliferation and apoptosis for the different treatment regimes in both sub-clones. Proliferation was measured using IdU staining (see Fig. 5.20 for representative examples of IdU immunohistochemistry). These, and CC3 staining below, were taken from four mice for each treatment, making 12 mice in total. A section of a tumour from each mouse was then quantified in 3 different areas. These were further quantified by looking at the percentage of red (IdU) stained nuclei. This is shown grouped according to sub-clone in Figure 5.21a and by treatment in Figure 5.21b. This suggests that in all cases, the mean cytostatic effect is stronger for the myc-low clone than the myc-high clone.

To assess the significance of these differences, I apply Welch's t-test, as described in Chapter 2.5.4. The full results are shown in Appendix C.3.2. The difference between sub-clones is significant in the case of PD-0325901 ($p = 0.0419$) and Licofelone ($p = 0.0133$), but not in the case of the Control or combination treatment. This is as predicted by my model for the single drug therapies, which showed it was very difficult to significantly lower proliferation in the myc-high clone with a single drug or even a pair of drugs, other than by targeting cell cycle machinery directly. However, the model also predicted a difference for the combination therapy, but this was not significant. This discrepancy may be that in the case of combination therapy, the cooperation between the sub-clones begins to collapse, leading to lower proliferation for the myc-high sub-clone, which I discuss further in Section 5.7.3.

Further, the mean proliferation after Mek inhibition by PD-0325901 is lower than COX2 inhibition by Licofelone, in the myc-low sub-clone. This is again, as predicted by the model (see Table 5.1). In order to assess this further, I conducted a two-factor ANOVA for the myc-low and the myc-high sub-clones. This showed that while there were significant differences between each treatment and control for the myc-low sub-clone, the difference between PD-0325901 and Licofelone treatment was not significant for the myc-low sub-clone (see Appendix Table C.16).

Unexpectedly, there was also an effect on proliferation in the myc-high clone, again, with the mean effect of combination therapy being more than Mek inhibition, which in turn is more

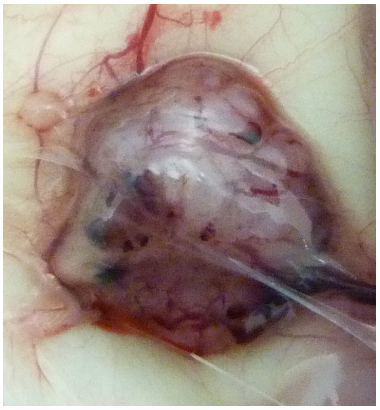

(a) Control

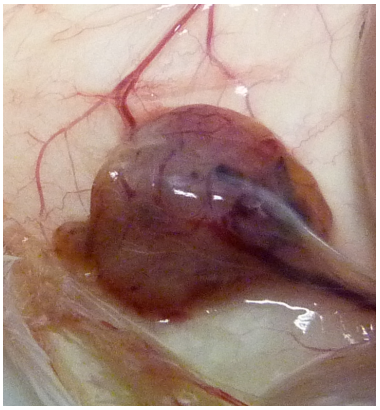

(b) Lico: tumour treated with COX2 inhibitor shows reduced tumour volume, with fewer dark regions indicative of cell death than with Mek inhibition

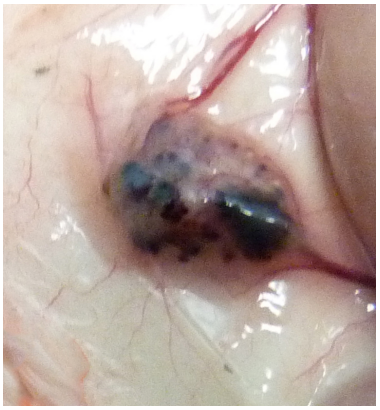

(c) PD: tumour treated with Mek inhibitor shows reduced tumour volume, as well as areas of cell death (dark regions)

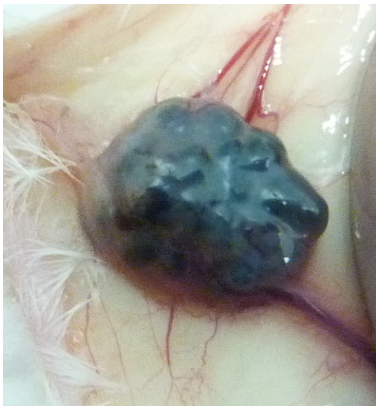

(d) Lico+PD: Combination of Mek and COX2 inhibitor shows the most cell death, with very few regions of intact tissue remaining. The tumour looks larger than the PD-0325901 treatment, but is mostly blood and necrosis.

Fig. 5.19 Comparison of the morphology of representative heterogeneous tumours under no treatment, monotherapy and combination therapy, at the end of treatment, showing the effect on tumour volume and amounts of cell death and necrosis. Quantification of the change in tumour size is shown in Figure 5.18. Proliferation and apoptosis are quantified from tumour sections, with representative histology shown in Figure 5.20 and Figure 5.23, and quantification in Figure 5.20 and Figure 5.22, respectively.

than COX2 inhibition. As above, I conducted an ANOVA, which showed that while the effect of PD-0325901 was significant, the effect of Licofelone was not, and that the interaction was also non-significant (see Appendix Table C.17 and C.18). That PD-0325901 is unexpectedly effective on the myc-high sub-clone may suggest that the model over-estimates the strength of myc-driven proliferation, but this matched well with what was observed in the pure myc-low and myc-high tumours. Another reason for this underestimation may be that the model takes initial conditions for the healthy heterogeneous tumours, and predicts how treatment will change the behaviour of the sub-clones under those conditions. However, if as in this case, one sub-clone is slowed in proliferation, it cannot support the other sub-clone to the same degree, and so these external conditions change. Thus this drop in proliferation in the myc-high clone may be partly due to lower Wnt1 from the myc-low sub-clone, which is being directly slowed by the treatment. I discuss this further, and how future work on the model may improve its ability to predict changes in the cooperation between the sub-clones in Chapter 7.3.3.

5.7.3 Mek and COX2 inhibition both have cytotoxic effects against both sub-clones

Apoptosis was measured by staining for Cleaved-Caspase 3, as shown in Figure 5.23. Figure 5.22 shows quantification of the effect of treatment both singly and in combination, compared to control, grouped by sub-clone (Fig. 5.22a) or by treatment (Fig. 5.22b), on apoptosis. Apoptosis is measured by the percentage of Cleaved Caspase-3 (CC3) positive pixels in tumour immunohistochemistry, where sub-clones where identified by GFP staining of a consecutive section. Overall tumour growth by volume is shown in Figure 5.18 and representative images of tumours in Figure 5.19.

My model predicted that the Mek inhibitor would have a larger effect on the myc-high clone than on the myc-low when applied singly. Figure 5.22b shows that, as the model predicted, the trend amongst the mice is that the Mek inhibitor has a larger mean effect on the myc-high clone than the myc-low, and Figure 5.22a shows that this treatment has the least effect on the myc-low clone, other than no treatment at all. Indeed, it is only slightly higher than the Control. Conversely, the COX2 inhibition has a similar effect on both sub-clones, and is less than the effect of Mek inhibition. However, the differences are less pronounced than in the case for proliferation. Applying Welch's t-test shows that the differences between myc-low and myc-high sub-clones is not significant in any treatment regime (see Appendix Table C.14), contrary to the predictions of the model.

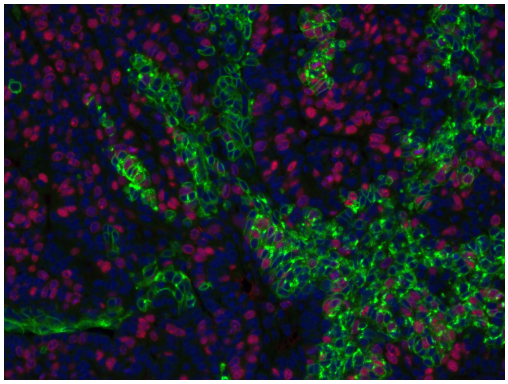

(a) Control: Proliferation is present throughout the tumour in both the myc-high and myc-low sub-clones.

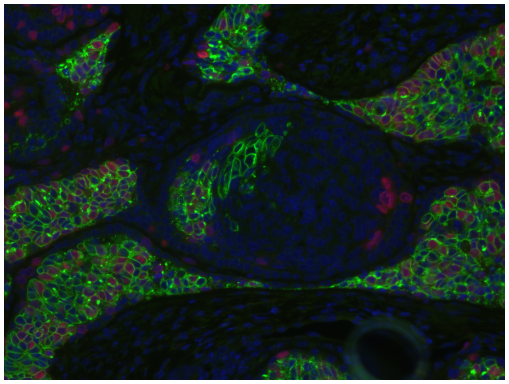

(b) Lico: Proliferation decreases across both sub-clones, but still present in both, such as the large red area in the centre-right.

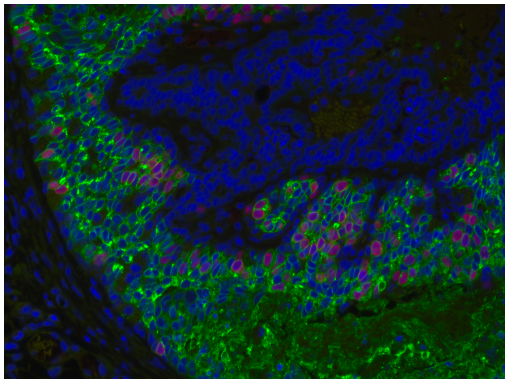

(c) PD: Very little proliferation in the myc-low regions, as predicted, but remains in the myc-high.

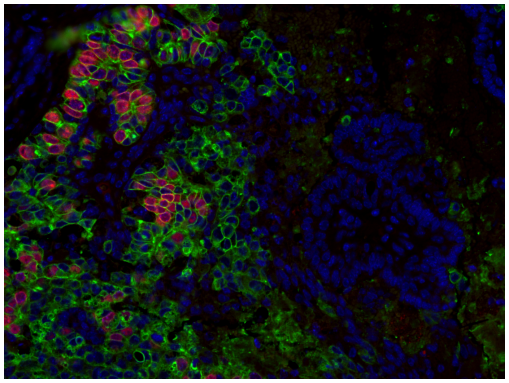

(d) Lico+PD: Proliferation is strongly suppressed relative to control, but the myc-high cells continue to grow.

Fig. 5.20 Representative examples of IdU staining for proliferation (red). Increased numbers of red stained tumour cells indicates higher proliferation. Green stain indicates myc-high cells, uncoloured cells are myc-low or stroma. Myc-high cells are detected with a GFP antibody, not endogenous GFP used for the FACS sorting (see Chapter 2.5.1). Original RFP and GFP are inactivated during fixing process, and so do not interfere with IdU staining. Stains are of tumour samples taken on Day 3 post-treatment, at the end of treatment. Quantification for proliferation is shown in Figure 5.21

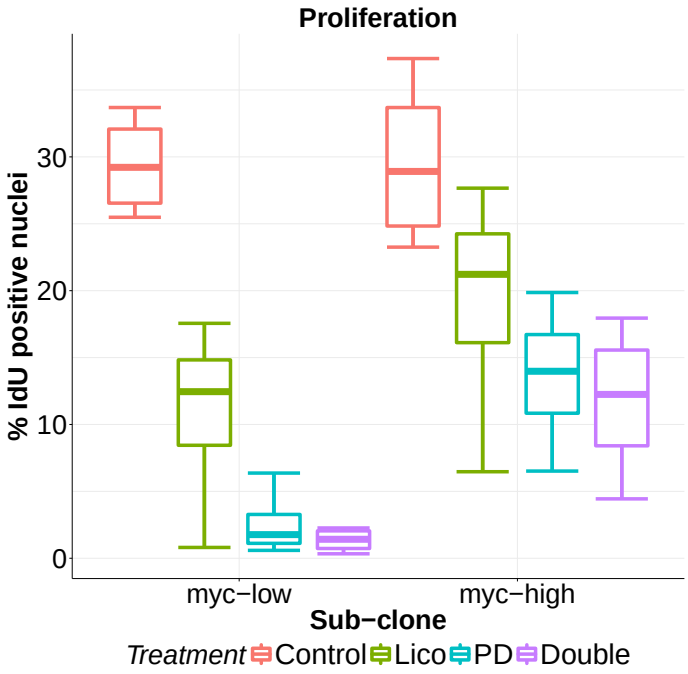

(a) Grouped by sub-clone.

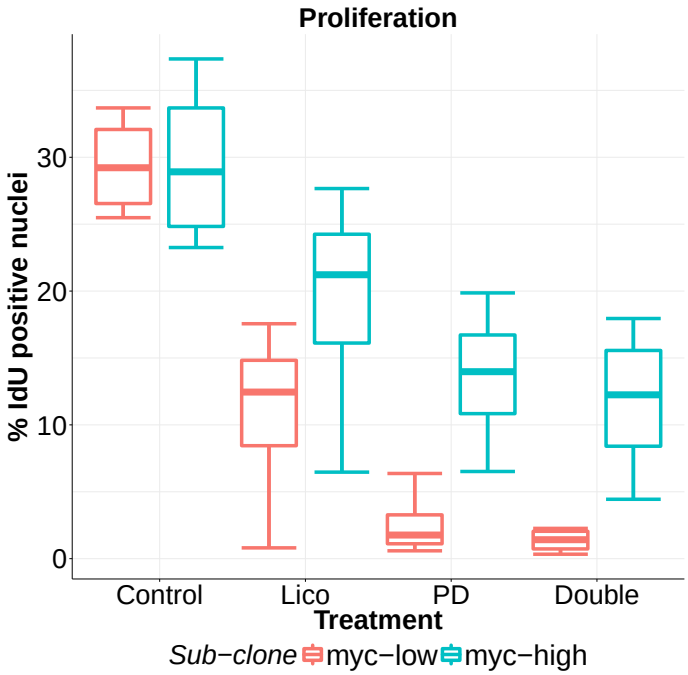

(b) Grouped by drug applied.

Fig. 5.21 Quantification of IdU staining for different treatments and control. Outliers (circles) are cases which are more than 1.5 times the interquartile range from the first or third quartile. Each treatment was replicated in four mice, so each box represents 4 replicates, and both sub-clones are measured in the same tumour, staining was performed on the last day of treatment as this could only be performed on tumour sections. Data, their means and standard deviations, shown in Appendix C.1. Statistical analysis is detailed in Appendix C.3 and C.4 and discussed in Section 5.7.2.

.

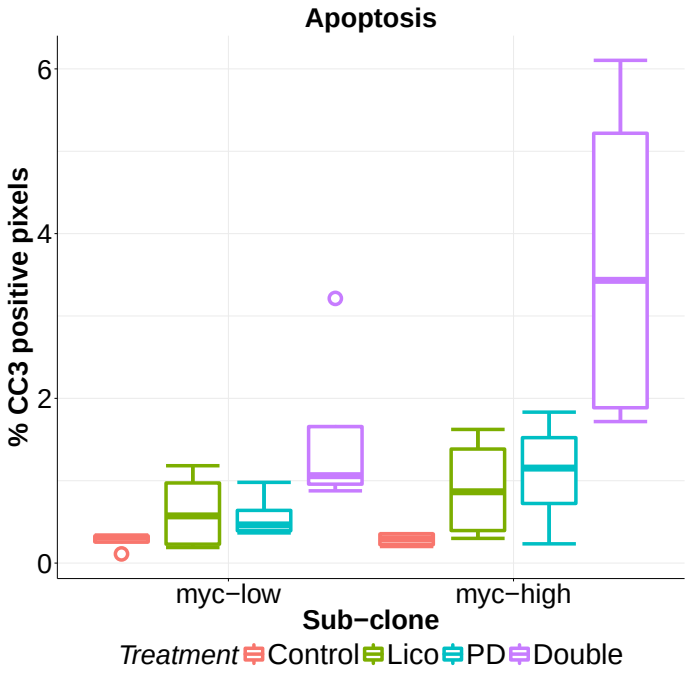

(a) Grouped by sub-clone.

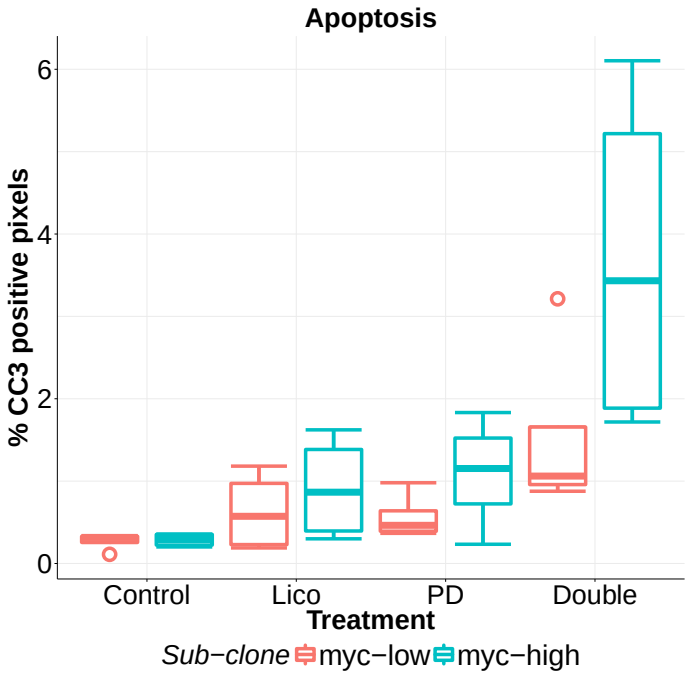

(b) Grouped by drug applied.

Fig. 5.22 Quantification of CC3 staining for different treatments and control. Outliers (circles) are cases which are more than 1.5 times the interquartile range from the first or third quartile. Each treatment was replicated in four mice, so each box represents 4 replicates, and both sub-clones are measured in the same tumour, staining performed on the last day of treatment as this could only be performed on tumour sections. Data, means and standard deviations, are shown in Appendix C.1. Statistical analysis is detailed in Appendix C.3 and C.5 and discussed in Section 5.7.3.

Unexpectedly, the mean apoptosis for the myc-high clone is relatively similar for COX2 and Mek inhibition, suggesting either that COX2 inhibition is more effective, or Mek inhibition is less effective than expected. This is confirmed by ANOVA analysis, which shows that both Mek and COX2 inhibition are have a significant effect against both the myc-low and myc-high sub-clones (see Appendix Table C.20 and C.22 respectively), where the model predicted that Mek alone should be ineffective against the myc-low sub-clone. Similarly, while the growth curves for these tumours (Fig. 5.18) suggest that Mek inhibition is more effective overall, despite being less effective against the myc-low tumour, there was no significant difference between the single treatments (Appendix Table C.12). This may be due to the fact that while the model distinguishes between the sub-clones, it does so using different initial conditions. This means they must be run separately, and so the effect on COX2 against VEGF is only taken into account for one sub-clone, not both, and so may have had more of an effect on hypoxia than expected. Similarly, it may be that that the combination therapy would also reduce the cooperation between sub-clones. For example, the myc-high clone would receive less Wnt1. Further, we focus on the stable state of the model, whereas effects on angiogenesis are likely to change as the tumour grows. So this could be improved by adding more detail temporally to the model.

5.7.4 Synergy in Combination Therapy

As shown in Figure 5.18 and Appendix Table C.12, combination therapy was more effective than applying either drug singly.

In order to investigate this further, I conducted a two-factor ANOVA for both sub-clones for both proliferation and apoptosis (shown in Appendix C.4 and C.5 respectively). The factors were the presence or absence of Mek or COX2 inhibition. Specifically, I investigated whether there was a significant interaction between the two drugs applied, which would be an indication of synergy beyond a merely additive effect.

In the case of proliferation there was a significant interaction in the myc-low sub-clone (see Appendix Table C.15) but not in the case of the myc-high clone (see Appendix Table C.17). This is in line with the predictions of the model, which suggested that there would be a greater effect in combination in the myc-low sub-clone, but no such benefit in the myc-high sub-clone.

In terms of apoptosis, the model further predicts that a combination of Mek and COX2 inhibition will be more effective than inhibiting either alone.

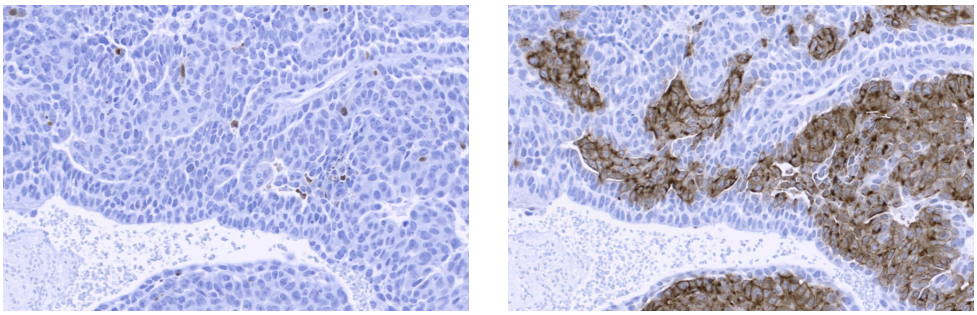

CC3 GFP

(a) Control: Some apoptosis in both sub-clones without treatment

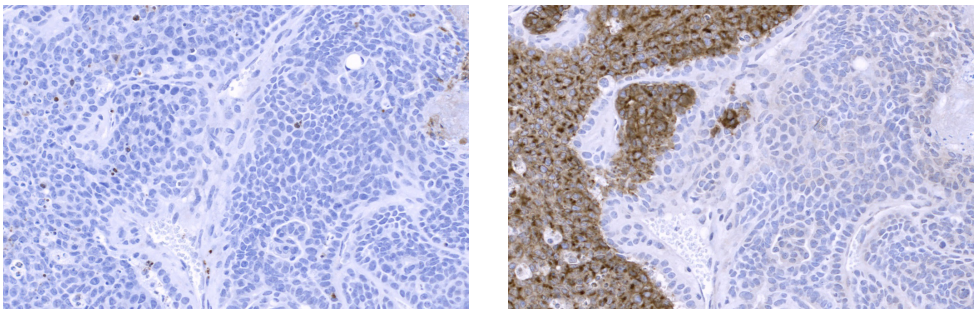

CC3 GFP

(b) Lico: Increase in apoptosis across both sub-clones

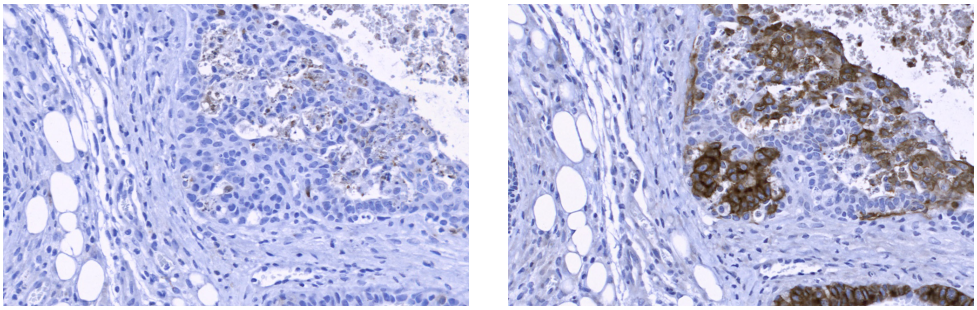

CC3 GFP

(c) PD: Increase in apoptosis, primarily in myc-high

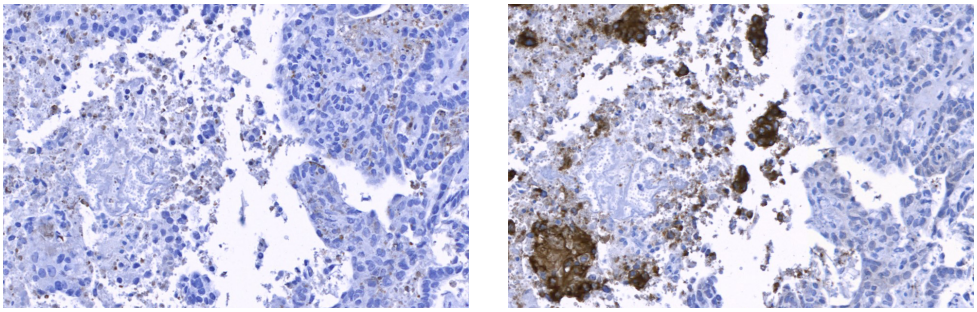

CC3 GFP

(d) Lico+PD: High apoptosis in both sub-clones

Fig. 5.23 Representative examples of tumour histochemistry for Cleaved-Caspase 3 (left, CC3), indicating apoptosis, and GFP antibody (right), indicating myc-high. Stains are of tumour samples taken on Day 3 post-treatment, at the end of treatment. Apoptosis, as measured by CC3, in areas of clonal intermingling is quantified in Figure 5.22.

However, ANOVA for apoptosis showed no significant interaction in either sub-clone (see Appendix Table C.19 and C.21). Nevertheless, in this case a log_{10} transform had been applied in order to correct for heteroscedasticity, which may have masked the effect of interaction, and so this is inconclusive.

In order to prove true synergy, rather than a cooperative effect, it would be better to find a combination of treatments in which one partner was wholly ineffective, but this would have yielded fewer insights into the system for the available funding for experiments. The model did predict maximum apoptosis for the myc-high sub-clone for Mek inhibition alone, whereas experimentally it could go yet higher in the combination case. This suggests that the sensitivity may need to be adjusted to make better use of the whole range of the granularity for apoptosis.

5.7.5 Summary of Model Validation

The model predicted (Table 5.1) that there would be a greater effect on proliferation in the myc-low sub-clone than the myc-high sub-clone. This difference was observed in the mean proliferation for all cases (Fig. 5.21), but the difference was significant only in the case of the monotherapies, not for the combination therapy (Appendix Table C.13).

In the case of apoptosis, the prediction was the reverse, that the myc-high clone would be more affected. While this trend was again observed (Fig. 5.22), none of these differences were significant (Appendix Table C.14).

Within sub-clones, for proliferation, the predictions were that the combination therapy would be more effective than the monotherapies in myc-low, but equally effective in myc-high. Figure 5.21 shows that the mean proliferation conforms to this, and ANOVA showed that while there was a significant interaction effect in myc-low (Appendix Table C.15), there was not in myc-high (Appendix Table C.17). However, Mek inhibition alone is effective in the myc-high sub-clone which is unexpected (Appendix Table C.18).

In apoptosis, it is predicted that the combination is more effective than either single treatment, but there is not significant interaction according to the ANOVA (Appendix Table C.19). However, both treatments have significant effects, which is as expected (Appendix Table C.20). Finally, for myc-high both treatments make a significant difference (Appendix Table C.22), with no significant interaction, as expected (Appendix Table C.21). However, as these ANOVA were applied following a transform, there may be an interaction which the transform hides.

The combined effect on tumour growth shows a significant difference when compared to either treatment alone, or control (Appendix Table C.12).

Overall, the increased effect of the combination therapy was recapitulated in the growth and proliferation data, with the latter indicating an interaction effect. The predictions for proliferation were generally in line with what the model predicted, although the effect of Mek in the myc-high sub-clone was more than expected. However, for apoptosis, while the treatments both had an effect, the predicted differences were in general insignificant. Therefore, overall the model shows an ability to find effective single and combination therapies, but the predictions of the fine grained differences between the level of effect of the single therapies and between the sub-clones is not validated, particularly in the case of apoptosis.

These differences may, in part, be due to the inability of the model to simulate the change in cooperation between sub-clones as the treatment continues. This may reduce some of the differences between sub-clones as the cooperative relationship breaks down. I discuss how the model can be improved to better simulate this in Chapter 7.3.3.

5.8 Conclusions

In this Chapter I demonstrate how the model can be used to classify the effects of combination therapies, identifying those which enhance one another, as well as those which are counter-productive. The model predicts that the most specific monotherapy is Mek inhibition, being cytotoxic to the myc-high clone preferentially. Supplementing this with COX2, which is less effective against either sub-clone than Mek inhibition is against the myc-high, is predicted to broaden the effect of the therapy against both sub-clones by improving the effect against the myc-low sub-clone to a higher level of apoptosis than either monotherapy. Through application of these therapies to an *in vivo* model of heterogeneous basal breast cancer in mice, my collaborators provide evidence that both treatments are effective, and have an enhanced effect in combination. However, the predicted differences within and between treatments, especially for the monotherapies, were not significant. As such the model requires further refinement and testing.

Chapter 6

Reconstructing Tumour Evolution

6.1 Introduction

Cancers must acquire a range of abilities in order to out-compete healthy tissue and survive in the new environment they carve out as they grow [190]. These hallmarks of cancer are acquired through mutations of the genome of these cells, as well as epigenetic changes. However, there are many safe-guards which have evolved to present such changes from being favourable to the cell, and so prevent the emergence of cancer. Cell autonomous safeguards include protection against DNA damage, to prevent oncogenic mutations in the first place [226]. In addition, tumour suppressor genes sense changes due to such mutations, and trigger growth arrest and apoptosis in response [35]. Non-cell autonomous protections include the immune system, which helps to prevent cancer by protecting against pathogens which induce abnormal cell growth [442]. It also actively detects and eliminates cells which express tumour specific antigens [429]. The possibility of enhancing this latter behaviour is now being explored as a possible method of treatment [386].

These safeguards mean that there is a degree of constraint on which mutations can lead to enough benefit for the cancer for them to be observed. The mutation rate in humans implies there must be many more occasions where mutations result in no change or adverse change for the development of cancer, and so go unobserved, given how rare, comparatively, the emergence of cancer is. In this Chapter, I use the model to explore how changes in proliferation and apoptosis due to mutations constrain the order in which oncogenic mutations are acquired. I first aim to show whether such constraints exist, or if any oncogene can emerge at any time. Second, if such constraints do exist, how do they vary for different combinations of oncogenes, and can this lead to better understanding of breast cancer development for diagnosis, prognosis and treatment?

In order to explore this, I applied the mutations from common cancer cell lines in all possible combinations, drawn from Hollestelle et al. [207] (see Table 6.1). These cell lines were originally derived from primary tumours, indicating that the final combination of these mutations should be tumour promoting. In addition, in all cases, there was a background of EGF and Wnt signalling (at activity 1) to simulate the supportive signalling from surrounding tissues as it would be *in vivo*. This is as opposed to the *in vitro* background used in Chapter 3.4.2 as I am modelling the initial development of these tumours. At each combination of mutations, I find all attractors for the network that are reachable with that mutation from any of the previous states using the BDD algorithm (see Chapter 2.1.10). As shown in Chapter 2.4, this produces a plot of the attractors of the network at every stage of the evolution of the tumour (Fig. 2.7). I then score these by the level of proliferation and apoptosis, taking the mean value in the case of loops. This allows me to show the optimum path through the powerset to minimise apoptosis and maximise proliferation as early as possible. This is then the optimal order, for the evolution of the tumour, in which these mutations can be acquired.

Table 6.1 Mutations found in different cell lines

Cell Line	Source	Mutations										
		ErbB1	ErbB2	p53	PI3K	Ras	Raf-1	Myc	ARF	p16	pRb	PTEN
SKBR3	Hollestelle et al. [207]		2	0				2				
BT549	Hollestelle et al. [207]			0							0	0
SUM159PT	Hollestelle et al. [207]			0	0	0						
BT20	Hollestelle et al. [207]	2		0	2				0	0		

6.2 SKBR3 demonstrates tightly constrained path to cancer

SKBR3, which is an ER- basal epithelial cell line [208], shows how the order of mutation can be strongly constrained by apoptosis (Fig. 6.1). This diagram shows the effect on proliferation (blue) and apoptosis (red) at nodes representing different combinations of mutations. From the top of the powerset, representing the healthy cell, I apply more mutations one at a time. Each layer represents one more mutation, and the arrows are labelled with which mutation is acquired at each stage. These mutations are cumulative, so each point represents the phenotype of the cell when it has acquired all the mutations on the arrows leading to that point. The diagram converges at the bottom when all mutations seen in the cell line have been acquired. This then shows that, for example, if the first mutation is myc or ErbB2, then apoptosis rises, whereas if the first mutation acquired is p53 it stays the same (see Fig. 6.1b).

There is only one path from the healthy cell to the full set of mutations exhibited by the cell line that minimises apoptosis. This path is to acquire a p53 inactivation mutation first, followed by activation of ErbB2 and then finally myc. This shows that these phenotypes are sufficient to constrain the order of mutations due to selective pressures, and may help explain the ordering observed experimentally. This is due to the strong triggering of apoptosis by myc, mainly via p53, perhaps as a fail-safe for its potent proliferative effects [136]. This means that it is most tumour promoting dependent on several earlier mutations removing these safeguards, and I predict this encourages late mutation, as observed [68]. Proliferation is a weaker constraint for this cell line, with mutations which lead to high proliferation triggering higher apoptosis due to the coupling of the cell cycle to tumour suppression via p53, until this is mitigated by other mutations (Fig. 6.1a). Apoptosis remains lower if p53 mutates early, and so is to be expected if I assume that the order of mutations is more strongly constrained by negative selection, which, in my model, is due to apoptosis, than positive selection by proliferation. This contradicts some models of tumour development in other cancers [142, 216] but is consistent with experimental data for breast cancer [497, 401, 343] where p53 is often mutated early. In many cases of breast cancer myc mutations occur comparatively late [68]. This may be, in part, due to this particular path to breast cancer being tightly constrained, compared to the other cell lines I studied (Section 6.3), as there is only one optimal order for these mutations to emerge.

ErbB2 (a.k.a HER2) has a more contextual effect. It increases apoptosis if it is the first mutation, but offers some protection from the downsides of c-myc activation through the PI3K pathway if mutated after c-myc and p53. This is consistent with the known cooperation

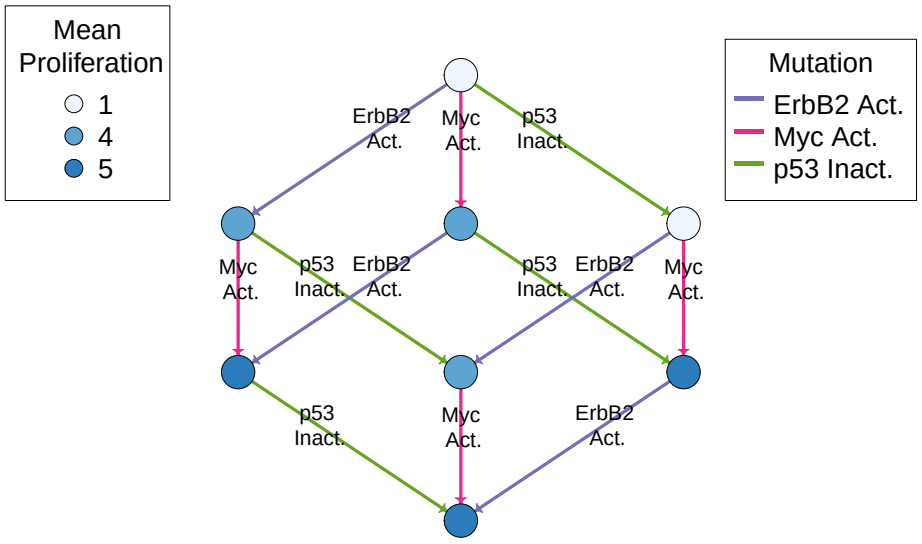

(a) The effect of mutations found in the SKBR3 cell line on proliferation

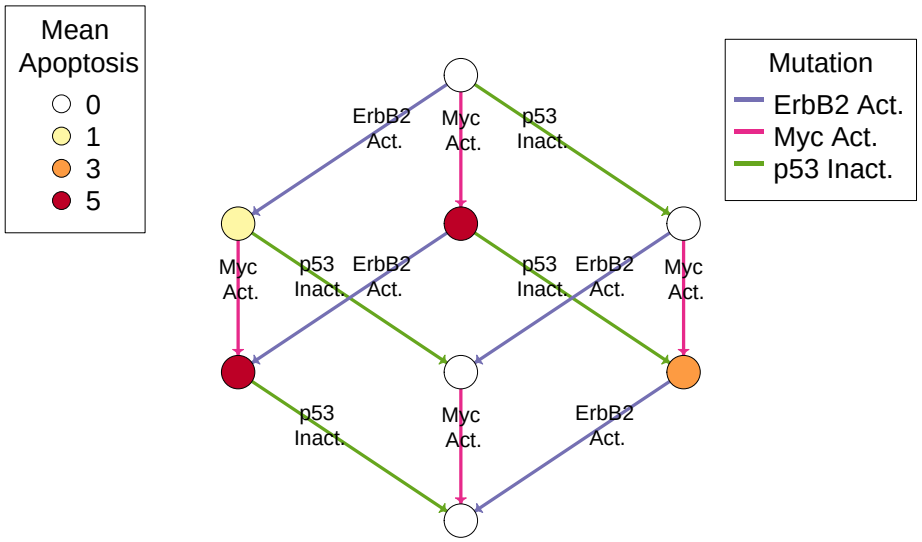

(b) The effect of mutations found in the SKBR3 cell line on Apoptosis

Fig. 6.1 How proliferation and apoptosis change as a tumour acquires the mutations seen in the SKBR3 cell line. The colour of the vertices corresponds to the level of proliferation (blue) and apoptosis (red). Edge colour and label corresponds to the mutation applied at each step, moving from top (healthy cell) to bottom (all mutations). Act. indicates and activatory mutation, and Inact. an inactivatory mutation, with nodes being set to take a constant value as detailed in Table 6.1.

between c-myc and Ras, which is downstream of ErbB2 [273] but suggests that the stage at which ErbB2 mutates depends on c-myc status. Such contextual behaviour will be important to map out as it will be a determinant of how tumours adapt to therapy.

6.3 Acquisition of mutations is constrained to varying degrees

While the mutations exhibited by the SKBR3 cell line can only be acquired optimally in a specific order, not all the combinations of mutations observed to produce viable cancer cell lines were so restrictive of tumour evolution. For example, SUM159PT [151] (Fig. 6.2) shows only 2 equally optimal paths to cancer, whereas BT549 shows a very loose ordering (Fig. 6.2). That there is such variance in the degree of constraint, even for phenotypically similar cell lines, implies some flexibility in the acquisition of mutations, but with underlying patterns. This may correlate with incidence of different combinations of mutations. I discuss this how this could be explored further in Chapter 7.4.2.

6.4 Difference in constraints from Proliferation and Apoptosis

While activation of tumour suppressor mechanisms places a strong negative selection pressure on tumour evolution, there must also be selection for increased proliferation. Strong constraints on oncogenes by apoptosis favour lineages in which c-myc, ErbB1 and ErbB2 mutate late. In the case of BT20 [276] however, there are many paths to cancer which are unconstrained by apoptosis (Fig. 6.3b). Nevertheless, there are still only a few optimal paths, and thus likely dominant clones, which can be taken to maximise proliferation without taking a hit from tumour suppressor mechanisms. Figure 6.3a shows that there are only two attractors of the model which maximise possible proliferation for this cell line after 3 mutations, without apoptosis, out of 10 possible attractors at this stage of evolution. This means there are only 4 of a possible 21 minimal apoptosis paths that lead to maximum proliferative benefit, showing how proliferation can place further constraints in addition to apoptosis.

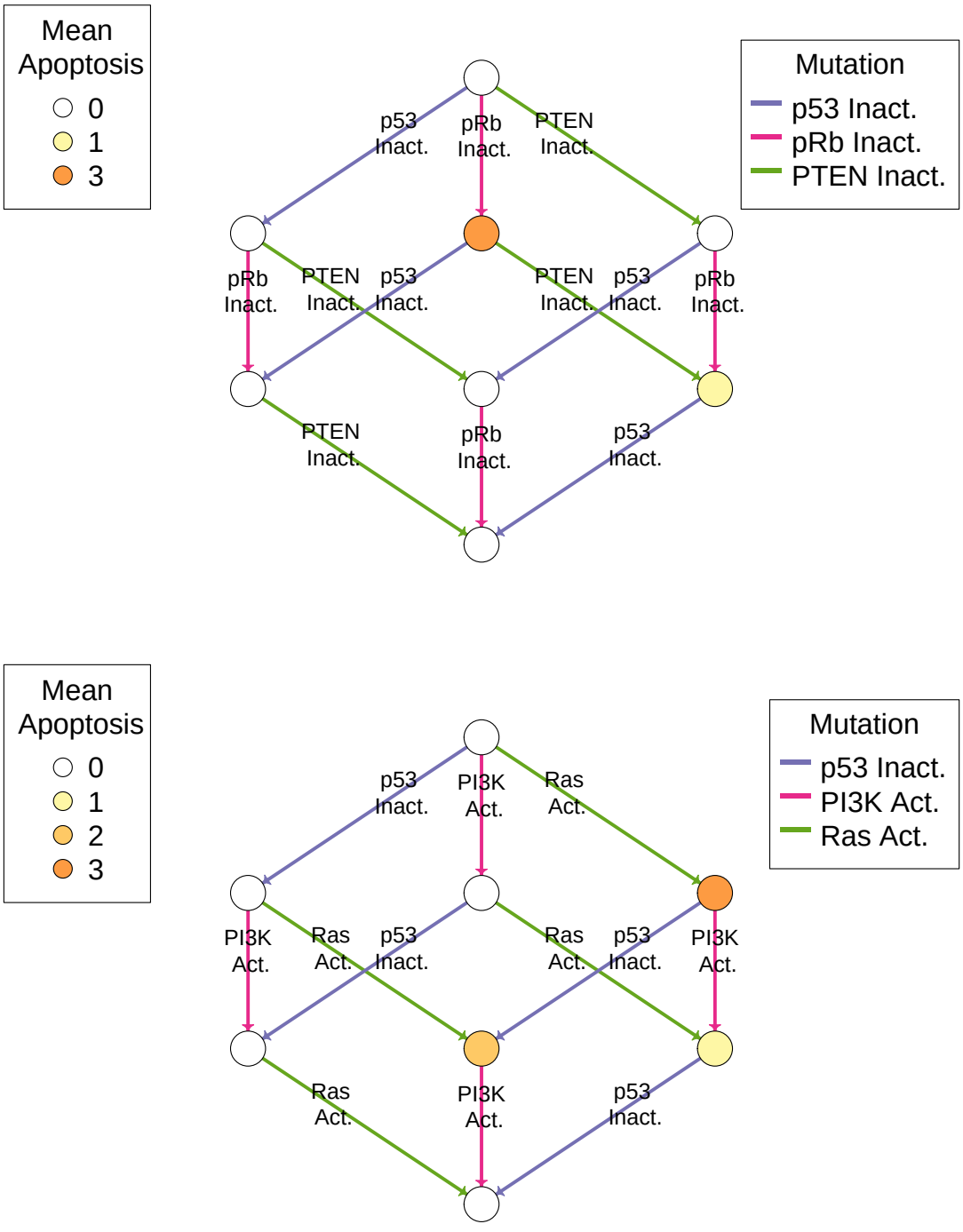

Fig. 6.2 Comparison of degree of constraint by apoptosis in different cell lines with an equal number of total mutations. The effect of mutations found in the BT549 cell line on apoptosis show the order can vary greatly, despite being phenotypically similar to SKBR3. The effect of mutations found in the SUM159PT cell line on apoptosis shows more flexibility than SKBR3. Act. indicates and activatory mutation, and Inact. an inactivatory mutation, with nodes being set to take a constant value as detailed in Table 6.1.

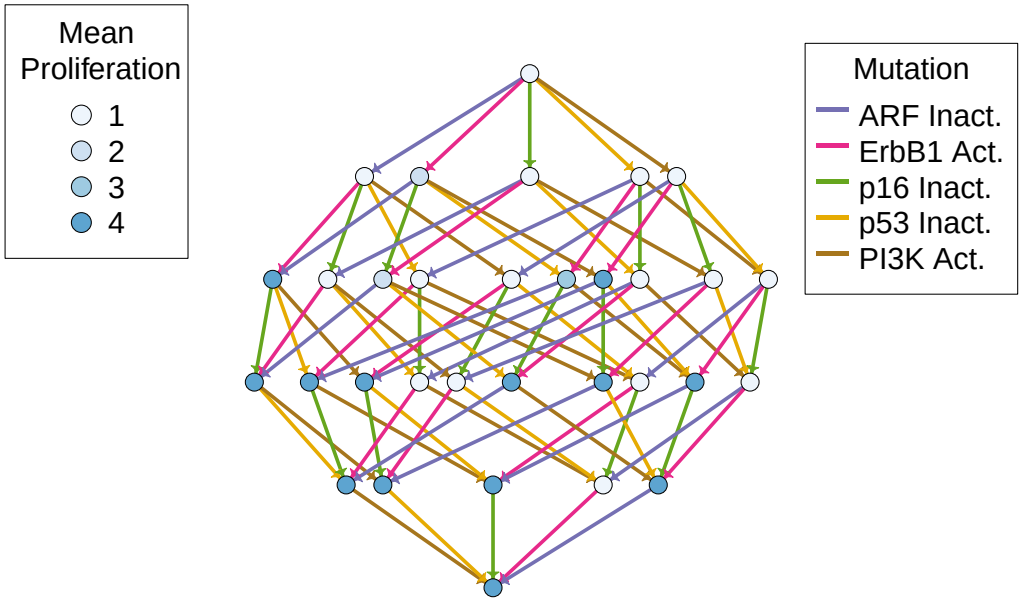

(a) The effect of mutations found in the BT20 cell line on proliferation

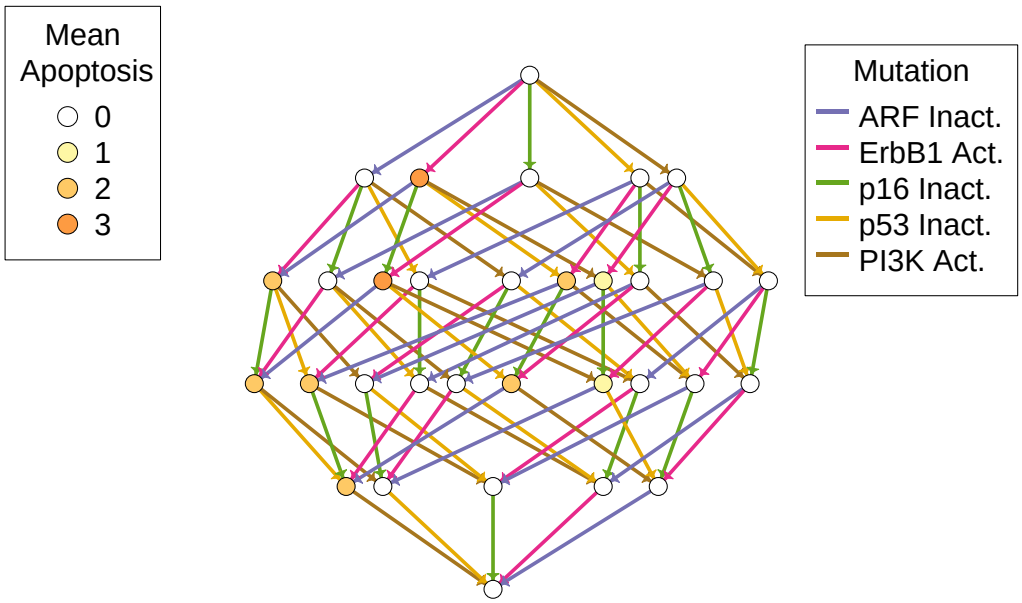

(b) The effect of mutations found in the BT20 cell line on Apoptosis

Fig. 6.3 Comparison of the role played in restriction of order of mutations in the BT20 cell line by proliferation vs apoptosis. Act. indicates and activatory mutation, and Inact. an inactivatory mutation, with nodes being set to take a constant value as detailed in Table 6.1.

6.5 Cell lines show redundancy in mutations

It might be expected that the optimum state, of maximum proliferation and minimum apoptosis, would emerge only with the full complement of mutations for each cell line. This is true in the case of SKBR3, where proliferation is maximised and apoptosis minimised only in the final combination of all the mutations observed in the cell line which apply to my model. However, this is not true for all cell lines. BT20 (Fig. 6.3), for example, gains no further benefit from mutation of p16 and ARF if p53 has been inactivated. And yet, while the full path is not selected for, neither is it selected against by apoptosis. This implies that this is partly a reflection of benefits not accounted for in my model. The current model only considers proliferation and apoptosis, but a cancer must also acquire other phenotypes in order to be successful enough to be a candidate for a cell line. For example, the impact of the mutations on invasiveness [487], differentiation [434], angiogenesis [38], and immune response [95] will also exert selective pressures. In the future, these can be taken into account with further refinements to the models input into this method. Further, I assume every mutation is perfectly effective, and so a mutation to p53 and ARF is not any more beneficial than one to p53 alone. This does not capture the full dynamics, especially considering heterozygous mutations. Different genes will respond differently to heterozygous and homozygous mutations, according to the two-hit tumour suppressor hypothesis, [253], although this has exceptions [352]. This is a better assumption to make initially than trying to guess how effective they should be, but could be supplemented by more experimental data to make a better assessment. This may also require higher granularity for the effected nodes to best capture the difference between different kinds of mutations. It is also likely that the constraints of a cell line *in vitro* are different to those of a cancer *in vivo*, which may require extra mutations from which a cancer would not benefit.

6.6 Conclusions

In this Chapter I demonstrate how proliferation and apoptosis, as predicted to change under mutation in my breast cancer model, can be used to constrain the order of mutations in the evolution of cancer. Further, I show that the degree of constraint varies with different observed combinations of oncogenic mutations, with some cell lines being tightly constrained by a need to avoid high apoptosis (see Section 6.2) or to increase proliferation (see Section 6.4). Other cell lines show little constrain in their ordering of the acquisition of mutations, such as BT549 (see Section 6.3). This may allow future work to use this ordering to better

estimate the stage and future evolution of observed cancers. The degree of constraint may also be related to the frequency with which different combinations of mutations will arise in the population. I discuss this further in the next Chapter.

Chapter 7

Discussion

7.1 Introduction

In this Chapter I will summarise the main findings of this Thesis. My aims were to: build and test a model of heterogeneous breast cancer, to predict and test the most effective targeted therapies for this cancer, and to model the evolution of such cancers in order to provide better diagnosis and prognosis. I show how I was able to build a model able to reproduce known breast cancer behaviour in Chapter 3. I then show how by applying this model to the case of breast cancer heterogeneous in myc expression I was able to the most promising therapies in Chapters 4 and 5. These treatments were shown to affect apoptosis and proliferation, and their combination was more effective against tumour growth than either alone, as shown in Chapter 5.7. discuss here how successful the model is in predicting the *in vivo* behaviour of the tumour, and how this might be improved further. The model is flexible enough to not only be applied to the specific case of this heterogeneous cancer, but to be able to give insights into the evolution of breast cancers in general. I demonstrate a method by which the model is able to predict tumour evolution in Chapter 6. Finally, in this Chapter, I discuss the limitations of the current model and the opportunities for further research, as well as how the techniques used in this thesis can be applied and expanded upon in other systems.

7.2 Building Discrete Qualitative Models

7.2.1 A Discrete Qualitative Network Model of the Gene Regulatory Network in Breast Cancer

In Chapter 3 I show how I built a model of the gene regulatory network in breast cancer comprising over 70 nodes and 140 edges, with the connections and interactions being supported by evidence drawn from the literature. This is able to match the behaviour of both *in vitro* experiments (Chapter 3.4.2) and the behaviour of the *in vivo* model (Chapter 3.5.2). I built this model as a Qualitative Network to better model the non-binary relationships that characterises many of the key interactions which define the behaviour of this system. This enables target functions which are able to model interactions such as: thresholds, such as inhibition of HIF1α at high levels of p53 activity [38]; competition for binding, such as between Myc and Mad [181]; and the effect of different binding partners, such as the effect of ErbB2 on other members of the ErbB family [496]. This level of detail was required to reproduce the behaviour of breast cancer *in vitro* and *in vivo*, as discussed in the next section.

7.2.2 Reproduction of *in vitro* and *in vivo* Behaviour

In order to ensure that the model was able to capture known behaviour of breast cancer, I compared the behaviour of the model to expected behaviour from experiments reported in the literature. I used cell line data so that I would be able to model the mutations of the cells, which are better reported for cell lines than for primary tumour data. This allowed the network to be given initial conditions to match their behaviour. However, cell line behaviour is not a perfect model for the behaviour of cells in tissues. This is partly because they lack interaction with the microenvironment, and are sustained by unnatural levels of survival factors. For example, in the model I consider the effect of hypoxia, and how it is controlled by angiogenesis by the tumour. By contrast a cell line cannot prompt angiogenesis in response to stress, although this may be possible to study *in vitro* in the future [221]. Cell lines are more successfully cultured from pleural effusions than primary cancers, and so are more similar to metastases [242]. In addition, they may also have mutations which differ from primary cancers, to adapt to their unique circumstances. Finally, within a single cell line, there may be mutations which are more representative of the one cancer it is derived from than breast cancer as a whole, and so it is important to compare many cell lines, as I did when testing the model (Chapter 3.4.2). These difficulties are reviewed by Lacroix and Leclercq [272], who conclude that while cell lines are not a perfect model, they are a still close enough to be a

useful one. Therefore I also compared the model with data drawn from the *in vivo* mouse model built by my collaborators. Here the model was able to exactly match the observations. This allowed me to balance the broader range of experiments available from cell line data with the more precise knowledge of the system from the experiments by my collaborators.

My model matched the behaviour of the *in vitro* experiments well, with the exception of lacking a loss of proliferation in the case of Akt inhibition for the SKBR3 cell line, as observed by She et al. [403]. This may be partly a problem of granularity, as the loss of proliferation for SKBR3 was the lowest of the cell lines observed. However, this may also highlight the difficulty of reproducing such a broad range of contexts. The amplification of myc observed in SKBR3 [207] is likely less than that induced by MycER^{T2} in the *in vivo* model, but my model does not have enough intermediate granularity to accommodate this. However, the strong proliferative effect of myc matched the behaviour of the *in vivo* model, and I prioritised this as this was closest to a real cancer, and to the system which my model was to predict treatments for. Overall, this shows the difficulty of making a general purpose model over one specialised to a specific system. However, the degree of success at reproducing *in vitro* results demonstrates how model can provide a base to such specialisation to different sub-types of breast cancer.

A limitation of the model is that by modelling, for example, p53 mutation as fixing the target function for that node at 0 constantly, I assume the mutations is perfectly effective, when in reality some mutations may be more effective than others. In the case of the experiments *in vivo*, the initial conditions were activation of Wnt1 and Myc, which could be reasonably assumed to be very strong effects, and so this was not an issue (see Table 3.11). Likewise, we assumed that the drugs used to test Mek and COX2 in the experimental validation (see Chapter 5.7) were effective. This assumption may be less appropriate for the mutations modelled for tumour evolution, and I discuss this further in Section 6.5. In future versions of the model different levels of mutation could be explored.

In building the model, it was necessary to choose a level of abstraction appropriate to the aims of the project. A more detailed model, with continuous variables and modelling of precise changes of the levels of different proteins could have been built, and may have accommodated some of the cases above better. However, overall, the questions I aimed to answer were addressed better with my simpler model, as this allowed me to include a wider range of data, and interactions for which such quantitative, fine-grained detail is not yet available. I could compare different sources of data more consistently at a lower granularity, as it is clearer how to relate a node which can take values $\{0,1,2\}$ to under-, normal and over-expression than it is for higher levels of granularity.

7.2.3 Further Work

Expanding the model

The model is currently limited to ER- cancer. This is due to the fact that MycER^{T2} is activated by 4-OHT Tamoxifen, and so the tumours in the mouse model were pretreated with Tamoxifen to ensure ER negativity. I therefore limited my model to this scenario. However, the model could be readily expanded to accommodate this pathway, as well as the progesterone pathway, and so expand to luminal breast cancer. Such a model could be easily verified as the MCF-7 ER+ breast cancer cell line is one of the most commonly used.

There was evidence of necrosis as well as apoptosis in the tumours (see Fig. 5.19d). I did not explicitly model necrosis as an outcome in my model in the same manner as I did proliferation and apoptosis, as it is not a controlled death, but the result of a more widespread failure. Necrosis can occur independently of, but also simultaneously with, apoptosis [130]. Indeed, necrosis and apoptosis may exist on a continuum, and are not mutually exclusive, with Zeiss [505] suggesting that the cell intrinsic mechanisms leading to necrosis cannot be distinguished from those leading to apoptosis, but rather that the final choice is dependent on the physiological context. For example, Fas-induced apoptosis requires ATP [127], and so a lack thereof increases the likelihood of necrosis over apoptosis. Therefore it might be possible in the future to use this contextual information, some of which is already present in the model in the form of the hypoxia pathway, to inform whether a cell will respond to these stresses by controlled apoptotic cell death or uncontrolled necrotic cell death. But this in turn would require more complex modelling of the metabolic processes of the cell.

Other areas in which more detail would have the most benefit are in immune evasion, the cell cycle and in angiogenesis. The mouse model was generated in immunocompromised SCID mice by necessity, to allow the repeated transfer of tumours. However, the interaction of the tumour with the immune system will be an important area to model in the future, especially as there is evidence of strong interaction between myc and the immune system [260].

In the case of the cell cycle, while it was not be useful for my aims to be able to model different stages explicitly, it could be useful in the future. There is growing interest in using a cytostatic drug in combination with a cytotoxic drug which affects one stage of the cycle preferentially. As shown by Jackson et al. [225], this takes advantage of the propensity of cancer cells to bypass cell cycle checkpoints to create a difference in cycle stage between cancer and healthy cells, and thus make the cytotoxic treatment more specific. My model is not yet detailed enough to explore this, but detailed models of the cell cycle exist [454] and

have recently been discretised [355], providing a roadmap for future inclusion. Similarly, as seen in Chapter 5, currently pRb knock-out is strongly proliferative in the model, due to a lack of routes to bypass it. There is evidence that CDK2 can drive proliferation in the presence of pRb [299]. This could therefore be an important area for expansion to model a wider range of breast cancers and the treatment thereof.

Modelling angiogenesis presents a limit of the Qualitative Network approach. It is well suited to examining different stable states, but has no explicit time component, making it difficult to model feedback.This is because feedback mechanisms often operate on different time-scales, whereas examining stability only would only show the final state after feedback has suppressed the initial effects of a perturbation. So for angiogenesis, VEGF and other similar factors may only be expressed transiently, but the effect of generated vasculature would have a longer term effect. BMA can accommodate this in simulation, but when examining the stable state behaviours such transient behaviour can be missed. This may partly explain why it was difficult to link hypoxia and VEGF production when initially characterising the pure tumours (see Chapter 3.5). This represents a case where the ability to compare many different cases, as in Chapters 4 and 5, requires a loss of detail compared to simulating a smaller set of cases in more detail.

Core Interactions

In order to find the most important interactions, I could analyse how close my model is to the minimal model needed to meet the specification of behaviours laid out in Chapter 3.4.2 and 3.5.2 by removing edges iteratively. This would allow me to see how many are not needed for the observed behaviours, and how many such subsets of the model are equally successful at reproducing observed behaviour. While it is to be expected that there is redundancy in gene regulatory network, the core edges might be better targets for therapy.

Improving Model Generation

Finally, at the time that I started this work, it was unclear whether network inference methods could produce networks suitable for computational simulation in the case of myc. There are two key problems. Firstly, such networks tend to be large and with a mixture of edges representing direct and indirect interactions (see Fig. 1.10). Secondly, how to derive the logic of such interactions, in our case the Target Functions. There are emerging methods to solve these problems. To better find the core functional network regulating the expression changes seen in micro-array data, there are new approaches merging expression with mutation and

phosphoproteomic data, as presented by Drake et al. [119]. Here, expression changes and mutation data are combined. As expression changes in cancer cells are a response to the mutations, connections between a mutated and a differentially expressed gene are prioritised. This helps reduce the size of the network inferred to something computationally tractable, but relies heavily on there being existing pathway data. In order to derive target functions, such smaller networks become amenable to network synthesis methods. This allows the derivation of target functions for a given network and a specification of expected behaviour, as presented by Dunn et al. [121]. There are also rich new sources of data enabling new techniques, such as synthesis of executable networks from single cell data [330, 62, 10, 15].

In addition, there are methods which could improve the integration of prior knowledge of network topology from the literature, which may help ameliorate the biases discussed in Chapter 2.1.4. This may counter the bias of a literature based approach by attempting to combine it with a data-driven one, and so take advantage of the strengths of both. For example, Zhou et al. [516] describes a method to integrate data from multiple independent sources. Going further, mixed methods have been proposed by Eduati et al. [126] and Kulkarni et al. [265] allow automated supplementation of a model inferred from expression data with information from the literature. Similarly, Saez-Rodriguez et al. [385] propose a method to generate Boolean network models from existing protein-interaction and protein-signalling networks, with the parameters fit to experimental data. Further, text-mining and machine learning techniques may be employed to apply a data-driven approach to the literature itself, see, for example, the work by Steele et al. [420], or more generally pathway databases produced automatically such Literome [364]. The above techniques may therefore in the future allow the automation of at least the generation of an initial network suitable for BMA modelling, even with the need for complex target functions, using these new methods.

Alternative Network Modelling Methods

I use a qualitative network to model more complex interactions than is possible with a Boolean network, while maintaining the ability to analyse the attractors for large networks, and integrate heterogeneous sources of data. This would be more difficult in mathematical models, such as those based on ODEs. Another way to bridge this divide is to model the network with fuzzy logic, as described by Aldridge et al. [5]. These offer a way to preserve the utility of the extensive methods of analysis developed for Boolean networks, while allowing the representation of intermediate levels of activity for nodes, which was a key reason for my choice to use qualitative network modelling. An example of the use of such methods is the modelling of liver inflammation by Morris et al. [333]. It is possible to add

fuzzy logic to existing discrete networks [5], where they allow advantages in modelling smooth transitions between different levels of activity for nodes. This could be assessed as to whether it would allow a better representation of interactions which the qualitative network struggled with, such as areas in which there are low level oscillations (see Chapter 3.2.8).

In my model I used the abstraction of a single constant level of perturbation to a node to simulate the effect of a drug. However, Behar et al. [24] demonstrate that different kinds of stimulus may be able to elicit different responses from the same genes, especially those which act as hubs in the network. This shows how different levels of abstraction allows for different and perhaps more specific treatments, and should be considered if any single part of this network model were to be expanded upon in more depth.

As shown in Chapter 1.8.4 there are many ways to generate network topology, and as shown Chapter 1.9 there are a wide array of different network modelling and analysis methods at a wide range of levels of abstraction. Any further development of this model must therefore be made with knowledge of, and taking advantage of, this rapidly developing field.

7.3 Adapting to and Taking Advantage of Tumour Heterogeneity in Treatment

7.3.1 Single Targeted Therapies Can Target Single Sub-clones

The model shows that monotherapies can be used to target the tumour both cytostatically and cytotoxically. Cytotoxic therapies offer the best options to attack both sub-clones at once, for example through inhibition of Ras. It is also possible to attack one sub-clone of the tumour preferentially, cytostatically for the myc-low sub-clone and cytotoxically for the myc-high sub-clone. The model identifies Mek inhibition as the best way to demonstrate this effect as it has a large difference between the effect on the two sub-clones in the heterogeneous case, both cytostatically and cytotoxically. This difference between sub-clones is shown in the experimental validation for cytostatic effects for the monotherapies, but not for cytotoxic.

A key aspect of these predictions is that they are based on understanding, encapsulated in the model, of the cross-talk and interplay between the different pathways, and using this understanding to find points vulnerable to targeted therapy. Furthermore, the model allows one to extrapolate from the major differences between sub-clones and to find treatments which are specific but not based upon those differences directly. This differs from other successful uses of targeted therapy, which often directly target the mutation which drives the cancer. For example, Vemurafenib targets melanoma by binding to mutant V600E BRAF

[63], or Imatinib targets leukaemia through binding to the oncogenic fusion gene Bcr-Abl [329]. These treatments are extremely effective in the short term but resistance quickly emerges [464]. By targeting the driver mutation, such therapy produces a selection pressure to bolster or work around the driver, and so the resistance mechanism runs the risk of being a net benefit for the tumour. My model finds targets based on the cancerous behaviour of the tumour, therefore providing more options for treatment and so more ways to counter resistance. This is especially important in cases of cooperating sub-clones, as in the case of the mouse model. For example, to target Wnt1 encourages the myc-high clone to acquire the mutations that release it from dependence upon the myc-low clone, making further treatment more difficult and possibly prompting competitive release [132]. Evidence of cancer heterogeneity [23, 11], and cooperation [317, 79, 510] continues to emerge, including myc heterogeneity [187], showing a need to model such cancers.

Specificity of treatment to one sub-clone offers another possibility for treatment which minimises resistance. Targeting one sub-clone minimises the number of cells treated, which lowers the pool of cells in which a resistant mutation might exist. But this still can be used to treat the tumour as a whole, in cases where the sub-clones are interdependent. It also allows for directed tumour evolution, as suggested by Basanta et al. [17]. Further, the model finds treatments which avoid apoptotic effects on the healthy tissue. This minimises side-effects and allows treatments to be applied at higher dosages and for longer time-periods [379]. Many of the treatments predicted by the model do lower proliferation in healthy tissue, but this is well tolerated in existing cytostatic drugs for breast cancer [503, 397].

Further Work

There are opportunities to expand these uses of the model. I currently model myc as constitutively active in the myc-high case, which matches the situation of the *in vivo* model where it is driven by MycER^{T2}. However, in many breast cancers myc over-expression may still be vulnerable to regulation at the post-transcriptional and post-translational levels, such as phosphorylation of the protein by GSK3β [498]. This means it may be more vulnerable to upstream effects than the model suggests, and this could be explored further by driving myc expression with a dummy node, while allowing myc itself to vary, as is the case with HypoxiaInitial and Hypoxia.

In Chapter 5 I chose to build upon the results of modelling monotherapies by looking for the best combinations of drugs. This multiplies the number of stability analyses by a factor equal to twice the number of nodes (to account for activation and inactivation). To do this for many triplicate or more combinations becomes prohibitively time-consuming. However,

one could apply mutations iteratively; after applying all possible single mutations, select the best treatments and repeat only in combination with those, and so on. This could help map the evolution of the tumour in response to treatment. I explore a similar concept in Chapter 6, where I reconstruct tumour evolution from existing sets of mutations, but one could also use the model to predict how the tumour might change in response to treatment and which mutations might best resist this.

7.3.2 Combination therapies can improve the effectiveness of single therapies

In Chapter 5 I demonstrate that treatments applied in combination increase the proportion of effective therapies for a given panel of possible drugs predicted by the model (see Figure 5.9). This is due to synergistic combinations, which enhances the effectiveness of drugs which would be of less useful alone. For example, Figure 5.12 shows how Akt inhibition, which is ineffective at increasing apoptosis alone in the heterogeneous myc-low sub-clone, enhances the effect of several other treatments, such as inhibition of the Bcl-2 family of proteins. This is important for sequential therapy, as in this paradigm combating resistance benefits from having more options to fall back on [424, 50]. It is also relevant for the emerging field of personalised medicine. As we gain the ability to learn in more detail about the differences between patients, there will be more opportunities to tailor therapies to these differences, but only if we can tailor our treatments with equal detail. As shown in 5.3, combination therapy allows more granular control of effect, as well as more ways to target different parts of the gene regulatory network. The specificity of treatment, demonstrated in Chapters 4 and 5, further aids this.

As well as showing how drugs can work together, I also demonstrate that there is potential for the combination to be more effective than either drug alone. Given that I consider only existing drugs (see Chapter 4.2.1), this shows how computational modelling can increase the uses for existing drugs. I chose to investigate the combination of COX2 and Mek inhibition to demonstrate the sub-clone specificity of Mek inhibition alone, and the synergistic effect of their combination.

Further Work

Combination therapy also reduces the chances of the tumour successfully acquiring resistance. The model, by analysing single and combination therapies separately, can determine which combinations are treatments which are independently effective, and which are only effective

in combination. In this thesis, I focus on the latter as it allowed me to test specificity and synergy together, but the predictions of independently effective combinations may be more effective at preventing resistance, as they are less likely to have a single mutation which provides resistance to both drugs simultaneously. Further, cases in which two singly effective drugs reduce their effectiveness in combination should be noted. For example Figure 5.12 shows that Mek inhibition increases the effectiveness of COX2 inhibition in causing apoptosis in the heterogeneous myc-low sub-clone, but reduces the effectiveness of other treatments such as Bcl-2 inhibition. This demonstrates that one cannot simply rely on any combination of anti-cancer drugs having an additive effect. Future work could explore further those combination which are independently effective and do not change their effect when combined, as these are less likely to have a cross-resistance mutation. It could also focus on those combinations which inhibit one another, despite being individually effective. This demonstrates the necessity of such models to better guide experiment and find effective treatments more effectively and efficiently.

In comparing such a large number of different drug combinations, it was necessary to use the VMCAI algorithm (see Chapter 2.1.8). This meant that for some treatments, the algorithm did not find a single fixed point for the behaviour of the model. This represents the instability of the system, with the possibility of it entering a stable loop or bifurcating into multiple stable states. While the SMT (see Chapter 2.1.9) algorithm proved too slow to be able to provide further insight in these cases for all the perturbations, in the future the BDD algorithm (see Chapter 2.1.10) may be more efficient. This presents the possibility of finding all the attractors for cases in a reasonable time, but as shown in Chapter 5.6, comparing a set of attractors to a single fixed point attractor still requires assumptions about the system.

In Chapter 5.6.2 I discussed the sensitivity of the main predictions to the assumptions of the model and its parameters. Analysis using the BDD algorithm could also enhance this, as it would allow one to enumerate all the attractors for all single and combination treatments, with those with more attractors being more sensitive to initial conditions.

Sensitivity analysis could be further improved by analysing the effect of other kinds of perturbation on the behaviour of the network, see for example the analysis presented by Bentele et al. [28]. A Boolean, or in my case qualitative, network can be perturbed in many ways. Different parameter types which can be perturbed are discussed by Kochi et al. [255]. These include the degree of nodes, which could be altered by removing or adding edges as artificial noise. However, the authors caution that not network properties can be separately perturbed. They compare network properties by finding the average Hamming distance between networks under different perturbation. This could be applied to my model

by considering the hamming distance between the stable states, under different perturbations. This could help identify the key parameters upon which the model behaviour depends.

7.3.3 Experimental Validation of Model Predictions

The experiments in the mouse model show that both single therapies affect the proliferation and apoptosis of the tumours, and that the combination has a greater effect on growth than either treatment applied alone, or the control. This demonstrates the utility of the model to find treatments, as well as predicting how combination therapies interact. However, the predicted differences in effect between the sub-clones and between the single treatments were not significant in all cases, showing areas in which further improvement and testing of the model is required.

Comparison to Existing Studies

The experimental results demonstrate the efficacy of combining Mek and COX2 inhibition in the treatment of heterogeneous breast cancer. This parallels results in other systems. Schmidt et al. [391] show that in hepatocellular carcinoma cell lines COX2 inhibition alone decreases apoptosis and increases Mek expression. When a Mek inhibitor is added they see apoptosis greater than the Mek inhibitor alone would provide. Both inhibitors lower proliferation, and again show a synergistic effect. Cusimano et al. [97] show similar results, again in hepatocellular cell lines. These two studies were performed *in vitro* and so do not take account of the effects of COX2 on angiogenesis. However, the model does not predict a compensatory change in Mek expression in response to COX2 inhibition. This would suggest the model would overestimate the effect of COX2 inhibition, when it rather appears the model underestimates it. Any differential effects of Mek inhibition on different sub-types of the cancer, as we observed are not explored to my knowledge. However, Tsuneoka and Mekada [447] show that Mek inhibition is more effective in cases where both myc and Ras are over-expressed. This is consistent with our prediction that it is more effective in the myc-high sub-clone. Erk activity did not change between the myc-low and myc-high sub-clones (see Chapter 3.5.2), implying similar levels of Ras expression.

My model not only predicts this combination, but provides a mechanistic explanation for the increased effectiveness of the combination over either treatment alone, as discussed in Chapter 5.6.1. This indicates that key elements of this interaction are in changes to VEGF and PGE2 production upon inhibition of COX2, as well as activation of BIM when Mek is inhibited. The model can therefore guide future investigation of this treatment to

better determine the mechanisms of action, as well as predict that these key nodes might also be routes to resistance. That the pathways converge on activation of BIM highlights a disadvantage of a synergistic treatment, that for the two treatments to support one another necessarily means there is overlap in the pathway, and so an opportunity for a single mutation to provide resistance. Bozic et al. [45] and Komarova et al. [256] suggest that such cross-resistance mutations do not eliminate the benefits of combination therapy in slowing the emergence of resistance, but it may reduce it. It may be more clinically useful therefore to combine therapies which the model predicts are independently effective and have no benefits from combination. However, in order to best test the dynamics of the computational model and the mouse model, a synergistic treatment provides more information.

Quantification of Proliferation and Apoptosis

The experiments of my collaborators show that, as predicted, that a combination of these two drugs is more effective than either applied singly in proliferation. However, the analysis of the CC3 staining of the tumours was complicated by the very effectiveness of the treatments. In the case of the combination therapy, there was very little tissue left to analyse. This may have lead to the high variance in the results observed.

Another consideration is that analysis of proliferation and apoptosis of these tumours by IdU and CC3 immunohistochemistry necessarily can only measure those cells which survived until Day 3 after the beginning of treatment. Therefore these cells are those which are more resistant to the treatments. However, this will be a similar systematic error across all the experiments and therefore does not have a major impact on differential measurements.

Further Work

As an initial study of an untested model, the number of mice on which treatments were tested was quite small. The differences between tumour growth for the combination therapy versus either monotherapy or control was significant, but further repeats are needed to clarify the differences between the monotherapies compared to one another, and treatment effects on different sub-clones. This is especially the case for the combination therapy, given the difficulty in quantifying the results of the tumour sections due to the small amount of surviving tumour tissue.

It is unclear whether the effect of combining the treatments is simply the additive effect of combining two treatments, as opposed to producing different effects in combination as predicted by the model. There was significant interaction between the therapies as measured

by ANOVA for proliferation, however this was inconclusive in the case of apoptosis. Further, ANOVA at a single dose, as is the case in this study, can only provide an initial indication of interaction. A full examination of how the response changes at different dose levels [435] is required for a full test of synergy as opposed to additivity.

The model does not predict that any two independently effective treatments can be combined, as shown by the many combinations that worsen effectiveness in Figures 5.10 to 5.13. By testing such a counter-productive combination, as well as a combination which is predicted to be equally effective as monotherapy, it would be possible to better determine the additive effects of treatments as compared to the cooperation between Mek and COX2 inhibition which the model predicts.

Furthermore, there was an effect from Mek inhibition in the myc-high sub-clone for proliferation, which was not predicted. This is likely as I had to simulate the network separately for each sub-clone, limiting the ability to predict the change in effect from one tumour to another as a result of treatment, and perhaps reducing the differences between tumour sub-clones. This is because the difference in the sub-clones in the model derives from the difference in the initial conditions, but as the sub-clones are treated, they can support one another less and so these initial conditions should gradually trend from the heterogeneous case to the pure myc-high and myc-low tumour case. This demonstrates the limitations of modelling a single cell at a time. To better predict these changes it would be necessary to include the spatial dynamics of the tumour.

Tissues and tumours are ensembles of cells that exhibit emergent properties in a population, and must be modelled as a group to understand the dynamics of tumours. My breast cancer model can simulate different sub-clones, but not how changes due to treatment in one sub-clone changes the microenvironment and structure of the tumour as a whole. There has been work on combining a physical model of individual cells with BMA models [189]. In such a model each cell would be represented by an automaton running an independent instance of BMA, but as they divide and die these cells interact in 3D space. This could be extended with cell signalling to better model how mixing of tumour cells and tumour structure affect and are affected by treatment. Such a multi-scale, hybrid model would combine the best features of two approaches: the discrete model of the cell's decision making; and a continuous model of how cells affect one another. The continuous elements of this model would allow better modelling of the transition from a tumour in which the sub-clones are intermingled and cooperating, and how this breaks down under treatment. Such a gradual change over time is better suited to a continuous rather than a discrete model. This would also improve modelling of angiogenesis, as the effect of transient VEGF on more long term

angiogenesis could be simulated in the spatial component of the model. This hybrid model would allow me to trace gross changes in tumour behaviour back to individual mutations and treatments, and vice-versa, and may show how the breakdown of cooperation between the sub-clones leads to a greater than predicted effectiveness of the combination therapy.

7.4 Tumour Evolution

The model predicts that the order of mutations will affect the level of apoptosis and proliferation that a cancer will pass through as mutations accumulate. Further, it predicts that the level of apoptosis at each stage can be minimised with by acquiring mutations in a specific order. A cell cannot choose the order of mutations, but this is likely to constrain which cells survive, and so which orders of mutations are observed. Thus, there are constraints on which orders are most beneficial to the cancer, and this differs for different sub-types of breast cancer, as represented by different cell lines. For example, the SKBR3 cell line is tightly constrained, with only one "path" through the powerset of all possible combinations of subsets of mutations (Fig. 6.1b). Meanwhile, other cell lines are less constrained, such as BT549, where most paths are equally viable for the tumour (Fig. 6.2).

However, the evolution of the tumour is not only constrained by apoptosis but also by a need to increase proliferation, to out-compete other clones. This may be a stronger constraint on which path is optimal, as in the case of BT20 (Fig. 6.3).

7.4.1 Assumptions of the Model

In this model, I assumed that, in choosing between a point in the powerset with high apoptosis and high proliferation, or a point with low apoptosis with low proliferation, that the latter would be preferred. That is, that apoptosis overrides proliferation. Under these assumptions it is possible to form a general order of mutations across cell lines, with tumour suppressors in general mutating earlier. However, this assumption could be explored further experimentally, as it may be that a highly apoptotic but proliferative clone outweighs the disadvantage with a faster rate of mutation, due to faster division, and so might pass through this phase faster. In this way the clone could out-compete a more healthy but slower growing one. This might explain why p53 is often, but not always, a founder mutation in breast cancer [401].

Other assumptions made in this model simplify the type and number of mutations. Firstly, it assumes that the mutations are all affecting a single gene at a time; i.e. point mutations rather than copy-number mutations or similar. Secondly, it assumes that these are maximally

effective, that is that a knock-out stops all function (see Section 6.5). Thirdly, it makes the assumption that each mutation occurs individually, independently and with equal probability. However, in reality, multiple mutations can be acquired together, and which mutations are acquired are not necessarily equally likely. There are also more complex events such as chromothripsis [92] and, especially in breast cancer, kataegis [437], which cause large scale changes in the DNA of the cell in a short time-frame. Currently the model assumes that mutation A and B acquired together will have the same stable points as if B is acquired after A or both together from the healthy state. However, the transitions between attractors upon mutation, i.e. the arrows in the powerset may change in the case that mutations are acquired together. This is because the model finds which attractors are reachable from the previous state, plus the new mutations. So if the network has three attractors for AB which are reachable from all initial states, but only two are reachable from the attractors of A alone plus the new mutation B, then this might connect the points of the powerset differently than going directly from the healthy state to AB. In other words it may be the case that one cannot reach some of the stable states of AB from A but one can from the healthy cell. The model can accommodate this, and so adding the ability to mutate multiple genes in one step is a possible expansion of the model.

In Chapter 6 I demonstrate the method for predicting the order of mutations using cell lines as a basis. However, it would be better to use primary tumour data on mutations. While a cell line derived from a patient would be expected to have the mutations required to be a successful cancer, it may also have acquired additional mutations to adapt to the niche of being a cell line. For example, the common cell line HeLa has been found to have developed some strains which are adapted to the lab environment and therefore have become more of a contaminant for other cultures than a useful model [278, 298]. Further, cell lines for breast cancer have been mostly cultured from pleural effusions, and so bear more similarity to metastases than to primary tumour data. This may be why some of the mutations in the cell lines seemed to be redundant (Chapter 6.5).

While, the model predicts constraints on the order in which mutations are acquired, it does not predict that different orders of mutations have an effect on the final phenotype of the tumour. Experimental evidence on this matter remains mixed, with some finding no influence on final phenotype from the tumour [142], and some evidence in favour [349]. This could be investigated further to find which interactions are required in the gene regulatory network of the cell to produce different phenotypes based on the evolutionary history of the tumour, despite the same final set of mutations.

7.4.2 Further Work

The method tested in this thesis could be extended to consider more phenotypes, although this requires assumptions about how to balance the priorities of a tumour. It would be important to consider, for example, how important invasiveness is to successful tumourigenesis compared to proliferation at different stages.

I also currently use the method to reconstruct the history of known tumours, but it could also be used to predict how a larger set of mutations interacts. Instead of using a set of mutations drawn from the literature, I could construct a larger powerset of many possible oncogenic mutations. However, analysing this becomes difficult. The powerset of n mutations has 2^n members, and the number of paths through the powerset is equal to the number of permutations of these mutations, i.e. n factorial. The number of possible paths to analyse grows very quickly, and so becomes too large to be computationally tractable. Therefore, whether this method can be applied to follow the evolution of a tumour from genesis through treatments and possible recurrence, depends on the number of mutations it must handle. Studies suggest that tumours might accumulate as many as 70 amino-acid-changing mutations [463]. However, as few as 5 of these are under positive selection, and are therefore key driver mutations [315], although which are selected for may change at different stages. Depending on how many mutations are needed may mean the model is be better suited to early stages of the tumour. To model a longer time-frame may require the model to be improved to stop following paths which have high apoptosis early, rather than mapping out every possible combination of mutations.

Instead, the model could be used to see whether the degree of constraint in the order of mutations correlates with incidence of said combinations in the population. This might be expected as a combination of mutations for which there are fewer constraints is more likely to occur in the optimal order. However, this assumes similar rates of mutation for all the genes. To test this, data on mutations in primary breast cancer, for example from the METABRIC dataset [96], could be used to construct powersets, which could be assessed to compare which cancer promoting combinations of mutations are predicted to be strongly and weakly constrained in the order in which they can be acquired. These could then be compared to incidence of those combinations of mutations in the population. I would hypothesise that the more constrained combinations of tumour promoting mutations, such as those seen in SKBR3 (see Chapter 6.2) might be rarer than those which weakly constrained. This could then lead to better understanding of the incidence of different breast cancer sub-types, and support using the model to predict how a cancer might evolve further under treatment.

By better predicting which mutations occur early and late in tumour development, the model could also be used to better diagnose at which stage a tumour is, based on the combination of mutations observed, as suggested by Durinck et al. [122]. This could then lead to better prognosis. Furthermore, if a cancer appears to be developing along a non-optimum path, this might help choose which treatments to use to encourage it to remain on that path, and so guide its evolution [17]. If the model predicts a certain order of mutations leading to a dead-end, it may even help reduce unnecessary treatment.

The method could also be expanded to consider not only how mutations are selected in tumour evolution, but also in response to treatment. In addition to oncogenic mutations, nodes could be perturbed to model the effect of treatments, as in Chapters 4 and 5 , but at different stages of tumour evolution. In addition, the current set of oncogenes could be supplemented with common resistance mutations. It would then be possible to evaluate the effects of different sequences of treatments on tumour evolution, examine the possible resistance mutations which might be selected for in response, and see how different treatment regimes affect the course of tumour development. This is an active area of research, as reviewed by Foo and Michor [155]. For example, Chmielecki et al. [70] use model the evolution of cancer in response to treatment to find the optimal dosing strategy, while Mumenthaler et al. [335] use such models to search for optimal sequential treatment timing. As different sub-clones with different orders of mutations may diverge in their future evolution under therapy, this could be combined with the game theoretic approaches discussed in Chapter 1.9.2 to provide a comprehensive model of how a tumour changes under therapy.

Finally, while my model broadly agrees with the existing literature on the order of mutations in breast cancer, the timescales are very different. Individual mutations can now be applied sequentially using emerging techniques such as CRISPR-Cas9 [388]. This would allow experiments, guided by our model to most closely recapitulate the early stages of tumour evolution.

7.5 Conclusions and Outlook

Cancer is a complex set of diseases, with subtle differences between and within tumours of different tissues. This is complicated further by the fact that every tumour is actively adapting, competing and cooperating within itself, and continues to do so in response to perturbation and treatment. To cope with this complexity, computational methods are required to guide experiment in order to better understand and treat cancer.

My aims for this thesis were to reproduce the behaviour of heterogeneous breast cancer, and to predict the most effective therapies. Cancer heterogeneity poses a major obstacle to successful treatment, as different sub-clones will react differently to treatment. As these sub-clones exist as part of an ecosystem of cooperation and competition, this can lead to unindented negative outcomes, such as competetive release of one sub-clone. Heterogeneity also provides a pool of possible resistance mutations, making cancer recurrence more likely.

There are three possible ways in which to tackle this heterogeneity. Firstly, one can embrace it as a key aspect of the cancer, and try and find treatments which compensate for it, and still affect the majority of the tumour. In Chapter 4 I show how the model can be used to predict the best cytostatic and cytotoxic therapies, both for pure and heterogeneous tumours, and in Chapter 5 how combination can be used to expand the possible treatments, and broaden the effect on both sub-clones within a heterogeneous tumour.

Secondly, one can attempt to exploit this heterogeneity, by balancing sub-clones against one another , or targeting the driver clone in the hopes of causing the other clones to collapse. This has the added benefit of targeting smaller populations of cells and so decreasing the chances of resistance. In Chapter 4 I show how the model can identify treatments which are specific to one sub-clone and so are best suited to this treatment paradigm. Experiments from my collaborators show that the combination therapy that I predict as the best against both tumours is significantly more effective than either single therapy (Section 5.7.4, Appendix Table C.12). However, the prediction of differences between sub-clones and treatments were not always significant, highlighting areas in which the model can be improved.

Thirdly, one can avoid the heterogeneity all together. Most cancers evolve from a single celland split into different sub-clones as they develop. If one can understand the order of mutations, then one can predict which mutations are likely to be at the root of the phylogenetic tree of the cancer, and which in the leaves. Targeting the root, or founder mutations, offers the opportunity to sidestep this heterogeneity altogether. In Chapter 6 I demonstrate a method for predicting how the gene regulatory network constrains the order of mutations. This can be used to predict founder mutations, and so the best treatments for affecting the majority of sub-clones.

All these analyses are agnostic of the kind of cancer which is being modelled, and these methods can be applied to any BMA model, such as those developed for Chronic Myeloid Leukemia [75] and Acute Myeloid Leukemia [408]. As the cost of genome sequencing continues to come down, the data required to extend these methods to patients in the form of personalised medicine will become more available.

In this thesis, with my collaborators, I have predicted and tested a new combination therapy for breast cancer. Clinically approved inhibitors of both Mek and COX2 are already available, for example, Trametenib is approved for Mek inhibition [252], and Celecoxib for COX2 [138]. This makes it possible to quickly develop this therapy further in the future, showing the potential of these computational methods to predict cancer behaviour and evolution, in order to find new treatments.

References

[1] Agency for Healthcare Research and Quality (2011). *Methods guide for effectiveness and comparative effectiveness reviews*. Agency for Healthcare Research and Quality.

[2] Agoston, V., Csermely, P., and Pongor, S. (2005). Multiple weak hits confuse complex systems: a transcriptional regulatory network as an example. *Physical review. E, Statistical, nonlinear, and soft matter physics*, 71(5 Pt 1):051909.

[3] Ahmed, I., Sutton, A. J., and Riley, R. D. (2012). Assessment of publication bias, selection bias, and unavailable data in meta-analyses using individual participant data: A database survey. *BMJ (Online)*, 344(7838):1–10.

[4] Al-azawi, D., Ilroy, M. M., Kelly, G., Redmond, A. M., Bane, F. T., Cocchiglia, S., Hill, A. D. K., and Young, L. S. (2008). Ets-2 and p160 proteins collaborate to regulate c-Myc in endocrine resistant breast cancer. *Oncogene*, 27(21):3021–31.

[5] Aldridge, B. B., Saez-Rodriguez, J., Muhlich, J. L., Sorger, P. K., and Lauffenburger, D. A. (2009). Fuzzy Logic Analysis of Kinase Pathway Crosstalk in TNF/EGF/Insulin-Induced Signaling. *PLoS Computational Biology*, 5(4).

[6] Amador-Noguez, D., Feng, X. J., Fan, J., Roquet, N., Rabitz, H., and Rabinowitz, J. D. (2010). Systems-level metabolic flux profiling elucidates a complete, bifurcated tricarboxylic acid cycle in Clostridium acetobutylicum. *Journal of Bacteriology*, 192(17):4452–4461.

[7] Amati, B., Alevizopoulos, K., and Vlach, J. (1998). Myc and the cell cycle. *Frontiers in bioscience : a journal and virtual library*, 3:d250–68.

[8] An, W. G., Kanekal, M., Simon, M. C., Maltepe, E., Blagosklonny, M. V., and Neckers, L. M. (1998). Stabilization of wild-type p53 by hypoxia-inducible factor 1alpha. *Nature*, 392(6674):405–408.

[9] Andersen, M. R., Nielsen, M. L., and Nielsen, J. (2008). Metabolic model integration of the bibliome, genome, metabolome and reactome of Aspergillus niger. *Molecular Systems Biology*, 4(178):178.

[10] Angerer, P., Simon, L., Tritschler, S., Wolf, F. A., Fischer, D., and Theis, F. J. (2017). Single cells make big data: New challenges and opportunities in transcriptomics. *Current Opinion in Systems Biology*, 4:85–91.

[11] Aparicio, S. and Caldas, C. (2013). The implications of clonal genome evolution for cancer medicine. *The New England journal of medicine*, 368(9):842–51.

[12] Aplin, A. E., Stewart, S. A., Assoian, R. K., and Juliano, R. L. (2001). Integrin-mediated adhesion regulates ERK nuclear translocation and phosphorylation of Elk-1. *Journal of Cell Biology*, 153(2):273–281.

[13] Autier, P., Boniol, M., La Vecchia, C., LaVecchia, C., Vatten, L., Gavin, A., Héry, C., and Heanue, M. (2010). Disparities in breast cancer mortality trends between 30 European countries: retrospective trend analysis of WHO mortality database. *BMJ (Clinical research ed.)*, 341:c3620.

[14] Ayer, D. E., Kretzner, L., and Eisenman, R. N. (1993). Mad: a heterodimeric partner for Max that antagonizes Myc transcriptional activity. *Cell*, 72(2):211–22.

[15] Babtie, A. C., Chan, T. E., and Stumpf, M. P. (2017). Learning regulatory models for cell development from single cell transcriptomic data. *Current Opinion in Systems Biology*, 5:72–81.

[16] Barabási, A.-L. and Oltvai, Z. N. (2004). Network biology: understanding the cell's functional organization. *Nature reviews. Genetics*, 5(2):101–13.

[17] Basanta, D., Gatenby, R. A., and Anderson, A. R. A. (2012). Exploiting evolution to treat drug resistance: Combination therapy and the double bind. *Molecular Pharmaceutics*, 9(4):914–921.

[18] Basanta, D., Hatzikirou, H., and Deutsch, A. (2008). Studying the emergence of invasiveness in tumours using game theory. *European Physical Journal B*, 63(3):393–397.

[19] Bates, D. (2005). Fitting linear mixed models in R. Using the lme4 package. *R News*, 5(May):27–30.

[20] Bates, D., Mächler, M., Bolker, B., and Walker, S. (2015). Fitting Linear Mixed-Effects Models Using {lme4}. *Journal of Statistical Software*, 67(1):1–48.

[21] Bates, S., Phillips, A. C., Clark, P. A., Stott, F., Peters, G., Ludwig, R. L., and Vousden, K. H. (1998). p14ARF links the tumour suppressors RB and p53. *Nature*, 395(September):124–125.

[22] Becskei, A. and Serrano, L. (2000). Engineering stability in gene networks by autoregulation. *Nature*, 405(6786):590–593.

[23] Bedard, P. L., Hansen, A. R., Ratain, M. J., and Siu, L. L. (2013). Tumour heterogeneity in the clinic. *Nature*, 501(7467):355–64.

[24] Behar, M., Barken, D., Werner, S. L., and Hoffmann, A. (2013). The dynamics of signaling as a pharmacological target. *Cell*, 155(2):448–461.

[25] Behrens, J., von Kries, J., Kühl, M., Bruhn, L., Wedlich, D., Grosschedl, R., and Birchmeier, W. (1996). Functional Interaction of β-Catenin with the Transcription Factor LEF-1.

[26] Bell, R. (2002). What can we learn from Herceptin trials in metastatic breast cancer? *Oncology*, 63 Suppl 1:39–46.

[27] Benque, D., Bourton, S., Cockerton, C., Cook, B., Fisher, J., Ishtiaq, S., Piterman, N., Taylor, A., and Vardi, M. Y. (2012). BMA: Visual Tool for Modeling and Analyzing Biological Networks. *Computer Aided Verification*, pages 686–692.

[28] Bentele, M., Lavrik, I., Ulrich, M., Stößer, S., Heermann, D. W., Kalthoff, H., Krammer, P. H., and Eils, R. (2004). Mathematical modeling reveals threshold mechanism in CD95-induced apoptosis. *Journal of Cell Biology*, 166(6):839–851.

[29] Berns, K., Horlings, H. M., Hennessy, B. T., Madiredjo, M., Hijmans, E. M., Beelen, K., Linn, S. C., Gonzalez-Angulo, A. M., Stemke-Hale, K., Hauptmann, M., Beijersbergen, R. L., Mills, G. B., van de Vijver, M. J., and Bernards, R. (2007). A Functional Genetic Approach Identifies the PI3K Pathway as a Major Determinant of Trastuzumab Resistance in Breast Cancer. *Cancer Cell*, 12(4):395–402.

[30] Berra, E., Benizri, E., Ginouvès, A., Volmat, V., Roux, D., and Pouysségur, J. (2003). HIF prolyl-hydroxylase 2 is the key oxygen sensor setting low steady-state levels of HIF-1α in normoxia. *EMBO Journal*, 22(16):4082–4090.

[31] Bertheau, P., Lehmann-Che, J., Varna, M., Dumay, A., Poirot, B., Porcher, R., Turpin, E., Plassa, L.-F., de Roquancourt, A., Bourstyn, E., de Cremoux, P., Janin, A., Giacchetti, S., Espié, M., and de Thé, H. (2013). P53 in Breast Cancer Subtypes and New Insights Into Response To Chemotherapy. *The Breast*, 22:S27–S29.

[32] Beverly, L. J. and Varmus, H. E. (2009). MYC-induced myeloid leukemogenesis is accelerated by all six members of the antiapoptotic BCL family. *Oncogene*, 28(9):1274–9.

[33] Beyer, A., Thomason, P., Li, X., Scott, J., and Fisher, J. (2010). Mechanistic Insights into Metabolic Disturbance during Type-2 Diabetes and Obesity Using Qualitative Networks. In Priami, C., Breitling, R., Gilbert, D., Heiner, M., and Uhrmacher, A., editors, *Transactions on Computational Systems Biology XII SE - 4*, volume 5945 of *Lecture Notes in Computer Science*, pages 146–162. Springer Berlin Heidelberg.

[34] Bhanot, P., Brink, M., Samos, C. H., Hsieh, J. C., Wang, Y., Macke, J. P., Andrew, D., Nathans, J., and Nusse, R. (1996). A new member of the frizzled family from Drosophila functions as a Wingless receptor.

[35] Bieging, K. T., Mello, S. S., and Attardi, L. D. (2014). Unravelling mechanisms of p53-mediated tumour suppression. *Nature reviews. Cancer*, 14(5):359–70.

[36] Bilic, J., Huang, Y.-L., Davidson, G., Zimmermann, T., Cruciat, C.-M., Bienz, M., and Niehrs, C. (2007). Wnt induces LRP6 signalosomes and promotes dishevelled-dependent LRP6 phosphorylation. *Science (New York, N.Y.)*, 316(5831):1619–1622.

[37] Billen, L. P., Kokoski, C. L., Lovell, J. F., Leber, B., and Andrews, D. W. (2008). Bcl-XL Inhibits Membrane Permeabilization by Competing with Bax. *PLoS Biology*, 6(6):e147.

[38] Blagosklonny, M. V., An, W. G., Romanova, L. Y., Trepel, J., Fojo, T., and Neckers, L. (1998). p53 inhibits hypoxia-inducible factor-stimulated transcription. *The Journal of biological chemistry*, 273(20):11995–8.

[39] Blagosklonny, M. V. and El-Deiry, W. S. (1996). In vitro evaluation of a p53-expressing adenovirus as an anti-cancer drug. *International journal of cancer*, 67(3):386–92.

[40] Blancher, C., Moore, J. W., Robertson, N., and Harris, a. L. (2001). Effects of ras and von Hippel-Lindau (VHL) gene mutations on hypoxia-inducible factor (HIF)-1alpha, HIF-2alpha, and vascular endothelial growth factor expression and their regulation by the phosphatidylinositol 3'-kinase/Akt signaling pathway. *Cancer research*, 61(19):7349–7355.

[41] Blaydes, J. P. and Wynford-Thomas, D. (1998). The proliferation of normal human fibroblasts is dependent upon negative regulation of p53 function by mdm2. *Oncogene*, 16(January):3317–3322.

[42] Bleris, L., Xie, Z., Glass, D., Adadey, A., Sontag, E., and Benenson, Y. (2014). Synthetic incoherent feedforward circuits show adaptation to the amount of their genetic template. *Molecular Systems Biology*, 7(1):519–519.

[43] Boras-Granic, K. and Wysolmerski, J. J. (2008). Wnt signaling in breast organogenesis. *Organogenesis*, 4(2):116–122.

[44] Bosma, M., Schuler, W., and Bosma, G. (1988). The scid mouse mutant. *Current topics in microbiology and immunology*, 137:197–202.

[45] Bozic, I., Reiter, J. G., Allen, B., Antal, T., Chatterjee, K., Shah, P., Moon, Y. S., Yaqubie, A., Kelly, N., Le, D. T., Lipson, E. J., Chapman, P. B., Diaz, L. A., Vogelstein, B., and Nowak, M. A. (2013). Evolutionary dynamics of cancer in response to targeted combination therapy. *eLife*, 2:e00747.

[46] Bray, F., McCarron, P., and Parkin, D. M. (2004). The changing global patterns of female breast cancer incidence and mortality. *Breast Cancer Research*, 6(6):229.

[47] Brunet, A., Sweeney, L. B., Sturgill, J. F., Chua, K. F., Greer, P. L., Lin, Y., Tran, H., Ross, S. E., Mostoslavsky, R., Cohen, H. Y., Hu, L. S., Cheng, H.-L., Jedrychowski, M. P., Gygi, S. P., Sinclair, D. A., Alt, F. W., and Greenberg, M. E. (2004). Stress-dependent regulation of FOXO transcription factors by the SIRT1 deacetylase. *Science (New York, N.Y.)*, 303(5666):2011–5.

[48] Bunz, F., Dutriaux, A., Lengauer, C., Waldman, T., Zhou, S., Brown, J. P., Sedivy, J. M., Kinzler, K. W., and Vogelstein, B. (1998). Requirement for p53 and p21 to sustain G2 arrest after DNA damage. *Science (New York, N.Y.)*, 282(April):1497–1501.

[49] Calbo, J., van Montfort, E., Proost, N., van Drunen, E., Beverloo, H. B., Meuwissen, R., and Berns, A. (2011). A Functional Role for Tumor Cell Heterogeneity in a Mouse Model of Small Cell Lung Cancer. *Cancer Cell*, 19(2):244–256.

[50] Calvo, E., Schmidinger, M., Heng, D. Y., Grünwald, V., and Escudier, B. (2016). Improvement in survival end points of patients with metastatic renal cell carcinoma through sequential targeted therapy. *Cancer Treatment Reviews*, 50:109–117.

[51] Campone, M., Campion, L., Roché, H., Gouraud, W., Charbonnel, C., Magrangeas, F., Minvielle, S., Genève, J., Martin, A. L., Bataille, R., and Jézéquel, P. (2008). Prediction of metastatic relapse in node-positive breast cancer: Establishment of a clinicogenomic model after FEC100 adjuvant regimen. *Breast Cancer Research and Treatment*, 109(3):491–501.

[52] Campone, M., Noël, B., Couriaud, C., Grau, M., Guillemin, Y., Gautier, F., Gouraud, W., Charbonnel, C., Campion, L., Jézéquel, P., Braun, F., Barré, B., Coqueret, O., Barillé-Nion, S., and Juin, P. (2011). c-Myc dependent expression of pro-apoptotic Bim renders HER2-overexpressing breast cancer cells dependent on anti-apoptotic Mcl-1. *Molecular cancer*, 10(1):110.

[53] Cao, Y. (2004). Antiangiogenic cancer therapy. *Seminars in Cancer Biology*, 14(2):139–145.

[54] Capuco, A. V., Li, M., Long, E., Ren, S., Hruska, K. S., Schorr, K., and Furth, P. a. (2002). Concurrent pregnancy retards mammary involution: effects on apoptosis and proliferation of the mammary epithelium after forced weaning of mice. *Biology of reproduction*, 66(5):1471–6.

[55] Caradec, J., Sirab, N., Keumeugni, C., Moutereau, S., Chimingqi, M., Matar, C., Revaud, D., Bah, M., Manivet, P., Conti, M., and Loric, S. (2010). Desperate house genes: The dramatic example of hypoxia. *British Journal of Cancer*, 102(6):1037–1043.

[56] Cardone, M. H. (1998). Regulation of Cell Death Protease Caspase-9 by Phosphorylation. *Science*, 282(5392):1318–1321.

[57] Carracedo, A., Ma, L., Teruya-feldstein, J., Rojo, F., and Salmena, L. (2008). Inhibition of mTORC1 leads to MAPK pathway activation through a PI3K- dependent feedback loop in human cancer. *Journal of Clinical Investigation*, 118(9):3065–3074.

[58] Carrillo, M., Góngora, P. A., and Rosenblueth, D. A. (2012). An overview of existing modeling tools making use of model checking in the analysis of biochemical networks. *Frontiers in plant science*, 3(July):155.

[59] Casás-Selves, M. and DeGregori, J. (2011). How Cancer Shapes Evolution and How Evolution Shapes Cancer. *Evolution: Education and Outreach*, 4(4):624–634.

[60] Caspari, T. (2000). Checkpoints: How to activate p53. *Current Biology*, 10(8):315–317.

[61] Castelo-Branco, G., Wagner, J., Rodriguez, F. J., Kele, J., Sousa, K., Rawal, N., Pasolli, H. A., Fuchs, E., Kitajewski, J., and Arenas, E. (2003). Differential regulation of midbrain dopaminergic neuron development by Wnt-1, Wnt-3a, and Wnt-5a. *Proceedings of the National Academy of Sciences of the United States of America*, 100(22):12747–12752.

[62] Chan, T. E., Stumpf, M. P., and Babtie, A. C. (2017). Gene Regulatory Network Inference from Single-Cell Data Using Multivariate Information Measures. *Cell Systems*, 5(3):251–267.e3.

[63] Chapman, P. B., Hauschild, A., Robert, C., Haanen, J. B., Ascierto, P., Larkin, J., Dummer, R., Garbe, C., Testori, A., Maio, M., Hogg, D., Lorigan, P., Lebbe, C., Jouary, T., Schadendorf, D., Ribas, A., O'Day, S. J., Sosman, J. A., Kirkwood, J. M., Eggermont,

A. M., Dreno, B., Nolop, K., Li, J., Nelson, B., Hou, J., Lee, R. J., Flaherty, K. T., and McArthur, G. A. (2011). Improved Survival with Vemurafenib in Melanoma with BRAF V600E Mutation. *New England Journal of Medicine*, 364(26):2507–2516.

[64] Chen, D., Li, M., Luo, J., and Gu, W. (2003). Direct interactions between HIF-1 alpha and Mdm2 modulate p53 function. *The Journal of biological chemistry*, 278(16):13595–8.

[65] Chen, J. C., Alvarez, M. J., Talos, F., Dhruv, H., Rieckhof, G. E., Iyer, A., Diefes, K. L., Aldape, K., Berens, M., Shen, M. M., and Califano, A. (2014). Identification of causal genetic drivers of human disease through systems-level analysis of regulatory networks. *Cell*, 159(2):402–14.

[66] Chen, L., Willis, S. N., Wei, A., Smith, B. J., Fletcher, J. I., Hinds, M. G., Colman, P. M., Day, C. L., Adams, J. M., and Huang, D. C. (2005). Differential Targeting of Prosurvival Bcl-2 Proteins by Their BH3-Only Ligands Allows Complementary Apoptotic Function. *Molecular Cell*, 17(3):393–403.

[67] Chen, S., Guttridge, D. C., You, Z., Zhang, Z., Fribley, A., Mayo, M. W., Kitajewski, J., and Wang, C.-y. (2001). WNT-1 Signaling Inhibits Apoptosis by Activating β-Catenin/T Cell Factor–Mediated Transcription. *The Journal of Cell Biology*, 152(1):87–96.

[68] Chen, Y. and Olopade, O. I. (2008). MYC in breast tumor progression. *Expert Review of Anticancer Therapy*, 8(10):1689–1698.

[69] Cheng, M., Sexl, V., Sherr, C. J., and Roussel, M. F. (1998). Assembly of cyclin D-dependent kinase and titration of p27Kip1 regulated by mitogen-activated protein kinase kinase (MEK1). *Proceedings of the National Academy of Sciences of the United States of America*, 95(3):1091–6.

[70] Chmielecki, J., Foo, J., Oxnard, G. R., Hutchinson, K., Ohashi, K., Somwar, R., Wang, L., Amato, K. R., Arcila, M., Sos, M. L., Socci, N. D., Viale, A., de Stanchina, E., Ginsberg, M. S., Thomas, R. K., Kris, M. G., Inoue, A., Ladanyi, M., Miller, V. A., Michor, F., and Pao, W. (2011). Optimization of dosing for EGFR-mutant non-small cell lung cancer with evolutionary cancer modeling. *Science translational medicine*, 3(90):90ra59.

[71] Cho, H., Berger, B., and Peng, J. (2016). Compact Integration of Multi-Network Topology for Functional Analysis of Genes. *Cell Systems*, 3(6):540–548.e5.

[72] Chong, C. R. and Jänne, P. A. (2013). The quest to overcome resistance to EGFR-targeted therapies in cancer. *Nature medicine*, 19(11):1389–400.

[73] Chonghaile, T. N. and Letai, A. (2008). Mimicking the BH3 domain to kill cancer cells. *Oncogene*, 27(0 1):S149–S157.

[74] Chowdhury, S. and Sarkar, R. R. (2015). Comparison of human cell signaling pathway databases - Evolution, drawbacks and challenges. *Database*, 2015(July):1–25.

[75] Chuang, R., Hall, B. A., Benque, D., Cook, B., Ishtiaq, S., Piterman, N., Taylor, A., Vardi, M., Koschmieder, S., Gottgens, B., and Fisher, J. (2015). Drug Target Optimization in Chronic Myeloid Leukemia Using Innovative Computational Platform. *Scientific Reports*, 5:8190.

[76] Chung, S. S., Lee, J. S., Kim, M., Ahn, B. Y., Jung, H. S., Lee, H. M., Kim, J. W., and Park, K. S. (2012). Regulation of Wnt/β-catenin signaling by CCAAT/enhancer binding protein β during adipogenesis. *Obesity*, 20(3):482–487.

[77] Clark, A., Galpin, V., Gilmore, S., Guerriero, M. L., and Hillston, J. (2012). Formal Methods for Checking the Consistency of Biological Models. In Goryanin, I. I. and Goryachev, A. B., editors, *Advances in Systems Biology*, pages 461–475. Springer, New York, NY.

[78] Clarke, E. M., Grumberg, O., and Peled, D. A. (1999). *Model checking*. MIT Press.

[79] Cleary, A. S., Leonard, T. L., Gestl, S. A., and Gunther, E. J. (2014). Tumour cell heterogeneity maintained by cooperating subclones in Wnt-driven mammary cancers. *Nature*, 508(7494):113–117.

[80] Cleveland, C., Liao, D., and Austin, R. (2012). Physics of cancer propagation: A game theory perspective. *AIP Advances*, 2(1):1–10.

[81] Clevers, H., Loh, K. M., and Nusse, R. (2014). An integral program for tissue renewal and regeneration: Wnt signaling and stem cell control. *Science*, 346(6205):1248012–1248012.

[82] Cnaan, A., Laird, N. A. N. M., and Slasor, P. (1997). Using the general linear mixed model to analyse unbalanced repeated measures and longitudinal data. *Stat.Med.*, 16(20):2349–2380.

[83] Cobb, M. H. (1999). MAP kinase pathways. *Progress in Biophysics and Molecular Biology*, 71(3-4):479–500.

[84] Coller, H. A., Grandori, C., Tamayo, P., Colbert, T., Lander, E. S., Eisenman, R. N., and Golub, T. R. (2000). Expression analysis with oligonucleotide microarrays reveals that MYC regulates genes involved in growth, cell cycle, signaling, and adhesion. *Proceedings of the National Academy of Sciences of the United States of America*, 97(7):3260–5.

[85] Collins, N. L., Reginato, M. J., Paulus, J. K., Sgroi, D. C., Labaer, J., and Brugge, J. S. (2005). G1/S cell cycle arrest provides anoikis resistance through Erk-mediated Bim suppression. *Molecular and cellular biology*, 25(12):5282–91.

[86] Colman, M. S., Afshari, C. A., and Barrett, J. C. (2000). Regulation of p53 stability and activity in response to genotoxic stress. *Mutation research*, 462(2-3):179–88.

[87] Conacci-Sorrell, M., McFerrin, L., and Eisenman, R. N. (2014). An overview of MYC and its interactome. *Cold Spring Harbor Perspectives in Medicine*, 4(1):a014357.

[88] Cook, B., Fisher, J., Hall, B. A., Ishtiaq, S., Juniwal, G., and Piterman, N. (2014). Finding instability in biological models. *Lecture Notes in Computer Science (including subseries Lecture Notes in Artificial Intelligence and Lecture Notes in Bioinformatics)*, 8559 LNCS:358–372.

[89] Cook, B., Fisher, J., Krepska, E., and Piterman, N. (2011). Proving Stabilization of Biological Systems. In *VMCAI*, volume 11, pages 134–149. Springer.

[90] Cook, S. A. (1971). The complexity of theorem-proving procedures. *Proceedings of the 3rd {IEEE} Symposium on the Theory of Computation*, pages 151–158.

[91] Corda, G. and Sala, A. (2017). Non-canonical WNT/PCP signalling in cancer: Fzd6 takes centre stage. *Oncogenesis*, 6(7):e364.

[92] Crasta, K., Ganem, N. J., Dagher, R., Lantermann, A. B., Ivanova, E. V., Pan, Y., Nezi, L., Protopopov, A., Chowdhury, D., and Pellman, D. (2012). DNA breaks and chromosome pulverization from errors in mitosis. *Nature*, 482(7383):53–58.

[93] Crawley, M. J. (2012). *The R book*. John Wiley & Sons.

[94] Csermely, P., Korcsmaros, T., Kiss, H. J. M., London, G., and Nussinov, R. (2012). Structure and dynamics of molecular networks: A novel paradigm of drug discovery. A comprehensive review. *Pharmacology and Therapeutics*, 138(3):333–408.

[95] Cui, Y. and Guo, G. (2016). Immunomodulatory function of the tumor suppressor p53 in host immune response and the tumor microenvironment. *International Journal of Molecular Sciences*, 17(11).

[96] Curtis, C., Shah, S. P., Chin, S.-F., Turashvili, G., Rueda, O. M., Dunning, M. J., Speed, D., Lynch, A. G., Samarajiwa, S., Yuan, Y., Gräf, S., Ha, G., Haffari, G., Bashashati, A., Russell, R., McKinney, S., Langerød, A., Green, A., Provenzano, E., Wishart, G., Pinder, S., Watson, P., Markowetz, F., Murphy, L., Ellis, I., Purushotham, A., Børresen-Dale, A.-L., Brenton, J. D., Tavaré, S., Caldas, C., and Aparicio, S. (2012). The genomic and transcriptomic architecture of 2,000 breast tumours reveals novel subgroups. *Nature*, 486(7403):346–52.

[97] Cusimano, A., Foderà, D., D'Alessandro, N., Lampiasi, N., Azzolina, A., Montalto, G., and Cervello, M. (2007). Potentiation of the antitumor effects of both selective cyclooxygenase-1 and cyclooxygenase-2 inhibitors in human hepatic cancer cells by inhibition of the MEK/ERK pathway. *Cancer biology & therapy*, 6(9):1461–8.

[98] Dai, X., Li, T., Bai, Z., Yang, Y., Liu, X., Zhan, J., and Shi, B. (2015). Breast cancer intrinsic subtype classification, clinical use and future trends. *Am J Cancer Res*, 5(10):2929–2943.

[99] Dang, C. V., Kim, J.-w., Gao, P., and Yustein, J. (2008). The interplay between MYC and HIF in cancer. *Nature reviews. Cancer*, 8(1):51–6.

[100] Dang, C. V., O'Donnell, K. A., Zeller, K. I., Nguyen, T., Osthus, R. C., and Li, F. (2006). The c-Myc target gene network. *Seminars in cancer biology*, 16(4):253–64.

[101] Dang, C. V., Reddy, E. P., Shokat, K. M., and Soucek, L. (2017). Drugging the 'undruggable' cancer targets. *Nature Reviews Cancer*, 17(8):502–508.

[102] Das, S. K., Menezes, M. E., Bhatia, S., Wang, X.-Y., Emdad, L., Sarkar, D., and Fisher, P. B. (2015). Gene Therapies for Cancer: Strategies, Challenges and Successes. *Journal of Cellular Physiology*, 230(2):259–271.

[103] Davidich, M. and Bornholdt, S. (2008). The transition from differential equations to Boolean networks: A case study in simplifying a regulatory network model. *Journal of Theoretical Biology*, 255(3):269–277.

[104] Davidson, E. H. (2010). Emerging properties of animal gene regulatory networks. *Nature*, 468(7326):911–920.

[105] Davis, A., Gao, R., and Navin, N. (2017). Tumor evolution: Linear, branching, neutral or punctuated? *Biochimica et Biophysica Acta - Reviews on Cancer*, 1867(2):151–161.

[106] De, A. (2011). Wnt/Ca2+ signaling pathway: a brief overview. *Acta Biochimica et Biophysica Sinica*, 43(10):745–756.

[107] de Moura, L. and Bjørner, N. (2008). Z3: An Efficient SMT Solver. In Ramakrishnan, C. R. and Rehof, J., editors, *Tools and Algorithms for the Construction and Analysis of Systems*, pages 337–340. Springer Berlin Heidelberg, Berlin, Heidelberg.

[108] Depowski, P. L., Rosenthal, S. I., and Ross, J. S. (2001). Loss of expression of the PTEN gene protein product is associated with poor outcome in breast cancer. *Modern pathology : an official journal of the United States and Canadian Academy of Pathology, Inc*, 14(7):672–676.

[109] Dewson, G., Kratina, T., Sim, H. W., Puthalakath, H., Adams, J. M., Colman, P. M., and Kluck, R. M. (2008). To trigger apoptosis, Bak exposes its BH3 domain and homodimerizes via BH3:groove interactions. *Molecular cell*, 30(3):369–80.

[110] Dhillon, A. S., Hagan, S., Rath, O., and Kolch, W. (2007). MAP kinase signalling pathways in cancer. *Oncogene*, 26(22):3279–3290.

[111] Diehl, J. A., Cheng, M., Roussel, M. F., and Sherr, C. J. (1998). Glycogen synthase kinase-3beta regulates cyclin D1 proteolysis and subcellular localization. *Genes & development*, 12(22):3499–3511.

[112] Dijkers, P. F., Medema, R. H., Pals, C., Banerji, L., Thomas, N. S., Lam, E. W., Burgering, B. M., Raaijmakers, J. A., Lammers, J. W., Koenderman, L., and Coffer, P. J. (2000). Forkhead transcription factor FKHR-L1 modulates cytokine-dependent transcriptional regulation of p27(KIP1). *Mol Cell Biol*, 20(24):9138–9148.

[113] Ding, L., Ley, T. J., Larson, D. E., Miller, C. A., Koboldt, D. C., Welch, J. S., Ritchey, J. K., Young, M. A., Lamprecht, T., McLellan, M. D., McMichael, J. F., Wallis, J. W., Lu, C., Shen, D., Harris, C. C., Dooling, D. J., Fulton, R. S., Fulton, L. L., Chen, K., Schmidt, H., Kalicki-Veizer, J., Magrini, V. J., Cook, L., McGrath, S. D., Vickery, T. L., Wendl, M. C., Heath, S., Watson, M. A., Link, D. C., Tomasson, M. H., Shannon, W. D., Payton, J. E., Kulkarni, S., Westervelt, P., Walter, M. J., Graubert, T. A., Mardis, E. R., Wilson, R. K., and DiPersio, J. F. (2012). Clonal evolution in relapsed acute myeloid leukaemia revealed by whole-genome sequencing. *Nature*, 481(7382):506–510.

[114] Ding, Q., Xia, W., Liu, J. C., Yang, J. Y., Lee, D. F., Xia, J., Bartholomeusz, G., Li, Y., Pan, Y., Li, Z., Bargou, R. C., Qin, J., Lai, C. C., Tsai, F. J., Tsai, C. H., and Hung, M. C. (2005). Erk associates with and primes GSK-3β for its inactivation resulting in upregulation of β-catenin. *Molecular Cell*, 19(2):159–170.

[115] Doehn, U., Hauge, C., Frank, S. R., Jensen, C. J., Duda, K., Nielsen, J. V., Cohen, M. S., Johansen, J. V., Winther, B. R., Lund, L. R., Winther, O., Taunton, J., Hansen, S. H., and Frödin, M. (2009). RSK is a principal effector of the RAS-ERK pathway for eliciting a coordinate promotile/invasive gene program and phenotype in epithelial cells. *Molecular cell*, 35(4):511–22.

[116] Dong, A., Wodziak, D., and Lowe, A. W. (2015). Epidermal growth factor receptor (EGFR) signaling requires a specific endoplasmic reticulum thioredoxin for the post-translational control of receptor presentation to the cell surface. *Journal of Biological Chemistry*, 290(13):8016–8027.

[117] Downward, J. (2003). Targeting RAS signalling pathways in cancer therapy. *Nature reviews. Cancer*, 3(1):11–22.

[118] Draetta, G. F. (1994). Mammalian G1 cyclins. *Current Opinion in Cell Biology*, 6(6):842–846.

[119] Drake, J. M., Paull, E. O., Graham, N. A., Lee, J. K., Smith, B. A., Titz, B., Stoyanova, T., Faltermeier, C. M., Uzunangelov, V., Carlin, D. E., Fleming, D. T., Wong, C. K., Newton, Y., Sudha, S., Vashisht, A. A., Huang, J., Wohlschlegel, J. A., Graeber, T. G., Witte, O. N., and Stuart, J. M. (2016). Phosphoproteome Integration Reveals Patient-Specific Networks in Prostate Cancer. *Cell*, 166(4):1041–1054.

[120] Duarte, N. C., Becker, S. A., Jamshidi, N., Thiele, I., Mo, M. L., Vo, T. D., Srivas, R., and Palsson, B. O. (2007). Global reconstruction of the human metabolic network based on genomic and bibliomic data. *Proceedings of the National Academy of Sciences*, 104(6):1777–1782.

[121] Dunn, S.-J., Martello, G., Yordanov, B., Emmott, S., and Smith, a. G. (2014). Defining an essential transcription factor program for naïve pluripotency. *Science (New York, N.Y.)*, 344(6188):1156–60.

[122] Durinck, S., Ho, C., Wang, N. J., Liao, W., Jakkula, L. R., Collisson, E. A., Pons, J., Chan, S. W., Lam, E. T., Chu, C., Park, K., woo Hong, S., Hur, J. S., Huh, N., Neuhaus, I. M., Yu, S. S., Grekin, R. C., Mauro, T. M., Cleaver, J. E., Kwok, P. Y., LeBoit, P. E., Getz, G., Cibulskis, K., Aster, J. C., Huang, H., Purdom, E., Li, J., Bolund, L., Arron, S. T., Gray, J. W., Spellman, P. T., and Cho, R. J. (2011). Temporal dissection of tumorigenesis in primary cancers. *Cancer Discovery*, 1(2):137–143.

[123] Dutkowski, J., Kramer, M., Surma, M. A., Balakrishnan, R., Cherry, J. M., Krogan, N. J., and Ideker, T. (2013). A gene ontology inferred from molecular networks. *Nature biotechnology*, 31(1):38–45.

[124] Dytham, C. (2011). *Choosing and using statistics: a biologist's guide*. Blackwell Science, Oxford, 3rd edition.

[125] Easterbrook, P., Gopalan, R., Berlin, J., and Matthews, D. (1991). Publication bias in clinical research. *The Lancet*, 337(8746):867–872.

[126] Eduati, F., De Las Rivas, J., Di Camillo, B., Toffolo, G., and Saez-Rodriguez, J. (2012). Integrating literature-constrained and data-driven inference of signalling networks. *Bioinformatics*, 28(18):2311–2317.

[127] Eguchi, Y., Srinivasan, A., Tomaselli, K. J., Shimizu, S., and Tsujimoto, Y. (1999). ATP-dependent steps in apoptotic signal transduction. *Cancer Research*, 59(9):2174–2181.

[128] Eilers, M., Schirm, S., and Bishop, J. M. (1991). The MYC protein activates transcription of the alpha-prothymosin gene. *The EMBO journal*, 10(1):133–41.

[129] Eldar-Finkelman, H., Seger, R., Vandenheede, J. R., and Krebs, E. G. (1995). Inactivation of glycogen synthase kinase-3 by epidermal growth factor is mediated by mitogen-activated protein kinase/p90 ribosomal protein S6 kinase signaling pathway in NIH/3T3 cells. *Journal of Biological Chemistry*, 270(3):987–990.

[130] Elmore, S. (2007). Apoptosis: A Review of Programmed Cell Death. *Toxicologic Pathology*, 35(4):495–516.

[131] Emmert-Streib, F., Glazko, G. V., Altay, G., and Simoes, R. d. M. (2012). Statistical inference and reverse engineering of gene regulatory networks from observational expression data. *Frontiers in Genetics*, 3(FEB):1–15.

[132] Enriquez-Navas, P. M., Kam, Y., Das, T., Hassan, S., Silva, A., Foroutan, P., Ruiz, E., Martinez, G., Minton, S., Gillies, R. J., and Gatenby, R. A. (2016). Exploiting evolutionary principles to prolong tumor control in preclinical models of breast cancer. *Science Translational Medicine*, 8(327):327ra24–327ra24.

[133] Eroglu, Z. and Ribas, A. (2016). Combination therapy with BRAF and MEK inhibitors for melanoma: latest evidence and place in therapy. *Therapeutic Advances in Medical Oncology*, 8(1):48–56.

[134] Esteva, F. J., Hortobagyi, G. N., Sahin, a. a., Smith, T. L., Chin, D. M., Liang, S. Y., Pusztai, L., Buzdar, a. U., and Bacus, S. S. (2001). Expression of erbB/HER receptors, heregulin and P38 in primary breast cancer using quantitative immunohistochemistry. *Pathology oncology research : POR*, 7(3):171–7.

[135] Evan, G. I. and Vousden, K. H. (2001). Proliferation, cell cycle and apoptosis in cancer. *Nature*, 411(May):342–348.

[136] Evan, G. I., Wyllie, A. H., Gilbert, C. S., Littlewood, T. D., Land, H., Brooks, M., Waters, C. M., Penn, L. Z., and Hancock, D. C. (1992). Induction of apoptosis in fibroblasts by c-myc protein. *Cell*, 69(1):119–28.

[137] Ewer, M. S., Vooletich, M. T., Durand, J.-B., Woods, M. L., Davis, J. R., Valero, V., and Lenihan, D. J. (2005). Reversibility of trastuzumab-related cardiotoxicity: new insights based on clinical course and response to medical treatment. *Journal of clinical oncology : official journal of the American Society of Clinical Oncology*, 23(31):7820–6.

[138] Faich, G., Goldstein, J. L., Simon, L. S., Pincus, T., Whelton, A., Stenson, W. F., Burr, A. M., Zhao, W. W., Kent, J. D., Lefkowith, J. B., and Geis, G. S. (2000). Gastrointestinal Toxicity With Celecoxib vs. *JAMA : the journal of the American Medical Association*, 284(10):1247–1255.

[139] Fanale, D., Bazan, V., Corsini, L. R., Caruso, S., Insalaco, L., Castiglia, M., Cicero, G., Bronte, G., and Russo, A. (2013). HIF-1 is involved in the negative regulation of AURKA expression in breast cancer cell lines under hypoxic conditions. *Breast Cancer Research and Treatment*, pages 1–13.

[140] Farago, M., Dominguez, I., Landesman-Bollag, E., Xu, X., Rosner, A., Cardiff, R. D., and Seldin, D. C. (2005). Kinase-inactive glycogen synthase kinase 3beta promotes Wnt signaling and mammary tumorigenesis. *Cancer research*, 65(13):5792–801.

[141] Farkas, I. J., Korcsmaros, T., Kovacs, I. A., Mihalik, A., Palotai, R., Simko, G. I., Szalay, K. Z., Szalay-Beko, M., Vellai, T., Wang, S., and Csermely, P. (2011). Network-Based Tools for the Identification of Novel Drug Targets. *Science Signaling*, 4(173):pt3–pt3.

[142] Fearon, E. R. and Vogelstein, B. (1990). A genetic model for colorectal tumorigenesis. *Cell*, 61(5):759–767.

[143] Feng, X. H., Liang, Y. Y., Liang, M., Zhai, W., and Lin, X. (2002). Direct interaction of c-Myc with Smad2 and Smad3 to inhibit TGF-β-mediated induction of the CDK inhibitor p15Ink4B. *Molecular Cell*, 9(1):133–143.

[144] Ferlay, J., Soerjomataram, I., Dikshit, R., Eser, S., Mathers, C., Rebelo, M., Parkin, D. M., Forman, D., and Bray, F. (2015). Cancer incidence and mortality worldwide: Sources, methods and major patterns in GLOBOCAN 2012. *International Journal of Cancer*, 136(5):E359–E386.

[145] Fernandez-Pol, J. A., Talkad, V. D., Klos, D. J., and Hamilton, P. D. (1987). Suppression of the EGF-dependent induction of c-myc proto-oncogene expression by transforming growth factor beta in a human breast carcinoma cell line. *Biochemical and biophysical research communications*, 144(3):1197–205.

[146] Finch, A. J., Soucek, L., Junttila, M. R., Swigart, L. B., and Evan, G. I. (2009). Acute Overexpression of Myc in Intestinal Epithelium Recapitulates Some but Not All the Changes Elicited by Wnt/ -Catenin Pathway Activation. *Molecular and Cellular Biology*, 29(19):5306–5315.

[147] Fisher, J., Piterman, N., Hajnal, A., and Henzinger, T. a. (2007). Predictive modeling of signaling crosstalk during C. elegans vulval development. *PLoS computational biology*, 3(5):e92.

[148] Fisher, J., Piterman, N., and Vardi, M. Y. (2011). The Only Way Is Up. In Butler, M. and Schulte, W., editors, *FM 2011: Formal Methods: 17th International Symposium on Formal Methods, Limerick, Ireland, June 20-24, 2011. Proceedings*, pages 3–11. Springer Berlin Heidelberg, Berlin, Heidelberg.

[149] Fisher, R. A. (1950). *Statistical methods for research workers.* Biological monographs and manuals. Oliver and Boyd, Edinburgh, 11th edition.

[150] Fitzgerald, J. B., Schoeberl, B., Nielsen, U. B., and Sorger, P. K. (2006). Systems biology and combination therapy in the quest for clinical efficacy. *Nature Chemical Biology*, 2(9):458–466.

[151] Flanagan, L., Van Weelden, K., Ammerman, C., Ethier, S. P., and Welsh, J. (1999). SUM-159PT cells: a novel estrogen independent human breast cancer model system. *Breast cancer research and treatment*, 58(3):193–204.

[152] Fletcher, M. N. C., Wang, X., Santiago, I. D., Reilly, M. O., Chin, S.-F., Rueda, O. M., Caldas, C., Ponder, B. A. J., Markowetz, F., Meyer, K. B., Castro, M. A. A., Wang, X., de Santiago, I., O'Reilly, M., Chin, S.-F., Rueda, O. M., Caldas, C., Ponder, B. A. J., Markowetz, F., and Meyer, K. B. (2013). Master regulators of FGFR2 signalling and breast cancer risk. *Nature communications*, 4:2464.

[153] Folger, O., Jerby, L., Frezza, C., Gottlieb, E., Ruppin, E., and Shlomi, T. (2011). Predicting selective drug targets in cancer through metabolic networks. *Molecular Systems Biology*, 7(501):1–10.

[154] Fomchenko, E. I., Dougherty, J. D., Helmy, K. Y., Katz, A. M., Pietras, A., Brennan, C., Huse, J. T., Milosevic, A., and Holland, E. C. (2011). Recruited cells can become transformed and overtake PDGF-induced murine gliomas in vivo during tumor progression. *PLoS ONE*, 6(7).

[155] Foo, J. and Michor, F. (2014). The evolution of accuired resistance to anti-cancer therapy. *J. Theor Biol.*, 0:10–20.

[156] Forbes, S. A., Beare, D., Boutselakis, H., Bamford, S., Bindal, N., Tate, J., Cole, C. G., Ward, S., Dawson, E., Ponting, L., Stefancsik, R., Harsha, B., YinKok, C., Jia, M., Jubb, H., Sondka, Z., Thompson, S., De, T., and Campbell, P. J. (2017). COSMIC: Somatic cancer genetics at high-resolution. *Nucleic Acids Research*, 45(D1):D777–D783.

[157] Franke, T. F., Kaplan, D. R., and Cantley, L. C. (1997). PI3K: downstream AKTion blocks apoptosis. *Cell*, 88(4):435–7.

[158] Friedlander, M. L. and Stockman, S. J. (1983). Anchoring and publicity effects in clinical judgment. *Journal of Clinical Psychology*, 39(4):637–644.

[159] Friedmann-Morvinski, D. and Verma, I. M. (2014). Dedifferentiation and reprogramming: Origins of cancer stem cells. *EMBO Reports*, 15(3):244–253.

[160] Fumiã, H. F. and Martins, M. L. (2013). Boolean Network Model for Cancer Pathways: Predicting Carcinogenesis and Targeted Therapy Outcomes. *PLoS ONE*, 8(7).

[161] Furlong, L. I. (2013). Human diseases through the lens of network biology. *Trends in Genetics*, 29(3):150–159.

[162] Furuuchi, K., Tada, M., Yamada, H., Kataoka, A., Furuuchi, N., Hamada, J., Takahashi, M., Todo, S., and Moriuchi, T. (2000). Somatic mutations of the APC gene in primary breast cancers. *The American journal of pathology*, 156(6):1997–2005.

[163] Gadadhar, S. and Karande, A. A. (2015). Targeted Cancer Therapy: History and Development of Immunotoxins. In Verma, R. S. and Bonavida, B., editors, *Resistance to Immunotoxins in Cancer Therapy*, pages 1–31. Springer International Publishing.

[164] Gajewski, T. F., Schreiber, H., and Fu, Y.-X. (2013). Innate and adaptive immune cells in the tumor microenvironment. *Nature Immunology*, 14(10):1014–1022.

[165] Gao, R., Davis, A., McDonald, T. O., Sei, E., Shi, X., Wang, Y., Tsai, P.-C., Casasent, A., Waters, J., Zhang, H., Meric-Bernstam, F., Michor, F., and Navin, N. E. (2016). Punctuated copy number evolution and clonal stasis in triple-negative breast cancer. *Nature genetics*, 48(10):1119–30.

[166] Garg, A., Di Cara, A., Xenarios, I., Mendoza, L., and De Micheli, G. (2008). Synchronous versus asynchronous modeling of gene regulatory networks. *Bioinformatics*, 24(17):1917–1925.

[167] Garg, A., Xenarios, I., Mendoza, L., and DeMicheli, G. (2007). An Efficient Method for Dynamic Analysis of Gene Regulatory Networks and in silico Gene Perturbation Experiments. In *Research in Computational Molecular Biology*, pages 62–76. Springer Berlin Heidelberg, Berlin, Heidelberg.

[168] Gatenby, R. A., Silva, A. S., Gillies, R. J., and Frieden, B. R. (2009). Adaptive therapy. *Cancer research*, 69(11):4894–903.

[169] Gelebart, P., Hegazy, S. A., Wang, P., Bone, K. M., Anand, M., Sharon, D., Hitt, M., Pearson, J. D., Ingham, R. J., Ma, Y., and Lai, R. (2012). Aberrant expression and biological significance of Sox2, an embryonic stem cell transcriptional factor, in ALK-positive anaplastic large cell lymphoma. *Blood Cancer Journal*, 2(8):1–11.

[170] Gerlinger, M., McGranahan, N., Dewhurst, S. M., Burrell, R. A., Tomlinson, I., and Swanton, C. (2014). Cancer: evolution within a lifetime. *Annual Review of Genetics*, 48:215–236.

[171] Germain, M., Milburn, J., and Duronio, V. (2008). MCL-1 inhibits BAX in the absence of MCL-1/BAX Interaction. *The Journal of biological chemistry*, 283(10):6384–92.

[172] Giacomantonio, C. E. and Goodhill, G. J. (2010). A boolean model of the gene regulatory network underlying mammalian cortical area development. *PLoS Computational Biology*, 6(9).

[173] Gianni, L., Eiermann, W., Semiglazov, V., Manikhas, A., Lluch, A., Tjulandin, S., Zambetti, M., Vazquez, F., Byakhow, M., Lichinitser, M., Climent, M. A., Ciruelos, E., Ojeda, B., Mansutti, M., Bozhok, A., Baronio, R., Feyereislova, A., Barton, C., Valagussa, P., and Baselga, J. (2010). Neoadjuvant chemotherapy with trastuzumab followed by adjuvant trastuzumab versus neoadjuvant chemotherapy alone, in patients with HER2-positive locally advanced breast cancer (the NOAH trial): a randomised controlled superiority trial with a parallel HER. *Lancet (London, England)*, 375(9712):377–84.

[174] Gibson, L., Holmgreen, S. P., Huang, D. C., Bernard, O., Copeland, N. G., Jenkins, N. A., Sutherland, G. R., Baker, E., Adams, J. M., and Cory, S. (1996). bcl-w, a novel member of the bcl-2 family, promotes cell survival. *Oncogene*, 13(4):665–75.

[175] Gilmore, A. P., Valentijn, A. J., Wang, P., Ranger, A. M., Bundred, N., O'Hare, M. J., Wakeling, A., Korsmeyer, S. J., and Streuli, C. H. (2002). Activation of BAD by therapeutic inhibition of epidermal growth factor receptor and transactivation by insulin-like growth factor receptor. *The Journal of biological chemistry*, 277(31):27643–50.

[176] Glass, L. and Kauffman, S. A. (1973). The logical analysis of continuous, non-linear biochemical control networks. *Journal of Theoretical Biology*, 39(1):103–129.

[177] Glöckner, S., Buurman, H., Kleeberger, W., Lehmann, U., and Kreipe, H. (2002). Marked intratumoral heterogeneity of c-myc and cyclinD1 but not of c-erbB2 amplification in breast cancer. *Laboratory investigation; a journal of technical methods and pathology*, 82(10):1419–1426.

[178] Goel, S., Chin, E. N., Fakhraldeen, S. A., Berry, S. M., Beebe, D. J., and Alexander, C. M. (2012). Both LRP5 and LRP6 receptors are required to respond to physiological Wnt ligands in mammary epithelial cells and fibroblasts. *Journal of Biological Chemistry*, 287(20):16454–16466.

[179] Gradishar, W., Kaklamani, V., Prasad Sahoo, T., Lokanatha, D., Raina, V., Bondarde, S., and Jain, M. (2014). A Double-Blind, Randomized, Placebo-Controlled, Phase 2b Study Evaluating the Efficacy and Safety of Sorafenib (SOR) in Combination with Paclitaxel (PAC) as a First-Line Therapy in Patients (pts) with Locally Recurrent or Metastatic Breast Cancer (BC). *Cancer Research*, 69(24 Supplement).

[180] Grafen, A. and Hails, R. (2002). *Modern statistics for the life sciences*. Oxford University Press, Oxford.

[181] Grandori, C., Cowley, S. M., James, L. P., and Eisenman, R. N. (2000). The Myc/Max/Mad network and the transcriptional control of cell behavior. *Annual review of cell and developmental biology*, 16:653–99.

[182] Gray, R., Bhattacharya, S., Bowden, C., Miller, K., and Comis, R. L. (2009). Independent review of E2100: A phase III trial of bevacizumab plus paclitaxel versus paclitaxel in women with metastatic breast cancer. *Journal of Clinical Oncology*, 27(30):4966–4972.

[183] Greaves, M. and Maley, C. C. (2012). Clonal evolution in cancer. *Nature*, 481(7381):306–13.

[184] Greenman, C. D., Pleasance, E. D., Newman, S., Yang, F., Fu, B., Nik-Zainal, S., Jones, D., Lau, K. W., Carter, N., Edwards, P. A., Futreal, P. A., Stratton, M. R., and Campbell, P. J. (2012). Estimation of rearrangement phylogeny for cancer genomes. *Genome Research*, 22(2):346–361.

[185] Greijer, A. E. and van der Wall, E. (2004). The role of hypoxia inducible factor 1 (HIF-1) in hypoxia induced apoptosis. *Journal of clinical pathology*, 57(10):1009–14.

[186] Greil, R., Moik, M., Reitsamer, R., Ressler, S., Stoll, M., Namberger, K., Menzel, C., and Mlineritsch, B. (2009). Neoadjuvant bevacizumab, docetaxel and capecitabine combination therapy for HER2/neu-negative invasive breast cancer: Efficacy and safety in a phase II pilot study. *European Journal of Surgical Oncology*, 35(10):1048–1054.

[187] Gupta, N., Jung, K., Wu, C., Alshareef, A., Alqahtani, H., Damaraju, S., Mackey, J. R., Ghosh, S., Sabri, S., Abdulkarim, B. S., Bigras, G., and Lai, R. (2017). High Myc expression and transcription activity underlies intra-tumoral heterogeneity in triple-negative breast cancer. *Oncotarget*, 8(17):28101–28115.

[188] Gutteridge, E., Agrawal, A., Nicholson, R., Cheung, K. L., Robertson, J., and Gee, J. (2010). The effects of gefitinib in tamoxifen-resistant and hormone-insensitive breast cancer: A phase II study. *International Journal of Cancer*, 126(8):1806–1816.

[189] Hall, B. A., Piterman, N., Hajnal, A., and Fisher, J. (2015). Emergent stem cell homeostasis in the C. elegans germline is revealed by hybrid modeling. *Biophysical journal*, 109(2):428–38.

[190] Hanahan, D. and Weinberg, R. A. (2011). Hallmarks of cancer: The next generation. *Cell*, 144(5):646–674.

[191] Harris, S. L. and Levine, A. J. (2005). The p53 pathway: positive and negative feedback loops. *Oncogene*, 24:2899–2908.

[192] Hartman, J. L., Garvik, B., and Hartwell, L. (2001). Principles for the buffering of genetic variation. *Science (New York, N.Y.)*, 291(5506):1001–4.

[193] Harvey, W. R. (1966). Least-squares analysis of data with unequal subclass numbers. *Technical Report ARS-20-8*.

[194] He, B., You, L., Uematsu, K., Xu, Z., Lee, A. Y., Matsangou, M., McCormick, F., and Jablons, D. M. (2004a). A monoclonal antibody against Wnt-1 induces apoptosis in human cancer cells. *Neoplasia (New York, N.Y.)*, 6(1):7–14.

[195] He, G., Siddik, Z. H., Huang, Z., Wang, R., Koomen, J., Kobayashi, R., Khokhar, A. R., and Kuang, J. (2005). Induction of p21 by p53 following DNA damage inhibits both Cdk4 and Cdk2 activities. *Oncogene*, 24(18):2929–43.

[196] He, T. C., Sparks, A. B., Rago, C., Hermeking, H., Zawel, L., da Costa, L. T., Morin, P. J., Vogelstein, B., and Kinzler, K. W. (1998). Identification of c-MYC as a target of the APC pathway. *Science*, 281(5382):1509–1512.

[197] He, X., Semenov, M., Tamai, K., and Zeng, X. (2004b). LDL receptor-related proteins 5 and 6 in Wnt/beta-catenin signaling: arrows point the way. *Development (Cambridge, England)*, 131(8):1663–77.

[198] Hegde, P. S., Rusnak, D., Bertiaux, M., Alligood, K., Strum, J., Gagnon, R., and Gilmer, T. M. (2007). Delineation of molecular mechanisms of sensitivity to lapatinib in breast cancer cell lines using global gene expression profiles. *Mol. Cancer Ther.*, 6(5):1629–40.

[199] Heiser, L. M., Wang, N. J., Talcott, C. L., Laderoute, K. R., Knapp, M., Guan, Y., Hu, Z., Ziyad, S., Weber, B. L., Laquerre, S., Jackson, J. R., Wooster, R. F., Kuo, W., Gray, J. W., and Spellman, P. T. (2009). Integrated analysis of breast cancer cell lines reveals unique signaling pathways. *Genome Biology*, 10(3):R31.

[200] Hermeking, H., Rago, C., Schuhmacher, M., Li, Q., Barrett, J. F., Obaya, A. J., O'Connell, B. C., Mateyak, M. K., Tam, W., Kohlhuber, F., Dang, C. V., Sedivy, J. M., Eick, D., Vogelstein, B., and Kinzler, K. W. (2000). Identification of CDK4 as a target of c-MYC. *Proceedings of the National Academy of Sciences of the United States of America*, 97(5):2229–34.

[201] Hill, C. S. and Treisman, R. (1995). Differential activation of c-fos promoter elements by serum, lysophosphatidic acid, G proteins and polypeptide growth factors. *The EMBO journal*, 14(20):5037–5047.

[202] Hinck, A. P. (2012). Structural studies of the TGF-βs and their receptors - insights into evolution of the TGF-β superfamily. *FEBS letters*, 586(14):1860–70.

[203] Hobor, S., Van Emburgh, B. O., Crowley, E., Misale, S., Di Nicolantonio, F., and Bardelli, A. (2014). TGFα and amphiregulin paracrine network promotes resistance to EGFR blockade in colorectal cancer cells. *Clinical Cancer Research*, 20(24):6429–6438.

[204] Hochhaus, A., Erben, P., Ernst, T., and Mueller, M. C. (2007). Resistance to Targeted Therapy in Chronic Myelogenous Leukemia. *Seminars in Hematology*, 44(SUPPL. 1):15–24.

[205] Hoeben, A. N. N., Landuyt, B., Highley, M. S. M., Wildiers, H., Oosterom, A. T. V. A. N., Bruijn, E. A. D. E., Van Oosterom, A. T., and De Bruijn, E. A. (2004). Vascular endothelial growth factor and angiogenesis. *Pharmacological reviews*, 56(4):549–580.

[206] Holbro, T., Beerli, R. R., Maurer, F., Koziczak, M., Barbas, C. F., and Hynes, N. E. (2003). The ErbB2/ErbB3 heterodimer functions as an oncogenic unit: ErbB2 requires ErbB3 to drive breast tumor cell proliferation. *Proceedings of the National Academy of Sciences of the United States of America*, 100(15):8933–8.

[207] Hollestelle, A., Nagel, J. H. A., Smid, M., Lam, S., Elstrodt, F., Wasielewski, M., Ng, S. S., French, P. J., Peeters, J. K., Rozendaal, M. J., Riaz, M., Koopman, D. G., Ten Hagen, T. L. M., De Leeuw, B. H. C. G. M., Zwarthoff, E. C., Teunisse, A., Van Der Spek, P. J., Klijn, J. G. M., Dinjens, W. N. M., Ethier, S. P., Clevers, H., Jochemsen, A. G., Den Bakker, M. A., Foekens, J. A., Martens, J. W. M., and Schutte, M. (2010). Distinct gene mutation profiles among luminal-type and basal-type breast cancer cell lines. *Breast Cancer Research and Treatment*, 121(1):53–64.

[208] Holliday, D. L. and Speirs, V. (2011). Choosing the right cell line for breast cancer research. *Breast cancer research : BCR*, 13:215.

[209] Holm, S. (1979). A Simple Sequentially Rejective Multiple Test Procedure. *Scandinavian Journal of Statistics*, 6(2):65–70.

[210] Hong, C., Hwang, J., Cho, K. H., and Shin, I. (2015). An efficient steady-state analysis method for large Boolean networks with high maximum node connectivity. *PLoS ONE*, 10(12):1–19.

[211] Hopewell, S., Clarke, M., and Mallett, S. (2006). Grey Literature and Systematic Reviews. *Publication Bias in Meta-Analysis*, pages 49–72.

[212] Horiuchi, D., Anderton, B., and Goga, A. (2014). Taking on Challenging Targets: Making MYC Druggable. *American Society of Clinical Oncology Educational Book*, 34(415):e497–e502.

[213] Hortobagyi, G. N., Stemmer, S. M., Burris, H. A., Yap, Y.-S., Sonke, G. S., Paluch-Shimon, S., Campone, M., Blackwell, K. L., André, F., Winer, E. P., Janni, W., Verma, S., Conte, P., Arteaga, C. L., Cameron, D. A., Petrakova, K., Hart, L. L., Villanueva, C., Chan, A., Jakobsen, E., Nusch, A., Burdaeva, O., Grischke, E.-M., Alba, E., Wist, E., Marschner, N., Favret, A. M., Yardley, D., Bachelot, T., Tseng, L.-M., Blau, S., Xuan, F., Souami, F., Miller, M., Germa, C., Hirawat, S., and O'Shaughnessy, J. (2016). Ribociclib

as First-Line Therapy for HR-Positive, Advanced Breast Cancer. *New England Journal of Medicine*, 375(18):1738–1748.

[214] Howe, L. R., Crawford, H. C., Subbaramaiah, K., Hassell, J. a., Dannenberg, a. J., and Brown, a. M. (2001). PEA3 is up-regulated in response to Wnt1 and activates the expression of cyclooxygenase-2. *The Journal of biological chemistry*, 276(23):20108–15.

[215] Howe, L. R., Watanabe, O., Leonard, J., and Brown, A. M. C. (2003). Twist is up-regulated in response to Wnt1 and inhibits mouse mammary cell differentiation. *Cancer Research*, 63(8):1906–1913.

[216] Hruban, R. H., Goggins, M., Parsons, J., and Kern, S. E. (2000). Progression model for pancreatic cancer. *Clinical cancer research : an official journal of the American Association for Cancer Research*, 6(8):2969–72.

[217] Huang, L. E. (2008). Carrot and stick: HIF-alpha engages c-Myc in hypoxic adaptation. *Cell death and differentiation*, 15(4):672–677.

[218] Huang, S., Eichler, G., Bar-Yam, Y., and Ingber, D. E. (2005). Cell fates as high-dimensional attractor states of a complex gene regulatory network. *Physical Review Letters*, 94(12):1–4.

[219] Hummert, S., Bohl, K., Basanta, D., Deutsch, A., Werner, S., Theißen, G., Schroeter, A., and Schuster, S. (2014). Evolutionary game theory: cells as players. *Mol. BioSyst.*, 10(12):3044–3065.

[220] Hurvitz, S. and Mead, M. (2015). Triple-negative breast cancer. *Current Opinion in Obstetrics and Gynecology*, page 1.

[221] Ibrahim, M. and Richardson, M. K. (2017). Beyond organoids: In vitro vasculogenesis and angiogenesis using cells from mammals and zebrafish. *Reproductive Toxicology*, 73:292–311.

[222] Independent UK Panel on Breast Cancer Screening (2012). The benefits and harms of breast cancer screening: an independent review. *Lancet (London, England)*, 380(9855):1778–86.

[223] Inoue, M. and Kaneko, K. (2013). Cooperative Adaptive Responses in Gene Regulatory Networks with Many Degrees of Freedom. *PLoS Computational Biology*, 9(4):e1003001.

[224] Inukai, M., Toyooka, S., Ito, S., Asano, H., Ichihara, S., Soh, J., Suehisa, H., Ouchida, M., Aoe, K., Aoe, M., Kiura, K., Shimizu, N., and Date, H. (2006). Presence of epidermal growth factor receptor gene T790M mutation as a minor clone in non-small cell lung cancer. *Cancer Research*, 66(16):7854–7858.

[225] Jackson, R. C., Di Veroli, G. Y., Koh, S.-B., Goldlust, I., Richards, F. M., and Jodrell, D. I. (2017). Modelling of the cancer cell cycle as a tool for rational drug development: A systems pharmacology approach to cyclotherapy. *PLOS Computational Biology*, 13(5):e1005529.

[226] Jackson, S. P. and Bartek, J. (2010). The DNA-damage response in human biology and disease. *Nature*, 461(7267):1071–1078.

[227] Jelinek, T., Catling, A. D., Reuter, C. W., Moodie, S. A., Wolfman, A., and Weber, M. J. (1994). RAS and RAF-1 form a signalling complex with MEK-1 but not MEK-2. *Molecular and cellular biology*, 14(12):8212–8.

[228] Jögi, A., Vaapil, M., Johansson, M., and Påhlman, S. (2012). Cancer cell differentiation heterogeneity and aggressive behavior in solid tumors. *Upsala Journal of Medical Sciences*, 117(2):217–224.

[229] Johnson, D. G., Schwarz, J. K., Cress, W. D., and Nevins, J. R. (1993). Expression of transcription factor E2F1 induces quiescent cells to enter S phase. *Nature*, 365(6444):349–352.

[230] Johnston, L. A., Prober, D. A., Edgar, B. A., Eisenman, R. N., Gallant, P., Amati, B., Amati, B., Land, H., Armelin, H., Armelin, M., Kelly, K., Stewart, T., Leder, P., Cochran, B., Stiles, C., Ashburner, M., Blackwood, E., Kretzner, L., Eisenman, R., Böhni, R., Riesgo-Escovar, J., Oldham, S., Brogiolo, W., Stocker, H., Andruss, B., Beckingham, K., Hafen, E., Charron, J., Malynn, B., Fisher, P., Stewart, V., Jeannotte, L., Goff, S., Robertson, E., Alt, F., Conlon, I., Raff, M., Craig, R., Buchan, H., Civin, C., Kastan, M., Dang, C., Davis, A., Wims, M., Spotts, G., Hann, S., Bradley, A., Downs, K., Martin, G., Bishop, J., Eilers, M., Schirm, S., Bishop, J., Galaktionov, K., Chen, X., Beach, D., Gallant, P., Shiio, Y., Cheng, P., Parkhurst, S., Eisenman, R., García-Bellido, A., Merriam, J., Grandori, C., Eisenman, R., Grandori, C., Mac, J., Siebelt, F., Ayer, D., Eisenman, R., Hann, S., Thompson, C., Eisenman, R., Hay, B., Wolff, T., Rubin, G., He, T.-C., Sparks, A., Rago, C., Hermeking, H., Zawel, L., da Costa, L., Morin, P., Vogelstein, B., Kinzler, K., Heikkila, R., Schwab, G., Wickstrom, E., Loke, S., Pluznik, D., Watt, R., Neckers, L., Henriksson, M., Luscher, B., Johnston, L., Edgar, B., Karn, J., Watson, J., Lowe, A., Green, S., Vedeckis, W., Kelly, K., Cochran, B., Stiles, C., Leder, P., Kessler, D., Duyao, M., Spicer, D., Sonenshein, G., Lambertsson, A., Lehman, D., Patterson, B., Johnston, L., Balzer, T., Britton, J., Saint, R., Edgar, B., Leone, G., DeGregori, J., Sears, R., Jakol, L., Nevins, J., Li, L., Nerlov, K., Prendergast, G., MacGregor, D., Ziff, E., Mateyak, M., Obaya, A., Adachi, S., Sedivy, J., McCabe, J., French, V., Partridge, L., Milan, M., Campuzano, S., García-Bellido, A., Milan, M., Campuzano, S., García-Bellido, A., Moens, C., Auerbach, A., Conlon, R., Joyner, A., Rossant, J., Morata, G., Ripoll, P., Neufeld, T., de la Cruz, A., Johnston, L., Edgar, B., O'Brochta, D., Bryant, P., Phillips, R., Whittle, J., Pignoni, F., Zipursky, S., Polymenis, M., Schmidt, E., Raff, M., Roussel, M., Cleveland, J., Shurtleff, S., Sherr, C., Sawai, S., Shimono, A., Wakamatsu, Y., Palmes, C., Hanaoka, K., Kondoh, H., Schreiber-Agus, N., Stein, D., Chen, K., Goltz, J., Stevens, L., DePinho, R., Simpson, P., Morata, G., Sorrentino, V., Drozdoff, V., McKinney, M., Zeitz, L., Fleissner, E., Stanton, B., Perkins, A., Tessarollo, L., Sassoon, D., Parada, L., Stern, D., Emlen, D., Stern, D., Roberts, A., Roche, N., Sporn, M., Weinberg, R., Struhl, G., Basler, K., Thomas, B., Gunning, D., Cho, J., Zipursky, S., van de Wetering, M., Cavallo, R., Dooijes, D., van Beest, M., van Es, J., Loureiro, J., Ypma, A., Hursh, D., Jones, T., Bejsovec, A., Al., E., Wakamatsu, Y., Watanabe, Y., Shimono, A., Kondoh, H., Xu, T., Rubin, G., Zaffran, S., Chartier, A., Gallant, P., Astier, M., Arquier, N., Doherty, D., Gratecos, D., Semeriva, M., Zornig, M., and Evan, G. (1999). Drosophila myc regulates cellular growth during development. *Cell*, 98(6):779–90.

[231] Jolly, M. K. and Levine, H. (2017). Computational systems biology of epithelial-hybrid-mesenchymal transitions. *Current Opinion in Systems Biology*, 3:1–6.

[232] Jong, H. D. (2002). Modeling and simulation of genetic regulatory systems: a literature review. *Journal of Computational Biology*, 9(1):67–103.

[233] Jonsson, P. F. and Bates, P. A. (2006). Global topological features of cancer proteins in the human interactome. *Bioinformatics (Oxford, England)*, 22(18):2291–7.

[234] Júlvez, J., Dikicioglu, D., and Oliver, S. G. (2018). Handling variability and incompleteness of biological data by flexible nets: a case study for Wilson disease. *npj Systems Biology and Applications*, 4(1):7.

[235] Junttila, M. R. and de Sauvage, F. J. (2013). Influence of tumour micro-environment heterogeneity on therapeutic response. *Nature*, 501(7467):346–354.

[236] Juven-Gershon, T. and Oren, M. (1999). Mdm2: the ups and downs. *Molecular Medicine*, 5(12):71–83.

[237] Kabir, M., Noman, N., and Iba, H. (2010). Reverse engineering gene regulatory network from microarray data using linear time-variant model. *BMC Bioinformatics*, 11(SUPPLL.1):1–15.

[238] Kaczmarek, J. C., Kowalski, P. S., and Anderson, D. G. (2017). Advances in the delivery of RNA therapeutics: from concept to clinical reality. *Genome Medicine*, 9(1):60.

[239] Kanehisa, M., Furumichi, M., Tanabe, M., Sato, Y., and Morishima, K. (2017). KEGG: new perspectives on genomes, pathways, diseases and drugs. *Nucleic acids research*, 45(D1):D353–D361.

[240] Kanehisa, M. and Goto, S. (2000). KEGG: kyoto encyclopedia of genes and genomes. *Nucleic acids research*, 28(1):27–30.

[241] Kanehisa, M., Sato, Y., Kawashima, M., Furumichi, M., and Tanabe, M. (2016). KEGG as a reference resource for gene and protein annotation. *Nucleic acids research*, 44(D1):D457–62.

[242] Kao, J., Salari, K., Bocanegra, M., Choi, Y. L., Girard, L., Gandhi, J., Kwei, K. A., Hernandez-Boussard, T., Wang, P., Gazdar, A. F., Minna, J. D., and Pollack, J. R. (2009). Molecular profiling of breast cancer cell lines defines relevant tumor models and provides a resource for cancer gene discovery. *PLoS ONE*, 4(7).

[243] Kaplan, A. (1964). *The conduct of inquiry; methodology for behavioral science.* Chandler publications in anthropology and sociology. Chandler Pub. Co, San Francisco.

[244] Karn, J., Watson, J. V., Lowe, A. D., Green, S. M., and Vedeckis, W. (1989). Regulation of cell cycle duration by c-myc levels. *Oncogene*, 4(6):773–87.

[245] Kaur, M. and Cole, M. D. (2013). MYC acts via the PTEN tumor suppressor to elicit autoregulation and genome-wide gene repression by activation of the Ezh2 methyltransferase. *Cancer Research*, 73(2):695–705.

[246] Ke, X. and Shen, L. (2017). Molecular targeted therapy of cancer: The progress and future prospect. *Frontiers in Laboratory Medicine*, 1(2):69–75.

[247] Kim, H., Yang, J., Kim, M. J., Choi, S., Chung, J. R., Kim, J. M., Yoo, Y. H., Chung, J., and Koh, H. (2016). Tumor necrosis factor receptor-associated protein 1 (TRAP1) mutation and TRAP1 inhibitor gamitrinibtriphenylphosphonium (G-TPP) induce a forkhead box O (FOXO)-dependent cell protective signal from mitochondria. *Journal of Biological Chemistry*, 291(4):1841–1853.

[248] Kim, M. S., Lee, E. J., Kim, H. R. C., and Moon, A. (2003). p38 kinase is a key signaling molecule for H-ras-induced cell motility and invasive phenotype in human breast epithelial cells. *Cancer Research*, 63(17):5454–5461.

[249] Kirk, R. E. (2013). Chapter 3: Fundamental Assumptions in Analysis of Variance. In *Experimental Design: Procedures for the Behavioral Sciences*, pages 77–124. SAGE Publications, Inc., 2455 Teller Road, Thousand Oaks California 91320 United States, 4th edition.

[250] Kirouac, D. C., Du, J. Y., Lahdenranta, J., Overland, R., Yarar, D., Paragas, V., Pace, E., McDonagh, C. F., Nielsen, U. B., and Onsum, M. D. (2013). Computational Modeling of ERBB2-Amplified Breast Cancer Identifies Combined ErbB2/3 Blockade as Superior to the Combination of MEK and AKT Inhibitors. *Science Signaling*, 6(288):ra68–ra68.

[251] Klapper, L. N., Glathe, S., Vaisman, N., Hynes, N. E., Andrews, G. C., Sela, M., and Yarden, Y. (1999). The ErbB-2/HER2 oncoprotein of human carcinomas may function solely as a shared coreceptor for multiple stroma-derived growth factors. *Proceedings of the National Academy of Sciences of the United States of America*, 96(9):4995–5000.

[252] Knispel, S., Zimmer, L., Kanaki, T., Ugurel, S., Schadendorf, D., and Livingstone, E. (2018). The safety and efficacy of dabrafenib and trametinib for the treatment of melanoma. *Expert opinion on drug safety*, 17(1):73–87.

[253] Knudson, A. G. (1971). Mutation and Cancer: Statistical Study of Retinoblastoma. *Proceedings of the National Academy of Sciences*, 68(4):820–823.

[254] Knuefermann, C., Lu, Y., Liu, B., Jin, W., Liang, K., Wu, L., Schmidt, M., Mills, G. B., Mendelsohn, J., and Fan, Z. (2003). HER2/PI-3K/Akt activation leads to a multidrug resistance in human breast adenocarcinoma cells. *Oncogene*, 22:3205–3212.

[255] Kochi, N., Helikar, T., Allen, L., Rogers, J. A., Wang, Z., and Matache, M. T. (2014). Sensitivity analysis of biological Boolean networks using information fusion based on nonadditive set functions. *BMC Systems Biology*, 8(1):1–14.

[256] Komarova, N. L., Katouli, A. A., and Wodarz, D. (2009). Combination of two but not three current targeted drugs can improve therapy of chronic myeloid leukemia. *PloS one*, 4(2):e4423.

[257] Komiya, Y. and Habas, R. (2008). Wnt signal transduction pathways. *Organogenesis*, 4(2):68–75.

[258] Kong, W., He, L., Richards, E. J., Challa, S., Xu, C.-X., Permuth-Wey, J., Lancaster, J. M., Coppola, D., Sellers, T. a., Djeu, J. Y., and Cheng, J. Q. (2014). Upregulation of miRNA-155 promotes tumour angiogenesis by targeting VHL and is associated with poor prognosis and triple-negative breast cancer. *Oncogene*, 33(November 2012):679–89.

[259] Korinek, V., Barker, N., Morin, P. J., van Wichen, D., de Weger, R., Kinzler, K. W., Vogelstein, B., and Clevers, H. (1997). Constitutive transcriptional activation by a b-catenin-Tcf complex in APC-/- colon carcinoma. *Science*, 275(March):1784–1787.

[260] Kortlever, R. M., Sodir, N. M., Wilson, C. H., Burkhart, D. L., Pellegrinet, L., Brown Swigart, L., Littlewood, T. D., and Evan, G. I. (2017). Myc Cooperates with Ras by Programming Inflammation and Immune Suppression. *Cell*, 171(6):1301–1315.

[261] Koshiji, M., Kageyama, Y., Pete, E. a., Horikawa, I., Barrett, J. C., and Huang, L. E. (2004). HIF-1alpha induces cell cycle arrest by functionally counteracting Myc. *The EMBO journal*, 23(9):1949–56.

[262] Krepska, E., Bonzanni, N., Feenstra, A., Fokkink, W., Kielmann, T., Bal, H., and Heringa, J. (2008). Design Issues for Qualitative Modelling of Biological Cells with Petri Nets. In Fisher, J., editor, *Formal Methods in Systems Biology*, pages 48–62, Berlin, Heidelberg. Springer Berlin Heidelberg.

[263] Kreso, A., O'Brien, C. A., van Galen, P., Gan, O. I., Notta, F., Brown, A. M. K., Ng, K., Ma, J., Wienholds, E., Dunant, C., Pollett, A., Gallinger, S., McPherson, J., Mullighan, C. G., Shibata, D., and Dick, J. E. (2013). Variable clonal repopulation dynamics influence chemotherapy response in colorectal cancer. *Science (New York, N.Y.)*, 339(6119):543–8.

[264] Kress, T. R., Sabò, A., and Amati, B. (2015). MYC: connecting selective transcriptional control to global RNA production. *Nature reviews. Cancer*, 15(10):593–607.

[265] Kulkarni, V. V., Arastoo, R., Bhat, A., Subramanian, K., Kothare, M. V., and Riedel, M. C. (2012). Gene regulatory network modeling using literature curated and high throughput data. *Systems and Synthetic Biology*, 6(3-4):69–77.

[266] Kundu, N., Yang, Q., Dorsey, R., and Fulton, a. M. (2001). Increased cyclooxygenase-2 (cox-2) expression and activity in a murine model of metastatic breast cancer. *International journal of cancer. Journal international du cancer*, 93(5):681–6.

[267] Kuukasjärvi, T., Karhu, R., Tanner, M., Kähkönen, M., Schäffer, A., Nupponen, N., Pennanen, S., Kallioniemi, A., Kallioniemi, O. P., and Isola, J. (1997). Genetic heterogeneity and clonal evolution underlying development of asynchronous metastasis in human breast cancer. *Cancer research*, 57(8):1597–604.

[268] Kuznetsova, A., Brockhoff, P. B., and Christensen, R. H. B. (2017). {lmerTest} Package: Tests in Linear Mixed Effects Models. *Journal of Statistical Software*, 82(13):1–26.

[269] Kwon, Y. S., Chun, S. Y., Nam, K. S., and Kim, S. (2015). Lapatinib sensitizes quiescent MDA-MB-231 breast cancer cells to doxorubicin by inhibiting the expression of multidrug resistance-associated protein-1. *Oncology Reports*, 34(2):884–890.

[270] Kyriakis, J. M., App, H., Zhang, X. F., Banerjee, P., Brautigan, D. L., Rapp, U. R., and Avruch, J. (1992). Raf-1 activates MAP kinase-kinase. *Nature*, 358(6385):417–21.

[271] Lacher, M. D., Siegenthaler, A., Jäger, R., Yan, X., Hett, S., Xuan, L., Saurer, S., Lareu, R. R., Dharmarajan, A. M., and Friis, R. (2003). Role of DDC-4/sFRP-4, a secreted Frizzled-related protein, at the onset of apoptosis in mammary involution. *Cell Death and Differentiation*, 10(5):528–538.

[272] Lacroix, M. and Leclercq, G. (2004). Relevance of Breast Cancer Cell Lines as Models for Breast Tumours: An Update. *Breast Cancer Research and Treatment*, 83(3):249–289.

[273] Land, H., Chen, A. C., Morgenstern, J. P., Parada, L. F., and Weinberg, R. A. (1986). Behavior of myc and ras oncogenes in transformation of rat embryo fibroblasts. *Molecular and Cellular Biology*, 6(6):1917–1925.

[274] Lane, H. A., Motoyama, A. B., Beuvink, I., and Hynes, N. E. (2001). Modulation of p27/Cdk2 complex formation through 4D5-mediated inhibition of HER2 receptor signaling. *Annals of oncology : official journal of the European Society for Medical Oncology*, 12 Suppl 1(Supplement 8):S21–2.

[275] Larkin, J., Chiarion-Sileni, V., Gonzalez, R., Grob, J. J., Cowey, C. L., Lao, C. D., Schadendorf, D., Dummer, R., Smylie, M., Rutkowski, P., Ferrucci, P. F., Hill, A., Wagstaff, J., Carlino, M. S., Haanen, J. B., Maio, M., Marquez-Rodas, I., McArthur, G. A., Ascierto, P. A., Long, G. V., Callahan, M. K., Postow, M. A., Grossmann, K., Sznol, M., Dreno, B., Bastholt, L., Yang, A., Rollin, L. M., Horak, C., Hodi, F. S., and Wolchok, J. D. (2015). Combined Nivolumab and Ipilimumab or Monotherapy in Untreated Melanoma. *The New England journal of medicine*, 373(1):23–34.

[276] Lasfargues, E. Y. and Ozzello, L. (1958). Cultivation of human breast carcinomas. *Journal of the National Cancer Institute*, 21(6):1131–47.

[277] Laughner, E., Taghavi, P., Chiles, K., Mahon, P. C., and Semenza, G. L. (2001). HER2 (neu) signaling increases the rate of hypoxia-inducible factor 1alpha (HIF-1alpha) synthesis: novel mechanism for HIF-1-mediated vascular endothelial growth factor expression. *Molecular and cellular biology*, 21(12):3995–4004.

[278] Lavappa, K. S. (1978). Survey of ATCC stocks of human cell lines for HeLa contamination. *In vitro*, 14(5):469–75.

[279] Layek, R., Datta, A., Bittner, M., and Dougherty, E. R. (2011). Cancer therapy design based on pathway logic. *Bioinformatics*, 27(4):548–555.

[280] Le Novere, N. (2015). Quantitative and logic modelling of molecular and gene networks. *Nature Reviews Genetics*, 16(3):146–158.

[281] Ledford, H. (2016). Cocktails for cancer with a measure of immunotherapy. *Nature*, 532(7598):162–4.

[282] Lehtinen, M. K., Yuan, Z., Boag, P. R., Yang, Y., Villén, J., Becker, E. B. E., DiBacco, S., de la Iglesia, N., Gygi, S., Blackwell, T. K., and Bonni, A. (2006). A conserved MST-FOXO signaling pathway mediates oxidative-stress responses and extends life span. *Cell*, 125(5):987–1001.

[283] Lemma, S., Avnet, S., Salerno, M., Chano, T., and Baldini, N. (2016). Identification and validation of housekeeping genes for gene expression analysis of cancer stem cells. *PLoS ONE*, 11(2):1–19.

[284] Lenth, R. V. (2016). Least-Squares Means: The {R} Package {lsmeans}. *Journal of Statistical Software*, 69(1):1–33.

[285] Leung, J. Y., Andrechek, E. R., Cardiff, R. D., and Nevins, J. R. (2012). Heterogeneity in MYC-induced mammary tumors contributes to escape from oncogene dependence. *Oncogene*, 31(20):2545–54.

[286] Levene, H. (1961). Robust tests for equality of variances. *Contributions to Probability and Statistics. Essays in Honor of Harold Hotelling*, pages 279–292.

[287] Levine, E. and Hwa, T. (2007). Stochastic fluctuations in metabolic pathways. *Proceedings of the National Academy of Sciences*, 104(22):9224–9229.

[288] Li, P., Burke, S., Wang, J., Chen, X., Ortiz, M., Lee, S.-C., Lu, D., Campos, L., Goulding, D., Ng, B. L., Dougan, G., Huntly, B., Gottgens, B., Jenkins, N. A., Copeland, N. G., Colucci, F., and Liu, P. (2010). Reprogramming of T Cells to Natural Killer-Like Cells upon Bcl11b Deletion. *Science*, 329(5987):85–89.

[289] Li, X., Kolomeisky, A. B., and Valleriani, A. (2014). Pathway structure determination in complex stochastic networks with non-exponential dwell times. *The Journal of chemical physics*, 140(18):184102.

[290] Li, Y., Liu, J., Liu, X., Xing, K., Wang, Y., Li, F., and Yao, L. (2006). Resveratrol-induced cell inhibition of growth and apoptosis in MCF7 human breast cancer cells are associated with modulation of phosphorylated Akt and caspase-9. *Applied biochemistry and biotechnology*, 135(3):181–192.

[291] Lin, C. Y., Lovén, J., Rahl, P. B., Paranal, R. M., Burge, C. B., Bradner, J. E., Lee, T. I., and Young, R. a. (2012). Transcriptional amplification in tumor cells with elevated c-Myc. *Cell*, 151(1):56–67.

[292] Lin, S. Y., Xia, W., Wang, J. C., Kwong, K. Y., Spohn, B., Wen, Y., Pestell, R. G., and Hung, M. C. (2000). Beta-catenin, a novel prognostic marker for breast cancer: its roles in cyclin D1 expression and cancer progression. *Proceedings of the National Academy of Sciences of the United States of America*, 97(8):4262–4266.

[293] Littlewood, T. D., Hancock, D. C., Danielian, P. S., Parker, M. G., and Evan, G. I. (1995). A modified oestrogen receptor ligand-binding domain as an improved switch for the regulation of heterologous proteins. *Nucleic acids research*, 23(10):1686–90.

[294] Littlewood, T. D., Kreuzaler, P., and Evan, G. I. (2012). All things to all people. *Cell*, 151(1):11–3.

[295] Low-Nam, S. T., Lidke, K. A., Cutler, P. J., Roovers, R. C., van Bergen en Henegouwen, P. M. P., Wilson, B. S., and Lidke, D. S. (2011). ErbB1 dimerization is promoted by domain co-confinement and stabilized by ligand binding. *Nature Structural & Molecular Biology*, 18(11):1244–1249.

[296] Lozano, R., Naghavi, M., Foreman, K., Lim, S., Shibuya, K., Aboyans, V., Abraham, J., Adair, T., Aggarwal, R., Ahn, S. Y., Alvarado, M., Anderson, H. R., Anderson, L. M., Andrews, K. G., Atkinson, C., Baddour, L. M., Barker-Collo, S., Bartels, D. H., Bell, M. L., Benjamin, E. J., Bennett, D., Bhalla, K., Bikbov, B., Bin Abdulhak, A., Birbeck, G., Blyth, F., Bolliger, I., Boufous, S., Bucello, C., Burch, M., Burney, P., Carapetis, J., Chen, H., Chou, D., Chugh, S. S., Coffeng, L. E., Colan, S. D., Colquhoun, S., Colson, K. E., Condon, J., Connor, M. D., Cooper, L. T., Corriere, M., Cortinovis, M., de Vaccaro, K. C., Couser, W., Cowie, B. C., Criqui, M. H., Cross, M., Dabhadkar, K. C., Dahodwala, N., De Leo, D., Degenhardt, L., Delossantos, A., Denenberg, J., Des Jarlais, D. C., Dharmaratne, S. D., Dorsey, E. R., Driscoll, T., Duber, H., Ebel, B., Erwin, P. J., Espindola, P., Ezzati, M., Feigin, V., Flaxman, A. D., Forouzanfar, M. H., Fowkes, F. G. R., Franklin, R., Fransen, M., Freeman, M. K., Gabriel, S. E., Gakidou, E., Gaspari, F., Gillum, R. F., Gonzalez-Medina, D., Halasa, Y. a., Haring, D., Harrison, J. E., Havmoeller, R., Hay, R. J., Hoen, B., Hotez, P. J., Hoy, D., Jacobsen, K. H., James, S. L., Jasrasaria, R., Jayaraman, S., Johns, N., Karthikeyan, G., Kassebaum, N., Keren, A., Khoo, J.-P., Knowlton, L. M., Kobusingye, O., Koranteng, A., Krishnamurthi, R., Lipnick, M., Lipshultz, S. E., Ohno, S. L., Mabweijano, J., MacIntyre, M. F., Mallinger, L., March, L., Marks, G. B., Marks, R., Matsumori, A., Matzopoulos, R., Mayosi, B. M., McAnulty, J. H., McDermott, M. M., McGrath, J., Mensah, G. a., Merriman, T. R., Michaud, C., Miller, M., Miller, T. R., Mock, C., Mocumbi, A. O., Mokdad, A. a., Moran, A., Mulholland, K., Nair, M. N., Naldi, L., Narayan, K. M. V., Nasseri, K., Norman, P., O'Donnell, M., Omer, S. B., Ortblad, K., Osborne, R., Ozgediz, D., Pahari, B., Pandian, J. D., Rivero, A. P., Padilla, R. P., Perez-Ruiz, F., Perico, N., Phillips, D., Pierce, K., Pope, C. A., Porrini, E., Pourmalek, F., Raju, M., Ranganathan, D., Rehm, J. T., Rein, D. B., Remuzzi, G., Rivara, F. P., Roberts, T., De León, F. R., Rosenfeld, L. C., Rushton, L., Sacco, R. L., Salomon, J. a., Sampson, U., Sanman, E., Schwebel, D. C., Segui-Gomez, M., Shepard, D. S., Singh, D., Singleton, J., Sliwa, K., Smith, E., Steer, A., Taylor, J. a., Thomas, B., Tleyjeh, I. M., Towbin, J. a., Truelsen, T., Undurraga, E. a., Venketasubramanian, N., Vijayakumar, L., Vos, T., Wagner, G. R., Wang, M., Wang, W., Watt, K., Weinstock, M. a., Weintraub, R., Wilkinson, J. D., Woolf, A. D., Wulf, S., Yeh, P.-H., Yip, P., Zabetian, A., Zheng, Z.-J., Lopez, A. D., Murray, C. J. L., AlMazroa, M. a., and Memish, Z. a. (2012). Global and regional mortality from 235 causes of death for 20 age groups in 1990 and 2010: a systematic analysis for the Global Burden of Disease Study 2010. *Lancet*, 380(9859):2095–128.

[297] Lu, C., Shen, Q., DuPré, E., Kim, H., Hilsenbeck, S., and Brown, P. H. (2005). cFos is critical for MCF-7 breast cancer cell growth. *Oncogene*, 24(43):6516–24.

[298] Lucey, B. P., Nelson-Rees, W. A., and Hutchins, G. M. (2009). Historical Perspective Henrietta Lacks, HeLa Cells, and Cell Culture Contamination. *Arch Pathol Lab Med*, 133(9):1463–1467.

[299] Lukas, J., Herzinger, T., Hansen, K., Moroni, M. C., Resnitzky, D., Helin, K., Reed, S. I., and Bartek, J. (1997). Cyclin E-induced S phase without activation of the pRb/E2F pathway. *Genes and Development*, 11(11):1479–1492.

[300] Lukas, J., Parry, D., Aagaard, L., Mann, D. J., Bartkova, J., Strauss, M., Peters, G., and Bartek, J. (1995). Retinoblastoma-protein-dependent cell-cycle inhibition by the tumour suppressor p16.

[301] Luke, S. G. (2017). Evaluating significance in linear mixed-effects models in R. *Behavior Research Methods*, 49(4):1494–1502.

[302] Lüscher, B. and Vervoorts, J. (2012). Regulation of gene transcription by the oncoprotein MYC. *Gene*, 494(2):145–60.

[303] Lyng, M. B., Lænkholm, A. V., Pallisgaard, N., and Ditzel, H. J. (2008). Identification of genes for normalization of real-time RT-PCR data in breast carcinomas. *BMC Cancer*, 8:1–11.

[304] MacDonald, B. T. and He, X. (2012). Frizzled and LRP5/6 receptors for Wnt/β-catenin signaling. *Cold Spring Harbor perspectives in biology*, 4(12):a007880–a007880.

[305] Mack, F. A., Patel, J. H., Biju, M. P., Haase, V. H., and Simon, M. C. (2005). Decreased growth of Vhl-/- fibrosarcomas is associated with elevated levels of cyclin kinase inhibitors p21 and p27. *Molecular and cellular biology*, 25(11):4565–78.

[306] MacKay, D. J. C. (2003). *Information Theory, Inference, and Learning Algorithms*. Cambridge University Press, Cambridge, 7.2 edition.

[307] MacNeil, L. T. and Walhout, A. J. M. (2011). Gene regulatory networks and the role of robustness and stochasticity in the control of gene expression. *Genome Research*, 21(5):645–657.

[308] Maestro, R., Dei Tos, A. P., Hamamori, Y., Krasnokutsky, S., Sartorelli, V., Kedes, L., Doglioni, C., Beach, D. H., and Hannon, G. J. (1999). Twist Is a Potential Oncogene That Inhibits Apoptosis. *Genes and Development*, 13(17):2207–2217.

[309] Maetschke, S. R., Madhamshettiwar, P. B., Davis, M. J., and Ragan, M. A. (2014). Supervised, semi-supervised and unsupervised inference of gene regulatory networks. *Briefings in Bioinformatics*, 15(2):195–211.

[310] Mahmood, T. and Yang, P.-C. (2012). Western blot: technique, theory, and trouble shooting. *North American journal of medical sciences*, 4(9):429–34.

[311] Majumder, M., Xin, X., Liu, L., Tutunea-Fatan, E., Rodriguez-Torres, M., Vincent, K., Postovit, L.-M., Hess, D., and Lala, P. K. (2016). COX-2 Induces Breast Cancer Stem Cells via EP4/PI3K/AKT/NOTCH/WNT Axis. *STEM CELLS*.

[312] Maley, C. C., Galipeau, P. C., Finley, J. C., Wongsurawat, V. J., Li, X., Sanchez, C. A., Paulson, T. G., Blount, P. L., Risques, R.-A., Rabinovitch, P. S., and Reid, B. J. (2006). Genetic clonal diversity predicts progression to esophageal adenocarcinoma. *Nature genetics*, 38(4):468–73.

[313] Margolin, A. A., Nemenman, I., Basso, K., Wiggins, C., Stolovitzky, G., Dalla Favera, R., Califano, A., Favera, R. D., and Califano, A. (2006). ARACNE: An Algorithm for the Reconstruction of Gene Regulatory Networks in a Mammalian Cellular Context. *BMC bioinformatics*, 7(Suppl 1):S7.

[314] Markowetz, F. and Spang, R. (2007). Inferring cellular networks–a review. *BMC bioinformatics*, 8 Suppl 6(Suppl 6):S5.

[315] Martincorena, I., Raine, K. M., Gerstung, M., Dawson, K. J., Haase, K., Van Loo, P., Davies, H., Stratton, M. R., and Campbell, P. J. (2017). Universal Patterns of Selection in Cancer and Somatic Tissues. *Cell*, 171(5):1029–1041.e21.

[316] Martins, C. P., Brown-Swigart, L., and Evan, G. I. (2006). Modeling the Therapeutic Efficacy of p53 Restoration in Tumors. *Cell*, 127(7):1323–1334.

[317] Marusyk, A., Tabassum, D. P., Altrock, P. M., Almendro, V., Michor, F., and Polyak, K. (2014). Non-cell-autonomous driving of tumour growth supports sub-clonal heterogeneity. *Nature*, 6(2):54–58.

[318] Massacesi, C., Di Tomaso, E., Urban, P., Germa, C., Quadt, C., Trandafir, L., Aimone, P., Fretault, N., Dharan, B., Tavorath, R., and Hirawat, S. (2016). PI3K inhibitors as new cancer therapeutics: implications for clinical trial design. *OncoTargets and Therapy*, 9:203.

[319] Matsuda, Y., Schlange, T., Oakeley, E. J., Boulay, A., and Hynes, N. E. (2009). WNT signaling enhances breast cancer cell motility and blockade of the WNT pathway by sFRP1 suppresses MDA-MB-231 xenograft growth. *Breast cancer research : BCR*, 11(3):R32.

[320] McGlynn, L. M., Kirkegaard, T., Edwards, J., Tovey, S., Cameron, D., Twelves, C., Bartlett, J. M., and Cooke, T. G. (2009). Ras/Raf-1/MAPK pathway mediates response to tamoxifen but not chemotherapy in breast cancer patients. *Clinical Cancer Research*, 15(4):1487–1495.

[321] McGranahan, N. and Swanton, C. (2015). Biological and therapeutic impact of intratumor heterogeneity in cancer evolution. *Cancer Cell*, 27(1):15–26.

[322] McNeill, R. E., Miller, N., and Kerin, M. J. (2007). Evaluation and validation of candidate endogenous control genes for real-time quantitative PCR studies of breast cancer. *BMC Molecular Biology*, 8:1–13.

[323] Mellor, H. R. and Harris, A. L. (2007). The role of the hypoxia-inducible BH3-only proteins BNIP3 and BNIP3L in cancer. *Cancer and Metastasis Reviews*, 26(3-4):553–566.

[324] Meyer, N. and Penn, L. Z. (2008). Reflecting on 25 years with MYC. *Nature Reviews Cancer*, 8(12):976–990.

[325] Michalak, E. M., Villunger, A., Adams, J. M., and Strasser, A. (2008). In several cell types tumour suppressor p53 induces apoptosis largely via Puma but Noxa can contribute. *Cell death and differentiation*, 15(6):1019–1029.

[326] Miles, D., von Minckwitz, G., and Seidman, A. D. (2002). Combination versus sequential single-agent therapy in metastatic breast cancer. *The oncologist*, 7 Suppl 6(suppl 6):13–9.

[327] Miller, R. G. (1986). *Beyond ANOVA : basics of applied statistics*. Wiley series in probability and mathematical statistics. Applied probability and statistics. Wiley, New York.

[328] Mitchell, K. O. and El-Deiry, W. S. (1999). Overexpression of c-Myc inhibits p21WAF1/CIP1 expression and induces S-phase entry in 12-O-tetradecanoylphorbol-13-acetate (TPA)-sensitive human cancer cells. *Cell growth & differentiation : the molecular biology journal of the American Association for Cancer Research*, 10(4):223–30.

[329] Moen, M. D., McKeage, K., Plosker, G. L., and Siddiqui, M. A. A. (2007). Imatinib: a review of its use in chronic myeloid leukaemia. *Drugs*, 67(2):299–320.

[330] Moignard, V., Woodhouse, S., Haghverdi, L., Lilly, A. J., Tanaka, Y., Wilkinson, A. C., Buettner, F., Macaulay, I. C., Jawaid, W., Diamanti, E., Nishikawa, S.-I., Piterman, N., Kouskoff, V., Theis, F. J., Fisher, J., and Göttgens, B. (2015). Decoding the regulatory network of early blood development from single-cell gene expression measurements. *Nature Biotechnology*, 33(3):269–76.

[331] Molinelli, E. J., Korkut, A., Wang, W., Miller, M. L., Gauthier, N. P., Jing, X., Kaushik, P., He, Q., Mills, G., Solit, D. B., Pratilas, C. A., Weigt, M., Braunstein, A., Pagnani, A., Zecchina, R., and Sander, C. (2013). Perturbation Biology: Inferring Signaling Networks in Cellular Systems. *PLoS Computational Biology*, 9(12).

[332] Morris, M., Hepburn, P., and Wynford-Thomas, D. (2002). Sequential extension of proliferative lifespan in human fibroblasts induced by over-expression of CDK4 or 6 and loss of p53 function. *Oncogene*, 21(27):4277–88.

[333] Morris, M. K., Saez-Rodriguez, J., Clarke, D. C., Sorger, P. K., and Lauffenburger, D. A. (2011). Training signaling pathway maps to biochemical data with constrained fuzzy logic: Quantitative analysis of liver cell responses to inflammatory stimuli. *PLoS Computational Biology*, 7(3).

[334] Moulder, S. L., Yakes, F. M., Muthuswamy, S. K., Bianco, R., Simpson, J. F., and Arteaga, C. L. (2001). Epidermal growth factor receptor (HER1) tyrosine kinase inhibitor ZD1839 (Iressa) inhibits HER2/neu (erbB2)-overexpressing breast cancer cells in vitro and in vivo. *Cancer research*, 61(24):8887–95.

[335] Mumenthaler, S. M., Foo, J., Leder, K., Choi, N. C., Agus, D. B., Pao, W., Mallick, P., and Michor, F. (2011). Evolutionary modeling of combination treatment strategies to overcome resistance to tyrosine kinase inhibitors in non-small cell lung cancer. *Mol Pharm*, 8(October):2069–2079.

[336] Muthalagu, N., Junttila, M. R., Wiese, K. E., Wolf, E., Morton, J., Bauer, B., Evan, G. I., Eilers, M., and Murphy, D. J. (2014). BIM Is the Primary Mediator of MYC-Induced Apoptosis in Multiple Solid Tissues. *Cell reports*, 8(5):1347–53.

[337] Nakano, K. and Vousden, K. H. (2001). PUMA, a Novel Proapoptotic Gene, Is Induced by p53. *Molecular Cell*, 7(3):683–694.

[338] Nass, S. J. and Dickson, R. B. (1998). Epidermal growth factor-dependent cell cycle progression is altered in mammary epithelial cells that overexpress c-myc. *Clinical Cancer Research*, 4(7):1813 LP – 1822.

[339] Nelder, J. A. (1977). A Reformulation of Linear Models. *Journal of the Royal Statistical Society. Series A (General)*, 140(1):48.

[340] Nesbit, C. E., Tersak, J. M., and Prochownik, E. V. (1999). MYC oncogenes and human neoplastic disease. *Oncogene*, 18(19):3004–16.

[341] Nickerson, R. (1998). Confirmation bias: A unique phenomenon in many guises. *Review of General Psychology*, 2(2):175–220.

[342] Nie, Z., Hu, G., Wei, G., Cui, K., Yamane, A., Resch, W., Wang, R., Green, D. R., Tessarollo, L., Casellas, R., Zhao, K., and Levens, D. (2012). c-Myc is a universal amplifier of expressed genes in lymphocytes and embryonic stem cells. *Cell*, 151(1):68–79.

[343] Nik-Zainal, S., Van Loo, P., Wedge, D. C., Alexandrov, L. B., Greenman, C. D., Lau, K. W., Raine, K., Jones, D., Marshall, J., Ramakrishna, M., Shlien, A., Cooke, S. L., Hinton, J., Menzies, A., Stebbings, L. A., Leroy, C., Jia, M., Rance, R., Mudie, L. J., Gamble, S. J., Stephens, P. J., McLaren, S., Tarpey, P. S., Papaemmanuil, E., Davies, H. R., Varela, I., McBride, D. J., Bignell, G. R., Leung, K., Butler, A. P., Teague, J. W., Martin, S., Jönsson, G., Mariani, O., Boyault, S., Miron, P., Fatima, A., Langerød, A., Aparicio, S. A. J. R., Tutt, A., Sieuwerts, A. M., Borg, Å., Thomas, G., Salomon, A. V., Richardson, A. L., Børresen-Dale, A.-L., Futreal, P. A., Stratton, M. R., Campbell, P. J., Langerod, A., Aparicio, S. A. J. R., Tutt, A., Sieuwerts, A. M., Borg, Å., Thomas, G., Salomon, A. V., Richardson, A. L., Borresen-Dale, A. L., Futreal, P. A., Stratton, M. R., Campbell, P. J., and Breast Cancer Working Group of the International Cancer Genome Consortium (2012). The life history of 21 breast cancers. *Cell*, 149(5):994–1007.

[344] Nikiforov, M. A., Riblett, M., Tang, W.-H., Gratchouck, V., Zhuang, D., Fernandez, Y., Verhaegen, M., Varambally, S., Chinnaiyan, A. M., Jakubowiak, A. J., and Soengas, M. S. (2007). Tumor cell-selective regulation of NOXA by c-MYC in response to proteasome inhibition. *Proceedings of the National Academy of Sciences of the United States of America*, 104(49):19488–93.

[345] Obaya, A. J., Mateyak, M. K., and Sedivy, J. M. (1999). Mysterious liaisons: the relationship between c-Myc and the cell cycle. *Oncogene*, 18(19):2934–41.

[346] Ohtani, N., Zebedee, Z., Huot, T. J., Stinson, J. A., Sugimoto, M., Ohashi, Y., Sharrocks, A. D., Peters, G., and Hara, E. (2001). Opposing effects of Ets and Id proteins on p16INK4a expression during cellular senescence. *Nature*, 409(6823):1067–1070.

[347] Oltvai, Z. N., Milliman, C. L., and Korsmeyer, S. J. (1993). Bcl-2 heterodimerizes in vivo with a conserved homolog, Bax, that accelerates programed cell death. *Cell*, 74(4):609–619.

[348] O'Reilly, K. E., Rojo, F., She, Q. B., Solit, D., Mills, G. B., Smith, D., Lane, H., Hofmann, F., Hicklin, D. J., Ludwig, D. L., Baselga, J., and Rosen, N. (2006). mTOR inhibition induces upstream receptor tyrosine kinase signaling and activates Akt. *Cancer Research*, 66(3):1500–1508.

[349] Ortmann, C. A., Kent, D. G., Nangalia, J., Silber, Y., Wedge, D. C., Grinfeld, J., Baxter, E. J., Massie, C. E., Papaemmanuil, E., Menon, S., Godfrey, A. L., Dimitropoulou, D., Guglielmelli, P., Bellosillo, B., Besses, C., Döhner, K., Harrison, C. N., Vassiliou, G. S., Vannucchi, A., Campbell, P. J., and Green, A. R. (2015). Effect of Mutation Order on Myeloproliferative Neoplasms. *The New England journal of medicine*, 372(7):601–612.

[350] Pacheco, J. M., Santos, F. C., and Dingli, D. (2014). The ecology of cancer from an evolutionary game theory perspective. *Interface Focus*, 4(4):20140019–20140019.

[351] Pacold, M. E., Suire, S., Perisic, O., Lara-Gonzalez, S., Davis, C. T., Walker, E. H., Hawkins, P. T., Stephens, L., Eccleston, J. F., and Williams, R. L. (2000). Crystal Structure and Functional Analysis of Ras Binding to Its Effector Phosphoinositide 3-Kinase γ. *Cell*, 103(6):931–944.

[352] Paige, A. J. W. (2003). Redefining tumour suppressor genes: exceptions to the two-hit hypothesis. *Cellular and molecular life sciences : CMLS*, 60(10):2147–63.

[353] Papazisis, K. T., Habeshaw, T., Miles, D. W., Leonard, R., Jones, A., Twelves, C., Coleman, R., Makris, A., Earl, H., Highley, M., Price, C., McKinna, F., Perren, T., Le Vay, J., McAleer, A., Houston, S., Crawford, M., Johnston, S., Howell, A., Wardley, A., Harris, A., O'Reilly, S., O'Byrne, K., Verrill, M., Hickish, T., Mansi, J. L., Barrett-Lee, P. J., Davidson, N., Stein, R., Rowland, C., Symmonds, P., Bailey, N., Chan, S., and Soukop, M. (2004). Safety and efficacy of the combination of trastuzumab with docetaxel for HER2-positive women with advanced breast cancer. A review of the existing clinical trials and results of the expanded access programme in the UK. *International Journal of Clinical Practice*, 58(6):581–586.

[354] Park, P. J. (2009). ChIP-seq: Advantages and challenges of a maturing technology. *Nature Reviews Genetics*, 10(10):669–680.

[355] Paterson, Y. Z., Shorthouse, D., Pleijzier, M. W., Piterman, N., Bendtsen, C., Hall, B. A., and Fisher, J. (2018). A toolbox for discrete modelling of cell signalling dynamics. *Integrative Biology*, 10(6):370–382.

[356] Paull, E. O., Carlin, D. E., Niepel, M., Sorger, P. K., Haussler, D., and Stuart, J. M. (2013). Discovering causal pathways linking genomic events to transcriptional states using Tied Diffusion Through Interacting Events (TieDIE). *Bioinformatics (Oxford, England)*, 29(21):2757–64.

[357] Pavelic, Z. P., Pavelic, K., Carter, C. P., and Pavelic, L. (1992). Heterogeneity of c-myc expression in histologically similar infiltrating ductal carcinomas of the breast. *Journal of Cancer Research and Clinical Oncology*, 118(1):16–22.

[358] Peleg, M., Rubin, D., and Altman, R. B. (2005). Using Petri Net Tools to Study Properties and Dynamics of Biological Systems. *J Am Med Inform Assoc.*, 12(2):181–199.

[359] Peña, J. M., Björkegren, J., and Tegnér, J. (2005). Growing Bayesian network models of gene networks from seed genes. *Bioinformatics*, 21(SUPPL. 2):224–229.

[360] Petit, A. M., Rak, J., Hung, M. C., Rockwell, P., Goldstein, N., Fendly, B., and Kerbel, R. S. (1997). Neutralizing antibodies against epidermal growth factor and ErbB-2/neu receptor tyrosine kinases down-regulate vascular endothelial growth factor production by tumor cells in vitro and in vivo: angiogenic implications for signal transduction therapy of so. *The American journal of pathology*, 151(6):1523–30.

[361] Petri, C. A. (1966). *Communication with automata*. PhD thesis, Universität Hamburg.

[362] Piao, S., Lee, S. H., Kim, H., Yum, S., Stamos, J. L., Xu, Y., Lee, S. J., Lee, J., Oh, S., Han, J. K., Park, B. J., Weis, W. I., and Ha, N. C. (2008). Direct inhibition of GSK3β by the phosphorylated cytoplasmic domain of LRP6 in Wnt/β-catenin signaling. *PLoS ONE*, 3(12).

[363] Piccart-Gebhart, M. J., Procter, M., Leyland-Jones, B., Goldhirsch, A., Untch, M., Smith, I., Gianni, L., Baselga, J., Bell, R., Jackisch, C., Cameron, D., Dowsett, M., Barrios, C. H., Steger, G., Huang, C.-S., Andersson, M., Inbar, M., Lichinitser, M., Láng, I., Nitz, U., Iwata, H., Thomssen, C., Lohrisch, C., Suter, T. M., Rüschoff, J., Süto, T., Greatorex, V., Ward, C., Straehle, C., McFadden, E., Dolci, M. S., and Gelber, R. D. (2005). Trastuzumab after Adjuvant Chemotherapy in HER2-Positive Breast Cancer. *New England Journal of Medicine*, 353(16):1659–1672.

[364] Poon, H., Quirk, C., DeZiel, C., and Heckerman, D. (2014). Literome: PubMed-scale genomic knowledge base in the cloud. *Bioinformatics*, 30(19):2840–2842.

[365] Posternak, V. and Cole, M. D. (2016). Strategically targeting MYC in cancer. *F1000Research*, 5:408.

[366] Prochazka, L., Benenson, Y., and Zandstra, P. W. (2017). Synthetic gene circuits and cellular decision-making in human pluripotent stem cells. *Current Opinion in Systems Biology*, 5(September):93–103.

[367] Puisieux, A., Valsesia-Wittmann, S., and Ansieau, S. (2006). A twist for survival and cancer progression. *British journal of cancer*, 94:13–17.

[368] Purvis, J. E., Karhohs, K. W., Mock, C., Batchelor, E., Loewer, A., and Lahav, G. (2012). p53 Dynamics Control Cell Fate. *Science*, 336(6087):1440–1444.

[369] Quinn, G. and Keough., M. J. (2002). *Experimental design and data analysis for biologists*. Cambridge University Press, New York.

[370] R Core Team (2017). *R: A Language and Environment for Statistical Computing*. R Foundation for Statistical Computing, Vienna, Austria.

[371] Ray, A., James, M. K., Larochelle, S., Fisher, R. P., and Blain, S. W. (2009). p27Kip1 inhibits cyclin D-cyclin-dependent kinase 4 by two independent modes. *Molecular and cellular biology*, 29(4):986–999.

[372] Reader, J., Holt, D., and Fulton, A. (2011). Prostaglandin E2 EP receptors as therapeutic targets in breast cancer. *Cancer metastasis reviews*, 30(3-4):449–63.

[373] Rimerman, R. A., Gellert-Randleman, A., and Diehl, J. A. (2000). Wnt1 and MEK1 cooperate to promote cyclin D1 accumulation and cellular transformation. *Journal of Biological Chemistry*, 275(19):14736–14742.

[374] Robert, C., Karaszewska, B., Schachter, J., Rutkowski, P., Mackiewicz, A., Stroiakovski, D., Lichinitser, M., Dummer, R., Grange, F., Mortier, L., Chiarion-Sileni, V., Drucis, K., Krajsova, I., Hauschild, A., Lorigan, P., Wolter, P., Long, G. V., Flaherty, K., Nathan, P., Ribas, A., Martin, A.-M., Sun, P., Crist, W., Legos, J., Rubin, S. D., Little, S. M., and Schadendorf, D. (2015). Improved Overall Survival in Melanoma with Combined Dabrafenib and Trametinib. *New England Journal of Medicine*, 372(1):30–39.

[375] Rodrik, V., Gomes, E., Hui, L., Rockwell, P., and Foster, D. A. (2006). Myc stabilization in response to estrogen and phospholipase D in MCF-7 breast cancer cells. *FEBS Letters*, 580(24):5647–5652.

[376] Romond, E. H., Perez, E. A., Bryant, J., Suman, V. J., Geyer, C. E., Davidson, N. E., Tan-Chiu, E., Martino, S., Paik, S., Kaufman, P. A., Swain, S. M., Pisansky, T. M., Fehrenbacher, L., Kutteh, L. A., Vogel, V. G., Visscher, D. W., Yothers, G., Jenkins, R. B., Brown, A. M., Dakhil, S. R., Mamounas, E. P., Lingle, W. L., Klein, P. M., Ingle, J. N., and Wolmark, N. (2005). Trastuzumab plus Adjuvant Chemotherapy for Operable HER2-Positive Breast Cancer. *New England Journal of Medicine*, 353(16):1673–1684.

[377] Rosfjord, E. C. and Dickson, R. B. (1999). Growth factors, apoptosis, and survival of mammary epithelial cells. *Journal of mammary gland biology and neoplasia*, 4(2):229–37.

[378] Ross, A. J., Amy, S. P., Mahar, P. L., Lindsten, T., Knudson, C. M., Thompson, C. B., Korsmeyer, S. J., and MacGregor, G. R. (2001). BCLW mediates survival of postmitotic Sertoli cells by regulating BAX activity. *Developmental biology*, 239(2):295–308.

[379] Rowinsky, E. K. (2000). The pursuit of optimal outcomes in cancer therapy in a new age of rationally designed target-based anticancer agents. *Drugs*, 60 Suppl 1:1–14; discussion 41–2.

[380] Rubin, E. H. and Gilliland, D. G. (2012). Drug development and clinical trials - The path to an approved cancer drug. *Nature Reviews Clinical Oncology*, 9(4):215–222.

[381] Ruths, D., Muller, M., Tseng, J. T., Nakhleh, L., and Ram, P. T. (2008). The signaling petri net-based simulator: A non-parametric strategy for characterizing the dynamics of cell-specific signaling networks. *PLoS Computational Biology*, 4(2).

[382] Sabò, A., Kress, T. R., Pelizzola, M., de Pretis, S., Gorski, M. M., Tesi, A., Morelli, M. J., Bora, P., Doni, M., Verrecchia, A., Tonelli, C., Fagà, G., Bianchi, V., Ronchi, A., Low, D., Müller, H., Guccione, E., Campaner, S., and Amati, B. (2014). Selective transcriptional regulation by Myc in cellular growth control and lymphomagenesis. *Nature*, 511(7510):488–492.

[383] Sachs, L. (1984). *Applied Statistics*. Springer Series in Statistics. Springer New York, New York, NY, 2nd edition.

[384] Sackmann, A., Heiner, M., and Koch, I. (2006). Application of Petri net based analysis techniques to signal transduction pathways. *BMC Bioinformatics*, 7:1–17.

[385] Saez-Rodriguez, J., Alexopoulos, L. G., Epperlein, J., Samaga, R., Lauffenburger, D. A., Klamt, S., and Sorger, P. K. (2009). Discrete logic modelling as a means to link protein signalling networks with functional analysis of mammalian signal transduction. *Molecular Systems Biology*, 5(331):1–19.

[386] Sagiv-Barfi, I., Czerwinski, D. K., Levy, S., Alam, I. S., Mayer, A. T., Gambhir, S. S., and Levy, R. (2018). Eradication of spontaneous malignancy by local immunotherapy. *Sci. Transl. Med*, 10(31).

[387] Samaga, R., Saez-Rodriguez, J., Alexopoulos, L. G., Sorger, P. K., and Klamt, S. (2009). The logic of EGFR/ErbB signaling: theoretical properties and analysis of high-throughput data. *PLoS computational biology*, 5(8):e1000438.

[388] Sánchez-Rivera, F. J. and Jacks, T. (2015). Applications of the CRISPR-Cas9 system in cancer biology. *Nature reviews. Cancer*, 15(7):387–95.

[389] Sandhu, C., Garbe, J., Bhattacharya, N., Daksis, J., Pan, C. H., Yaswen, P., Koh, J., Slingerland, J. M., and Stampfer, M. R. (1997). Transforming growth factor beta stabilizes p15INK4B protein, increases p15INK4B-cdk4 complexes, and inhibits cyclin D1-cdk4 association in human mammary epithelial cells. *Molecular and cellular biology*, 17(5):2458–2467.

[390] Schaub, M. A., Henzinger, T. A., and Fisher, J. (2007). Qualitative networks: a symbolic approach to analyze biological signaling networks. *BMC systems biology*, 1:4.

[391] Schmidt, C. M., Wang, Y., and Wiesenauer, C. (2003). Novel Combination of Cyclooxygenase-2 and MEK Inhibitors in Human Hepatocellular Carcinoma Provides a Synergistic Increase in Apoptosis. *Journal of Gastrointestinal Surgery*, 7(8):1024–1033.

[392] Schmidt, M., Fernandez de Mattos, S., van der Horst, A., Klompmaker, R., Kops, G. J. P. L., Lam, E. W.-F., Burgering, B. M. T., and Medema, R. H. (2002). Cell Cycle Inhibition by FoxO Forkhead Transcription Factors Involves Downregulation of Cyclin D. *Molecular and Cellular Biology*, 22(22):7842–7852.

[393] Schulze, W. X., Deng, L., and Mann, M. (2005). Phosphotyrosine interactome of the ErbB-receptor kinase family. *Molecular Systems Biology*, 1(1):E1–E13.

[394] Scott, P. A., Gleadle, J. M., Bicknell, R., and Harris, A. L. (1998). Role of the hypoxia sensing system, acidity and reproductive hormones in the variability of vascular endothelial growth factor induction in human breast carcinoma cell lines. *International journal of cancer*, 75(5):706–12.

[395] Searle, S. R., Speed, F. M., and Milliken, G. A. (1980). Population Marginal Means in the Linear Model: An Alternative to Least Squares Means. *The American Statistician*, 34(4):216–221.

[396] Sears, R., Nuckolls, F., Haura, E., Taya, Y., Tamai, K., and Nevins, J. R. (2000). Multiple Ras-dependent phosphorylation pathways regulate Myc protein stability. *Genes & Development*, 14(19):2501–2514.

[397] Seidman, A., Hudis, C., Pierri, M. K., Shak, S., Paton, V., Ashby, M., Murphy, M., Stewart, S. J., and Keefe, D. (2002). Cardiac dysfunction in the trastuzumab clinical trials experience. *Journal of clinical oncology : official journal of the American Society of Clinical Oncology*, 20(5):1215–21.

[398] Semenza, G. L. (2003). Targeting HIF-1 for cancer therapy. *Nature reviews. Cancer*, 3(10):721–32.

[399] Seoane, J., Pouponnot, C., Staller, P., Schader, M., Eilers, M., and Massagué, J. (2001). TGFbeta influences Myc, Miz-1 and Smad to control the CDK inhibitor p15INK4b. *Nature cell biology*, 3(4):400–8.

[400] Shah, S. P., Morin, R. D., Khattra, J., Prentice, L., Pugh, T., Burleigh, A., Delaney, A., Gelmon, K., Guliany, R., Senz, J., Steidl, C., Holt, R. A., Jones, S., Sun, M., Leung, G., Moore, R., Severson, T., Taylor, G. A., Teschendorff, A. E., Tse, K., Turashvili, G., Varhol, R., Warren, R. L., Watson, P., Zhao, Y., Caldas, C., Huntsman, D., Hirst, M., Marra, M. A., and Aparicio, S. (2009). Mutational evolution in a lobular breast tumour profiled at single nucleotide resolution. *Nature*, 461(7265):809–813.

[401] Shah, S. P., Roth, A., Goya, R., Oloumi, A., Ha, G., Zhao, Y., Turashvili, G., Ding, J., Tse, K., Haffari, G., Bashashati, A., Prentice, L. M., Khattra, J., Burleigh, A., Yap, D., Bernard, V., McPherson, A., Shumansky, K., Crisan, A., Giuliany, R., Heravi-Moussavi, A., Rosner, J., Lai, D., Birol, I., Varhol, R., Tam, A., Dhalla, N., Zeng, T., Ma, K., Chan, S. K., Griffith, M., Moradian, A., Cheng, S.-W. G., Morin, G. B., Watson, P., Gelmon, K., Chia, S., Chin, S.-F., Curtis, C., Rueda, O. M., Pharoah, P. D., Damaraju, S., Mackey, J., Hoon, K., Harkins, T., Tadigotla, V., Sigaroudinia, M., Gascard, P., Tlsty, T., Costello, J. F., Meyer, I. M., Eaves, C. J., Wasserman, W. W., Jones, S., Huntsman, D., Hirst, M., Caldas, C., Marra, M. A., and Aparicio, S. (2012). The clonal and mutational evolution spectrum of primary triple-negative breast cancers. *Nature*, 486(7403):395–399.

[402] Shapiro, S. S. and Wilk, M. B. (1965). An Analysis of Variance Test for Normality (Complete Samples). *Biometrika*, 52(3/4):591.

[403] She, Q.-B., Chandarlapaty, S., Ye, Q., Lobo, J., Haskell, K. M., Leander, K. R., DeFeo-Jones, D., Huber, H. E., and Rosen, N. (2008). Breast tumor cells with PI3K mutation or HER2 amplification are selectively addicted to Akt signaling. *PloS one*, 3(8):e3065.

[404] Shen, F., Fan, X., Liu, B., Jia, X., Gao, A., Du, H., Ye, M., You, B., Huang, C., and Shi, X. (2008). Downregulation of cyclin D1-CDK4 protein in human embryonic lung fibroblasts (HELF) induced by silica is mediated through the ERK and JNK pathway. *Cell Biology International*, 32(10):1284–1292.

[405] Shih, Y. C. T., Smieliauskas, F., Geynisman, D. M., Kelly, R. J., and Smith, T. J. (2015). Trends in the cost and use of targeted cancer therapies for the privately insured nonelderly: 2001 To 2011. *Journal of Clinical Oncology*, 33(19):2190–2196.

[406] Siegal, M. L. and Bergman, A. (2002). Waddington's canalization revisited: Developmental stability and evolution. *Proceedings of the National Academy of Sciences*, 99(16):10528–10532.

[407] Siegel, P. M., Shu, W., and Massagué, J. (2003). Mad upregulation and Id2 repression accompany transforming growth factor (TGF)-β-mediated epithelial cell growth suppression. *Journal of Biological Chemistry*, 278(37):35444–35450.

[408] Silverbush, D., Grosskurth, S., Wang, D., Powell, F., Gottgens, B., Dry, J., and Fisher, J. (2017). Cell-Specific Computational Modeling of the PIM Pathway in Acute Myeloid Leukemia. *Cancer research*, 77(4):827–838.

[409] Sinn, E., Muller, W., Pattengale, P., Tepler, I., Wallace, R., and Leder, P. (1987). Coexpression of MMTV/v-Ha-ras and MMTV/c-myc genes in transgenic mice: Synergistic action of oncogenes in vivo. *Cell*, 49(4):465–475.

[410] Slamon, D., Clark, G., Wong, S., Levin, W., Ullrich, A., and McGuire, W. (1987). Human breast cancer: correlation of relapse and survival with amplification of the HER-2/neu oncogene. *Science*, 235(4785):177–182.

[411] Smalley, M. J. and Dale, T. C. (2001). Wnt signaling and mammary tumorigenesis. *Journal of mammary gland biology and neoplasia*, 6(1):37–52.

[412] Smet, R. D. and Marchal, K. (2010). Advantages and limitations of current network inference methods. *Nature Publishing Group*, 8(10):717–729.

[413] Sokal, R. and Rohlf, F. (1987). *Introduction to Biostatistics*. W. H. Freeman and Company, New York, 2nd edition.

[414] Sotiriou, C., Neo, S.-Y. Y., McShane, L. M., Korn, E. L., Long, P. M., Jazaeri, A., Martiat, P., Fox, S. B., Harris, A. L., and Liu, E. T. (2003). Breast cancer classification and prognosis based on gene expression profiles from a population-based study. *Proceedings of the National Academy of Sciences of the United States of America*, 100(18):10393–10398.

[415] Soucek, L., Whitfield, J., Martins, C. P., Finch, A. J., Murphy, D. J., Sodir, N. M., Karnezis, A. N., Swigart, L. B., Nasi, S., and Evan, G. I. (2008). Modelling Myc inhibition as a cancer therapy. *Nature*, 455(7213):679–83.

[416] Sowter, H. M., Ratcliffe, P. J., Watson, P., Greenberg, A. H., and Harris, A. L. (2001). HIF-1-dependent regulation of hypoxic induction of the cell death factors BNIP3 and NIX in human tumors. *Cancer Research*, 61(18):6669–6673.

[417] Sprouffske, K., Pepper, J. W., and Maley, C. C. (2011). Accurate Reconstruction of the Temporal Order of Mutations in Neoplastic Progression. *Cancer Prevention Research*, 4(7):1135–1144.

[418] Stambolic, V., MacPherson, D., Sas, D., Lin, Y., Snow, B., Jang, Y., Benchimol, S., and Mak, T. W. (2001). Regulation of PTEN transcription by p53. *Molecular cell*, 8(2):317–25.

[419] Stasinopoulos, I. A., Mironchik, Y., Raman, A., Wildes, F., Winnard, P., and Raman, V. (2005). HOXA5-twist interaction alters p53 homeostasis in breast cancer cells. *Journal of Biological Chemistry*, 280(3):2294–2299.

[420] Steele, E., Tucker, A., 't Hoen, P. A. C., and Schuemie, M. J. (2009). Literature-based priors for gene regulatory networks. *Bioinformatics (Oxford, England)*, 25(14):1768–74.

[421] Stern, H. M., Gardner, H., Burzykowski, T., Elatre, W., O'Brien, C., Lackner, M. R., Pestano, G. A., Santiago, A., Villalobos, I., Eiermann, W., Pienkowski, T., Martin, M., Robert, N., Crown, J., Nuciforo, P., Bee, V., Mackey, J., Slamon, D. J., and Press, M. F. (2015). PTEN loss is associated with worse outcome in HER2-Amplified breast cancer patients but is not associated with trastuzumab resistance. *Clinical Cancer Research*, 21(9):2065–2074.

[422] Stewart-Ornstein, J., Cheng, H. W. J., and Lahav, G. (2017). Conservation and Divergence of p53 Oscillation Dynamics across Species. *Cell Systems*, 5(4):410–417.e4.

[423] Student (1908). The Probable Error of a Mean. *Biometrika*, 6(1):1–25.

[424] Sun, M., Shariat, S. F., Trinh, Q.-D., Meskawi, M., Bianchi, M., Hansen, J., Abdollah, F., Perrotte, P., and Karakiewicz, P. I. (2013). An evidence-based guide to the selection of sequential therapies in metastatic renal cell carcinoma. *Therapeutic Advances in Urology*, 5(2):121–128.

[425] Sun, Q.-Y., Ding, L.-W., Tan, K.-T., Chien, W., Mayakonda, A., Lin, D.-C., Loh, X.-Y., Xiao, J.-F., Meggendorfer, M., Alpermann, T., Garg, M., Lim, S.-L., Madan, V., Hattori, N., Nagata, Y., Miyano, S., Yeoh, A. E. J., Hou, H.-A., Jiang, Y.-Y., Takao, S., Liu, L.-Z., Tan, S.-Z., Lill, M., Hayashi, M., Kinoshita, A., Kantarjian, H. M., Kornblau, S. M., Ogawa, S., Haferlach, T., Yang, H., and Koeffler, H. P. (2017). Ordering of mutations in acute myeloid leukemia with partial tandem duplication of MLL (MLL-PTD). *Leukemia*, 31(1):1–10.

[426] Sundvall, M., Iljin, K., Kilpinen, S., Sara, H., Kallioniemi, O. P., and Elenius, K. (2008). Role of ErbB4 in breast cancer. *Journal of Mammary Gland Biology and Neoplasia*, 13(2):259–268.

[427] Sunters, A., Fernández De Mattos, S., Stahl, M., Brosens, J. J., Zoumpoulidou, G., Saunders, C. A., Coffer, P. J., Medema, R. H., Coombes, R. C., and Lam, E. W.-F. W. (2003). FoxO3a transcriptional regulation of Bim controls apoptosis in paclitaxel-treated breast cancer cell lines. *The Journal of biological chemistry*, 278(50):49795–805.

[428] Sunters, A., Madureira, P. A., Pomeranz, K. M., Aubert, M., Brosens, J. J., Cook, S. J., Burgering, B. M., Coombes, R. C., and Lam, E. W. (2006). Paclitaxel-induced nuclear translocation of FOXO3a in breast cancer cells is mediated by c-Jun NH2-terminal kinase and Akt. *Cancer Research*, 66(1):212–220.

[429] Swann, J. B. and Smyth, M. J. (2007). Review series Immune surveillance of tumors. *The Journal of Clinical Investigation*, 117(5):1137–1146.

[430] Swisher, S. G., Roth, J. A., Komaki, R., Gu, J., Lee, J. J., Hicks, M., Ro, J. Y., Hong, W. K., Merritt, J. A., Ahrar, K., Atkinson, N. E., Correa, A. M., Dolormente, M., Dreiling, L., El-Naggar, A. K., Fossella, F., Francisco, R., Glisson, B., Grammer, S., Herbst, R., Huaringa, A., Kemp, B., Khuri, F. R., Kurie, J. M., Liao, Z., McDonnell, T. J., Morice, R., Morello, F., Munden, R., Papadimitrakopoulou, V., Pisters, K. M., Putnam, J. B., Sarabia, A. J., Shelton, T., Stevens, C., Shin, D. M., Smythe, W. R., Vaporciyan, A. A., Walsh, G. L., and Yin, M. (2003). Induction of p53-regulated genes and tumor regression in lung cancer patients after intratumoral delivery of adenoviral p53 (INGN 201) and radiation therapy. *Clinical Cancer Research*, 9(1 I):93–101.

[431] Tabassum, D. P. and Polyak, K. (2015). Tumorigenesis: it takes a village. *Nature Reviews Cancer*, 15(8):473–483.

[432] Taelman, V. F., Dobrowolski, R., Plouhinec, J.-L., Fuentealba, L. C., Vorwald, P. P., Gumper, I., Sabatini, D. D., and De Robertis, E. M. (2010). Wnt signaling requires sequestration of glycogen synthase kinase 3 inside multivesicular endosomes. *Cell*, 143(7):1136–48.

[433] Tait, S. W. and Green, D. R. (2010). Mitochondria and cell death: outer membrane permeabilization and beyond. *Nature reviews.Molecular cell biology*, 11(9):621–632.

[434] Takahashi, K. and Yamanaka, S. (2006). Induction of pluripotent stem cells from mouse embryonic and adult fibroblast cultures by defined factors. *Cell*, 126(4):663–76.

[435] Tallarida, R. J. (2006). An Overview of Drug Combination Analysis with Isobolograms. *Journal of Pharmacology and Experimental Therapeutics*, 319(1):1–7.

[436] Tamai, K., Zeng, X., Liu, C., Zhang, X., Harada, Y., Chang, Z., and He, X. (2004). A Mechanism for Wnt Coreceptor Activation. *Molecular Cell*, 13(1):149–156.

[437] Taylor, B. J. M., Nik-Zainal, S., Wu, Y. L., Stebbings, L. A., Raine, K., Campbell, P. J., Rada, C., Stratton, M. R., and Neuberger, M. S. (2013). DNA deaminases induce break-associated mutation showers with implication of APOBEC3B and 3A in breast cancer kataegis. *eLife*, 2013(2):1–14.

[438] Tepera, S. B., McCrea, P. D., and Rosen, J. M. (2003). A beta-catenin survival signal is required for normal lobular development in the mammary gland. *Journal of cell science*, 116(Pt 6):1137–1149.

[439] Teuliere, J., Faraldo, M. M., Deugnier, M. A., Shtutman, M., Ben-Ze'ev, A., Thiery, J. P., and Glukhova, M. A. (2005). Targeted activation of beta-catenin signaling in basal mammary epithelial cells affects mammary development and leads to hyperplasia. *Development*, 132(2):267–277.

[440] Thakar, J., Pilione, M., Kirimanjeswara, G., Harvill, E. T., and Albert, R. (2007). Modeling systems-level regulation of host immune responses. *PLoS Computational Biology*, 3(6):1022–1039.

[441] Thliveris, A. T., Schwefel, B., Clipson, L., Plesh, L., Zahm, C. D., Leystra, A. A., Washington, M. K., Sullivan, R., Deming, D. A., Newton, M. A., and Halberg, R. B. (2013). Transformation of epithelial cells through recruitment leads to polyclonal intestinal tumors. *Proceedings of the National Academy of Sciences of the United States of America*, 110(28):11523–11528.

[442] Thompson, M. P. and Kurzrock, R. (2004). Epstein-Barr virus and cancer. *Clinical cancer research : an official journal of the American Association for Cancer Research*, 10(3):803–21.

[443] Thurnherr, T., Singer, F., Stekhoven, D. J., and Beerenwinkel, N. (2016). Genomic variant annotation workflow for clinical applications. *F1000Research*, 5(0):1963.

[444] Timoshenko, A. V., Lala, P. K., and Chakraborty, C. (2004). PGE2-mediated upregulation of iNOS in murine breast cancer cells through the activation of EP4 receptors. *International Journal of Cancer*, 108(3):384–389.

[445] Trimarchi, J. M. and Lees, J. A. (2002). Sibling rivalry in the E2F family. *Nature Reviews Molecular Cell Biology*, 3(1):11–20.

[446] Tsukamoto, A. S., Grosschedl, R., Guzman, R. C., Parslow, T., and Varmus, H. E. (1988). Expression of the int-1 gene in transgenic mice is associated with mammary gland hyperplasia and adenocarcinomas in male and female mice. *Cell*, 55(4):619–625.

[447] Tsuneoka, M. and Mekada, E. (2000). Ras/MEK signaling suppresses Myc-dependent apoptosis in cells transformed by c-myc and activated ras. *Oncogene*, 19(1):115–23.

[448] Tukey, J. W. (1949). Comparing Individual Means in the Analysis of Variance. *Biometrics*, 5(2):99.

[449] Turajlic, S., McGranahan, N., and Swanton, C. (2015). Inferring mutational timing and reconstructing tumour evolutionary histories. *Biochimica et Biophysica Acta - Reviews on Cancer*, 1855(2):264–275.

[450] Turke, A. B., Zejnullahu, K., Wu, Y.-L., Song, Y., Dias-Santagata, D., Lifshits, E., Toschi, L., Rogers, A., Mok, T., Sequist, L., Lindeman, N. I., Murphy, C., Akhavanfard, S., Yeap, B. Y., Xiao, Y., Capelletti, M., Iafrate, a. J., Lee, C., Christensen, J. G., Engelman, J. a., and Jänne, P. a. (2010). Preexistence and Clonal Selection of MET Amplification in EGFR Mutant NSCLC. *Cancer Cell*, 17(1):77–88.

[451] Turner, N. C. and Reis-Filho, J. S. (2012). Genetic heterogeneity and cancer drug resistance. *The Lancet Oncology*, 13(4):e178–e185.

[452] Tversky, A. and Kahneman, D. (1975). Judgment under Uncertainty: Heuristics and Biases. *Utility, Probability, and Human Decision Making*, 185:141–162.

[453] Tyson, J. J., Chen, K. C., and Novak, B. (2003). Sniffers, buzzers, toggles and blinkers: dynamics of regulatory and signaling pathways in the cell. *Current opinion in cell biology*, 15(2):221–31.

[454] Tyson, J. J. and Novák, B. (2015). Models in biology: lessons from modeling regulation of the eukaryotic cell cycle. *BMC Biology*, 13(1):46.

[455] Untch, M., Rezai, M., Loibl, S., Fasching, P. A., Huober, J., Tesch, H., Bauerfeind, I., Hilfrich, J., Eidtmann, H., Gerber, B., Hanusch, C., Kuehn, T., Du Bois, A., Blohmer, J. U., Thomssen, C., Dan Costa, S., Jackisch, C., Kaufmann, M., Mehta, K., and Von Minckwitz, G. (2010). Neoadjuvant treatment with trastuzumab in HER2-positive breast cancer: Results from the GeparQuattro study. *Journal of Clinical Oncology*, 28(12):2024–2031.

[456] Villunger, A., Michalak, E. M., Coultas, L., Müllauer, F., Böck, G., Ausserlechner, M. J., Adams, J. M., and Strasser, A. (2003). p53- and drug-induced apoptotic responses mediated by BH3-only proteins puma and noxa. *Science (New York, N.Y.)*, 302:1036–1038.

[457] Vita, M. and Henriksson, M. (2006). The Myc oncoprotein as a therapeutic target for human cancer. *Seminars in Cancer Biology*, 16(4):318–330.

[458] Vogel, C. L., Cobleigh, M. A., Tripathy, D., Gutheil, J. C., Harris, L. N., Fehrenbacher, L., Slamon, D. J., Murphy, M., Novotny, W. F., Burchmore, M., Shak, S., Stewart, S. J., and Press, M. (2002). Efficacy and Safety of Trastuzumab as a Single Agent in First-Line Treatment of HER2 -Overexpressing Metastatic Breast Cancer. *Journal of Clinical Oncology*, 20(3):719–726.

[459] Vogel, C. L. and Franco, S. X. (2003). Clinical Experience with Trastuzumab (Herceptin). *The Breast Journal*, 9(6):452–462.

[460] Vogler, M. (2012). BCL2A1: the underdog in the BCL2 family. *Cell Death and Differentiation*, 19(1):67–74.

[461] von Lintig, F. C., Dreilinger, A. D., Varki, N. M., Wallace, A. M., Casteel, D. E., and Boss, G. R. (2000). Ras activation in human breast cancer. *Breast cancer research and treatment*, 62(1):51–62.

[462] Vranic, S., Gatalica, Z., and Wang, Z. Y. (2011). Update on the molecular profile of the MDA-MB-453 cell line as a model for apocrine breast carcinoma studies. *Oncology Letters*, 2(6):1131–1137.

[463] Waclaw, B., Bozic, I., Pittman, M. E., Hruban, R. H., Vogelstein, B., and Nowak, M. a. (2015). A spatial model predicts that dispersal and cell turnover limit intratumour heterogeneity. *Nature*, 525(7568):261–264.

[464] Wagle, N., Emery, C., Berger, M. F., Davis, M. J., Sawyer, A., Pochanard, P., Kehoe, S. M., Johannessen, C. M., MacConaill, L. E., Hahn, W. C., Meyerson, M., and Garraway, L. A. (2011). Dissecting therapeutic resistance to RAF inhibition in melanoma by tumor genomic profiling. *Journal of Clinical Oncology*, 29(22):3085–3096.

[465] Wagner, A. H., Coffman, A. C., Ainscough, B. J., Spies, N. C., Skidmore, Z. L., Campbell, K. M., Krysiak, K., Pan, D., McMichael, J. F., Eldred, J. M., Walker, J. R., Wilson, R. K., Mardis, E. R., Griffith, M., and Griffith, O. L. (2016). DGIdb 2.0: Mining clinically relevant drug-gene interactions. *Nucleic Acids Research*, 44(D1):D1036–D1044.

[466] Wang, H., Mannava, S., Grachtchouk, V., Zhuang, D., Soengas, M. S., Gudkov, A. V., Prochownik, E. V., and Nikiforov, M. A. (2008). c-Myc depletion inhibits proliferation of human tumor cells at various stages of the cell cycle. *Oncogene*, 27(13):1905–15.

[467] Wang, X., Ling, M. T., Guan, X.-Y., Tsao, S. W., Cheung, H. W., Lee, D. T., and Wong, Y. C. (2004). Identification of a novel function of TWIST, a bHLH protein, in the development of acquired taxol resistance in human cancer cells. *Oncogene*, 23(2):474–82.

[468] Wang, Y., Waters, J., Leung, M. L., Unruh, A., Roh, W., Shi, X., Chen, K., Scheet, P., Vattathil, S., Liang, H., Multani, A., Zhang, H., Zhao, R., Michor, F., Meric-Bernstam, F., and Navin, N. E. (2014). Clonal evolution in breast cancer revealed by single nucleus genome sequencing. *Nature*, 512(7513):155–160.

[469] Watanabe, O., Imamura, H., Shimizu, T., Kinoshita, J., Okabe, T., Hirano, A., Yoshimatsu, K., Konno, S., Aiba, M., and Ogawa, K. (2004). Expression of twist and Wnt in human breast cancer. *Anticancer Research*, 24(6):3851–3856.

[470] Watson, C. J. (2006). Post-lactational mammary gland regression: molecular basis and implications for breast cancer. *Expert reviews in molecular medicine*, 8(32):1–15.

[471] Watson, P. H., Pon, R. T., and Shiu, R. P. (1991). Inhibition of c-myc expression by phosphorothioate antisense oligonucleotide identifies a critical role for c-myc in the growth of human breast cancer. *Cancer research*, 51(15):3996–4000.

[472] Weber, J. D., Taylor, L. J., Roussel, M. F., Sherr, C. J., and Bar-Sagi, D. (1999). Nucleolar Arf sequesters Mdm2 and activates p53. *Nature cell biology*, 1(May):20–26.

[473] Wei, M. C., Zong, W.-X., Cheng, E. H.-Y., Lindsten, T., Panoutsakopoulou, V., Ross, A. J., Roth, K. A., MacGregor, G. R., Thompson, C. B., and Korsmeyer, S. J. (2001). Proapoptotic BAX and BAK: A Requisite Gateway to Mitochondrial Dysfunction and Death. *Science (New York, N.Y.)*, 292(April):727–730.

[474] Weinberg, R. A. (1995). The retinoblastoma protein and cell cycle control. *Cell*, 81(3):323–330.

[475] Welch, B. L. (1947). The Generalization of 'Student's' Problem when Several Different Population Variances are Involved. *Biometrika*, 34(1/2):28.

[476] Welcker, M., Singer, J., Loeb, K. R., Grim, J., Bloecher, A., Gurien-West, M., Clurman, B. E., and Roberts, J. M. (2003). Multisite phosphorylation by Cdk2 and GSK3 controls cyclin E degradation. *Molecular Cell*, 12(2):381–392.

[477] West, J., Bianconi, G., Severini, S., and Teschendorff, A. E. (2012). Differential network entropy reveals cancer system hallmarks. *Scientific Reports*, 2.

[478] Whitfield, J. R., Beaulieu, M.-E., and Soucek, L. (2017). Strategies to Inhibit Myc and Their Clinical Applicability. *Frontiers in Cell and Developmental Biology*, 5(February):1–13.

[479] Whitmarsh, A. J. and Davis, R. J. (2000). A central control for cell growth. *Nature*, 403(6767):255–256.

[480] Widakowich, C., de Castro, G., de Azambuja, E., Dinh, P., and Awada, A. (2007). Review: Side Effects of Approved Molecular Targeted Therapies in Solid Cancers. *The Oncologist*, 12(12):1443–1455.

[481] Wodarz, D., Newell, A. C., and Komarova, N. L. (2018). Passenger mutations can accelerate tumour suppressor gene inactivation in cancer evolution. *Journal of The Royal Society Interface*, 15(143):20170967.

[482] Wollbold, J., Huber, R., Pohlers, D., Koczan, D., Guthke, R., Kinne, R. W., and Gausmann, U. (2009). Adapted Boolean network models for extracellular matrix formation. *BMC systems biology*, 3:77.

[483] Won, K. a. and Reed, S. I. (1996). Activation of cyclin E/CDK2 is coupled to site-specific autophosphorylation and ubiquitin-dependent degradation of cyclin E. *The EMBO journal*, 15(16):4182–4193.

[484] Wu, A., Liao, D., Tlsty, T. D., Sturm, J. C., and Austin, R. H. (2014). Game theory in the death galaxy: interaction of cancer and stromal cells in tumour microenvironment. *Interface focus*, 4(4):20140028.

[485] Wu, F., Zhang, J., Wang, P., Ye, X., Jung, K., Bone, K. M., Pearson, J. D., Ingham, R. J., McMullen, T. P., Ma, Y., and Lai, R. (2012). Identification of two novel phenotypically distinct breast cancer cell subsets based on Sox2 transcription activity. *Cellular Signalling*, 24(11):1989–1998.

[486] Wu, M., Sirota, M., Butte, A. J., and Chen, B. (2015). Characteristics of drug combination therapy in oncology by analyzing clinical trial data on ClinicalTrials.gov. *Pacific Symposium on Biocomputing. Pacific Symposium on Biocomputing*, pages 68–79.

[487] Wu, X., Sun, L., Wang, X., Su, P., Li, Z., Zhang, C., Wang, Y., Gao, P., and Ma, R. (2016). Breast Cancer Invasion and Metastasis by mPRα Through the PI3K/Akt Signaling Pathway. *Pathology oncology research : POR*, 22(3):471–6.

[488] Wu, Z. L., Zheng, S. S., Li, Z. M., Qiao, Y. Y., Aau, M. Y., and Yu, Q. (2010). Polycomb protein EZH2 regulates E2F1-dependent apoptosis through epigenetically modulating Bim expression. *Cell death and differentiation*, 17(5):801–810.

[489] Wynn, M. L., Consul, N., Merajver, S. D., and Schnell, S. (2012). Logic-based models in systems biology: a predictive and parameter-free network analysis method. *Integrative Biology*, 4(11):1323.

[490] Xiong, S., Grijalva, R., Zhang, L., Nguyen, N. T., Pisters, P. W., Pollock, R. E., and Yu, D. (2001). Up-regulation of vascular endothelial growth factor in breast cancer cells by the heregulin-beta1-activated p38 signaling pathway enhances endothelial cell migration. *Cancer research*, 61(4):1727–32.

[491] Yanase, K., Tsukahara, S., Asada, S., Ishikawa, E., Imai, Y., and Sugimoto, Y. (2004). Gefitinib reverses breast cancer resistance protein-mediated drug resistance. *Molecular cancer therapeutics*, 3(September):1119–1125.

[492] Yang, B. S., Gilbert, J. D., and Freytag, S. O. (1993). Overexpression of Myc suppresses CCAAT transcription factor/nuclear factor 1-dependent promoters in vivo. *Mol Cell Biol*, 13(5):3093–3102.

[493] Yang, J.-Y., Zong, C. S., Xia, W., Yamaguchi, H., Ding, Q., Xie, X., Lang, J.-Y., Lai, C.-C., Chang, C.-J., Huang, W.-C., Huang, H., Kuo, H.-P., Lee, D.-F., Li, L.-Y., Lien, H.-C., Cheng, X., Chang, K.-J., Hsiao, C.-D., Tsai, F.-J., Tsai, C.-H., Sahin, A. A., Muller, W. J., Mills, G. B., Yu, D., Hortobagyi, G. N., and Hung, M.-C. (2008). ERK promotes tumorigenesis by inhibiting FOXO3a via MDM2-mediated degradation. *Nature cell biology*, 10(2):138–48.

[494] Yang, S. and Han, H. (2014). Effect of cycloxygenase-2 silencing on the malignant biological behavior of MCF-7 breast cancer cells. *Oncology letters*, 8(4):1628–1634.

[495] Yang, W., Shen, J., Wu, M., Arsura, M., FitzGerald, M., Suldan, Z., Kim, D. W., Hofmann, C. S., Pianetti, S., Romieu-Mourez, R., Freedman, L. P., and Sonenshein, G. E. (2001). Repression of transcription of the p27(Kip1) cyclin-dependent kinase inhibitor gene by c-Myc. *Oncogene*, 20(14):1688–1702.

[496] Yarden, Y. and Sliwkowski, M. X. (2001). Untangling the ErbB signalling network. *Nature reviews. Molecular cell biology*, 2(2):127–137.

[497] Yates, L. R., Gerstung, M., Knappskog, S., Desmedt, C., Gundem, G., Van Loo, P., Aas, T., Alexandrov, L. B., Larsimont, D., Davies, H., Li, Y., Ju, Y. S., Ramakrishna, M., Haugland, H. K., Lilleng, P. K., Nik-Zainal, S., McLaren, S., Butler, A., Martin, S., Glodzik, D., Menzies, A., Raine, K., Hinton, J., Jones, D., Mudie, L. J., Jiang, B., Vincent,

D., Greene-Colozzi, A., Adnet, P.-Y., Fatima, A., Maetens, M., Ignatiadis, M., Stratton, M. R., Sotiriou, C., Richardson, A. L., Lønning, P. E., Wedge, D. C., and Campbell, P. J. (2015). Subclonal diversification of primary breast cancer revealed by multiregion sequencing. *Nature Medicine*, 21(7):751–759.

[498] Yeh, E., Cunningham, M., Arnold, H., Chasse, D., Monteith, T., Ivaldi, G., Hahn, W. C., Stukenberg, P. T., Shenolikar, S., Uchida, T., Counter, C. M., Nevins, J. R., Means, A. R., and Sears, R. (2004). A signalling pathway controlling c-Myc degradation that impacts oncogenic transformation of human cells. *Nature cell biology*, 6(4):308–18.

[499] Yordanov, B., Dunn, S.-J., Kugler, H., Smith, A., Martello, G., and Emmott, S. (2016). A Method to Identify and Analyze Biological Programs through Automated Reasoning. *NPJ systems biology and applications*, 2(1):16010.

[500] You, Z., Saims, D., Chen, S., Zhang, Z., Guttridge, D. C., Guan, K. L., MacDougald, O. A., Brown, A. M. C., Evan, G., Kitajewski, J., and Wang, C. Y. (2002). Wnt signaling promotes oncogenic transformation by inhibiting c-Myc-induced apoptosis. *Journal of Cell Biology*, 157(3):429–440.

[501] Yu, J., Zhang, L., Hwang, P. M., Kinzler, K. W., and Vogelstein, B. (2001). PUMA Induces the Rapid Apoptosis of Colorectal Cancer Cells. *Molecular Cell*, 7(3):673–682.

[502] Zaman, N., Li, L., Jaramillo, M., Sun, Z., Tibiche, C., Banville, M., Collins, C., Trifiro, M., Paliouras, M., Nantel, A., O'Connor-McCourt, M., and Wang, E. (2013). Signaling Network Assessment of Mutations and Copy Number Variations Predict Breast Cancer Subtype-Specific Drug Targets. *Cell Reports*, 5(1):216–223.

[503] Zambelli, A., Della Porta, M. G., Eleuteri, E., De Giuli, L., Catalano, O., Tondini, C., and Riccardi, A. (2011). Predicting and preventing cardiotoxicity in the era of breast cancer targeted therapies. Novel molecular tools for clinical issues. *Breast*, 20(2):176–183.

[504] Zañudo, J. G., Steinway, S. N., and Albert, R. (2018). Discrete dynamic network modeling of oncogenic signaling: Mechanistic insights for personalized treatment of cancer. *Current Opinion in Systems Biology*, 9:1–10.

[505] Zeiss, C. J. (2003). The apoptosis-necrosis continuum: Insights from genetically altered mice. *Veterinary Pathology*, 40(5):481–495.

[506] Zevedei-Oancea, I. and Schuster, S. (2005). A theoretical framework for detecting signal transfer routes in signalling networks. *Computers and Chemical Engineering*, 29(3):597–617.

[507] Zhai, D., Jin, C., Huang, Z., Satterthwait, A. C., and Reed, J. C. (2008). Differential regulation of Bax and Bak by anti-apoptotic Bcl-2 family proteins Bcl-B and Mcl-1. *Journal of Biological Chemistry*, 283(15):9580–9586.

[508] Zhang, H.-F., Wu, C., Alshareef, A., Gupta, N., Zhao, Q., Xu, X.-E., Jiao, J.-W., Li, E.-M., Xu, L.-Y., and Lai, R. (2016). The PI3K/AKT/c-MYC Axis Promotes the Acquisition of Cancer Stem-Like Features in Esophageal Squamous Cell Carcinoma. *Stem Cells*, 34(8):2040–2051.

[509] Zhang, H. Y., Liang, F., Jia, Z. L., Song, S. T., and Jiang, Z. F. (2013). PTEN mutation, methylation and expression in breast cancer patients. *Oncology Letters*, 6(1):161–168.

[510] Zhang, M., Tsimelzon, A., Chang, C.-H. C.-H., Fan, C., Wolff, A., Perou, C. M., Hilsenbeck, S. G., Rosen, J. M., and ZhangA., M. (2015). Intratumoral heterogeneity in a p53 null mouse model of human breast cancer. *Cancer Discovery*, 5(5):520–533.

[511] Zhang, S. Q., Hayashida, M., Akutsu, T., Ching, W. K., and Ng, M. K. (2007). Algorithms for finding small attractors in boolean networks. *Eurasip Journal on Bioinformatics and Systems Biology*, 2007.

[512] Zhang, X., Podsypanina, K., Huang, S., Mohsin, S. K., Chamness, G. C., Hatsell, S., Cowin, P., Schiff, R., and Li, Y. (2005). Estrogen receptor positivity in mammary tumors of Wnt-1 transgenic mice is influenced by collaborating oncogenic mutations. *Oncogene*, 24(26):4220–31.

[513] Zheng, D., Yang, G., Li, X., Wang, Z., Liu, F., and He, L. (2013). An Efficient Algorithm for Computing Attractors of Synchronous And Asynchronous Boolean Networks. *PLoS ONE*, 8(4):1–7.

[514] Zhou, B. P., Liao, Y., Xia, W., Spohn, B., Lee, M. H., and Hung, M. C. (2001). Cytoplasmic localization of p21Cip1/WAF1 by Akt-induced phosphorylation in HER-2/neu-overexpressing cells. *Nature cell biology*, 3(3):245–252.

[515] Zhou, N., Hu, Z., Wu, C., and Bao, J. (2018). CM-viewer: Visualizing interaction network of co-mutated and mutually exclusively mutated cancer genes. *BioSystems*, 166:37–42.

[516] Zhou, N., Zhang, J., Feng, L., Lu, B., Wang, Z., Sun, R., Wu, C., and Bao, J. (2013). IntApop: A web service for predicting apoptotic protein interactions in humans. *BioSystems*, 114(3):238–244.

[517] Ziello, J. E., Jovin, I. S., and Huang, Y. (2007). Hypoxia-Inducible Factor (HIF)-1 regulatory pathway and its potential for therapeutic intervention in malignancy and ischemia. *Yale Journal of Biology and Medicine*, 80(2):51–60.

[518] Zimmerman, D. W. (2004). A note on preliminary tests of equality of variances. *British Journal of Mathematical and Statistical Psychology*, 57(1):173–181.

[519] Zindy, F., Eischen, C. M., Randle, D. H., Kamijo, T., Cleveland, J. L., Sherr, C. J., and Roussel, M. F. (1998). Myc signaling via the ARF tumor suppressor regulates p53-dependent apoptosis and immortalization. *Genes and Development*, 12:2424–2433.

[520] Zou, Y., Tsai, W.-B., Cheng, C.-J., Hsu, C., Chung, Y. M., Li, P.-C., Lin, S.-H., and Hu, M. C. T. (2008). Forkhead box transcription factor FOXO3a suppresses estrogen-dependent breast cancer cell proliferation and tumorigenesis. *Breast cancer research : BCR*, 10(1):R21.

[521] Zundel, W. and Giaccia, A. (1998). Inhibition of the anti-apoptotic PI(3)K/Akt/Bad pathway by stress. *Genes and Development*, 12(13):1941–1946.

Appendix A

Supplementary Tables and Data

A.1 Number of Drugs which interact with genes in the network

Table A.1 Number of distinct drugs which are known to interact with each node in the network. Drawn from the Drug-Gene Interaction Database [465] accessed using the package rDGIdb [443].

Node	GeneID	Distinct Drug Count
A1	BCL2A1	1
Akt	AKT1	43
ARF	CDKN2A	20
BAD	BAD	2
BAXBAK	BAX	54
BAXBAK	BAK	0
Bcl-2	BCL2	54
Bcl-W	BCL2L2	6
Bcl-xl	BCL2L1	6
Beta-Catenin	CTNNB1	9
BIM	BCL2L11	2
BNIP3	BNIP3	0
Caspase3	CASP3	9
Caspase9	CASP9	3
CDK2	CDK2	142
CDK2	CCNE1	6

Table A.1 continued from previous page

Node	GeneID	Distinct Drug Count
CDK4	CDK4	32
CDK4	CCND1	16
cFos	FOS	17
COX2	PTGS2	95
Dishevelled	DVL1	0
E2F-1	E2F1	18
Elk-1	ELK1	1
EP4	PTGER4	31
ErbB1	EGFR	146
Erk	MAPK1	29
Ets-2	ETS2	2
EZH2	EZH2	7
FoxO	FOXO3	0
Frizzled	FZD1	1
GSK3	GSK3B	35
HIF1	HIF1A	12
LRP	LRP5	0
LRP	LRP6	0
Mad	MXD1	0
Max	MAX	0
Mcl1	MCL1	10
mdm2	MDM2	2
Mek	MAP2K1	38
MOMP	MOMP	0
Myc	MYC	48
Noxa	PMAIP1	1
p15	CDKN2B	1
p16	CDKN2A	20
p21	CDKN1A	24
p27	CDKN1B	13
p38	MAPK14	95
p53	TP53	108

Table A.1 continued from previous page

Node	GeneID	Distinct Drug Count
PEA3	ETV4	1
PGE2	PGE2	0
PHD2	EGLN1	7
PI3K	PIK3CA	149
pRb	RB1	22
PTEN	PTEN	104
PUMA	BBC3	0
Raf-1	RAF1	21
Ras	KRAS	148
Rsk	RPS6KA1	7
TCF	TCF7L1	0
TGFBeta	TGFB1	37
TGFR	TGFBR1	10
TRAP1	TRAP1	1
Twist	TWIST1	0
VEGF	VEGFA	33
VHL	VHL	16

A.1.1 Node Categories

Table A.2 Categories given to nodes so that general patterns can be identified.

Node	Category
A1	Apoptosis
Akt	PI3K-Akt
BAD	Apoptosis
BAXBAK	Apoptosis
Bcl-2	Apoptosis
Bcl-W	Apoptosis
Bcl-xl	Apoptosis
Beta-Catenin	Wnt
BIM	Apoptosis
BNIP3	Apoptosis
Caspase3	Apoptosis
Caspase9	Apoptosis
CDK2	Cycle
CDK4	Cycle
cFos	MAPK
COX2	Hypoxia
Dishevelled	Wnt
E2F-1	Cycle
Elk-1	MAPK
EP4	PI3K-Akt
ErbB1	EGF
ErbB1-ErbB1	EGF
Erk	MAPK
Ets-2	MAPK
EZH2	PI3K-Akt
FoxO	Growth Antagonist
Frizzled	Wnt
GSK3	Growth Antagonist
GSK3-Axin-APC-CK1	Wnt
HIF1	Hypoxia

Table A.2 continued from previous page

Hypoxia	Hypoxia
HypoxiaInitial	Hypoxia
LRP	Wnt
Mad	Myc
Max	Myc
Mcl1	Apoptosis
mdm2	Growth Antagonist
Mek	MAPK
MOMP	Apoptosis
Myc	Myc
Noxa	Apoptosis
p15	Growth Antagonist
p16	Growth Antagonist
ARF	Growth Antagonist
p21	Growth Antagonist
p27	Growth Antagonist
p38	Growth Antagonist
p53	Growth Antagonist
PEA3	Wnt
PGE2	Hypoxia
PHD2	Hypoxia
PI3K	PI3K-Akt
pRb	Cycle
PTEN	Growth Antagonist
PUMA	Apoptosis
Raf-1	MAPK
Ras	EGF
Rsk	MAPK
TCF	Wnt
TGFBeta	Growth Antagonist
TGFR	Growth Antagonist
TRAP1	Myc
Twist	Wnt
VEGF	Hypoxia

Table A.2 continued from previous page

VHL	Hypoxia

A.1.2 Sources for all Nodes and Edges

Table A.3 Table of sources for all nodes and edges in the network.

Group	From	To	Type	Cell Line/Tissue	Evidence
Myc	MycMax	Activatory	Review	Grandori et al. [181]	Review
	MadMax	Inhibitory	Review	Grandori et al. [181]	Review
Max	MycMax	Activatory	Review	Grandori et al. [181]	Review
Max	MadMax	Activatory	Review	Grandori et al. [181]	Review
Mad	MycMax	Inhibitory	Review	Grandori et al. [181]	Review
	MadMax	Activatory	Review	Grandori et al. [181]	Review
MycMax	TRAP1	Activatory	WI38 Fibroblasts	Coller et al. [84]	Microarray Expression Analysis of response to myc
MycMax	ARF	Activatory	MEF	Zindy et al. [519]	Response to retroviral induction of myc measured by Western and Northern blot
MycMax	p21	Inhibitory	WI38 Fibroblasts	Coller et al. [84]	Microarray Expression Analysis of response to myc
MycMax	p21	Inhibitory	SKBR3 breast cancer epithelial	Mitchell and El-Deiry [328]	Response to adenovirus induction of myc measured by Western blot

Table A.3 continued from previous page

MycMax	PTEN	Activatory	IMEC Immortalised Epithelial Mammary Cells	Kaur and Cole [245]	Comparison of normal and myc-null cells for changes in mRNA (measured by RTPCR) and protein (measured by Western blot)
MycMax	p27	Inhibitory	Primary Human Mammary Tissue and Mouse Mammary Cell Lines HC14)	Nass and Dickson [338]	Response to retroviral induction of myc measured by Western
MycMax	p27	Inhibitory	Hs578T breast cancer cells	Yang et al. [495]	Activity of p27 promotor reporter construct in presence or absence of myc vector
MycMax	CDK4	Activatory	Rat1 Fibroblasts	Hermeking et al. [200]	Response to adenovirus induction of myc measured by Western and Northern blot

Table A.3 continued from previous page

CDK4	Proliferation	Activatory	HCA2 Human Fibroblasts	Morris et al. [332]	Overexpression of CDK4 by retrovirus extends lifespan, measured by population doublings over time in cell culture
MycMax	CDK2	Activatory	WI38 Fibroblasts	Coller et al. [84]	Microarray Expression Analysis of response to myc
MycMax	CDK2	Activatory	Primary Human Mammary Tissue and Mouse Mammary Cell Lines HC14)	Nass and Dickson [338]	Response to retroviral induction of myc measured by Western blot
MycMax	BIM	Activatory	MEF	Muthalagu et al. [336]	Response to activation of MycER measured by Northern blot and ChIP-seq
MycMax	BIM	Activatory	BT474, SKBR3 and MCF7	Campone et al. [52]	Response to inhibition of c-myc by siRNA, measured by Western blot

Table A.3 continued from previous page

MycMax	Noxa	Activatory	MDA-MB-231	Nikiforov et al. [344]	ChIP binding of myc to Noxa promotor, and effect of c-myc inhibition by shRNA, measured by Western blot
TRAP1	FoxO	Inhibitory	MCF7	Kim et al. [247]	Response to TRAP1 inhibitor, measured by Western blot
TGFBeta	TGFR	Activatory	Review	Hinck [202]	Review
TGFR	Myc	Inhibitory	MDA-MB-468	Fernandez-Pol et al. [145]	Response of myc mRNA to TGFBeta exposure measured by Northern blot
TGFR	Mad	Activatory (Indirect)	NMuMG mouse mammary epithelial	Siegel et al. [407]	Response to TGFBeta exposure measured by Northern and Western blot and ChIP
TGFR	p15	Activatory	HaCaT	Seoane et al. [399]	Response to TGFBeta exposure measured by Northern blot

Table A.3 continued from previous page

MycMax	p15	Inhibitory	HaCaT	Feng et al. [143]	Physical interactions measured by yeast-two hybrid assay, and response to myc plasmid measured by Western blot
MycMax	p16	Inhibitory	Review	Amati et al. [7]	Review
EGF	ErbB1-ErbB1	Activatory	Review	Yarden and Sliwkowski [496]	Review
ErbB1-ErbB1		Expression in breast	MCF10A	Dong et al. [116]	ErbB1-ErbB1 detected by Western blot.
EGF	ErbB1-ErbB2	Activatory	T47D	Klapper et al. [251]	Immunoblot to determine phosphorylation of receptor in different conditions
EGF	ErbB2-ErbB3	Activatory	SKBR3, MDA-MB-361, BT474	Holbro et al. [206]	Immunoblot to determine phosphorylation of receptor in different conditions
ErbB1	ErbB1-ErbB1	Activatory	Review	Yarden and Sliwkowski [496]	Review

Table A.3 continued from previous page

ErbB1	ErbB1-ErbB1	Activatory	A431 Human Squamous Carcinoma	Low-Nam et al. [295]	Two-color quantum dot tracking to visualise dimerisation in response to ligands
ErbB1	ErbB1-ErbB2	Activatory	Review	Yarden and Sliwkowski [496]	Review
ErbB1	ErbB1-ErbB2	Activatory	T47D	Klapper et al. [251]	Immunoblot to determine phosphorylation of receptor in different conditions
ErbB2	ErbB1-ErbB2	Activatory	Review	Yarden and Sliwkowski [496]	Review
ErbB2	ErbB1-ErbB2	Activatory	T47D	Klapper et al. [251]	Immunoblot to determine phosphorylation of receptor in different conditions
ErbB2	ErbB2-ErbB3	Activatory	Review	Yarden and Sliwkowski [496]	Review

Table A.3 continued from previous page

ErbB2	ErbB2-ErbB3	Activatory	T47D	Klapper et al. [251]	Immunoblot to determine phosphorylation of receptor in different conditions
ErbB3	ErbB2-ErbB3	Activatory	Review	Yarden and Sliwkowski [496]	Review
ErbB3	ErbB2-ErbB3	Activatory	T47D	Klapper et al. [251]	Immunoblot to determine phosphorylation of receptor in different conditions
ErbB1-ErbB1	Ras	Activatory	HeLa	Schulze et al. [393]*	Co-immunoprecipitation to assay protein-protein interaction
ErbB1-ErbB2	Ras	Activatory	HeLa	Schulze et al. [393]	Co-immunoprecipitation to assay protein-protein interaction

Table A.3 continued from previous page

ErbB2-ErbB3	PI3K	Activatory	SKBR3, MDA-MB-361, BT474	Holbro et al. [206]	Immunoblot to determine phosphorylation of receptor in different conditions
Ras	Raf-1	Activatory	3T3 Fibroblasts	Jelinek et al. [227]*	Binding assays carried out on cell lysates
		Activatory	Primary Breast Tissue	McGlynn et al. [320]	Immunohistochemistry for Ras, Raf-1 and MAPK pathway expression.
Raf-1	Mek	Activatory	3T3 Fibroblasts	Jelinek et al. [227]*	Binding assays carried out on cell lysates
		Activatory	Primary Breast Tissue	McGlynn et al. [320]	Immunohistochemistry for Ras, Raf-1 and MAPK pathway expression.
		Activatory	3T3 Fibroblasts	Kyriakis et al. [270]*	Effect on Mek from Raf-1 transfection, measured by chromatography
Mek	Erk	Activatory	Review	Cobb [83]*	Review

Table A.3 continued from previous page

		Activatory	Primary Breast Tissue	McGlynn et al. [320]	Immunohistochemistry for Ras, Raf-1 and MAPK pathway expression.
Erk	Elk-1	Activatory	3T3 Fibroblasts	Aplin et al. [12]	Response to constitutively active Mek measured by immunoprecipitation of anti-Elk1 antibody
Elk-1	cFos	Activatory	3T3 Fibroblasts	Hill and Treisman [201]*	Response of transfected cFos promotor to growth factor induced signals detected by mRNA immunoblot
cFos	Myc	Activatory (Indirect)	MCF7	Lu et al. [297]	Effect of inhibition of cFos with dominant negative mutant measured by Western blot

Table A.3 continued from previous page

Erk	Myc	Activatory	REF52 Fibroblasts	Sears et al. [396]*	Stability of myc under different Ras-pathway dependent phosphorylations measured by immunoprecipitation of myc over time.
Erk	Rsk	Activatory	MCF10A Breast	Doehn et al. [115]	Effect of inhibition of cFos with dominant negative mutant measured by Western blot
Rsk	GSK3	Inhibitory	3T3 Fibroblasts	Eldar-Finkelman et al. [129]	Phosphorylation of GSK3 in presence or absence of Rsk determined by immunoprecipitation
Rsk	GSK3	Inhibitory	Primary Human Colon Carcinoma	Ding et al. [114]	Effect of dominant negative Erk on phosphorylation of GSK3 determined by immunoprecipitation

Table A.3 continued from previous page

Rsk	BAD	Inhibitory	Primary mouse mammary epithelial cells	Gilmore et al. [175]	Effect of Rsk on BAD phosphorylation determined by immunoprecipitation
Ets-2	p16	Activatory	TIG3, Hs68 Human Fibroblasts	Ohtani et al. [346]	ChIP of interaction between Ets-2 and p16
Erk	Ets-2	Activatory	SKBR3	Al-azawi et al. [4]	ChIP to measure interactions in presence or absence of EGF
Ets-2	Myc	Activatory	SKBR3	Al-azawi et al. [4]	ChIP to measure interactions in presence or absence of EGF
Mek	p38	Activatory	Primary Human Breast Tissue	Esteva et al. [134]	Analysis of coexpression in breast cancer samples
Ras	p38	Activatory (indirect)	MDA-MB-231	Kwon et al. [269]	Response to lapatinib, measured by Western blot
Ras	p38	Activatory (indirect)	MCF10A	Kim et al. [248]	Response to Ras as measured by immunoblot, and effect of p38 inhibition on Ras effects

Table A.3 continued from previous page

p38	VEGF	Activatory	MCF7, SKBR3	Xiong et al. [490]	Western and Northern blot analysis of VEGF, and requirement of p38 for its activation by HRG-β1
Erk	FoxO	Inhibitory	MCF7	Yang et al. [493]	Immunoblot of FoxO in response to Erk activation by consitutively active Mek
Erk	BIM	Inhibitory	MCF10A	Collins et al. [85]	Immunoblot for BIM with and without Erk inhibition during G1/S arrest
Erk	CDK4	Activatory	Review	Whitmarsh and Davis [479]	Review
Erk	CDK4	Activatory	3T3 Fibroblasts	Cheng et al. [69]	Immunoblot following Erk activation by consitutively active Mek

Table A.3 continued from previous page

Erk	CDK4	Activatory	Human Lung Fibroblast	Shen et al. [404]	Blocking Erk prevented activation of CDK4CyclinD by silica exposure, as measured by immunoblot.
Ras	PI3K	Activatory	COS-7	Pacold et al. [351]*	In vitro and in vivo interaction assay and crystal structure of Ras-PI3K complex
PI3K	Akt	Activatory	Review	Franke et al. [157]*	Review
Akt	HIF1	Activatory	MDA-MB-468	Blancher et al. [40]	Western blot analysis with and without kinase inhibitors
Akt	p21	Inhibitory	MDA-MB-453	Zhou et al. [514]	p21 phosphorylation determined with Western blot with and without PI3K inhibitor LY294002
Akt	GSK3	Inhibitory	MCF7	Knuefermann et al. [254]*	Western blot analysis following transfection of consitutively active Akt

Table A.3 continued from previous page

Akt	BAD	Inhibitory	MCF7	Knuefermann et al. [254]	Western blot analysis following transfection of consitutively active Akt
Akt	EZH2	Inhibitory	IMEC Immortalised Epithelial Mammary Cells	Kaur and Cole [245]	Phosphorylation of EZH2 measured by immunoblot following Akt inhibition
Akt	Apoptosis	Inhibitory	Rat1 Fibroblasts	Zundel and Giaccia [521]	Effect on apoptosis by Akt inhibitor ceremide
Akt	Caspase9	Inhibitory	293T HEK	Cardone [56]	Phosphorylation of Caspase9 in response to Akt transfection, measured by immunoprecipitation.
Akt	Caspase9	Inhibitory	MCF7	Li et al. [290]	Resveratol leads to Akt phosphorylation, followed by Caspase 9 phosphorylation

Table A.3 continued from previous page

Akt	FoxO	Inhibitory	MCF7	Sunters et al. [428]	Translocation of FoxO3a measured with confocal microscopy, and is dependent on Akt signalling.
EZH2	BIM	Inhibitory	MCF7	Wu et al. [488]	Bim response to activation and inhibition of EZH2 measured by immunoblot and RT-PCR
EZH2	Myc	Inhibitory	IMEC Immortalised Epithelial Mammary Cells	Kaur and Cole [245]	Response of Myc to EZH2 inhibition by siRNA measured by RT-PCR
PTEN	Akt	Inhibitory	IMEC Immortalised Epithelial Mammary Cells	Kaur and Cole [245]	Comparison of normal and myc-null cells for changes in protein (measured by Western blot)

Table A.3 continued from previous page

EZH2	BIM	Inhibitory	MCF7	Wu et al. [488]	Bim response to activation and inhibition of EZH2 measured by immunoblot and RT-PCR
FoxO	BIM	Activatory	MCF7, MDA-MB-231	Sunters et al. [427]	Immunoblot of FoxO and BIM in response to paclitaxel, and BIM response is dependent on FoxO activity
FoxO	CDK4CylindD	Inhibitory	MEF	Schmidt et al. [392]*	Response to retrovirally induced FoxO measured by Western blot.
FoxO	p21	Activatory	MCF7	Zou et al. [520]	Comparison of expression in FoxO and FoxO-null cells, measured by immunoblot.
FoxO	p27	Activatory	Ba/F3 Murine pre-B-cell	Dijkers et al. [112]	Immunoblot of p27 in with and without FoxO inhibition.

Table A.3 continued from previous page

FoxO	p27	Activatory	MCF7, MDA-MB-231	Sunters et al. [427]	Immunoblot of FoxO and p27 in response to paclitaxel, and BIM response is dependent on FoxO activity
GSK3	MycMax	Inhibitory	MCF7	Rodrik et al. [375], Yeh et al. [498]*	Western blot of myc phosphorylation under modulation of GSK3 activity by different inhibitors
mdm2	p53	Inhibitory	HCA2 Fibroblasts	Blaydes and Wynford-Thomas [41]	Response of p53 reporter in response to anti-mdm2 antibody
ARF	mdm2	Inhibitory	MEF	Weber et al. [472]	Change in mdm2 localisation in response to Arf measured by immunofluorescence
p53	PUMA	Activatory	MCF7	Nakano and Vousden [337]	Northern blot in p53-inducible cells

Table A.3 continued from previous page

p53	PUMA	Activatory	MEF	Villunger et al. [456]	Comparison of loss of PUMA and Noxa in ameliorating p53-induced apoptosis due to radiation
p53	Noxa	Activatory	MEF	Villunger et al. [456]	Comparison of loss of PUMA and Noxa in ameliorating p53-induced apoptosis due to radiation
p53	p21	Activatory	HCT116 Human Colorectal	Bunz et al. [48]	Immunoblot following p53 activation by radiation
p53	PTEN	Activatory	SAOS-2 Osteosarcoma	Stambolic et al. [418]	Measurement of mRNA and protein by immunoblot following p53 activation by radiation
p53	HIF1	Inhibitory	MCF7 Breast Cancer	Blagosklonny et al. [38]	Comparison of expression of HIF1 reporter constructs in presence or absence of transfected p53

Table A.3 continued from previous page

mdm2	FoxO	Inhibitory	MCF7 Breast Cancer	Yang et al. [493]	Immunoblot of FoxO in response in mdm2 normal and mdm2 null cells, in response to Erk
p53	PTEN	Activatory	MEF	Stambolic et al. [418]	Measurement of mRNA and protein by immunoblot following p53 activation by radiation
Wnt1	Frizzled	Activatory	Mammary (Review)	Boras-Granic and Wysolmerski [43]	Review
			Mammary (Review)	Smalley and Dale [411]	Review
			Drosophila, Human Embryonic Kidney (HEK293)	Bhanot et al. [34]	Immunostaining of Wnt1 binding to Frizzled, transfected into HEK293 cells
Wnt1	LRP	Activatory	Mammary HC11 Cells	Goel et al. [178]	Comparison of response to Wnt by normal and lrp-null cells by TOP-FLASH assay

Table A.3 continued from previous page

			Human Embryonic Kidney (HEK293)	Tamai et al. [436]	Stimulation of cells with Wnt1 induced phosphorylation of LRP as measured by immunoblot.
Frizzled	Dishevelled	Activatory	Mammary (Review)	Boras-Granic and Wysolmerski [43]	Review
			Mammary (Review)	Smalley and Dale [411]	Review
			HeLa	Bilic et al. [36]	Dishevelled is required for LRP phosphorylation and aggregation, which works with Frizzled, as measured by immunoblot and real-time confocal microscopy.
LRP	Dishevelled	Activatory	Mammary (Review)	Boras-Granic and Wysolmerski [43]	Review
			Mammary (Review)	Smalley and Dale [411]	Review

Table A.3 continued from previous page

			HeLa	Bilic et al. [36]	Dishevelled is required for LRP phosphorylation and aggregation, which works with Frizzled, as measured by immunoblot and real-time confocal microscopy.
Dishevelled	GSK3-Axin-APC-CK1	Inhibitory	Mammary (Review)	Boras-Granic and Wysolmerski [43]	Review
			Mammary (Review)	Smalley and Dale [411]	Review
			Review	MacDonald and He [304]	Review
Dishevelled	GSK3		Review	MacDonald and He [304]	Review
			Human Fibroblast 3T3 cells	Taelman et al. [432]	GSK3 translocation in response to Wnt measured by cryo-electron microscopy

Table A.3 continued from previous page

GSK3-Axin-APC-CK1	Beta-Catenin	Inhibitory	C57MG mouse mammary epithelial	Farago et al. [140]	Response to GSK3 transfection, measured by immunoblot
Beta-Catenin	TCF	Activatory	Mammary (Review)	Boras-Granic and Wysolmerski [43]	Review
			Mammary (Review)	Smalley and Dale [411]	Review
			Xenopus	Behrens et al. [25]	Beta-Catenin LEF complexes detected by co-immunoprecipitation
			HT29 Colon Cancer	Korinek et al. [259]	TOPFLASH assay for Beta-Catenin TCF interaction
TCF	Myc		HT29 Colon Cancer	He et al. [196]	Northern blot of myc following TCF induction by APC in APC-inducible cell line
			Mouse Mammary	Teuliere et al. [439]	RT-PCR of myc in mice with consitutively active beta-catenin

Table A.3 continued from previous page

TCF	CDK4	Activatory	MCF7	Lin et al. [292]	Response to Beta-catenin plasmid, measured by Western blot
Wnt1	p27	Inhibitory (Indirect)	Neuronal cells	Castelo-Branco et al. [61]	Effect of Wnt1 on p27 mRNA measured by RT-PCR
Wnt1	p27	Inhibitory (Indirect)	3T3 Fibroblasts	Rimerman et al. [373]	Immunoblot of p27 in Wnt and Mek overexpressing cells
TCF	PEA3	Activatory	Mouse Mammary Epithelial	Howe et al. [214]	Immunoblot of PEA3 expression in Wnt1 overexpressing cells
TCF	Twist	Activatory	HC11, C57MG mouse mammary and *in vivo*	Howe et al. [215]	Immunoblot of Twist expression in Wnt1 overexpressing cells
Wnt1	Twist	Activatory (Indirect)	Human Primary Breast Cancer samples	Watanabe et al. [469]	Twist expression correlated with Wnt expression, as measured by RT-PCR
Twist	p53	Inhibitory (Indirect)	MCF7	Stasinopoulos et al. [419]	Twist expressing cells have compromised p53 response to radiation

Table A.3 continued from previous page

Twist	p53	Inhibitory	HNE1-T3 and HNE1 nasopharangeal cancer	Wang et al. [467]	Expression of Twist increases mdm2 expression, measured by RT-PCR
Twist	Apoptosis	Inhibitory	HNE1-T3 and HNE1 nasopharangeal cancer	Wang et al. [467]	Ectopic Twist leads to resistance to paclitaxel and vincristine
Twist	ARF	Inhibitory	Review (Neuroblastoma)	Puisieux et al. [367]	Review
Twist	Apoptosis	Inhibitory	Human breast cancer (unpublished data)	Puisieux et al. [367]	Review
Twist	ARF	Inhibitory	MEFs	Maestro et al. [308]	Immunoblot shows lower ARF in cells ectopically expressing Twist

Table A.3 continued from previous page

p21	CDK4	Inhibitory	MCF7	He et al. [195]	Immunoprecipitated crude cell lysates, after activation of p53-p21 pathway by DNA-damaging agent, with anti-Cdk4 or anti-cyclin D antibodies for the Cdk4 complex and with anti-Cdk2 or anti-cyclin E antibodies for the Cdk2 complex and immunoblotted the precipitated proteins with anti-p21 antibodies.

Table A.3 continued from previous page

p21	CDK2	Inhibitory	MCF7	He et al. [195]	Immunoprecipitated crude cell lysates, after activation of p53-p21 pathway by DNA-damaging agent, with anti-Cdk4 or anti-cyclin D antibodies for the Cdk4 complex and with anti-Cdk2 or anti-cyclin E antibodies for the Cdk2 complex and immunoblotted the precipitated proteins with anti-p21 antibodies.
p27	CDK4	Inhibitory	Mv1Lu Lung Epithelial	Ray et al. [371]	Immunoprecipitation of p27 binding to cdks and immunoblot of phosphorylation

Table A.3 continued from previous page

p27	CDK2	Inhibitory	BT-474 Cells	Lane et al. [274]	Expression and association of p27 with cdk2 measured after treatment with anti-HER2 monoclonal antibody.
p16	CDK4	Inhibitory	BALB/c mice	Lukas et al. [300]	In vitro association assay of p16 and CDK4CyclinD binding
p15	CDK4	Inhibitory	Human Mammary Epithelial Cell (HMEC)	Sandhu et al. [389]	Immunoprecipitation assay of p15 CDK4CyclinD binding
GSK3	CDK4	Inhibitory	Cell Free, 3T3 Fibroblasts	Diehl et al. [111]	Phosphorylation of CDK4CyclinD by GSK3 in vitro measured by autoradiography.
GSK3	CDK2	Inhibitory	Cell Free, Rat Fibroblasts	Welcker et al. [476]	Tryptic phosphopeptide maps show effects of GSK3
CDK2	pRb	Inhibitory	Review	Draetta [118]	Review
CDK4	pRb	Inhibitory	Review	Weinberg [474]	Review
pRb	E2F-1	Inhibitory	Review	Weinberg [474]	Review

Table A.3 continued from previous page

E2F-1	ARF	Activatory	SAOS-2 Osteosarcoma	Bates et al. [21]	Western blot of ARF in cells with inducible E2F-1
E2F-1	Proliferation	Activatory	REF52 Rat	Johnson et al. [229]	Proliferation measured by BrdU incorporation in response to E2F1 plasmid
E2F-1	EZH2	Activatory	MCF7	Wu et al. [488]	Western blot of EZH2 in responset to E2F1 activation using cells transformed by oncogene E1A
PUMA	Bcl-2	Inhibitory	DLD1, SW48, HCT116 Colorectal	Yu et al. [501]	PUMA Bcl-2 binding assessed with immunoprecipitation
PUMA	Bcl-2	Inhibitory	SAOS-2 Osteosarcoma	Nakano and Vousden [337]	PUMA Bcl-2 binding assessed with immunoprecipitation

Table A.3 continued from previous page

PUMA	Bcl-2	Inhibitory	All (cell free) and MEFs	Chen et al. [66]	Affinity and competition assays on recombinant proteins, and targets of proteins in mammalian cells assessed with co-immunoprecipitation.
PUMA	Bcl-xl	Inhibitory	All (cell free) and MEFs	Chen et al. [66]	Affinity and competition assays on recombinant proteins, and targets of proteins in mammalian cells assessed with co-immunoprecipitation.
PUMA	Mcl1	Inhibitory	All (cell free) and MEFs	Chen et al. [66]	Affinity and competition assays on recombinant proteins, and targets of proteins in mammalian cells assessed with co-immunoprecipitation.

Table A.3 continued from previous page

PUMA	Bcl-W	Inhibitory	All (cell free) and MEFs	Chen et al. [66]	Affinity and competition assays on recombinant proteins, and targets of proteins in mammalian cells assessed with co-immunoprecipitation.
PUMA	A1	Inhibitory	All (cell free) and MEFs	Chen et al. [66]	Affinity and competition assays on recombinant proteins, and targets of proteins in mammalian cells assessed with co-immunoprecipitation.
BIM	Bcl-2	Inhibitory	All (cell free) and MEFs	Chen et al. [66]	Affinity and competition assays on recombinant proteins, and targets of proteins in mammalian cells assessed with co-immunoprecipitation.

Table A.3 continued from previous page

BIM	Bcl-xl	Inhibitory	All (cell free) and MEFs	Chen et al. [66]	Affinity and competition assays on recombinant proteins, and targets of proteins in mammalian cells assessed with co-immunoprecipitation.
BIM	Mcl1	Inhibitory	All (cell free) and MEFs	Chen et al. [66]	Affinity and competition assays on recombinant proteins, and targets of proteins in mammalian cells assessed with co-immunoprecipitation.
BIM	Bcl-W	Inhibitory	All (cell free) and MEFs	Chen et al. [66]	Affinity and competition assays on recombinant proteins, and targets of proteins in mammalian cells assessed with co-immunoprecipitation.

Table A.3 continued from previous page

BIM	A1	Inhibitory	All (cell free) and MEFs	Chen et al. [66]	Affinity and competition assays on recombinant proteins, and targets of proteins in mammalian cells assessed with co-immunoprecipitation.
BAD	Bcl-2	Inhibitory	All (cell free) and MEFs	Chen et al. [66]	Affinity and competition assays on recombinant proteins, and targets of proteins in mammalian cells assessed with co-immunoprecipitation.
BAD	Bcl-xl	Inhibitory	All (cell free) and MEFs	Chen et al. [66]	Affinity and competition assays on recombinant proteins, and targets of proteins in mammalian cells assessed with co-immunoprecipitation.

Table A.3 continued from previous page

BAD	Bcl-W	Inhibitory	All (cell free) and MEFs	Chen et al. [66]	Affinity and competition assays on recombinant proteins, and targets of proteins in mammalian cells assessed with co-immunoprecipitation.
Noxa	Mcl1	Inhibitory	All (cell free) and MEFs	Chen et al. [66]	Affinity and competition assays on recombinant proteins, and targets of proteins in mammalian cells assessed with co-immunoprecipitation.
Noxa	A1	Inhibitory	All (cell free) and MEFs	Chen et al. [66]	Affinity and competition assays on recombinant proteins, and targets of proteins in mammalian cells assessed with co-immunoprecipitation.

Table A.3 continued from previous page

Bcl-2	BAXBAK	Inhibitory	All (Co-IP)	Oltvai et al. [347]	Bcl-2 BAX binding assessed with immunoprecipitation
Bcl-xl	BAXBAK	Inhibitory	Cell free	Billen et al. [37]	Mitochondria from mice were incubated with Bcl-xl to assess effect on membrane permealization. Bcl-xl BAX binding assessed by co-immunoprecipitation.
Mcl1	BAXBAK	Inhibitory	MEF, HeLa	Germain et al. [171]	Cytochrome c release measured in cells transfected with Mcl1 and BAX. Bcl-xl BAX binding assessed by co-immunoprecipitation.
Bcl-W	BAXBAK	Inhibitory	Mouse Myeloid Cells	Gibson et al. [174]	Enforced expression of bcl-w protected cells against cytotoxic conditions

Table A.3 continued from previous page

Bcl-W	BAXBAK	Inhibitory	Mouse Sertolli	Ross et al. [378]	Bcl-W deficient cells undergo increased apoptosis, measured by counting cells overtime by histology. BAX-null cells are protected.
A1	BAXBAK	Inhibitory	Review	Vogler [460]	Review
A1	BAXBAK	Inhibitory	Co-IP, GST assay	Zhai et al. [507]	GST pulldown assay of A1 (Bfl1) binding BAX
			Expressed in human breast	Beverly and Varmus [32]	Western blot of tumours from mice, and qPCR of human tissue samples
			Expressed in human breast	Campone et al. [51]	Measured expression in tissue samples using microarray
A1	Apoptosis	Inhibitory (Indirect)	Mouse breast	Capuco et al. [54]	In mice with reduced mammary involution, and thus death, A1 (Bfl1) was elevated as measured by RNase protection assay

Table A.3 continued from previous page

BAXBAK	MOMP	Activatory	MEF	Wei et al. [473]	BAX knockout protects against intrinsic cell death signals, measured by enzyme-linked immunosorbent assay of apoptotic DNA fragmentation, and quatification of Caspase3 activity.
BAXBAK	MOMP	Activatory	MEF	Dewson et al. [109]	BAK mutants protect against apoptosis, assayed by measuring nonviable cells by flow cytometry following exposure to propidium iodide.
MOMP	Apoptosis	Activatory	Review	Tait and Green [433]	Review
Caspase9	Caspase3	Activatory	Review	Tait and Green [433]	Review
Caspase3	Apoptosis	Activatory	Review	Tait and Green [433]	Review
HypoxiaInitial	Hypoxia			Used to fix external pressures on the cell	NA

Table A.3 continued from previous page

Hypoxia	FoxO	Inhibitory	MCF7	Kim et al. [247]	TRAP1 mutation induces resistance to oxidative stress, measured by in vivo reactive oxygen species, mediated by FoxO
Hypoxia	PHD2	Inhibitory	CAL51 breast epithelial	Berra et al. [30]	Silencing of PHD2 by siRNA upregulates HIF1 in normoxia, measured by Western blot
PHD2	HIF1	Inhibitory	CAL51 breast epithelial	Berra et al. [30]	Silencing of PHD2 by siRNA upregulates HIF1 in normoxia, measured by Western blot
VHL	HIF1	Inhibitory	BT474 Mammary Epithelial human	Kong et al. [258]	miR-155 induction and repression induces and represses angiogenesis, dependent on VHL expression
HIF1	BNIP3	Activatory	Review	Greijer and van der Wall [185]	Review

Table A.3 continued from previous page

HIF1	BNIP3	Activatory	MCF7	Sowter et al. [416]	BNIP3 induced by hypoxia, dependent on HIF1, measured by Western blot
BNIP3	Apoptosis (Indirect)	Activatory	MCF7	Sowter et al. [416]	BNIP3 induced by hypoxia, dependent on HIF1, measured by Western blot
BNIP3	BAXBAK	Activatory	Review	Mellor and Harris [323]	Review
HIF1	p53	Activatory (Indirect)	MCF7	An et al. [8]	HIF1 potentiates p53 dependent PG13-luciferase activity, and co-immunoprecipitates with p53
HIF1	mdm2	Inhibitory	MEF	Chen et al. [64]	GST pulldown assay for HIF1 and mdm2 interaction and protection of p53 from mdm2 mediated degradation by HIF1 measured by Western blot

Table A.3 continued from previous page

HIF1	p21	Activatory	HCT116 cells	Koshiji et al. [261]	HIF1 increases expression of p21 in normoxia, as measured by Northern blot, and induces cell cycle arrest as measured by BrdU incorporation.
HIF1	p21	Activatory	MEF	Mack et al. [305]	Comparison of p21 expression in VHL normal and VHL null cells by immunoblot.
HIF1	p21	Activatory	MCF7, MDA-MB-231	Fanale et al. [139]	Gene expression by microarray showed p21 upregulated in hypoxia in breast cancer cell lines
HIF1	p27	Activatory	MEF	Mack et al. [305]	Comparison of p27 expression in VHL normal and VHL null cells by immunoblot

Table A.3 continued from previous page

HIF1	VEGF	Activatory	MCF7	Laughner et al. [277]	HIF1 expression correlates with VEGF expression, as measured by immunoblot
PEA3	COX2	Activatory	Mouse Mammary Epithelial	Howe et al. [214]	Transfection of PEA3 increased expression of COX2 as measured by Northern blot
COX2	Akt	Activatory (Indirect)	MCF-7, SKBR3	Majumder et al. [311]	Comparison of Western blot for Akt in COX2 normal and overexpressing cell lines
COX2	PGE2	Activatory	Mouse Mammary Epithelial	Kundu et al. [266]	COX2 and PGE2 expression correlate in samples, and inhibition of COX2 inhibits PGE2

Table A.3 continued from previous page

PGE2	EP4	Activatory	C3L5 Mouse Mammary	Timoshenko et al. [444]	EP receptor antagonists decrease PGE2 dependent iNOS production, while agonists increase, as measured by Nitrate/Nitrite Colorimetric Assay Kit
EP4	PI3K	Activatory	Review (breast)	Reader et al. [372]	Review
COX2	VEGF	Activatory	MCF7	Yang and Han [494]	RNAi silencing of COX2 inhibits VEGF production, as measured by Western blotting
VEGF	Angiogenesis	Activatory	Review	Hoeben et al. [205]	Review

A.1.3 Full Attractors for COX2 and Mek inhibition in Heterogeneous Myc-Low

Table A.4 Proliferation for all attractors with Mek inhibition for heterogeneous myc-low. Each column shows the level of proliferation over a loop stable state. The network stabilises into one of these loops based on changes in the initial conditions not set explicitly according to Table 3.11.

Attractor	A	B	C	D	E
	1	0	1	0	1
	0	0	1	0	1
	0				
	1				
	1				
Proliferation	1				
	1				
	0				
	0				
	0				
	0				
Mean (3sf)	0.455	0	1	0	1
Overall Mean (3sf)	0.491				

Table A.5 Apoptosis for all attractors with Mek inhibition for heterogeneous myc-low. Each column shows the level of apoptosis over a loop stable state. The network stabilises into one of these loops based on changes in the initial conditions not set explicitly according to Table 3.11.

Attractor	A	B	C	D	E
	3	3	2	4	3
	4	2	3	3	4
	2				
	2				
	3				
Apoptosis	1				
	0				
	1				
	0				
	0				
	4				
Mean (3sf)	1.82	2.5	2.5	3.5	3.5
Overall Mean (3sf)	2.76				

Table A.6 Proliferation for all attractors with COX2 inhibition for heterogeneous myc-low. Each column shows the level of proliferation over a loop stable state. The network stabilises into one of these loops based on changes in the initial conditions not set explicitly according to Table 3.11.

Attractor	A	B	C	D	E	F	G	H	I	J	K	L	M
	4	3	3	3	4	3	4	3	3	4	3	4	3
	4	2	2	2	3	2	3	2	2	3	2	3	2
	4												
	3												
	2												
Proliferation	3												
	4												
	2												
	1												
	1												
	1												
Mean (3sf)	2.64	2.5	2.5	2.5	3.5	2.5	3.5	2.5	2.5	3.5	2.5	3.5	2.5
Overall Mean (3sf)	2.82												

Table A.7 Apoptosis for all attractors with COX2 inhibition for heterogeneous myc-low. Each column shows the level of apoptosis over a loop stable state. The network stabilises into one of these loops based on changes in the initial conditions not set explicitly according to Table 3.11.

Attractor	A	B	C	D	E	F	G	H	I	J	K	L	M
	4	3	2	3	3	2	2	2	3	3	2	2	3
	5	4	3	4	4	3	3	3	4	4	3	3	4
	5												
	4												
	3												
Apoptosis	2												
	3												
	1												
	0												
	1												
	2												
Mean (3sf)	2.73	3.5	2.5	3.5	3.5	2.5	2.5	2.5	3.5	3.5	2.5	2.5	3.5
Overall Mean (3sf)	2.98												

Appendix B

Supplementary Figures

B.1 Monotherapy Unfiltered Heat maps

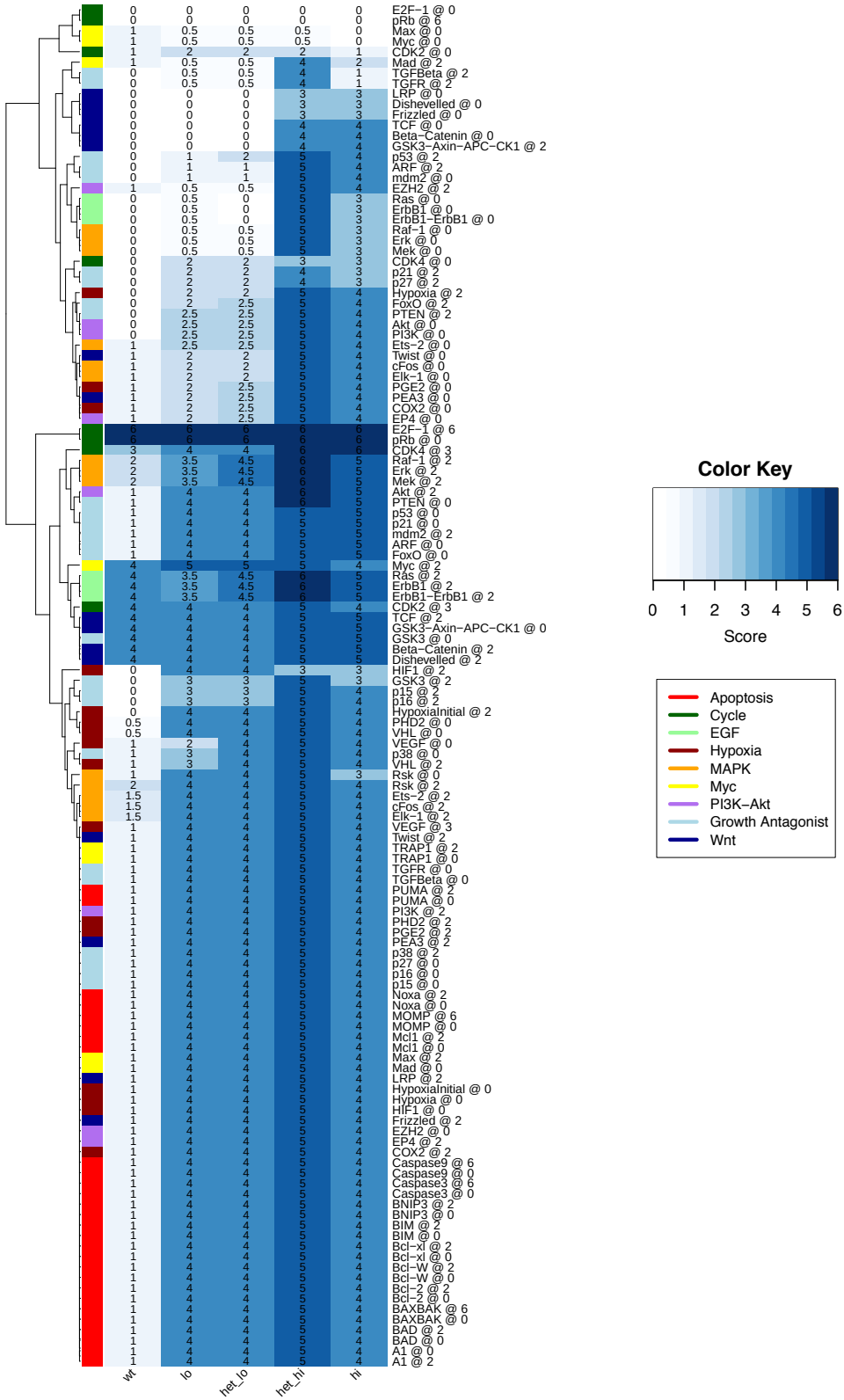

Fig. B.1 Heat map showing the mean value of proliferation under all possible perturbations, for the different possible sub-clones and the healthy cell (wt), shown as columns. Darker blue indicates higher proliferation, with colours on the left giving an indication of the pathways for the nodes perturbed. Results are clustered by Euclidean hierarchical clustering, as shown by the dendrogram on the left.

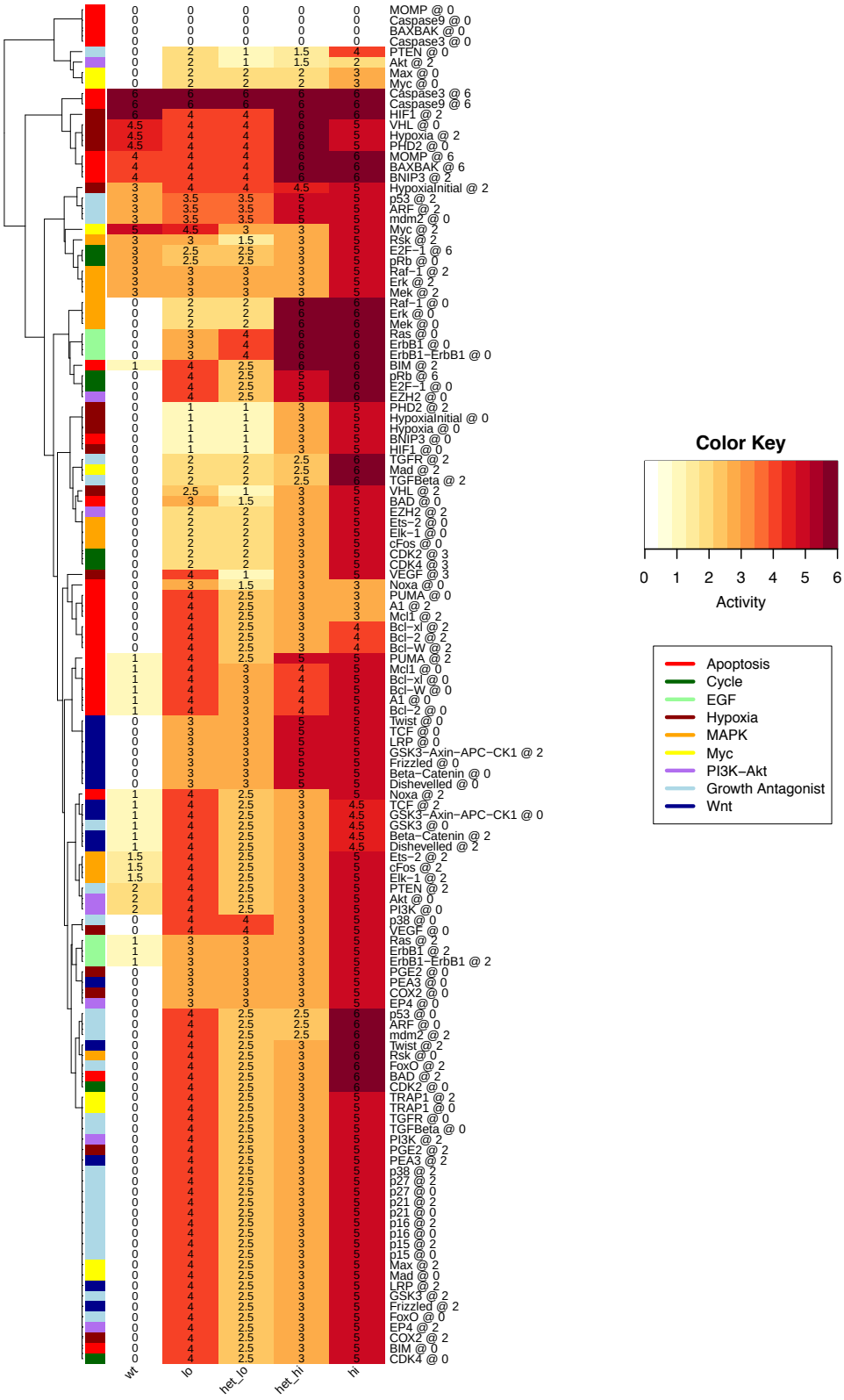

Fig. B.2 Heat map showing the mean value of apoptosis under all possible perturbations, for the different possible sub-clones and the healthy cell (wt), shown as columns. Darker red indicates higher apoptosis, with colours on the left giving an indication of the pathways for the nodes perturbed. Results are clustered by Euclidean hierarchical clustering, as shown by the dendrogram on the left.

B.2 Monotherapy Range Restriction Heat maps

B.3 Combination Therapy Unfiltered Heat Maps

Heat maps showing the effect of all possible pairwise combinations of node activations or inactivations. Black cells indicate combinations which are nonsensical such as an activation combined with an inactivation of the same node.

B.3.1 Cytostatic

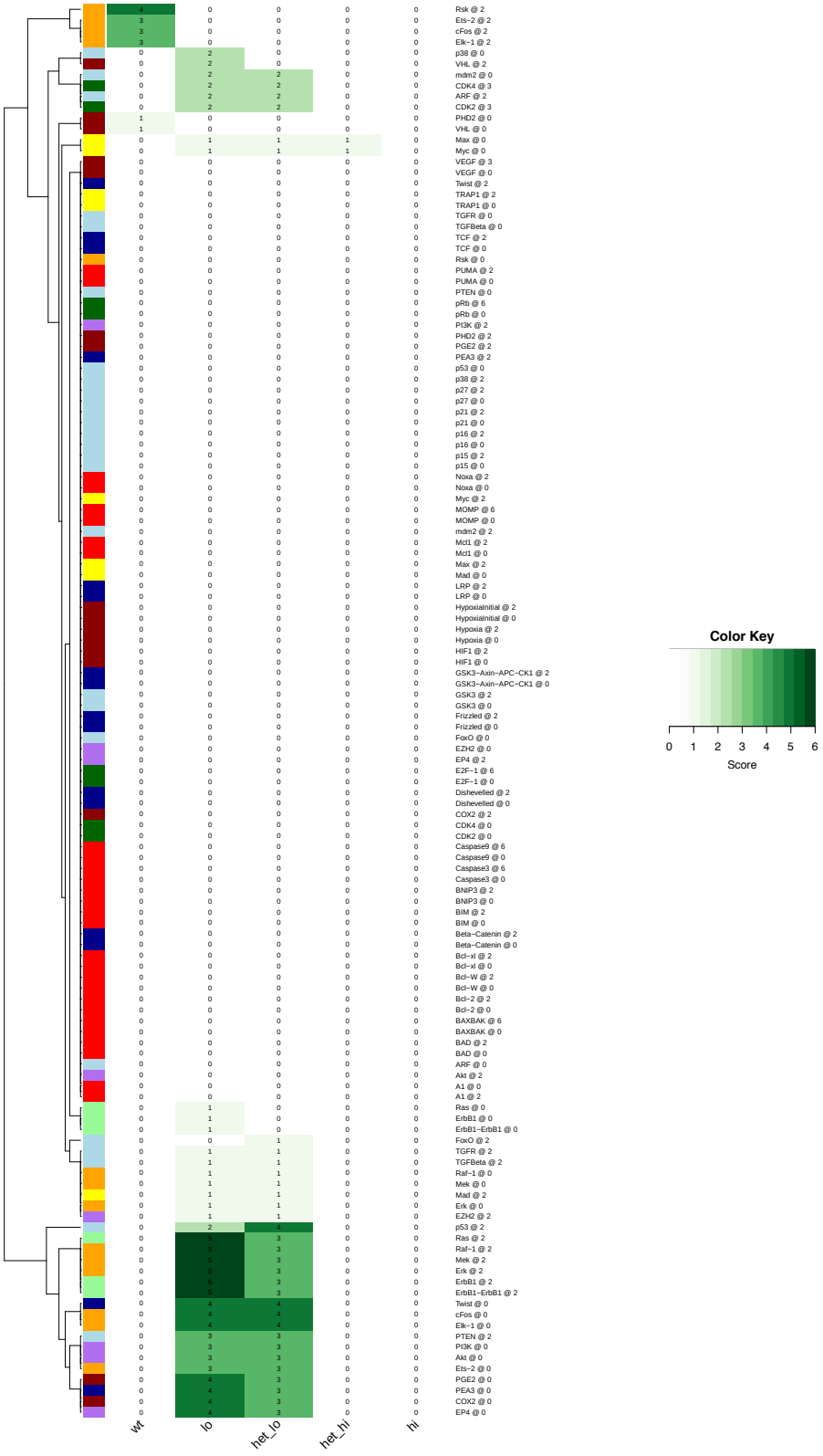

Fig. B.3 Heat map showing the range to which the proliferation node has been restricted by the VMCAI algorithm. Non-zero cases indicate bifurcation or oscillation within that range.

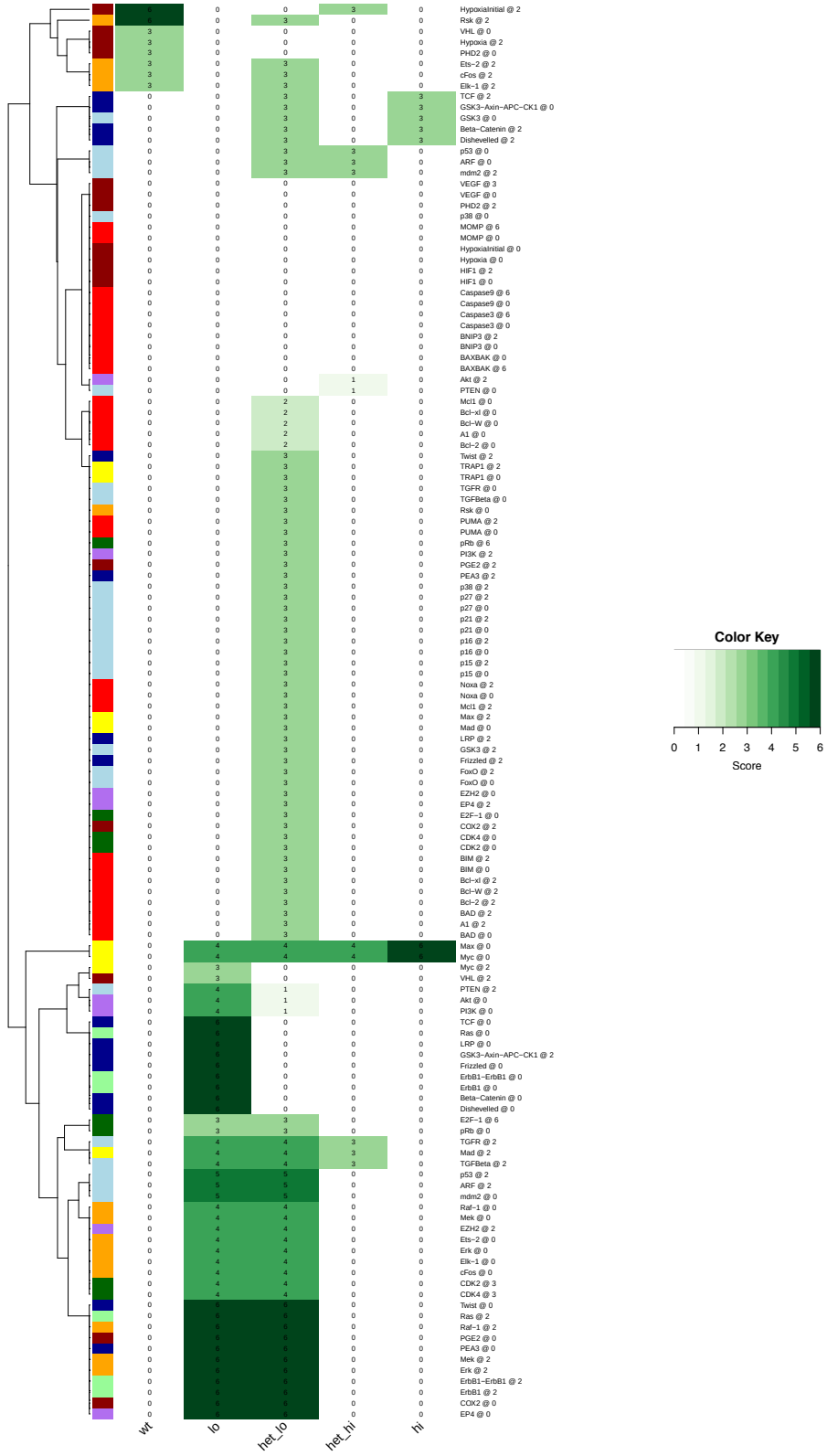

Fig. B.4 Heat map showing the range to which the apoptosis node has been restricted by the VMCAI algorithm. Non-zero cases indicate bifurcation or oscillation within that range.

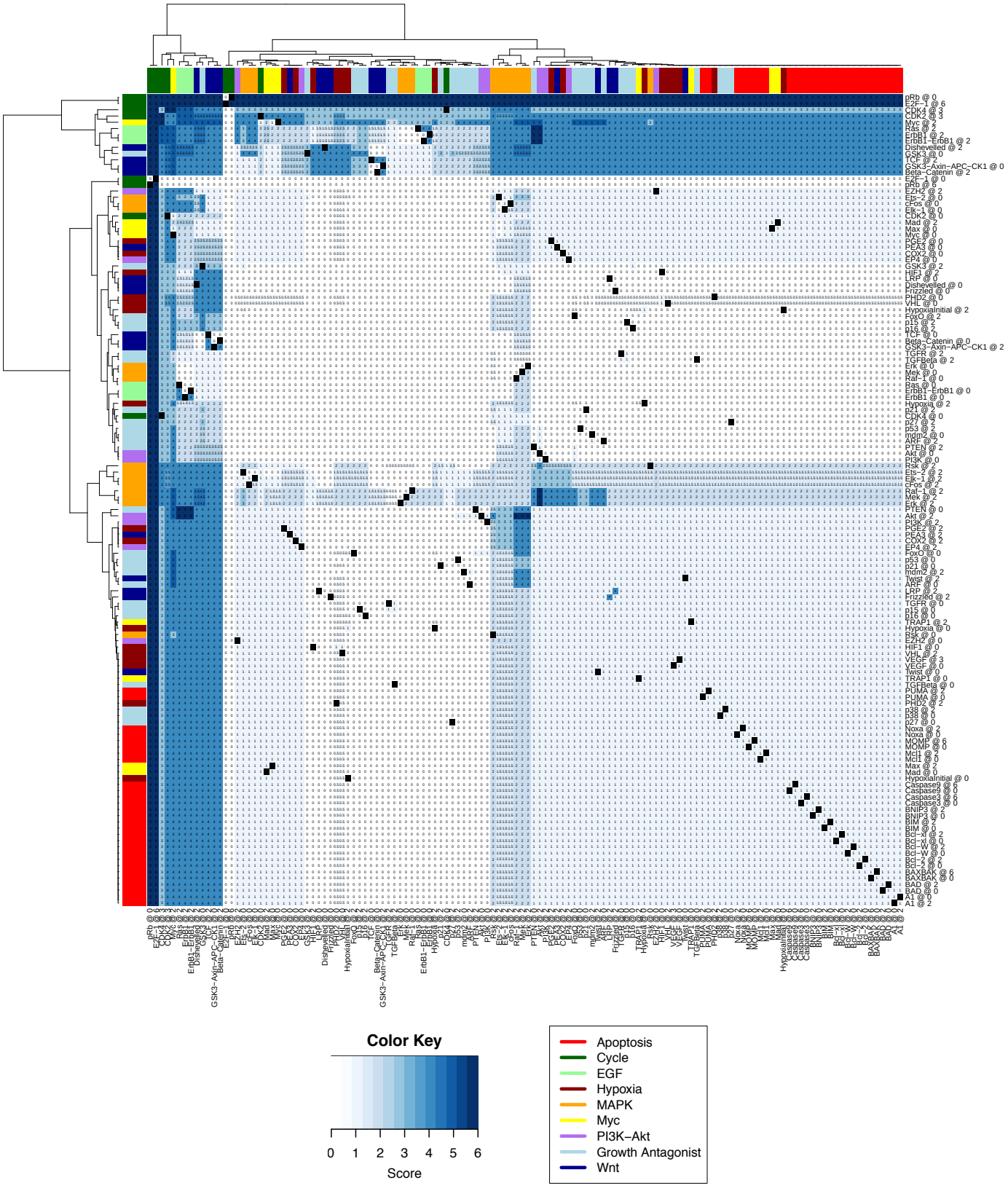

Fig. B.5 Proliferation under combination of perturbations for the healthy (wt) cell. Darker blue indicates higher proliferation.

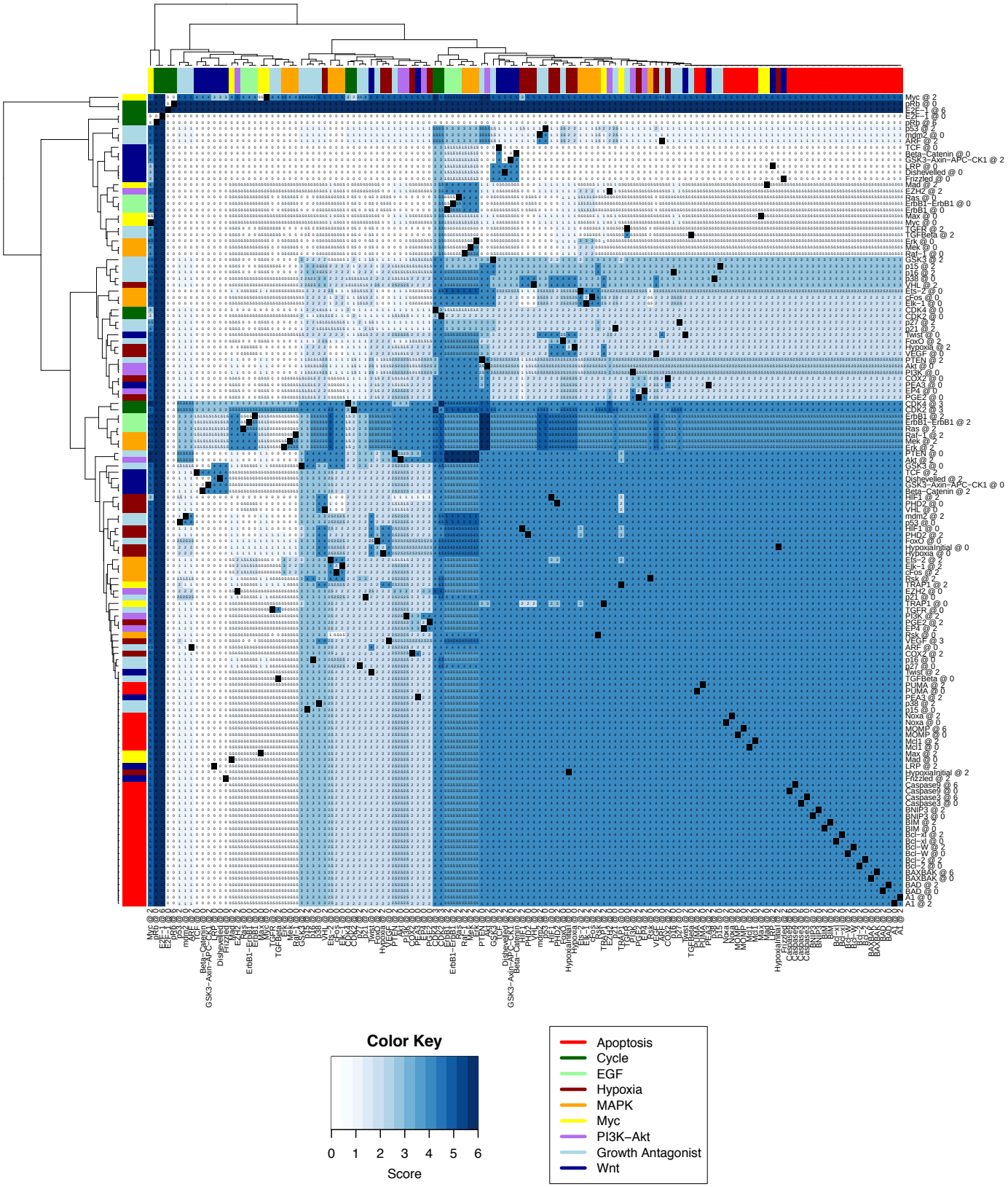

Fig. B.6 Proliferation under combination of perturbations for the pure myc-low tumours. Darker blue indicates higher proliferation.

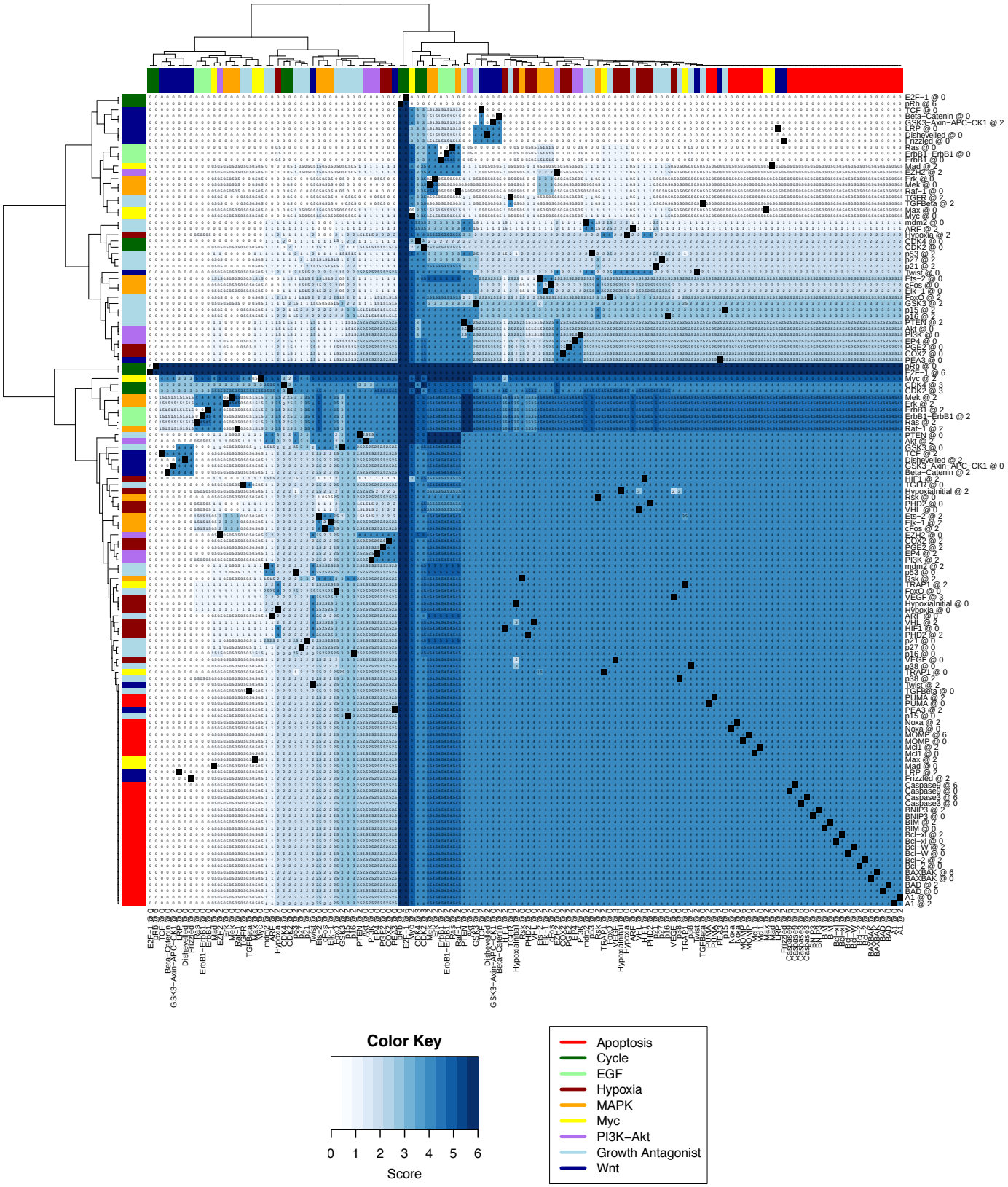

Fig. B.7 Proliferation under combination of perturbations for the heterogeneous myc-low sub-clone. Darker blue indicates higher proliferation.

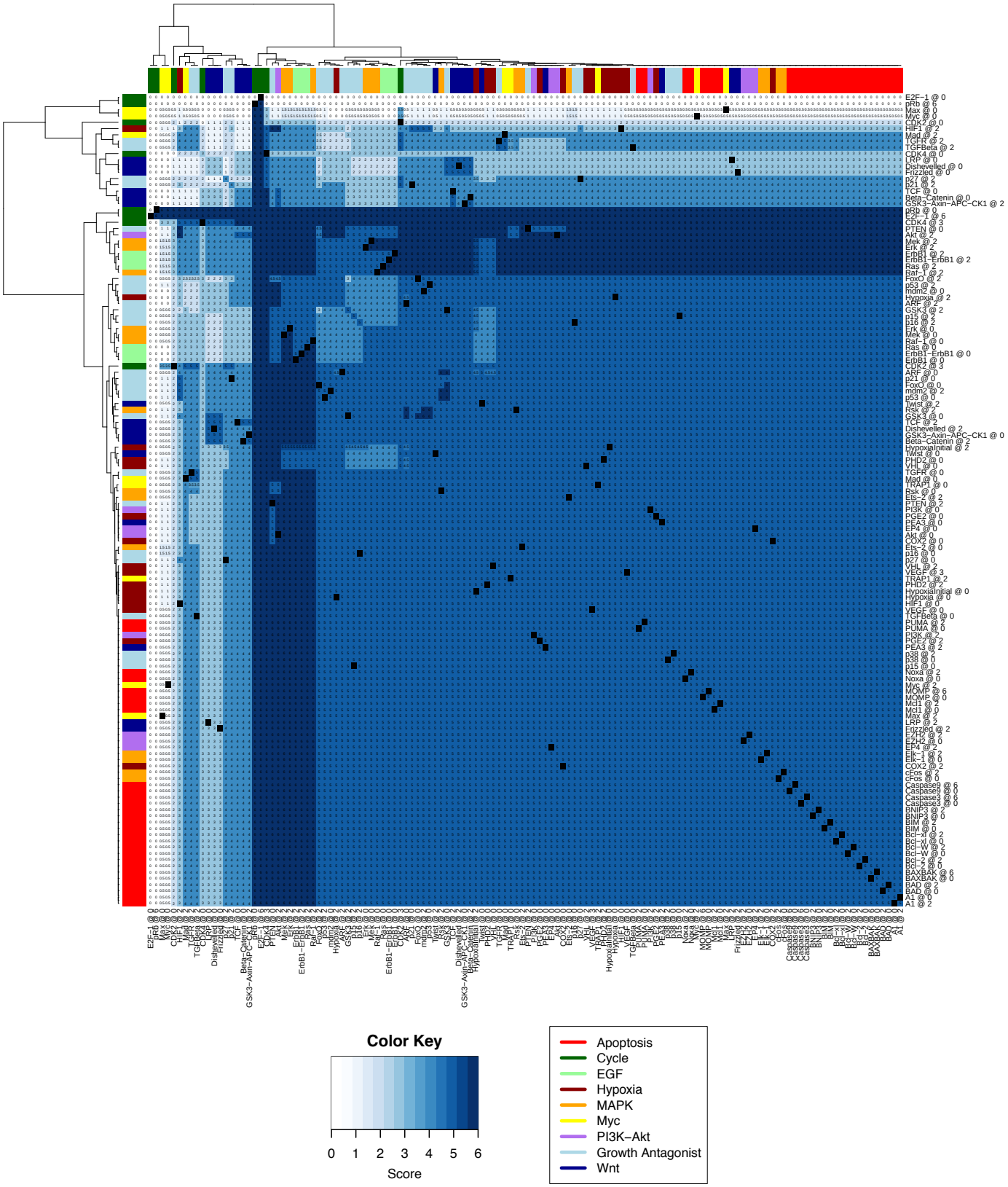

Fig. B.8 Proliferation under combination of perturbations for the heterogeneous myc-high sub-clone. Darker blue indicates higher proliferation.

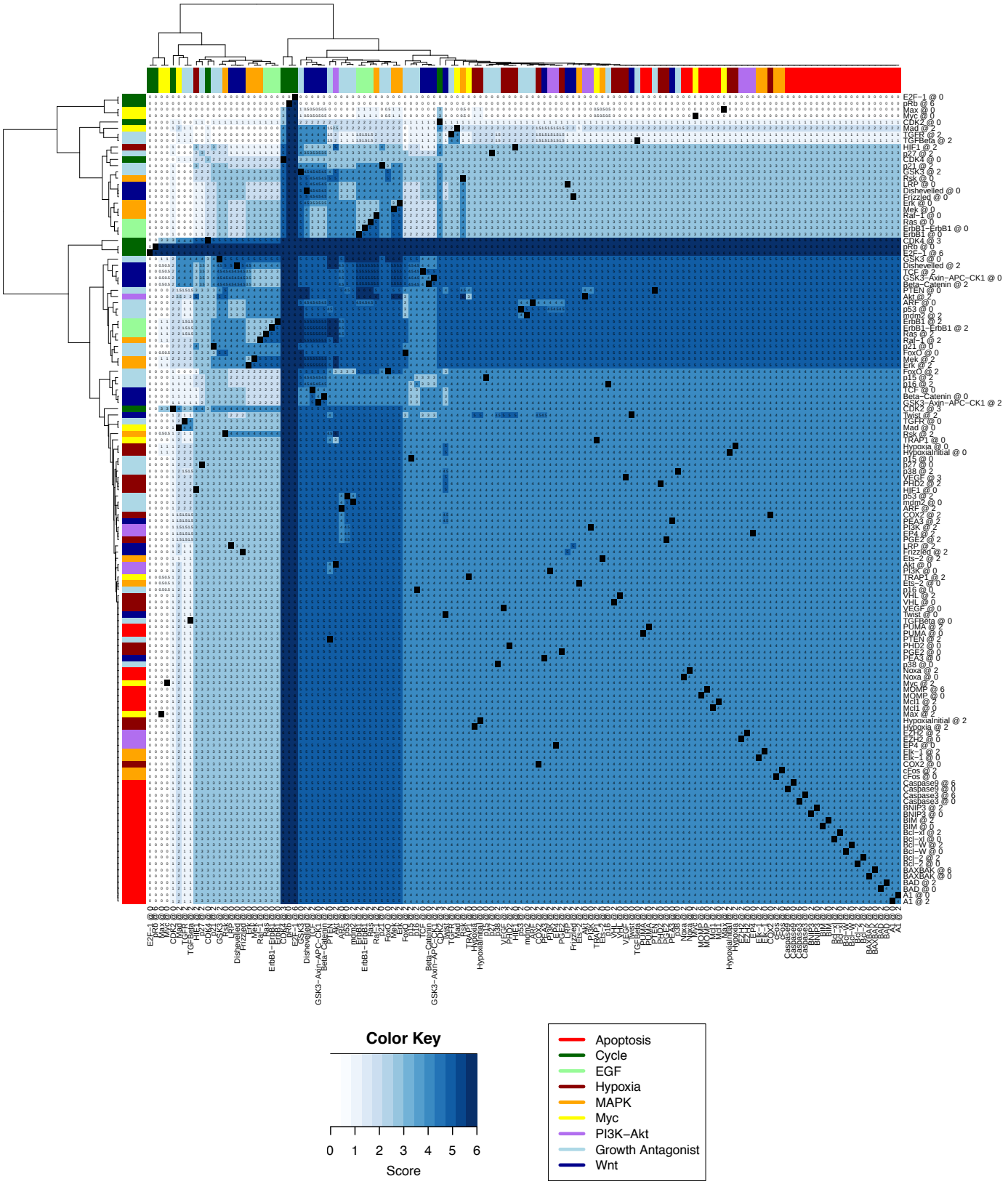

Fig. B.9 Proliferation under combination of perturbations for the pure myc-high tumours. Darker blue indicates higher proliferation.

B.3.2 Cytotoxic

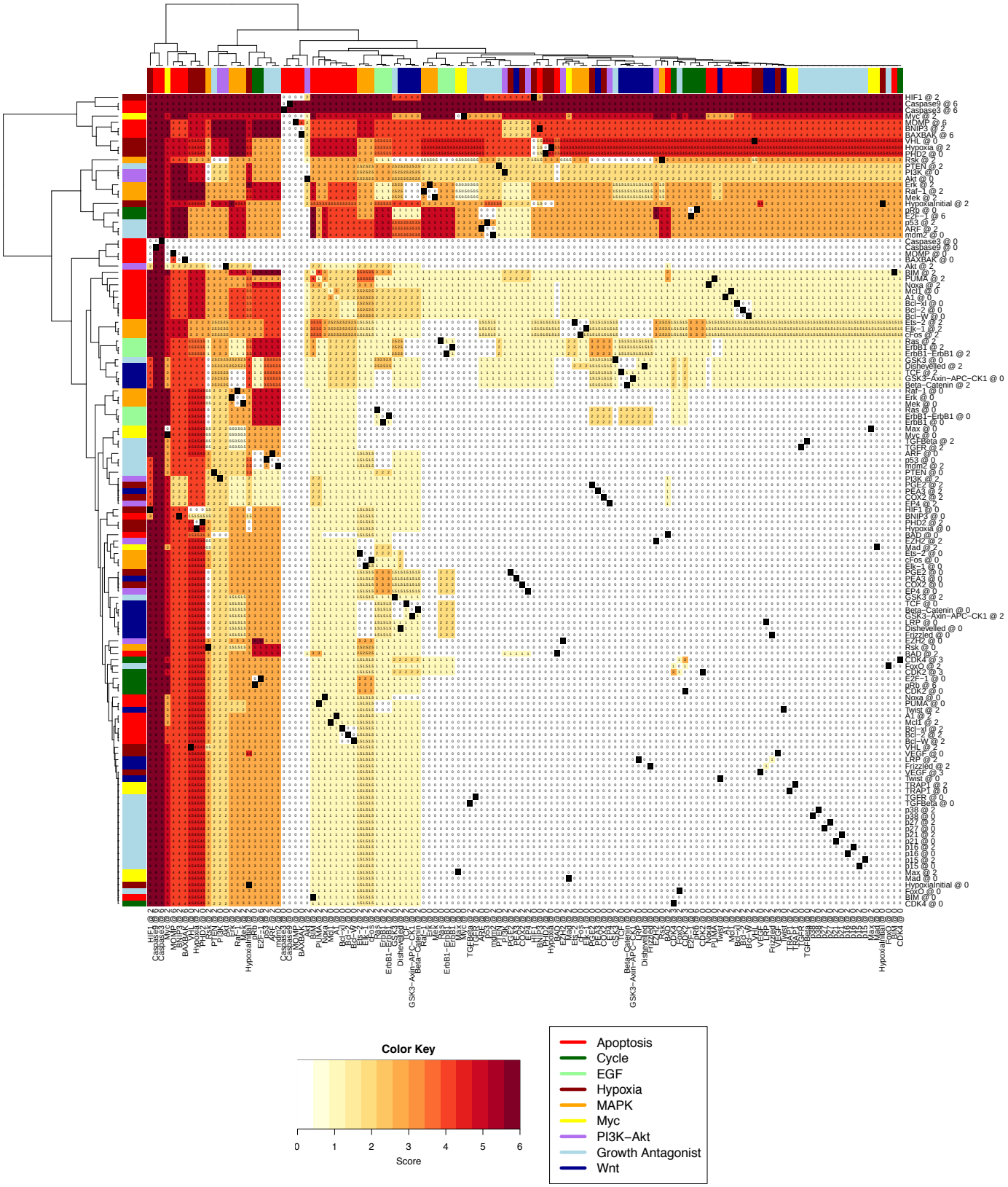

Fig. B.10 Apoptosis under combination of perturbations for healthy (wt) cells. Darker red indicates higher apoptosis.

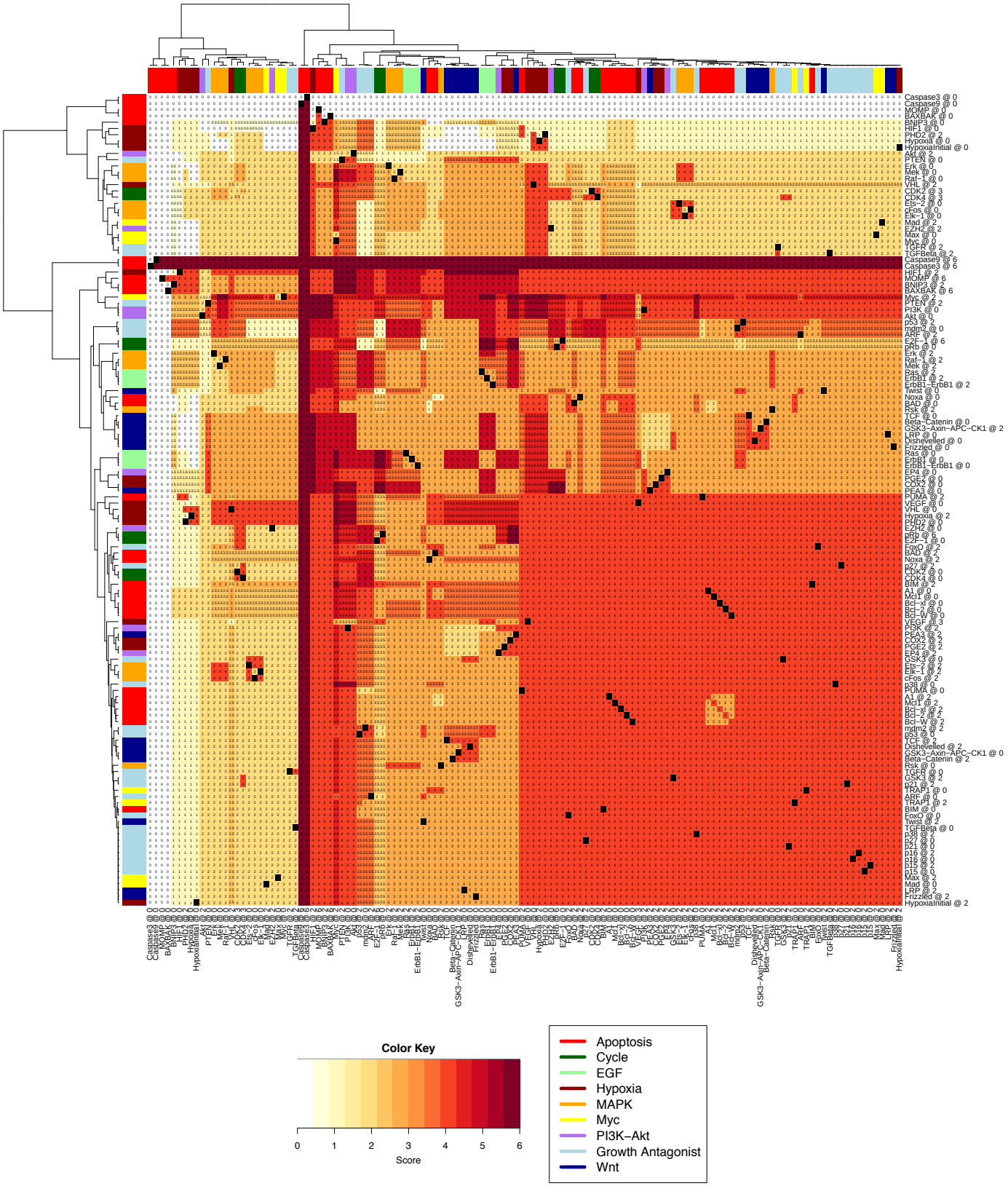

Fig. B.11 Apoptosis under combination of perturbations for pure myc-low cells. Darker red indicates higher apoptosis.

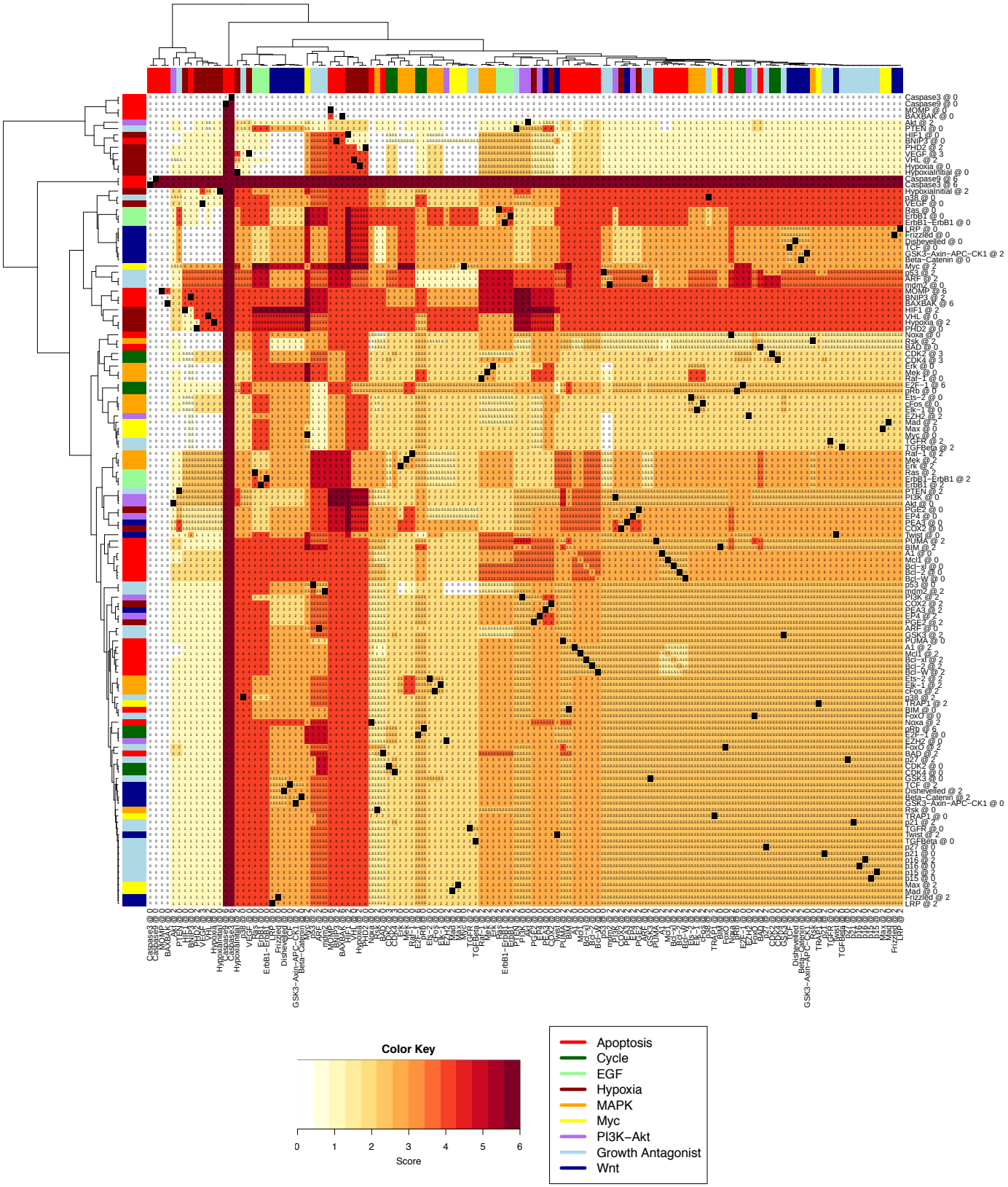

Fig. B.12 Apoptosis under combination of perturbations for heterogeneous myc-low cells. Darker red indicates higher apoptosis.

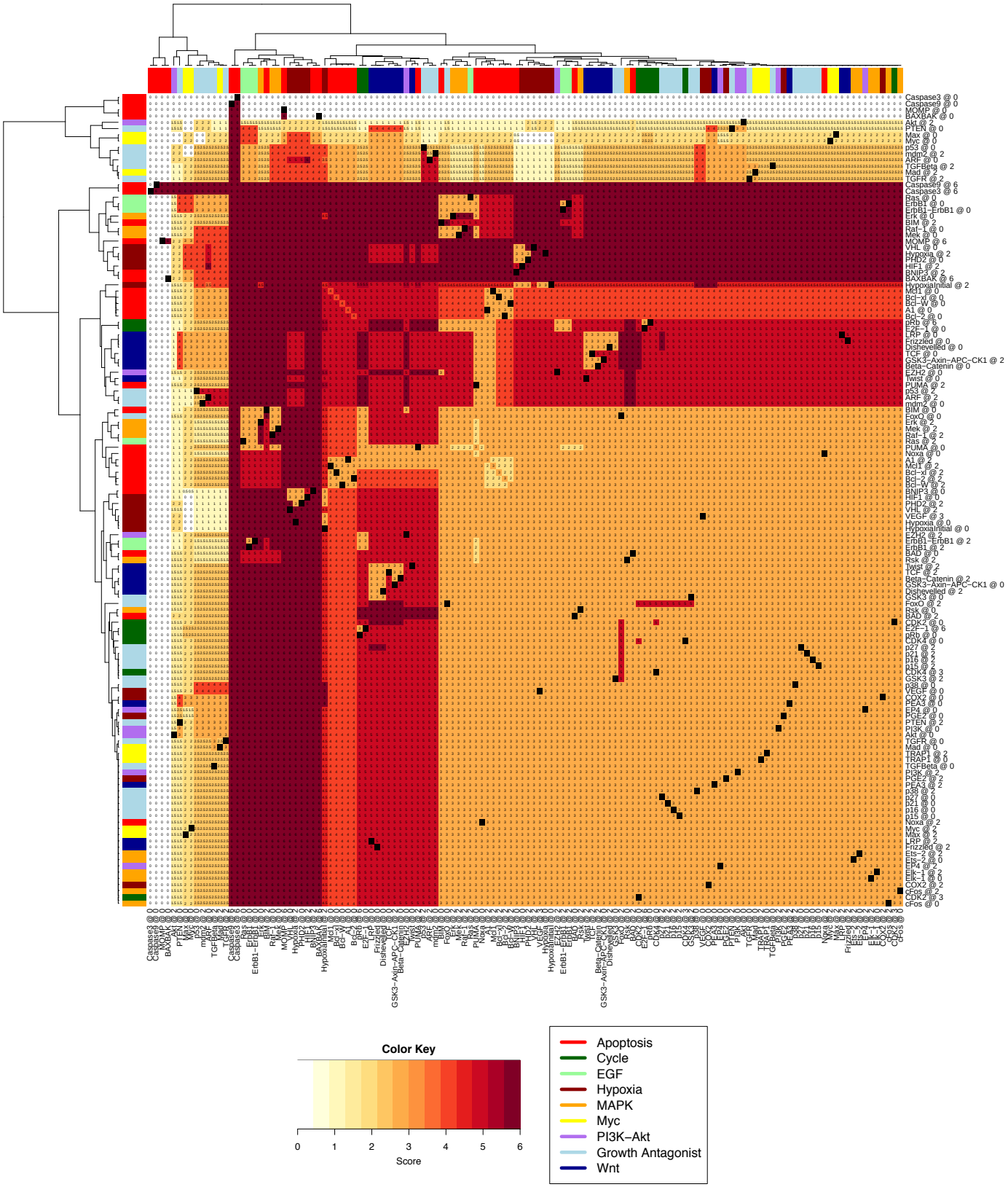

Fig. B.13 Apoptosis under combination of perturbations for heterogeneous myc-high cells. Darker red indicates higher apoptosis.

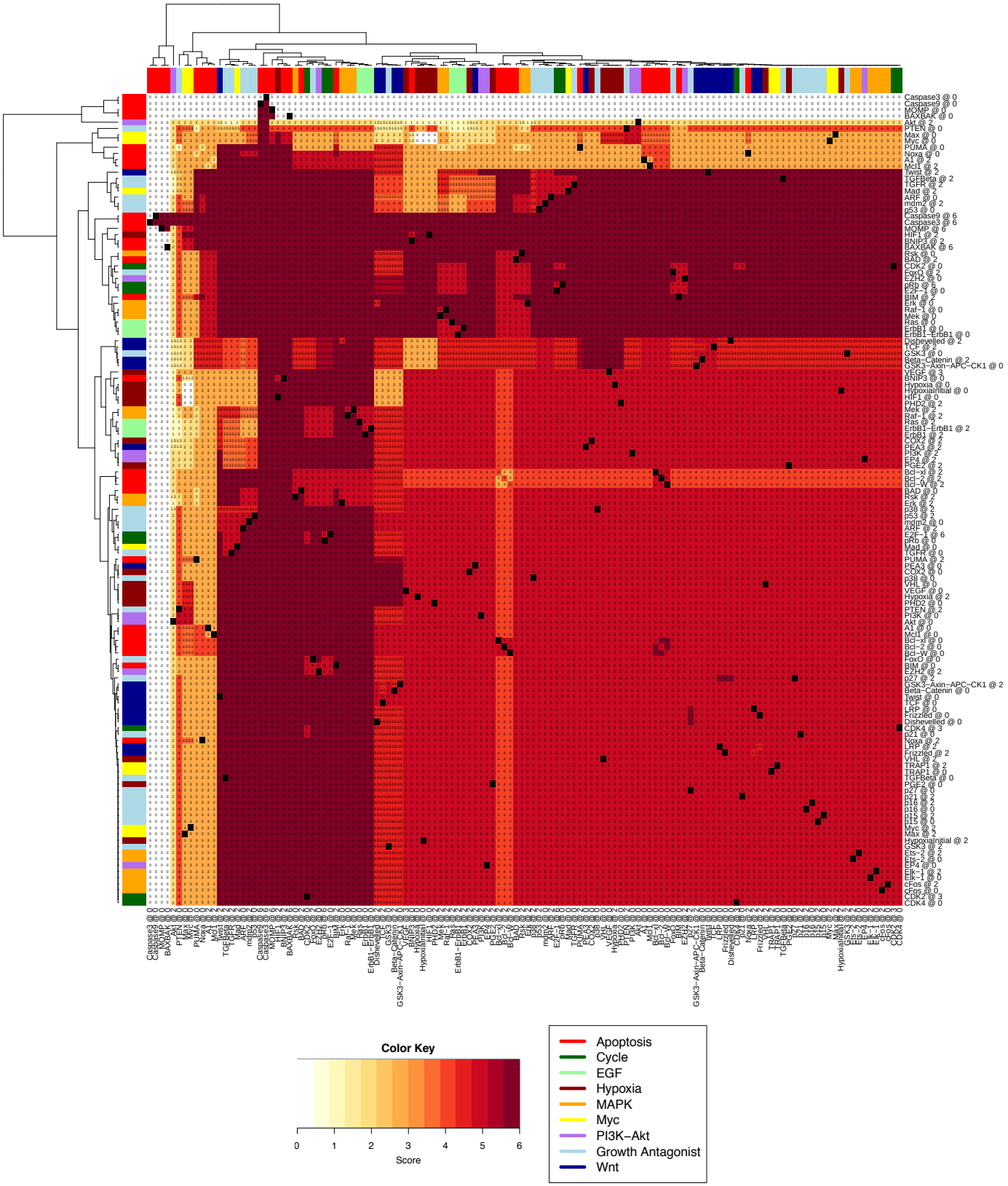

Fig. B.14 Apoptosis under combination of perturbations for pure myc-high cells. Darker red indicates higher apoptosis.

B.4 Combination Therapy Unfiltered Range Restriction Heat Maps

B.4.1 Cytostatic

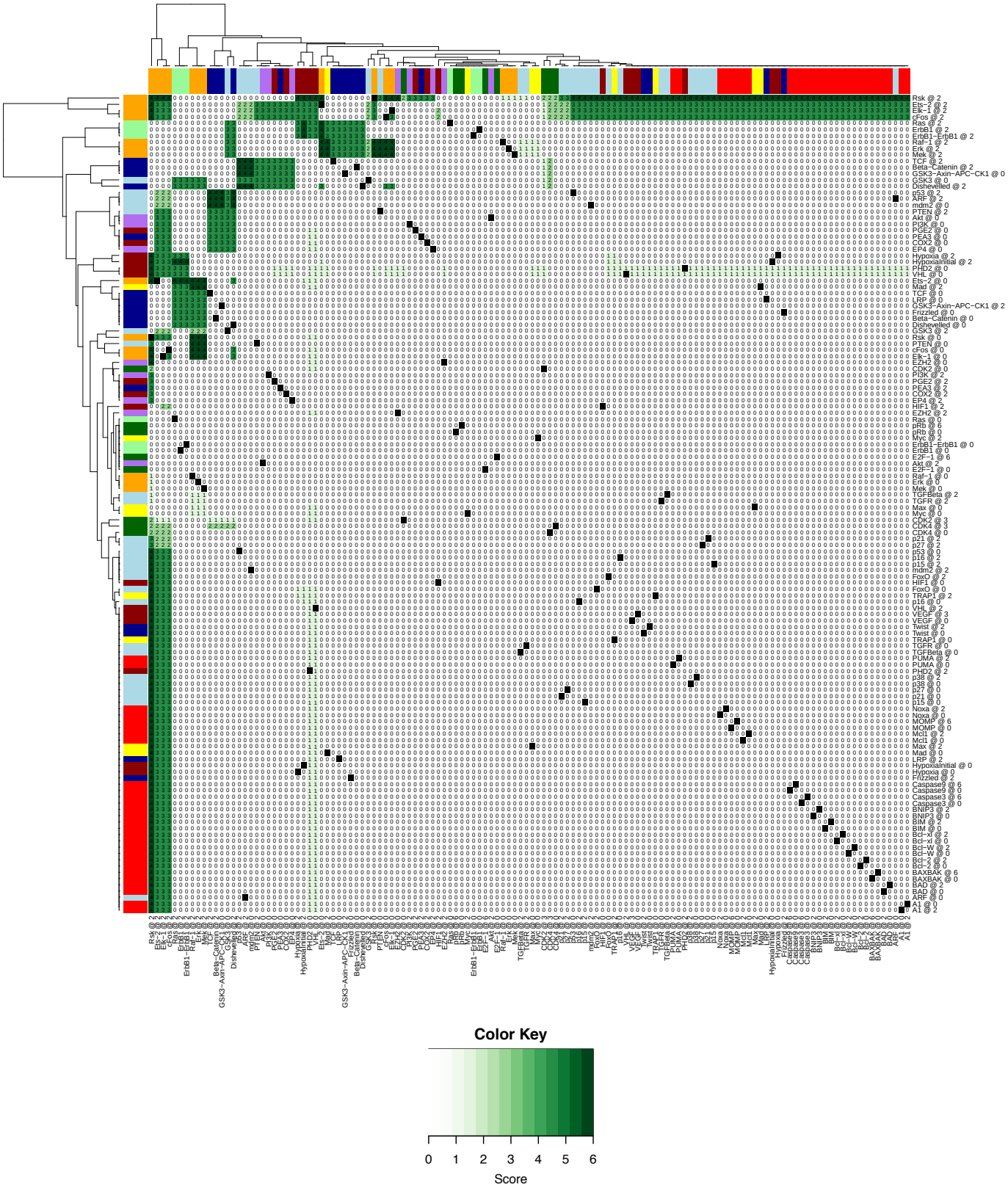

Fig. B.15 Heat map showing the range to which the proliferation node has been restricted by the VMCAI algorithm for healthy cells. Non-zero cases indicate bifurcation or oscillation within that range.

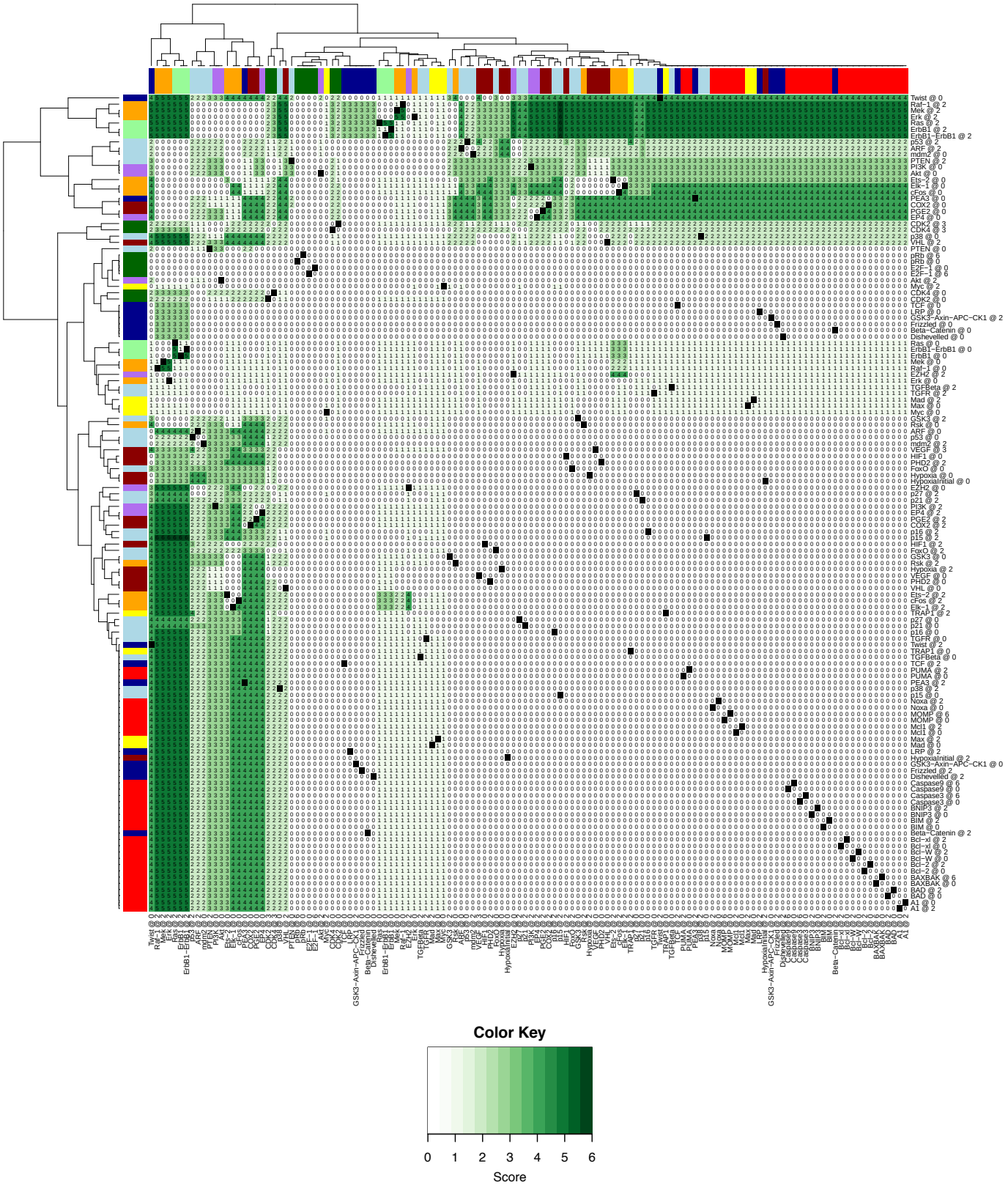

Fig. B.16 Heat map showing the range to which the proliferation node has been restricted by the VMCAI algorithm for the pure myc-low sub-clone. Non-zero cases indicate bifurcation or oscillation within that range.

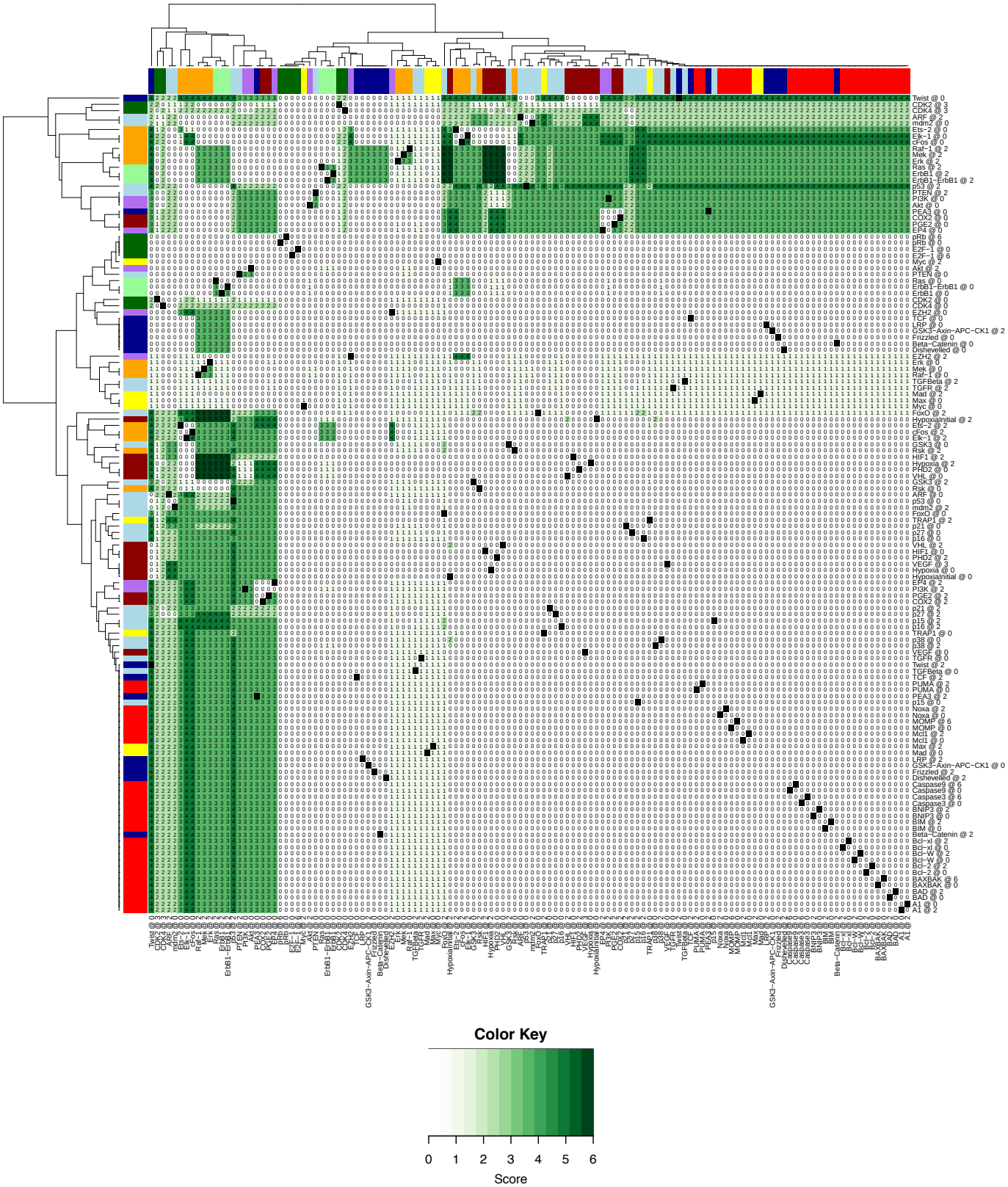

Fig. B.17 Heat map showing the range to which the proliferation node has been restricted by the VMCAI algorithm for the heterogeneous myc-low sub-clone. Non-zero cases indicate bifurcation or oscillation within that range.

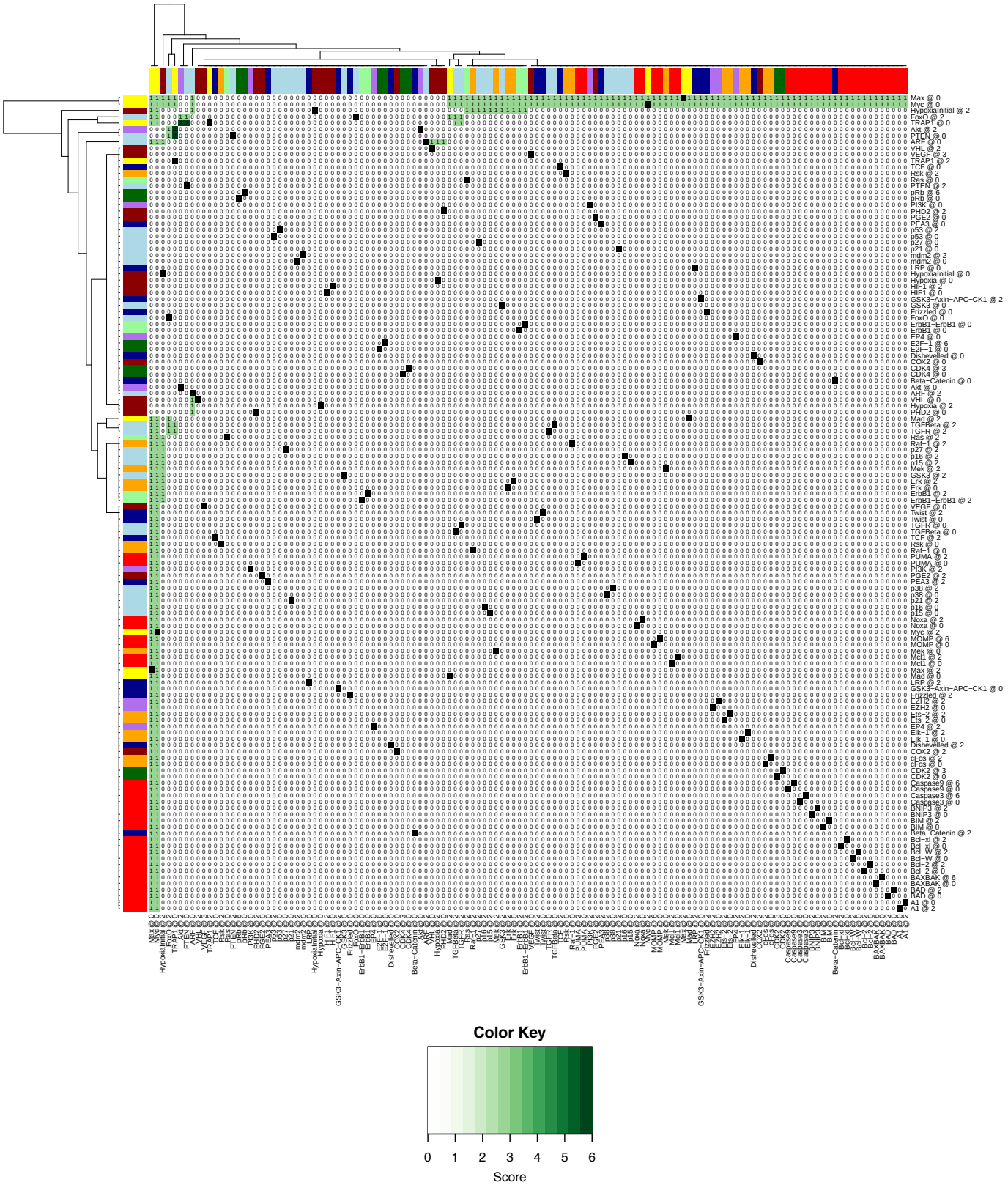

Fig. B.18 Heat map showing the range to which the proliferation node has been restricted by the VMCAI algorithm for the heterogeneous myc-high sub-clone. Non-zero cases indicate bifurcation or oscillation within that range.

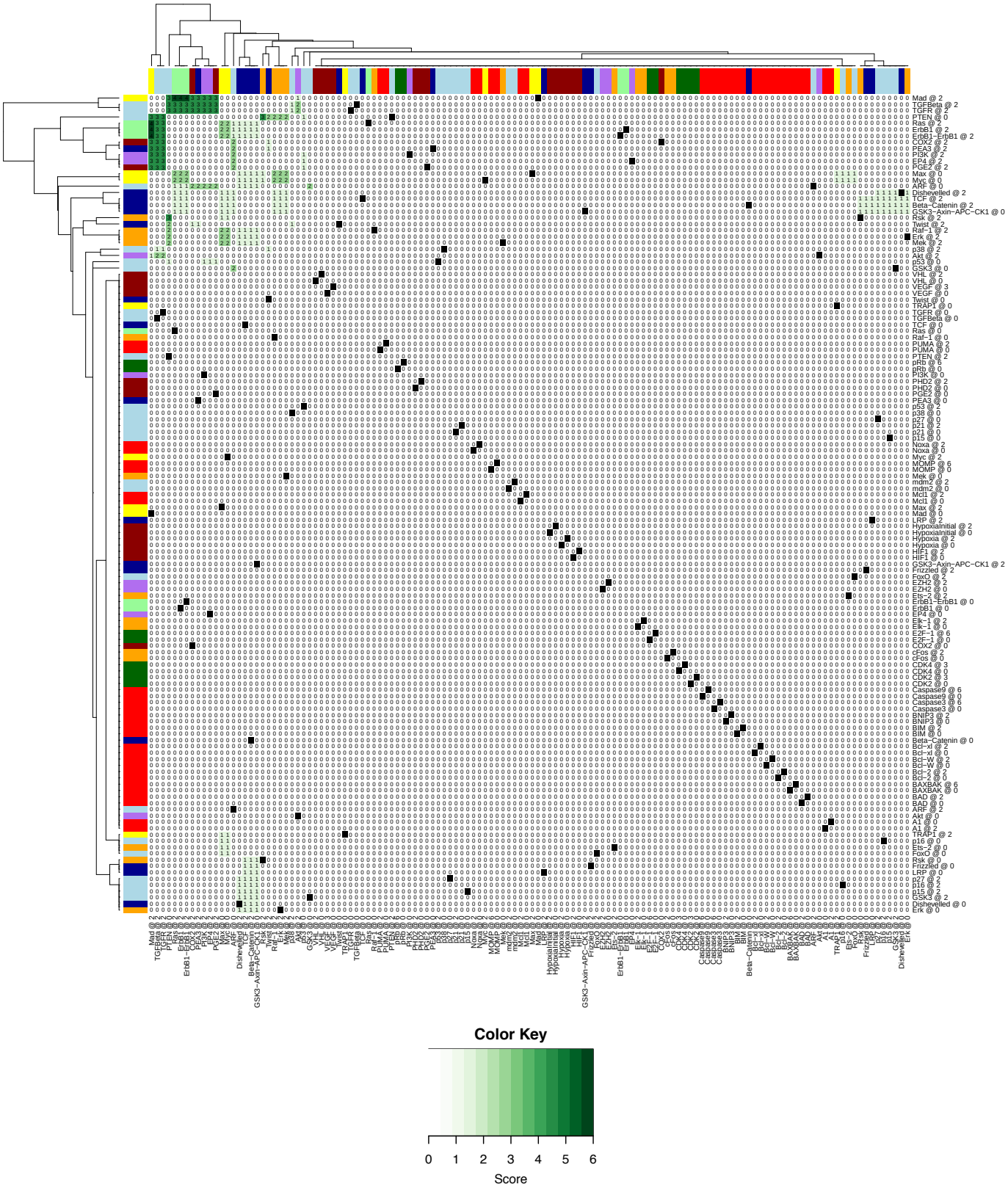

Fig. B.19 Heat map showing the range to which the proliferation node has been restricted by the VMCAI algorithm for the pure myc-high sub-clone. Non-zero cases indicate bifurcation or oscillation within that range.

B.4.2 Cytotoxic

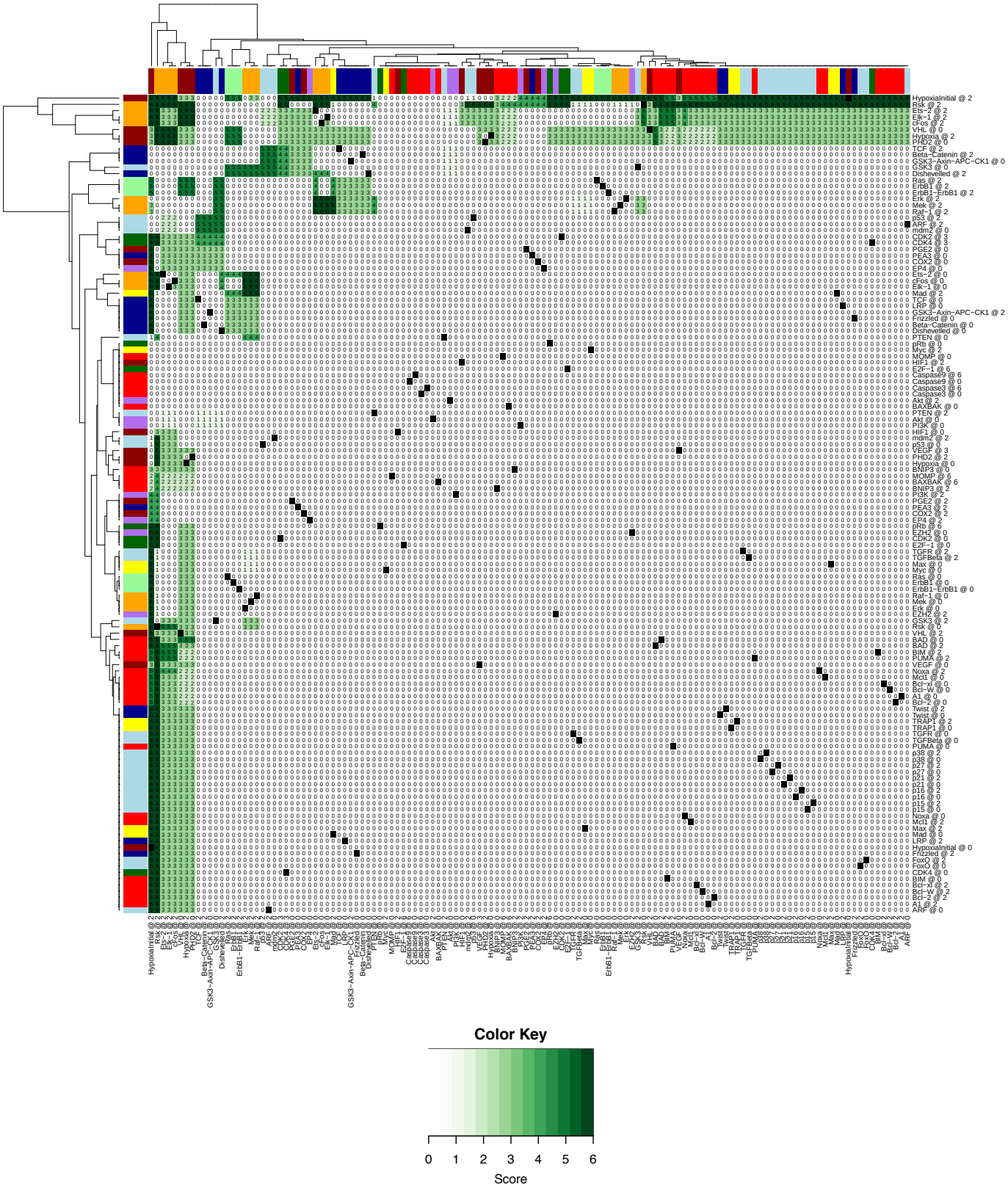

Fig. B.20 Heat map showing the range to which the apoptosis node has been restricted by the VMCAI algorithm for healthy cells. Non-zero cases indicate bifurcation or oscillation within that range.

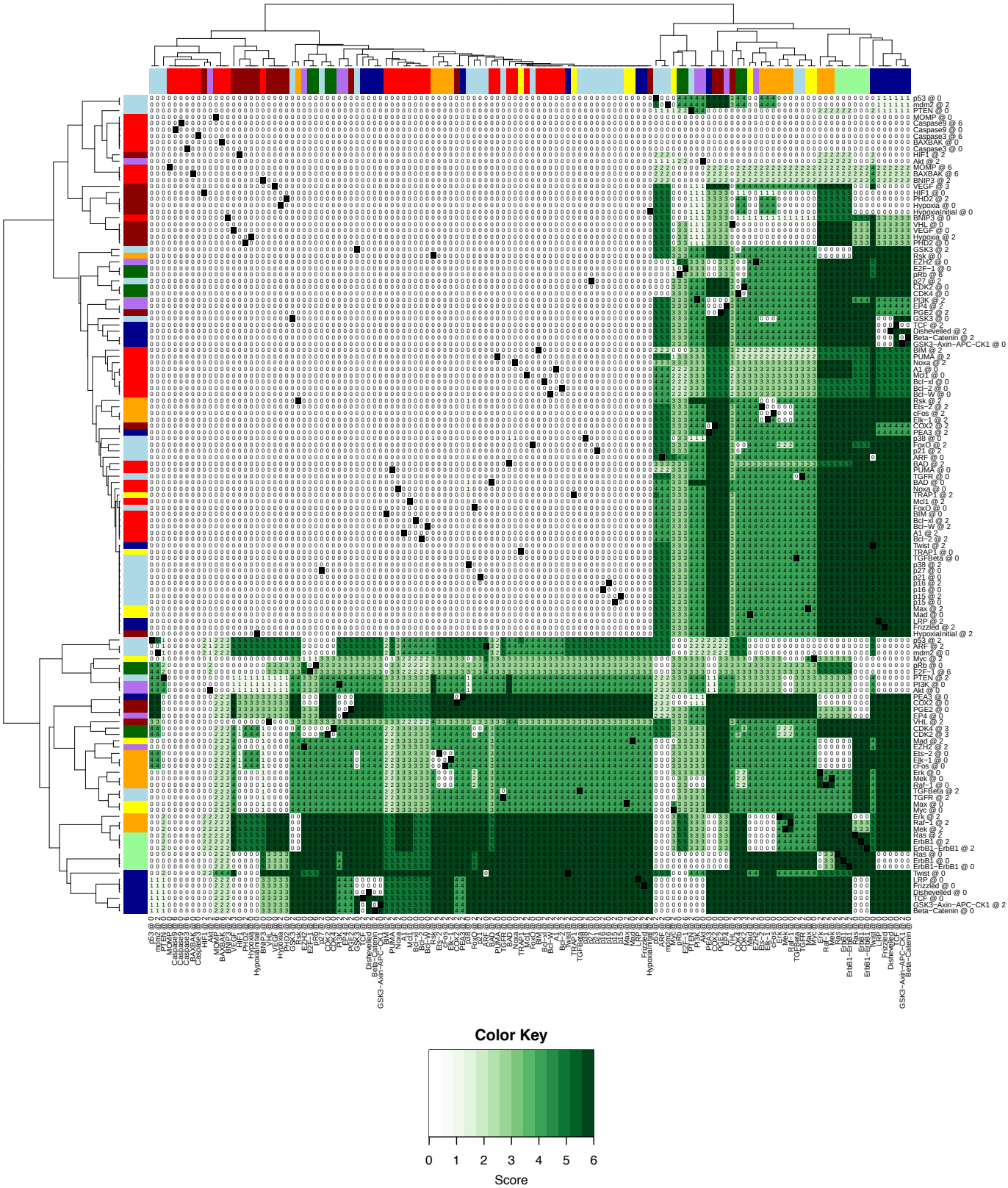

Fig. B.21 Heat map showing the range to which the apoptosis node has been restricted by the VMCAI algorithm for the pure myc-low sub-clone. Non-zero cases indicate bifurcation or oscillation within that range.

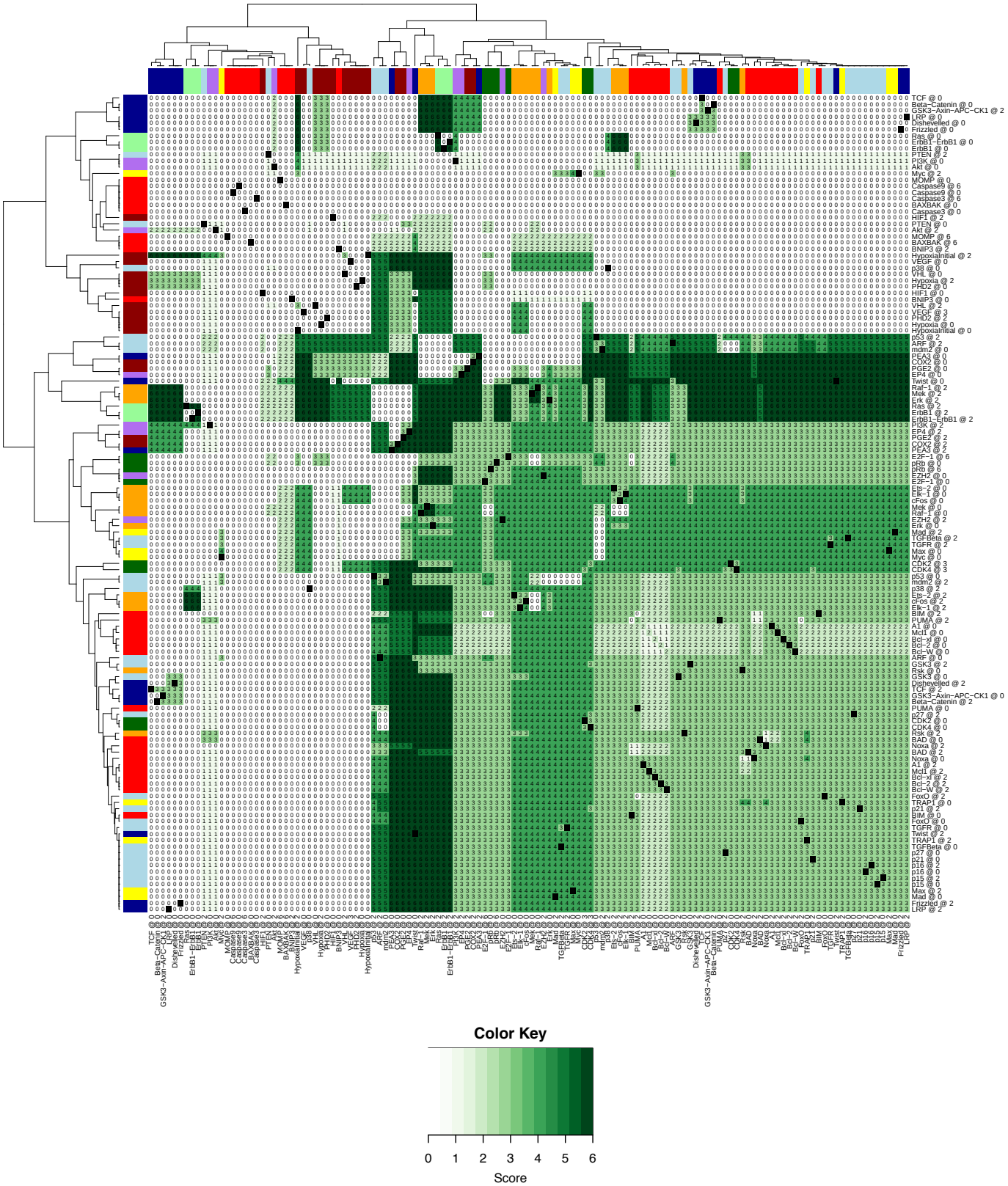

Fig. B.22 Heat map showing the range to which the apoptosis node has been restricted by the VMCAI algorithm for the heterogeneous myc-low sub-clone. Non-zero cases indicate bifurcation or oscillation within that range.

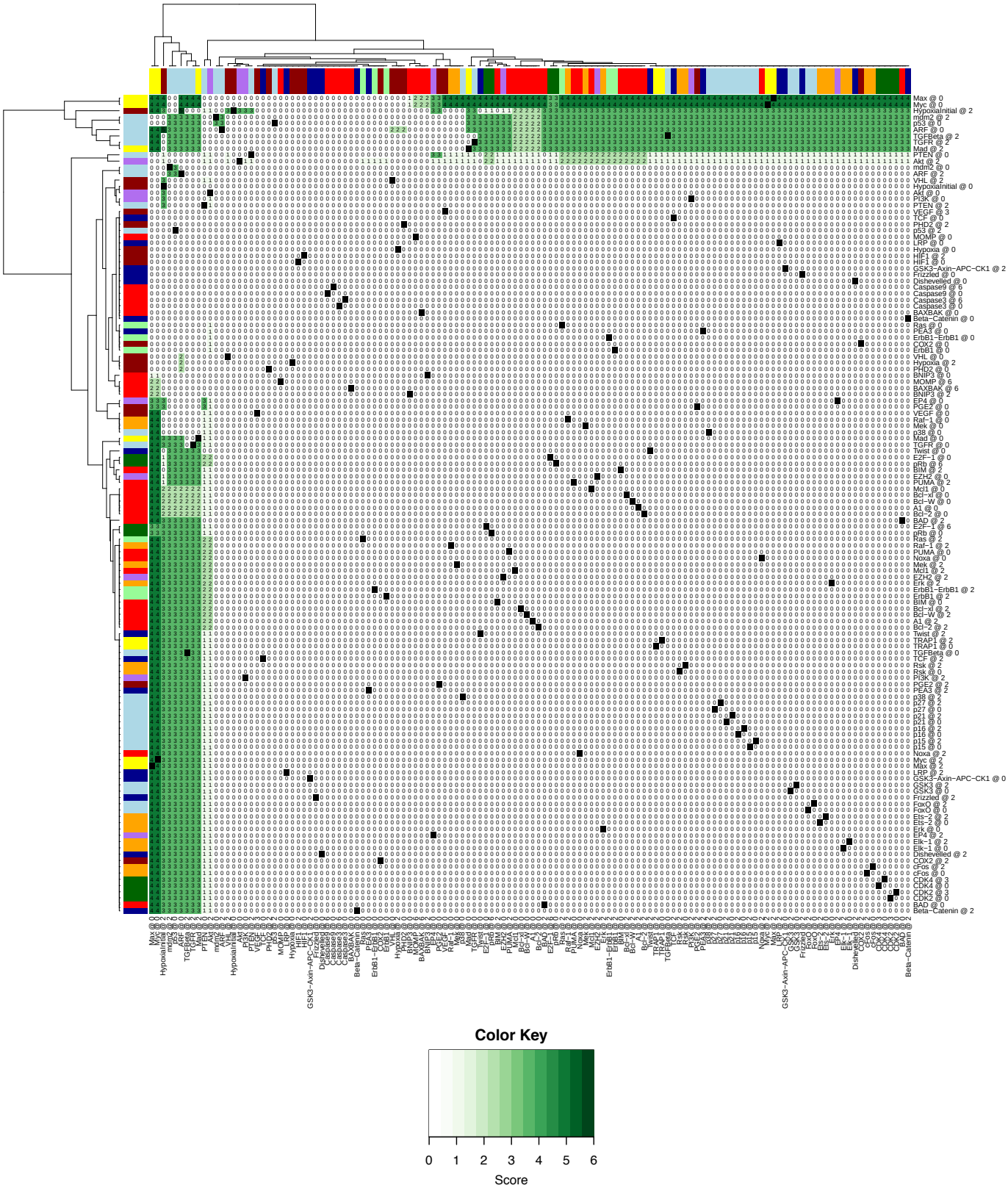

Fig. B.23 Heat map showing the range to which the apoptosis node has been restricted by the VMCAI algorithm for the heterogeneous myc-high sub-clone. Non-zero cases indicate bifurcation or oscillation within that range.

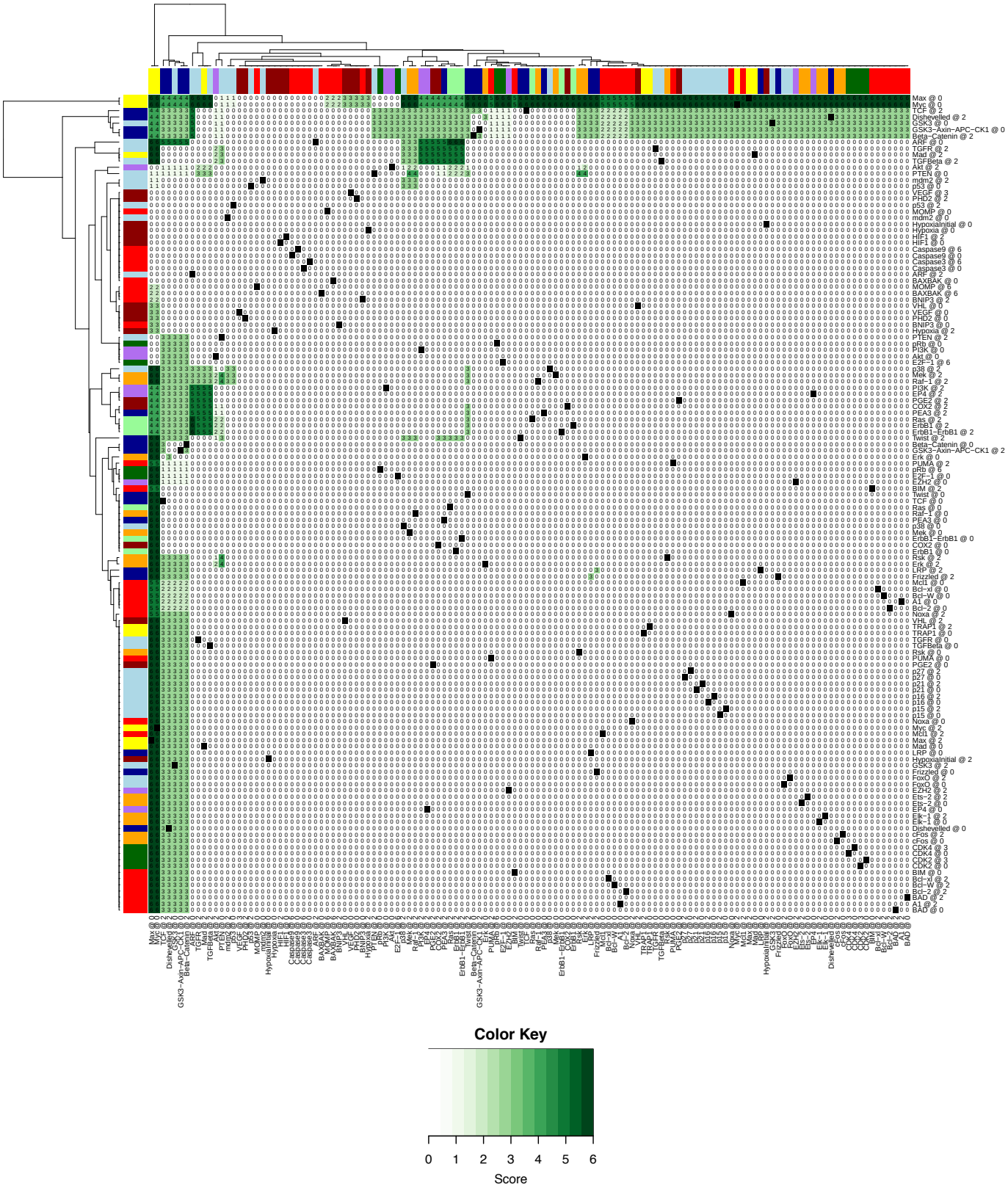

Fig. B.24 Heat map showing the range to which the apoptosis node has been restricted by the VMCAI algorithm for the pure myc-high sub-clone. Non-zero cases indicate bifurcation or oscillation within that range.

B.5 Change due to addition of Second Drug for All Perturbations

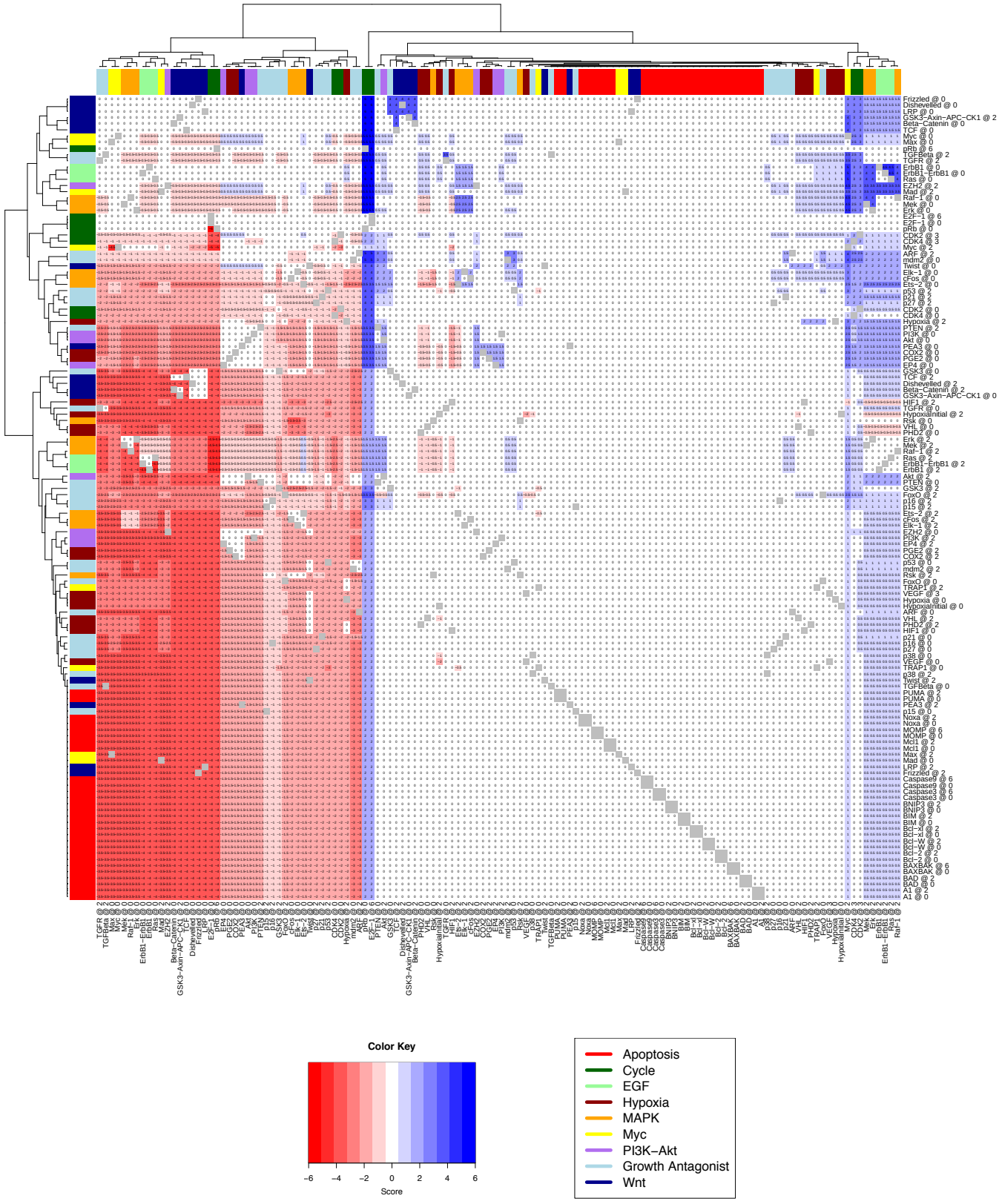

Fig. B.25 Change in mean proliferation in the heterogeneous myc-low sub-clone when adding a second drug to a drug shown to be effective in monotherapy. y-axis shows first drug, x-axis the drug which is added in combination. Grey boxes are combinations which are nonsensical (two different treatments of the same node).

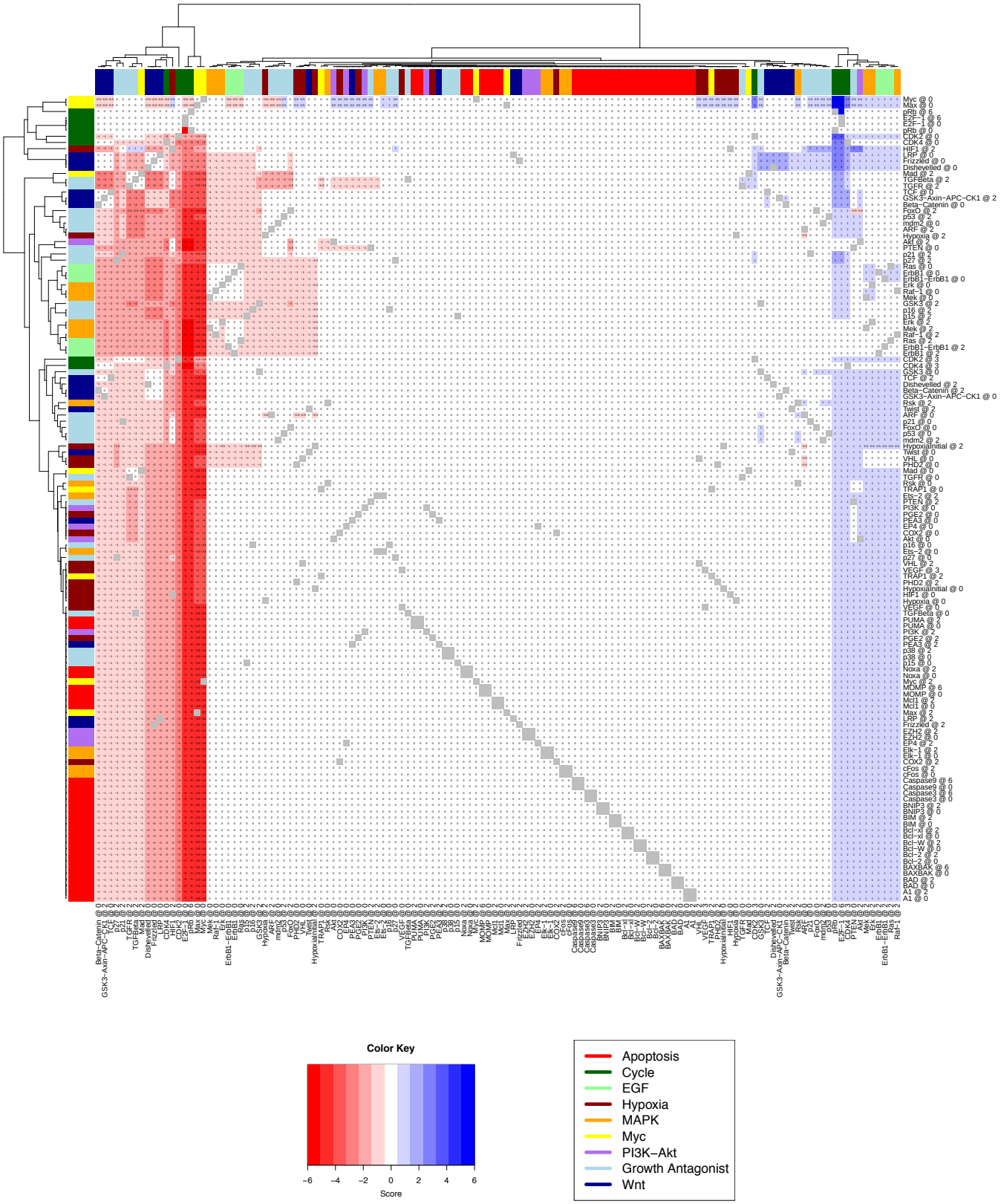

Fig. B.26 Change in mean proliferation in the heterogeneous myc-high sub-clone when adding a second drug to a drug shown to be effective in monotherapy. y-axis shows first drug, x-axis the drug which is added in combination. Grey boxes are combinations which are nonsensical (two different treatments of the same node).

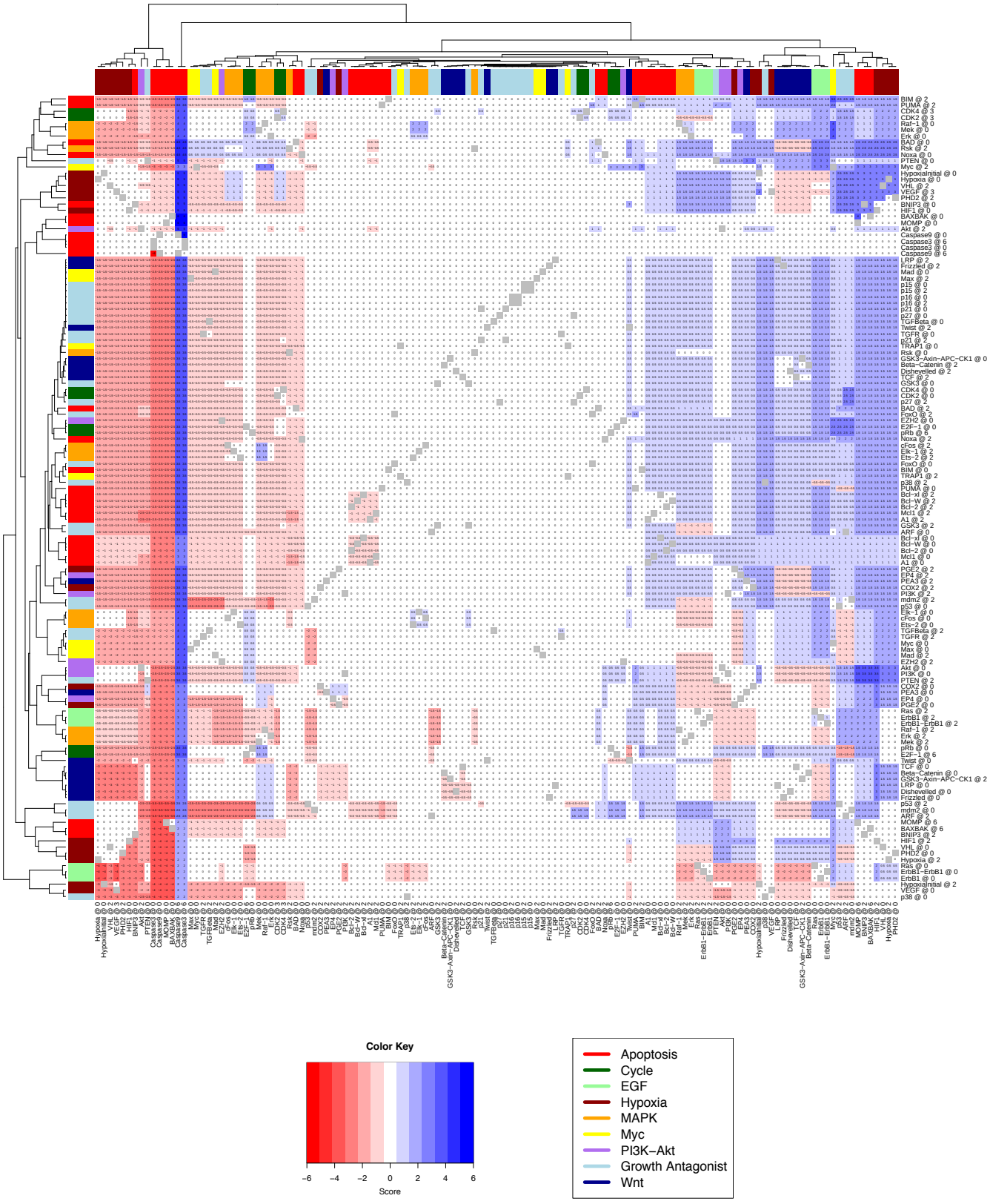

Fig. B.27 Change in mean apoptosis in the heterogeneous myc-low sub-clone when adding a second drug to a drug shown to be effective in monotherapy. y-axis shows first drug, x-axis the drug which is added in combination. Grey boxes are combinations which are nonsensical (two different treatments of the same node).

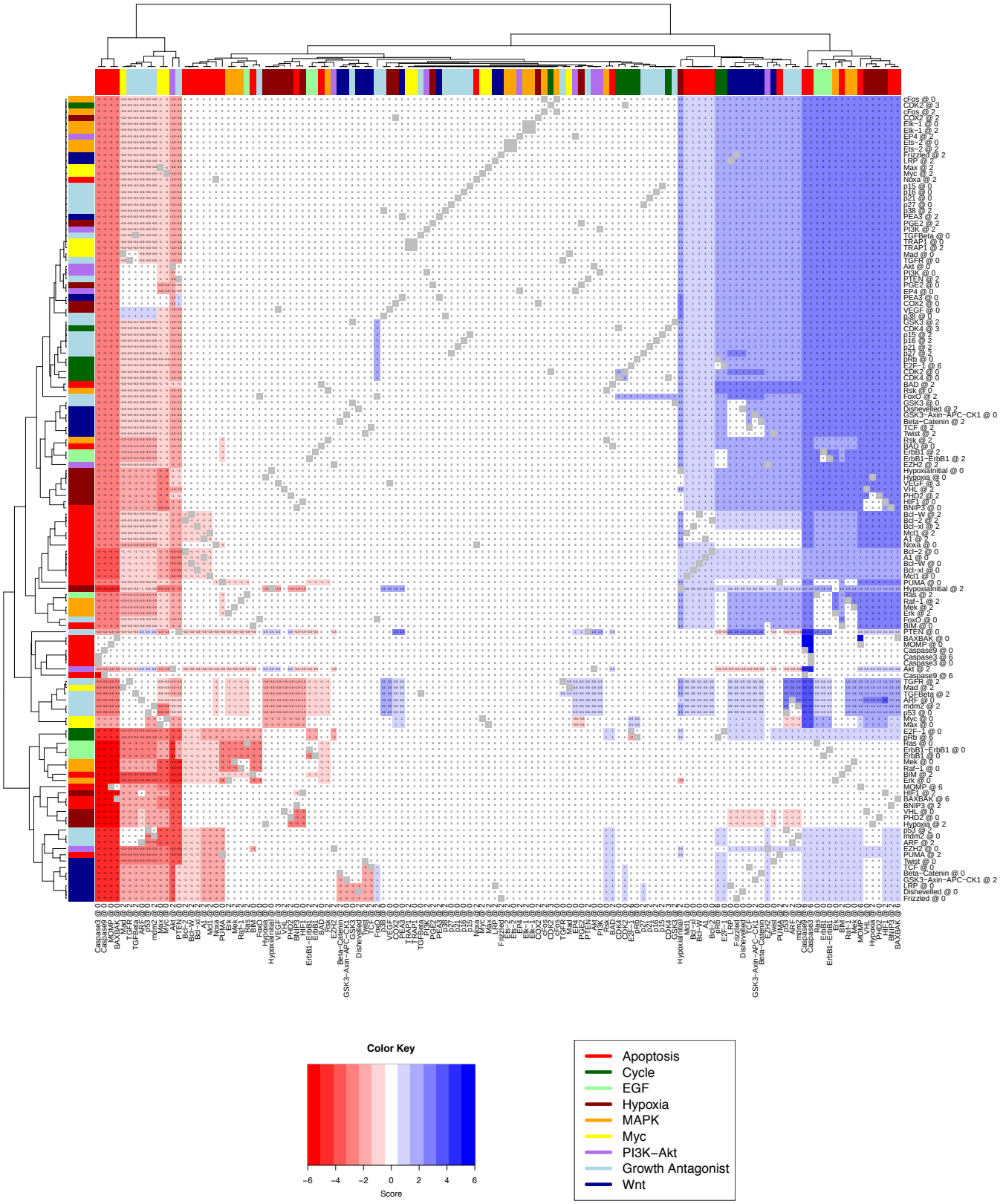

Fig. B.28 Change in mean apoptosis in the heterogeneous myc-high sub-clone when adding a second drug to a drug shown to be effective in monotherapy. y-axis shows first drug, x-axis the drug which is added in combination. Grey boxes are combinations which are nonsensical (two different treatments of the same node).

B.6 Pathways Involved in Effective Treatments

B.6.1 Monotherapy

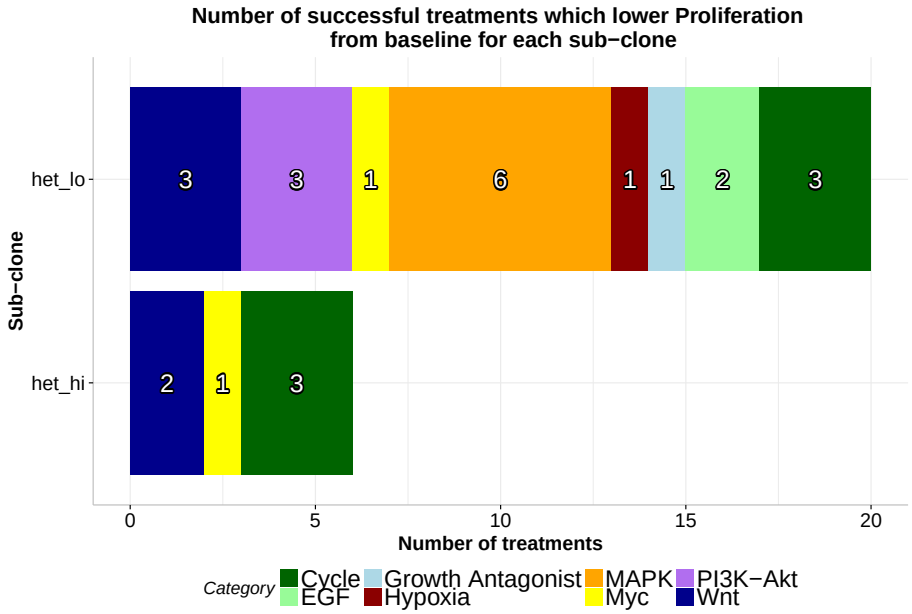

(a) Proportion of successful cytostatic treatments involving different pathways.

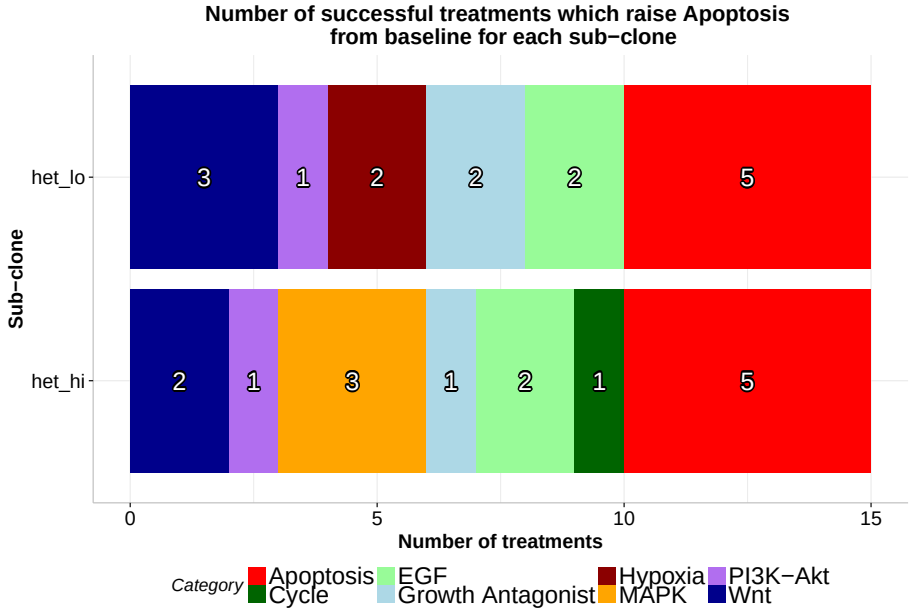

(b) Proportion of successful cytotoxic treatments involving different pathways.

Fig. B.29 Number of successful cytostatic and cytotoxic treatments involving different pathways. Successful are those which lower proliferation below the baseline for the respective sub-clone, or apoptosis above the baseline. How I group nodes in the network into pathways is broken down in Appendix A.2. Note that sections of the bar indicate all the treatments which fit that category, rather than being cumulative, as indicated by labels.

B.6.2 Combination Therapy

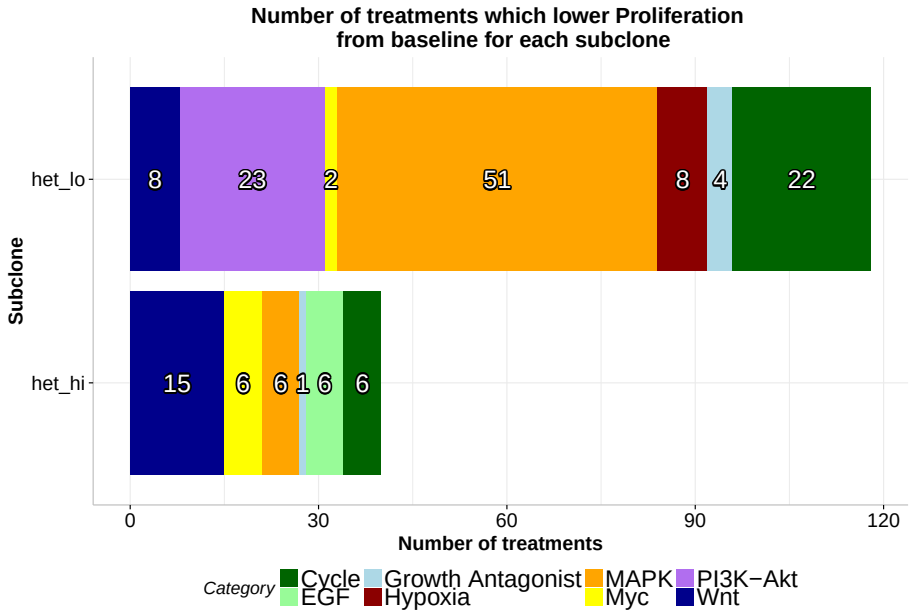

(a) Number of cytostatic treatments which lower proliferation below the baseline for the respective sub-clone involving different pathways.

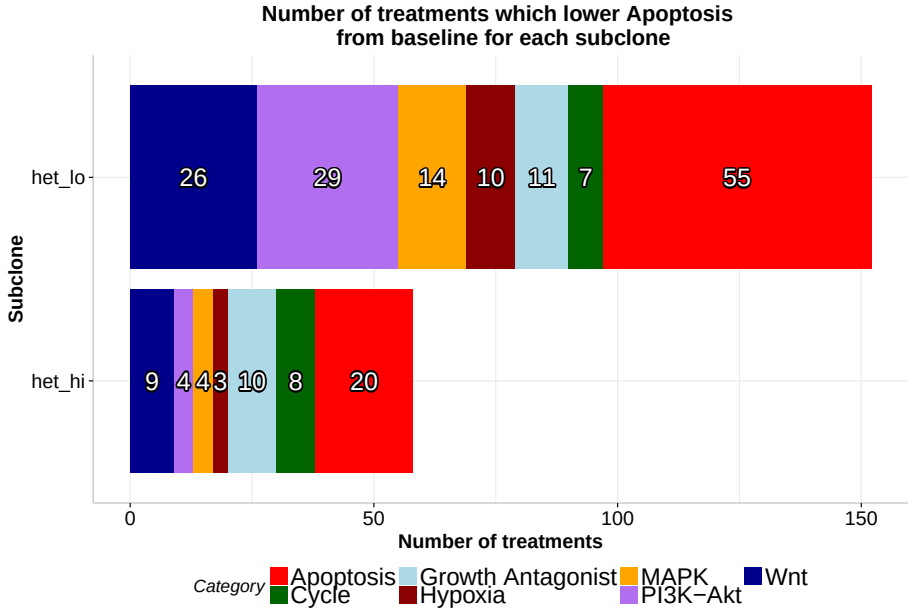

(b) Number of cytotoxic treatments which raise apoptosis above the baseline for the respective sub-clone involving different pathways.

Fig. B.30 Number of successful cytostatic and cytotoxic treatments involving different pathways. This includes only those which improved over the monotherapy case to avoid describing the effects of a monotherapy and a neutral passenger.

Appendix C

Statistical Analysis

C.1 Data from Experimental Validation of Model Predictions

C.1.1 Tumour Growth

Table C.1 Percentage change in tumour size, relative to size on Day 0, for mice under different treatment regimes, measured over 3 days of treatment.

Mouse	Treatment	Day 0	Day 1	Day 2	Day 3
M00235975	Double	100	66.99	76.56	66.99
M00235977	Double	100	114.29	83.97	73.47
M00235979	Double	100	60.49	53.77	70.23
M00235990	Double	100	79.01	100.00	90.00
M00235969	Double	100	114.29	62.97	62.97
M00235978	Lico	100	100.00	100.00	125.00
M00235971	Lico	100	100.00	137.17	150.89
M00235985	Lico	100	100.00	112.50	142.38
M00235972	Lico	100	144.23	132.21	132.21
M00235980	PD	100	123.43	123.43	123.43
M00235981	PD	100	100.00	140.00	97.22
M00235984	PD	100	130.61	100.00	100.00
M00235991	PD	100	144.00	144.00	83.33
M00235973	Control	100	100.00	227.30	289.29
M00235970	Control	100	108.33	121.00	180.00
M00235982	Control	100	100.00	140.65	140.65
M00235983	Control	100	89.10	100.00	110.00

Table C.2 Mean percentage tumour size, relative to size on Day 0, and standard deviation for each treatment regime.

Treatment	Day	Mean	SD	Percentage SD
Control	0	100.00	0.00	0.00
Control	1	99.36	7.89	7.94
Control	2	147.24	55.89	37.96
Control	3	179.98	78.30	43.50
Lico	0	100.00	0.00	0.00
Lico	1	111.06	22.12	19.91
Lico	2	120.47	17.32	14.37
Lico	3	137.62	11.36	8.26
PD	0	100.00	0.00	0.00
PD	1	124.51	18.43	14.80
PD	2	126.86	20.00	15.76
PD	3	101.00	16.64	16.47
Double	0	100.00	0.00	0.00
Double	1	87.01	25.77	29.61
Double	2	75.45	18.04	23.91
Double	3	72.73	10.41	14.31

C.1.2 Proliferation in Tumour Sections

Table C.3 Percentage of IdU positive nuclei in tumour sections, taken on the third day after the commencement of treatment, for myc-high and myc-low sub-clones.

Mouse	Treatment	Sub-clone	Percent IdU positive nuclei
M00235969	Double	myc-high	9.73
M00235975	Double	myc-high	14.77
M00235977	Double	myc-high	17.95
M00235979	Double	myc-high	4.44
M00235971	Lico	myc-high	6.47
M00235972	Lico	myc-high	27.66
M00235978	Lico	myc-high	23.11
M00235985	Lico	myc-high	19.33
M00235980	PD	myc-high	15.67
M00235981	PD	myc-high	6.52
M00235984	PD	myc-high	19.86
M00235991	PD	myc-high	12.28
M00235970	Control	myc-high	25.36
M00235973	Control	myc-high	32.47
M00235982	Control	myc-high	23.25
M00235983	Control	myc-high	37.35
M00235969	Double	myc-low	2.26
M00235975	Double	myc-low	0.33
M00235977	Double	myc-low	0.86
M00235979	Double	myc-low	1.97
M00235971	Lico	myc-low	0.81
M00235972	Lico	myc-low	17.56
M00235978	Lico	myc-low	13.92
M00235985	Lico	myc-low	10.99
M00235980	PD	myc-low	1.29
M00235981	PD	myc-low	2.24
M00235984	PD	myc-low	6.37
M00235991	PD	myc-low	0.59
M00235970	Control	myc-low	26.89
M00235973	Control	myc-low	31.54
M00235982	Control	myc-low	33.69
M00235983	Control	myc-low	25.49

Table C.4 Mean and standard deviation of percentage of IdU positive nuclei in tumour sections, taken on the third day after the commencement of treatment, for myc-high and myc-low sub-clones.

Treatment	Sub-clone	Mean	SD	Percentage SD
Control	myc-low	29.40	3.86	13.11
Control	myc-high	29.61	6.49	21.94
Lico	myc-low	10.82	7.19	66.50
Lico	myc-high	19.14	9.11	47.59
PD	myc-low	2.62	2.59	98.67
PD	myc-high	13.58	5.64	41.52
Double	myc-low	1.36	0.91	67.18
Double	myc-high	11.72	5.92	50.49

C.1.3 Apoptosis in Tumour Sections

Table C.5 Percentage of CC3 positive pixels in tumour sections, taken on the third day after the commencement of treatment, for myc-high and myc-low sub-clones.

Mouse	Treatment	Sub-clone	Percent CC3 positive pixels
M00235975	Double	myc-high	1.72
M00235977	Double	myc-high	1.94
M00235979	Double	myc-high	6.10
M00235969	Double	myc-high	4.92
M00235978	Lico	myc-high	1.62
M00235971	Lico	myc-high	0.30
M00235985	Lico	myc-high	1.30
M00235972	Lico	myc-high	0.43
M00235980	PD	myc-high	0.23
M00235981	PD	myc-high	1.42
M00235984	PD	myc-high	0.89
M00235991	PD	myc-high	1.83
M00235973	Control	myc-high	0.36
M00235970	Control	myc-high	0.23
M00235982	Control	myc-high	0.20
M00235983	Control	myc-high	0.35
M00235975	Double	myc-low	0.99
M00235977	Double	myc-low	0.88
M00235979	Double	myc-low	3.21
M00235969	Double	myc-low	1.14
M00235978	Lico	myc-low	0.19
M00235971	Lico	myc-low	0.24
M00235985	Lico	myc-low	0.90
M00235972	Lico	myc-low	1.18
M00235980	PD	myc-low	0.53
M00235981	PD	myc-low	0.98
M00235984	PD	myc-low	0.40
M00235991	PD	myc-low	0.37
M00235973	Control	myc-low	0.30
M00235970	Control	myc-low	0.11
M00235982	Control	myc-low	0.34
M00235983	Control	myc-low	0.33

Table C.6 Mean and standard deviation of percentage of CC3 positive pixels in tumour sections, taken on the third day after the commencement of treatment, for myc-high and myc-low sub-clones.

Treatment	Sub-clone	Mean	SD	Percentage SD
Control	myc-low	0.27	0.11	39.47
Control	myc-high	0.29	0.08	28.31
Lico	myc-low	0.63	0.49	78.04
Lico	myc-high	0.91	0.65	71.23
PD	myc-low	0.57	0.28	49.80
PD	myc-high	1.09	0.69	63.26
Double	myc-low	1.55	1.11	71.59
Double	myc-high	3.67	2.18	59.44

C.2 Linear Mixed Effects Modelling of Tumour Growth

C.2.1 Without Transformation

I fit a linear mixed effects model to account for the repeated measures of tumour growth made for each mouse. The fixed effects were application or absence of PD-0325901 (PD) and Licofelone (Lico), and the day of treatment (Day). The random effect was the mouse to which the treatment was applied.

I then use a residual (Figure C.1a) and quartile-quartile plot (Figure C.1b) to assess the model for adherence to the assumptions of homoscedasticity and normality respectively.

As residuals increase with fitted values, I apply a negative inverse transformation.

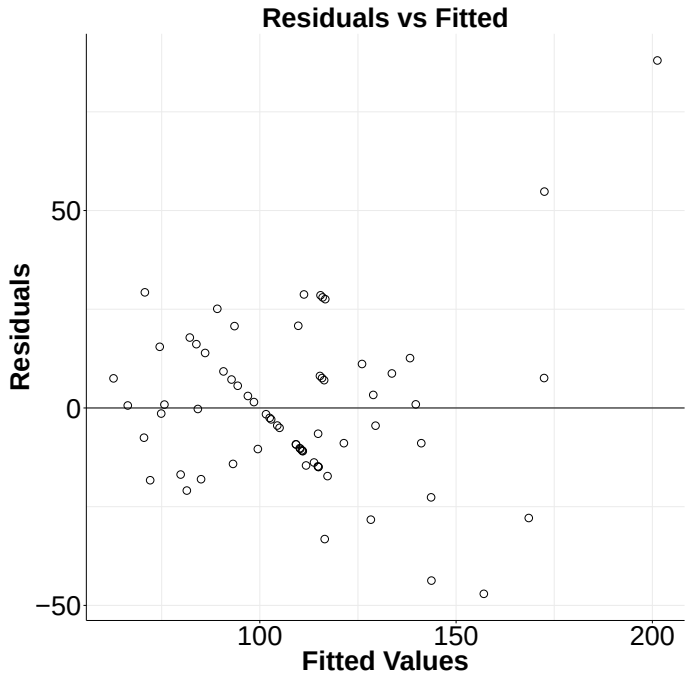

(a) Residuals vs fitted values for linear mixed effects model of tumour growth, measured as percentage change in volume, considering interactions.

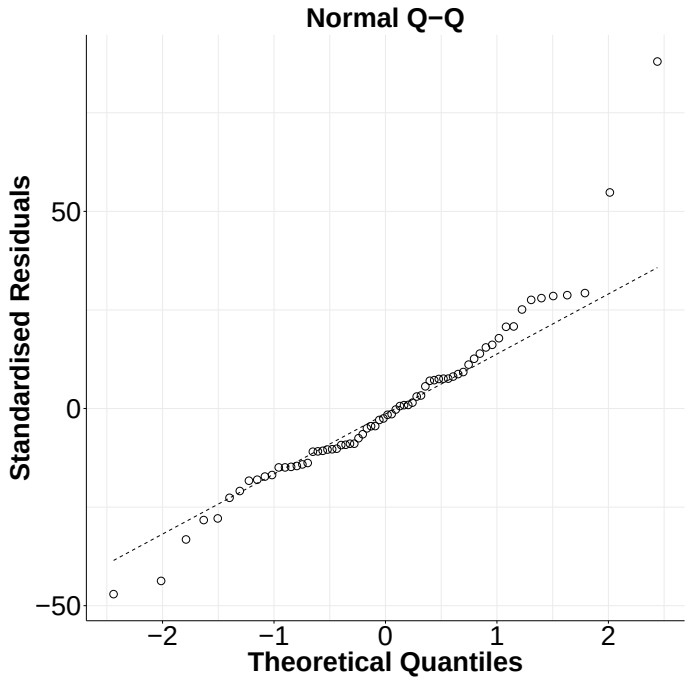

(b) Quantile-quantile plot of tumour growth, measured as percentage change in volume.

Fig. C.1 Residual and quantile-quantile plots for linear mixed effects model of tumour growth, measured as percentage change in volume, considering interactions.

Table C.7 Coefficients and estimators of fit for linear mixed effects model of negative inverse tumour growth, fit using REML. Numbers in brackets indicate standard errors.

	Linear mixed-effects model of tumour growth
(Intercept)	88.47029 (11.92543)
Day	28.78261 (5.29515)
PD1	23.82030 (16.86511)
Lico1	10.47563 (16.86511)
Day:PD1	−28.24910 (7.48847)
Day:Lico1	−16.55478 (7.48847)
PD1:Lico1	−24.96191 (23.24694)
Day:PD1:Lico1	6.68547 (10.32214)
AIC	604.13762
BIC	626.33270
Log Likelihood	-292.06881
Num. obs.	68
Num. groups: Mouse	17
Var: Mouse (Intercept)	176.32369
Var: Residual	560.77128

Table C.8 Coefficients and estimators of fit for linear mixed effects model of negative inverse tumour growth, fit using REML. Numbers in brackets indicate standard errors.

	Without Correlation
(Intercept)	−0.01053 (0.00081)
Day	0.00138 (0.00038)
PD1	0.00147 (0.00114)
Lico1	0.00045 (0.00114)
Day:PD1	−0.00139 (0.00054)
Day:Lico1	−0.00049 (0.00054)
PD1:Lico1	−0.00192 (0.00157)
Day:PD1:Lico1	−0.00084 (0.00074)
AIC	-544.04939
BIC	-521.85432
Log Likelihood	282.02470
Num. obs.	68
Num. groups: Mouse	17
Var: Mouse (Intercept)	0.00000
Var: Residual	0.00000

C.2.2 Negative Inverse Transformation

Fitted with REML, with growth now transformed by the negative inverse, this has parameters:

I then use a residual (Figure C.2a) and quartile-quartile plot (Figure C.2b) to assess the model for adherence to the assumptions of homoscedasticity and normality respectively.

The transformation has improved both the homoscedasticity of the data.

I then assess the significance of the contribution of the main effects and interactions in the model by conducting a Type III ANOVA with Satterthwaite's method [301], as detailed in Chapter 2.5.4.

As the third-way interaction is insignificant, I remove it, in line with the principle of marginality [339].

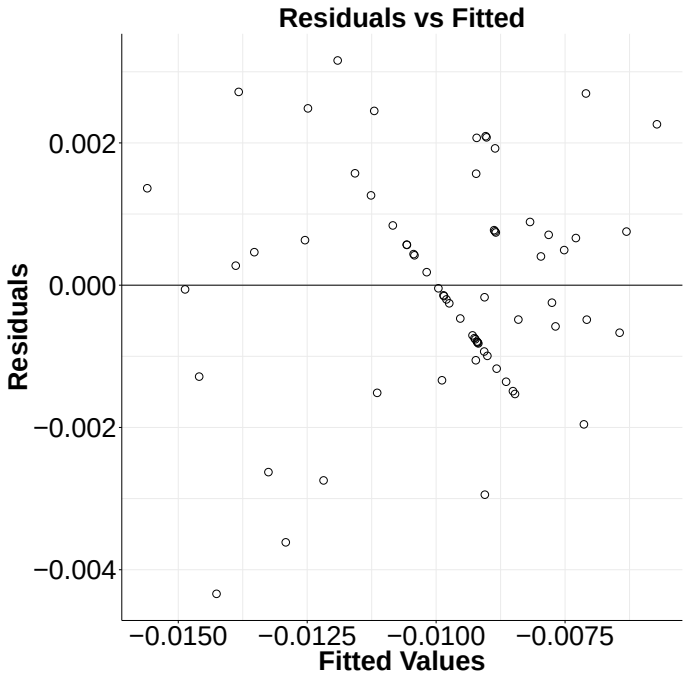

(a) Residuals vs fitted values for linear mixed effects model of negative inverse of tumour growth, measured as percentage change in volume, considering interactions.

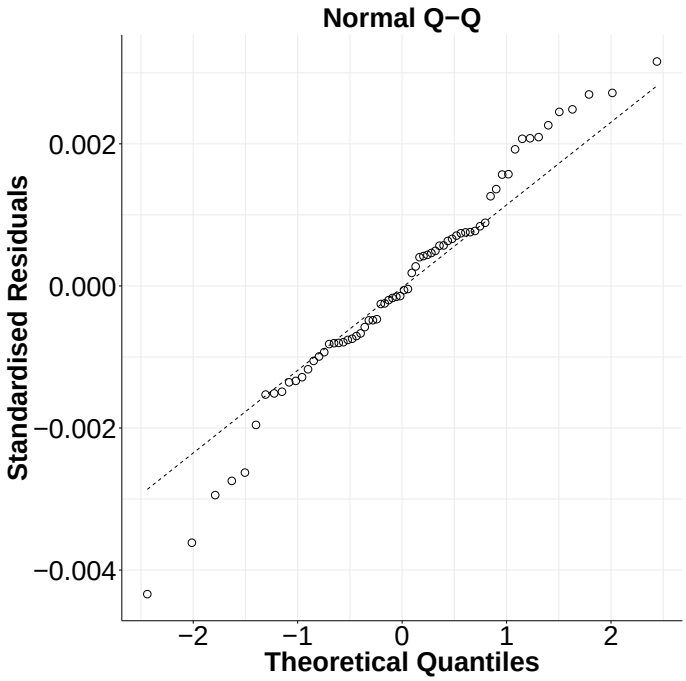

(b) Quantile-quantile plot of the negative inverse of tumour growth, measured as percentage change in volume.

Fig. C.2 Residual and quantile-quantile plot for linear mixed effects model of negative inverse of tumour growth, measured as percentage change in volume, considering interactions.

Table C.9 Type III Analysis of Variance Table with Satterthwaite's method for linear mixed effects model of negative inverse of tumour growth with all possible interactions.

	Sum Sq	Mean Sq	NumDF	DenDF	F value	Pr(>F)
Day	4.32E-06	4.32E-06	1	4.70E+01	1.51E+00	0.226
PD	1.21E-06	1.21E-06	1	4.03E+01	4.22E-01	0.519
Lico	1.20E-06	1.20E-06	1	4.03E+01	4.19E-01	0.521
Day:PD	6.91E-05	6.91E-05	1	4.70E+01	2.41E+01	0.000
Day:Lico	1.73E-05	1.73E-05	1	4.70E+01	6.04E+00	0.018
PD:Lico	4.29E-06	4.29E-06	1	4.03E+01	1.50E+00	0.228
Day:PD:Lico	3.71E-06	3.71E-06	1	4.70E+01	1.29E+00	0.261

Table C.10 Coefficients and estimators of fit for linear mixed effects model of negative inverse tumour growth, fit using REML. Numbers in brackets indicate standard errors.

	Without Correlation
(Intercept)	−0.01086 (0.00075)
Day	0.00160 (0.00033)
PD1	0.00214 (0.00098)
Lico1	0.00112 (0.00098)
PD1:Lico1	−0.00318 (0.00112)
Day:PD1	−0.00183 (0.00037)
Day:Lico1	−0.00093 (0.00037)
AIC	-557.34267
BIC	-537.36710
Log Likelihood	287.67134
Num. obs.	68
Num. groups: Mouse	17
Var: Mouse (Intercept)	0.00000
Var: Residual	0.00000

Remove marginal terms

Fitting without the interaction between *Day*, *PD* and *Lico*:

Residuals are shown in Figure C.3a and quartile-quartile plots in Figure C.3b.

In Table C.11 I assess the significance of the contribution of the main effects and interactions in the model by conducting a Type III ANOVA with Satterthwaite's method. This shows that there are significant effects from PD and Lico over time, as well as between PD and Lico. Assessing the the significance of the main effects, given that the interactions are significant, is likely to be misleading, due to the principle of marginality.

As there are significant interactions, I perform a pairwise comparison between the groups based on treatment regime, using least square means [193, 395] and correcting for multiple testing by Tukey's HSD test [448].

This shows a significant difference between the combination therapy $(1,1)$ and either of the single treatments (PD alone $1,0$ and Lico alone $0,1$) or control $(0,0)$.

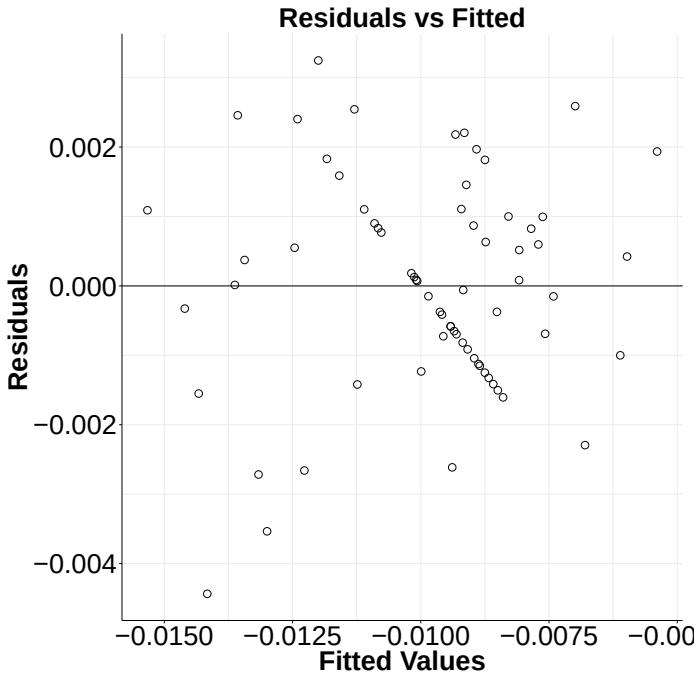

(a) Residuals vs fitted values for linear mixed effects model of negative inverse of tumour growth, measured as percentage change in volume, considering main effects and pairwise interactions.

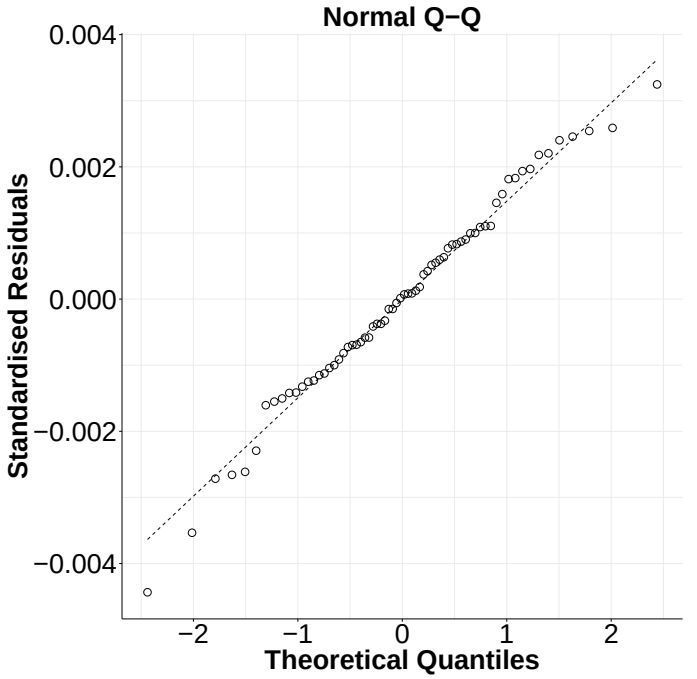

(b) Quantile-quantile plot of the negative inverse of tumour growth, measured as percentage change in volume.

Fig. C.3 Residual and quantile-quantile plots for linear mixed effects model of negative inverse of tumour growth, measured as percentage change in volume, considering main effects and pairwise interactions.

Table C.11 Type III Analysis of Variance Table with Satterthwaite's method for linear mixed effects model of negative inverse of tumour growth without third order interaction.

	Sum Sq	Mean Sq	NumDF	DenDF	F value	Pr(>F)
Day	3.92E-06	3.92E-06	1	4.80E+01	1.36E+00	0.24964
PD	1.38E-06	1.38E-06	1	4.06E+01	4.78E-01	0.49324
Lico	1.06E-06	1.06E-06	1	4.06E+01	3.66E-01	0.54850
PD:Lico	2.34E-05	2.34E-05	1	1.30E+01	8.12E+00	0.01369
Day:PD	7.10E-05	7.10E-05	1	4.80E+01	2.46E+01	0.00001
Day:Lico	1.82E-05	1.82E-05	1	4.80E+01	6.31E+00	0.01539

Table C.12 Pairwise comparison of treatments using least square means and TukeyHSD correction for multiple comparisons. Order of contrasts is PD, Lico with 0 indicating absence of drug and 1 indicating presence.

contrast	estimate	SE	df	t.ratio	p.value
0,0 - 1,0	0.0006	0.0008	13	0.758	0.8715
0,0 - 0,1	0.0003	0.0008	13	0.343	0.9855
0,0 - 1,1	0.0041	0.0008	13	5.300	0.0007
1,0 - 0,1	-0.0003	0.0008	13	-0.415	0.9748
1,0 - 1,1	0.0035	0.0008	13	4.501	0.0029
0,1 - 1,1	0.0038	0.0008	13	4.939	0.0014

P value adjustment: tukey method for comparing a family of 4 estimates

C.3 Welch's t-test comparing Proliferation and Apoptosis Between Sub-clones

C.3.1 Proliferation without transformation

I conduct a Welch's t-test [475] to compare the proliferation between the myc-low and myc-high sub-clones for different treatment regimes (see Tables C.3 and C.4). I adjust for multiple comparisons with Holm's method [209].

I first assess the normality of the data with a quantile-quantile plot, Fig. C.4.

As the data has a slight right skew, I apply a square-root transformation.

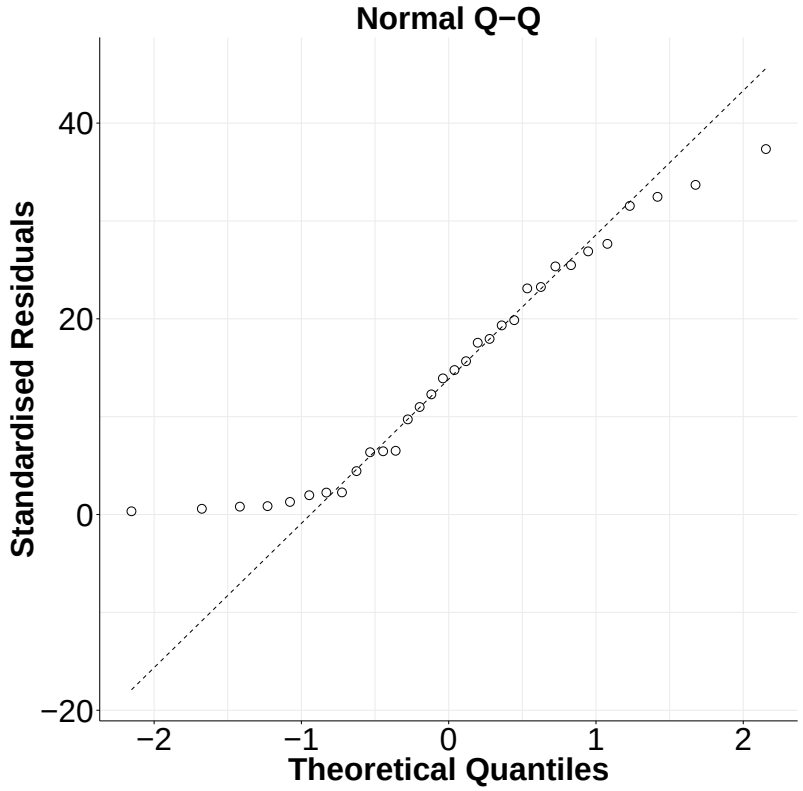

Fig. C.4 Quantile-quantile plot of the proliferation, measured as percentage IdU stained nuclei, in myc-low and myc-high sub-clones across all treatments.

C.3.2 Proliferation with square root transformation

I re-assess the normality of the data following square-root transformation (Fig. C.5), and judge it to be acceptable.

The results of the Welch's t-test and multiple testing correction is shown in Table C.13.

Table C.13 Paired Welch test for difference between myc-low and myc-high sub-clone proliferation, measured as percentage IdU stained nuclei.

Treatment	t	df	p	p.adj
Control	0.0075	3	0.99451	0.9945
Lico	8.5725	3	0.00334	0.0133
PD	5.1782	3	0.01398	0.0419
Double	3.4604	3	0.04063	0.0813

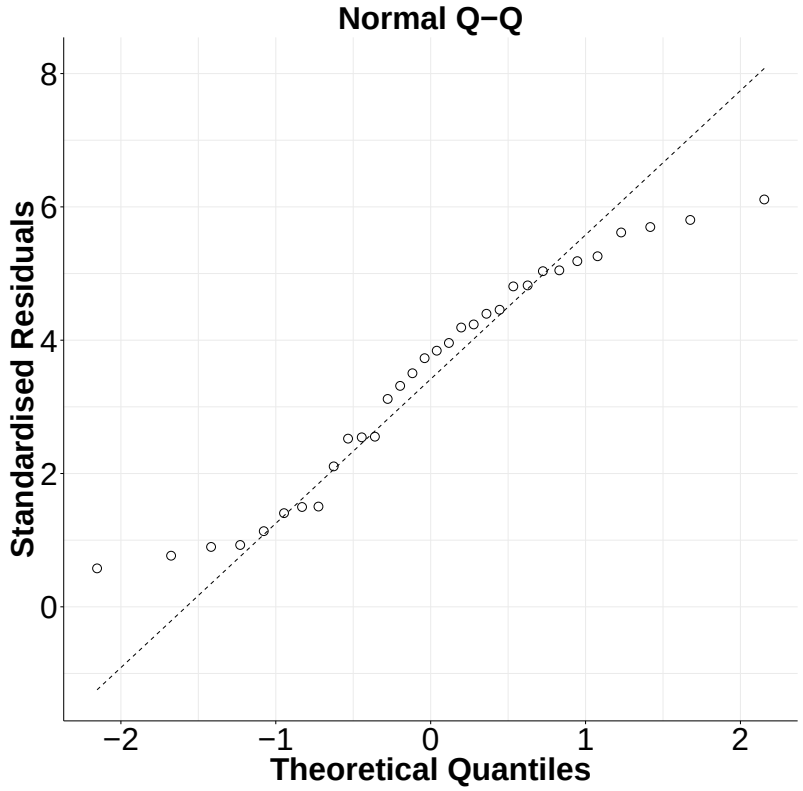

Fig. C.5 Quantile-quantile plot of the square root of proliferation, measured as percentage IdU stained nuclei, in myc-low and myc-high sub-clones across all treatments.

C.3.3 Apoptosis without transformation

I first assess the normality of the data with a quantile-quantile plot, Fig. C.6.

As there is a right-skew, I apply a log_{10} transformation.

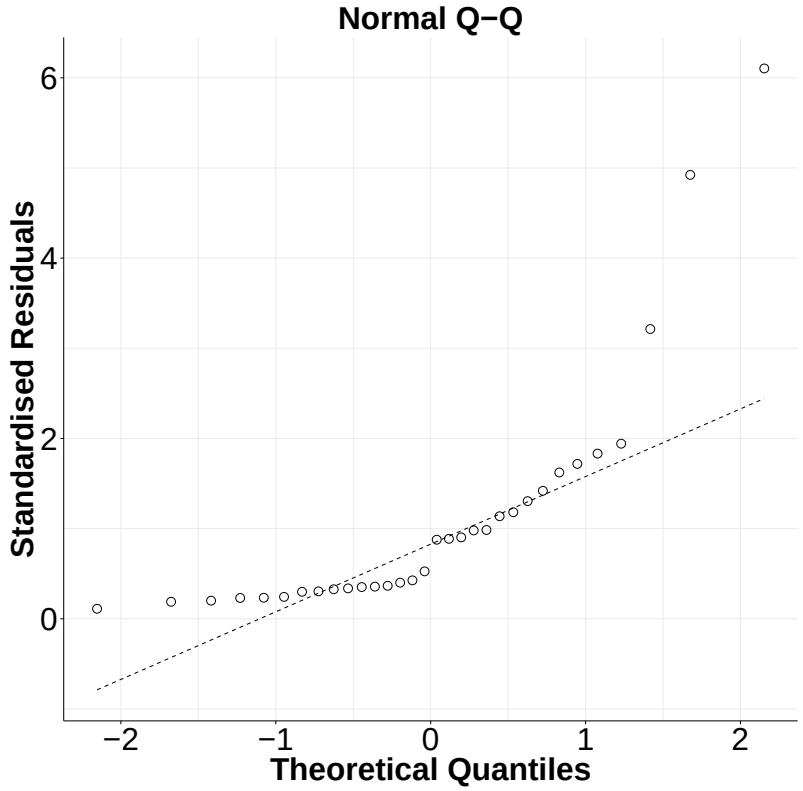

Fig. C.6 Quantile-quantile plot of apoptosis, measured as percentage CC3 positive-pixels, in myc-low and myc-high sub-clones across all treatments.

C.3.4 Apoptosis with log_{10} transformation

I re-assess the normality of the data following square-root transformation (Fig. C.7), and judge it to be acceptable.

The results of the Welch's t-test and multiple testing correction is shown in Table C.14.

Table C.14 Paired Welch test for difference between the log_{10} of myc-low and myc-high sub-clone apoptosis, measured as percentage CC3 positive-pixels.

Treatment	t	df	p	p.adj
Control	0.4320	3	0.6949	1.000
Lico	0.6546	3	0.5595	1.000
PD	0.9724	3	0.4026	1.000
Double	4.1909	3	0.0248	0.099

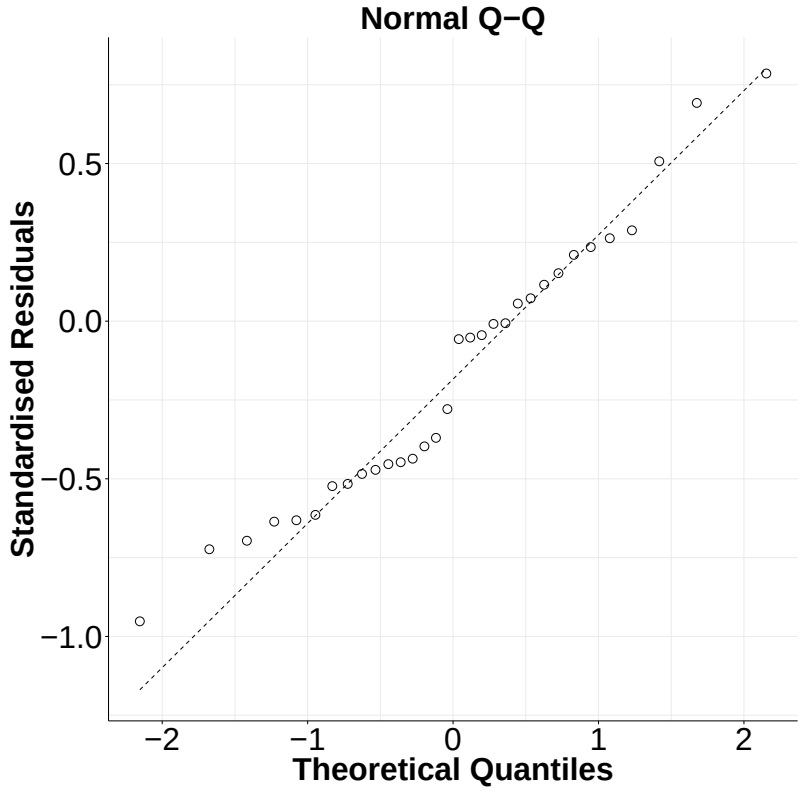

Fig. C.7 Quantile-quantile plot of log_{10} of apoptosis, measured as percentage CC3 positive-pixels, in myc-low and myc-high sub-clones across all treatments.

C.4 Two-Factor Analysis of Variance of Proliferation

I conducted two-factor Analysis of Variance (ANOVA) for the proliferation data (see Tables C.3 and C.4), with the presence or absence of treatment by PD or Lico being the factors.

C.4.1 Myc-low sub-clone

Interactive

The data conform to the assumptions of homoscedasticity (Fig. C.8a) and normality (Fig. C.8b) without transformation.

Table C.15 ANOVA for proliferation of the myc-low sub-clone measured as percentage IdU stained nuclei, considering interactions.

	Df	Sum Sq	Mean Sq	F value	Pr(>F)
PD	1	1313	1313	70.9	2.23E-06
Lico	1	394	394	21.3	6.00E-04
PD:Lico	1	300	300	16.2	1.69E-03
Residuals	12	222	19		

As the interaction term was significant, I consider the pairwise contrasts between the two factors, using TukeyHSD to correct for multiple comparisons (Table C.16).

Table C.16 Pairwise comparison of treatments using least square means and TukeyHSD correction for multiple comparisons. Order of contrasts is PD:Lico.

	diff	lwr	upr	p adj
1:0-0:0	-26.8	-35.8	-17.7	7.32E-06
0:1-0:0	-18.6	-27.6	-9.5	2.68E-04
1:1-0:0	-28.0	-37.1	-19.0	4.51E-06
0:1-1:0	8.2	-0.8	17.2	8.02E-02
1:1-1:0	-1.3	-10.3	7.8	9.75E-01
1:1-0:1	-9.5	-18.5	-0.4	3.93E-02

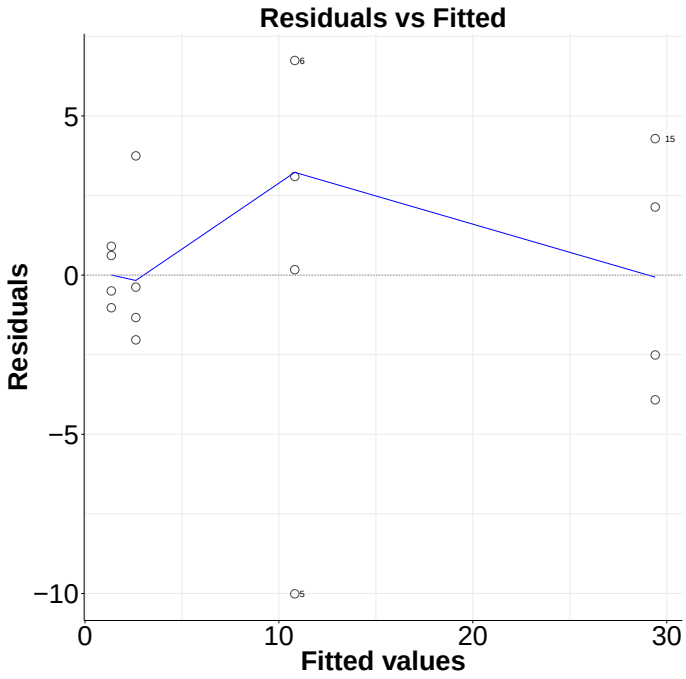

(a) Residuals vs fitted values for ANOVA of proliferation of the myc-low sub-clone, measured as percentage IdU stained nuclei, considering interactions.

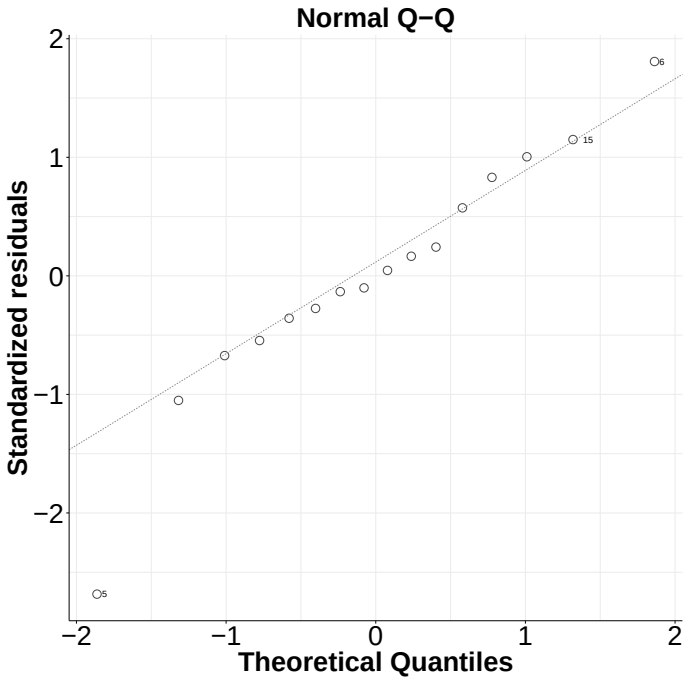

(b) Quantile-quantile plot of proliferation, measured as percentage IdU stained nuclei, in myc-low sub-clone across all treatments.

Fig. C.8 Residual and quantile-quantile plots for ANOVA of proliferation of the myc-low sub-clone, measured as percentage IdU stained nuclei, considering interactions.

C.4.2 Myc-high sub-clone

Interactive

The data conform to the assumptions of homoscedasticity (Fig. C.9a) and normality (Fig. C.9b) without transformation.

I first consider the model with an interaction term (Table C.17).

Table C.17 ANOVA for proliferation of the myc-high sub-clone measured as percentage IdU stained nuclei, considering interactions.

	Df	Sum Sq	Mean Sq	F value	Pr(>F)
PD	1	550	550	11.45	5.43E-03
Lico	1	152	152	3.17	1.01E-01
PD:Lico	1	74	74	1.54	2.38E-01
Residuals	12	576	48		

As the the interaction term is insignificant, I remove it according to the principle of marginality.

Additive

The data conform to the assumptions of homoscedasticity (Fig. C.10a) and normality (Fig. C.10b) without transformation.

The results of the ANOVA without the interaction term are shown in Table C.18.

Table C.18 ANOVA for proliferation of the myc-high sub-clone measured as percentage IdU stained nuclei, not considering interactions.

	Df	Sum Sq	Mean Sq	F value	Pr(>F)
PD	1	550	549.8	10.99	0.00558
Lico	1	152	151.9	3.04	0.10489
Residuals	13	650	50.0		

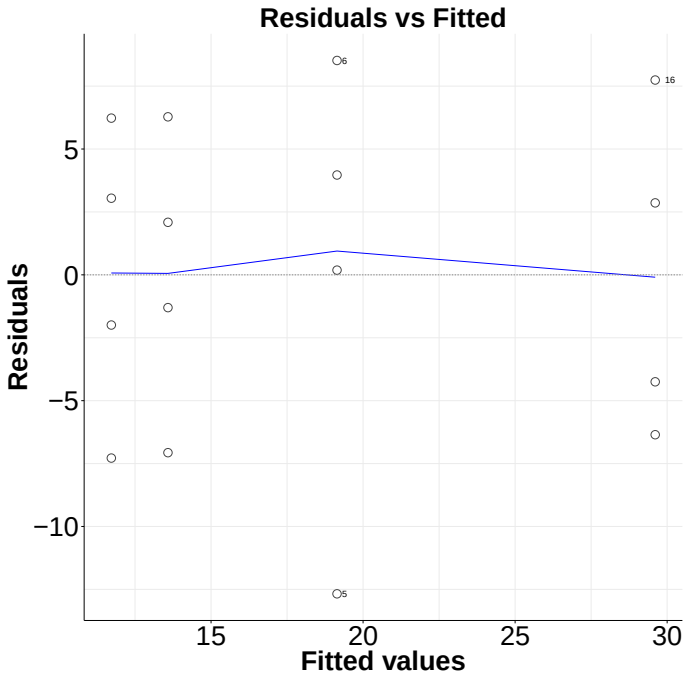

(a) Residuals vs fitted values for ANOVA of proliferation of the myc-high sub-clone, measured as percentage IdU stained nuclei, considering interactions.

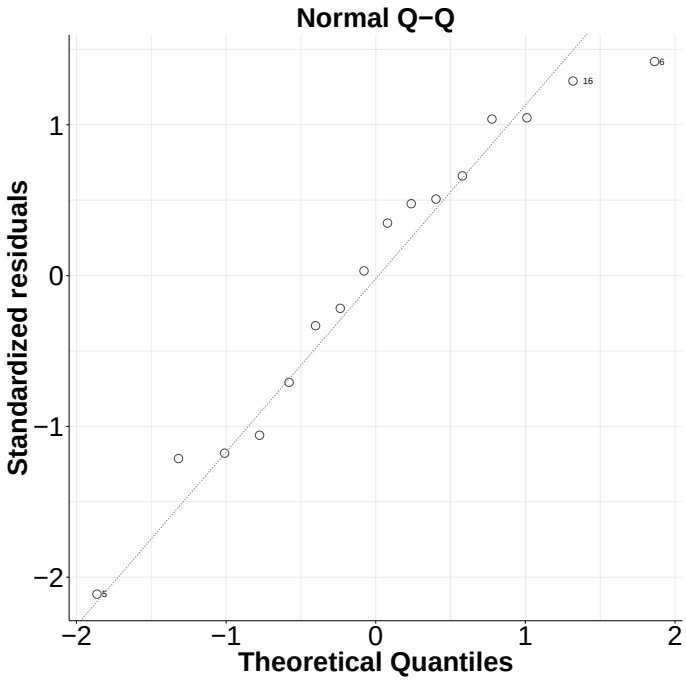

(b) Quantile-quantile plot of proliferation, measured as percentage IdU stained nuclei, in myc-high sub-clone across all treatments.

Fig. C.9 Residual and quantile-quantile plots for ANOVA of proliferation of the myc-high sub-clone, measured as percentage IdU stained nuclei, considering interactions.

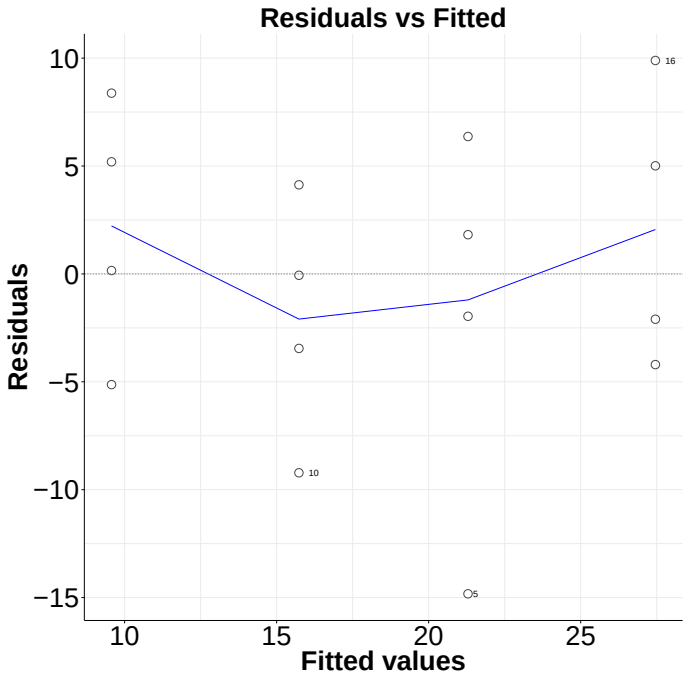

(a) Residuals vs fitted values for ANOVA of proliferation of the myc-high sub-clone, measured as percentage IdU stained nuclei, not considering interactions.

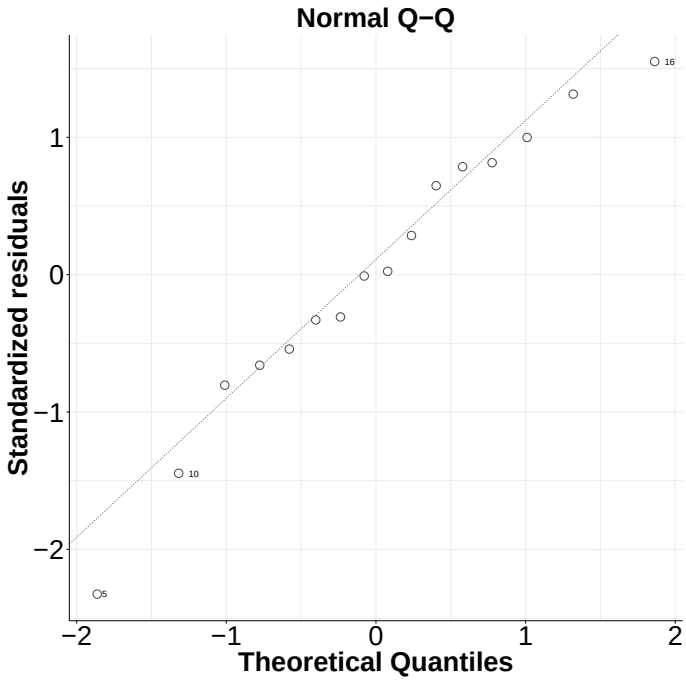

(b) Quantile-quantile plot of proliferation, measured as percentage IdU stained nuclei, in myc-high sub-clone across all treatments.

Fig. C.10 Residual and quantile-quantile plots for ANOVA of proliferation of the myc-high sub-clone, measured as percentage IdU stained nuclei, not considering interactions.

C.5 Two-Factor Analysis of Variance of Apoptosis

I conducted two-factor Analysis of Variance (ANOVA) for the apoptosis data (see Tables C.5 and C.6), with the presence or absence of treatment by PD or Lico being the factors.

C.5.1 Myc-low sub-clone

Interactive without transformation

The data do not conform to the assumptions of homoscedasticity (Fig. C.11a) and normality (Fig. C.11b) without transformation.

Due to high heteroscedasticity in Figure C.11a I apply a log_{10} transform.

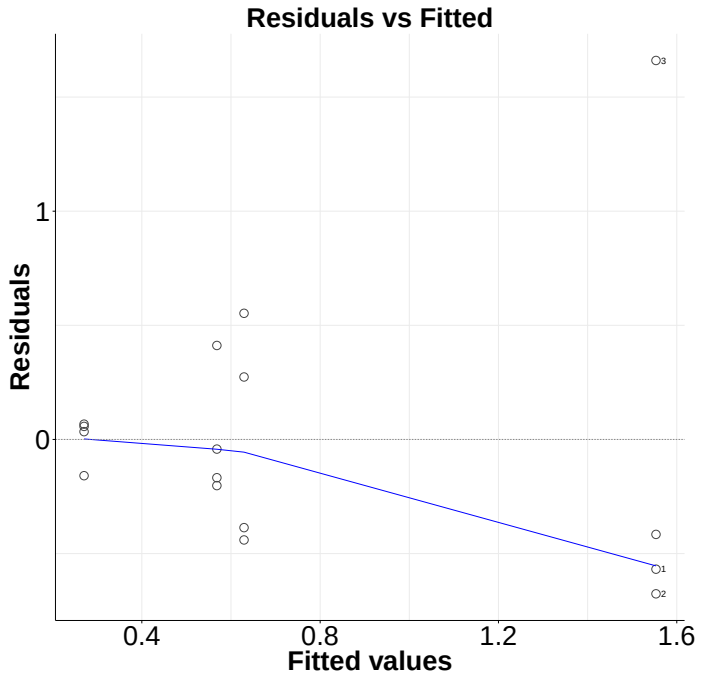

(a) Residuals vs fitted values for ANOVA of apoptosis of the myc-low sub-clone, measured as percentage CC3 positive-pixels, considering interactions.

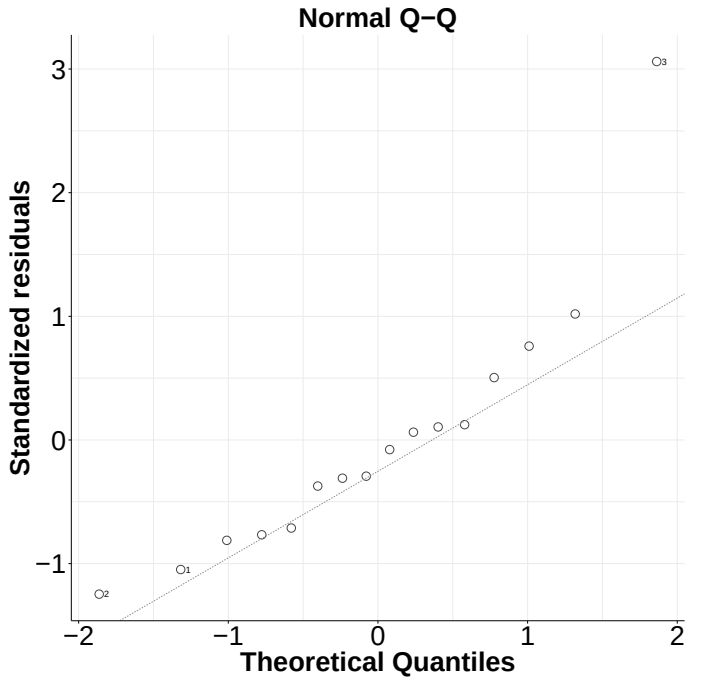

(b) Quantile-quantile plot of apoptosis, measured as percentage CC3 positive-pixels, in myc-low sub-clone across all treatments.

Fig. C.11 Residual and quantile-quantile plots for ANOVA of apoptosis of the myc-low sub-clone, measured as percentage CC3 positive-pixels, considering interactions.

Interactive with log_{10} transformation

The homoscedasticity (C.12a) is improved by this transformation.

Table C.19 shows that the interaction is not significant, so I remove it, in line with the principle of marginality.

Table C.19 ANOVA for log_{10} of apoptosis of the myc-low sub-clone measured as percentage CC3 positive-pixels, considering interactions.

	Df	Sum Sq	Mean Sq	F value	Pr(>F)
PD	1	0.6055	0.6055	7.626	0.0172
Lico	1	0.4676	0.4676	5.889	0.0319
PD:Lico	1	0.0160	0.0160	0.201	0.6618
Residuals	12	0.9528	0.0794		

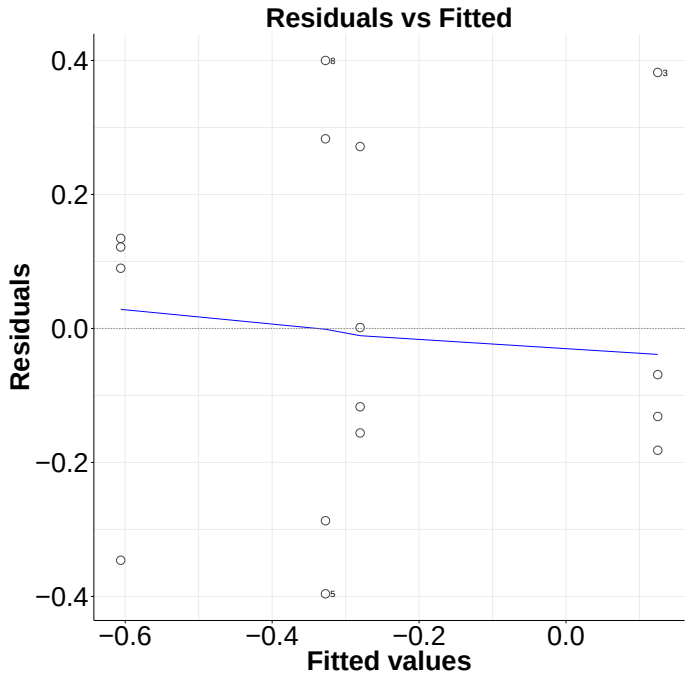

(a) Residuals vs fitted values for ANOVA of log_{10} apoptosis of the myc-low sub-clone, measured as percentage CC3 positive-pixels, considering interactions.

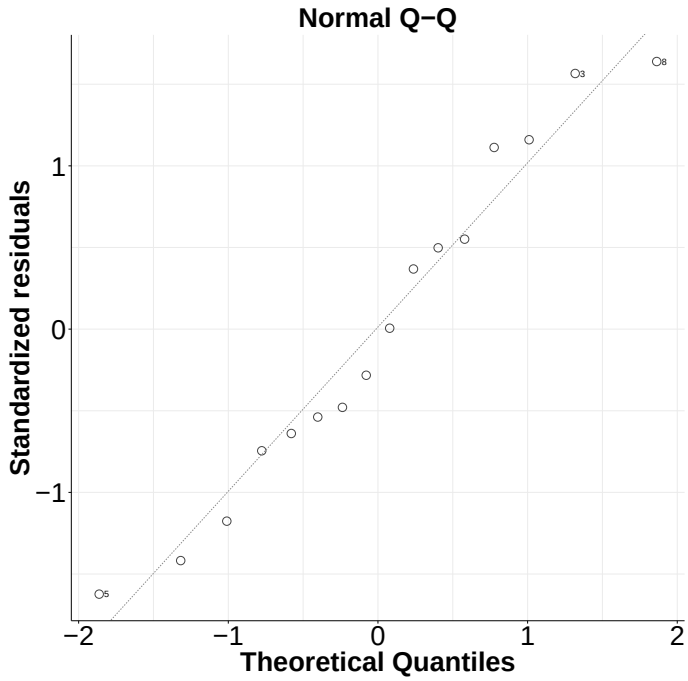

(b) Quantile-quantile plot of log_{10} apoptosis, measured as percentage CC3 positive-pixels, in myc-low sub-clone across all treatments.

Fig. C.12 Residual and quantile-quantile plots for ANOVA of log_{10} apoptosis of the myc-low sub-clone, measured as percentage CC3 positive-pixels, considering interactions.

Additive with log_{10} transformation

The data conform to the assumptions of homoscedasticity (Fig. C.13a) and normality (Fig. C.13b) without an interaction term.

The results of the ANOVA without the interaction term are shown in Table C.20.

Table C.20 ANOVA for log_{10} apoptosis of the myc-low sub-clone measured as percentage CC3 positive-pixels, not considering interactions.

	Df	Sum Sq	Mean Sq	F value	Pr(>F)
PD	1	0.606	0.606	8.125	0.0136
Lico	1	0.468	0.468	6.275	0.0263
Residuals	13	0.969	0.075		

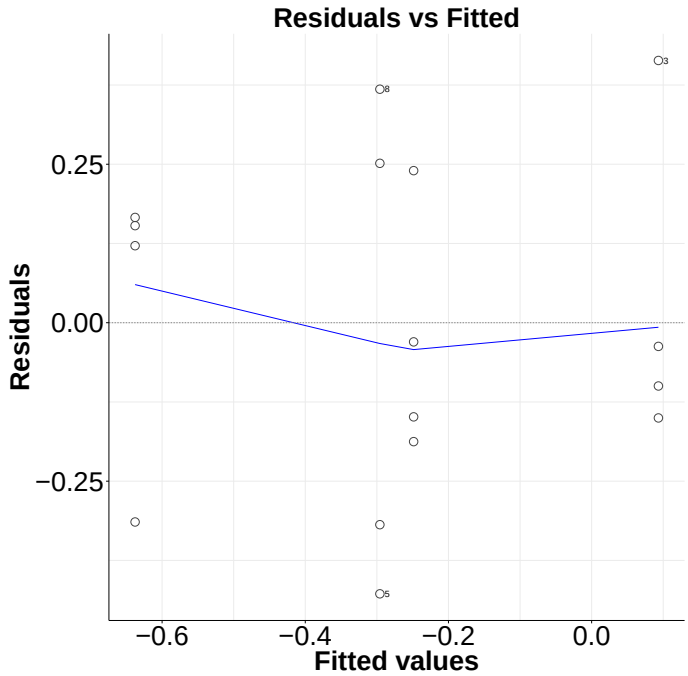

(a) Residuals vs fitted values for ANOVA of log_{10} apoptosis of the myc-low sub-clone, measured as percentage CC3 positive-pixels, not considering interactions.

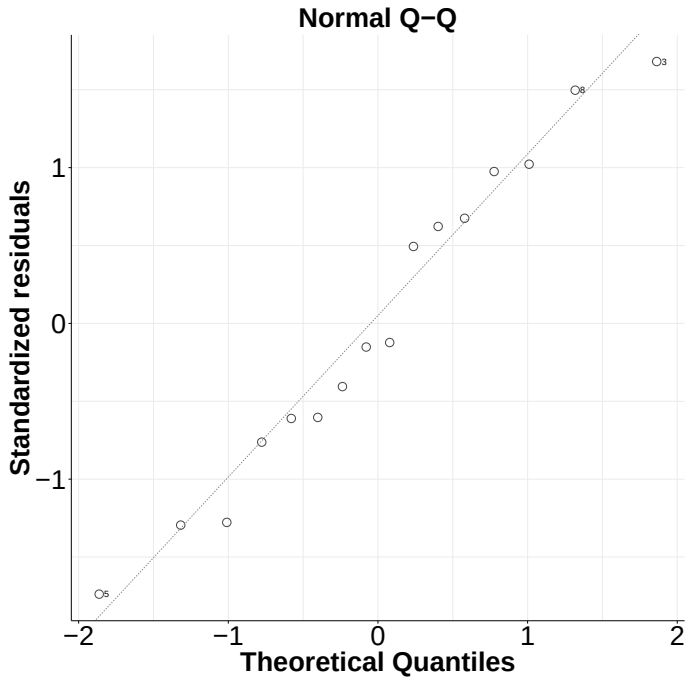

(b) Quantile-quantile plot of log_{10} apoptosis, measured as percentage CC3 positive-pixels, in myc-low sub-clone across all treatments.

Fig. C.13 Residual and quantile-quantile plots for ANOVA of log_{10} apoptosis of the myc-low sub-clone, measured as percentage CC3 positive-pixels, not considering interactions.

C.5.2 Myc-high sub-clone

Interactive without transformation

The data do not conform to the assumptions of homoscedasticity (Fig. C.14a) and normality (C.14b) without transformation.

Due to high heteroscedasticity in Figure C.14a I apply a log_{10} transform.

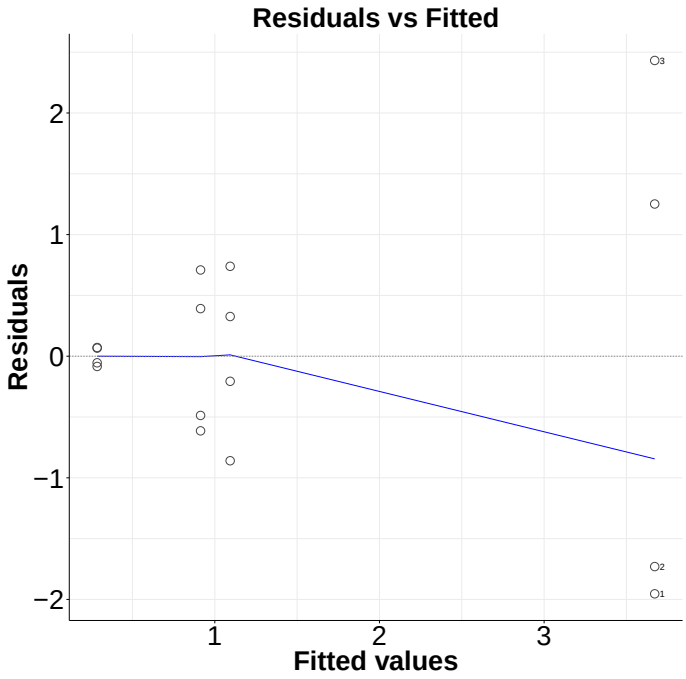

(a) Residuals vs fitted values for ANOVA of apoptosis of the myc-high sub-clone, measured as percentage CC3 positive-pixels, considering interactions.

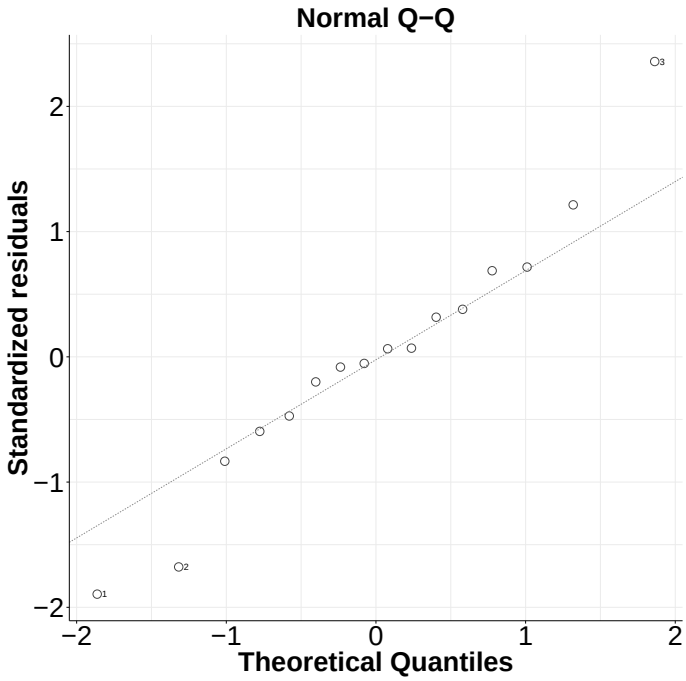

(b) Quantile-quantile plot of apoptosis, measured as percentage CC3 positive-pixels, in myc-high sub-clone across all treatments.

Fig. C.14 Residual and quantile-quantile plots for ANOVA of apoptosis of the myc-high sub-clone, measured as percentage CC3 positive-pixels, considering interactions.

Interactive with $log10$ transformation

The homoscedasticity (C.15a) is improved by this transformation.

As with the myc-low sub-clone, the interaction term is insignificant (see Table C.21) and so I remove it.

Table C.21 ANOVA for log_{10} apoptosis of the myc-high sub-clone measured as percentage CC3 positive-pixels, considering interactions.

	Df	Sum Sq	Mean Sq	F value	Pr(>F)
PD	1	1.2845	1.2845	13.455	0.00322
Lico	1	0.9678	0.9678	10.138	0.00786
PD:Lico	1	0.0228	0.0228	0.239	0.63396
Residuals	12	1.1456	0.0955		

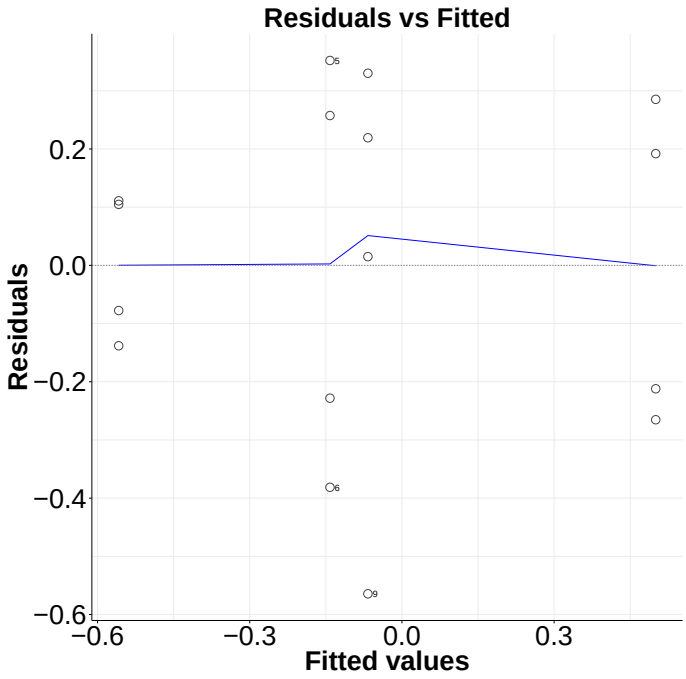

(a) Residuals vs fitted values for ANOVA of log_{10} apoptosis of the myc-high sub-clone, measured as percentage CC3 positive-pixels, considering interactions.

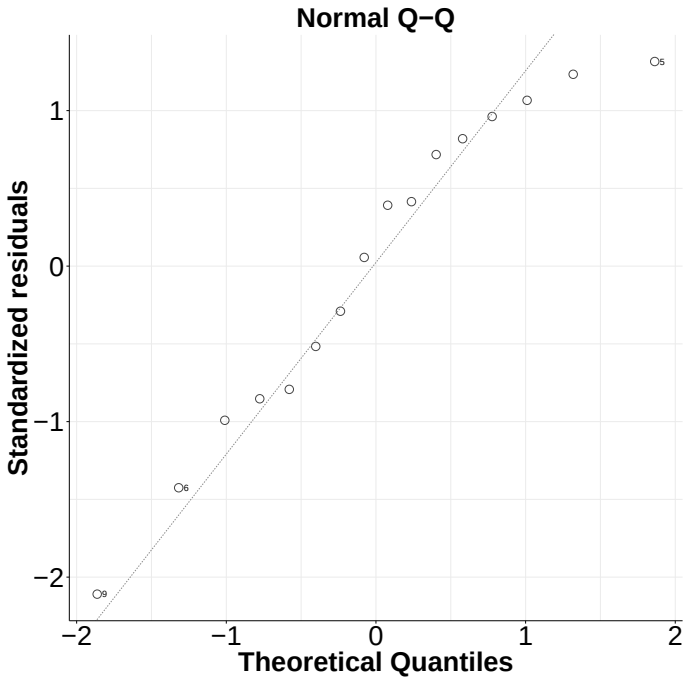

(b) Quantile-quantile plot of log_{10} apoptosis, measured as percentage CC3 positive-pixels, in myc-high sub-clone across all treatments.

Fig. C.15 Residual and quantile-quantile plots for ANOVA of log_{10} apoptosis of the myc-high sub-clone, measured as percentage CC3 positive-pixels, considering interactions.

Additive model with log_{10} transform

The data conform to the assumptions of homoscedasticity (Fig. C.16a) and normality (Fig. C.16b) without an interaction term.

The results of the ANOVA without the interaction term are shown in Table C.22.

Table C.22 ANOVA for log_{10} apoptosis of the myc-high sub-clone measured as percentage CC3 positive-pixels, not considering interactions.

	Df	Sum Sq	Mean Sq	F value	Pr(>F)
PD	1	1.285	1.285	14.292	0.00229
Lico	1	0.968	0.968	10.769	0.00595
Residuals	13	1.168	0.090		

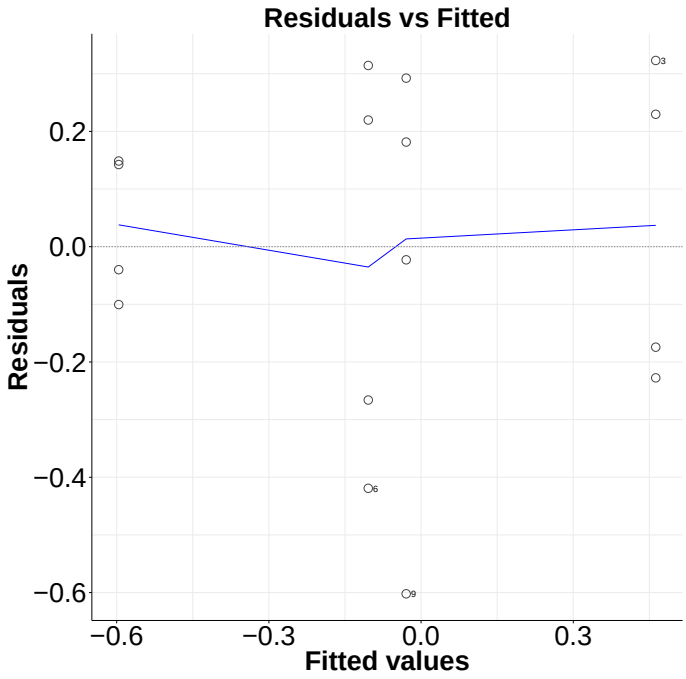

(a) Residuals vs fitted values for ANOVA of log_{10} apoptosis of the myc-high sub-clone, measured as percentage CC3 positive-pixels, not considering interactions.

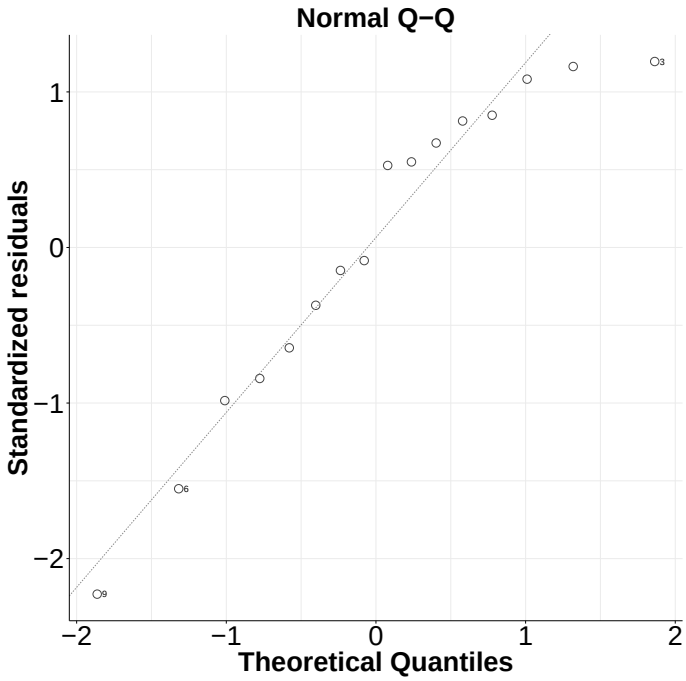

(b) Quantile-quantile plot of log_{10} apoptosis, measured as percentage CC3 positive-pixels, in myc-high sub-clone across all treatments.

Fig. C.16 Residual and quantile-quantile plots for ANOVA of log_{10} apoptosis of the myc-high sub-clone, measured as percentage CC3 positive-pixels, not considering interactions.

Appendix D

Log of Major Changes to the Network

Table D.1 A history of the major changes made to the model as it was built and tested, as described in Chapter 3. Shows the version which was changed, the new version that resulted, a brief summary of the aims of the changes, and details of the specific change for each node.

Version		Summary of Change	Node	Change from	Change to
From	To				
	1	First draft of network	EGF		Added, Target Function: $avg(pos) - avg(neg)$, Range: 0-2
					Activatory edge to EGF Receptor
			TGFBeta		Added, Target Function: $avg(pos) - avg(neg)$, Range: 0-2
					Activatory edge to EGF-Beta-Receptor
			EGF-Receptor		Added, Target Function: $avg(pos) - avg(neg)$, Range: 0-2
					Activatory edge to Myc
					Activatory edge to Fibronectin
			TGF-Beta-Receptor		Added, Target Function: $avg(pos) - avg(neg)$, Range: 0-2
					Inhibitory edge to Myc
					Activatory edge to Mad
					Activatory edge to COL3A1
					Activatory edge to Fibronectin
					Activatory edge to pINK4b/CDKN2B
			Myc		Added, Target Function: $avg(pos) - avg(neg)$, Range: 0-2
					Inhibitory edge to p21
					Activatory edge to MycMax
			Max		Added, Target Function: $const(2)$, Range: 0-2

Table D.1 continued from previous page

	Activatory edge to MycMax
	Activatory edge to MadMax
Mad	Added, Target Function: $avg(pos) - avg(neg)$, Range: 0-2
	Activatory edge to MadMax
MycMax	Added, Target Function: $min(var(Myc), var(Max)) - var(MadMax)$, Range: 0-2
	Activatory edge to alpha prothymosin
	Activatory edge to TRAP1
	Activatory edge to eIF4E
	Inhibitory edge to Differentiation
	Inhibitory edge to COL3A1
	Inhibitory edge to Fibronectin
	Activatory edge to cdk4
	Activatory edge to Miz1MycMax
	Inhibitory edge to MadMax
MadMax	Added, Target Function: $min(var(Mad), var(Max)) - var(MycMax)$, Range: 0-2
	Inhibitory edge to MadMax
CD95/Fas	Added, Target Function: $max((var(CD95L) * var(MycMax)), var(CD95L))$, Range: 0-2
	Activatory edge to Apoptosis
CD95L	Added, Target Function: $avg(pos) - avg(neg)$, Range: 0-2

Table D.1 continued from previous page

		Activatory edge to CD95/Fas
	p21	Added, Target Function: $avg(pos) - avg(neg)$, Range: 0-2
		Inhibitory edge to Proliferation
	alpha prothymosin	Added, Target Function: $avg(pos) - avg(neg)$, Range: 0-2
		Activatory edge to proliferation
	TRAP1	Added, Target Function: $avg(pos) - avg(neg)$, Range: 0-2
		Inhibitory edge to apoptosis
	eIF4E	Added, Target Function: $avg(pos) - avg(neg)$, Range: 0-2
		Activatory edge to Protein Synthesis
	COL3A1	Added, Target Function: $avg(pos) - avg(neg)$, Range: 0-2
		Activatory edge to Cell Adhesion
	Fibronectin	Added, Target Function: $avg(pos) - avg(neg)$, Range: 0-2
		Activatory edge to Cell Adhesion
	cdk4	Added, Target Function: $avg(pos) - avg(neg)$, Range: 0-2
		Inhibitory edge to senescence
	Miz1	Added, Target Function: $const(2)$, Range: 0-2
		Activatory edge to Miz1MycMax
		Activatory edge to pINK4b/CDKN2B

Table D.1 continued from previous page

			Miz1MycMax		Added, Target Function: $min(var(Miz1), var(MycMax))$, Range: 0-2
			pINK4b/CDKN2B		Added, Target Function: $avg(pos) - avg(neg)$, Range: 0-2
					Inhibitory edge to cdk4
			Proliferation		Added, Target Function: $avg(pos) - avg(neg)$, Range: 0-2
			Apoptosis		Added, Target Function: $avg(pos) - avg(neg)$, Range: 0-2
			Protein Synthesis		Added, Target Function: $avg(pos) - avg(neg)$, Range: 0-2
			Differentiation		Added, Target Function: $avg(pos) - avg(neg)$, Range: 0-2
			Cell Adhesion		Added, Target Function: $avg(pos) - avg(neg)$, Range: 0-2
			Senescence		Added, Target Function: $avg(pos) - avg(neg)$, Range: 0-2
1	2	No feedback from Miz1MycMax to Miz1 and MycMax to reflect the depletion of the latter two in the formation of the trimer	MycMax	$min(var(Myc), var(Max)) - var(MadMax)$	$min(var(Myc), var(Max)) - var(MadMax) - var(Miz1MycMax)$
			Miz1	$avg(pos) - avg(neg)$	$2 - var(Miz1MycMax)$
2	3	Given that Myc, Max, and Mad are not depleted by formation of dimers, neither should activity of Miz1 be affected by the formation of the MycMaxMiz1 trimer	Miz1	$2 - var(Miz1MycMax)$	$avg(pos) - avg(neg)$

Table D.1 continued from previous page

3	4	Given the correct conditions, MycMax, MadMax and Miz1MycMax can lock up	MycMax	$min(var(Myc), var(Max)) - var(MadMax) - var(Miz1MycMax)$	$min(var(Myc), var(Max)) - min(var(Mad), var(Max)) - min(min(var(Myc), var(Max)), var(Miz1))$
		Also added dependency on Miz1MycMax to MadMax as it must compete with this trimer for Max, if not Myc or Miz1	MadMax	$min(var(Mad), var(Max)) - var(MycMax)$	$min(var(Mad), var(Max)) - min(var(Myc), var(Max)) - min(min(var(Myc), var(Max)), var(Miz1))$
			Miz1MycMax	$min(var(Miz1), var(MycMax))$	$min(min(var(Myc), var(Max)), var(Miz1)) - min(var(Myc), var(Max)) - min(var(Mad), var(Max))$
		Miz1 had no target function	Miz1	$avg(pos) - avg(neg)$	$2 - var(MycMaxMiz1)$
4	5	Addition of Ras network	EGFR		Added, Target Function: $avg(pos) - avg(neg)$, Range: 0-2
					Activatory edge to Ras
			Ras		Added, Target Function: $avg(pos) - avg(neg)$, Range: 0-2
					Activatory edge to Raf-1
					Activatory edge to Akt
			PI3K		Added, Target Function: $avg(pos) - avg(neg)$, Range: 0-2
					Activatory edge to Akt
			Raf-1		Added, Target Function: $avg(pos) - avg(neg)$, Range: 0-2

Table D.1 continued from previous page

	Activatory edge to Mek
Akt	Added, Target Function: $avg(pos) - avg(neg)$, Range: 0-2
	Inhibitory edge to p21
	Inhibitory edge to GSK3
	Inhibitory edge to Bad
	Inhibitory edge to Caspase9
Mek	Added, Target Function: $avg(pos) - avg(neg)$, Range: 0-2
	Activatory edge to Erk
Caspase9	Added, Target Function: $avg(pos) - avg(neg)$, Range: 0-2
	Activatory edge to Caspase9
Bad	Added, Target Function: $avg(pos) - avg(neg)$, Range: 0-2
	Activatory edge Apoptosis
BIM	Added, Target Function: $avg(pos) - avg(neg)$, Range: 0-2
	Activatory edge to Apoptosis
Bcl-2	Added, Target Function: $avg(pos) - avg(neg)$, Range: 0-2
	Inhibitory edge to Bim
Ets-1	Added, Target Function: $avg(pos) - avg(neg)$, Range: 0-2
	Activatory edge to p16
GSK3	Added, Target Function: $avg(pos) - avg(neg)$, Range: 0-2
	Inhibitory edge to CDK4_CyclinD

Table D.1 continued from previous page

			Rsk	Added, Target Function: $avg(pos) - avg(neg)$, Range: 0-2
				Inhibitory edge to GSK3
			Elk-1	Added, Target Function: $avg(pos) - avg(neg)$, Range: 0-2
				Activatory edge c-Fos
			c-Fos	Added, Target Function: $avg(pos) - avg(neg)$, Range: 0-2
				Activatory edge to Myc
			ERF	Added, Target Function: $avg(pos) - avg(neg)$, Range: 0-2
				Inhibitory edge to Myc
			p27	Added, Target Function: $avg(pos) - avg(neg)$, Range: 0-2
				Inhibitory edge CDK4_CyclinD
			p16	Added, Target Function: $avg(pos) - avg(neg)$, Range: 0-2
				Inhibitory edge CDK4_CyclinD
			Erk	Added, Target Function: $avg(pos) - avg(neg)$, Range: 0-2
				Activatory edge to Myc
				Inhibitory edge to ERF
5	6	Addition of pathway to allow Ras to regulate extrinsic (Fas) apoptosis via PI(3)K pathway.	FoxO	Added, Target Function: $avg(pos) - avg(neg)$, Range: 0-2
				Activatory edge to CD95L
			JNK	Added, Target Function: $avg(pos) - avg(neg)$, Range: 0-2

Table D.1 continued from previous page

				Activatory edge to STAT3
				Activatory edge to c-jun
			STAT3	Added, Target Function: $avg(pos) - avg(neg)$, Range: 0-2
				Activatory edge to STAT3_c-jun
			c-jun	Added, Target Function: $avg(pos) - avg(neg)$, Range: 0-2
				Activatory edge to STAT3_c-jun
			STAT3_c-jun	Added, Target Function: $min(var(STAT3), var(c-jun))$, Range 0-2
				Activatory edge to CD95
			CD95	Added, Target Function: $avg(pos) - avg(neg)$, Range: 0-2
				Activatory edge to CD95_CD95L
			CD95_CD95L	Added, Target Function: $min(var(CD95), var(CD95L))$, Range: 0-2
				Activatory edge to apoptosis
			Akt	Inhibitory edge to FoxO
			Akt	Inhibitory edge to JNK
6	7	Addition of p53 Core	p53	Constitutively expressed at 2
			p53_active	$avg(pos) - avg(neg)$
			mdm2	$avg(pos) - avg(neg)$
			p14ARF	$avg(pos) - avg(neg)$
			p14ARF	Myc now upregulates
			p21	Now upregulated by p53_active
			CDK2	Added and now suppressed by p21

Table D.1 continued from previous page

			Growth Arrest		Now suppressed by CDK2
			PUMA		Added and activated by p53_active, and activates Apoptosis
			BAX		Added and activated by p53_active, and activates Apoptosis
			Noxa		Added and activated by p53_active, and activates Apoptosis
			mdm2		Erk now upregulates mdm2
			Rb		Added, and has Target Function 2-var(pRb) to show that these two convert into one another. Currently effectively Constitutively expressed.
			pRB		Upregulated by CDK4, supresses Rb and upregulates E2F1
			E2f-1		Upregulated by pRb and upregulates ARF
			CDK4		Now upregulated by Erk and upregulates pRb
7	8	Test change to connection of E2F-1	E2F-1	Connected to ARF	Now connects directly to p53_active due to evidence laid out in \citet{Lindstrom2003}
8	9	Simplifications to pathways which were half-implemented	Akt		Removed a downregulatory edge between Akt and Ras.
			Bax		Temporarily removed
			Noxa		Temporarily removed
			CDK2		Temporarily removed
			Caspase-9 and Akt	Akt downregulates Caspase9 which upregulates Apoptosis	Removed Caspase9 and now Akt directly downregulates apoptosis
			Miz1		Temporarily disabled

Table D.1 continued from previous page

9	10		MycMax and MadMax	Target function was essentially: $(myc*myc)/(myc+max)$	$ceil(var(Myc)/2) - ceil(var(Myc)/2) * (1 - floor(var(Myc)/2)) * floor(var(Mad)/2) + floor(var(Myc)/2) * (1 - ceil(var(Mad)/2))$
			MycMax and MadMax	Target function was essentially: $(myc*myc)/(myc+max)$	$ceil(var(Mad)/2) - ceil(var(Mad)/2) * (1 - floor(var(Mad)/2)) * floor(var(Myc)/2) + floor(var(Mad)/2) * (1 - ceil(var(Myc)/2))$
10	11		Apoptosis	$avg(pos) - avg(neg)$	$var(Bim) + var(Bad) + var(CD95\_CD95L) + var(PUMA) - var(TRAP1) - var(Akt)$
11	12	Bcl-2 currently redundant	Bcl2	Present, connecting to Bad and Bim (inhibitory)	Removed
		Change connection to Bim	Bim, Myc, MycMax	Connection from Myc to Bim	Connection from MycMax to Bim
		Remove redundant link from p21 to Growth arrest as via CDK4	p21, CDK4_CyclinD	p21 upregulates growth arrest and down regulates CDK4_CyclinD	p21 only downregulates CDK4_CyclinD
		Change Target Function of Growth Arrest node	Growth Arrest	$avg(pos) - avg(neg)$	$2 - var(CDK4\_CyclinD)$
		Renamed alpha prothymosin to PTMA and removed all underscores in node names			

Table D.1 continued from previous page

12	13	Change MycMax and MadMax target functions simplified without functional change	MycMax	$ceil(var(Myc)/2) - ceil(var(Myc)/2) * (1 - floor(var(Myc)/2)) * floor(var(Mad)/2) + floor(var(Myc)/2) * (1 - ceil(var(Mad)/2))$	$min(var(Myc), var(Max)) - min(1, floor(min(var(Myc), var(Max)) * min(var(Mad), var(Max))/2))$
			MadMax	$ceil(var(Mad)/2) - ceil(var(Mad)/2) * (1 - floor(var(Mad)/2)) * floor(var(Myc)/2) + floor(var(Mad)/2) * (1 - ceil(var(Myc)/2))$	$min(var(Mad), var(Max)) - min(1, floor(min(var(Mad), var(Max)) * min(var(Myc), var(Max))/2))$
		Avoids double negative connection	JNK	$avg(pos) - avg(neg)$	$2 - var(Akt)$
13	14	Added first parts of Wnt Pathway	Wnt		Added
			LRP		Added
			Frizzled		Added
			Dishevelled		Added
			Beta Catenin		Added
			TCF		Added
			Axin		Added
			APC		Added
			Ck1		Added
14	15	Added Rest of Wnt Pathway	ROR2		Added
			rac1		Added

Table D.1 continued from previous page

			DAAM1		Added
			Prolifin		Added
			Rho		Added
			ROCK		Added
			TCF		Added
			Invasiveness		Added
15	16	Added HER2 Pathway	NRG		Added
			HER2		Added
			ErbB3		Added
			ErbB3-HER		Added
			EGFR	$avg(pos) - avg(neg)$	$var(HER2) * var(EGF)$
			PI3K	Upregulated by Ras	Upregulated by ErbB3-HER2
16	17	Merged GSK3, Axin, Apc and CK1 nodes into one degradation complex	GSK3-Axin-APC-CK1	Were separate Nodes	Combined, although there is still a separate GSK3
		Corrected effect of GSK3-Axin-APC-CK1 on Beta-catenin, Did not rise unless degraded	Beta-Catenin		$2 - var(GSK3 - Axin - APC - CK1)$
17	18	Made Myc Target Function more sensitive, avg function could not handle more than 10 inputs	Myc	$avg(pos) - avg(neg)$	$var(EGFR) - var(TGFR) + var(cFos) + var(Erk) + var(ERF) - var(GSK3) + var(Ets - 1) + var(TCF4)$
		Made CDK4CyclinD1 Target Function more sensitive, avg function could not handle more than 10 inputs	CDK4CyclinD1	$avg(pos) - avg(neg)$	$var(MycMax) - var(p21) - var(p15) + var(Erk) - var(GSK3) - var(p27) + var(TCF4) - var(FoxO) - var(p16)$

Table D.1 continued from previous page

18	19	Changed Myc Target Function to match known response to perturbations in Wnt and HER2, c-fos and ERK were overweighted due to a fork in the network	Myc	$var(EGFR) - var(TGFR) + var(cFos) + var(Erk) + var(ERF) - var(GSK3) + var(Ets-1) + var(TCF4)$	$var(TCF) + var(EGFR) - var(TGFR) + 0.5(var(cFos) + var(Erk)) + var(ERF) - var(GSK3) + var(Ets-1)$
		Added link from TCF to Myc	Myc		TCF now upregulates
19	20	Changed EGF, HER2 and ErbB3 to reflect the dimeric nature of the receptors more accurately.	EGFR	Cell surface receptor	Gene coding for the cell surface receptor, renamed to ErbB1 for consistency
			HER2	Cell surface receptor	Gene coding for the cell surface receptor, renamed to ErbB2 for consistency
			ErbB3	Cell surface receptor	Gene coding for the cell surface receptor
		Added receptor dimers	ErbB1-ErbB1		$min(var(ErbB1), var(ErbB1)) * var(EGF)$
			ErbB1-ErbB2		$min(var(ErbB1), var(ErbB2)) * var(EGF) * var(ErbB2)$
			ErbB2-ErbB3		$min(var(ErbB2), var(ErbB3)) * var(NRG) * var(HER2)$
			EGF	Edge to EGFR	Edge to ErbB1-ErbB1 and ErbB1-ErbB2
			NRG	Edge to ErbB3	Edge ErbB2-ErbB3
			Myc	$var(TCF) + var(EGF) - var(TGFR) + 0.5(var(cFos) + var(Erk)) + var(ERF) - var(GSK3) + var(Ets-1)$	$var(TCF) + avg(var(ErbB1 - ErbB1), var(ErbB1 - ErbB2)) - var(TGFR) + 0.5(var(cFos) + var(Erk)) + var(ERF) - var(GSK3) + var(Ets-1)$
			Dishevelled		Changed the names of both to Dishevelled1 and 2 to avoid confusion

Table D.1 continued from previous page

20	21	BMA does not interpret 0.5 correctly, change to /2	Myc	$var(TCF)+avg(var(ErbB1-ErbB1),var(ErbB1-ErbB2))-var(TGFR)+0.5(var(cFos)+var(Erk))+var(ERF)-var(GSK3)+var(Ets-1)$	$var(TCF)+avg(var(ErbB1-ErbB1),var(ErbB1-ErbB2))-var(TGFR)+(var(cFos)+var(Erk))/2+var(ERF)-var(GSK3)+var(Ets-1)$
21	22	Ets-1, cFos and Erk are all activated from the same node, so averaging counteracts an artificial amplification of the signal	Myc	$var(TCF)+avg(var(ErbB1-ErbB1),var(ErbB1-ErbB2))-var(TGFR)+(var(cFos)+var(Erk))/2+var(ERF)-var(GSK3)+var(Ets-1)$	$var(TCF)+avg(var(ErbB1-ErbB1),var(ErbB1-ErbB2))-var(TGFR)+(var(cFos)+var(Erk)+var(Ets-1))/3+var(ERF)-var(GSK3)$
22	23	Removed activation from EGFR independent of Ras	Myc	$var(TCF)+avg(var(ErbB1-ErbB1),var(ErbB1-ErbB2))-var(TGFR)+(var(cFos)+var(Erk)+var(Ets-1))/3+var(ERF)-var(GSK3)$	$var(TCF)-var(TGFR)+(var(cFos)+var(Erk)+var(Ets-1))/3+var(ERF)-var(GSK3)$
23	24	Change to more complex model of apoptosis, to assess which part of pathway are driving response	Noxa		Added, upregulated by p53
			Bcl-2		$2-avg(var(PUMA),var(BIM),var(BAD))$
			Bcl-xl		$2-avg(var(PUMA),var(BIM),var(BAD))$
			Bcl-W		$2-avg(var(PUMA),var(BIM),var(BAD))$
			Mcl1		$2-avg(var(PUMA),var(BIM),var(Noxa))$

Table D.1 continued from previous page

			A1		$2-avg(var(Noxa), var(PUMA), var(BIM))$
			BAX		$ceil(2-avg(var(Bcl-2), var(Bcl-xl), var(Mcl1), var(Bcl-W), var(A1)))$
			MOMP		Activated by BAX
			Caspase9		Upregulated by MOMP, downregulated by Akt
			Caspase3		Upregulated by Capase9
			Apoptosis		Upregulated by Caspase3
			TRAP1	Directly downregulated apoptosis	Now affects oxidative stress, which may later affect apoptosis
			Apoptosis	$avg(pos)-avg(neg)$	$var(Caspase3)+var(CD95CD95L)$
24	25	Cannot stabilise due to loop in p53 to CDK4 to Rb to p53	E2F-1	Link directly to p53.active	Upregulates p14ARF much like Myc
25	26	mdm2 was not fully inhibited by fully active ARF because it was averaging the effects of ARF, Erk and p53. Thus had effective max of 1	mdm2	$avg(pos)-avg(neg)$ with Arf inhibiting and Erk and p53 activating	$var(p53)+var(Erk)-var(p14ARF)$
		Network could not stabilise	p14ARF	$avg(pos)-avg(neg)$	$max(var(MycMax), var(E2F-1))$
			p14ARF		Changed name to p19ARF
26	27	Apoptosis not sensitive enough to p53	Bcl-2	$2-avg(var(PUMA), var(BIM), var(BAD))$	$floor(2-avg(var(PUMA), var(BIM), var(BAD)))$
			Bcl-xl	$2-avg(var(PUMA), var(BIM), var(BAD))$	$floor(2-avg(var(PUMA), var(BIM), var(BAD)))$
			Bcl-W	$2-avg(var(PUMA), var(BIM), var(BAD))$	$floor(2-avg(var(PUMA), var(BIM), var(BAD)))$

Table D.1 continued from previous page

			Mcl1	$2 - avg(var(PUMA), var(BIM), var(Noxa))$	$floor(2 - avg(var(PUMA), var(BIM), var(Noxa)))$
			A1	$2 - avg(var(Noxa), var(PUMA), var(BIM))$	$floor(2 - avg(var(Noxa), var(PUMA), var(BIM)))$
27	28		Growth Arrest	$2 - var(CDK4CyclinD)$	$1 - ceil(var(CDK4CyclinD))$
28	29	Added nodes for HIF1 pathway	HIF1		Added
			PHD2		$floor(2 - avg(var(PUMA), var(BIM), var(BAD), var(BNIP3)))$
			VHL		$floor(2 - avg(var(PUMA), var(BIM), var(BAD), var(BNIP3)))$
			MT1-MMP		Added
			MMP2		Added
			IAP2		Added
			BNIP3		Added
			IGF2		Added
			VEGF		Added
			BNIP3		Added, edge to Caspase3
29	30	Changed Target Function for mdm2 to accommodate HIF1	MDM2	$var(p53) + var(Erk) - var(p19ARF)$	$var(p53) + var(Erk) - var(p19ARF) - var(HIF1)$
			BNIP3		Added, edge to Caspase3
		Changed VHL range	VHL	$2 - var(rac1)$, Range 0-2	$1 - var(rac1)$, Range 0-1
30	31	Added COX2 connections	COX2		
			PGE2		
			PGE2 (outside)		
			PEA3		Connected to Beta-catenin

Table D.1 continued from previous page

			MMP1		
			MMP9		
			Inflammation		
			Angiogenesis		
			SuppressTcell		
			SuppressDenrtitic		
			SuppressMacrophage		
			Immunosuppression		
31	32	Removed Angiogenesis module to allow changes to Myc Autoregulation	Angiogenesis Module		Removed
		Added Node "Placeholder" which should allow merger of jsons after fork	Placeholder		Added
		Split names of Dishevelled	Dishevelled		Changed Dishevelled to Dishevelled2 so that no duplicate node names
32	33	Added Myc Autoregulation and PTEN	PTEN		$1 + var(MycMax)$
			Akt		PTEN now inhibits Akt
			MycMax		Connects to PTEN
			Akt		Connects to EZH2
			EZH2		$2 - var(Akt)$
		Connect EZH2 to Myc and adjust Target Function accordingly	Myc	$var(TCF) - var(TGFR) + (var(cFos) + var(Erk) + var(Ets - 1))/3 + var(ERF) - var(GSK3)$	$var(TCF) - var(TGFR) + (var(cFos) + var(Erk) + var(Ets - 1))/3 + var(ERF) - var(GSK3) - var(EZH2)$
		PI3K should be able to be raised to 2 when Ras is overexpressed	PI3K	$avg(pos) - avg(neg)$	$var(Ras) + var(ErbB2 - ErbB3)$

Table D.1 continued from previous page

33	34	BioCheck cannot change nodes whose range is of form 1-1	ErbB2	Range 1-1, Target Function: $avg(pos) - avg(neg)$	Range 0-2, Target Function: 1
			ErbB1	Range 1-1, Target Function: $avg(pos) - avg(neg)$	Range 0-2, Target Function: 1
			ErbB3	Range 1-1, Target Function: $avg(pos) - avg(neg)$	Range 0-2, Target Function: 1
			p53	Range 2-2, Target Function: $avg(pos) - avg(neg)$	Range 0-2, Target Function: 2
34	35	BioCheck cannot change nodes whose range is of form 1-1	ErbB2	Range 1-1, Target Function: $avg(pos) - avg(neg)$	Range 0-2, Target Function: 1
			ErbB1	Range 1-1, Target Function: $avg(pos) - avg(neg)$	Range 0-2, Target Function: 1
			ErbB3	Range 1-1, Target Function: $avg(pos) - avg(neg)$	Range 0-2, Target Function: 1
			p53	Range 2-2, Target Function: $avg(pos) - avg(neg)$	Range 0-2, Target Function: 2
35	35.1	Test network	GSK	$avg(pos) - avg(neg)$	$2 - var(Rsk)$
35	35.2	Test network	Fox0	$avg(pos) - avg(neg)$	$2 - var(Akt)$
35	35.3	Test network	Erf	$avg(pos) - avg(neg)$	$2 - var(Erk)$
35.1	35.2	Include Akt in Target Function	GSK3	2-var(Rsk)	$2 - avg(var(Rsk), var(Akt))$
		Connect GSK3 to Erk	GSK3	Inhibits Myc	Inhibits Erk
35.2	35.3	Connect GSK3 to Erk	GSK3	Suppress Erk	Suppress Erk part of Myc Target Function
			Myc	$var(TCF) - var(TGFR) + (var(cFos) + var(Erk) + var(Ets - 1))/3 + var(ERF)$	$var(TCF) - var(TGFR) + (var(cFos) + max(0, var(Erk) - var(GSK3)) + var(Ets - 1))/3 + var(ERF)$

Table D.1 continued from previous page

35.3	35.4	CyclinD1/CDK4 Oversensitive	CyclinD1CDK4	$var(MycMax) - var(p21) - var(p15) + var(Erk) - var(GSK3) - var(p27) + var(TCF) - var(FoxO) - var(p16)$	$avg(pos) - avg(neg)$
35.4	35.5	Myc now suppresses p21,p15 and p27	p21		Suppressed by Myc
			p15		Suppressed by Myc
			p27		Suppressed by Myc
35.5	35.6	Both GSK3 and Gox0 constitutively activated	Fox0	$avg(pos) - avg(neg)$	$2 - var(Akt)$
35.6	35.7	Myc suppressing p21 rather than Myc Max	p21	Suppressed by Myc	Suppressed by MycMax
		Myc suppressing p15 rather than Myc Max	p15	Suppressed by Myc	Suppressed by MycMax
		Myc suppressing p27 rather than Myc Max	p27	Suppressed by Myc	Suppressed by MycMax
		Changed level of FoxO constitutive expression	FoxO	$2 - var(Akt)$	$1 - var(Akt)$
35.7	35.8	FoxO upregulated in response to O2 stress	FoxO	$1 - var(Akt)$	$1 - var(Akt) + min(1, (var(Akt))) * var(OxidativeStress)$
		FoxO upregulates BIM	FoxO	No effect on BIM	Activatory edge to BIM
35.8	35.9	Erf upregulates Myc rather than downregulates	Erf	Activatory edge to myc	Inhibitory edge to myc
		Turn on Erf	Erf	$avg(pos) - avg(neg)$	$2 - var(Erk)$

Table D.1 continued from previous page

		Target Function of Myc has Erf as activatory not inhibitory	Myc	$var(TCF) - var(TGFR) + (var(cFos) + max(0, var(Erk) - var(GSK3)) + var(Ets - 1))/3 + var(ERF)$	$var(TCF) - var(TGFR) + (var(cFos) + max(0, var(Erk) - var(GSK3)) + var(Ets - 1))/3 - var(ERF)$
35.9	40	Re-implementing Myc autoregulation stuff on top of changes made to GSK3, FoxO and ERF			
		Added Myc Autoregulation and PTEN	PTEN		$1 + var(MycMax)$
			Akt		PTEN now inhibits
			MycMax		Connects to PTEN
			Akt		Connects to EZH2
			EZH2		$2 - var(Akt)$
		Connect EZH2 to Myc and adjust Target Function accordingly	Myc	$var(TCF) - var(TGFR) + (var(cFos) + var(Erk) + var(Ets - 1))/3 + var(ERF) - var(GSK3)$	$var(TCF) - var(TGFR) + (var(cFos) + var(Erk) + var(Ets - 1))/3 - var(ERF) - var(GSK3) - var(EZH2)$
		PI3K should be able to be raised to 2 when Ras is overexpressed	PI3K	$avg(pos) - avg(neg)$	$var(Ras) + var(ErbB2 - ErbB3)$
35.9	35.9.	Remove factor of 1/3	Myc	$var(TCF) - var(TGFR) + (var(cFos) + max(0, var(Erk) - var(GSK3))/3 + var(Ets - 1)) - var(ERF)$	$var(TCF) - var(TGFR) + (var(cFos) + max(0, var(Erk) - var(GSK3)) + var(Ets - 1)) - var(ERF)$
		PI3K should be able to be raised to 2 when Ras is overexpressed	PI3K	$avg(pos) - avg(neg)$	$var(Ras) + var(ErbB2 - ErbB3)$

Table D.1 continued from previous page

35.9.1	41	Remove factor of 1/3	Myc	$var(TCF) - var(TGFR) + (var(cFos) + max(0, var(Erk) - var(GSK3))/3 + var(Ets - 1)) - var(ERF)$	$var(TCF) - var(TGFR) + (var(cFos) + max(0, var(Erk) - var(GSK3)) + var(Ets - 1)) - var(ERF)$
35.9.1	35.9.	PUMA knockout no more effective than Noxa Knockout, fix by changing granularity of all nodes below BAX inclusive to granularity 3 to allow enough levels to see this	BAX	Range 0-2	Range 0-3
			BAX	$ceil(2 - avg(var(Bcl - 2), var(Bcl - xl), var(Mcl1), var(Bcl - W), var(A1)))$	$ceil(3 - avg(var(Bcl - 2), var(Bcl - xl), var(Mcl1), var(Bcl - W), var(A1)))$
			MOMP	Range 0-2	Range 0-3
			Caspase9	Range 0-2	Range 0-3
			Caspase3	Range 0-2	Range 0-3
			Apoptosis	Range 0-2	Range 0-3
41	42	PUMA knockout no more effective than Noxa Knockout, fix by changing granularity of all nodes below BAX inclusive to granularity 3 to allow enough levels to see this	BAX	Range 0-2	Range 0-3
			BAX	$ceil(2 - avg(var(Bcl - 2), var(Bcl - xl), var(Mcl1), var(Bcl - W), var(A1)))$	$ceil(3 - avg(var(Bcl - 2), var(Bcl - xl), var(Mcl1), var(Bcl - W), var(A1)))$
			MOMP	Range 0-2	Range 0-3
			Caspase9	Range 0-2	Range 0-3

Table D.1 continued from previous page

			Caspase3	Range 0-2	Range 0-3
			Apoptosis	Range 0-2	Range 0-3
42	43	Added Connection from EGF to ErbB3	ErbB2-ErbB3	$min(var(ErbB2), var(ErbB3)) * var(NRG) * var(ErbB2)$	$min(var(ErbB2), var(ErbB3)) * var(NRG) * var(ErbB2)$ and edge from EGF to this node
		PI3K back to $avg(pos) - avg(neg)$	PI3K	$var(Ras) + var(ErbB2 - ErbB3)$	$avg(pos) - avg(neg)$
		Erk downregulate FoxO3a		$1 - avg(var(Akt)) + min(1, (var(Akt))) * var(OxidativeStress)$	$1 - avg(var(Akt), min(var(mdm2), var(Erk))) + min(1, (var(Akt))) * var(OxidativeStress)$
43	44	Connect p53 to PTEN	PTEN	Only regulated by Myc	Regulated by Myc and p53
		Change PTEN Target Function to $avg(pos) - avg(neg)$		$1 + var(MycMax)$	$avg(pos) - avg(neg)$
44	45	Change Myc Target Function to average		$var(TCF) - var(TGFR) + (var(cFos) + max(0, var(Erk) - var(GSK3)) + var(Ets - 1)) - var(ERF) - var(EZH2)$	$avg(var(TCF), var(cFos), var(Ets - 1), max(0, var(Erk) - var(GSK3))) - avg(var(TGFR), var(ERF), var(EZH2))$
		Correct Target Function of ErbB2-ErbB3	ErbB2-ErbB3	$min(var(ErbB2), var(ErbB3)) * var(NRG) * var(ErbB2) * var(EGF)$	$min(var(ErbB2), var(ErbB3)) * avg(var(NRG), var(EGF)) * var(ErbB2)$
45	46	Change Akt Target Function to lower power of PTEN		$avg(pos) - avg(neg)$	$min(1, 2 - var(PI3K)) * (var(PI3K) - var(PTEN)) + (1 - min(1, 2 - var(PI3K))) * var(PI3K)$
46	47	Increase range of PI3K so it can better integrate range of inputs.	PI3K	Range of 0-2	Range of 0-4

Table D.1 continued from previous page

47	48	Decrease basal activity of GSK3	GSK3	$2-avg(var(Rsk),var(Akt))$	$1-avg(var(Rsk),var(Akt))$
48	49	Integrate HIF	Added from Network 35		
49	50	Removed HIF1 upregulation of PHD2	PHD2	$2-var(HIF1)-var(LowOxygen)$	$2-var(LowOxygen)$
		Removed connection of Rac1 to VHL	VHL	$2-var(rac1)$	$const(2)$
50	51	Change Target Function of Akt, as PTEN not effective	Akt	$min(1,2-var(PI3K))*(var(PI3K)-var(PTEN))+(1-min(1,2-var(PI3K)))*var(PI3K)$	$var(PI3K)-floor(var(PTEN)/2)$
51	52	Change Target Function of Myc	Myc not quite sensitive enough	$avg(var(TCF),var(cFos),var(Ets-1),max(0,var(Erk)-var(GSK3)))-avg(var(TGFR),var(ERF),var(EZH2))$	$ceil(avg(var(TCF),var(cFos),var(Ets-1),max(0,var(Erk)-var(GSK3))))-avg(var(TGFR),var(ERF),var(EZH2))$
52	53	Change Target Function of Akt, as PTEN not effective	Akt	$var(PI3K)-floor(var(PTEN)/2)$	$var(PI3K)-var(PTEN)+(1-min(1,2-var(PI3K)))$
53	54	Test of whether PI3K does need granularity of 4 or if it can be granularity of 2	PI3K	Range 0-4	Range 0-2
54	55	Revert PI3K to granularity 4 as easier for batch script, change back after		Range 0-2	Range 0-4
		Put IAP2 to 0 until can put in network more completely	IAP2	$avg(pos)-avg(neg)$	const(0)
55	56	Allow VEGF to counteract hypoxia	VEGF		VEGF inhibits LowOxygen $avg(pos)-avg(neg)$

Table D.1 continued from previous page

		Node to set initial level of hypoxia	LowOxygenInitial		LowOxygenInitial upregulates LowOxygen $avg(pos) - avg(neg)$
56	57	COX2 now upregulates Akt	Akt	$var(PI3K) - var(PTEN) + (1 - min(1, 2 - var(PI3K)))$	$avg(var(COX2), var(PI3K)) - var(PTEN) + (1 - min(1, 2 - var(PI3K)))$
57	58	Renamed LowOxygen to Hypoxia			
		Removed VEGF to Hypoxia loop for validation testing			
58	59	VEGF upregulates Hypoxia directly, when it should be via Angiogenesis	VEGF		Removed inhibitory link to Hypoxia
			Angiogenesis		Added inhibitory link to Hypoxia
59	60	Change name of LowOxygen and LowOxygen Initial to Hypoxia	LowOxygen	LowOxygen	Hypoxia
			LowOxygenInitial	LowOxygenInitial	HypoxiaInitial
		Remove link from COX2 to Akt	COX2	Activatory Link to Akt	Removed
			Akt	Activatory Link from COX2	Removed
		Changed Akt Target Function back to pre-COX2 version	Akt	$avg(var(COX2), var(PI3K)) - var(PTEN) + (1 - min(1, 2 - var(PI3K)))$	$var(PI3K) - var(PTEN) + (1 - min(1, 2 - var(PI3K)))$
		Made PGE2 node external	PGE2	Internal (red) node	External (grey) node
		Add EP4 Node	EP4		Added EP4 as receptor (green) node
		Connect EP4 to PI3K	EP4		Activatory link to PI3K
			PI3K		Activatory link from EP4
		Connection from COX2 to VEGF	COX2		Activatory link to VEGF
			VEGF		Activatory link from COX2
60	61	HypoxiaInitial was hard coded to be fixed at 2, throwing off results.	HypoxiaInitial	$const(2)$	$avg(pos) - avg(neg)$

Table D.1 continued from previous page

61	62	Made separate Apoptosis bubble for clarity about high level behaviours	Apoptosis		Made into own module
62	63	Added links from EGF to VEGF	ErbB1-ErbB1		Activatory link to p38
			ErbB1-ErbB2		Activatory link to p38
			p38		Created node, range 0-2
			p38		Activatory link from EGF and to VEGF
			VEGF		Activatory link from p38
63	64	Changed connection from EGFR and HER2 to p38 to be via Ras/Mek	ErbB1-ErbB1	Activatory link to p38	Removed
			ErbB1-ErbB2	Activatory link to p38	Removed
			p38	Activatory link from ErbB1-ErbB1	Removed
			p38	Activatory link from ErbB1-ErbB2	Removed
			Mek		Activatory link to p38
			p38		Activatory link from p38
64	65	Add activation of p21 and p27 by HIF1	HIF1		Activatory link to p21
			HIF1		Activatory link to p27
			p21		Activatory link from p21
			p27		Activatory link from p27
65	66	Add inhibition of p21 and p27 by COX2	COX2		Inhibitory link to p21
			COX2		Inhibitory link to p27
			p21		Inhibitory link from COX2
			p27		Inhibitory link from COX2
66	67	Remove links from COX2 to p21 and p27	COX2	Inhibitory link to p21	Removed

Table D.1 continued from previous page

			COX2	Inhibitory link to p27	Removed
			p21	Inhibitory link from COX2	Removed
			p27	Inhibitory link from COX2	Removed
		Raise granularity of VEGF to 3	VEGF	Range 0-2	Range 0-3
		Remove link from HypoxiaInitial to Myc	HypoxiaInitial	Inhibitory Link to myc (not effective as not in Target Function)	Removed
			Myc	Inhibitory Link from HypoxiaInitial	Removed
		Change p21 Target Function to let HIF1 stop myc repression as well as activating p21	p21	$avg(pos) - avg(neg)$	$var(HIF1) - max(0, (var(MycMax) - var(HIF1)))$
		Change p27 Target Function to let HIF1 stop myc repression as well as activating p27	p27	$avg(pos) - avg(neg)$	$avg(var(FoxO), var(HIF1)) - max(0, (var(MycMax) - var(HIF1)))$
		Increase granularity of CDK4CyclinD	CDK4CyclinD	Range 0-2	Range 0-3
		Increase granularity of Growth Arrest	Growth Arrest	Range 0-2	Range 0-3
		Change Target Function of Growth Arrest to allow new granularity	Growth Arrest	$2 - var(CDK4CyclinD)$	$3 - var(CDK4CyclinD)$
67	68	Erk downregulates Bim	Erk		Inhibitory node to BIM
			BIM		Inhibitory nodes from Erk
		Remove STAT3 CD95 pathway	JNK		Removed
			STAT3		Removed
			c-jun		Removed
			STAT3c-jun		Removed
			CD95CD95L		Removed
			CD95		Removed

Table D.1 continued from previous page

			CD95L		Removed
			Apoptosis	$var(Caspase3) + var(CD95CD95L)$	$var(Caspase3)$
68	69	Myc upregulates Noxa	Myc		Activatory link to Noxa
			Noxa		Activatory link from Myc
69	70	BNIP3 activates Bax directly, not via Bcl proteins	BNIP3	Inhibitory link to Bcl-2 and Bcl-xl	Activatory link to Bax
			Bcl-2	Inhibitory link from BNIP3	
			Bcl-xl	Inhibitory link from BNIP3	
			Bcl-2	$floor(2 - avg(var(PUMA), var(BIM), var(B$	$floor(2 - avg(var(PUMA), var(BIM), var(BAD)))$
			Bcl-xl	$floor(2 - avg(var(PUMA), var(BIM), var(B$	$floor(2 - avg(var(PUMA), var(BIM), var(BAD)))$
			Bax	$ceil(3 - avg(var(Bcl-2), var(Bcl-xl), var(Mcl1), var(Bcl-W), var(A1)))$	$ceil(3 - avg(var(Bcl-2), var(Bcl-xl), var(Mcl1), var(Bcl-W), var(A1)))$
70	71	Add p53 influence to p21	p21	$var(HIF1) - max(0, (var(MycMax) - var(HIF1)))$	$var(HIF1) + var(p53.active) - avg(var(Akt), max(0, (var(MycMax) - var(HIF1))))$
71	72	Adjust sensitivity of mdm2	mdm2	$var(p53) + var(Erk) - var(p19ARF) - var(HIF1)$	$avg(var(p53), var(Erk)) - var(p19ARF) - var(HIF1)$
72	73	Correct Erk mechanism of p53 suppression	Erk	Activate mdm2	Inhibit p53.active
			mdm2	Inhibition by Erk	
			p53.active		Activated by Erk

Table D.1 continued from previous page

			mdm2	$avg(var(p53), var(Erk)) - var(p19ARF) - var(HIF1)$	$var(p53) - var(p19ARF) - var(HIF1)$
73	74	Remove influence of HIF1	p21	$var(HIF1) + var(p53.active) - avg(var(Akt), max(0, (var(MycMax) - var(HIF1))))$	$var(p53.active) - avg(var(Akt), max(0, (var(MycMax) - var(HIF1))))$
74	75	Adjust HIF1 Target Function	HIF1	$var(Akt) - var(VHL) * (var(PHD2)) - (var(p53.active) * (1 - var(p53.active)))$	$1 + var(Akt) - var(VHL) * (var(PHD2)) - (var(p53.active) * min(1, (var(p53.active) - 1)))$
		VHL gets multiplied in another Target Function, so misleading to be $const(2)$	VHL	$const(2)$	$const(1)$
75	76	Proliferation should be the same granularity as other phenotypes	Proliferation	Range 0-2	Range 0-3
		Invasiveness should be the same granularity as other phenotypes	Invasiveness	Range 0-2	Range 0-3
76	77	Increase sensitivity to mitogenic signals so there is proliferation in MCF10A	CDK4CylinD	$avg(pos) - avg(neg)$	$var(MycMax) + var(Erk) + var(TCF) - avg(var(p21), var(p16), var(GSK3), var(p27), var(FoxO), var(p15))$
77	78	Introduce threshold for PUMA and Noxa activation by p53	PUMA	$avg(pos) - avg(neg)$	$max(0, var(p53.active) - 1) * 2$
			Noxa	$avg(pos) - avg(neg)$	$avg((max(0, var(p53.active) - 1) * 2), var(MycMax))$
78	79		mdm2	$var(p53) - var(p19ARF) - var(HIF1)$	$avg(pos) - avg(neg)$

Table D.1 continued from previous page

			Caspase 9	$avg(pos) - avg(neg)$	$var(MOMP) - 2 * var(Akt)/3$
79	80		mdm2	$avg(pos) - avg(neg)$	$var(p53) - var(p19ARF) - var(HIF1)/2$
			p19ARF	$max(var(MycMax), var(E2F - 1))$	$avg(pos) - avg(neg)$
80	81.1	Expand BIM regulation	E2F1		Activate BIM
			E2F1		Activate EZH2
			EZH2	$2 - var(Akt)$	$var(E2F1) - var(Akt)$
			EZH2		Inhibit BIM
			BIM		Activated by E2F1
			BIM		Inhibited by EZH2
			Myc	$avg(var(TCF), var(cFos), var(Ets - 1), max(0, var(Erk) - var(GSK3))) - avg(var(TGFR), var(ERF), var(EZH2))$	$floor(avg(var(TCF), var(cFos), var(Ets - 1), max(0, var(Erk) - var(GSK3))) - avg(var(TGFR), var(ERF), var(EZH2)))$
81.1	81.2	Add VEGF Myc interaction	Myc	Activates VEGF	Remove
			VEGF	Activated by Myc	Remove
		Make HIF a stronger regulator of VEGF than COX2 and p38	VEGF	$avg(pos) - avg(neg)$	$var(HIF1) + avg(var(COX2), var(p38))$
81.2	81.3	Observed that p27 low when myc is low	TCF		Inhibit p27
			p27	$avg(var(FoxO), var(HIF1)) - max(0, (var(MycMax) - var(HIF1)))$	$avg(var(FoxO), var(HIF1)) - avg(var(TCF), max(0, (var(MycMax) - var(HIF1))))$

Table D.1 continued from previous page

81.3	81.4	Myc too well autorepressed	Myc	$floor(avg(var(TCF),$ $var(cFos), var(Ets-1),$ $max(0, var(Erk)-var(GSK3)))$ $-avg(var(TGFR), var(ERF),$ $var(EZH2)))$	$avg(var(TCF), var(cFos), var(Ets-1),$ $max(0, var(Erk)-var(GSK3)))$ $-avg(var(TGFR), var(ERF),$ $min(1, var(EZH2)))$
			CDK4CylinD	$var(MycMax)+var(Erk)$ $+var(TCF)-avg(var(p21),$ $var(p16), var(GSK3),$ $var(p27), var(FoxO),$ $var(p15))$	$avg(pos)-avg(neg)$
81.1	82	Keep same but rename for testing			
81.2	82.1	Keep same but rename for testing			
81.3	82.2	Keep same but rename for testing			
81.4	82.3	Keep same but rename for testing			
81.3	82.4	Default mdm2	mdm2	$var(p53)-var(p19ARF)-$ $var(HIF1)/2$	$avg(pos)-avg(neg)$
81.3	82.5	Mdm2 normal weighting	mdm2	$var(p53)-var(p19ARF)-$ $var(HIF1)/2$	$var(p53)-var(p19ARF)-var(HIF1)$
81.3	82.6	Add back HIF to p21	p21	$var(p53.active)-$ $avg(var(Akt), max(0, (var(MycMax$ $var(HIF1))))$	$var(HIF1)+var(p53.active)-$ $avg(var(Akt), max(0, (var(MycMax)-$ $var(HIF1))))$
82.6	83	Add transactivation of EGFR by Wnt	Wnt1		Activate ErbB1-ErbB1
			ErbB1-ErbB1		Activated by Wnt1
			ErbB1-ErbB1	$min(var(ErbB1), var(ErbB1))*$ $var(EGF)$	$min(var(ErbB1), var(ErbB1))*$ $max(var(EGF), var(Wnt1))$

Table D.1 continued from previous page

				$avg(var(TCF),$ $var(cFos),var(Ets-1),$ $max(0,var(Erk)-var(GSK3)))$ $-avg(var(TGFR),var(ERF),$ $min(1,var(EZH2)))$	$floor(avg(var(TCF),$ $var(cFos),var(Ets-1),$ $max(0,var(Erk)-var(GSK3)))$ $-avg(var(TGFR),var(ERF),$ $min(1,var(EZH2))))$
83	84	Myc oscillating	Myc		
84	85	Change VEGF sensitivity to HIF1	VEGF	$var(HIF1)+$ $avg(var(COX2),var(p38))$	$var(HIF1)+$ $avg(var(COX2),var(p38))/2$
85	86	Increase Apoptosis sensitivity	Bax	$ceil(3-avg(var(Bcl-$ $2),var(Bcl-$ $xl),var(Mcl1),var(Bcl-$ $W),var(A1))+var(BNIP3))$	$ceil(6-avg(var(Bcl-2),var(Bcl-$ $xl),var(Mcl1),var(Bcl-W),var(A1))+$ $var(BNIP3))$
			Bax	Range 0-3	Range 0-6
			MOMP	Range 0-3	Range 0-6
			Caspase3	Range 0-3	Range 0-6
			Caspase9	Range 0-3	Range 0-6
			Apoptosis	Range 0-3	Range 0-6
			IAP2		Remove
86	87	Add back Apoptosis thresholding	PUMA	$avg(pos)-avg(neg)$	$max(0,var(p53.active)-1)*2$
			Noxa	$avg(pos)-avg(neg)$	$avg((max(0,var(p53.active)-1)*$ $2),var(MycMax))$
		Add Apoptosis_short node	Apoptosis_short		Activated by Apoptosis
					Range 0-3
86	88	Erk overrides effect of mdm2 on p53	p53.active	$avg(pos)-avg(neg)$	$var(p53)-$ $max(var(mdm2),(var(Erk)/2))$
		E2F1 potentiates p19ARF, but does not trigger it	p19ARF	$avg(pos)-avg(neg)$	$var(MycMax)*var(E2F-1)$

Table D.1 continued from previous page

88	89	Add "Apoptosis Long" node, so that final apoptosis node is only 0-3	Apoptosis		Rename to ApoptosisLong with 0-6 range
			Apoptosis		New node of range 0-3
89	90	E2F1 only activates p19ARF above a threshold	p19ARF	$var(MycMax) * var(E2F-1)$	$var(MycMax) + (var(E2F-1) * min(1,(var(E2F-1)-1)))$
90	91	Simplify PI3K/Akt Target Function	Akt	$var(PI3K) - var(PTEN) + (1 - min(1, 2 - var(PI3K)))$	$avg(pos) - avg(neg)$
			PI3K	Range 0-4	Range 0-2
91	92	Simplify Myc Target Function	cFos		Remove
			ERF		Remove
			Elk-1		Remove
			Myc	$floor(avg(var(TCF), var(cFos), var(Ets-1), max(0, var(Erk) - var(GSK3))) - avg(var(TGFR), var(ERF), min(1, var(EZH2))))$	$floor(avg(var(TCF), var(Ets-1), max(0, var(Erk) - var(GSK3))) - avg(var(TGFR), min(1, var(EZH2))))$
		Add Akt to Raf1 feedback	Akt		Inhibits Raf-1
			Raf-1		inhibited by Akt
		Add activation of ARF by Wnt1	TCF		Activate p19ARF
			p19ARF		Activated by TCF
			p19ARF	$var(MycMax) + (var(E2F-1) * min(1,(var(E2F-1)-1)))$	$max(var(MycMax), max((var(E2F-1) * min(1,(var(E2F-1)-1))), (var(TCF) * min(1,(var(TCF)-1)))))$
92	93	Allow high Ras to override Akt inhibition	Raf-1	$avg(pos) - avg(neg)$	$min(var(Ras), 2 - var(Akt))$

Table D.1 continued from previous page

		Low GSK3 cannot substitute for Dishevelled	GSK3-Axin-APC-CK1	$avg(pos) - avg(neg)$	$min(var(GSK3), 2 - var(Dishevelled))$
		TCF only affects ARF at high levels	p19ARF	$max(var(MycMax), max((var(E2F 1) * min(1, (var(E2F - 1) - 1))), (var(TCF) * min(1, (var(TCF) - 1)))))$	$max(var(MycMax), max((var(E2F - 1) * min(1, (var(E2F - 1) - 1))), (1 - min(1, 2 - var(TCF)))))$
93	94	Re-add Akt Target Function for non-basal cells as experiment	Akt	$avg(pos) - avg(neg)$	$var(PI3K) - var(PTEN) + (1 - min(1, 2 - var(PI3K)))$
95	96	Make Dishevelled the rate limiting factor in TCF degradation. If Dishevelled is 0 but GSK3 is 1, TCF being 1, making it look like Wnt1 is 1 is a bit too powerful	GSK3-Axin-APC-CK1	$min(var(GSK3), 2 - var(Dishevelled))$	$min(1, var(GSK3)) * (2 - var(Dishevelled))$
		Fix Raf-1, current Target Function blocks Ras activation entirely if Akt is 2. Change so that Akt can only control Raf by a max of 1		$min(var(Ras), 2 - var(Akt))$	$var(Ras) - min(1, var(Akt))$
91	97	Make Dishevelled the rate limiting factor in TCF degradation. If Dishevelled is 0 but GSK3 is 1, TCF being 1, making it look like Wnt1 is 1 is a bit too powerful	GSK3-Axin-APC-CK1	$(var(GSK3) - var(Dishevelled))$	$min(1, var(GSK3)) * (2 - var(Dishevelled))$
97	98	Block p19ARF by Wnt1	Wnt1		Inhibitory edge to p19ARF
			p19ARF		Inhibitory edge from Wnt1
			p19ARF	$var(MycMax) + (var(E2F - 1) * min(1, (var(E2F - 1) - 1)))$	$var(MycMax) + (var(E2F - 1) * min(1, (var(E2F - 1) - 1))) - var(Wnt1)$

Table D.1 continued from previous page

98	99	Move suppression of p19ARF from Wnt1 to TCF as seems to go via beta-cat at least	Wnt1	Inhibitory edge to p19ARF	Removed
			p19ARF	Inhibitory edge from Wnt1	Removed
			TCF		Inhibitory edge to p19ARF
			p19ARF		inhibitory edge from TCF
		Blockade of p19ARF by Wnt1 too strong	p19ARF	$var(MycMax) + (var(E2F-1) * min(1,(var(E2F-1)-1))) - var(Wnt1)$	$var(MycMax) + (var(E2F-1) * min(1,(var(E2F-1)-1))) - var(TCF)/2$
		Change Erk effect on p53	Erk	Inhibitory edge to p53.active	Removed
			p53.active	Inhibitory edge from Erk	Removed
			p53.active	$var(p53) - max(var(mdm2),(var(Erk)/2))$	$var(p53) - var(mdm2)$
			Erk		Inhibitory edge to p21
			p21		Inhibitory edge from Erk
			p21	$var(p53.active) - avg(var(Akt), max(0,(var(MycMax) - var(HIF1))))$	$var(p53.active) - avg(var(Erk),var(Akt), max(0,(var(MycMax) - var(HIF1))))$
99	100	Add Twist as effector of Wnt effects on p19ARF	TCF	Inhibitory edge to p19ARF	Activatory edge to Twist
			p19ARF	Inhibitory edge from TCF	Inhibitory edge from Twist
			Twist		Inhibitory edge from TCF
			Twist		Inhibitory Edge to p19ARF
			p19ARF	$var(MycMax) + (var(E2F-1) * min(1,(var(E2F-1)-1))) - var(TCF)/2$	$var(MycMax) + (var(E2F-1) * min(1,(var(E2F-1)-1))) - var(Twist)/2$

Table D.1 continued from previous page

100	101	Bad could not activate	Bad		$2 - avg(var(Rsk), var(Akt))$
			Rsk		Inhibitory edge to Bad
			Bad		Inhibitory edge from Rsk
101	102	Remove PTMA	CDK4CyclinD	$avg(pos) - avg(neg)$	$ceil(avg(var(MycMax), var(Erk), var(TCF)) - avg(var(p21), var(p16), var(GSK3), var(p27), var(FoxO), var(p15)))$
		Wnt transactivation	Wnt1	Activatory edge to ErbB1-ErbB1	Removed
			ErbB1-ErbB1	Activatory edge from Wnt1	Removed
			ErbB1-ErbB1	$min(var(ErbB1), var(ErbB1)) * max(var(EGF), var(Wnt1))$	$min(var(ErbB1), var(ErbB1)) * var(EGF)$
		Myc inhibits p16	Myc		Inhibitory edge to p16
			p16		Inhibitory edge from Myc
		Dishevelled inhibits GSK3	GSK3	$2 - avg(var(Rsk), var(Akt))$	$2 - avg(var(Rsk), var(Akt), var(Dishevelled))$
			Dishevelled		Inhibitory edge to GSK3
			GSK3		Inhibitory edge from Dishevelled
			PTMA		Removed
98	103	Move suppression of p19ARF from Wnt1 to TCF	Wnt1	Inhibitory edge to p19ARF	Removed
			p19ARF	Inhibitory edge from Wnt1	Removed
			TCF		Inhibitory edge to p19ARF
			p19ARF		inhibitory edge from TCF
		Blockade of p19ARF by Wnt1 too strong	p19ARF	$var(MycMax) + (var(E2F-1) * min(1, (var(E2F-1) - 1))) - var(Wnt1)$	$var(MycMax) + (var(E2F-1) * min(1, (var(E2F-1) - 1))) - var(TCF)/2$

Table D.1 continued from previous page

Change Erk effect on p53	Erk	Inhibitory edge to p53.active	Removed
	p53.active	Inhibitory edge from Erk	Removed
	p53.active	$var(p53) - max(var(mdm2), (var(Erk)/2))$	$var(p53) - var(mdm2)$
	Erk		Inhibitory edge to p21
	p21		Inhibitory edge from Erk
	p21	$var(p53.active) - avg(var(Akt), max(0, (var(MycMax) - var(HIF1))))$	$var(p53.active) - avg(var(Erk), var(Akt), max(0, (var(MycMax) - var(HIF1))))$
Add Twist as effector of Wnt effects on p19ARF	TCF	Inhibitory edge to p19ARF	Activatory edge to Twist
	p19ARF	Inhibitory edge from TCF	Inhibitory edge from Twist
	Twist		Inhibitory edge from TCF
	Twist		Inhibitory Edge to p19ARF
	p19ARF	$var(MycMax) + (var(E2F-1) * min(1, (var(E2F-1) - 1))) - var(TCF)/2$	$var(MycMax) + (var(E2F-1) * min(1, (var(E2F-1) - 1))) - var(Twist)/2$
Bad could not activate	Bad		$2 - avg(var(Rsk), var(Akt))$
	Rsk		Inhibitory edge to Bad
	Bad		Inhibitory edge from Rsk
Remove PTMA	CDK4CyclinD	$avg(pos) - avg(neg)$	$ceil(avg(var(MycMax), var(Erk), var(TCF)) - avg(var(p21), var(p16), var(GSK3), var(p27), var(FoxO), var(p15)))$
Wnt transactivation	Wnt1	Activatory edge to ErbB1-ErbB1	Removed
	ErbB1-ErbB1	Activatory edge from Wnt1	Removed

Table D.1 continued from previous page

		Removal of min	ErbB1-ErbB1	$min(var(ErbB1), var(ErbB1)) * max(var(EGF), var(Wnt1))$	$var(ErbB1) * var(EGF)$
		Myc inhibits p16	MycMax		Inhibitory edge to p16
			p16		Inhibitory edge from Myc
		Dishevelled inhibits GSK3	GSK3	$2 - avg(var(Rsk), var(Akt))$	$2 - avg(var(Rsk), var(Akt), var(Dishevelled))$
			Dishevelled		Inhibitory edge to GSK3
			GSK3		Inhibitory edge from Dishevelled
			PTMA		Removed
		Remove ERF	ERF		Removed
		Remove c-Fos	c-Fos		Removed
		Remove Elk-1	Elk-1		Removed
102	104	GSK3-Axin-APC-CK1 corrected	GSK3-Axin-APC-CK1	$var(GSK3) - var(Dishevelled)$	$min(1, var(GSK3)) * (2 - var(Dishevelled))$
		Change Myc mediated suppression of p16 to be via MycMax	Myc	Inhibitory edge to p16	Removed
			p16	Inhibitory edge from Myc	Inhibitory edge from MycMax
			MycMax		Inhibitory edge to p16
104	105	Add CDK2 with activation by Myc and suppression by p21 and p27	CDK2CyclinE		Added
			MycMax		Activatory edge to CDK2
			CDK2CyclinE		Activatory edge to from MycMax
			p21		Inhibitory edge to CDK2
			CDK2CyclinE		Inhibitory edge from p21
			p27		Inhibitory edge to CDK2
			CDK2CyclinE		Inhibitory edge from p27
			Rb		Removed

Table D.1 continued from previous page

		Connect E2F to Proliferation to integrate the CDKs	E2F1		Raise granularity to 3
			E2F1		Activatory edge to Proliferation
			CDK4CyclinD	Activatory edge to Proliferation	Removed
			Proliferation		Activatory edge from Proliferation
		Increase Range	pRb	$avg(pos) - avg(neg)$	$3 - avg(var(CDK4CyclinD), var(CDK2))$
		Invert pRb as inhibits E2F	pRb	Activatory edge to E2F1	Inhibitory edge to E2F1
			CDK4CyclinD	Activatory edge to pRb	Inhibitory edge to pRb
			CDK2	Activatory edge to pRb	Inhibitory edge to pRb
			CDK4CyclinD		$(avg(var(MycMax), var(Erk), var(TCF)) - avg(var(p21), var(p16), var(GSK3), var(p27), var(FoxO), var(p15)))$
			CDK2		$ceil(var(MycMax) - avg(var(p21), var(p27)))$
		Remove Erk inhibition of p21	p21	$var(p53.active) - avg(var(Erk), var(Akt), max(0, (var(MycMax) - var(HIF1))))$	$var(p53.active) - avg(var(Akt), max(0, (var(MycMax) - var(HIF1))))$
			Erk	Inhibitory edge to p21	Removed
			p21	Inhibitory edge from Erk	Removed
105	106	FoxO inhibits p21	p21	$var(p53.active) - avg(var(Akt), max(0, (var(MycMax$ $var(HIF1))))$	$avg(var(p53.active), var(FoxO)) - avg(var(Akt), max(0, (var(MycMax) - var(HIF1))))$

Table D.1 continued from previous page

			FoxO		Activatory edge to p21
			p21		Activatory edge from p21
		GSK3 inhibits CDK2	CDK2	$ceil(var(MycMax) - avg(var(p21), var(p27)))$	$ceil(var(MycMax) - avg(var(p21), var(p27), var(GSK3)/2))$
			GSK3		Inhibitory edge to CDK2
			CDK2		Inhibitory edge from GSK3
		Bad too active	BAD	$2 - avg(var(Rsk), var(Akt))$	$2 - max(var(Rsk), var(Akt))$
		Remove p53 p53.active split	p53		Removed
			p53.active	$var(p53) - var(mdm2)$	$2 - var(mdm2)$
			mdm2	$var(p53) - var(p19ARF) - var(HIF1)/2$	$2 - var(p19ARF) - var(HIF1)/2$
106	107	p19ARF		$var(MycMax) + (var(E2F-1) * min(1, (var(E2F-1)-1))) - var(Twist)/2$	$max(var(MycMax), (var(E2F-1) * min(1, (var(E2F-1)-1)))) - var(Twist)/2$
107	108	Test of ko of BAD	BAD	$2 - max(var(Akt), var(Rsk))$	$const(0)$
107	109	Test of hypoxia from being fixed at 1 for hetlo to being CAPPED at 1 for hetlo	Hypoxia	$avg(pos) - avg(neg)$	$min(1, var(HypoxiaInitial) - var(Angiogenesis))$
107	110	Corrected link from E2F1 to Proliferation	CDK4	Activatory Edge to Proliferation	Removed
			E2F-1		Activatory Edge to Proliferation
			Proliferation	Activatory Edge from CDK4	Activatory Edge from E2F-1
			pRb	$3 - avg(var(CDK4CyclinD), var(CDK2)$	$3 - ceil(avg(var(CDK2), var(CDK4CyclinD)))$

Table D.1 continued from previous page

			CDK4	$ceil(avg(var(MycMax), var(Erk), var(TCF)) - avg(var(p21), var(p16), var(GSK3), var(p27), var(FoxO), var(p15)))$	$(avg(var(MycMax), var(Erk), var(TCF)) - avg(var(p21), var(p16), var(GSK3), var(p27), var(FoxO), var(p15)))$
110	111	Test of removal of ErbB3	ErbB3		Removed
			NRG		Removed
			VEGF	$var(HIF1) + avg(var(COX2), var(p38))/2$	$avg(var(HIF1), var(COX2)/2)$
			p38		Removed
			ROR2		Removed
			Dishevelled2		Removed
			DAAM1		Removed
			Prolifin		Removed
			Rho		Removed
			ROCK		Removed
			rac1		Removed
			Invasiveness		Removed
			MMP1		Removed
			MMP9		Removed
			PEA3		Removed
			MMP2		Removed
			MT1-MMP		Removed
			Inflammation		Removed
			IGF2		Removed
			Elk-1		Removed
			cFos		Removed

Table D.1 continued from previous page

			ERF		Removed
107	112	Add Het node to switch on cap on hypoxia	Het		Default Target Function of 2, switch to 1 in het case
					Activatory edge from Het to Hypoxia
			Hypoxia	$var(HypoxiaInitial) - var(Angiogenesis)$	$min(var(Het), var(HypoxiaInitial) - var(Angiogenesis)/2)$
108	113		Remove p38		
			Adjust VEGF	$var(HIF1) + avg(var(COX2), var(p38))/2$	$avg(var(HIF1), var(COX2)/2)$
			Normalise VEGF Range	0-3	0-2
			BAX	$ceil(6 - avg(var(Bcl-2), var(Bcl-xl), var(Mcl1), var(Bcl-W), var(A1)) + var(BNIP3))$	$ceil(6 - avg(var(Bcl-2), var(Bcl-xl), var(Mcl1), var(Bcl-W), var(A1)) + var(BNIP3)/2)$
109	114		BAX	$ceil(6 - avg(var(Bcl-2), var(Bcl-xl), var(Mcl1), var(Bcl-W), var(A1)) + var(BNIP3)/2)$	$ceil(6 - avg(var(Bcl-2), var(Bcl-xl), var(Mcl1), var(Bcl-W), var(A1)) + var(BNIP3))$
111	115		VEGF		$var(HIF1) + avg(var(COX2), var(p38))/2$
			p38	Added back	
114	116		Revert VEGF Target Function		
110	117		Remove NRG but leave ErbB3 as important differentiator between HER2 and EGFR		
			Added CDKN2A node		

Table D.1 continued from previous page

			removed ERF etc		
			Added back cFos and Elk-1 but left out ERF		
117	118		removed ERF but left cFos and Elk-1 as makes more stable		
118	119	Consolidated effect of hypoxia and TRAP1 into FoxO Target Function to remove Oxidative Stress node	Oxidative Stress	Removed	
			FoxO	$1 - avg(var(Akt), min(var(mdm2), var(Erk)))$ $+ min(1, (var(Akt)))$ $* (var(OxidativeStress))$	$1 - avg(var(Akt), min(var(mdm2), var(Erk)))$ $+ min(1, (var(Akt)))$ $* (var(Hypoxia) - var(TRAP1))$
		Remove Unused Nodes	Immunosuppression		
			IGF2		
			Inflammation		
			ROR2		
			Dishevelled2		
			rac1		
			DAAM1		
			Prolifin		
			Rho		
			ROCK		
			MT1-MMP		
			MMP2		
			MMP1		
			MMP9		

Table D.1 continued from previous page

		Invasiveness	
		GrowthArrest	
		Change Apop back to 0-6 or just remove apop long?	Removed ApoptosisLong
		VEGF 0-2 or 0-3?	
		VEGF as phenotype?	Switched to normal external protein
		Angiogenesis 0-3	Changed range to 0-3 as phenotype
		p53.active	Changed name to p53
		p19ARF	Rename to ARF
119	120	Rename Ets-1 to Ets-2	